Exploring the Limits of Hydrogen Assisted Jet Ignition

by

Ferenc Hamori
B.Eng. (Mech)(Hons)

Submitted in total fulfilment of the requirements
of the degree of Doctor of Philosophy
March 2006

Department of Mechanical and Manufacturing Engineering
The University of Melbourne

Produced on archival quality paper

“If I have seen further it is by standing on shoulders of giants”

Isaac Newton (February 5, 1676)

Abstract

Homogeneously charged spark ignition (SI) engines are unable to stabilise the combustion in ultra lean mixtures, therefore they operate with a near stoichiometric air-fuel ratio (AFR) at all load points. This produces high engine out NO_x and CO emissions with a compromise on fuel consumption. Moreover, stoichiometric operation is needed for effective operation of a three way catalyst, which is not adequate to meet future fuel consumption targets.

The ignition and combustion of lean homogeneous mixtures offers the potential to simultaneously lower pollutant emissions, and improve thermal efficiency. However, lean burn is not well suited to catalytic control because even though HC and CO catalyst efficiencies are high, lean NO_x catalyst efficiencies are low. To take full advantage of lean homogeneous burn, and meet future emission targets without relying on a NO_x catalyst, combustion must be stabilised in ultra-lean mixtures, where NO_x emissions are near zero.

This thesis describes an investigation into the use of a lean mixture ignition system with supercharging, to simultaneously reduce engine out NO_x and improve the thermal efficiency of an internal combustion engine across the entire load range. Furthermore, the combustion characteristics of the lean mixture ignition system were compared to the baseline SI engine.

Combustion stability and enhancement in ultra lean mixtures was achieved using hydrogen assisted jet ignition (HAJI) fitted to a boosted single cylinder CFR research engine. The engine was tested in both gasoline and hydrogen main chamber fuel supply modes at various manifold air pressures, compression ratios (CR) and AFRs to explore the limits of performance.

Experimental results have shown that at all load points, the HAJI fitted CFR engine in gasoline mode has increased thermal efficiency by up to 41%, reduced CO by 90% and increased HC emissions by up to 3.5 times while maintaining an almost zero NO_x capability (<0.1 g/kWh) over its spark ignition gasoline counterpart. The

same tests performed with a hydrogen fuel supply, increased thermal efficiency by up to 10% over its spark ignition hydrogen counterpart and reduced CO, HC and NO_x emissions to near zero levels.

Quantitative theoretical analysis has shown that in SI mode the initial flame is laminar which later develops into a turbulent flame. In contrast the HAJI analysis indicates that the initial flame speeds are up to 7 times higher than laminar flame speeds, consequently the flame is almost turbulent for the entire burn duration. This phenomenon is primarily responsible for the short burn durations and stable combustion in lean mixtures.

While the experimental and theoretical investigations were carried out, an interesting pressure oscillation phenomena was observed, which was named “Jet Knock”. Unlike end gas knock, which occurs near the end of combustion and has an amplitude 10 to 30 time higher, Jet Knock manifests at the start of ignition as the hydrogen jet exits the nozzle at high velocity. Jet Knock was observed in all HAJI modes, even in the absence of main chamber fuel and was found to have no affect on engine performance, durability or emissions formation.

Declaration

I herby declare that this thesis comprises only my original work towards the PhD and contains no material previously written or published by another person, except where duly referenced and acknowledged in the text. I further certify that this thesis contains less than 100,000 words, exclusive of tables, maps, bibliographies and appendices.

Ferenc Hamori

Acknowledgements

I am forever indebted to my loving parents, whom without I would not be here. They provided me with the most valuable thing in the world - opportunity. I would like to express my gratitude to my brother who not only helped generously throughout my many years of study, but was also my best friend.

Many thanks to my wife, who without the use of words is able to remind me that the purpose of life does not revolve around engineering alone. Thank you for supporting me throughout this very long journey.

Many thanks to Professor Harry Watson, who not only shared his incredible wisdom unselfishly, but also reminded me without the use of any words that the purpose of life does indeed revolve around engineering.

My grateful appreciation cannot be expressed in words to fellow research student and closest friend George Zakis, who was always up for a brainstorming session and always made time to philosophise about engineering problems and life in general. Furthermore I am extremely grateful for your efforts in reading and correcting the language in this thesis.

A lot of credit goes to Mr. Ted Grange, who always overwhelmed me with his knowledge in design, manufacturing and workplace philosophy.

And last but not least I would like to thank my collages and friends for their generous assistance at various stages throughout my PhD. These include Dr Gavin Dober, Dr Deanna Wang, Paul Baker, Elisa Toulson and Can Ertekin. Thanks for having time for me when I most needed it.

Nomenclature

Symbols

A	Surface area	(m^2)
C_1, C_2	Woschni heat transfer correction coefficients	(m/s.K)
c_p	Specific heat at constant pressure	(J/kg.K)
c_v	Specific heat at constant volume	(J/kg.K)
D	Diameter of piston	(m)
Da	Damkohler number: the ratio of turbulent (integral) to chemical time-scale	
F	Force	(N)
h_c	Heat transfer	($W/m^2.K$)
L_K	Kolmogorov scale	(m)
L_T	Taylor microscale	(m)
N	Engine rotational speed	(r/min)
P	Pressure	(Pa)
P_m	Motoring pressure	(Pa)
Q	Heat transfer	(J)
Re_T	Turbulent Reynolds number	
r_c	Compression ratio	
R	Gas constant	(kJ/kg.K)
S_L	Laminar flame speed	(m/s)
S_p	Average liner piston velocity	(m/s)
$S_{T,a}$	Actual turbulent flame speed	(m/s)
$S_{T,t}$	Theoretical turbulent flame speed	(m/s)
T	Temperature	(kelvin)
u'	Turbulence intensity	(m/s)
U	Internal energy	(kJ/kg)
V	Voltage, Volume	(V, m^3)
W	Work transfer	(J)

α	Angle	degrees (°)
γ	Ratio of specific heats (c_p/c_v)	
η_{th}	Efficiency, thermal	(%)
θ	Crank Angle	degrees (°)
λ	Relative air fuel ratio (AFR/AFR_{stoic})	
Λ	Integral length scale	(m)
ν	Kinematic viscosity	(m^2/s)
ρ	Density	(kg/m^3)
ϕ	Equivalence ratio (FAR/FAR_{stoic})	
ω	Average gas velocity in combustion chamber	(m/s)

Abbreviations

ABDC	After bottom dead center	
AFR	Air fuel ratio	
ASTM	American society for testing materials	
ATDC	After top dead center	
BBDC	Before bottom dead center	
BDC	Bottom dead center	
BMEP	Brake mean effective pressure	(kPa)
BTDC	Before top dead center	
CAD	Crank angle degree	degrees (°)
E-CoBRA	Experimental combustion burn rate analysis (software)	
P-CoBRA	Predictive combustion burn rate analysis (software)	
CFD	Computational fluid dynamics	
CFR	Cooperative fuels research	
CI	Compression ignition	
CO	Carbon monoxide	
CO_2	Carbon dioxide	
CoV	Coefficient of variation (standard deviation/mean)	(%)
CR	Compression ratio	
DISI	Direct injection spark ignition	
ECU	Electronic control unit	

EGR	Exhaust gas re-circulation	
FAR	Fuel air ratio ($mass_{fuel}/mass_{air}$)	
FSM Factor	Flame speed multiplying factor (FSR_a/FSR_t)	
FSR_a	Actual flame speed ratio ($S_{T,a}/S_L$)	
FSR_t	Theoretical flame speed ratio ($S_{T,t}/S_L$)	
FTP	Federal test procedure	
GDI	Gasoline direct injection	
H_2	Hydrogen	
H^+	Hydrogen radical	
HAJI	Hydrogen Assisted Jet Ignition	
HAJI-G	Hydrogen Assisted Jet Ignition in gasoline mode (pre-chamber H_2, main chamber gasoline)	
HAJI-H_2	Hydrogen Assisted Jet Ignition in H_2 mode (pre-chamber H_2, main chamber H_2)	
HUCR	Highest useful compression ratio	
HC	Hydrocarbon	
IC	Internal combustion	
IMEP	Indicated mean effective pressure (for the entire cycle)	(kPa)
ISFC	Indicated specific fuel consumption	(g/kWh)
IVC	Inlet valve closing	
IVO	Inlet valve opening	
KI	Knock intensity	
LH_2	Liquid hydrogen	
LNV	Lowest normalised value	
MAP	Manifold absolute pressure	(kPa)
MBR	Mass burn rate	(%/CA)
MBT	Maximum brake torque (minimum spark advance for best torque)	°BTDC
MFB	Mass fraction burned	(%)
MPI	Multi-point (fuel) injection	
NEDC	New European drive cycle	
NMOG	Non-methane organic gases	
NO	Nitric oxide	
NO_2	Nitric dioxide	

NO_x	Oxides of nitrogen (mainly NO and NO_2). In this thesis all calculated and measured NO_x values are made up of NO.
ODE	Ordinary differential equation
OH^-	Hydroxyl radical
ONR	Octane number requirement
OPL	Optimum performance line (dotted line in Chapter 5 and 6) where NO_x<=0.1g/kWh, CoV of IMEP<=5% for HAJI-G and CoV of IMEP<=3% for HAJI-H_2
PC	Personal computer
PFI	Port fuel injection
PMEP	Pumping mean effective pressure (kPa)
ppm	Parts per million
r/min	Crankshaft revolution per minute
RON	Research octane number
SI	Spark ignition
SIDI	Spark ignition direct injection
TDC	Top dead center
TWC	Three-way catalyst
VBA	Visual Basic for Applications
VOC	Volatile organic compounds
WOT	Wide open throttle

Common Subscripts

b	burned mixture
u	unburned mixture

Contents

List of Figures

List of Tables

CHAPTER 1
Introduction

1.1 Global Air Pollution - The Problem

1.1.1 Sources and Output of Transport Emissions

In developing countries, the adoption of cars in both private and corporate sectors began after World War II. In 1950, there were only 70 million cars, trucks and buses on the world's roads (Figure 1.1). However, by 1994, there was about nine times that number, or 630 million.

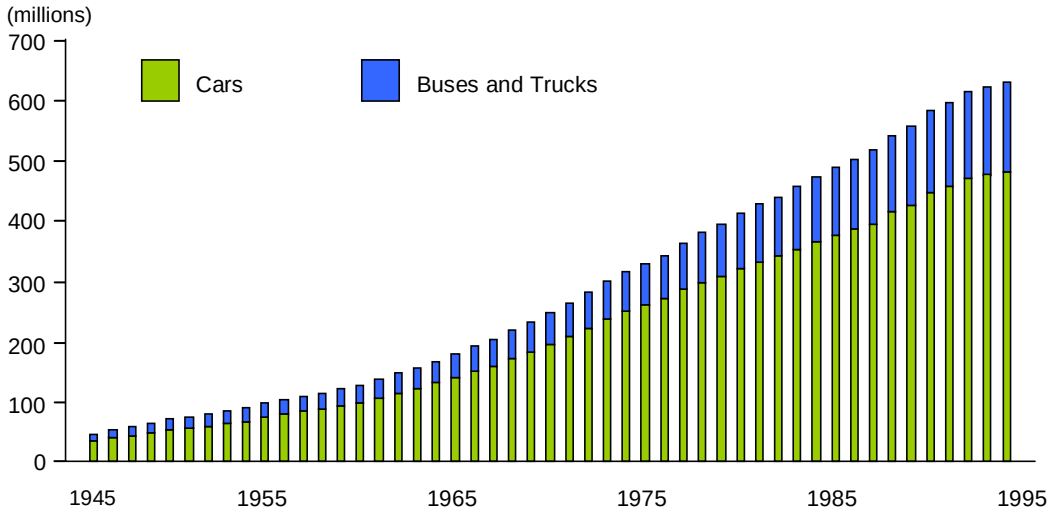

Figure 1.1: Trends in global motor vehicle registration, Year: 1945-95 [13].

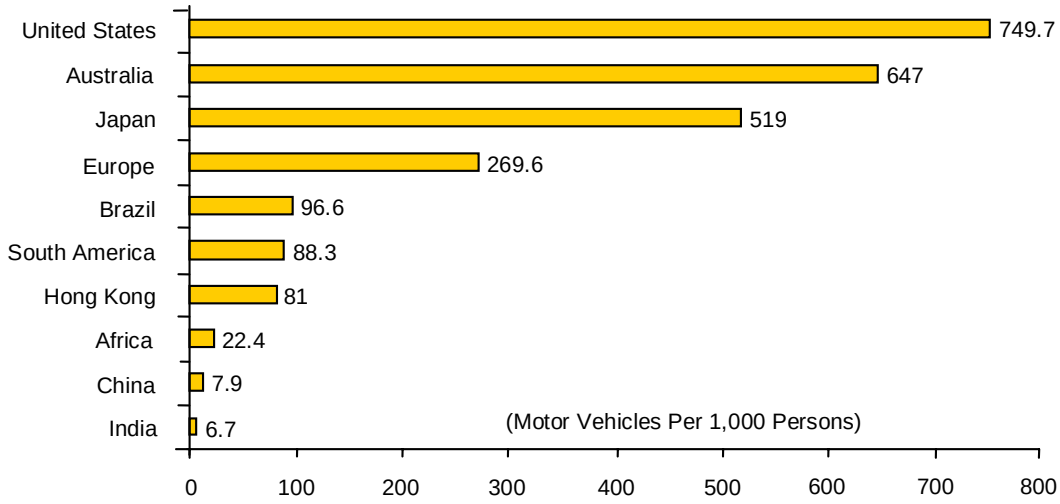

Figure 1.2: Motor vehicle registrations per 1000 persons in selected countries and regions, Year: 1994 [12].

Since about 1970, the global fleet has been growing at a steady rate of about 16 million vehicles per year. Interestingly, this expansion has been accompanied by a similar linear growth in fuel consumption [228].

If this kind of linear vehicle growth continues, by the year 2025 there will be well over 1 billion vehicles on the world's roads [13]. Per capita, car ownership is high in the wealthy nations of North America, Europe, and Japan, but it is still low in most developing nations (Figure 1.2). Growth potential is especially great in the rapidly developing economies of Asia. In China, for example, there are only about 8 registered vehicles per 1,000 persons, and in India, only 7 per 1,000 persons. In contrast, there are about 750 motor vehicles registered per 1,000 persons in the United States [12].

According to Andrews [14], motor vehicles on average contribute 69% carbon monoxide (CO), 47% unburned hydrocarbons (HC) and 63% oxides of nitrogen (NO_x) to the total airborne pollution in western cities. As shown in Figure 1.3, on a typical summer weekday in Melbourne, the air pollution contribution from motor vehicles is 60% for NO_x emissions and 44% for volatile organic compounds (VOC). The major vehicle emissions of concern are CO which is toxic at high concentrations, NO_x which as NO_2 can cause respiratory illness, and HC, including non-methane organic gases (NMOG) and VOC, which can be carcinogenic (Table A.2.).

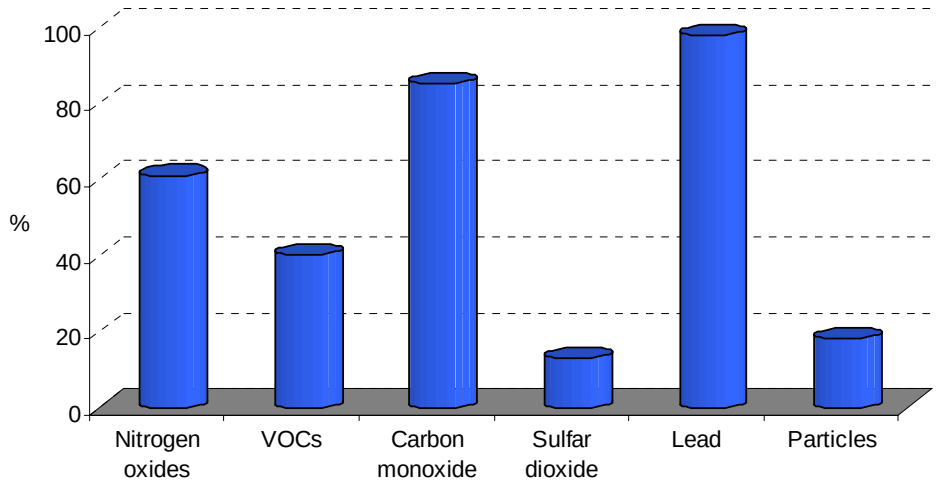

Figure 1.3: Percentage contribution to air pollution emissions by motor vehicles in Melbourne on a typical summer day [98].

1.1.2 The Cost of Air Pollution

The World Health Organization (WHO) found that due to vehicle emissions including particulate matter in Austria, Switzerland and France, around 40,000 people die every year [77]. WHO also reports that globally about 2.7 million people die each year from air pollution - 900,000 in cities and 1.8 million in rural areas. As a consequence of so many people being affected by emissions, the health treatment costs are enormous. Table 1.1 summarises the financial benefits of reducing health treatment costs if Australian air quality standards were achieved.

Table 1.1: Financial benefits in Australia upon meeting air quality standards [64].

Pollutant	Estimated monetary benefit of achieving the proposed air quality standard
CO	$34 million - reduced health treatment costs
NO2	$4.5 million - reduced health treatment costs
O3	$95 - 285 million - reduced health treatment costs
SO2	$12.5 million - reduced health treatment costs
PM10 / PM2.5*	$850 million - reduced health treatment costs $4 billion - avoided deaths

*PM10 is particulate matter composed of particles less than 10 micron in diameter; while PM2.5 is composed of fine particles less than 2.5 microns in diameter.

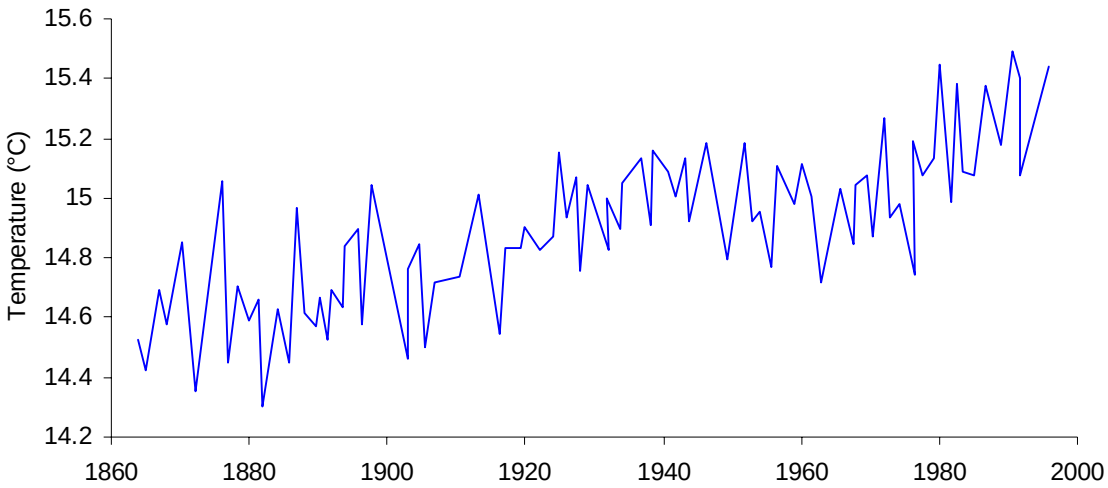

Figure 1.4: Global mean surface air temperatures, Year: 1865-1995 [211].

1.1.3 Vehicle Emissions and Global Warming

The rising concentration of CO_2 in our atmosphere is effecting an average planetary temperature rise (Figure 1.4). Motor vehicle emissions contribute to global warming with carbon dioxide (CO_2) and NO_x greenhouse gases. Relatively speaking, the nitrous oxide (N_2O) in NO_x has a greenhouse impact 270 times that of CO_2 [14], but CO_2 still contributes 64% to the total greenhouse effect. (Figure 1.5). Motor vehicles produce approximately 900 million tonnes of CO_2 each year which corresponds to about 15 per cent of the total anthropogenic global output. The “Intergovernmental Panel on Climate Change” estimates that by 2100, the expected average global temperature rise from 1990 will be between 1.4 - 5.8 °C.

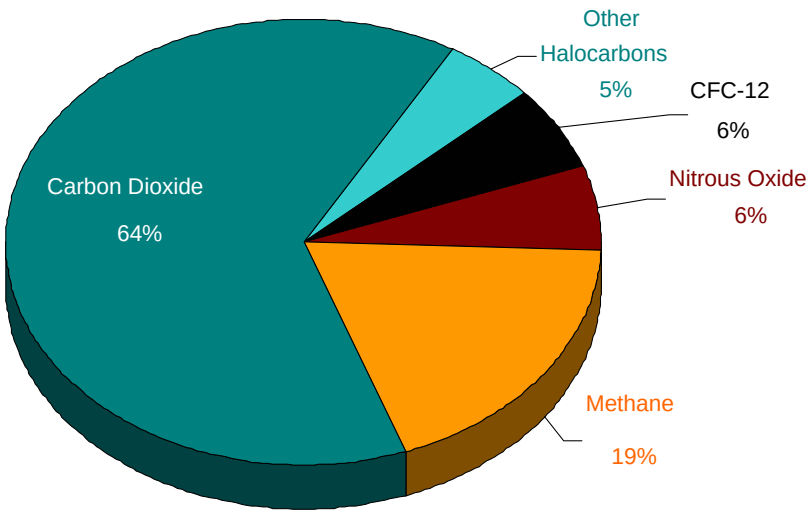

Figure 1.5: Share of greenhouse warming due to different greenhouse gases [100].

This rise in temperature is predicted to increase the frequency of extreme rainfalls and will trigger an increase in sea level due to melting of the polar icecaps.

1.1.4 The CO_2 Challenge

When using oil based hydrocarbon fuels, CO_2 output and fuel consumption is primarily a function of engine thermal efficiency. Vehicle manufacturers are thus continually pressured by governments and consumers to improve thermal efficiency. From the consumer side, the global drive for more efficient engines is primarily motivated by the erratic and steadily increasing cost of oil based fuel which is considered to be a finite natural resource.

From an environmental perspective, the growing emphasis on reducing greenhouse gas CO_2 has forced European institutions and legislative bodies to instigate CO_2 targets (Figure 1.6). These CO_2 targets can only be achieved by reducing fuel consumption or by increasing the hydrogen to carbon ratio of the fuel, where an infinitely high ratio corresponds to pure H_2.

To combat the CO_2 problem using conventional fuels such as gasoline and diesel, whilst simultaneously controlling emissions, engine manufactures are constantly trying to develop cost-effective new technologies. Figure 1.7 highlights that from 1987 onwards, improvement in fuel consumption for cars has been small. For

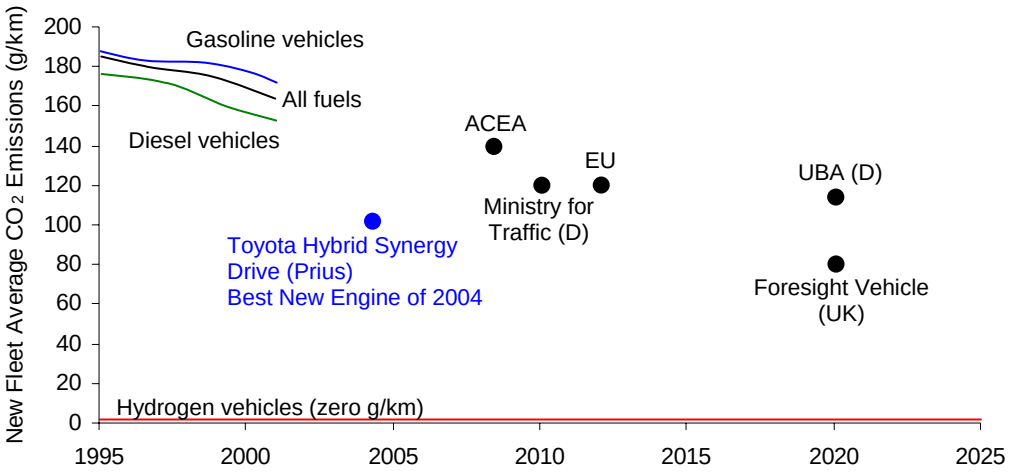

Figure 1.6: Targets for NEDC (New European Drive Cycle) drive-cycle fleet average CO_2 emissions [40, 129].

trucks, fuel economy has actually declined since 1987 which indicates that any technological improvements which have increased engine efficiencies in the past have been offset by the increase in vehicle weight. The hydrogen to carbon ratio of fuel will change little in the future and the fuel economy of internal combustion engines will only improve marginally. Consequently, internal combustion engines will only be free of CO_2 emissions if they are fueled by H_2.

1.1.5 Emissions Legislation

For the last decade, the Californian Air Resources Board (CARB) and the European Union (EU) have led the world in the introduction of the tightest emissions standards for new vehicles (Table A.3). For passenger cars running on gasoline, CARB is currently phasing in “low emission vehicle” (LEV_2) standards to reduce NO_x by 76% and PM by 75-87% with respect to LEV_1. The EU introduced Euro 4 standards for 2005, to reduce HC by 50%, NO_x by 46%, and CO by 65% relative to previous Euro 3 requirements [227]. The EU also proposes to phase in Euro 5 from 2010 (Table A.5) which requires a 73% reduction in NO_x for passenger cars compared to Euro 3 [185]. This would approximately correspond to a NO_x output of 0.123g/kWh (Appendix A.4) over the New European Drive Cycle (NEDC).

As well as urban emissions, CO_2 is a major contributor to global warming and therefore requires some form of legislative control. Currently neither the EU nor

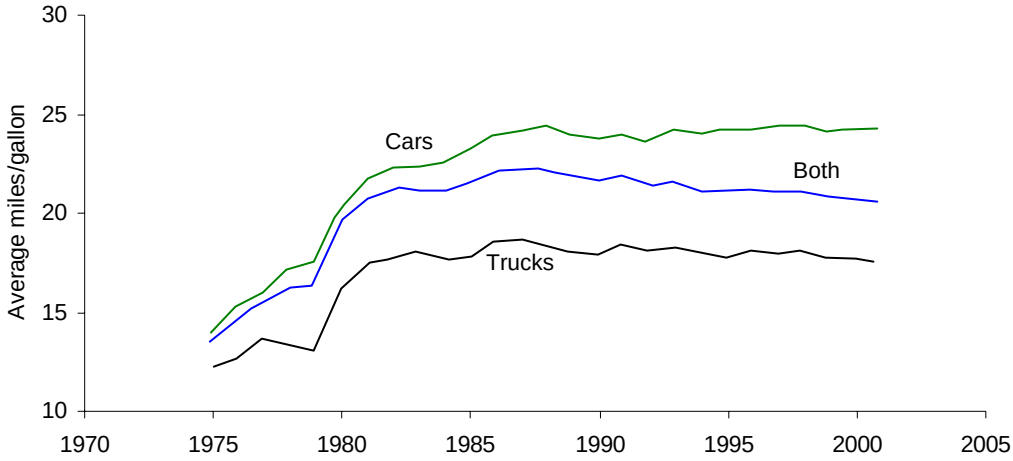

Figure 1.7: Fuel economy by model year in US [137].

CARB has formal legislation pertaining to CO_2 emissions and only "targets" are available (Figure 1.6). France and the United Kingdom on the other hand deal with the CO_2 problem through a tax law which factors in the CO_2 output. Other OECD (Organisation for Economic Co-Operation and Development) member countries determine tax rates simply according to the level of exhaust emissions causing air pollution and fuel efficiency losses. Still, others (such as Japan) carry out special tax reductions or tax exemptions on vehicles with low environmental loads, e.g. electric vehicles [113].

1.2 Current Engine Technology

1.2.1 Performance Limits in Catalyst Equipped Vehicles

Since the introduction of the Euro 1 emissions standards in 1992, emissions have been reduced on average by 97 percent [152]. This has been accomplished with the development and continuous improvement of catalytic converters. Catalytic converters reduce/oxidize engine-out NO_x, CO and HC emissions to CO_2 and N_2. Conversion efficiencies exceed 99% for CO, HC and NO_x emissions. Because catalytic converter technology has almost fully matured, in order to keep up with emissions regulations beyond Euro 4, the following limitations must be addressed or substitute technologies will be required:

- Catalyst conversion efficiency varies greatly with AFR. The 80% conversion efficiency window requires an AFR deviation of less than 0.1AFR from stoichiometric (Figure 1.8) [96].
- Noble metal prices have increased dramatically: rhodium >700%, platinum >200%, palladium >300% [191].
- It typically takes 40 seconds to achieve "light-off" (reach 50% conversion efficiency). Consequently in a typical drive cycle up to 95% of CO, 84% of HC and 65% of NO_x emissions are collected in the period prior to light off.
- Lean air-fuel operation prompts irreversible reactions of rhodium with other metal oxides when the converter bed temperature reaches 700°C. Also, base metals which act as oxygen storage components are irreversibly converted to a less reactive form as a result of lean air-fuel operation.

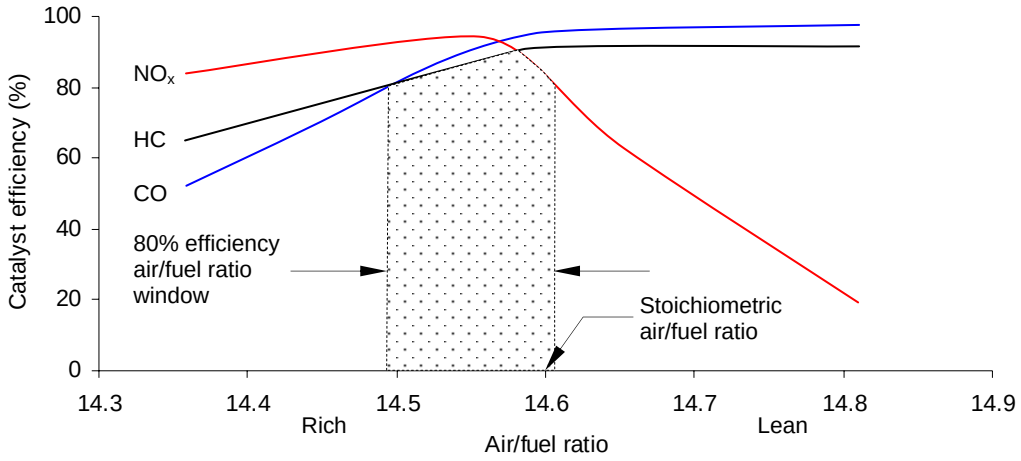

Figure 1.8: Conversion efficiency for NO_x, CO, HC for a three-way catalyst as a function of exhaust gas air-fuel ratio [96].

- In addition to cyanide and hydrogen sulphide, if there are any chlorine residues, phosgene (COCI2) is formed. This is a dangerous combat gas, which attacks the lung membrane [166].
- In petrol, MTBE (Methy-tert-btutyl-ether) is used to replace lead and ZDTP (zinc-dithiphosphate) is an additive used to prevent oil chain breakdown and loss of lubricant potential. In the presence of heat, these two react to form phosphoric acid esters (nerve gas) over platinum, which causes lung cancer.

It is worth noting that CO and HC converter efficiencies increase as the mixture is leaned (Figure 1.8), however NO_x efficiency drops dramatically. This would favor the operation of lean burn engines which produce lower NO_x and higher HC emissions compared to a λ=1 engine.

1.2.2 Inability to Reduce Engine out Emissions at λ=1

As vehicle out emissions are becoming difficult and expensive to reduce further with catalytic converters, powertrain engineers are looking to reduce the pre-catalyst emissions in the combustion chamber. Early improvements in specific emissions output for SI (spark ignition) engines were largely due to improvements in specific fuel consumption (and thermal efficiency). This progress stagnated in 1987 (Figure 1.7) as the improvement in fuel economy slowed down for cars.

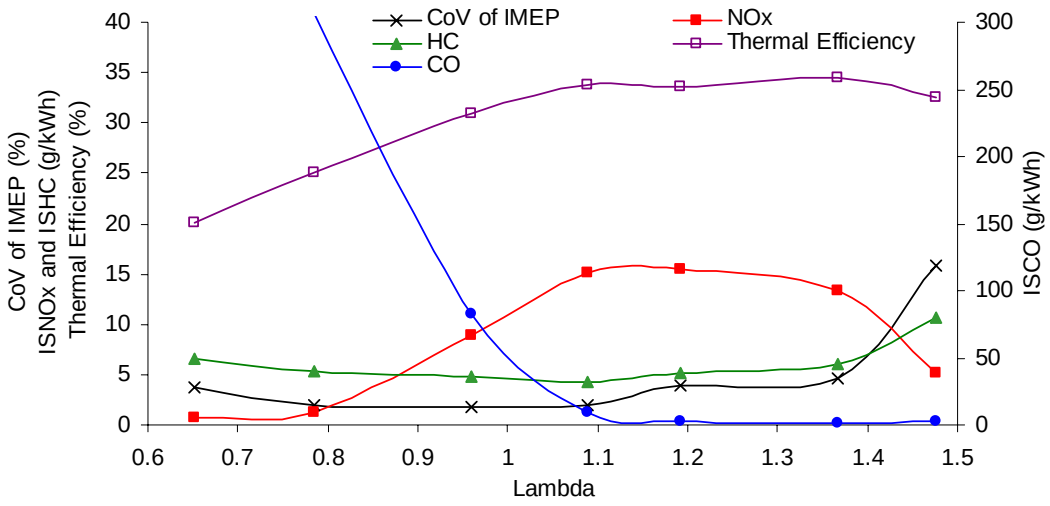

Figure 1.9: SI engine out emissions and thermal efficiency at different Lambda.

SI engines have been running on a homogeneous air-fuel mixture and around stoichiometric (λ=1) or slightly richer ever since the first engine was run in 1885 by Nicholas Otto. The reason SI engines have been charged homogeneously with a stoichiometric mixture is because it maximises engine torque for a given engine capacity, provides good combustion stability (Figure 1.9) and allows the catalytic converter to operate at optimum conversion efficiency (Figure 1.8). The disadvantages of running at or near λ=1 are that, engine out emissions of NO_x, CO and HC are high near this point and peak efficiency is compromised as it occurs lean of stoichiometric air-fuel ratios (Figure 1.9). Above all, for the last 120 years, engine designers were only able to stabilise combustion and therefore achieve maximum engine smoothness at near stoichiometric air-fuel ratios and thus unable to realise the simultaneous improvements in thermal efficiency and reduced emissions of ultra-lean burn.

1.3 Current and Future Technologies for Reduced Engine out Emissions

1.3.1 SI Engines

Although the challenges of meeting emissions targets are large, there are many different mechanisms and theories to simultaneously decrease engine out

emissions and increase the thermal efficiency. Currently the most developed gasoline SI engine technologies use different techniques such as EGR, direct injection and lean burn to reduce emissions whilst maintaining or increasing thermal efficiency (Figure 1.10).

EGR is an effective way to decrease engine-out NO_x whilst maintaining a $\lambda=1$ mixture and therefore compatibility with catalysts. Thermal efficiency usually increases slightly (primarily due to reduced pumping losses) whilst spark timing becomes more advanced as the %EGR increases. It also decreases exhaust gas temperature, which requires caution due to the temperature and AFR sensitivity of catalytic converter efficiency [96].

Bosch believes that “by 2007, every second new spark-ignition engine will have direct injection." [24]. SIDI (spark ignition direct injection) decreases fuel consumption by as much as 15% over PFI (port fuel injection), however the stratification of the charge begins to create similar emission problems to diesels. In addition to this, in excess of 50% load and engine speed, the engine must switch to homogeneous mode in order to avoid further degradation in emissions and combustion stability.

1.3.2 SI Compared to Diesel

Presently, it is undisputed that SI and diesel engines are the most popular and developed internal combustion engines in passenger cars. Although this thesis is

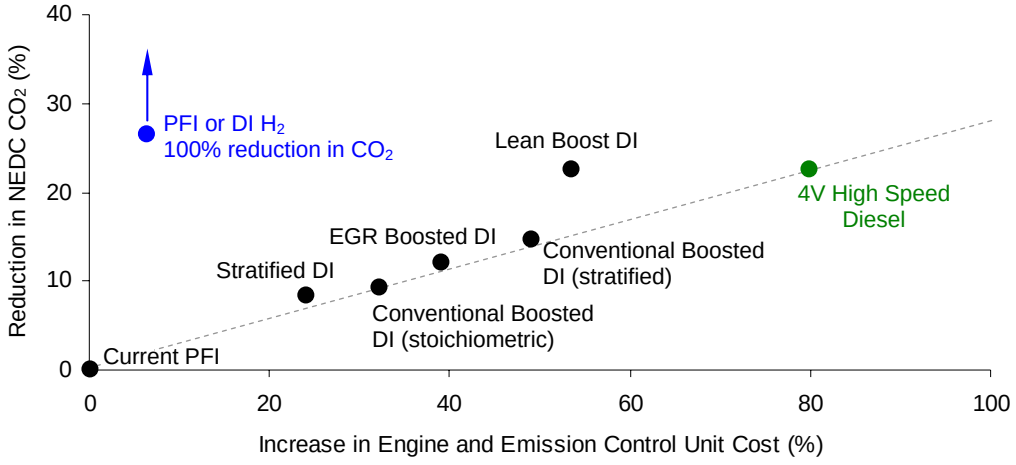

Figure 1.10: Cost benefit analysis for low CO_2 technology [129].

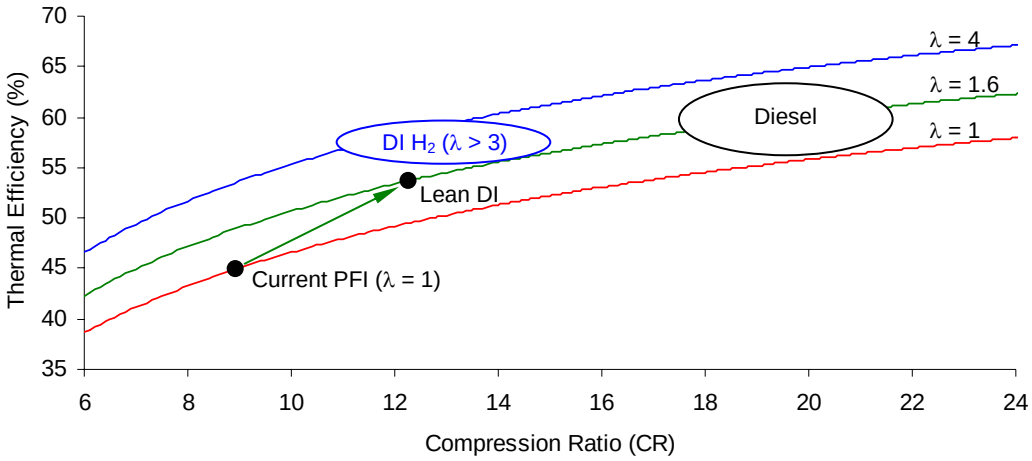

Figure 1.11: Ideal thermal efficiencies for different compression ratios and air/fuel ratios.

focused on SI engine technology, diesel engines deserve mention here due to their popularity and advanced lean-burn capability. With respect to the basic PFI SI engines, diesels can theoretically consume as much as 30% less fuel (assuming that the heating value of the two fuels on a volumetric basis are the same) by operating un-throttled, at high compression ratio, and with lean stratified mixtures (Figure 1.11). In reality this figure is closer to 20-25% [152] and when considering that the density of diesel fuel is higher than gasoline (heating values are similar per kg) then diesel engines are only 15% more thermal efficient than its PFI SI engine counterpart. From the emissions standpoint, diesel engines suffer from smoke, particulate emissions, and high NO_x compared to SI engines and aftertreatment of lean exhausts is also difficult and expensive. Furthermore, diesels are noisier and struggle to operate above 4000 r/min.

Any technology that provides better thermal efficiency is more likely to meet the proposed CO_2 emission requirements shown in Figure 1.6. In fact a 4V high speed diesel can already provide a reduction of approximately 22% in CO_2 emissions over a standard PFI engine. Unfortunately, this benefit comes at an increased engine and emissions control unit cost of 80% (Figure 1.10) compared to a PFI engine. Recently developed state of the art SI engines using lean boosted DI (direct injection) technology can now provide the same 22% improvement in CO_2 but at an engine unit cost only 53% more expensive (Figure 1.10).

Interestingly, Figure 1.10 clearly demonstrates that if the PFI engine is fueled with H_2 then the CO_2 benefits would approach 100% and the increase in unit cost of an engine would be approximately 0%.

1.3.3 Future Technologies

Due primarily to their lower fuel consumption, diesel engines have the potential to eliminate SI engines in the passenger car market segment if urban pollutants such as NO_x and PM can be minimised and total engine system cost lowered. In contrast, SI engines have the potential to do the same if they can be made more fuel efficient (comparable to diesel), whilst maintaining their low urban emissions and cost advantage. The head to head competition between SI and diesel is clear, and this is pushing future engine technology towards a direction that shares useful concepts from both engine technologies.

Based on the apparent technological convergence between diesel and SI engines, future engines are likely to be boosted with high compression ratios. Unlike the lean boosted DI or diesel engines in Figure 1.11, a lean homogeneous charge will most likely be utilised to lower in-cylinder emissions and yield even higher thermal efficiency compared to current diesel and SI engines.

With this in mind, researchers for many decades have been interested in homogeneous lean burning technologies. Unfortunately, due to the narrow flammability limits of most fuels it is quite a challenge to stabilise combustion. In addition to this, the catalytic NO_x converter efficiency starts dropping as the air-fuel ratio increases (Figure 1.8). Therefore, to maintain the same vehicle out emissions, a huge reduction in engine out NO_x emissions is required. This would require the engine to operate in the ultra lean region (λ>1.5) in homogeneous mode (Figure 1.8). However, at present there are no ignition systems available in production that can stabilise combustion in such a lean homogeneous mixture.

Toyota [103] already has engines in production capable of running at AFR=22:1. The Mitsubishi gasoline direct injection (GDI) engine [105] has been in production since 1996, which in stratified mode can operate up to an AFR=30. Regrettably,

while most lean burning SI technologies are unable to run at λ=2 in homogeneous mode, others suffer from great mechanical complexity. Consequently, a boosted ultra-lean mixture combustion technology that is simple and cost effective is needed to reduce emissions and increase thermal efficiency in a homogeneously charged, otherwise similar, SI engine. Furthermore, engines are needed to be fueled with H_2 in the longer term to maximise all the emissions and thermal efficiency benefits.

1.4 Current and Future Transport Fuels

At present, the dominant global transport fuel for SI engines is gasoline. There are however, many alternative fuels being considered for future use such as: ethanol, methanol, CNG, LNG, LPG, hydrogen etc... After reviewing alternative fuels for SI and Diesel engines, Grant [80] concluded that excluding H_2, there is a significant greenhouse benefit from renewable fuels, however higher processing inputs makes the benefits lower than expected. Also, natural gas provides the most benefits over other fuels. Finally, Grant concluded that gaseous fuels provide air quality benefits and depending on priority, biofuels can be used as well. When H_2 is included the result is somewhat different. When the engine is operated on lean H_2 it produces the lowest engine out emissions of any gaseous, liquid or biofuel, leaving no doubt that it is the cleanest of all the available alternative fuels.

There is a much stronger interest in liquid H_2 projects in Europe and Japan, compared to the US and Canada. IC engines and fuel cell projects are popular in Europe and Japan, but the US seems to be focusing only on fuel cell technology [43, 56, 110]. In 2002 the European Union committed 3.56 billion euros to prepare a plan to reduce the region's dependency on oil with the development of a H_2 economy becoming fast the center of attention [106][1].

[1] It is worth noting that while this plan is getting prepared consumers globally spend a minimum of 30 billion euros per year due to the increased unit cost of the SI and diesel engine required to meet emissions and fuel economy targets. This is assuming that 60 million engines are sold a year, where each is 500 euros more expensive than a basic PFI engine.

One of the disadvantages of H_2 fueled engines is the reduction in power by up to 30% with respect to gasoline fueled engines. This is due to the gaseous nature of the H_2 fuel, which displaces the air in the combustion chamber. The other problem is that if the engine operates at λ=1 then it produces more NO_x emissions than any HC based fuel, which is due to the high flame temperature of H_2. This is unacceptable since in the absence of HC and CO, the NO_x conversion efficiency of a catalytic converter plummets to zero. Consequently, post-catalyst NO_x emissions would fail emission regulations.

In contrast, H_2 possesses some unique properties such as extreme flammability limits, fast mass diffusivity, and high flame velocity. This allows H_2 to ignite very rich or lean as well as mix with air exceptionally well. The small quench gap of H_2 also makes it ideal as a pre-chamber fuel where surface to volume ratios are large. With these advantages in mind a typical H_2 engine could always operate in ultra lean mode. With boosting (supercharging) the H_2 engine can produce the same power as a liquid HC fueled engine whilst simultaneously reducing engine out NO_x emissions.

The major barriers to mainstream H_2 usage are the implementation of infrastructure for fueling stations and vehicle on board storage. To get reasonably high density, H_2 needs to be stored as a liquid (LH_2) at -253°C at 2bar. The cryogenic temperature drawback is that it needs super-insulation to keep the boil-off losses (amount fuel lost to cooling) within acceptable limits, typically below 2% per day for vehicles.

The energy required to liquefy H_2 is 0.95 kWh/liter or about one-third of its lower calorific value. If it were available today at the fuel station, it would cost between \$2.30 to \$3.30 per kg H_2 in comparison to gasoline, which is \$2.50 for the same amount of energy [56]. Interestingly, when methanol and LH_2 were considered to be supplied to Europe from remote hydropower facilities and compared to crude oil gasoline, the results showed that the overall efficiency of the crude oil-gasoline-vehicle system was about 19%, compared to about 9% for methanol and slightly less for LH_2.

1.5 The HAJI Phenomena

Hydrogen assisted jet ignition (HAJI) (Figure 1.12) operates by injecting H_2 fuel consisting of 0.5 to 4% of the total fuel energy into a pre-chamber volume, which is as little as 0.7 to 1.5 % of the main chamber clearance volume [128, 136]. The process of combusting any main chamber fuel starts with the induction of air and fuel into the main chamber - if the main chamber fuel is direct injected then only air is drawn into the main chamber. After inlet valve closure, the main chamber mixture is compressed. Hydrogen is injected into the pre-chamber 90° BTDC and the injection duration lasts approximately 10 degrees of crank rotation. After injection, the inflowing air-fuel mixture begins to diffuse and mix with the H_2 inside the pre-chamber. Ignition is initiated by a small sparkplug which ignites the H_2-air-fuel mixture. This ignition generates up to six turbulent jets depending on the number of orifices in the pre-chamber. The jets then flow into the main chamber at high speeds, both mixing and igniting the main chamber charge.

The prechamber contains a rich mixture, therefore combustion is incomplete and the jets are seeded with residual active species such as OH^- and H^+ [54, 85, 128]. Using this system, the physically and chemically active jets create multiple ignition sources, which consequently overcome the problems associated with poorly mixed main chamber charges and the slow burn of fuels under lean conditions.

The HAJI technology was developed and patented by Watson in 1992 [219]. The research and development work done in the past by Kyaw [128], Lumsden [143]

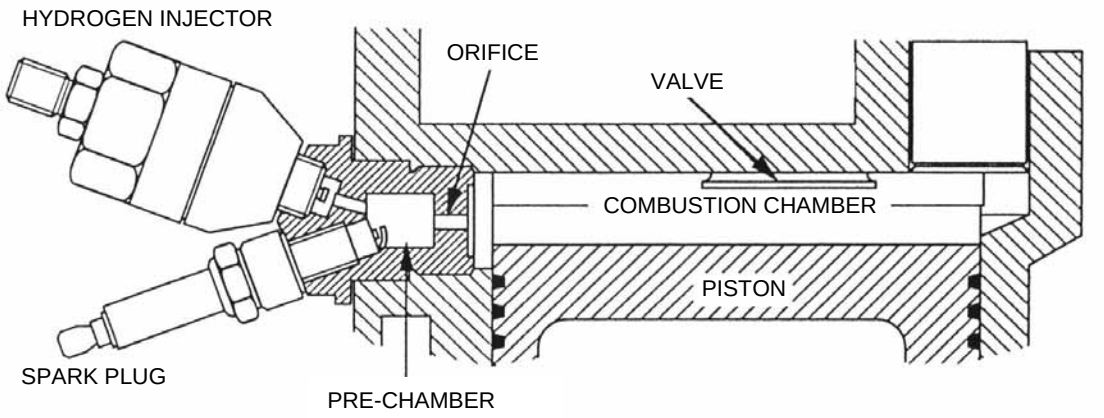

Figure 1.12: HAJI in a single cylinder Co-operative Fuel Research (CFR) Engine.

Glasson et al. [76], Lawrence [136], Dober [55], Wang [217], and Zakis [232] have already proven HAJI to be a practical low emission technology with high thermal efficiency. This is achieved through reduced pumping, heat, and chemical dissociation losses and increased ratio of specific heats. In addition, the higher turbulent flame speed caused by the jets and chemically controlled active species results in a shorter burn duration [218].

The performance limits of HAJI with gasoline and H_2 at different compression ratios and high inlet pressure via boosting are yet to be investigated. In addition, the use of HAJI as a bridging technology between HC based fuels and H_2, by using HAJI and H_2 alone in the main chamber, is also an avenue yet to be explored.

1.6 Research Objectives

The number of cars on our roads is increasing. Consequently, more harmful emissions are being released into the atmosphere, which has a devastating effect on the health of our planet and society. Reducing the rate of emission formation in the combustion chamber is required to reduce engine-out, and consequently vehicle-out emissions. Current SI engines are only able to stabilise the combustion at or near stoichiometric air-fuel mixtures. This thesis for the first time explores and demonstrates how a HAJI equipped SI engine in both gasoline and H_2 main chamber modes can simultaneously reduce emissions and increase thermal efficiency at all loads by utilising ultra lean air-fuel ratios - lean mixture combustion well beyond the stability limit of standard homogeneously charged SI engines. The specific objectives of this thesis are the following:

1. Set up and calibrate a standard SI CFR engine to run naturally aspirated and boosted in HAJI gasoline and H_2 mode;
2. To determine the optimum CR, lambda, and boost in a HAJI fitted gasoline and H_2 engine which provides acceptable combustion stability with the lowest NO_x;
3. To experimentally demonstrate the performance, emissions and thermal efficiency benefits of HAJI over its SI counterpart;
4. Develop a two-zone combustion model (E-CoBRA) with chemical equilibrium formation and a spherical flamelet model to diagnostically analyse the

combustion characteristics such as combustion temperatures, combustion burn rates, flame speed and knocking characteristics of HAJI and then compare it to the base SI engine.

1.7 Outline of Thesis

The present chapter introduces global and urban air pollution problems and informs awareness of the damage human technology has brought upon our world. Engine emissions and thermal efficiency problems have been identified as contributors to global warming. HAJI, the homogeneous ultra lean combustion initiator, has been recognised as a long term solution to simultaneously decrease engine out emissions and increase thermal efficiency. The detailed investigation of HAJI in gasoline and H_2 mode is described in this thesis.

Chapter 2 begins with a literature review on emission formation mechanisms and how thermal efficiency can be increased. This is followed by a discussion on *"Why lean burn and not EGR?"*, and then discusses engine knock limitations and how to assist lean combustion. The chapter is closed by reviewing the leaders of lean burn technology and identifying a solution to our global emissions problem.

Chapter 3 describes the theoretical framework, development and implementation of a two-zone quasi dimensional model (E-CoBRA). It reviews in detail the chemical equilibrium model, adiabatic flame temperature, flame speed models and dedicates special attention to explain the regimes of combustion.

Chapter 4 describes the experimental apparatus, instrumentation and data processing. It continues by describing the hypotheses of this thesis and test methodology used.

Chapter 5 describes in depth the behavior of HAJI-Gasoline (HAJI-G) at various compression ratios and fixed MAP=90kPa. Additionally, a fixed optimum compression ratio of 11 at variable MAP and λ conditions is described in terms of performance, emissions and combustion characteristics.

Chapter 6 is similar to Chapter 5, however it describes in depth the behavior of HAJI-Hydrogen (HAJI-H_2). This chapter together with chapter 5 completely satisfies objective number 2.

Chapter 7 partially satisfies objective number 3. It begins with a series of sensitivity studies of the HAJI system and, where appropriate, comparisons are made to SI. The chapter also closely examines an interesting knocking phenomenon that was observed in all HAJI modes.

Chapter 8 begins by comparing HAJI to SI with respect to combustion characteristics, satisfying the second part of objective number 4. This chapter also completes the requirements of objective number 3 by comparing HAJI to SI with respect to performance and emissions benefits. It finishes by attempting to put HAJI into perspective by discussing its merits and potential to meet future emissions regulations.

Chapter 9 summarises the research achievements and discusses the future work required to further understand the HAJI system and bring the technology one step closer to production.

Appendix A describes the properties of common fuels, effects of engine out pollutants on health, and provides information on current and future emission regulations. Appendix B briefly examines combustion enhancement through SIDI engine technology, which has been developed by leading industry vehicle manufacturers, and three common turbulence mechanisms - squish, tumble, and swirl. Appendix C presents important calibration curves developed prior taking any data point. Appendix D descries the fundamental equations applied in combustion modelling. Appendix E shows essential information about the exhaust gas analysis and together with Appendix C and Chapter 4, satisfies objective number 1. Appendix F provides an insight into important engine variables such as MBT and HUCR. Appendix G shows the source code for the combustion modelling software (E-CoBRA), which together with Appendix D and Chapter 3 satisfies the modelling part of objective number 4.

CHAPTER 2
Engine and Emission Concepts and Review

2.1 Introduction

Low engine out emissions and high thermal efficiency are conflicting design requirements in engine development. High thermal efficiency means more useful work out of the fuel. In general, this is achieved in the four stroke engine by means of a short combustion duration close to top dead center (TDC) at the highest useful compression ratio (HUCR). Stoichiometric air-fuel ratios (AFR) have traditionally been used over the last two decades to maximise the conversion efficiency of the exhaust three-way catalyst (TWC) at the expense of combustion efficiency and engine out emissions. In contrast, a simultaneous improvement in efficiency and engine emissions can be achieved with lean mixtures, but lean burn engines have been avoided due to slow and unstable combustion and their incompatibility with after treatment devices.

This chapter begins with a detailed overview of the three critical legislated SI engine emissions: NO_x, CO, and HC. The nature of these pollutants formation is explained and the factors affecting thermal efficiency are explored. This is followed by a review of a comparison between EGR and lean burn, engine knock, load control strategies, advanced lean burn technologies and in-cylinder

techniques to assist lean combustion. Finally, the chapter concludes by describing the potential of hydrogen to solve the problem of urban and global air pollution from the transport sector as outlined in Chapter 1.

2.2 Emission Formation

2.2.1 Oxides of Nitrogen - NO_x

This thesis deals with two oxides of nitrogen (NO_x) gases. These are nitric oxide (NO) and nitrogen dioxide (NO_2).

Free Radicals

Free radicals such as hydroxyl, and nitric oxide possess unpaired electrons, which makes them extremely reactive with other molecules. They are also unstable and can cause cellular damage that leads to the pathology of stroke, heart disease, and numerous other illnesses [70].

NO_2

NO_2 is extremely hazardous to health and in high concentrations it can cause fatality. In lower concentrations as in urban areas, it can create chronic and acute health problems. Further to this, NO_2 in the presence of sunlight splits into NO and oxygen atoms (O). The oxygen atom may react with molecular oxygen (O_2) to produce photochemical smog also known as ozone (O_3) [74]. Smog causes respiratory tract irritation, breathing difficulties and headaches [60].

Only small quantities of NO_2 are emitted from internal combustion engines. The proportion of NO_2 in NO_x in spark ignition engines is less than 2% whereas for diesels it is an order of magnitude higher at between 10-20% [96]. Over time, the majority of NO_2 forms outside the combustion chamber because NO is slowly oxidised to NO_2 in the upper atmosphere. In addition, NO is oxidised to NO_2 by ozone (O_3) which then depletes the ozone layer responsible for protecting the earth from the harmful ultraviolet radiation emitted by the sun [1].

In summary, NO_2 either directly from the exhaust or local oxidation of NO, creates O_3 in urban areas, however depletes O_3 as it is being created from NO in the

atmosphere. NO_2 dissolves into water to produce a mixture of nitric acid (HNO_3) and nitrous acid (HNO_2) and in the form of acid rain it is responsible for the degradation of many buildings around the world.

NO

Unlike most radicals, NO has both life saving and life threatening properties. In small quantities NO assists to regulate blood pressure and defends the body from pathogens. In high quantities however, NO can cause inappropriate enzyme activation and oxidative damage to vital cellular systems [134].

Figure 2.1 shows the amount of NO in the exhaust of the CFR SI engine. Zeldovich was the first to discover the exponential increase of NO as a function of temperature, which is described in detail in Chapter 3.

There are three factors contributing to NO_x formation in engines and these are temperature, oxygen concentration and residence time. Peak flame temperature occurs in slightly rich mixtures, however peak NO occurs in slightly lean mixtures (where the temperature of the flame is about 100°C lower) due to excess availability of oxygen. Further dilution of the mixture with air reduces NO exponentially because flame temperature drops rapidly.

NO cannot form instantaneously and is kinetically controlled. In a typical engine cycle, the temperature decreases so rapidly during the expansion stroke that the

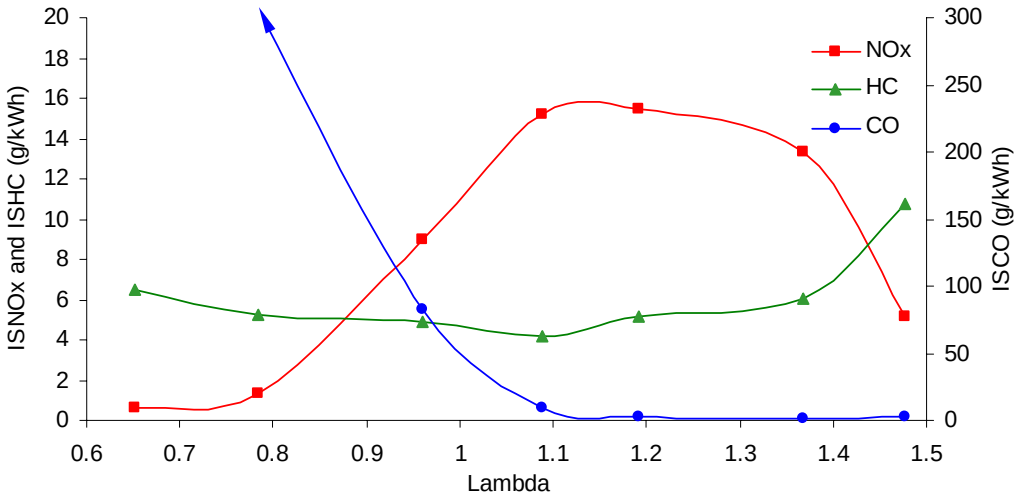

Figure 2.1: CFR SI engine - 1800r/min, CR=9, MAP=90kPa, MBT.

rate at which NO dissociates is not fast enough to reach equilibrium so the NO concentration becomes “frozen” in the cylinder. In lean mixtures, NO freezes at the beginning of the expansion process just after peak cylinder pressure. In rich mixtures, due to the higher flame temperatures, NO freezes later in the expansion stroke after substantial NO decomposition has occurred [119].

2.2.2 NO_x Formation in Engines

Of all the harmful engine out emissions, NO_x is the major focus of this thesis. The following section summarises the effects of different engine parameters on NO_x formation.

Effects of Compression Ratio and Spark Timing

As commented by Heywood [96], there are mixed reports on the effects of CR on NO_x formation. Predominantly, NO_x emissions decrease as the CR is increased because the increased density promotes faster combustion. Often, to avoid engine knock the spark timing is retarded, which reduces residence time, and combustion temperatures. In contrast when an engine is not knock limited, advancing spark timing will increase NO_x formation, since it increases residence time, and combustion temperature.

Effect of Diluents/EGR

Introducing diluents, usually EGR, into an engine will reduce the NO_x formation by two mechanisms. First, it reduces the adiabatic flame temperature and therefore lowers combustion temperatures. Second, it reduces the availability of O_2 in the combustion chamber therefore slowing down the rate formation of NO_x further.

Effects of Load and Speed

As the load increases, the amount of NO_x also increases. This is due to the higher average combustion temperatures and a reduction in internal EGR. The effect of speed is interesting because in principle, as it increases, it should decrease the rate formation of NO_x, due to a reduction in residence time. However, in practice an increase in engine speed usually translates into an increase in NO_x. This is due to a reduction in EGR (as the volumetric efficiency increases from low speed to the

engine speed at maximum torque), increase in combustion temperatures due to the reduction in heat loss per cycle and an extension in burn duration that is usually corrected by advancing spark timing, consequently increasing peak pressures and temperatures.

Effect of AFR and AFR gradient

The AFR gradient in the combustion chamber can have a significant effect on the local temperatures and oxygen concentrations. Consequently, the rate of NO_x can vary significantly as shown in Figure 2.2. For S=0 the mixture is homogeneous and for S=0.5 the mixture can be considered a stratified charge. For lean mixtures below φ=0.8 (λ=1.25) NO_x formation is lowest when uniformity is high due to the absence of higher temperature, stoichiometric and rich regions. At a stoichiometric AFR (λ=1), a high degree of non-uniformity reduces NO_x because rich and lean mixtures are burning; both of which have lower flame temperatures than stoichiometric flames.

2.2.3 Carbon Monoxide

Carbon monoxide (CO) is extremely toxic and even fatal in concentrations as low as 200ppm. CO is able to combine with hemoglobin molecules in blood to form carboxyhemoglobin which prevents the blood from carrying oxygen [217]. In small concentrations CO can damage arteries in the heart and even decrease pregnancy rates [232].

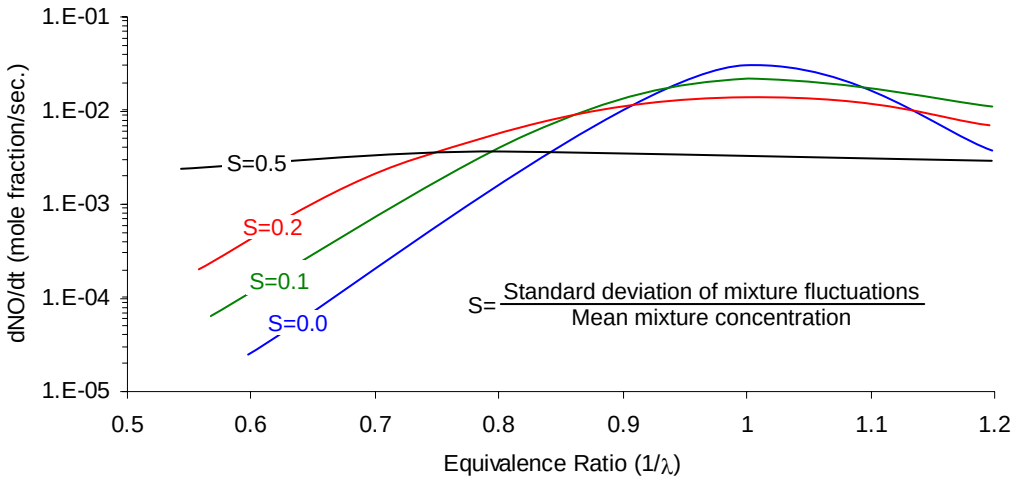

Figure 2.2: Effect of non uniformity of mixture on rate of NO_x formation [14].

High CO concentrations in SI engines are the result of incomplete combustion. As shown in Figure 2.1, only small quantities of CO form in mixtures leaner than λ=1.2. When a stoichiometric or richer AFR is established in the combustion chamber, the availability of O_2 is inadequate to convert all the reactants to CO_2.

Similar to NO, CO formation is also kinetically controlled. Typically, the rate of cooling of burned gases is so high during expansion that the CO levels become frozen. Therefore, levels of CO are significantly higher than equilibrium values in the exhaust gases [96] (Section 3.3.1 and Figure 3.2).

2.2.4 Unburned Hydrocarbons

Care must be taken when evaluating the health and environmental risks associated with hydrocarbon emissions (HC) since measurements are usually unable to provide sufficient information about the relative concentration of different species. Benzene and 1,3-butadine are known carcinogens and increase the risk of leukemia and bone marrow cancer [134]. HCs and NO_2 in the presence of sunlight react to form a photochemical smog containing compounds such as peroxyacetyl nitrate, hence can indirectly contribute to respiratory tract irritation, breathing difficulties and headaches.

HCs are formed due to incomplete combustion. Unlike NO_x and CO emissions, HCs are emitted from an engine mainly due to partial or total lack of oxidation. To prevent this, careful design of the combustion chamber and ignition system is required. The following will describe briefly the sources of HC emissions and some common techniques adopted to reduce them.

HC sources

In Table 2.1 a review by Watson [220] illustrates the relative contribution of HC emissions in a conventional spark ignition engine. Steady state HC emissions from a well-maintained engine were of interest in this study. Points 5 and 7 are therefore omitted from further discussion since it was estimated that valve leakage was small, and that the engine was operated warm. H_2 and gasoline was port fuel injected. This allowed a considerable amount of time for gasoline to

Table 2.1 Contribution of individual sources to the total engine out HC source [220].

1. Wall quenching	15%
2. Piston and other crevice	20%
3. Oil film absorption/desorption	10%
4. Incomplete fuel preparation	15%
5. Additional quench due to cold surfaces at 1.5 minutes	15%
6. Valve overlap	15%
7. Valve leakage	10%

vaporise and mix with the air. Therefore liquid droplet atomisation and vaporisation issues were considered to be minor. Consequently, incomplete fuel preparation (point 4) was negligible. Points 1, 2, 3 and 6 are predicted to be the major sources of HC emissions and discussed in further detail.

Wall Quench

Quenching is known to be a phenomenon associated with the extinction of a flame. It may involve the loss of active species, however the flame front extinction primarily occurs when the energy loss due to heat transfer at the flame front is higher than the energy generated due to combustion [28]. The ratio of the heat release from the flame to the heat lost to the walls at the point of quench is approximately constant across all geometries, and is known as the Peclet number (P_e). This ratio is most easily studied with the configuration of two parallel plates. The distance between the two plates where the flame extinguishes is known as the quench gap (δ_{q2}) (Appendix A.1 shows the quench gap of different fuels). The quench gap for two-plate configuration is given by:

$$\delta_{q2} = \frac{P_{e2} k_b}{\rho_w C_{Pb} S_l} \tag{2.1}$$

Where δ_{q2} is the instantaneous quench distance (between two parallel plates), P_{e2} the Peclet number, k_b the conductivity of the burned gas, ρ_w the density at local wall temperature, C_{Pb} the specific heat, and S_l the laminar flame speed.

In the combustion chamber heat sinks resulting in quench occur significantly by conduction, rather than convection and radiation (Figure 2.3). Therefore, it is important to know the size of the quench gap as unburned HCs will be trapped

there. Lavoie modified [135] the original two-plate (or wall) Peclet formula (rearranging Equation 2.1) of $P_{e2} = \rho_w S_l c_{pb} \delta_{q2} / k_b$ to $P_{e2} = 2.2\lambda P^{0.26}$ [55, 96]. However, in the combustion chamber, the flame approaches the cylinder walls head-on or traveling parallel (side-on). For this reason, Lavoie developed a single-plate (or wall) quenching Peclet numbers (P_{e1}), which have been found to be directly proportional to the two-plate value (P_{e2}):

$$P_{e1} = 0.2 \cdot (2.2\lambda P^{0.26}) \qquad \text{head - on} \qquad (2.2)$$

$$P_{e1} = 0.4 \cdot (2.2\lambda P^{0.26}) \qquad \text{side - on} \qquad (2.3)$$

Where P is the gas pressure in kPa and λ is the relative air-fuel ratio. Equation 2.2 and 2.3 can be substituted into Equation 2.1 to find the quench distance (δ_{q1}) for single-plate (or wall) configurations.

In lean combustion the heat release per unit volume is low and so the cylinder pressure is lower compared to a λ=1 engine. Consequently, the quench gap increases because the pressure affects the Peclet number (Equation 2.2 and 2.3).

As shown in Figure 2.4, in a HAJI engine running at λ=2, Lawrence [136] estimated from measurements, that in the exhaust, unburned quenched HCs constitute 10.22% compared to 0.5% at λ=1 of the total supplied HCs. One of the major advantages of diesel and SIDI engine technologies is that they reduce or eliminate quenched HC emissions by positioning the fuel away from cool cylinder walls.

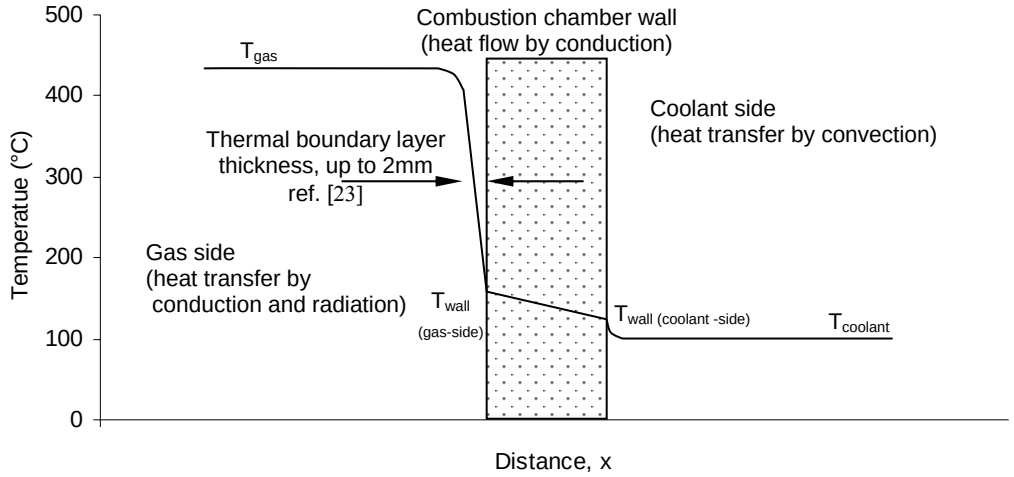

Figure 2.3 Temperature distribution in the region of the cylinder wall [96, 197].

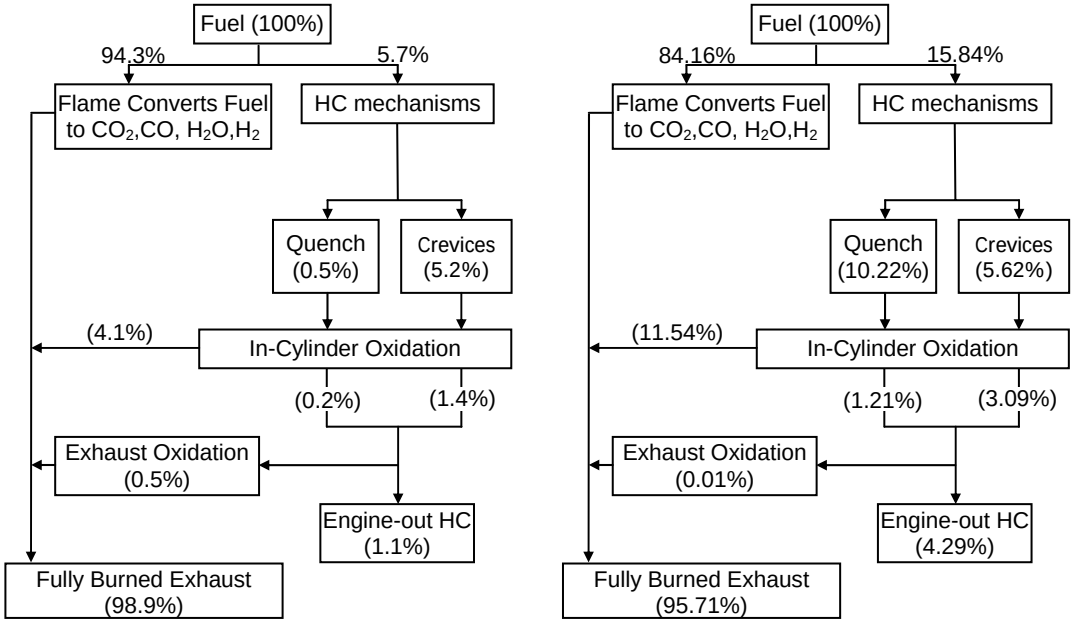

Figure 2.4 Hydrocarbon emission breakdown at λ=1(left) and λ=2(right) [136].

Crevice HC Emissions

Crevices are narrow volumes around the combustion chamber with a high surface to volume ratio, which prevent flame propagation regardless of the AFR. During compression of a homogeneous fuel-air mixture, these crevices are filled with fuel and air which escape the main combustion event, only to be released during the expansion stroke where some of the once trapped mixture is oxidised by the hot burned gases. Combustion chamber crevices include the piston top-land and rings, the head gasket, spark plug thread, the inlet and exhaust valve seats, and in the HAJI engine, the pre-chamber.

The ring crevice can contribute up to 30% of the total crevice HC emissions. This however can be eliminated by increasing the radial clearance between the piston and cylinder liner to sufficient width so that the flame can propagate into the crevice [8, 189]. This is not a feasible solution for lean mixtures where the quench gap can be as much as 4mm thick. Fortunately, the majority of piston crevice HCs are oxidised as they become trapped in the hot roll-up vortex [155] that forms in the piston crown - cylinder wall corner. The other crevices such as the head gasket and the spark plug are difficult to control as they are very close to the exhaust valve and are therefore the first to exit the cylinder upon the exhaust valve opening.

Oil Film Absorption

The gas phase driving force for solubility in oil is the partial pressure of each component of the fuel. This is proportional to the cylinder pressure and the component concentration. The solubility is also a function of the oil type, the temperature and the time of exposure to the concentration, since diffusion into the film layers takes time. Generally, solubility increases as the number of carbon atoms increase in the fuel [220]. Fuel is absorbed into the oil when the in-cylinder pressure rises and desorbs back into the cylinder as the pressure falls during the expansion stroke. Some of the desorbed fuel mixes with the hot burned mixture through interaction with the roll-up vortex. Even with partial post-combustion oxidation, it is estimated that of the total HC emissions, 10-15% are contributed by oil film absorption [26, 138].

Valve Overlap

It is possible for the air-fuel mixture to completely bypass the combustion chamber during the period of valve overlap, and therefore miss completely, the opportunity to oxidise. Variable valve timing can help remedy this problem, however engines with fixed valve timing, or engines operating un-throttled or boosted suffer the most.

During naturally aspirated mode and especially at low manifold pressure (i.e. idle), the inlet manifold pressure is lower than the exhaust backpressure allowing exhaust gas to flow back into the combustion chamber and this gas, together with residual gas, may flow into the inlet manifold. Consequently, little or no fresh charge bypasses the combustion chamber. At wide open throttle (WOT) or boosted, the inlet manifold pressure can be higher than the exhaust backpressure so during valve overlap, small quantities of fuel may bypass the combustion event, results in high unburned HC emissions. Since the CFR engine used in this research has fixed valve timing with approximately 20CAD vale overlap [131] and was operated at both low MAP (throttled) and high MAP (boosted) conditions, consideration of the abovementioned phenomena is important.

2.2.5 Particulate Emissions

Particulate matter (PM) emissions are an extremely serious public health issue costing Australia billions of dollars in health treatment (Table 1.1). PM causes breathing difficulties, respiratory diseases and can contain cancer producing materials.

Particulate matter (PM10 and PM2.5 – particles below 10μm and 2.5μm), form in rich AFR mixtures where an insufficient amount of oxygen is available to completely oxidise the fuel. PM is emitted directly from diesel and DI engines but additional quantities are generated from brake pads and tyre wear. Homogeneously charged SI engines do not suffer from PM emissions unless they are operated rich of stoichiometric for maximum power, which is only a small portion of a typical drive cycle.

2.3 Thermal Efficiency

2.3.1 Effects of Compression Ratio and AFR

The thermal efficiency of an engine running on the Otto-cycle (Figure 2.5) is equal to:

$$\eta_{th} = 1 - \frac{1}{r_c^{\gamma-1}} = \frac{W_{out}}{Q_{in}} \tag{2.4}$$

Where r_c is the compression ratio (maximum cylinder volume / clearance volume), and γ is the specific heat ratio equal to: (C_p / C_v *or* $C_p/(C_p\text{-}R_{gas})$).

To obtain the highest maximum thermal efficiency in an engine the gas pressure forces on the piston must be maximised for a given amount of fuel burned per cycle. This can be achieved by two methods.

Method 1 - is to burn all the fuel in the smallest volume near or at TDC whilst minimising combustion duration since the pressure rise due to combustion strongly depends on the volume in which combustion occurs (Equation 2.5). The pressure rise due to combustion is [19]:

$$\Delta P_{comb.} = \frac{\gamma - 1}{V} Q_{in} \tag{2.5}$$

Where V is the volume in which combustion occurs, and Q_{in} is the energy released due to combustion. Unfortunately, the magnitude of peak pressure and temperature in the combustion chamber is limited by the onset of knock, and this important point will be discussed further in Section 2.5.

Method 2 - is to increase γ, which is a function of AFR and combustion temperature. During the combustion phase in very rich and high temperature mixtures, γ can be as low as 1.2. Conversely, in very lean and low temperature mixtures, γ can be as high as 1.4. An increase in AFR boosts γ through two mechanisms: 1 - it increases the air mass fraction in the mixture which has the highest γ value of 1.4; 2 - it decreases the adiabatic flame temperatures and therefore decreases C_p which in turn increases γ [229].

Operating an engine lean can also decrease the exhaust gas temperatures, which means that engines equipped with stainless steel exhaust manifolds can be replaced with cast iron at one-fourth the cost. Furthermore, at high air-fuel ratios the heat transfer to the walls decreases, which in turn decreases the engine cooling requirements. This means the water pump and radiator can be reduced in size, opening up invaluable space in the engine bay area for packaging.

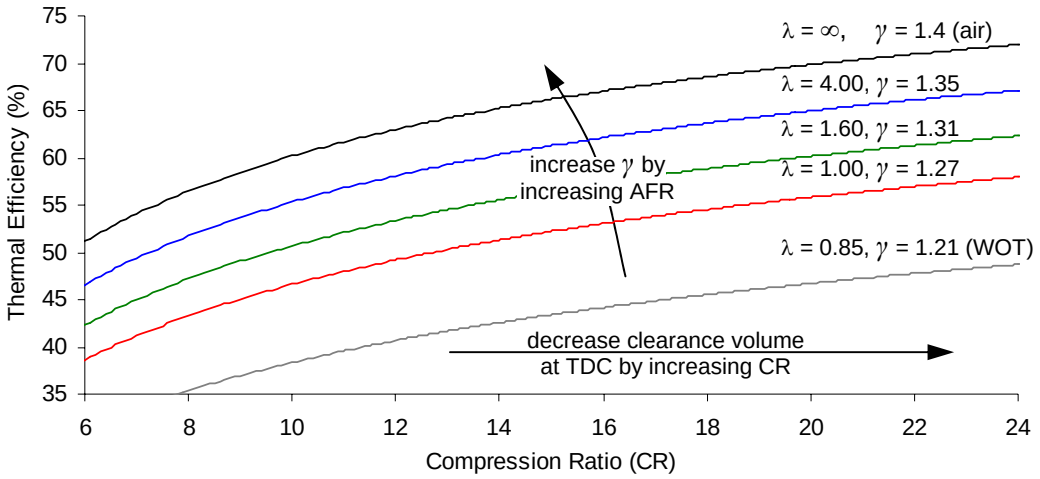

Figure 2.5: Ideal thermal efficiencies for different clearance volumes and constant γ.

2.3.2 Effects of Turbocharging and Downsizing

Turbocharging together with downsizing can provide an increase in thermal efficiency through a number of mechanisms: 1 - increasing the average MAP by using a compressor (powered by waste enthalpy instead of crank shaft work) to decrease the pumping losses; 2 - decreasing the engine size to reduce engine friction; 3 - reducing the combustion chamber surface area to lower the heat transfer through the walls, and lastly; 4 - increasing the mass flow rate across the inlet valves which enhances fuel atomisation.

The effect of turbocharging and supercharging together with downsizing has been described by many researchers throughout the literature [47, 57, 79, 88, 114, 123, 129, 173, 174, 175]. Petitjean et al. [175] captured these benefits through the data analysis of several hundred family sedan production vehicles, released over a ten-year period. They concluded that for the last ten-years, on average, for the same power, turbocharging enables gasoline engine downsizing by about 30%, improves fuel economy by 8-10%, and also improves torque and acceleration performance. Petitjean et al. [175] also ran vehicles through the New European Drive Cycle (NEDC) to capture the benefits of progressive downsizing and turbocharging. The results are shown in Figure 2.6. In this test they achieved a 19.6% reduction in fuel consumption by downsizing 40%. These results become even more impressive when one considers that the gains were achieved using a

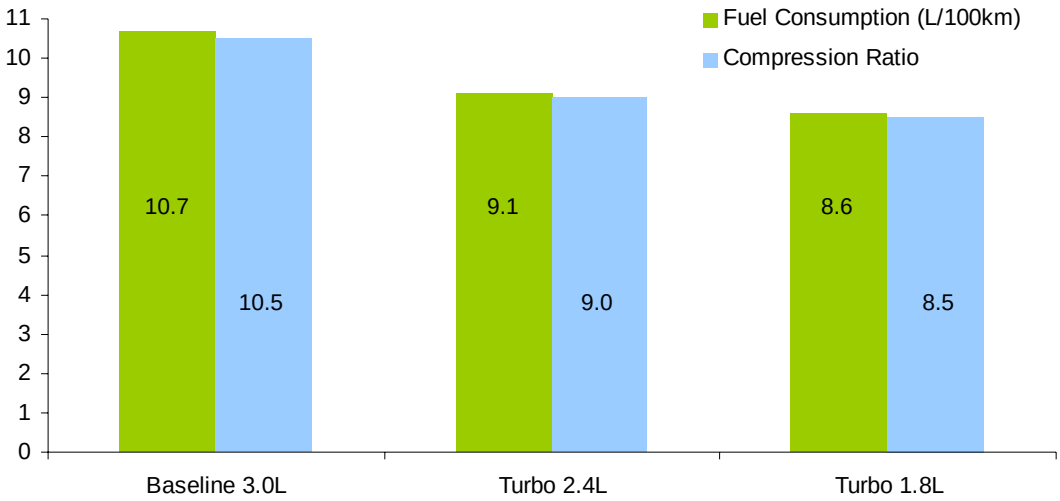

Figure 2.6: Fuel consumption and compression ratio of turbocharged and non-turbocharged engine in the same vehicle [175].

progressively lower compression ratio to avoid knock. Clearly, further gains in efficiency could be achieved if CR was maintained or increased whilst downsizing.

2.3.3 Effect of Poor Combustion Stability

Not all of the fuel is burned in an engine, especially as the mixture becomes rich or very lean. When combustion stability becomes compromised, such as in lean mixtures, the rate at which the fuel burns from cycle to cycle becomes variable. The first sign of compromised combustion stability manifests itself as an increase in burn duration. The usual description for combustion variability is the CoV of IMEP, which is used extensively throughout this thesis.

Further degradation in combustion results in a partially burned charge or at the extreme, an inability to ignite the mixture at all, resulting in misfire. Both partial burn and misfire can be measured by the LNV (lowest normalised value) of IMEP. To maximise thermal efficiency, extended burn duration, partial burns, and misfires must be avoided. Figure 2.7 shows that as CoV increases LNV drops dramatically and thermal efficiency decreases from 34.3% to 32.3% in the lean region - a relative thermal efficiency penalty of 5.8%.

In practice, good drivability will depend on many factors such as cylinder charge balance, torque converter characteristics and engine mount isolation. Equal or less

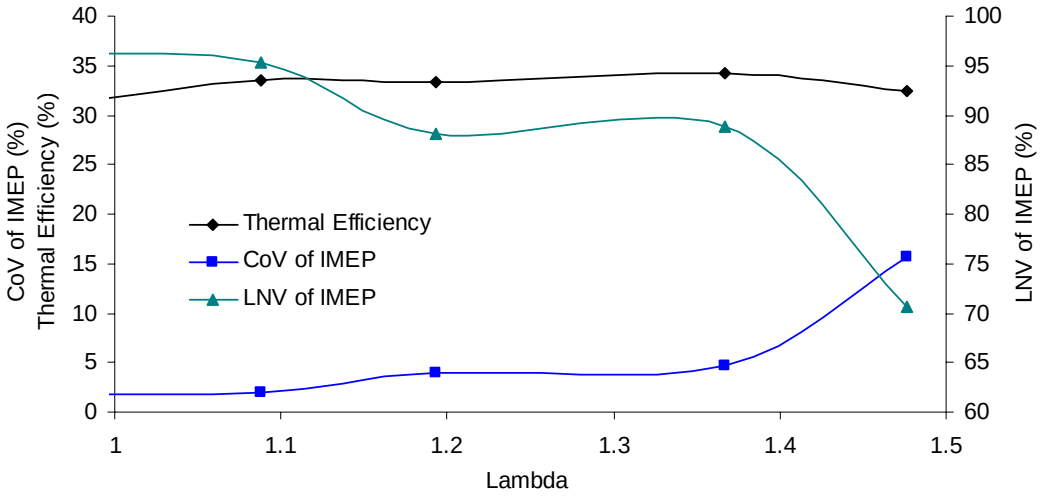

Figure 2.7: CoV and LNV of IMEP and indicated thermal efficiency as a function of Lambda, 1800r/min, MAP=90kPa, CFR-SI.

than 3% CoV of IMEP is considered best practice, 5% is good, and 10% is considered to be unacceptable not only because it decreases thermal efficiency, but because it results in poor customer satisfaction [34, 108, 176]. Since 5% CoV of IMEP is the upper limit of acceptable combustion, in this research it is considered as the lean limit of a combustion system.

2.4 Why Lean Burn and not EGR?

The dilution of the cylinder charge can be achieved by either increasing the AFR (lean burn) or by using an oxygen free substitute at an unchanged AFR, which is usually achieved by the recirculation of exhaust gases (EGR). The objective of each method is the same: to simultaneously increase thermal efficiency and reduce emissions. The major difference is that EGR, with a λ=1 mixture, allows the use of a conventional TWC. Not surprisingly, both methods have a very similar effect on the engine's thermodynamic behavior. These include:

- Reduced flame speed and flame temperature;
- Higher cycle-by-cycle variability (increase in CoV of IMEP);
- Reduced knock tendency and therefore higher allowable CR or boost pressure;
- Reducing pumping losses at equivalent load point at a given r/min.

The distinctions between lean burn and EGR are presented in Figure 2.8, which

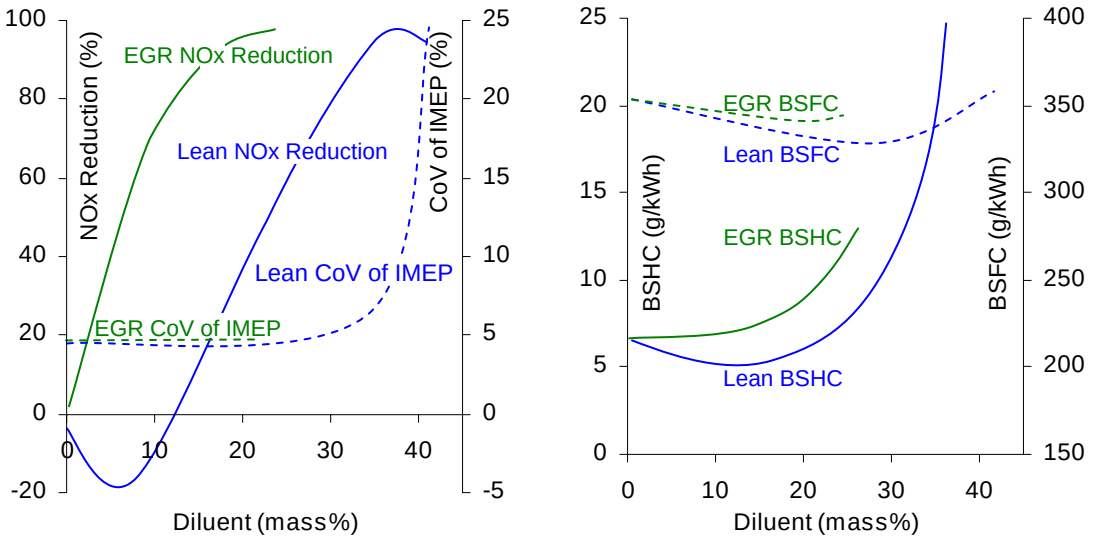

Figure 2.8: EGR vs lean burn, 4 cylinder, homogeneous charge, high swirl, 1500r/min, 262kPA BMEP, [142].

also demonstrates the effect of each dilution method on percentage NO_x reduction, CoV, fuel consumption and HC emissions. The lean burn NO_x peak is visible at about 5% dilution (λ=1.05), after which the rate of NO_x reduction as a function of dilution follows a similar path to EGR. The efficiency of the lean burn mode is clearly superior to EGR at a similar NO_x output. HC emissions are also lower for a given amount of charge dilution [142].

Lean burn is not popular in current production engines due to the incompatibility with the TWC converter. In addition, most ignition systems have problems stabilising combustion at mixtures leaner than λ=1.5 (Figure 2.9) where the lean burn NO_x benefits become significant. On the other hand EGR must be applied with care, because above 10% EGR rates, an undesirable increase in piston ring and cylinder liner wear arises, especially at high loads [50].

2.5 Knock

2.5.1 Normal and Abnormal Combustion

As shown in Figure 2.10, normal combustion is defined as a combustion process in which:

- the combustion event is initiated solely by a controlled spark event;
- the flame front propagates completely across the combustion chamber;
- the flame propagation is relatively uniform and consistent.

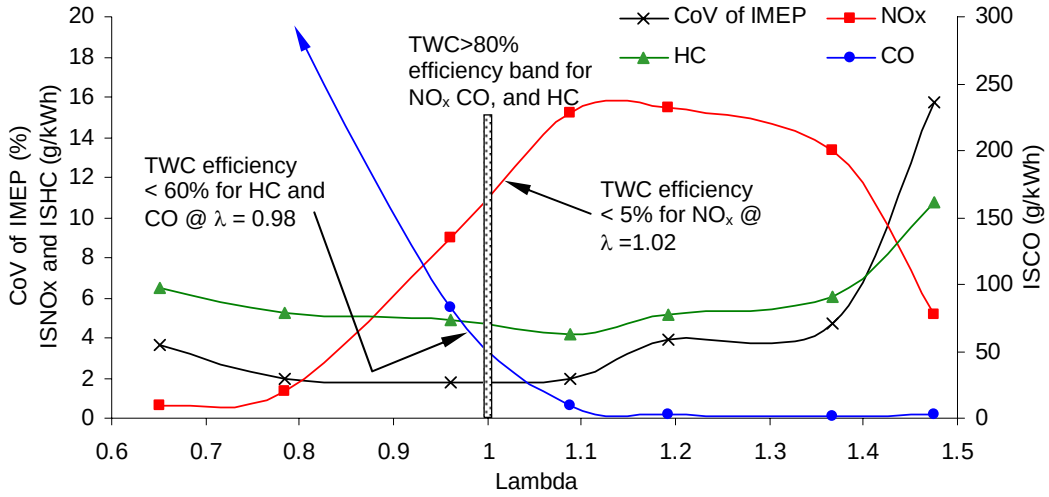

Figure 2.9: CFR SI engine - 1800r/min, CR=9, MAP=90kPa, MBT.

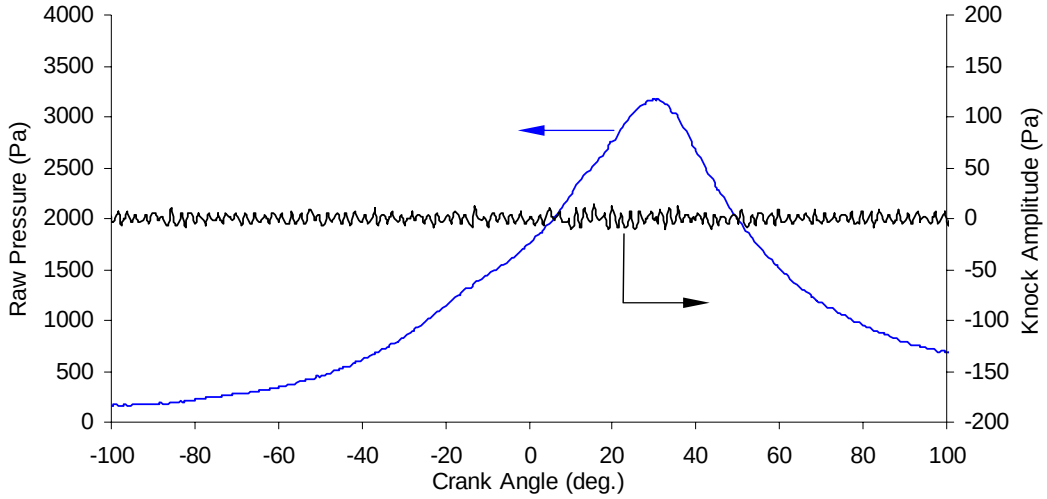

Figure 2.10: No knocking in the CFR-SI engine, Fuel=Gasoline, CR=9, 1800 r/min, λ=1, spark timing 15°BTDC.

Abnormal combustion can refer to a variety of situations in which one or more of the above definitions does not hold. This includes processes where the flame fails to completely consume all of the charge (partial burns and misfires), where the flame front is initiated prior to or after spark ignition by other means such as a hot spot in the chamber (preignition), or where some or all of the charge is consumed at extremely high rates (knock). This section only briefly reviews the important phenomena of knock and the reader is referred to detailed descriptions found in Heywood [96] and Stone [197].

2.5.2 Heavy Knock

As shown in Figure 2.11 heavy knock is characterised by a rapid rate of pressure rise up to 500 atm/ms compared to 30 atm/ms under normal combustion, but is less than the rise rate for a detonation wave. Heavy knock is initiated by sudden inflammation of the end gas, usually after most of the air-fuel mixture has been consumed. The propagation of the pressure shock wave velocities are in the order of 1000 m/s compared to 0.5 m/s for laminar flame speeds [208].

Knock is highly dependent on engine speed, as it defines the time available to heat up the end gas. As an example, the CFR engine knocks at 1800 r/min with 5 MPa of peak cylinder pressure, whereas a heavily boosted Formula 1 engine

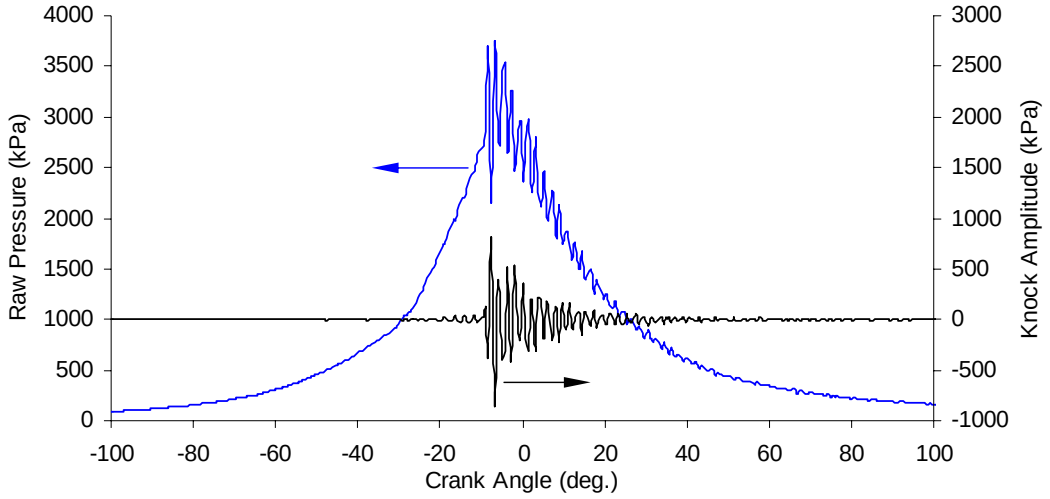

Figure 2.11: Heavy knocking in the CFR engine, Fuel=Gasoline CR=12, 1800 r/min, λ=1, Spark timing 20°BTDC, peak knock amplitude = 850kPa.

operates knock free at 12000 r/min with peak pressure in the order of 16 MPa. Consequently this creates a trend by which the octane requirements decrease as engine speed increases [173].

Heavy knock must be avoided in engines as it leads to structural damage such as piston surface erosion through high thermal stresses as well as audible noise. In addition, it reduces thermal efficiency due to an increase in heat transfer through the walls. In fact, the heat flux increases almost linearly with the amplitude of the pressure oscillation for oscillations greater than 0.5 MPa [139]. NO_x emissions and HC emission usually decrease. NO_x due to the reduced average bulk gas temperatures and HC due to the increased diffusion of unburned HC from crevices and quenched boundary layer, which is prompted by the vibration of the gas [111].

2.5.3 Jet Knock

Jet Knock is characterised by small pressure oscillations similar to conventional end-gas knock, only significantly smaller in magnitude and initiated at the start of ignition instead of towards the end of combustion. Jet Knock has been observed in high pressure direct injection studies [156, 162], direct injection of fuel on hot

surface investigations [72, 204] and in divided chamber engines [84, 172, 214, 215].

High Pressure Direct Injection and Hot Surface Ignition

When the H_2-air is ignited on a hot surface [72, 204], the small pressure oscillation (Figure 2.12 - left) is believed to be caused by the abrupt ignition of the mixture as it contacts the hot surface. This pressure oscillation leads to extremely high burning speed. Nakahira et al. [162] used the image analysis technique of shadow photography to analyse the shock wave generation around diesel fuel sprays (Figure 2.12 - right). They suspect that the multiple shock wave generation is related to the high velocity liquid fuel entering and breaking up in the main chamber.

Im et al. [102] examined the shock wave generation process during high pressure direct injection (135Mpa) of diesel fuel using Lagrangian spray simulations and also confirmed it experimentally with an X-ray radiographic technique. They have shown the development of conical shock wave formation at the tip of the jet as it penetrates into the combustion chamber.

Divided Chamber Ignition

Gupta et al. [84] in their study of pre-chamber shock generation, concluded that due to the pressure difference in the two chambers, both compression and

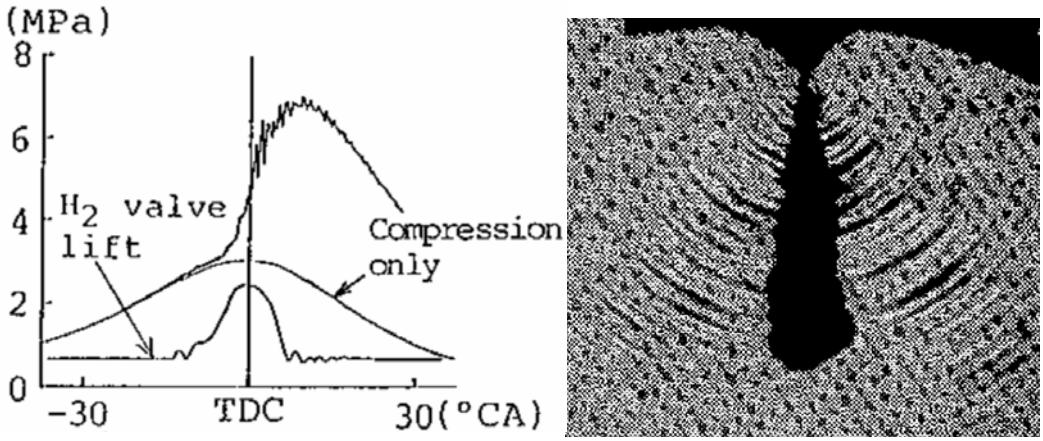

Figure 2.12: (left) pressure vibration on a H_2 fuel injection hot surface ignition engine [204], (right) multiple shock waves around diesel fuel spray [162].

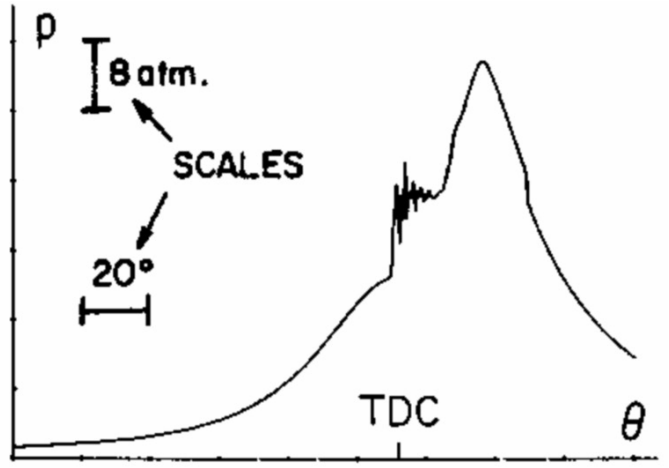

Figure 2.13: Pressure vibration as a result of 2D theoretical modelling of divided chamber engine, 1250r/min, spark time=3°BTDC, spark location is in middle of the pre-chamber, λ=1.17, orifice diameter=11.8mm [84].

expansion waves of high amplitudes are generated from the throat region (Figure 2.13). These shock waves propagate back and forth in the two chambers and are detected as pressure oscillations. The magnitude of oscillation is a function of the pressure difference between the two chambers and is also dependent on the strength and extent of the first pressure wave formed by the throat in the main chamber.

Wakai et al. [214, 215] experimentally verified the existence of pressure oscillations in a divided chamber combustion bomb. Figure 2.14 shows the

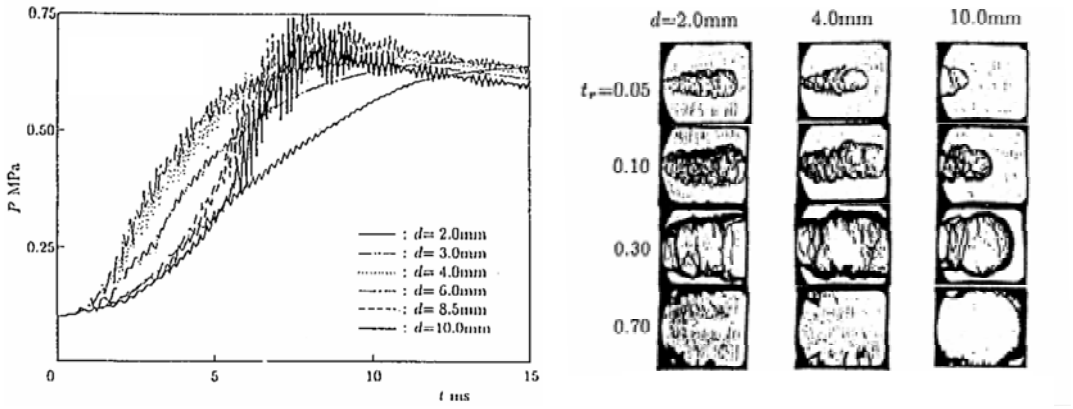

Figure 2.14: (left) Pressure vibration results, (right) flame images, methane-air mixture in a divided constant volume combustion chamber, main and pre-chamber is at λ=1, main chamber volume=300cm^3, pre-chamber volume=1.5cm^3, d=throat diameter [215].

variations in pressure oscillations as a function of throat diameter. Interestingly it is shown that the smallest pressure oscillation is caused by the smallest diameter nozzle (2mm).

A schlieren image taken by Oppenheim et al. [172] of a jet entering into the main chamber is shown on the left hand side of Figure 2.15. As the jet enters into the main chamber, a hemispherical shock wave is generated due to the mass addition associated with the jet. Oppenheim separated the two chambers with scotch tape and as the tape ruptured after combustion it traveled through the combustion chamber at supersonic velocity (Mach number = 1.6).

The linking characteristics between high-pressure liquid injection and pre-chamber ignited jets (which are gaseous), is the high jet velocities generated at relatively small throat areas by a large pressure ratio between the jet source and the main chamber. Consequently, when the jet velocity is equal to or exceeds Mach 1, a hemispherical or conical shock wave can be created in the combustion chamber, which is detected as a small pressure oscillation. Only a small amount of attention has been dedicated to the study of this field in IC engines, however it is interesting to note that in the field of fluid mechanics, the shock waves generated around high velocity jets are a well known phenomena (Figure 2.15 - right).

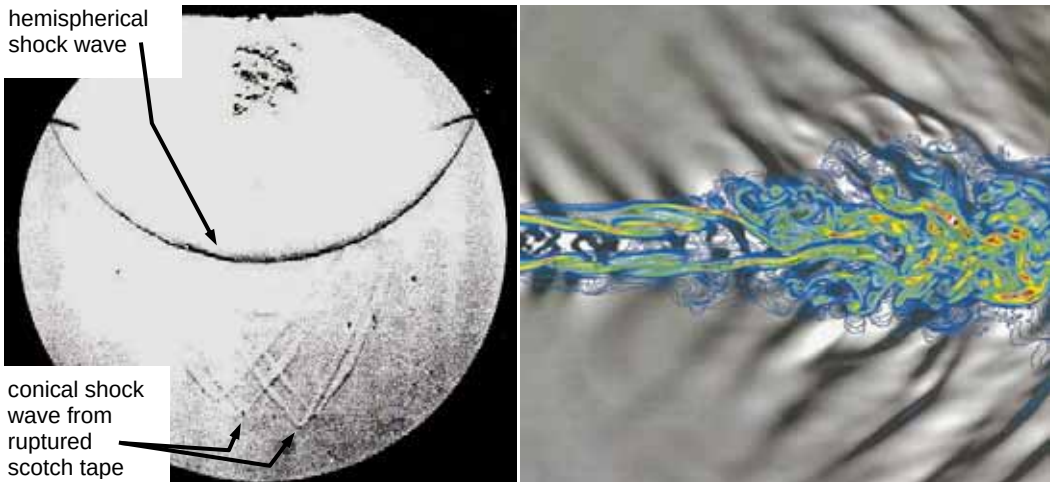

Figure 2.15: (left) single shock wave with jet ignition [172], (right) simulation result of turbulent jet at Mach 1.92 generating shocks, which dominate the near acoustic field [71].

2.6 Load Control Strategies

2.6.1 SI compared to Diesel

At a steady engine speed, the engine load (torque) is simply controlled by the amount of fuel drawn into the combustion chamber per cycle (and the thermal efficiency). In most current emission controlled SI engines, since the AFR is fixed to $\lambda=1$ the fuel flow is controlled indirectly by regulating the amount of air entering the combustion chamber. Consequently less air means less fuel or vise a versa. This is normally achieved by throttling, and often characterised as "quantity" controlled load matching.

In contrast, diesel engines operate un-throttled, which means that the amount of air entering into the combustion chamber is fixed at a given engine speed. Consequently, load is controlled by regulating the fuel flow and often characterised as "quality" load control matching. Current advanced engine technologies actually use a combination of both load control strategies; varying fuel flow and throttling. This is discussed in the following sections.

2.6.2 Throttling

In SI engines, the intake charge is expanded in the process of throttling. This is achieved at the expense of increasing the pumping work, which leads to higher negative work and therefore lower thermal efficiency. However, one of the benefits of throttling is the increased level of EGR, which can reduce NO_x emissions, while not affecting the TWC converter efficiency at $\lambda=1$.

Figure 2.16 shows the effect of AFR on specific fuel consumption (SFC), which is inversely proportional to efficiency, at different throttle position for a homogeneously charged SI engine. Evidently, at all throttle positions the best efficiency always occurs where the engine is charged with a lean mixture (point D). The best overall efficiency of the engine occurs at high load and this is another

disadvantage of throttling, since over the majority of the vehicle drive cycle the engine is actually throttled.

2.6.3 Fuel Flow Control and Inlet Boosting

As described earlier, when the engine load is regulated by fuel flow at a given engine speed, the amount of air entering into the combustion chamber is fixed. This operation is typical of a diesel engine, which simultaneously operates un-throttled and at a higher CR. The engine is un-throttled at all times, so at part load the engine operates lean (Figure 2.16 - point G to I) and at high loads the engine mixture moves closer to λ=1 (point F).

The fuel flow control method eliminates the efficiency losses at part load, since the engine is un-throttled and operates lean. However, at high load conditions close to λ=1, there is little advantage with respect to SI. The only way a diesel engine can operate lean at an equivalent load to a naturally aspirated SI engine is by inlet boosting. This means that at high load the fuel flow of SI and diesel engines is the same, however while the SI operates close to λ=1 the diesel engine is able to operate at very high λ values depending on the amount of boost. The advantages of operating in lean boosted mode are the realisation of simultaneous

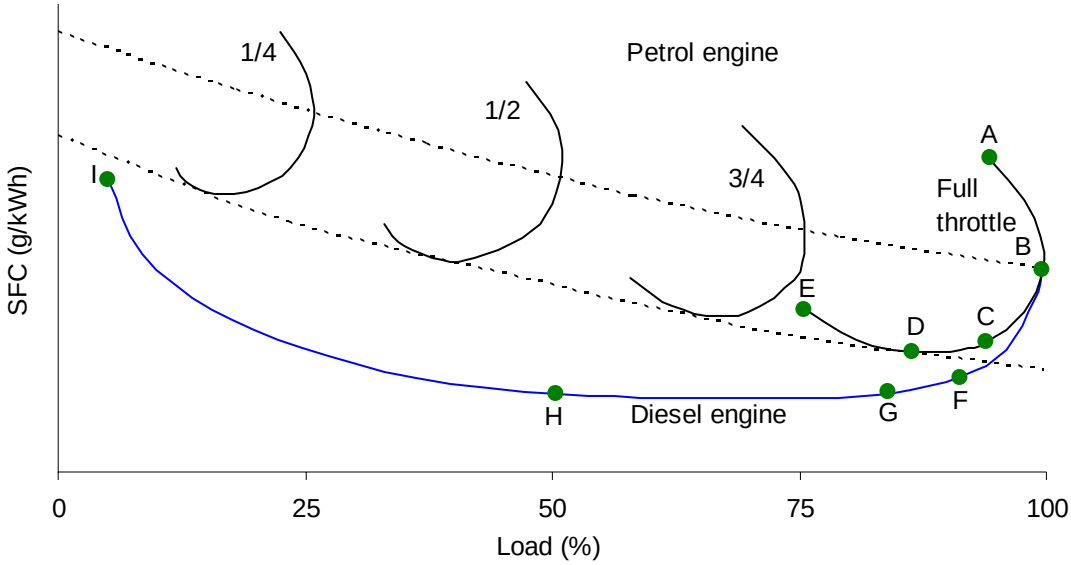

Figure 2.16: Comparison of fuel consumption loops for petrol and diesel engines (point A = very rich, B = rich, C = stoichiometric, D = slightly lean, E = lean limit, F = near stoichiometric, G = lean, H = very lean, I = extremely lean) [93].

increase in thermal efficiency, and reduction of NO_x to near zero levels. This is shown in Figure 2.17, which is based on actual engine data extrapolated to λ=2.5. The reduction of coolant heat rejection as AFR increases is also an important bonus as it could potentially decrease the radiator size, which would open up invaluable packaging space in the vehicle.

2.7 Assisting Lean Combustion

2.7.1 Introduction

Combustion must be stabilised at high air-fuel ratios in order to achieve the benefits of increased thermal efficiency and emissions reduction in the lean region. Most researchers in the past have made an effort to facilitate lean combustion by enhancing turbulence, enriching gasoline fueled engines with hydrogen, and increasing the amount of active species available in the mixture.

2.7.2 Turbulence

The flow process in the combustion chamber of an engine can be characterised as turbulent. Mixing rates due to turbulent flow are many times greater than those that could otherwise be achieved with molecular diffusion. Consequently, rates of

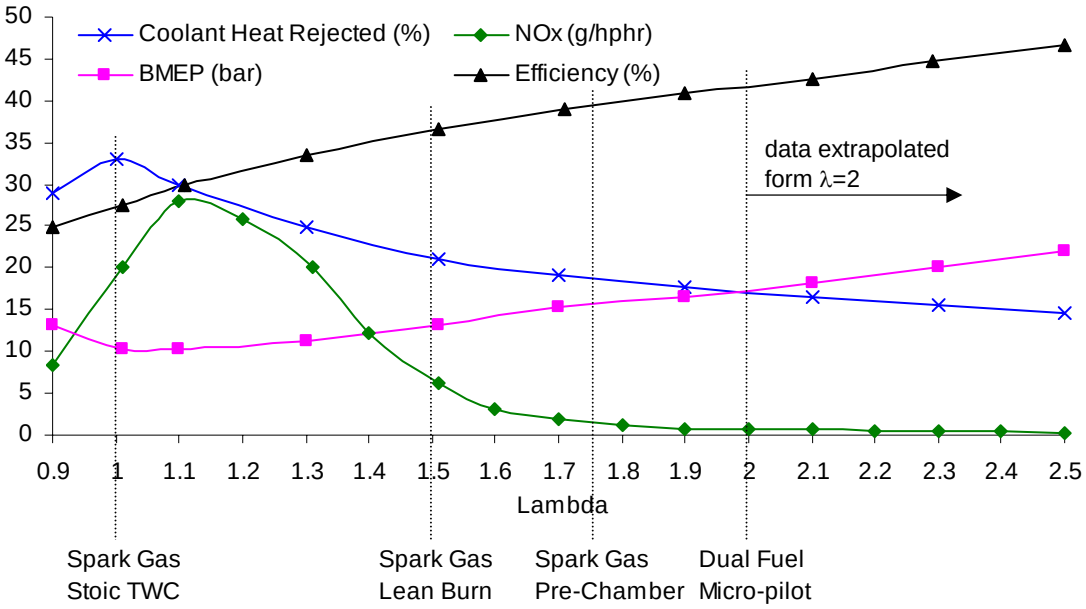

Figure 2.17: CNG engines optimum performance with lean burn [22].

momentum and heat and mass transfer are increased. Turbulence in the large scale flow field in engines is characterised as rotational, which include swirl, tumble, eddies etc... Each of these has high fluctuating vorticity. As turbulent flow is irregular and random, statistical methods are used to define the flow field. These definitions include the mean velocity, the fluctuating velocity about the mean (turbulence intensity), and several length and time scales [96].

Increasing turbulence has a number of benefits such as: enhanced breakup of liquid fuel droplets, better mixing of air and fuel, increased burning velocity, and increased postflame oxidation of HCs [55]. Contrary to the aforementioned benefits, turbulence enhancement must be carefully controlled, as it can be detrimental to thermal efficiency on account of increasing heat transfer to the walls and increasing unburned HCs [130, 170].

The lean limit of an engine can be extended by increasing the turbulence, since this has a positive effect on flame speed. Toyota Motor Corporation [103] demonstrated this in 1993 with their 3rd generation lean combustion system. This relationship is shown in Figure 2.18 and illustrates the possibility of extending the lean limit by increasing the mean turbulence intensity. From Figure 2.18 it can also be seen that any increase in turbulence intensity above 2 m/s has no ability to further increase the lean limit. This is most likely due to the reduced flame kernel growth rate caused by negative flame stretch, which is generated in lean mixtures exposed to high levels of turbulence [97].

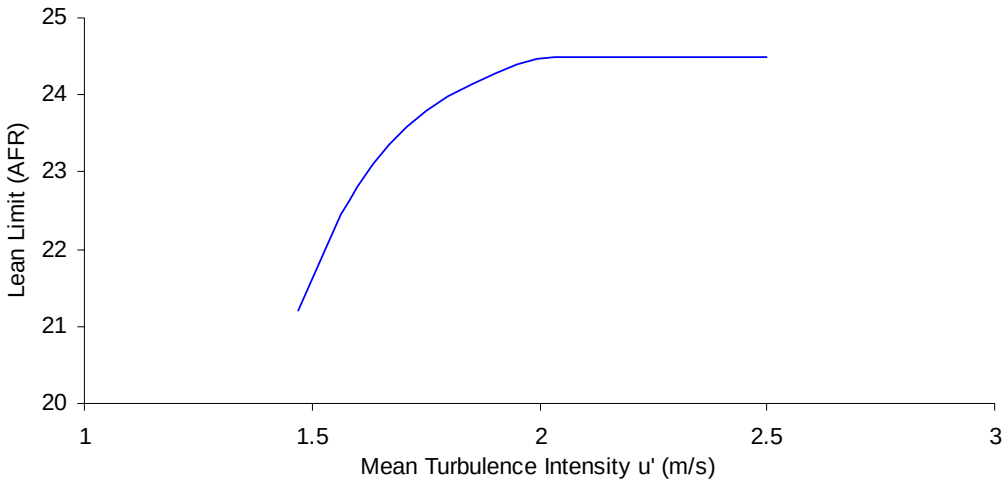

Figure 2.18: Extension of lean limit by increasing turbulence intensity, 1200r/min, homogeneous [103].

The flame kernel growth rate is strongly dependent on the ratio of turbulence intensity to the laminar flame speed as well as the expansion velocity [97]. Consequently, high initial expansion velocity can be used to delay the onset of the effects of turbulence on the flame kernel growth as this prevents negative flame stretch. This can be achieved by high ignition energy or with ignition systems similar to HAJI that can establish a rapidly expanding initial flame kernel.

The three most popular methods used to increase the turbulence intensity levels in the combustion chamber are: enhancing the level of squish, swirl and tumble. These methods are discussed further in Appendix B.2. Increasing turbulence requires careful design as it can reduce engine torque by up to 7% due to the potential energy (pressure difference across the valve and port) being converted to turbulent kinetic energy [116]. This reduction in torque may be unacceptable in production engines.

2.7.3 H_2 Assist

In order to make use of the unique properties of hydrogen, on-board H_2 reformers [9, 15, 81, 92, 209] have been developed to convert some of the HC fuel to H_2. This allows a standard gasoline fueled engine to be assisted with small quantities of H_2 with the aim of extending the lean limit and stabilising combustion in lean mixtures.

The lean flammability limit of hydrogen occurs at λ=10 compared to λ=1.32 for gasoline (Table A.1). Consequently, as shown in Figure 2.19, when 9% of the combustion energy is replaced with H_2 to assist a gasoline engine, the lean limit is extended to λ=1.42 [15, 81]. This extension of the lean flammability limit allows the engine to operate at lower combustion temperatures, which simultaneously reduces NO_x emissions and increases thermal efficiency [9, 15, 81, 209].

2.7.4 Chemical Control of Combustion

Free radicals such as hydrogen (H^+) and hydroxyl (OH^-) are molecules that possess unpaired electrons. This property makes them especially reactive with

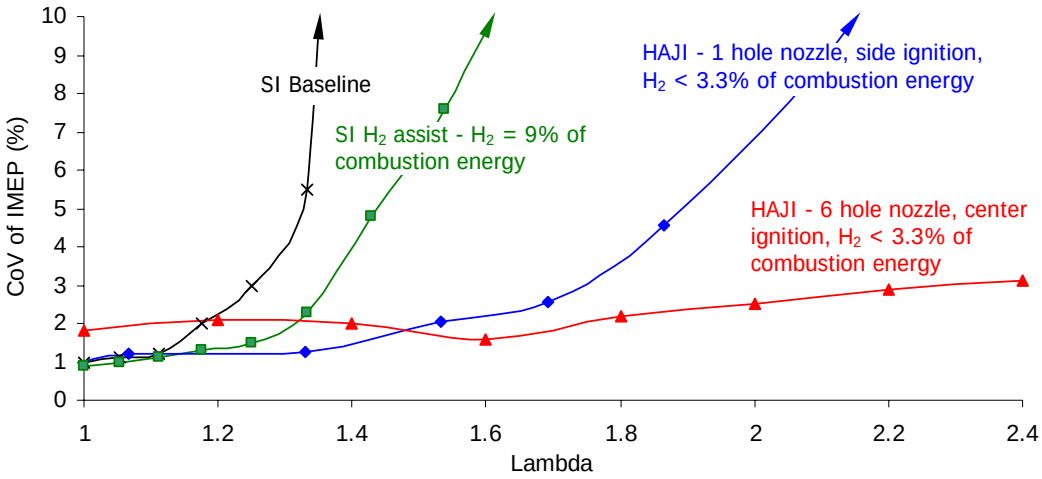

Figure 2.19: CoV of IMEP for SI, SI-H_2 assist [81], and HAJI (6 hole nozzle [136]).

other molecules. Combustion reactions involve a complex mechanism of chain reactions in which a radical (or atom) reacts with a stable molecule to give a product molecule another active specie which can propagate the chain. It is therefore possible to purposely produce radicals in the combustion chamber to increase the rate of combustion or to extend the flammability limit of a mixture. In an engine this can be achieved in rich mixtures where radicals are produced as the byproducts of combustion.

Gussak et al. [85, 86, 87] was one of the first to realise the importance of active radicals in lean burn engines and their production in fuel rich pre-chamber ignition systems. Since Gussak, many researchers have examined the benefits of active radicals with the use of a fuel rich pre-chamber [25, 94, 161, 171]. The majority of the fuel rich pre-chamber research uses a common fuel between the main chamber and the pre-chamber. HAJI however, utilises hydrogen in the pre-chamber irrespective of the type of fuel used in the main chamber. This is an important difference because hydrogen's rich ignitibility is the greatest out of all the surface transportational fuels (Table A.1). This special property may be responsible for hydrogen being able to produce more radicals than when a HC is used as the fuel in the pre-chamber.

It was shown in Figure 2.18 that turbulence alone cannot extend the lean limit beyond about 24.5:1 AFR, however with HAJI, it is possible to achieve stable

combustion between 30:1 to 45:1 AFRs (Figure 2.19). Kyaw [128] was the first to realise and suggest that together with turbulence, the ultra lean flammability limits are achieved by HAJI because the main chamber mixture is seeded with active radicals produced and issued from the pre-chamber. The active radicals H^+ and OH^- are the products of incomplete combustion in the hydrogen rich pre-chamber.

2.8 Leaders of Lean Burn Technology

Future ignition systems must be able to stabilise combustion in lean mixtures in order to both increase thermal efficiency and reduce emissions. To operate lean in an engine, the air fuel mixture can be administered homogeneously or stratified. As a generalisation, stratified mixtures are achieved via direct injection (DI) of the fuel into the combustion chamber, whereas homogeneous mixtures are usually premixed in the inlet port.

2.8.1 Diesel Engines

The diesel engine is an internal combustion engine in which a heavily stratified air-fuel mixture is formed, ignited and burnt in a high temperature environment, facilitated by the in-cylinder compression of air. Diesels are therefore commonly referred to as compression ignition (CI) engines and are predominantly fuelled by oil-based diesel fuel.

Diesel engines are capable of operating at ultra lean air-fuel ratios beyond the reach of SI engines. In contrast SI engines are less fuel efficient but have greater potential to produce less NO_x, CO and particulate emissions in comparison to diesels [29]. For this reason diesel engine technology is not discussed in detail in this thesis and all attention will be concentrated on the improvements in lean burn technology.

2.8.2 Spark-Ignition Direct-Injected (SIDI) Engines

The SIDI concept involves injecting gasoline fuel directly into the combustion chamber, as opposed to the intake port (typically on a closed valve), as with the

conventional PFI system. While this seems like a relatively subtle difference, it opens a new world of potential benefits such as:

- better transient response
- more complete combustion
- improved fuel economy
- no fuel pooling phenomena in intake ports
- less emissions - especially at start up

However, there are also the added complexities which must be considered and these are:

- more complex control system and calibration required
- when operating lean, NO_x aftertreatment is difficult
- potential to produce smoke and particulate emissions
- increased load on battery
- increased unit cost of engine

The primary reason for having a SIDI engine is to increase thermal efficiency and reduce emissions by operating lean or with EGR. A secondary reason is an increase in power.

SIDI is complex for two main reasons. First due to the short times available for the preparation of the mixture prior to combustion and second due to the desire to stratify the air-fuel mixture using the fuel spray and interacting gas dynamics. This thesis does not deal with DI technology in general. However it is an extension of PFI engine technology, which is being pursued by most of the engine manufacturing companies. Consequently, the reader is referred to Appendix B for information regarding DI injectors, their spray patterns and about the performance from leading manufactures of different SIDI engines.

2.8.3 H_2 Enrichment - with Onboard Reformers

As discussed in Section 2.7.3 and shown in Figure 2.19, the addition of H_2 can extend the lean limit of gasoline engines. Hydrogen can be made available by an

Table 2.2: Properties of different reformer types [9].

	Pro	Contra
C-POX Catalytic Partial Oxidation	+ quick start-up (<10s) + no H_2O necessary + compact + good dynamics	- low efficiency (85-93%) - low H_2 portion (≈20%) - low pressure operation (storage) - high temperature (≈1000°C)
STR Steam-Reforming	+ high H_2-portion (≈40%) + high pressure operation + high efficiency (90-93%)	- start-up, poor dynamics - size - H_2O required - temperature 600-700°C
ATR Autothermal-Reforming	+ high H_2-portion (≈30%) + quick start-up + efficiency (85-90%) + good dynamics	- size - temperature 800-900°C - pressure >1000kPa

onboard H_2 tank or with an onboard H_2 reformer. The most popular types of reformers are summarised in Table 2.2 with their pros and cons. The greatest disadvantages of these reformers are that they operate at high temperatures, increase the complexity of the engine management control system and add cost to the vehicle. It is worth noting that with maturing technology and the possibility of mass production in the future, theses disadvantages can be greatly reduced.

Green et al. [81] showed an increase in engine efficiency as the H_2 addition increased, however the overall system efficiency dropped due to the inefficiency of the reformer used in the experiment. In contrast, Tully et al. [209] showed that at the maximum thermal efficiency point, the overall system efficiency increased by 12.3% and NO_x decreased by 95%.

Allgeier et al. [9] at Bosch used a C-POX reformer, which produced 24% H_2 by volume. Results from experiments were used as inputs in a quasi-steady estimate on the New European Drive Cycle (NEDC) and with neither transient behavior nor

Table 2.3: Emission and energy consumption estimate of New European Drive Cycle [9].

NEDC	CO [g/km]	HC [g/km]	NO_x [g/km]	CO_2 [g/km]	Energy [MJ/km]
Gasoline	3.296	0.5386	0.2179	56.378	0.85
Reformed Gas	3.404	<0.0242	<0.0018	54.742	0.68
Variation	+3.3%	<-95.5%	<-99.2%	-2.9%	-20.0%

cold start taken into account, showed a dramatic decrease in emissions (Table 2.3). The levels achieved required no after-treatment of HCs and NO_x to meet Euro 4 emission requirements (Table 2.4). Allgeier also showed a decrease in fuel consumption of up to 20%.

2.8.4 HCCI

An alternative way of igniting a lean homogeneous charge is through HCCI (homogeneous charge compression ignition). In this form of combustion, the ignition sites are uniformly distributed throughout the combustion chamber so conventional flame propagation (and therefore end gas regions) are effectively eliminated, allowing the use of very high CR. Combustion is initiated by the auto-ignition of the mixture instead of by spark plug [196, 198].

HCCI technology has progressed substantially due to extensive worldwide studies. The Society of Automotive Engineers (SAE) alone published 13 papers related to HCCI between 1989 and 1999, however between 2000 and 2002 SAE has published 64 technical papers on this topic, some of which are referenced here. The strongest drivers of the HCCI technology has come from diesel engine manufacturers such as Caterpillar [58] which have been forced to meet future emission regulations (Figure 2.20).

HCCI engines can operate at CR=19, 2 bar boost pressure and up to λ=6 while maintaining stable combustion [45]. The thermal efficiency of HCCI engines is comparable to that of a stratified diesel engine, however it produces only 1-2ppm NO_x which translates into <0.04g/kWh depending on load and CR. In addition to

Table 2.4: Minimum catalyst conversion efficiency necessary to meet Euro 4 [9].

NEDC	CO [g/km]	HC [g/km]	NO_x [g/km]	CO_2 [g/km]	Energy [MJ/km]
Euro 4	1	0.1	0.08	-	-
Gasoline	69.7	81.4	63.4	-	-
Reformed Gas	70.6	0.0	0.0	-	-

this, running on gasoline, it generates no smoke [44]. HCCI is regarded as the 3rd ignition technology after SI and diesel. However, it must overcome the following limitations in order to be competitive in the future.

- Controlling the ignition timing and heat release rate is difficult due to the reliance on autoignition of the mixture.
- HC emissions are up to 5 times higher when compared to a standard SI engine (>20g/kWh at all times).
- The usable load range of HCCI engines is also quite narrow, even with the use of inlet heating and supercharging.
- Pressure rise is in the order of ~ 2MPa/deg, which can cause noise pollution.
- At room temperature, start up requires the engine to run in SI mode for 25 seconds to achieve a minimum oil temperature of 50°C - a prerequisite to HCCI operation.

2.8.5 Plasma, Torch, and Pulsed Jet Ignition

Plasma Jet Ignition (PJI) employs a large but very fast electrical discharge which creates a small plasma cloud, which penetrates 2mm into the combustion chamber in just 0.06ms [73]. This is quite remarkable compared to a spark plug which has a discharge duration of 1.7ms over a 0.8mm spark plug gap. PJI has been found to work well at low speed where the level of turbulence in the combustion chamber is low. However, high turbulence can extinguish the plasma cloud and consequently a reduction in the lean limit is observed [73].

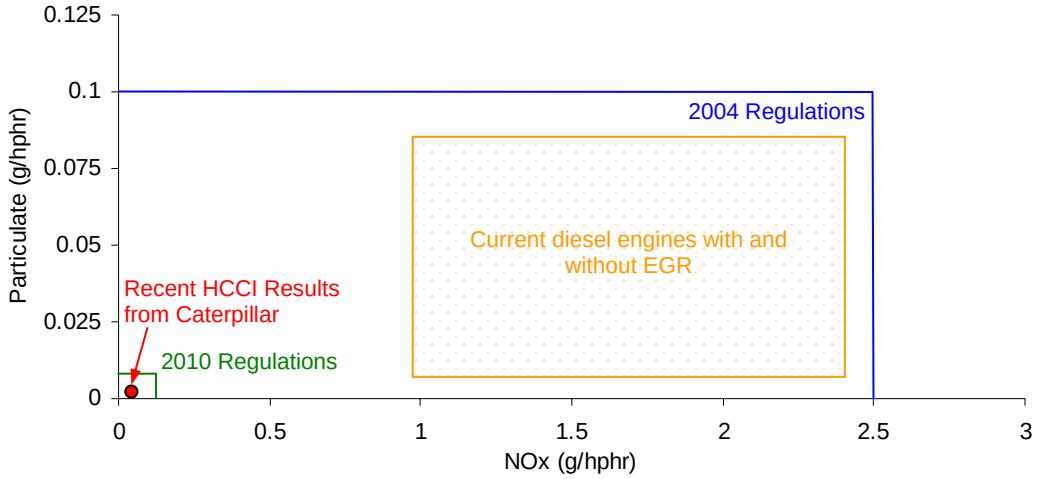

Figure 2.20: Heavy duty diesel emission requirements vs. diesel engine technology [58].

Torch Jet Ignition (TJI) usually employs a pre-chamber where the flame kernel is initiated. With this approach, the pre-chamber volume is usually 5 to 15 % of the clearance volume and the orifice diameter is larger than the quench gap of the air-fuel mixture. Once the pre-chamber mixture burns, the flame propagates into the main chamber without extinguishing due to the large orifice diameter. The pre-chamber can be scavenged through the pressure changes resulting from the compression and expansion processes. This however, results in high levels of residual gases. Honda solved this problem and went into production for a few years using the TJI system with separate pre-chamber and main chamber fuelling [49], they named the process CVCC (Compound Vortex Controlled Combustion).

As already mentioned in Section 2.7.4, Gussak et al. [85, 86, 87] was one of the first researchers to describe the importance of rich pre-chamber combustion in lean burn engines. Gussak's pre-chamber was 15% of the clearance volume (the same as the CVCC and TJI system), however his pre-chamber orifice was only 2 to 2.5mm in diameter. This means that combustion is extinguished by shear at the exit of the orifice and reignites in the main chamber. Gussak named his method of ignition the 'LAG' process (Avalanche Activation of Combustion). He discovered that active radicals were created in rich combustion and coined the term "chemically controlled combustion". Gussak then demonstrated that through chemical means, combustion reactions could be accelerated in a way that could not be achieved through fluid mechanics and enthalpy alone. In summary, he showed that radicals are produced in the rich pre-chamber which then issued via jets into the main combustion chamber, where the chemical reaction is enhanced and therefore the extension of lean flammability is realised. Unfortunately, Gussak had a lot of difficulty controlling combustion and especially HC emissions over a wide range of loads.

Oppenheim et al. [171] and other researchers [25, 94, 161] reformulated Gussak's findings by designing a more compact pre-chamber where the volume was less than 1% of the clearance volume. They called this a pulsed jet combustion (PJC) process, as the duration of the jet is shorter due to the smaller pre-chamber volume. The PJC device yields a turbulent combustion field that is said to control

combustion. The turbulent flame surface can be seen in Figure 2.21. When PJC is fitted to an engine it produces high HC emissions, similar to the LAG process.

An extension of the PJC system is seen in the APIR concept [184], a French abbreviation meaning Self-Ignition Triggered by Radical Injection. This concept is fundamentally similar to PJC, however a premixed rich mixture is injected into the pre-chamber and smaller diameter orifices (below 1mm) are used. The smaller orifices deliberately promote not only shear, but also quenching of the pre-chamber flame, thus uniformly seeding the main chamber with active radicals through the use of up to ten jets. It is claimed that these changes give better and faster ignition reproducibility compared to PJC. HC emissions are up to 260% higher in lean burn APIR mode compared to standard λ=1 SI operation. The lean limit of this concept is λ=1.8.

In summary plasma, torch, LAG, and pulsed jet ignition allow better control of turbulence and mean flow around the spark plug independently from the gas exchange process. The pre-chamber ensures that the air-fuel ratios are evenly prepared and of some optimal air-fuel ratio through separate fuelling. Ignition of the main chamber charge is extremely stable due to the large amount of energy available in the pre-chamber. The jets also create turbulence, which means that artificial turbulence generated from tumble and swirl can be relaxed, helping to reduce the associated pumping and heat transfer losses.

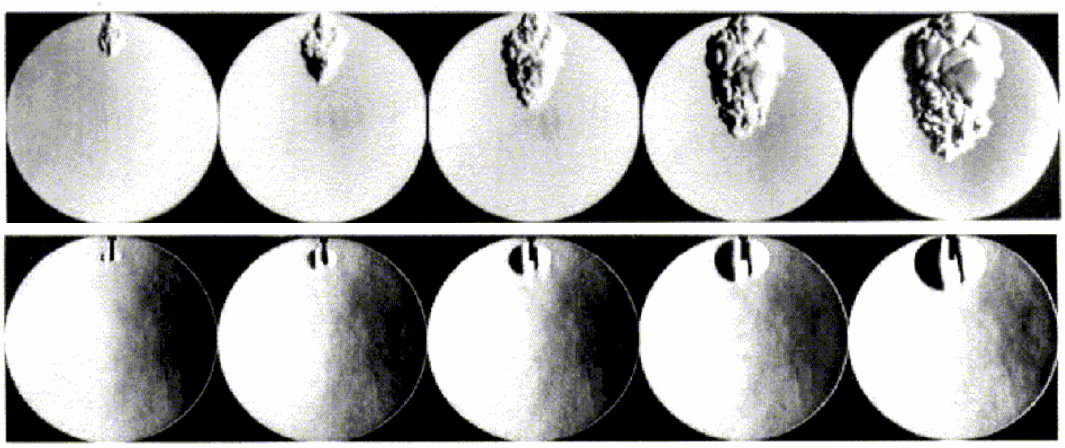

Figure 2.21: Schlieren records of combustion in methane-air mixture at an equivalence ratio of 0.8, Times: 1, 3, 5, 7, 9 ms after spark discharge, (top) PFJ, (bottom) SI, [182].

One of the more challenging aspects of pre-chamber ignition is to optimise the momentum of the jets over the wide range of throttle and speed settings required by modern SI engines. It is also important to control the depth of jet penetration as impingement on the piston and cylinder wall can cause surface erosion and wash the oil off the cylinder bore in addition to increasing heat losses.

2.8.6 Flame Jet Ignition - HAJI

As described in Section 1.5, hydrogen assisted jet ignition is a novel combustion initiation system, which allows a homogeneously charged spark ignition engine to operate stable at ultra lean air-fuel ratios. Fifteen years of continuous work has provided the foundation for this thesis. A brief history of knowledge captured by different researchers is now presented in chronological order.

Kyaw [128] and Watson [219] recognised that gasoline fuel is not an effective pre-chamber fuel due to the narrow flammability limits and large quench gap of gasoline fuel (Table A.1). By using hydrogen in the pre-chamber, HC emissions could be reduced and an extension of the lean limit could be achieved because of the production of active radicals which can only be generated in a H_2 rich pre-chamber. Finally they proved that an engine equipped with HAJI is able to run up to λ=5, which allows for the control of engine power output through air-fuel ratio adjustments rather than through throttling.

Lumsden and Watson [140] concluded through an optimisation process, that the most beneficial operating area of HAJI at a CR=9 was between λ=1.7 and λ=2. Within this range, values of ultra low emissions converge to values of high indicated net thermal efficiencies of 42%. They were also the first to take images of the HAJI process in an optical access engine (Figure 2.22). It is worth noting that the flame kernel in these images initiates away form the orifices. This implies that the jets momentarily extinguish as they propagate through the orifices and then re-ignite upon exit. Dober [55] has also shown this re-ignition phenomenon through 3D-KIVA modeling.

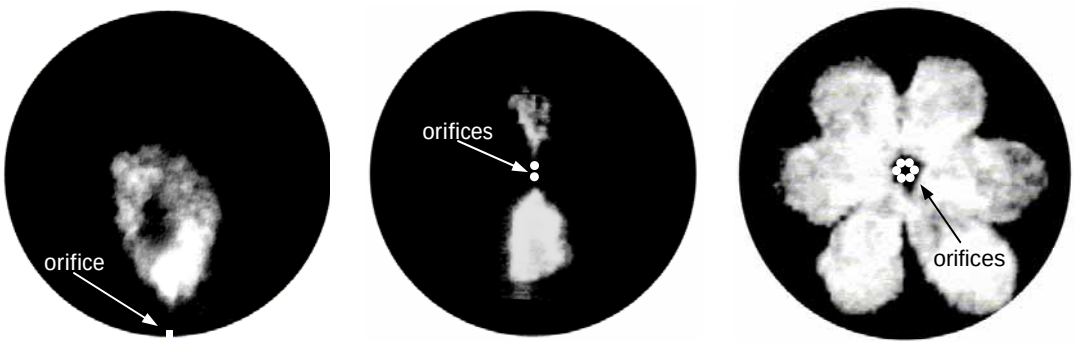

Figure 2.22: HAJI images showing flame propagation, optical access engine, (left) single nozzle - side ignition, (middle) 2 nozzles - central ignition, (right) 6 nozzle - central ignition [140].

Glasson et al. [76] developed a multi-cylinder spark ignition engine with the HAJI running in petrol mode. They showed a similar result to Lumsden [143] and Kyaw [128], which was a decrease in all exhaust gas emissions except HC which were higher in all operating conditions.

Lawrence [136] focused only on hydrocarbon emissions from the HAJI equipped ultra lean burn engine and identified the sources of the HC emissions. He concluded that HC emissions dramatically increase beyond λ=2. He also found that 72% of the HC emissions are sourced from the piston ring crevice.

Dober [54, 55] focused mainly on solving the HC emission problem through geometric control of HAJI nozzles as well as utilising direct cylinder injection of the main chamber fuel. He modelled the combustion in the pre-chamber, while varying the geometry of the pre-chamber and simulated the effect of different HAJI jet strength and direction. The effects of this were explored experimentally with DI fuel stratification and it was found that HC emissions could be reduced by at least 60% compared with homogeneous fueling, whilst maintaining a low NO_x (0.2g/kWh) capability.

In 2002, Zakis [232] installed a modified HAJI unit into a diesel engine to optimise lean burn CNG performance. He compared three ignition systems: SI, DPI (diesel pilot ignition) and HAJI to evaluate which of these gave best lean burn performance. He concluded that out of the three ignition systems, HAJI provided

the lowest NO_x, HC, CO and CO_2 emissions and also provided the greatest combustion stability.

Wang [217] examined the effect of DI injection timing on emissions and efficiency in a CNG fueled DI engine coupled with HAJI. She concluded that thermal efficiency, HC, NO_x, and CO emissions were all predominantly influenced by the end of injection time. Injecting later than 100° BTDC increased all three emissions and decreased efficiency.

2.9 Hydrogen Fueled Engines – The Solution to the Problem

In the world energy mix, the hydrogen to carbon ratio (H/C ratio) has grown from 0.28 since 1860 to 2.0 by 1990 [59]. This promises to be a positive trend towards decarbonisation and the only way towards sustainable economic growth. The lightest HC fuel today is methane (CH_4) with a H/C ratio of 4. The obvious progression from methane is the use of hydrogen (H_2) as it posses a H/C ratio of infinity. Currently, H_2 reflects 0% of all transportational energy consumption due to its lack of availability at fueling stations. To implement an appropriate infrastructure would take a minimum of 15 years and cost $500 billion [43]. One of the foreseeable economic advantages of reducing dependency on oil by implementing a H_2 infrastructure would be a better balance of powers between international consuming and producing nations, which may prevent events such as the Gulf War in 1991 [59].

Apart from the unavailability and storage difficulty of H_2, the extensive technical problems with H_2 should also be noted. These include residual gas ignition, hot surface and deposit ignition. These are considered to be serious problems, and therefore must be dealt with at the time of engine development. Watson et al. [222] successfully solved these problems while developing a 4 cylinder 2 liter engine. The solutions for the above problems included a delayed port admission of H_2, stringent oil control measures, selection of synthetic lubricating oil, high thermal conductivity aluminium coating of the combustion chamber surface, and water injection at high power outputs.

From the environmental point of view, many researchers, automotive companies and international organisations have realised the thermal efficiency improvement and emission reduction benefits of hydrogen fueled engines [23, 43, 59, 91, 106, 200, 222]. There is no doubt that H_2 produces the lowest engine out emissions of any of the gaseous, liquid or bio fuels and if the engine is boosted, it could possibly produce the equivalent torque and power to an otherwise naturally aspirated gasoline engine. Current engines would require only minor modifications in order to operate on H_2 reliably with equivalent durability to current SI engines. Lastly, contrary to popular belief, hydrogen is the safest fuel when ranked against gasoline and methane. Therefore in order to shift the public's perception of hydrogen as being a dangerous fuel, care must be taken when hydrogen is handled and dispensed to prevent careless accidents [210].

2.10 Summary

In this chapter we have seen how spark ignition engines emit large quantities of the three legislated emissions of NO_x, HC and CO. Their effect on human health and the environment is substantial. With current technology, to maximise both the efficiency of the catalytic converter and combustion stability in the combustion chamber, the SI engine must operate at a stoichiometric air-fuel ratio. In this mode, all three engine emissions are close to their maximum. The most effective way to reduce engine out emissions and increase thermal efficiency is to combust ultra lean air-fuel mixtures. This means operating at or above $\lambda=2$.

EGR has been shown to be an effective way to dilute the fuel-air mixture and has been used extensively because it does not affect the conversion efficiency of the TWC converter. EGR will be used in the near future, but if engine wear is to be reduced and thermal efficiency increased further, dilution of the mixture with air is the only alternative.

Knock was shown to be an interesting and important combustion characteristic. Heavy knock is undesirable due to the damage it can cause to the engine. A smaller but different phenomenon of small pressure oscillation was shown to exist

in hot surface ignition, DI, and divided chamber engines when the jet or fluid velocity equals or exceeds Mach 1 throughout the combustion process.

SI engines can only control engine load via throttling when the AFR is fixed at stoichiometric. This reduces their fuel economy considerably, since the NEDC vehicle test predominantly requires the engine to be throttled. In contrast, diesel engines can maintain stable combustion at all AFRs and therefore operate un-throttled with load variation via AFR change. When diesel engines are operated simultaneously lean and boosted they can produce the same or larger torque than an SI engine operating at WOT. Lean and boosted operation improves thermal efficiency and reduces engine out NO_x emissions. Furthermore, it is an indication that future ignition systems must be able to function un-throttled to harness these benefits.

It has been explained that there are a number of different mechanisms which can help extend the lean flammability limit of a gasoline air-fuel mixture. An increased level of turbulence can extend the lean limit (not exceeding 5% CoV of IMEP) by 0.23 λ, but at the expense of increased pumping losses. Replacing as little as 9% of the combustion energy with hydrogen can extend the lean limit by 0.1 λ, whereas seeding the combustion chamber with active radicals can extend the lean limit 1 to 2 λ, depending on the technology used.

The most popular lean burn SI technology at the moment is SIDI because engine management units and injector technology have matured to the point where they outperform their PFI counterparts. They perform best in stratified lean mode, however at high speeds and loads they suffer from smoke similar to diesels.

It is apparent that much effort and funding is going into developing engine technologies, primarily because we are persisting with HC based fuels as our energy source. A hydrogen based economy should eventually be established in order to stabilise powers between nations, reduce emissions generated by humans and establish equilibrium in the environment.

CHAPTER 3
Combustion Modelling

3.1 Introduction

This chapter describes the development, implementation and theoretical framework of a two-zone quasi dimensional model known as E-CoBRA (Experimental Combustion Burn Rate Analysis). This model was developed to analyse the characteristics of both SI and HAJI combustion. Over 500 experimental pressure traces were used as inputs to calculate more than 100 output parameters such as: IMEP, burn rate, flame speed, burned and unburned zone temperatures, knock amplitude and rate of NO_x formation. The large number of data points to be analysed required a computationally efficient model if results were to be obtained in a realistic time frame. An overview of various modelling options is therefore discussed and the most suitable modelling approach for this project is presented. It is shown that the modules implemented are highly flexible and computationally efficient algorithms.

This chapter discusses the important models implemented into E-CoBRA such as compression, combustion, expansion, chemical equilibrium, adiabatic flame temperature, turbulence, flame speed, NO_x formation and knock intensity. It also

reviews the regimes of combustion relevant to SI engines. The results of the theoretical analysis will be discussed in chapters 5, 6, 7 and 8.

3.2 Two-Zone Quasi Dimensional Modelling

3.2.1 Multi-dimensional Modelling

Over the last 15 years, multi-dimensional modelling has advanced steadily. Consequently, models are now capable of accurately predicting fluid flow, flame propagation rate and flame geometry throughout the entire cylinder. Unfortunately, their improvement is shadowed by the ever-growing demand on fast computational speed and more importantly, by today's complex combustion systems; in particular, single and multi fluid DI systems combined with tumble and swirl enhancements and other complex combustion systems such as HAJI.

When modelling complex combustion systems in 3D, such as HAJI combustion, the computation time still takes at least 1 week [217]. 2D models are also complex to implement, and at least 60 times slower than quasi dimensional models [21]. Consequently, it would be unrealistic to analyse hundreds of cases within the scope of this research project. As a result, a two-zone quasi dimensional model was chosen as it satisfies the timing requirements and level of sophistication required to study the differences in combustion behavior between SI and HAJI.

3.2.2 Commercial Diagnostic Software

The objectives of this research required that the model should be diagnostic (i.e.: to calculate IMEP, burn rate etc…), and to be predictive (to calculate the level of turbulence, rate of NO_x formation etc…).

There exists plenty of commercially available diagnostic software such as: Redline CAS, AVL Indicating Technology, Creative Technical Solutions Optimizer, Macao Osiris, Optimum Power PTrAn, REVelation, SMETec COMBI, and Dewetron. These mainstream software packages are however too expensive for university funded

research projects and are also difficult and restrictive in their ability to modify or add-in new algorithms.

Predictive two-zone quasi dimensional models have been developed by just about every academic institution with an interest in reciprocating engines and certainly every major engine manufacturer involved in engine research. These in-house models are however carefully guarded and therefore are not universally available.

Due to lack of funding, absence of flexibility in research groups models (BURN PBURN [149]), and the need to implement flamelet and chemical equilibrium modules, it was decided that a two-zone quasi dimensional model needed to be developed. This model would be based on the overwhelming availability of literature regarding the different techniques and algorithms.

3.2.3 Two-Zone Thermodynamic Cycle Analysis

The engine cycle simulation that models the compression and expansion strokes including combustion follows the formulation described by Ball et al. [19], Cheung and Heywood [42], Dai et al. [48], Guezennec and Hamama [83], Heywood [95, 96], Mattavi and Amman [147], Poulos and Heywood [177], Shrestha and Karim [193], Stone [197], and Taylor [205], and the reader is referred to these discussions for a comprehensive overview. In this chapter only a brief summary of salient points is included.

The E-CoBRA program is divided into three main loops: the compression of unburned charge, two-zone combustion including compression and expansion, and expansion of the completely burned products. The condition of the charge (pressure, temperature, AFR, type of fuel) and the engine specifications (speed, CR, MBT) at the start of the compression are required as inputs. A basic solution flowchart is shown in Figure 3.1, and a detailed derivation of all of the equations used in the program can be found in Appendix D. The software code implemented into VBA is contained in Appendix G.

All models are built around certain assumptions and the specific assumptions used in the formulation of the E-CoBRA model, these are similar to many other two-

zone engine models, as outlined here.

- The cylinder charge during combustion is assumed to be divided into two-zones - the burned products and unburned reactants.
- The two-zones are homogeneous and have uniform properties;
- The analysis is restricted to the closed valve period (IVO-EVO);
- The pressure at any time is uniform throughout the cylinder;
- Flame thickness is of null thickness;
- All crevice effects are ignored;
- There is no heat transfer between the two-zones;
- Gases behavior is ideal; and
- Leakage from the cylinder is negligible.

Residual Gas Mass Fraction

The residual gas fraction is estimated using the model developed at MIT by Fox et al. in 1993 [69]. This formula has been successfully used by General Motors Powertrain (GMPT) and also by Lumsden [143] in a HAJI CFR engine. The regression equation to predict residual fraction is the following:

$$X_r = 1.266 \frac{OF}{N} \left(\frac{p_i}{p_e} \right)^{-0.87} \sqrt{|p_e - p_i|} + 0.632 \frac{\phi (p_i / p_e)^{-0.74}}{CR} \qquad (3.1)$$

where: N = engine speed, P_i, P_e = intake and exhaust pressure respectively (kPa), CR = compression ratio, ϕ = fuel/air equivalence ratio, OF = overlap factor (mm^2 °/L)

The overlap factor is calculated using the following formula:

$$OF = \frac{1.45}{B} \left(107 + 7.8\Delta\theta + \Delta\theta^2 \right) \frac{L_{V,\max} D_V}{B^2} \qquad (3.2)$$

where: B = bore, $L_{V,max}$ = maximum valve lift, D_V = valve inner seat diameter (all dimensions are in [mm]), $\Delta\theta$ = valve overlap in crank angle degrees at 0.15mm valve lift (valve lift, inner seat diameter and valve overlap is published by Lancaster [131] for the CFR engine)

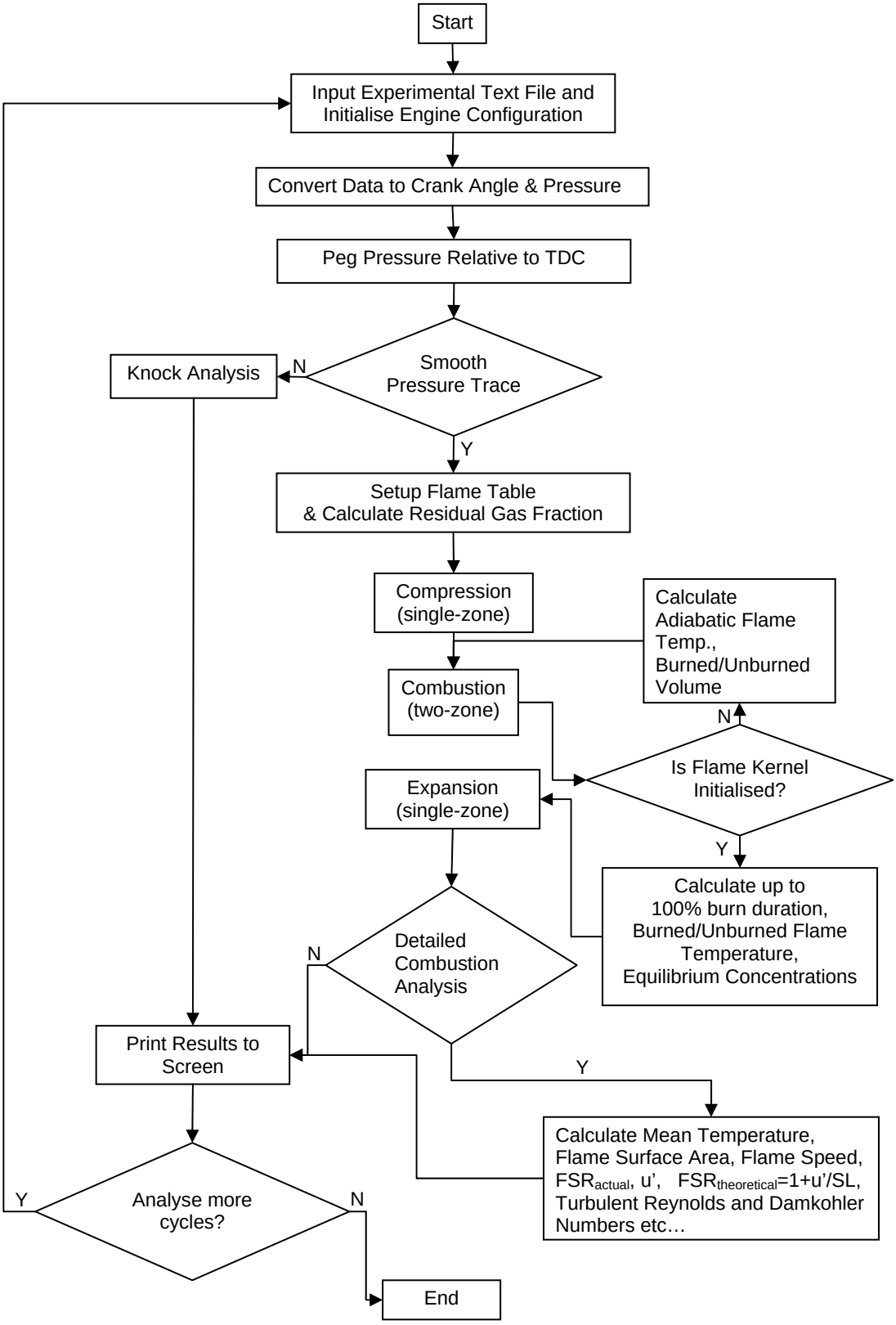

Figure 3.1: Solution procedure flow chart for E-CoBRA.

Compression and Expansion Strokes

When the First Law of thermodynamics is applied to the charge as a single zone during compression, before flame initiation, and during expansion following the completion of flame propagation, the following equation results:

$$\frac{dT}{d\theta} = T\left[\frac{1}{V}\frac{dV}{d\theta} + \frac{1}{P}\frac{dP}{d\theta}\right] \tag{3.3}$$

where: T = temperature, V = volume, P = pressure

Combustion Period

As mentioned, during the combustion phase the charge is assumed to be divided into two-zones. After some manipulation of the Equation of State, the First Law, and the conservation of mass and volume equation, the following three first order differential equations can be derived (Appendix D.2.2). These equations govern the combustion phase.

$$\frac{dT_u}{d\theta} = \frac{V_u}{m_u c_{p_u}}\frac{dP}{d\theta} + \frac{1}{m_u c_{p_u}}\frac{dQ_u}{d\theta} \tag{3.4}$$

$$\frac{dT_b}{d\theta} = \frac{P}{m_b R_b}\left[\frac{dV}{d\theta} - \frac{\left(R_b T_b - R_u T_u\right)}{P}\frac{dm_b}{d\theta} - \frac{R_u V_u}{P c_{p_u}}\frac{dP}{d\theta} - \frac{R_u}{P c_{p_u}}\frac{dQ_u}{d\theta} + \frac{V}{P}\frac{dP}{d\theta}\right] \tag{3.5}$$

$$\begin{aligned}\frac{dP}{d\theta} = \frac{-1}{\left[\frac{c_{u_u}}{c_{p_u}}V_u - \frac{c_{v_b}R_u}{R_b c_{p_u}}V_u + \frac{c_{v_b}}{R_b}V\right]}\Bigg\langle &\left[1+\frac{c_{v_b}}{R_b}\right]P\frac{dV}{d\theta} - \frac{dQ}{d\theta} \\ &+\left[\left(u_b - u_u\right) - c_{v_b}\left(T_b - \frac{R_u}{R_b}T_u\right)\right]\frac{dm_b}{d\theta} \\ &+\left[\frac{c_{v_u}}{c_{p_u}} - \frac{c_{v_b}}{R_b}\frac{R_u}{c_{p_u}}\right]\frac{dQ_u}{d\theta}\Bigg\rangle\end{aligned} \tag{3.6}$$

where: $R_{gas} = \frac{n}{m}R_{universal}$ $\quad c_v = c_p - R$ $\quad u = h - RT$

The equations are solved by simple substitution, which forms the basis for the crank angle marching finite difference solution. The first order differential equations (Equations 3.4 to 3.6) can be solved by the Adams-Moulton numerical method, detailed in Appendix D.5.

Heat Transfer

The bulk heat transfer was calculated by a method which has been extensively used throughout the literature. This method accounts for both convection and radiation (5% of total heat transfer) and assumes one-dimensional heat flow through the wall piston and cylinder head [96].

$$\frac{dQ}{d\theta} = \frac{30A}{N}\left[h_{c_u}(T_{g_u} - T_w) + \beta\sigma(T_{g_u}^4 - T_w^4\right] \tag{3.7}$$

where: A = surface area, N = engine rotational speed, h_c = convective heat transfer coefficients, β = 0.6, σ = Stefan-Boltzmann constant = $5.67*10^{-8}$ (W/m^2*K^4),

To estimate the heat transfer coefficient (h_c) the Woschni correlation is used. This correlation was extensively used in previous studies, because with the simple adjustment of constant *'C'* in Equation 3.8, the heat transfer coefficient of any engine can be correlated. For the CFR engine C = 30, however Guezennec and Hamama [83] reported C =110 for a 6 cylinder prototype engine.

$$h_c = C\left[D^{-0.2}P^{0.8}T^{-0.55}\omega^{0.8}\right] \tag{3.8}$$

where: D = diameter of piston, P = cylinder pressure in (kPA)
T = zone temperature (K)

Woschni hypothesised that the average gas velocity is proportional to the mean piston speed. To account for the change in density due to combustion he introduced a pressure rise due to combustion term (P-P_m). The average cylinder gas velocity is therefore expressed as follows:

$$\omega = C_1 S_P + C_2 \frac{V_d T_r}{P_r V_r}\left(P - P_m\right) \tag{3.9}$$

where: V_d = displaced volume, V_r, T_r, P_r represent the known state of the working gas related to inlet closure or ignition, S_p = average linear engine speed, P_m = corresponding motoring pressure in the absence of combustion, C_1 = 6.18 for gas exchange, C_1 = 2.28 for

compression and expansion, C_2 = 0 for gas exchange and compression, C_2 = 3.24*10^{-3}(m/sK) for combustion and expansion.

3.3 Chemical Equilibrium

3.3.1 Frozen, Chemically or Kinetically Controlled Chemistry

There are three popular methods used to calculate the concentrations of chemical species in the combustion chamber:

1. perfect combustion without chemical dissociation,
2. chemical equilibrium,
3. kinetically controlled chemistry.

Assuming perfect combustion is often used for performance estimations because it is computationally fast, however due to the exclusion of chemical dissociation this method overestimates the adiabatic flame temperatures by as much as 240°C at a stoichiometric AFR [96]. Chemical equilibrium calculations are adequate for computing adiabatic flame temperature and laminar flame speeds when it is assumed that in a given time step the mixture has reached chemical equilibrium. This is only valid for the combustion phase because during expansion the mixture has insufficient time to reach equilibrium due to the rapid temperature drop, consequently, some of the species freeze at higher concentrations. An example of this can be seen in Figure 3.2, where the bimolecular exchange reactions and the CO oxidization reaction were sufficiently fast to be continuously equilibrated. It was only during the later stages of the expansion stroke that the CO concentration was predicted to depart from equilibrium [96].

It is also worth noting that NO_x formation, like CO is also kinetically controlled. It is therefore important to develop a kinetically controlled combustion algorithm when emission predictions are to be made. The greatest disadvantage of detailed kinetic models is their extreme demand on computational time. For example, hexane (C_6H_{14}) which is less complex than gasoline, requires 450 species and

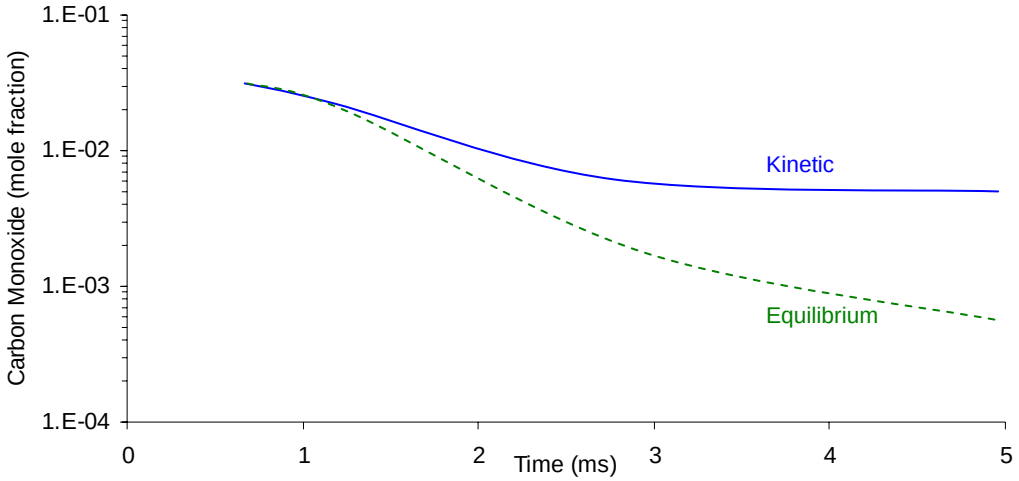

Figure 3.2: Kinetic vs. equilibrium calculations of CO concentration during expansion stroke following TDC combustion in SI engine [96].

1500 reactions to fully describe it kinetically. The purpose of this research does not require such detail and accuracy. Therefore a chemical equilibrium solver was implemented into the two-zone model.

3.3.2 Chemical Equilibrium Solver

The "rapid computation of chemical equilibrium compositions" (RCCEC) method calculating the concentration of chemical species was developed by Erickson and Prabhu at NASA [61] and was chosen because it is applicable to both hydrogen and hydrocarbon combustion.

The author re-derived, modified and implemented the RCCEC method into VBA as described in detail in Appendix D.6. The re-derivation was very important and is explained in further detail in Section 3.3.3. This method was chosen because it is up to 80 times faster than the often-used free-energy minimization method [61]. The chemical system is composed of four elements (C, H, O, N) and ten reacting species: H_2O, CO_2, CO, O_2, H_2, N_2, H, O, OH, and NO. Starting with an appropriate set of equilibrium equations and elemental balance equations, the ten equations are reduced to two equations and then to a single equation containing one unknown variable. This single equation was solved with a Newton iteration scheme. The chemical reactions considered in the scheme are:

$CO + H_2O$	$\rightarrow$	$CO_2 + H_2$	[1]
$2CO_2$	$\rightarrow$	$2CO + O_2$	[2]
H_2+O_2	$\rightarrow$	$2OH$	[3]
H_2	$\rightarrow$	$2H$	[4]
O_2	$\rightarrow$	$2O$	[5]
O_2+N_2	$\rightarrow$	$2NO$	[6]

The input parameters for this algorithm are temperature, density, equivalence ratio, H/C ratio, mol CO/ mol CO_2 ratio (initial guess), and nitrogen/oxygen ratio.

For all species, thermodynamic properties such as specific heat and enthalpy have been published by the National Institute of Standards and Technology [167] and are in the form of the "Shomate Equation". The accuracy of this format is equivalent to the more popular NASA polynomials [167].

3.3.3 Chemical Equilibrium Solver Accuracy

After implementation, the algorithm was not producing accurate information in comparison to published data in the literature [61, 62, 63, 96, 169]. Consequently, after considerable time debugging, the author re-derived the algorithm and corrected Equation D.64 and D.68 found in Appendix D. It was concluded that this was only a typing error in the paper published by Erickson and Prabhu [61], because upon implementing the changes, the program provided excellent correlation with published material.

When the chemical equilibrium solver was compared to packages developed by Olikara and Borman [169], and Eriksson [63], which used a similar number of chemical reactions and reacting species, the results were identical. The solver was also compared to the sophisticated NASA Lewis Chemical Equilibrium Code (CEC76) which was revised in 1976. Some of these results are published by Heywood [96] and Negus [165] and in general, the errors were less than 1.0% for the specific heat of burned mixtures at the pressures and temperatures of interest. The maximum error of 2.9% occurred at 2750K, 30atm, and at a

stoichiometric AFR. Based on the high accuracy and fast computational speed it was concluded by the author that the solver developed by Erickson and Prabhu [61] is more than adequate to satisfy the objectives of this research.

3.4 Adiabatic Flame Temperature

By definition, the adiabatic flame temperature is the temperature at which the enthalpy of reactants equals the enthalpy of the products [229]. It is an important parameter in two-zone modelling, because at the start of combustion the flame kernel is assumed to be at the adiabatic flame temperature. As previously stated, an inaccurate estimation of this temperature can result in an overestimate of initial flame temperature by up to 240°C for a H_2-air mixture and 110°C for a gasoline-air mixture.

3.4.1 Calculation Methods

Method 1 - Equilibrium Solver

The equilibrium solver described in the previous section (3.3.2), can be used to calculate the adiabatic flame temperature by rearranging the solver to iterate until the enthalpy of the reactants equals the enthalpy of the products.

Method 2 - Empirical Equation

An alternative method for calculating the adiabatic flame temperature is to use the empirical equations developed by Rhee et al. [183]. The study listed over 30 fuels including isooctane and hydrogen and the equations are a function of pressure, temperature and AFR. This method is applicable to mixtures ranging from stoichiometric to the lean flammability limit, initial mixture temperatures from 298K to self-ignition, and at reaction pressures of 1atm to 100atm. The method is only a few lines of computer code and requires no iteration and is therefore extremely computationally efficient.

Table 3.1: Accuracy of the adiabatic flame temperature for isooctane.

	Equilibrium Solver Erickson and Prabhu [61]	Empirical Equation Rhee and Chang [183]	No Dissociation
Rich (error)	< 2%	Can not operate	>> 6%
Stoichiometric (error)	< 2%	< 1%	> 6%
Lean (error)	<< 2%	< 1% (only operates to lean limit)	< 6%

3.4.2 Adiabatic Flame Speed Accuracy

Method 1 - Equilibrium Solver

The accuracy of the equilibrium solver directly affects the accuracy of the adiabatic flame temperature. This is demonstrated in Tables 3.1 and 3.2, which summarise the accuracy of different methods of calculation used for isooctane and hydrogen fuel. With the equilibrium solver, the adiabatic flame temperatures are within 2% of published results for isooctane, which was used in modelling instead of gasoline due to the unavailability of data in the literature. This assumption is consistent with other researchers [165, 197], since isooctane is a representative component of gasoline.

The H_2 fuel results are less accurate than those for isooctane because the solver was predominantly developed for HC fuels. Nevertheless, it provided a significant improvement over other methods which do not include dissociation. Based on this analysis, the equilibrium solver was used to calculate burned and unburned mixture properties such as C_p and γ, as well as the adiabatic flame temperature for rich mixtures.

Method 2 - Empirical Equation

The empirical equations provided superb accuracy with an error of less than 1% for a wide range of operating conditions, which is more than adequate for IC engine analysis (Tables 3.1 and 3.2). This method was used to calculate the adiabatic flame temperature for stoichiometric and lean mixtures and increased the computational speed by 30%, by eliminating the need for the equilibrium solver to iterate.

Table 3.2: Accuracy of the adiabatic flame temperature for hydrogen.

	Equilibrium Solver Erickson and Prabhu [61]	Empirical Equation Rhee and Chang [183]	No Dissociation
Rich (error)	< 4.5%	Can not operate	>> 9%
Stoichiometric (error)	< 4.5%	< 1%	> 9%
Lean (error)	<< 4.5%	< 1% (only operates to lean limit)	< 9%

3.5 Turbulence

3.5.1 Introduction to Laminar and Turbulent Flames

Before the modelling of turbulence is discussed, it is important to introduce and define laminar and turbulent flames, turbulence structure and regimes of combustion as they are frequently used in the thesis hereon.

The laminar flame's surface is smooth and has a relatively thin reaction zone. The velocity at which the flame propagates into a nonturbulent, premixed, unburned mixture ahead of the flame is termed the laminar burning velocity (S_L) [133, 197].

In IC engines, turbulent flames usually evolve from laminar flames. The smooth flame surface (laminar flame) can become wrinkled in the presence of turbulence (Figure 3.3) which causes the reaction zone to grow thicker. This wrinkled flame is known as the turbulent flame. Consequently, depending on the turbulence

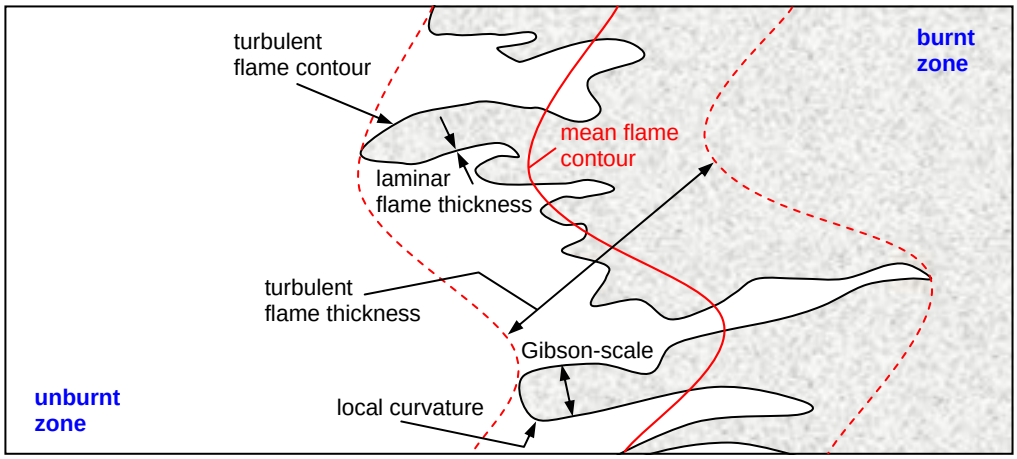

Figure 3.3: Schematic of wrinkled turbulent flame structure [95].

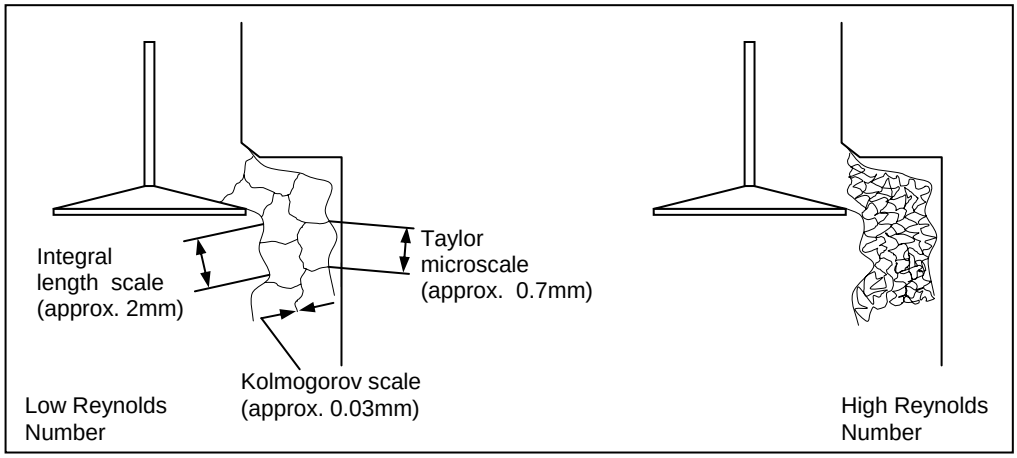

Figure 3.4: Turbulent structure of jet during intake, (left) low Re_T, (right) high Re_T, [96], length scales are from [95].

intensity, the turbulent flame speed (S_T) is several times larger than the laminar flame speed [8]. Both laminar and turbulent flames are discussed further in Section 3.6.

3.5.2 Turbulence Structure

As described in 2.7.2, turbulent flows are characterised by the turbulence intensity, which is the fluctuating velocity about the mean velocity. A turbulent flow possesses a number of length scales which characterize the turbulent structure. A graphical representation of a high and low turbulence structure during the intake stroke is shown in Figure 3.4. There are three length scales by which a turbulent structure is defined: integral, Kolmogorov, and Taylor length scales. These length scales measure the size of eddies or vortexes. In any turbulent flow, there is a distribution of energy over a continuous range of eddy sizes.

The largest eddies are measured by the integral length scale and these create velocity gradients in the flow which result in turbulent stresses. These stresses create smaller eddies measured by the Taylor length scale which in turn create still smaller eddies as measured by the Kolmogorov scale.

The integral length scale (Λ) is the largest scale structure of the flow field. It is also a measure of the size of the energy-containing eddies [3]. In an IC engine

the integral length scale is limited by the geometry of the combustion chamber. In combustion modelling the integral length scale has been estimated by using the following equation [27, 143]:

$$\Lambda = cH \tag{3.10}$$

where: c is = 0.2 to 0.5 [27, 143], H = combustion chamber height

The Kolmogorov scale (L_K) indicates the size or thickness of the smallest eddies (vortex tubes) [96, 202]. In an IC engine, these eddies are responsible for the dissipation of the turbulence energy into heat.

$$L_K = \left[\frac{\nu^3}{\varepsilon}\right]^{1/4} \tag{3.11}$$

where: ν is the kinematic viscosity, ε is the turbulent kinetic energy dissipation rate.

Assuming turbulence is homogeneous and isotropic (where: u' is the turbulence intensity).

$$\varepsilon = \frac{u'^3}{\Lambda} \tag{3.12}$$

The Taylor microscale (L_T) is defined by relating the fluctuating strain rate of the turbulent flow fields to the turbulence intensity [96] or, as defined by Tabaczynski et al. [202], is the spacing of the vortex tubes (smallest eddies) of Kolmogorov thickness.

$$L_T = 15^{1/2}\,\Lambda\,\mathrm{Re}_T^{-1/2} \tag{3.13}$$

The turbulent Reynolds number (Re_T) is generally determined for the reactant flow as the ratio of turbulence induced inertial forces to the viscous or dissipative forces. As Re_T increases the turbulence structure becomes fine (Figure 3.4).

$$Re_T = \frac{u'}{\Lambda\,\nu} \tag{3.14}$$

3.5.3 Regimes of Combustion

Turbulent combustion is often described in terms of "combustion regimes", and these can be defined using a domain of turbulent Reynolds number (Re_T) and Damkohler number (*Da*). Figure 3.5 is a widely accepted parameter-plane plot of these non-dimensional quantities [3].

The Damkohler number (*Da*) is the ratio of the characteristic turnover time (τ_t) of the largest eddies in the flow to the characteristic transient time (τ_L) through the laminar flame front.

$$Da = \frac{\tau_t}{\tau_L} = \frac{(\Lambda / u')}{(\delta_L / S_L)} = \frac{\Lambda}{u'} \frac{S_L}{\delta_L} = \frac{\Lambda}{u'} \frac{S_L}{\nu / S_L} \tag{3.15}$$

where: S_L is the laminar flame speed, and δ_L is laminar flame thickness equal to ν / S_L [2, 55].

Da is high when the flame front consumes the mixture faster than turbulence can distort it. This indicates weak levels of turbulence with respect to S_L. In contrast, *Da* is low when the chemical reaction in the flame reaction zone is slow compared to the high level of turbulence. This means that the turbulence has the opportunity to transport and mix the reacting mixture as the burning occurs.

In an IC engine, when the propagating flame is dominated by chemical reactions *Da* is high, when the combustion chamber is turbulence dominated, *Da* is low.

The precise boundaries of the "distributed-reaction" and "reaction sheet" regimes can be separated by the L_K/δ_L line. The ratio of L_K/δ_L (smallest turbulence to laminar flame thickness) is a measure of stretch to which the laminar flame is subjected in the turbulent flow [3]. The region that is greater than unity is considered to be the "reaction sheet" regime. In this region, turbulence does not affect the chemistry, and the flame is considered to be a discrete front or boundary between the burned and unburned mixture. For values of u'/S_L much

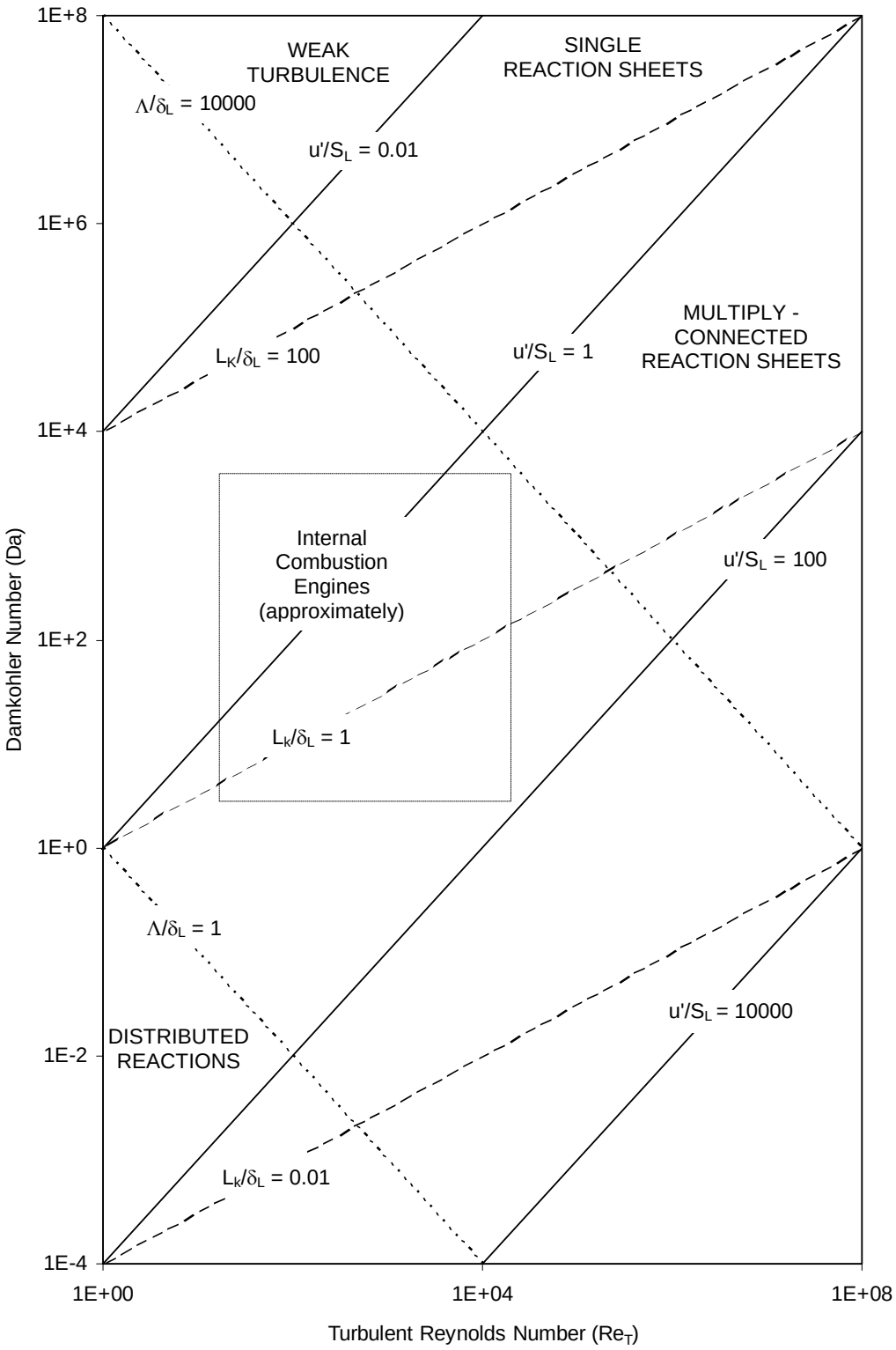

Figure 3.5: Illustration of regimes of turbulent combustion [3, 75].

less than one, the turbulence is relatively weak, and the flame can be considered to be a single sheet. Whereas when u'/S_L is much greater than one, the turbulence severely distorts the flame producing pockets of burned and unburned mixture in the vicinity of the flame front. This is called the "multiply-connected reaction sheet" regime. In contrast, the region where Λ/δ_L is less than one corresponds to the region of "distributed reaction" where the chemical reactions are significantly slower than the turbulent mixing and the flame profiles cannot be identified. This type of turbulent combustion can be visualised in a stirred reactor.

Abraham et al. [3] and Gillespie et al. [75] identified the different combustion regimes. They have concluded after examining a wide range of engine conditions that the combustion regimes of IC engines fall approximately into the area designated by the rectangle in Figure 3.5.

3.5.3 Effect of Turbulence on Flame Behavior

Some researchers have claimed that too much turbulence is not beneficial as it can extinguish the flame [3, 31, 96, 197]. Consequently the effects of turbulence on the flame behavior have been examined for a long time and the two parameters that are used to describe this are the Karlovitz and Lewis numbers.

As the turbulence intensity increases in the combustion chamber, the flame becomes wrinkled and consequently the area and the speed of the flame increases. Too much turbulence leads to flame thickening and a slowing of the reaction rates. Flame thickening is predominantly caused by turbulent flame stretch as described by the Karlovitz number (*Ka*). The Karlovitz number can be described in two ways. First, it is defined as the flame strain rate normalised by the flow through the laminar flame. Second it can be thought of as a ratio of chemical to eddy lifetimes:

$$Ka = \frac{u'}{L_M}\frac{\delta_L}{S_L} = \frac{\delta_L / S_L}{L_M / u'} \tag{3.16}$$

The Lewis number (*Le*) is the ratio of thermal diffusivity (α) to mass diffusivity (*D*) and affects both laminar and turbulent combustion:

$$Le = \frac{\alpha}{D} \tag{3.17}$$

The Lewis number describes whether reactant mass is diffused into the reaction zone or heat is diffused away from the reaction zone. When the *Le* < 1 combustion tends to intensify thereby wrinkling the flame. The flame is dominated by reactant mass diffusing into the reaction zone and therefore both the flame temperature and burning velocity increase. When the *Le* > 1 the thermal diffusivity is dominant and therefore the heat loss exceeds the reactant mass gain and the perturbations will tend to decay. Consequently, the flame temperature of the peak of the wrinkles will cool and the flame will reduce in speed.

3.5.4 Turbulence Modelling

The previous sections have highlighted that turbulence is a complex phenomenon that greatly affects the surface of the flame. The magnitude of turbulence intensity inside the combustion chamber is dependent on many variables such as the shape of the combustion chamber, the intake runners and the number and size of the intake valves. Data derived from experimental measurements are therefore of preference.

Lancaster [131] has made such measurement in the CFR engine with a hot wire anemometer. His data has been used extensively by many researchers for modelling and comparison [3, 27, 82, 96, 147, 197, 202]. The estimated error of the published data is less than 20% of the measured turbulent intensity values. Where 10% of the error is in the computed velocity and 10% is in the computed temperature. The published data was obtained in the following range: 1000-2000 r/min, 40-110kPa MAP, and CR = 6.5-10.5. For this project, the author required turbulence intensity over the following range: 1200-1800 r/min, MAP=40-200 kPa and CR=8-15. Due to the strong linear relationship between turbulence intensity,

MAP, and engine speed, a simple linear regression model was developed to predict u'_0, which is the turbulence intensity at 45° BTDC. CR had less effect on u'_0.

$$\begin{aligned} u'_0 &= 1.7 + (((((0.0012 * RPM - 0.2267) - 1.57 / 1.57) \\ &+ (((0.0083264 * MAP + 0.94107069) - 1.7) / 1.7) \\ &+ (((0.03783582 * CR + 1.1319092) - 1.46) / 1.46)) * 1.7) \end{aligned} \tag{3.18}$$

The average error of the linear regression line to the published data is 7.5% with a standard deviation of 3.21. This error is actually less than 5% at WOT where most of the data has been taken. Also, this error is relatively small compared to the estimated errors of < 20% in measured turbulent intensity values.

To calculate the turbulence intensity for the combustion period, the simplest form of the rapid-distortion theory was used [27, 82, 147, 199]. This form takes into consideration the conservation of angular momentum of a large eddy undergoing compression. Therefore the final form of the turbulence intensity is:

$$u' = u'_o \left[\frac{\rho}{\rho_0} \right]^{1/3} \tag{3.19}$$

where: ρ is unburned gas density and ρ_0 is the unburned gas density at 45° BTDC.

3.6 Flame Speed

3.6.1 Laminar Flame Speed Calculation

The important aspects of laminar and turbulent flame velocities using mathematical models relevant to IC engines have been discussed intensively in the literature [3, 27, 75, 95, 107, 133, 151, 154, 160, 202]. In this section, the formulation of laminar flame speeds is discussed and then followed by a review of the formulation of turbulent flame speed.

In theory, once the flame kernel is stabilised after ignition, it propagates away from the spark plug at the laminar flame speed (S_L). The laminar flame surface is smooth and has a thin reaction zone. In practice however, due to the expansion of the plasma and the conductive energy, the flame kernel needs to reach a radius of 10mm before it can become fully independent of the spark energy [32, 75, 133]. At this stage the flame kernel size is significant enough so that both large and small scale turbulence may distort the surface by wrinkling, thereby increasing the flame speed until it reaches the fully developed turbulent flame speed.

James [107] has reviewed the most popular laminar burning velocity correlations. The references were followed through and the author agrees with Heywood [95] that the most commonly used relationship in combustion modelling for laminar burning velocity is calculated by using the experimental correlations of Metghalchi and Keck [151]. Unfortunately, this and other correlations rapidly fall to zero at about λ=1.6, and therefore fail to predict the laminar flames speeds for the full range of pressures and temperatures experienced in an SI engine.

The most advanced analytic approximation for hydrogen, methane, ethylene, ethane, acetylene, and propane was developed by Gottgens et al. [78] and for n-heptane, iso-octane, and methanol were developed by Muller et al. [160]. The approximations are reproduced in the following form:

$$S_L = F Y_{F,u}^{m} \exp(-G/T^0) \frac{T_u}{T^0} \left[\frac{T_b - T^0}{T_b - T_u} \right]^n \qquad (3.20)$$

where: F, m, G and n are fitting coefficients (from reference 195), T_b is the adiabatic flame temperature, T^0 is the inner layer temperature (from reference 78), and $Y = 1/AFR$.

Each correlation is made up of 200 flames in the pressure range of 1 to 40 bar, for preheat temperatures ranging from 298 K to 800 K with λ=1 to λ=2 for isooctane and λ=1 to λ=2.5 for hydrogen. The correlation for hydrogen flame speed has a standard deviation of 7.6% and isooctane is within a few percent.

3.6.2 Turbulent Flame Speed Models

The most accepted explanation for the increase in flame speed due to turbulence considers the effects of turbulent eddies on a scale larger than the thickness of the flame front. These eddies are assumed to have no effect on the local flame velocity (laminar flame speed) but do distort the flame front so that its area is increased (Figure 3.3). Consequently, the increase in flame speed is then proportional to the increased area of the flame [133]. Damkohler was the first to propose this relationship in the following form:

$$FSR = \frac{S_T}{S_L} = \frac{A_T}{A_L} \tag{3.21}$$

where: *FSR* is the flame speed ratio, S_T is the turbulent flame speed, S_L is the laminar flame speed, A_T wrinkled flame area and A_L is the area of the smooth laminar flame.

Over the last 50 years many turbulent flame speed models have been developed. DeZylva [52] reviewed over 200 references and listed the 40 most popular turbulent flame speed models found in the literature. Between 1973-2002, SAE alone published 188 papers related to turbulent flames including a detailed discussion published by Abraham et al. [3] on the turbulent flame structure of a premixed charge with particular attention dedicated to turbulent flame speed

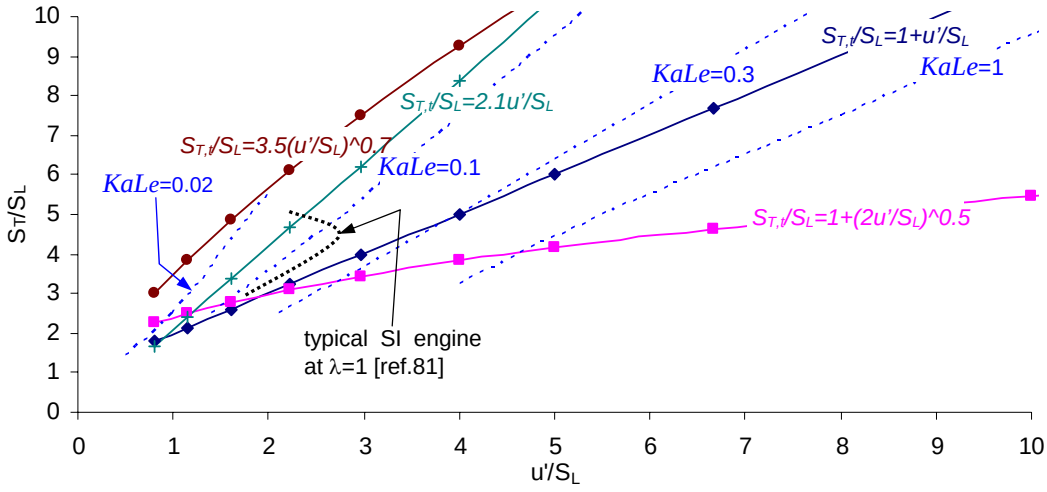

Figure 3.6: Different theoretical turbulent flamelet models with constant *KaLe* lines [3, 95, 197].

models. Some of these models are shown on Figure 3.6, and include constant lines based on the product of Karlovitz number and the Lewis number, *KaLe*.

In turbulent combustion, the product *KaLe* describes whether the flame is in the wrinkled laminar or quench region. For *KaLe* < 1 there is a continuous flame sheet indicating that the chemical processes are quicker than the fastest turbulent processes and that the structure of the flame is going to remain largely unaltered by the turbulent flow field. As *KaLe* increases, turbulence plays a more important role as the flame is increasingly distorted and wrinkled by the flow field. It is anticipated that when *KaLe* > 6, the flame surface is distorted and wrinkled so much that enhanced heat transfer can actually quench or extinguish the flame.

In Figure 3.6, $FSR_t=S_{T,t}/S_L=1+(2u'/S_L)^{0.5}$ is obtained experimentally for turbulence scales that are large enough for the laminar burning velocity to be unaffected by the turbulence. $S_{T,t}/S_L=1+u'/S_L$ correlates well to flames propagating through moderate turbulence. $S_{T,t}/S_L=2.1u'/S_L$ is developed on the basis of the evolution of probability density functions for wrinkled flames. $S_{T,t}/S_L=3.5(u'/S_L)^{0.7}$ has been obtained from theoretical approximations based on concepts of turbulent dispersion counterbalanced by wrinkled flame propagation. In a typical SI engine (as shown in Figure 3.6), as the flame growth is subjected to turbulence it follows a constant *KaLe* line, however in the later stages of combustion the turbulence intensity decreases and the higher pressures in the unburned gas lowers the laminar flame speed. Consequently the locus moves to the left with *KaLe* becoming smaller.

It is rather interesting to note that in Figure 3.6, a typical SI engine produces an $S_{T,a}/S_L$ ratio of less than 6. In fact, Bradley [31] developed a correlation based on over 1600 experimental results, where he concluded that the limit to turbulent flame speed enhancement is around $S_{T,t}/S_L$= 20. This would suggest that flame speed ratios near 30 are not realistic because the excessive turbulence levels would cause flame disruption and quenching. In contrast to Bradley's finding, high speed Formula 1 engines operating up to 12,000 r/min [173] develop an $S_{T,a}/S_L$ ratio in excess of 50 while providing stable combustion. Furthermore, Abraham et al. [3] and Gillespie et al. [75] defined the regimes of combustion of IC engines in

Figure 3.5 by the rectangular area, which suggests that it is possible for engines to operate at and above $S_{T,a}/S_L$=50.

3.6.3 Flame Geometry and Modelling

Actual Flame Speed

Up to this point, predictions of S_L and S_T in the combustion chamber as a function of pressure, temperature and turbulence intensity have been discussed. However, it is also possible to calculate the actual flame speed in the combustion chamber using experimental data with the following formula.

$$S_{T,a} = \frac{\dot{m}}{\rho_u A} \tag{3.22}$$

where: $\dot{m}$ is the unburned gas entrained into the flame front, A is the equivalent spherical flame surface area, and ρ_u is the unburned gas.

The flame speed due to the expansion of burned gas can be calculated with the following formula:

$$u_t = u_g + S_T \tag{3.23}$$

where the gas expansion velocity u_g behind the flame front is:

$$u_g = \frac{\dot{m}}{\rho_u A}\left[\frac{\rho_u - \rho_b}{\rho_u}\right] \tag{3.24}$$

Flame Speed Multiplying (FSM) Factor

There is no specific turbulent flamelet model developed for HAJI combustion. Lumsden [143] used a fractal based model and Dober [55] used a method which decoupled the chemistry and the flow field to reduce the complexity of modelling of the HAJI combustion. Both methods underestimated the turbulent flame speeds in lean mixtures, therefore both Lumsden and Dober used flame speed multiplying factors to compensate for the turbulent and chemical enhancement provided by the jets. The FSM factors were used for the entire combustion duration was near unity in stoichiometric mixtures and larger than unity in lean mixtures.

In this project, it was of interest to examine how this multiplying factor varied throughout the combustion event as this had never been examined before. Therefore the author adopted a simpler but very popular turbulent flamelet model [95]. This is in the form of $S_{T,t}=S_L+u'$ shown in Figure 3.6.

To track the interaction between actual (as determined by eq. 3.22) and theoretical flame speed $(S_{T,t}=S_L+u')$, the following relationship was used:

$$FSM\_Factor = \frac{S_L + u'}{\left[\frac{\dot{m}}{\rho_u A}\right]} = \frac{theoretical\_flame\_velocity}{actual\_flame\_velocity} \qquad (3.25)$$

Where the FSM factor is the "flame speed multiplying factor" that determines flame speed enhancements provided by the unaccounted chemical reactions and the turbulence intensity caused by the HAJI jets.

Spherical Flame Geometry

The HAJI flame kernel is assumed to be located ~20mm away from the nozzle exit (1/4 of bore diameter), which is consistent with images (Figure 2.22 - left) taken by Lumsden and Watson [140, 143] and observed through modelling by Dober [55]. This is a direct result of the flame quenching through the nozzle and then reigniting again away from the exit of the nozzle in the main chamber.

Through optical imaging, the shape of the jet is observed initially as an ellipsoid. However, it becomes progressively more spherical [55, 143]. Therefore, a spherical flamelet model has been implemented for the following reasons:

- It is consistent with previous HAJI modelling by Lumsden [143];
- The error in area is less than 8% between a sphere and a spheroid (with a 2:1 axis ratio);
- To calculate the perimeter of an ellipse, an elliptic integral of the second kind needs to be solved (which is computationally expensive), or the use of an approximation function is required;
- To calculate a segment of an ellipse a length iteration module is required;

- Unavailability of a mathematical function that describes the transition from an ellipsoid to a spherical flame during combustion;
- The overall development and validation time did not meet the project timing requirements.

The spherical flamelet model equations were implemented into VBA and are described in Appendix D.4. A sample result of the flamelet module is displayed in Figure 3.7, where a centrally ignited flame expands in a 4x4 (m) disc chamber.

Flame Lookup Table

In order to reduce the computational time to a minimum, a flame table was set up for different compression ratios as well as for the two different ignition positions of SI and HAJI. It took approximately 10 hours to set up each table on a Pentium III 866MHz PC, however using the flame table decreases the computational time by > 100 times by looking up tabulated flame geometry information at a specific CAD instead of calculating it at every 0.5 CAD. The table consists of 248 flames at 0.5 CAD intervals which translates to a 0.4mm resolution in flame radius. In addition to this fine resolution, when required, a linear interpolation is also performed between the flame increments. For lookup purposes, the flame table also provides: flame radius, burned and unburned volumes, flame surface area and the burned and unburned area of the cylinder head, piston and walls.

Accuracy of Flamelet Model

The flamelet model was validated against Poulos et al. [177] and arbitrarily

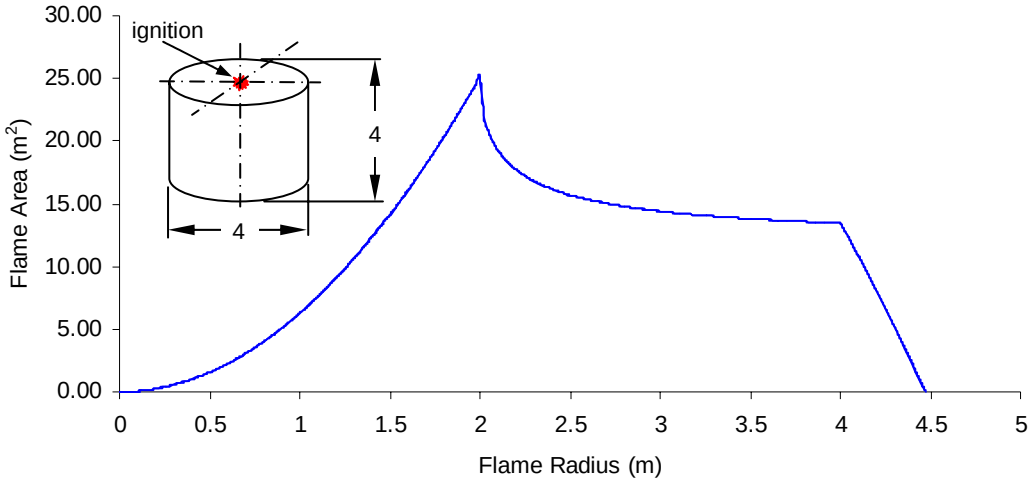

Figure 3.7: Flame radius vs. flame area for a 4x4 disc chamber, central ignition.

chosen geometries were implemented and then checked in Unigraphics. The author's results are excellent for a disc combustion chamber (same as the CFR engine). Furthermore the model is more accurate than Poulos [177] for a disc combustion chamber, however Poulos 'flat triangular' approximation can be used for hemi, open, and bowl in piston type combustion chambers.

3.7 NO_X Formation- Extended Zeldovich

As discussed previously, the interest in nitrogen oxide emissions is primarily due to their role in atmospheric pollution. The main sources of nitrogen oxide emissions in combustion are; oxidation of molecular nitrogen in the postflame zone, which is termed thermal NO, formation of NO in the flame zone termed prompt NO, and oxidation of nitrogen containing compounds in the fuel referred to as fuel-bound NO [28]. Postflame oxidization of NO is the main source of NO emissions in internal combustion engines and will therefore be the focus of this research.

NO has been measured experimentally, however to better understand the postflame oxidization of NO, the basic mechanisms for thermal NO production developed by Zeldovich were implemented. The mechanism consists of the following six reactions:

$$O + N_2 \underset{-1}{\overset{+1}{\Leftrightarrow}} NO + N \tag{3.26}$$

$$N + O_2 \underset{-2}{\overset{+2}{\Leftrightarrow}} NO + O \tag{3.27}$$

$$N + OH \underset{-3}{\overset{+3}{\Leftrightarrow}} NO + H \tag{3.28}$$

The first forward reaction predominantly controls the system but has high activation energy and is therefore very slow in lean, low temperature flames. The third reaction pair is included for rich mixtures where the O_2 concentration is low. The contribution from this reaction is consequently low for lean mixtures.

The rate of NO formation is given by the following form with rate constants (k) ±1, ±2, and ±3, which are available in Borman et al. [28] and Miller et al. [153].

$$\frac{d[NO]}{dt} = k_{+1}[O][N_2] - k_{-1}[NO][N] + k_{+2}[N][O_2] - k_{-2}[NO][O] + k_{+3}[N][OH] - k_{-3}[NO][H] \quad (3.29)$$

where:

$$[N] = \frac{k_{+1}[O][N_2] + k_{-2}[NO][O] + k_{-3}[NO][H]}{k_{-1}[NO] + k_{+2}[O_2] + k_{+3}[OH]} \quad (3.30)$$

and the rate constants (k) are of the following form:

$$k_c = A\exp(-B/T) \quad (3.31)$$

In order to evaluate the above equations, O, O_2, N_2, OH and H concentrations need to be determined. Due to high pressures and temperatures in SI engines the fuel oxidization is rapid and the reaction zone is thin. It has been shown, in this type of environment, that these species are in equilibrium [28, 96, 119]. The values were therefore obtained from the equilibrium solver described in Section 3.3.

As already described in Section 2.2.1 there are three factors which contribute to NO_x formation in IC engines: temperature, oxygen and residence time. NO_x formation is exponentially dependent on temperature as shown by Equation 3.31. O_2 must be present in order to produce NO_x, which is clearly shown by Equation 3.26 and 3.27. Finally the residence time at a given temperature will determine the amount of NO_x formation indicated by Equation 3.29. This is an interesting and complex factor, because extended time at a given temperature will drive the mixture towards the equilibrium values. This means that if enough time was available on the expansion stroke, the engine out NO_x could be minimised.

3.8 Knock Intensity

A second order high pass Butterworth digital filter developed by Rogers [186] in VBA was used to extract the knocking signal from the raw pressure trace. This

was the only module out of all the programming that was not developed and implemented by the author from first principles. The core filter module developed by Rogers [186] was adopted but I/O functions were changed to suit the combustion model. The input data sampling frequency was 20 kHz, which allowed the monitoring of first and second order pressure oscillations occurring at around 5 kHz and 10 kHz respectively in the engine.

Between Chun et al. [46] and Konig et al. [120], there are ten different methods to generate a knock intensity (KI) factor to describe the severity of pressure oscillation. From the ten, two methods were used to quantify knock.

Method 1

Maximum value of the high pass filter.

Method 2

Knock intensity factor calculation based on the intensity of the pressure oscillation over 30 CAD. Konig et al. [120] used this method as it correlates well with the development of knock damage in a combustion chamber. The equation is in the following form.

$$KI(30) = \sum_{i=1}^{N_{samp}} \left(P(i) - P_{mean}\right)^2 \frac{1}{N_{samp}} \tag{3.32}$$

where: P_{mean} (kPa) is the pressure without knock, $P(i)$ *(kPa)* is the actual pressure, and N_{samp} is the number of sample points.

It is worth noting that KI>60000 when heavy knock occurs with a ±800kPa pressure oscillation and KI>1500000 when severe knock occurs with a ±4000kPa pressure oscillation.

3.9 Summary

This chapter has described the framework and specific modules used in the development and implementation of a two-zone quasi-dimensional model known as (E-CoBRA). The two-zone model was chosen due to the fast computational

time, flexibly in modification, availability of similar fundamental frameworks in the literature and low implementation time which suited project timing. More complex 2D and 3D models including commercially available software were also considered and found to be unsuitable for project objectives.

The two-zone model consists of many different modules all with varying degrees of complexity. In this chapter, the more complex modelling processes of compression, combustion, and expansion have been reviewed. The combustion model was discussed in depth, especially chemical equilibrium, adiabatic flame temperature, turbulence, and flame speed. A brief discussion was also provided on the methodology to predict NO_x emissions and to calculate knock intensity.

To better understand Chapters 5 through to 8, a review of turbulence structure, combustion regimes and turbulent flamelet models was also provided.

CHAPTER 4
Experimental Method

4.1 Introduction

This chapter describes the experimental hypotheses and the test methodology used to formulate the test conditions, procedure and test matrix. The experimental apparatus and instrumentation used to obtain all experimental results is also presented here.

The principal aim of this thesis is to test the hypothesis that a HAJI equipped engine can outperform its spark ignition counterpart with respect to performance, emissions and thermal efficiency at all load points. It was hypothesised that this could be achieved through a combination of boosting, lean burn and HAJI.

To carry out this investigation, the research engine had to be capable of operating through a wide range of manifold air pressures (MAP) including boosted, at low and high compression ratios, and in spark ignition and HAJI combustion modes.

A brief discussion on the data post processing technique, which was carried out with E-CoBRA and other software, is also included.

4.2 Experimental Hypotheses

Based on the foundations laid down in Chapter 2 and 3 and consistent with the research objectives, the hypotheses to be tested by the apparatus and E-CoBRA were:

- Engine-out NO_x emissions can be controlled at all load points, with a simultaneous improvement in thermal efficiency over SI by coupling HAJI to a boosting device. More specifically, NO_x emission can be kept below 0.1g/kWh without aftertreatment, satisfying Euro 5 emission standards, with a simultaneous improvement in thermal efficiency.
- The flame speed multiplying factor varies throughout the combustion event because lean-mixture enhancement via HAJI is most dominant in the early phase of combustion where active radicals and turbulence are highest.
- As long as the pre-chamber is fueled with H_2 or gasoline mixtures, the small pressure oscillation "Jet Knock", which is generated in the combustion chamber upon ignition, exists independently of whether the main chamber is fueled or not.

Interestingly, the first and second hypotheses become the starting point of this research for further investigation by identifying a gap in the previous HAJI research work. The last hypothesis was generated upon discovering the existence of Jet Knock in HAJI combustion at the early stages of testing. Consequently, the above hypotheses enabled the experimental test matrix and methodology to be formulated.

4.3 Test Methodology

4.3.1 Test Conditions and Test Matrix

Previous HAJI work in the CFR engine completed by Lumsden [143], established that speed has less of an effect on emissions than AFR. A mid-speed of 1800 r/min, corresponding to a typical engine speed when a vehicle is being tested over

the NEDC cycle, was therefore chosen for this study. Inlet temperature, port-induced cylinder motion, cam timing, and combustion chamber shape were held constant throughout the experiments and direct injection and external EGR were not explored. Eliminating these variables enabled the target parameters such as CR, AFR, and MAP to be more thoroughly examined in the time available.

The experimental test matrix employed to test the hypotheses is shown in Table 4.1. The engine was operated in HAJI-Gasoline (HAJI-G), HAJI-Hydrogen (HAJI-H_2), SI-Gasoline (SI-G), and SI-Hydrogen (SI-H_2) modes. The SI modes provided the necessary baseline data for HAJI comparison. In addition, Lumsden's [143] results, at CR=9, at 1800 r/min and at 50, 70 and 90 kPa MAP were repeated to check that the engine and equipment were in order.

Table 4.1 shows that not all combustion modes were explored at high MAP. At low CR, the voids in the data set were due to both poor efficiency and emissions results. At high CR the lack of data was due to unacceptable levels of knock. Each

Table 4.1: Test Matrix at 1800r/min, rich < λ > lean limit.

MAP / CR	8	9	11	13	15
<=50 kPa	HAJI-G HAJI-H_2 - -	HAJI-G HAJI-H_2 SI-G SI-H_2	HAJI-G HAJI-H_2 SI-G SI-H_2	HAJI-G HAJI-H_2 SI-G SI-H_2	HAJI-G HAJI-H_2 - -
70 kPa	HAJI-G HAJI-H_2 - -	HAJI-G HAJI-H_2 SI-G SI-H_2	HAJI-G HAJI-H_2 SI-G SI-H_2	HAJI-G HAJI-H_2 SI-G SI-H_2	HAJI-G HAJI-H_2 - -
90 kPa	HAJI-G HAJI-H_2 - -	HAJI-G HAJI-H_2 SI-G SI-H_2	HAJI-G HAJI-H_2 SI-G SI-H_2	HAJI-G HAJI-H_2 SI-G SI-H_2	HAJI-G HAJI-H_2 - -
120 kPa	- - - -	HAJI-G - - -	HAJI-G HAJI-H_2 - -	HAJI-G - - -	- - - -
150 kPa	- - - -	HAJI-G - - -	HAJI-G HAJI-H_2 - -	HAJI-G - - -	- - - -
190 kPa	- - - -	- - - -	- HAJI-H_2 - -	- - - -	- - - -

condition in the test matrix was tested to at least 10% of CoV of IMEP. This is twice what the author considered as the lean limit of the combustion system, which in this research was defined as 5% CoV of IMEP.

In addition to the test matrix, supplementary sensitivity tests were conducted to gain an in-depth understanding of the most important variables affecting the combustion and performance of the HAJI system. These tests were selected based on their historical importance and common use in conventional engine optimisation and calibration.

The sensitivity tests included examining the effects of pre-chamber orifice length, pre-chamber H_2 quantity, engine speed, spark timing, CR, and λ. These tests were predominantly conducted at the engine conditions specified in Table 4.2. Furthermore, a detailed investigation of the Jet Knock phenomena was performed.

The data collected based on the test matrix and the additional sensitivity study resulted in approximately 500 data points, each consisting of 300 cycles of which 40 consecutive cycles were analysed with E-CoBRA. This comprehensive data base provided the foundation for the experimental and theoretical investigations.

Table 4.2: Parametric study test matrix.

Parametric Study	Speed (r/min)	CR	MAP (kPa)	λ	Spark Timing	Pre-chamber H_2 quantaty (% of total energy)
Pre-chamber orifice length	1800	9	90	1-2.6	MBT	optimum
Pre-chamber H_2 quantity	1800	9	90	1, 1.62, 2	MBT	1-5
Engine Speed	1800 /1200	9	50, 90	1-2.6	MBT	optimum
Spark Timing	1800	9	90	1, 1.62, 2	5 ATDC to 55 BTDC	optimum
Compression Ratio (CR)	1800	8-15	90	1, 1.6, 1.9	MBT	optimum
Lambda (λ)	1800	9	90	1-2.6	MBT	optimum

4.3.2 Test Procedure

Day to Day Preparation

Variations in coolant temperature can have a significant effect on HC emissions and can also affect mechanical friction and in-cylinder heat transfer characteristics. In addition, friction is dependent on oil temperature as it affects oil viscosity. Hence, sufficient time for attainment of equilibrium conditions must be given prior to any experimentation. Consequently, before any data was collected, the water jacket temperature circulating through the engine was consistently monitored and regulated to a steady value of 90°C. This also allowed the oil to warm up as the engine was run for approximately 15 minutes at λ=1.6 and 1800r/min. This warm up period allowed the IMEP and BMEP outputs to stabilise and the ADS9000 exhaust gas analyser to be warmed up and zeroed. This was accompanied by an inspection of both firing and motoring pressure traces and a test at a reference data point, to verify that all recorded outputs where within limits (less than +/- 1%).

Preparations for Boosting

Before commencing the boosted experiments, care was taken to remove excess water that may have condensed in the compressed air damping reservoir, as this would have significantly increased the humidity of the air stream. A change in humidity is known to have an affect on thermal efficiency and knock limits [205] (Appendix F.2). Most significant to this study however, is the effect of humidity on NO_x formation. An increase in humidity decreases NO_x for a given AFR because the inert water vapor dilutes the charge in a similar manner to EGR, hence reducing combustion temperature.

General Mapping Procedure

While avoiding heavy engine knock and high combustion variations throughout the experiments, the following basic procedure was used to gather experimental engine data.

(initial condition - all increments = 0)

1. Select CR=8+increment CR
2. Select MAP=30kPa+increment MAP
3. Select λ=1+increment λ
4. Find MBT (Appendix F.1) and optimum pre-chamber H_2 quantity
5. Increment MAP by min. 20kPa and go to (1) or if heavy knock detected or MAP=200kPa go to (6)
6. Increment λ by min. 0.2 and go to (1), if CoV of IMEP>20% go to (7)
7. Increment CR by min. 1 and go to (1)

4.4 The CFR Engine

4.4.1 Engine Specifications

The most important design parameters influencing the combustion process are: compression ratio, combustion chamber shape, ignition system, valve timing, inlet manifold air pressure and temperature, mixture preparation and engine speed. As can be seen, there are many variables that can be examined and it is difficult to conclude how these variables interact, especially when tests are performed on different engines. To help overcome this hurdle, the cooperative fuel research (ASTM-CFR) engine was established in the USA as a reference engine by the American Society for Testing Materials, initially for testing fuels, but now used worldwide for all types of research.

Due to its worldwide acceptance and the availability of experimental results in the literature, the CFR engine was chosen to obtain all experimental data points for this project. Its major specifications are summarised in Table 4.3 and a comprehensive manual written by McReynolds et al. [150] is published by ASTM. A schematic layout of the experimental set up is presented in Figure 4.1.

It should be noted that one of the unique engine specifications of the CFR engine is the inherently oversized piston-to-bore clearance and low tension piston rings. This is essential for the durability of this engine in boosted modes, however it can

Table 4.3: CFR engine specifications.

ASTM – CFR Single Cylinder Research Engine	
Manufacturer	Waukeshha Engine Co.
Capacity	611.7 cm^3
Bore x Stroke	82.6 x 114.3
Engine Control Unit	MOTEC
Compression Ratio	5 to 20 infinitely variable
Combustion Chamber	Plane Cylindrical
Inlet valve Opening	10° ATDC
Inlet valve Closing	34° ABDC
Exhaust Valve Opening	40° BBDC
Exhaust Valve Closing	15° ATDC
Dynamometer Type	AC, constant speed, belt driven to engine, variable pulley sizes for speed selection.
Fuel	Unleaded - 91 RON

cause higher than usual HC emissions due to an increase in oil consumption and high crevice HCs.

4.4.2 MOTEC M4

A Motec M4 engine control unit (ECU) was used to control spark timing and H_2 injector duration and timing in both SI and HAJI modes. The ECU also allowed for outputs to be logged in real-time via a computer interface.

The use of a reference wheel and a GT101 hall effect sensor fitted to the camshaft allowed the detection of both engine crank angle and cycle position. A Bosch ignition module (0227 100 124) was connected to a Bosch MEC 718 coil supplying energy to the spark plug with a transistorised coil ignition system.

A Delco 3 bar MAP sensor allowed the manifold air pressure to be monitored. In order to dampen fluctuations caused by pressure pulsations in the plenum, a small diameter copper tube restrictor was placed between the intake plenum and the MAP sensor.

Establishing the reference for the spark timing was performed with a timing light and later verified on a motoring curve. Figure 4.2 shows spark discharge at TDC

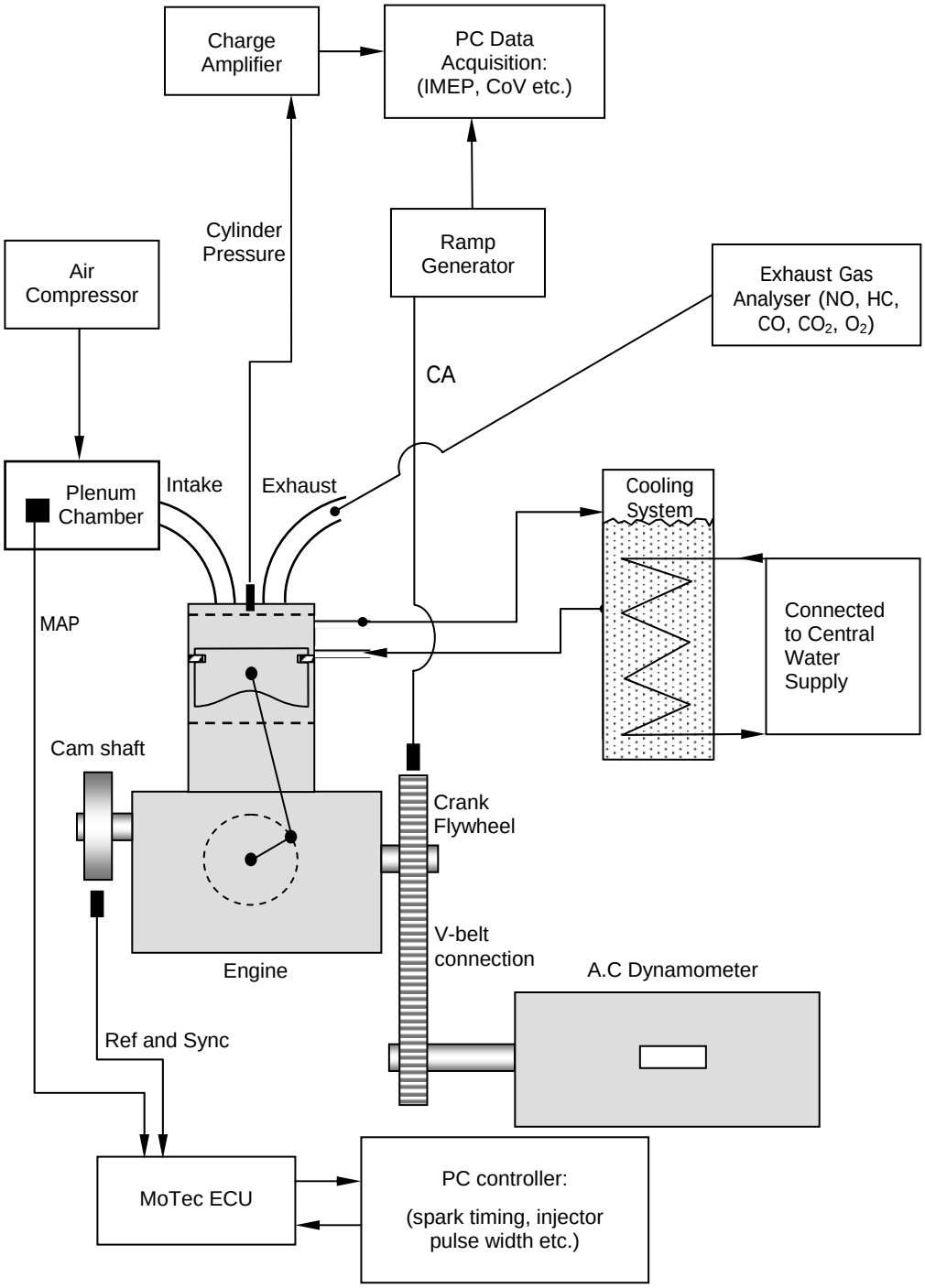

Figure 4.1 Experimental set up illustrating the basic schematic layout of the engine, including controllers, sensors and data acquisition systems. Combustion chamber detail is shown in Figure 1.12.

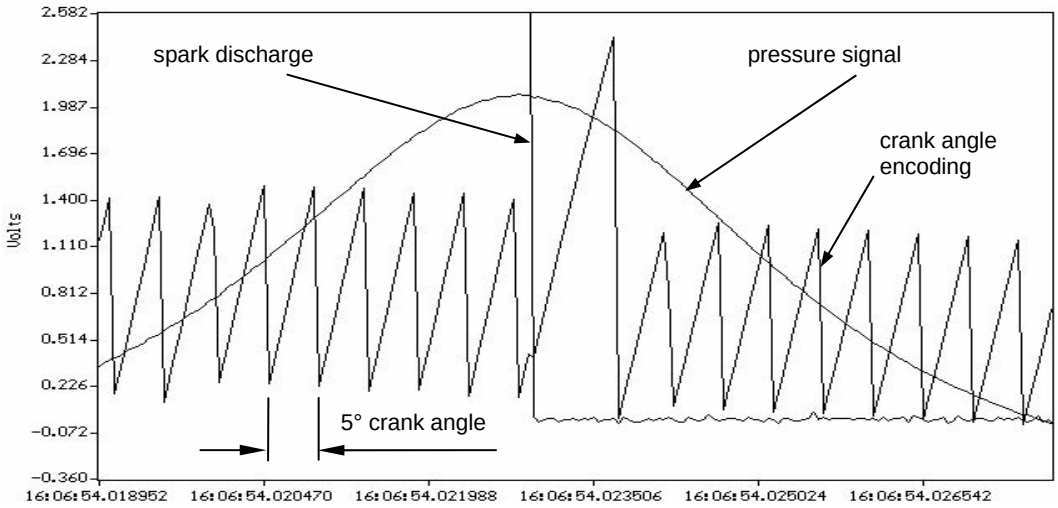

Figure 4.2: Motoring trace with spark discharge. Engine speed 1800 r/min, CR = 9, spark timing at 0°, results from Wave View on a time vs. voltage scale.

(0° crank angle). Considering peak cylinder pressure usually occurs at ~0.5-1.5° BTDC (Appendix C.1), the accuracy of phasing is estimated to within 0.5° CA.

4.4.3 HAJI System

In an SI engine, the role of the spark plug is vital for optimum engine operation. In contrast, the operation of the HAJI unit is not sensitive to the type of spark plug and is more dependent on the design of the prechamber volume, the number of orifices, and their diameters, length and orientation of these orifices. When implementing new combustion chambers and piston shapes pre-chamber optimisation must be considered. Table 4.4 may serve as starting point for a new application.

Pre-Chamber Design

The HAJI system has been redesigned and optimised several times in the past by Kyaw [128], Lumsden [143], Glasson et at. [76], Lawrence [136], Dober [55], Wang [217], and Zakis [232]. A brief summary of the important HAJI parameters is presented in Table 4.4.

Table 4.4: HAJI pre-chamber design by different researchers.

Charge - **S**tratified or **H**omogeneous	H	H	S	H	S	Diesel	H
Engine	Optical	Optical	Optical	CFR	Optical	Petter	CFR
Piston	flat	flat	flat	flat	flat	bowl	flat
Fuel main chamber	butane	butane	butane	gasoline	CNG	CNG	gasoline hydrogen
HAJI Location (**C**entral/**S**ide)	C	C	C	S	C	C	S
Number of Nozzles	6	6	6	1	6	1	1
Nozzle Diameter (mm)	1	1.25	1.25	2	1.25	1.2	2
Nozzle Angle (horizontal=0°)	45°	30°	30°	0°	30°	90°	0°
Nozzle Length	4mm	4mm	4mm	6mm	4mm	3mm	3mm
Pre-chamber Volume (cc)	0.85	1.3	1.3	1.5	1.3	0.85	0.9
Hydrogen Flow Rate (mg/s)	<3	<3	<3	<6	<2	<4	<4
Hydrogen EOI (°BTDC)	90°	96°	53°	90°	60°	90°	90°
HAJI Researcher	Lawrence [136]	Dober [55]	Dober [55]	Lumsden [143]	Wang [217]	Zakis [232]	Current Research

For a centrally mounted HAJI system used in an optical access engine, Lawrence [136] identified six nozzles with 1 mm orifices inclined 45° from the horizontal to be optimum. Although he was able to run with exceptional combustion stability (~3.1% CoV of IMEP) at λ=2.4, he had difficulties operating at stoichiometric air-fuel ratios. Dober [55] improved on the HAJI design and concluded that for both homogeneous and stratified charge, the optimum pre-chamber configuration was 6 x 1.25mm diameter nozzles inclined 30° from the horizontal. This design was successfully adopted by Wang [217].

Lumsden [143] used more H_2 and a larger pre-chamber volume compared to Lawrence [136], and Dober [55] in order to try to compensate for the inferior performance obtained when using a side mounted (CFR engine) single nozzle. Although using a centrally located HAJI in a diesel engine modified to operate on CNG, Zakis [232] made use of only a single nozzle. It was hypothesised that in order to engulf as much of the main chamber charge as possible, the jet needed to impinge onto the bowl of the diesel piston which would then redirect the jet

upward due to a combination of jet impingement and squish flow. This would consequently disperse the HAJI jet through more of the charge in addition to creating more turbulence.

Based on the abovementioned considerations, the HAJI nozzle used in this research was designed to have the following characteristics:

- Single orifice with a 2mm diameter to allow moderate jet penetration, maximise jet temperature, and allow the use of spherical flame modelling;
- 0.9cc pre-chamber as the international patent application by Watson [219] states that the prechamber must be sized between 0.5-2% of the clearance volume, which falls into the range of CR=4.4 to CR=15 respectively.
- 3mm orifice length which was determined via a parametric study and presented later in Chapter 7.

Pre-chamber Size vs. Standard Spark Plug

In the HAJI system, the main chamber charge is ignited by the jet (or jets) whereas in an SI engine a carefully designed spark plug is used. The pre-chamber is predominantly rich with highly flammable H_2, therefore the spark plug energy can be lower to consistently ignite the mixture. As a consequence, the HAJI unit uses a much smaller, 8mm NGK spark plug, compared to the standard 18mm spark plug used in standard engines.

The overall size of the HAJI unit including pre-chamber and spark plug was designed such that it was possible to screw into the side of the block using an M18 thread (standard spark plug hole). Consequently, when spark ignition was required, the HAJI unit was simply replaced with an 18mm spark plug.

Pre-chamber Durability

Kyaw [128], Lumsden [143], Glasson et al. [76], Lawrence [136], Dober [55], and Wang [217] all used aluminum pre-chambers and reported no durability issues. The author however eroded the aluminum pre-chamber after only a few hours of operation, which was concluded to be the result of poor cooling of the pre-chamber at high load operation in boosted mode. To combat this problem, a new

pre-chamber was manufactured from Inconel, which is a nickel-chromium-iron alloy 601 (Ni~60%, Cr~25%). Inconel is a general-purpose engineering material with outstanding resistance to high-temperature oxidation and is readily formed, machined and welded. The new Inconel pre-chamber was used throughout the research and was inspected after 100 hours of operation and showed no signs of surface erosion or any other changes to its original dimensions. Due to the poor durability of aluminium in heavy-duty applications, Zakis [232] used a less expensive mild steel pre-chamber in a diesel engine and he also found no durability issues with the steel pre-chamber.

4.4.4 Boosting with an Air Compressor

In order to operate the CFR engine in boosted mode, a 200 liter tank pressurized to 8 bar was connected to the engine. Two air compressors were used for pressurization. One of the compressors was a semi industrial grade 7.5HP Ingersoll-Rand Type 30 compressor able to deliver 10 liters/sec of air. The second was a small domestic grade compressor, which was able to increase the overall compressor capacity by 50%. With the use of these two compressors, a peak MAP of 190 kPa was sustained for over 3 minutes at 1800 r/min, which was more than adequate time for data logging.

It should be noted that all indicated thermal efficiency values throughout this thesis exclude the energy losses associated with the operation of the compressor.

4.5 Instrumentation and Data Processing

4.5.1 Data Logging and Pre-Processing of Data

Cylinder pressure analysis in internal combustion engines involves measuring large quantities of data. Over 500 data points were logged and each data point consisted of 40 engine cycles. Through two channels, the cylinder pressure and the corresponding crank angle was measured at every 0.5 CAD, corresponding to 2880 data points per cycle.

Output parameters that describe combustion, such as peak cylinder pressure were visualised in real-time with Wave View [224] and the rate of pressure rise and IMEP were calculated with Real Time IMEP [233]. More complex outputs such as mass fraction burned (MFB) and flame speed were evaluated by post-processing the pressure data with E-CoBRA.

A/D Converter

The data acquisition is achieved through both Wave View [224] and Real Time IMEP [233], which are based on the Eagle Development Resource (EDR) kit supplied for the PC-30D analogue to digital converter. Both programs have the capacity to collect and analyse data in real time and are also capable of post-processing.

The output data stream from the PC-30D A/D board is of 12 bit digital values between 0 and 4095. The board has a 20-volt digitization range giving a resolution of 20 volts per 2^{12} counts, or 0.004888 volt/count. Depending on the pressure transducer constant (Appendix C.3), this translates to a 3.97 kPa resolution over a 16 MPa pressure range.

Wave View

Wave View was used to visualise raw crank angle and pressure signals. The integrity of the signal was frequently checked to make sure that the pressure transducers and crank angle sensors were functioning properly. With Wave View, up to 4 sets of data and their power spectrums can be held in memory at any one time. The data was exported as ASCII text and saved to disk, which allowed further post-processing.

Real Time IMEP

Once the engine parameters are set and the calibration completed, in cylinder engine performance such as IMEP, coefficient of variation (CoV), knock, and misfire can be monitored in real time. The program has an oscilloscope mode to visually check the integrity of the data stream. Program features include: top dead center (TDC) alignment, log pressure vs. log volume diagram, multiple plot mode, and dynamic drift compensation.

4.5.2 Post Processing of Data - E-CoBRA and Sigmaplot

E-CoBRA

To complete the theoretical component of the project, E-CoBRA was developed to simultaneously calculate actual and theoretical flame speeds, so as to identify how much combustion enhancement the HAJI system provides and at what part of the burn duration. Furthermore, E-CoBRA had to be capable of filtering raw pressure traces to detect small and large pressure oscillations in the combustion chamber.

Throughout the project, E-CoBRA was used to analyse experimentally obtained data (in the form of a text file) from either Wave View or Real Time IMEP. The text file is loaded directly into E-CoBRA, which can analyse up to 40 consecutive engine cycles. The following list presents some of the 100 outputs derived by E-CoBRA. Where appropriate, 40 cycles are normally analysed including CoV:

- Power, torque, net/gross IMEP, PMEP, thermal efficiency, ISFC;
- Peak pressure location, rate of pressure rise;
- Mass fraction burned (MFB) and mass burned rate (MBR);
- Burn duration in degrees from: 0-10%, 0-90%, 10-90% and 0-100%;
- Knock: start, duration, peak amplitude and intensity;
- Flame speed: peak, location of peak, and flame speed ratio (FSR);
- Taylor length scale, turbulence intensity, turbulent Reynolds number and Damkohler number;
- NO_x prediction and NO_x rate formation.

Once the analysis of the 40 consecutive cycles was completed then it was possible to develop representative ensemble average diagrams for pressure vs. CA, MFB vs. CA, flame speed vs. CA etc... This was achieved by first analysing each of the 40 cycles, then simply calculating the average value of the 40 data points at every 0.5 CAD. Parameters such as IMEP, peak pressure, thermal efficiency etc... were determined first by calculating the value for each cycle and then a final value was established by calculating the average of 40 cycles. After the completion of experimental data analysis a database was set up to organise the 500 output files each with a size of 120MB.

DataFit and Sigmaplot

DataFit was used mainly for regression analysis (curve fitting). It has 298 pre-defined two dimensional regression models, and 242 three-dimensional nonlinear regression models, using the Levenberg-Marquardt method with double precision as a solver. One of the most useful applications of DataFit was curve fitting the chemical equilibrium constants. This was achieved by finding the fitting values of "a", "b", and "c" of the famous "Vapor Pressure Model", which is in the form of $exp(a+b/x+c*log(x))$. The final equations were used in the chemical equilibrium solver. Average fitting errors balanced out to be less than 0.006% with a standard deviation of +/- 0.38%.

Sigmaplot was used predominantly to plot all the 3D contour plots. Sigmaplot is a state-of-the-art technical graphing program designed to aid in documenting and publishing research by specialising in the graphical presentation of results. Throughout the experimentation it was next to impossible to maintain exact MAP and Lambda values from day to day. Unfortunately, Excel, Matlab, and Sigmaplot require an evenly spaced grid to create a 3D surface. Consequently, Sigmaplot's smoothing algorithms were used to resample data to a rectangular grid of MAP and Lambda. Out of the seven smoothing algorithms available in Sigmaplot the "Loess" smoothing method was found to be the best. It applies the tricube weight function to weight the data and the smoother can be a polynomial of degree 1, 2, or 3.

One of the disadvantages of smoothing is of course the error between the actual data point and the surface. It was found that the contour plots presented in Chapter 5 and 6 hold an error of less than 5%, however errors are as much as 10% in extreme conditions. This larger error predominantly occurs at the boundary of the smooth surface.

4.5.3 Exhaust Emissions Analyser

Exhaust gas emissions were measured using an ADS 9000 Super Four Gas Analyser. It measured the concentrations of CO(%), CO_2(%), O_2(%), HC(ppm), and NO(ppm) (In this thesis all calculated NO_x values are made up of NO). These

exhaust products were used to calculate AFR by performing a chemical balance of the reactants and products. In instances where two fuels were involved in the combustion process, such as HAJI, the appropriate change to the chemical reactants was made. Appendix E details the method used to obtain corrected emissions and AFR from the analyser.

The analyser was zeroed and spanned regularly using the manufacturer's recommended calibration gases, which were based on propane. The sensitivity of the analyser to NO was previously determined, showing linear response and a 1 to 1 sensitivity ratio to the calibration gas [55]. HC sensitivity was non-unity and this is discussed in further detail in Appendix E.2.

Unburned H_2 was not measured since Deslandes [51] has previously shown for an SI engine operating on H_2 fuel that the H_2 fraction in the exhaust was similar to the HC fraction in the exhaust of a petrol engine. Furthermore unburned H_2 is not considered an emission to which legislated limits apply.

4.5.4 Cylinder Pressure Measurement

A Kistler 601B1 piezoelectric pressure transducer mounted in the cylinder head was connected to a 462-A-05 PCP charge amplifier and used for in-cylinder pressure measurement. The transducer was calibrated statically using a dead weight tester based on a similar method to Lambe [130]. The transducer was subsequently tested in both motoring and firing engine mode based on the methods of Lancaster et al. [132].

During initial firing tests, a phenomena known as thermal shock was encountered. Thermal shock is caused by excessively high transducer temperatures following flame arrival and is characterised by a reduction in charge output. This was eliminated by placing RTV (high temperature silicone) over the transducer diaphragm. The reader is referred to Appendix C for further details.

4.5.5 Fuel and Air Flow Measurement

Gasoline (unleaded 91 RON) fuel flow was measured from the injector pulse width and also verified frequently by a calibrated sight glass and a stopwatch. The main chamber H_2 flow was measured with a series of sonic nozzles calibrated for H_2. The pre-chamber H_2 was measured by a digital Brooks 5860E gas flow meter. The H_2 quantity added to the HAJI mode is defined by equation 4.1 as the percentage of H_2 energy entering into the combustion chamber with respect to the total energy per cycle.

$$H_2(\%) = \frac{H_2(Joules)}{H_2(Joules) + Gasoline(Joules)} \times 100 \qquad (4.1)$$

The air flow through the engine was measured with a calibrated orifice meter and the corresponding calibration constants were developed based on the British Standard BS1042. Appendix C.2 provides a detailed description of both fuel and air flow measurements and calibration.

4.6 Summary

This chapter clearly identified the experimental hypotheses. The test matrix was explained and a brief description of the day-to-day preparations undertaken to assure that the experimental results were accurate was also included. Furthermore, the equipment and method used during the experimental and data analysis portion of the project have been summarised.

The author set up and calibrated all the testing and measuring equipment, maintained the research engine and carried out all of the data analysis. This allowed the collection of over 500 experimental data points with the highest confidence that they are free from any errors.

CHAPTER 5
Results of HAJI Gasoline

5.1 Introduction

This chapter presents the results of HAJI in gasoline mode (HAJI-G) in terms of performance, emissions and combustion characteristics. This was achieved by generating contour plots of the experimental data with the use of a smoothing algorithm. This algorithm provides an excellent tool for examining trends and behavior at different engine output parameters, namely: λ, CR, and MAP. All of the data is presented in contour plot form, with axes of λ and CR on the right hand side plots, and axes of MAP and λ on the left hand side plots at a fixed optimal CR=11 (Appendix F.3).

The optimal CR=11 was found after examining all of the data points and based on where thermal efficiency and emissions results are best balanced over all load conditions. This observation was consistent with Kyaw [128] and a detailed study on the effects of CR on different output parameters is discussed in Section 7.3.2.

Over 100 output parameters are tracked and as a result, more than 600 contour plots were generated. This chapter presents only the relevant graphs, those which best describe HAJI-G mode. Furthermore, an optimum performance line (OPL -

Table 5.1 CFR engine conditions for chapter 5 results.

Ignition Mode: HAJI-Gasoline (HAJI-G)		
Speed	-	1800 r/min
Spark Timing	-	MBT
CR vs. Lambda (λ) contour plots at	-	MAP = 90 kPa
Lambda (λ) vs. MAP contour plots at	-	CR = 11 (HUCR)

dotted line) is displayed on the λ vs. MAP contour plots, which indicates that the CoV of IMEP<=5% and NO_x<=0.1g/kWh while maximising thermal efficiency within the CoV and NO_x constraints. The actual engine conditions used in this chapter are shown in Table 5.1.

5.2 Performance

5.2.1 MBT - Minimum Spark Advance for Best Torque

All data points are recorded at MBT (Appendix F.1) to ensure maximum thermal efficiency at all operating points. MBT is usually limited by the onset of knock so as CR or MAP is increased for a given λ, spark timing is retarded to avoid heavy knock (Figure 5.1). Interestingly, MBT varies little as MAP is increased at λ>2. This occurs because the mixture is lean and MBT is not knock limited and also because burn durations are predominantly insensitive to variations in MAP (Figure 5.4).

5.2.2 IMEP

IMEP, throughout this thesis, is calculated for an entire engine cycle (IMEP = working loop - pumping loop), also referred to as the net indicated mean effective pressure [132]. IMEP strongly depends on λ and MAP so a decrease in λ (for λ>1) or an increase in MAP will tend to increase the magnitude of IMEP. The OPL (around λ=1.9) in Figure 5.1 clearly indicates that at CR=11 and speed=1800r/min, it is possible through the control of MAP to cover the entire load range from idle to high load and maintain excellent combustion stability at almost zero NO_x.

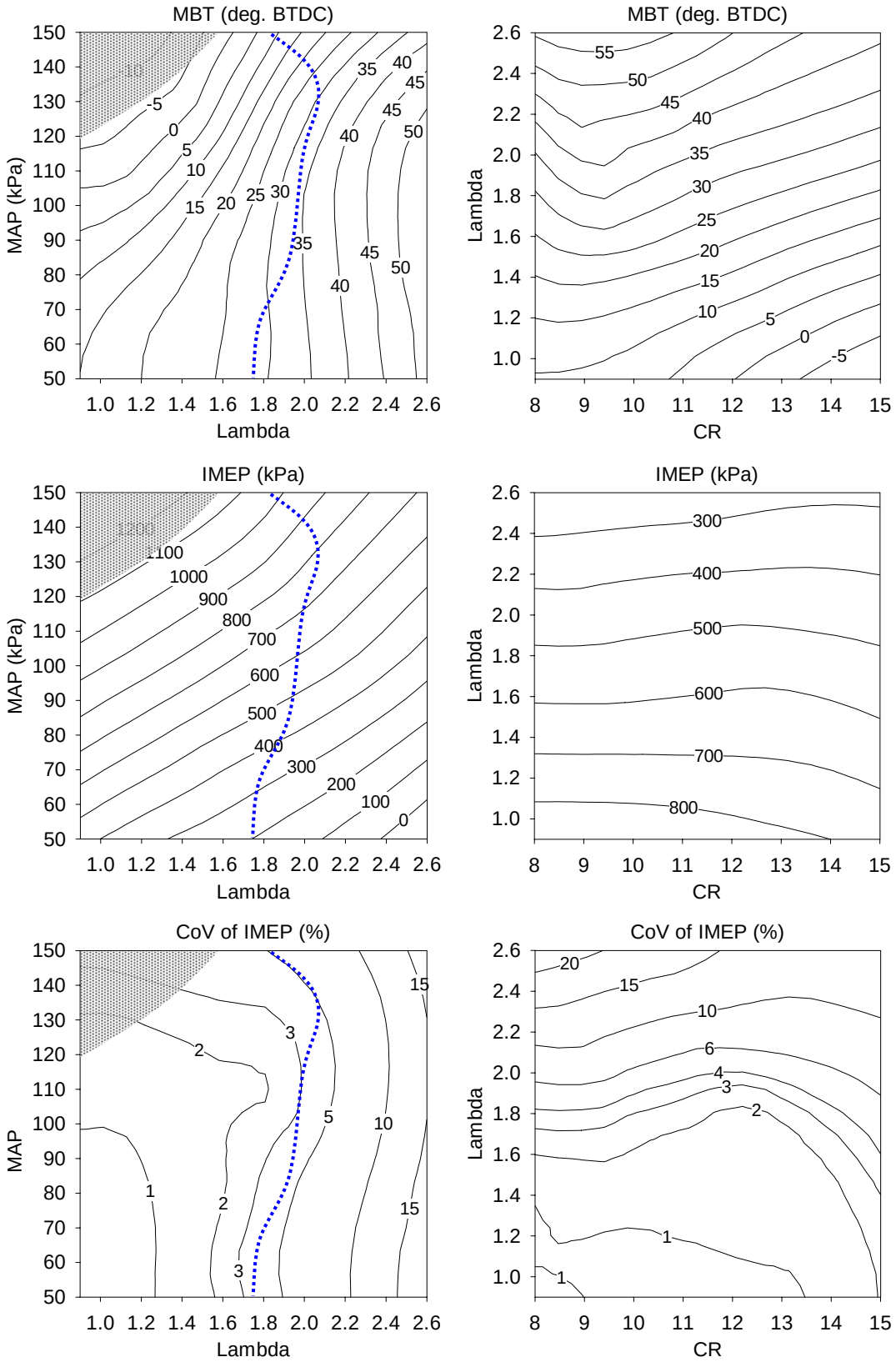

Figure 5.1: HAJI-G - (top) MBT, (middle) IMEP, (lower) CoV of IMEP.
(1800r/min, MBT, (left) CR=11, (right) MAP=90kPa, dark shaded area indicates where engine was not able to operate at all)

5.2.3 CoV of IMEP

It is clear from Figure 5.1 (bottom left), that combustion stability is compromised at high λ values. Beyond λ=2 CoV of IMEP increases to 10%, which is considered to be unacceptable as it can cause excessive Powertrain vibration.

5.2.4 Specific Fuel Consumption and Thermal Efficiency

Both the specific fuel consumption (g/kWh) and thermal efficiency (%) is shown in Figure 5.2. At MAP=90kPa and λ=1, the best efficiency occurs at a CR=9 with an ISFC of 260g/kWh, however at CR=11 and λ=1.6, the ISFC=230 g/kWh, which is an improvement of 11.5%. An overall 20% reduction in ISFC from 260g/kWh to 210g/kWh can be achieved by leaning the mixture to λ=2 and boosting MAP to 130kPa. The increase in thermal efficiency at high λ is made possible due to the stable throttleless operation (Figure 5.1) and low combustion temperatures (Figure 5.7), which reduce heat transfer.

5.2.5 %H_2 of Total Fuel Energy

As shown in Figure 5.2, H_2 consumption is a function of MAP and λ but is relatively independent of CR (Figure 5.2). At λ=1, the H_2 quantity is negligible and even without it the engine can operate stable. As λ increases, flame speed begins to drop, which affects combustion stability. At a given λ, the lack of stability becomes apparent at low MAP due to the increasing mass of residual gas, which further lowers flame speed. Consequently, as λ increases, the lower flame speed necessitates more H_2 to enhance flame speed and recover stability.

5.3 Emissions

5.3.1 ISHC - Unburned Fuel

Since the charge is premixed in the port, it is difficult not to increase HC emissions as λ and CR increase (Figure 5.2). This is due to an increase in quench gap and an

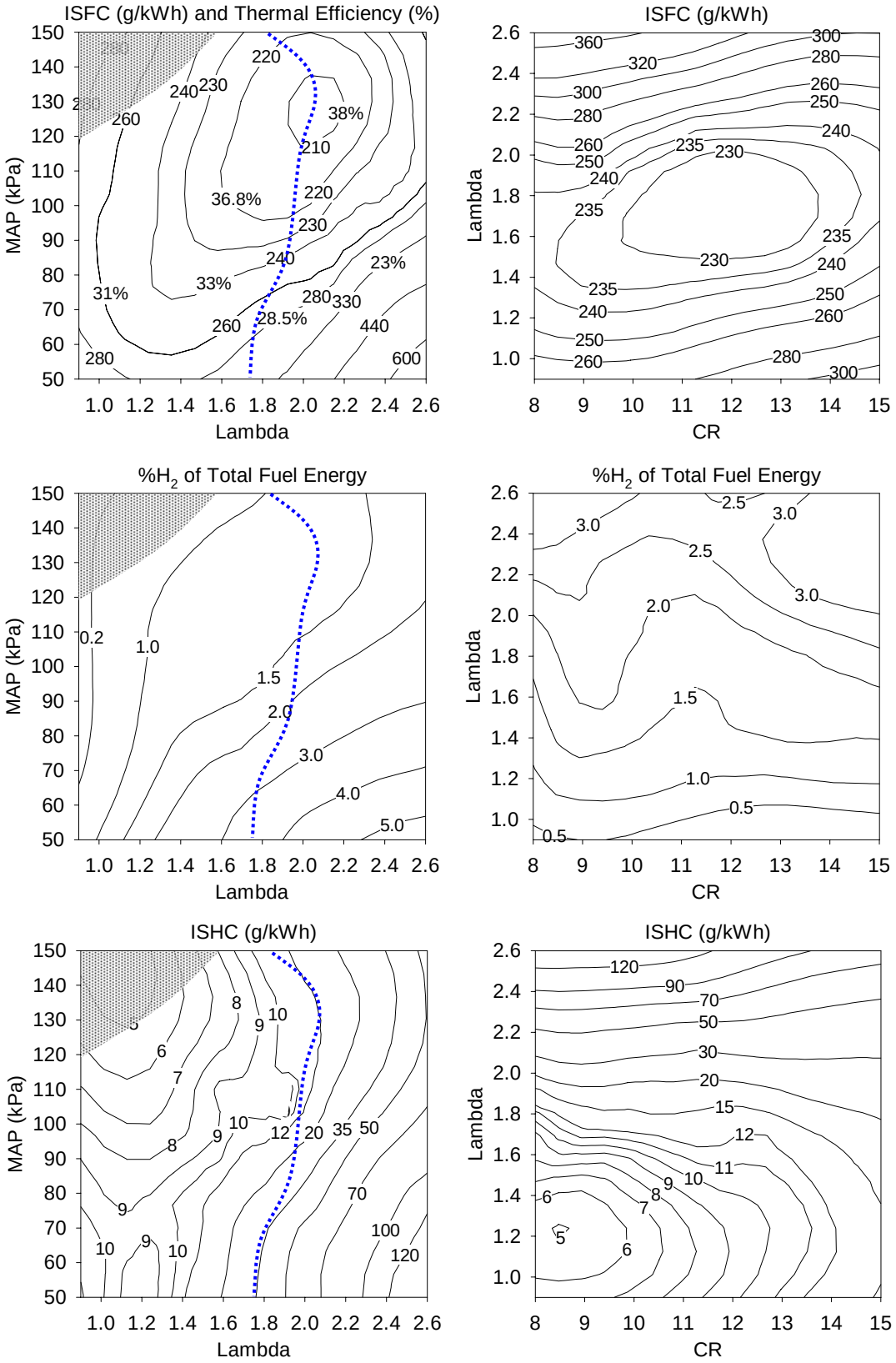

Figure 5.2: HAJI-G - (top) ISFC and Thermal Efficiency, (middle) % H_2 of total fuel energy, (lower) ISHC emission, (1800r/min, MBT, (left) CR=11, (right) MAP=90kPa, dark shaded area indicates where engine was not able to operate at all)

increase in the surface to volume ratio respectively. In addition, as shown in Figure 5.1(and Figure F.1), spark timing is usually retarded to avoid knock which can also increase the ISHC. It is worth noting that at λ=2, HAJI is able to provide higher thermal efficiency than at λ=1, even though the HC emissions increase by 2.5 times. This has advantages and disadvantages with regards to meeting Euro 5, which are discussed in more detail in Section 8.4.2.

5.3.2 $ISCO_2$

In Figure 5.3, on the OPL at low MAP values the CO_2 emissions level is equivalent to the λ=1 operating mode, which is due to the similarity in thermal efficiency. In contrast, where a 20% improvement in fuel economy is realised (Section 5.2.4) a 20% reduction in CO_2 emissions is also achieved. This improvement would directly assist in meeting the proposed EU emission targets set against CO_2.

5.3.3 ISCO

CO emission formation is independent of CR (Figure 5.3), however it is strongly influenced by λ. Minimum CO=1.5g/kWh occurs at λ=1.5. In ultra lean mixtures (λ=2.5) as much as 30 g/kWh can form, this is an undesirable operating point since the CoV of IMEP is quite high. In contrast, mixtures richer than λ=1 are often used to produce maximum power in SI engines and consequently, CO emissions may vary between 40g/kWh and 250g/kWh (Figure 2.9).

5.3.4 NO_x

NO_x emissions follow the opposite trend to HC emissions. As λ and CR are increased NO_x emissions decrease (Figure 5.3). This is due to the fact that high λ values produce low combustion temperatures and high CR desires retarded ignition timing, which also reduces combustion temperatures. At around λ=1.9 (OPL) a world class engine out emission of less than 0.1g/kWhr NO_x is realised with good combustion stabilities (CoV less than 5%). Beyond λ=2.5, NO_x emissions start to increase due to the increased residence time at high

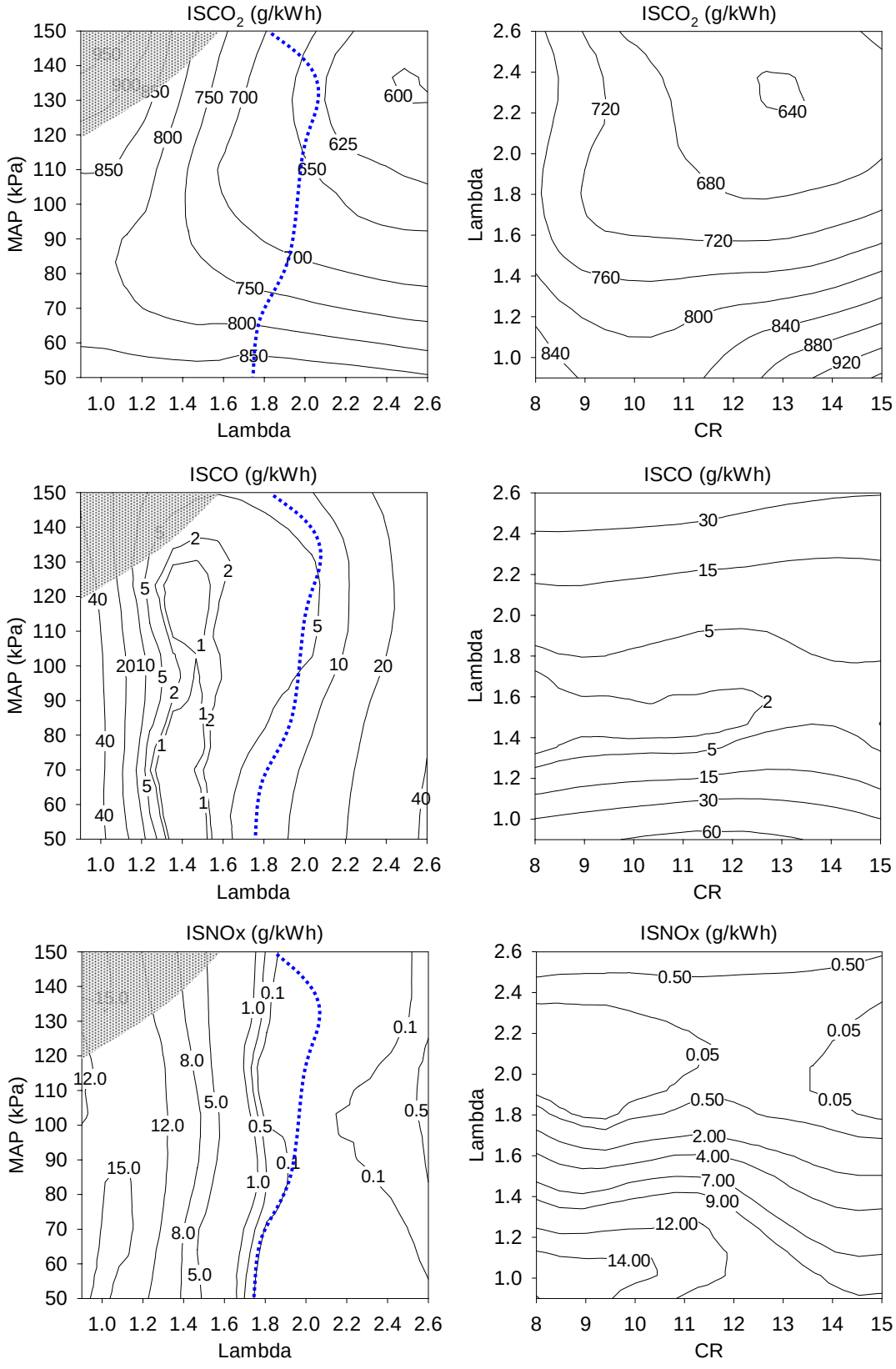

Figure 5.3: HAJI-G - (top) $ISCO_2$, (middle) ISCO, (lower) $ISNO_x$. (1800r/min, MBT, (left) CR=11, (right) MAP=90kPa, dark shaded area indicates where engine was not able to operate at all)

temperature and lower ISFC. This increase in emissions could be reversed by increasing combustion stability (by adding more H_2) and burn rate, which would retard spark timing.

5.4 Burn Characteristics

5.4.1 (0-10%) Burn Duration

In the flame initiation period, which is between spark initiation and the 10% mass fraction burned (MFB), the flame development and propagation is sensitive to large scale turbulence. Consequently, as burn duration increases (Figure 5.4) the CoV of IMEP (Figure 5.1) also increases. As MBT is retarded (Figure 5.1) at higher CR, the 0-10% burn duration decreases due to the higher pressures and temperatures.

As λ increases, the ability for the flame to become fully developed becomes more difficult. This is evidenced by an increase in duration of 0-10% MFB from 10 to 25 CAD as the mixture becomes leaner. As well as the strong affect of λ, lowering MAP increases the residual gases, which retards flame development, and therefore increases the 0-10% burn duration.

5.4.2 (10-90%) Burn Duration

In the 10-90% burn period, the flame is fully developed and both small and large scale turbulence can effect its development. As CR increases, the 10-90% burn duration (Figure 5.4) increases, unlike the 0-10% burn duration which decreases. This is attributed to the fact that at high CR the spark timing is retarded, which means that the 0-10% burn duration occurs near TDC, however the 10-90% burn duration occurs during the expansion stroke where both pressure and temperature are falling. The affect of λ and MAP on the 10-90% burn duration is similar to that observed for the 0-10% burn.

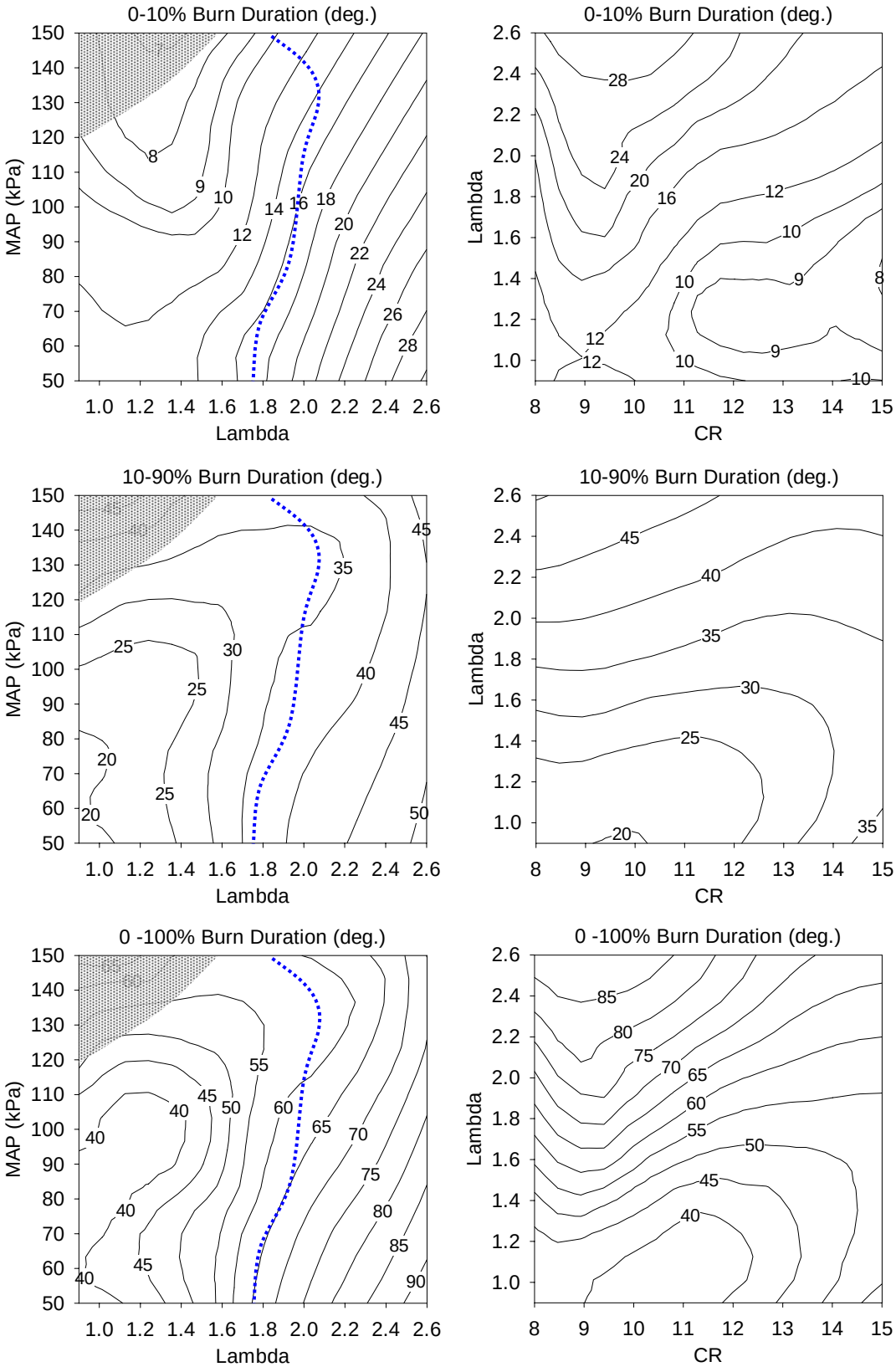

Figure 5.4: HAJI-G - (top) 0-10% Burn Duration, (middle) 10-90% Burn Duration, (lower) 0-100% Burn Duration. (1800r/min, MBT, (left) CR=11, (right) MAP=90kPa, dark shaded area indicates where engine was not able to operate at all)

5.4.3 (0-100%) Burn Duration

The total burn duration varies with CR, λ, and MAP. Most interestingly, in Figure 5.4 the duration of the last 10% MFB is consistently around 10 CAD, and therefore independent of CR, MAP and λ.

5.4.4 Peak MBR

The velocity of combustion is characterised by the mass burn rate (MBR), which is simply the derivative of MFB. As shown in Figure 5.5, at a given λ, CR only has a small affect on peak MBR which occurs at around CR=11. A decrease in MAP at a given λ decreases the peak MBR, which again is due to the presence of residual gas. In contrast, λ has the greatest effect on the magnitude of peak MBR. It is therefore no surprise that peak MBR occurs at λ=1, where mixture conditions are ideal for maximising combustion temperatures (Figure 5.7), which in turn maximises the rate of the chemical reaction necessary for rapid fuel oxidization.

5.4.5 Location of Peak MBR

Irrespective of the magnitude of CR, λ or MAP, the location of peak MBR always occurs after TDC (Figure 5.5). As CR increases at a given λ, the location of peak MBR becomes progressively more retarded. If λ is increased at a given CR or MAP, then the location of peak MBR becomes more advanced.

5.4.6 MFB at Peak MBR

It is expected that the peak MBR will occur in the fully developed flame region because that is where both large and small scale turbulence can wrinkle the surface of the flame, which enhances the rate at which the unburned mixture is consumed. This is clearly shown in Figure 5.5, where peak MBR occurs between 50-70% MFB at any given CR, MAP or λ. For low λ values, as CR or MAP increase, the MFB at peak MBR reaches maximum at CR=12 and MAP=100kPa respectively, then decrease. At high λ values, the MFB at peak MBR increases as either CR or MAP is increased.

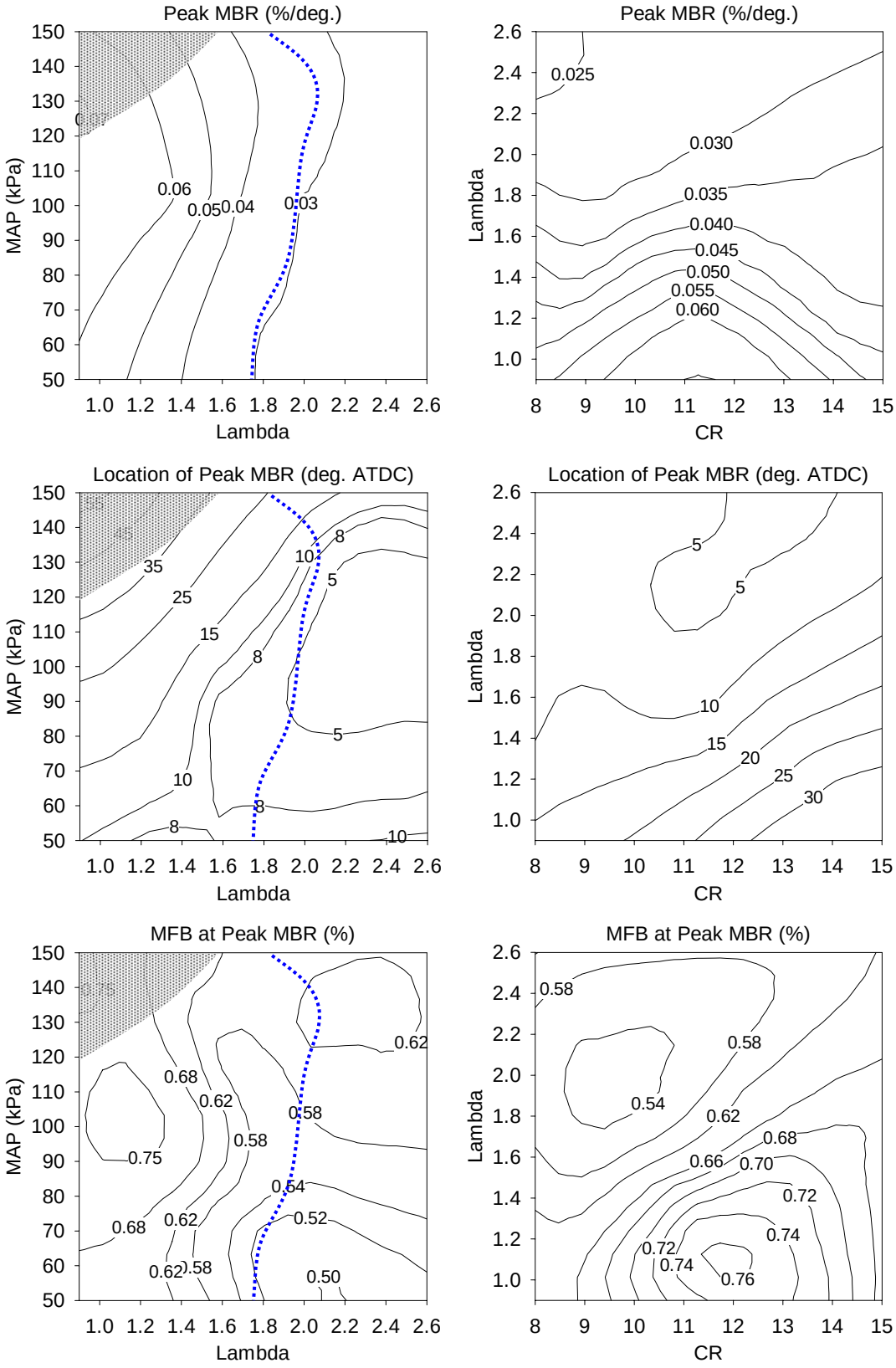

Figure 5.5: HAJI-G - (top) Peak MBR, (middle) Location of Peak MBR, (lower) MFB at Peak MBR. (1800r/min, MBT, (left) CR=11, (right) MAP=90kPa, dark shaded area indicates where engine was not able to operate at all)

5.5 Combustion Characteristics

5.5.1 Peak Pressure

When fuel burns in the combustion chamber it happens over a period of many CA degrees while the piston is moving. Therefore Cartwright and Fleck [38] adopted a simple but accurate (as long as the crank angle steps are small) method to calculate the pressure rise by summating the pressure rise due to combustion and the pressure change due to piston motion. This formulation is shown by Equation 5.1, where ΔQ_{in} is the heat released at the crank angle step.

$$\Delta P_{total} = \left[P_1 \left(\frac{V_1}{V_2} \right)^{\gamma} - 1 \right] + \left(\frac{\gamma - 1}{V_2} \right) \Delta Q_{in} \qquad (5.1)$$

In HAJI-G mode, peak pressure is a function of CR, MAP and λ as displayed in Figure 5.6. For low values of λ, as CR increases, peak pressure decreases. This behavior is counter intuitive and conflicts with Equation 5.1. The behavior, however, is a very real phenomenon not considered in Equation 5.1 and is due to the fact that combustion is heavily knock limited in this region (Figure F.1). In order to avoid knock at high CR, ignition timing was retarded by as much as 5 CAD after TDC. At low λ and high MAP conditions, ignition timing was retarded by as much as 5 CAD after TDC (Figure 5.1) for exactly the same reason.

5.5.2 Location of Peak Pressure

The location of peak pressure (see Figure F.4 where peak pressure usually occurs) is relatively insensitive to CR and MAP (Figure 5.6). However, for a given CR or MAP, as λ increases the location of peak pressure moves closer to TDC, which is due to the more advanced timing at high λ. Along the OPL, peak pressure location appears to stabilise at ~10° ATDC.

5.5.3 Peak *dp/dθ*

The rate of pressure rise is also an indicator of how fast combustion occurs. A very high rate of pressure rise (500kPa/deg.) is undesirable as it generates an

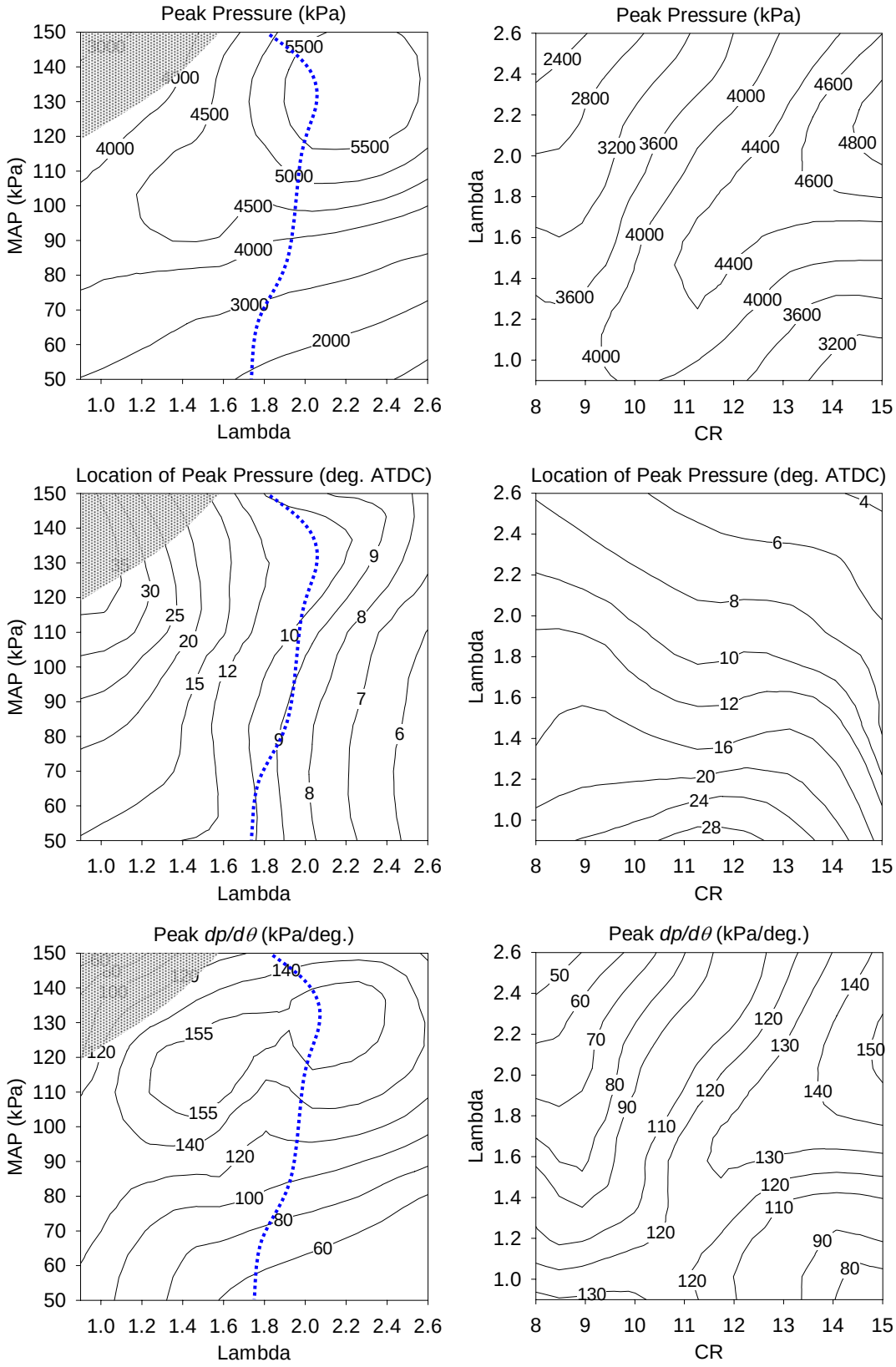

Figure 5.6: HAJI-G - (top) Peak Pressure, (middle) Location of Peak Pressure, (lower) Peak Rate of Pressure Rise (*dp/dθ*). (1800r/min, MBT, (left) CR=11, (right) MAP=90kPa, dark shaded area indicates where engine was not able to operate at all)

audible noise. In HAJI-G mode, the maximum rate of pressure rise is ~155 kPa/deg. (Figure 5.6). At low λ values, peak *dp/dθ* decreases only slightly as CR increases. However, at high λ it actually increases due to the advanced ignition timing. At low λ and high MAP operation, *dp/dθ* is very low, which again is due to the heavily retarded ignition timing used to avoid knock.

5.5.4 Location of Peak *dp/dθ*

As shown in Figure 5.7, at a given λ, the location of peak *dp/dθ* advances as CR is increased. At a fixed CR and low λ , peak *dp/dθ* occurs ATDC due to retarded MBT (Figure 5.1). As λ increases, the location of peak *dp/dθ* becomes advanced since MBT becomes progressively more advanced. At low λ, high MAP conditions where MBT occurs after TDC, peak *dp/dθ* is actually achieved on the compression stroke before ignition occurs. At lower MAP settings, as MBT is advanced, the location of peak *dp/dθ* becomes combustion dominated and spreads around TDC. At any given MAP at high λ where MBT is heavily advanced, peak *dp/dθ* is both compression and combustion dominated and therefore the location of peak *dp/dθ* during the compression stroke occurs between 7°-15° BTDC.

5.5.5 Peak Temperature

Combustion temperature is predominantly a function of λ and O_2 concentration. Consequently, as shown in Figure 5.7, CR and MAP have little influence on the peak combustion temperatures. At high λ and low MAP conditions, the effect of residual gases seems to drop the combustion temperatures, due to the additional dilution of charge with inert exhaust gases. Since λ is the most influential parameter effecting combustion temperatures, an increase in λ causes a drop in combustion temperature which is responsible for the observed reduction in NO_x emissions from 15g/kWh to 0.1g/kWh (Figure 5.3).

5.5.6 Location of Peak Temperature

Examining the location of peak temperature (Figure 5.7) and its correlation to MBT timing (Figure 5.1), shows that the location of peak temperature is closer to MBT

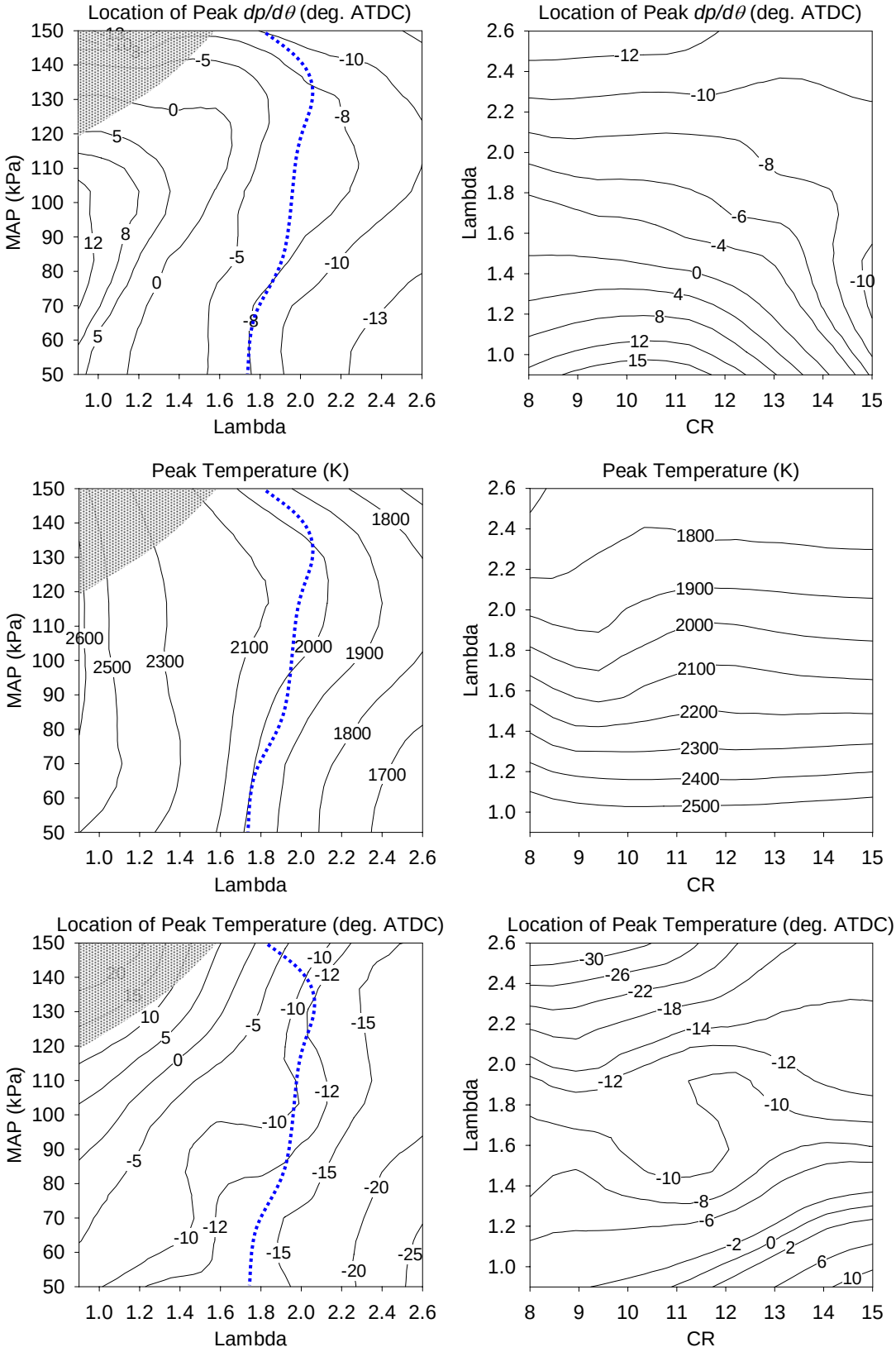

Figure 5.7: HAJI-G - (top) Location of Peak *dp/dθ*, (middle) Peak Temperature, (lower) Location of Peak Temperature. (1800r/min, MBT, (left) CR=11, (right) MAP=90kPa, dark shaded area indicates where engine was not able to operate at all)

if ignition timing occurs after TDC. This is because the rapidly expanding mixture is cooled by expansion and the rate of heat release is not high enough to counteract it. At high λ conditions where MBT is advanced, the location of peak temperature occurs between 10°BTDC and to 30°BTDC. One would expect this to be closer to TDC, however due to the general inaccuracy of two-zone modelling in relation to accurately predicting peak combustion temperatures, the author believes that these values are underestimated.

5.5.7 Peak Flame Speed

Peak flame speed varies with CR, λ and MAP as shown in Figure 5.8. For low λ values, when CR increases, peak flame speed increases up to CR=11 and then decreases as it approaches CR=15. At high λ values, peak flame speed increases with increasing CR. This is to be expected since the pressures and temperatures around TDC are higher at elevated CR. Flame speed relating to λ and MAP is complex, but generally high flame speeds occur around λ=1 mixtures or where MBT is advanced, such as at low MAP conditions. Moreover, flame speeds are affected by increased residuals, which may have an effect on radical concentration in the flame reaction zone, or perhaps HAJI jet penetration changes at different MAP and ignition timings.

5.5.8 Location of Peak Flame Speed

At low λ values, CR has little influence on the location of peak flame speed, and at high λ values the location varies between 10°-20° BTDC (Figure 5.8). MAP has little influence on the location of peak flame speed at high λ values. As MAP decreases at low λ values, the peak flame speed location becomes more advanced, which is a similar trend to that observed on the MBT plot.

5.6 Jet Knock

5.6.1 Knock Intensity - KI30

The knock intensity factor (KI30) describes the intensity of the pressure oscillation

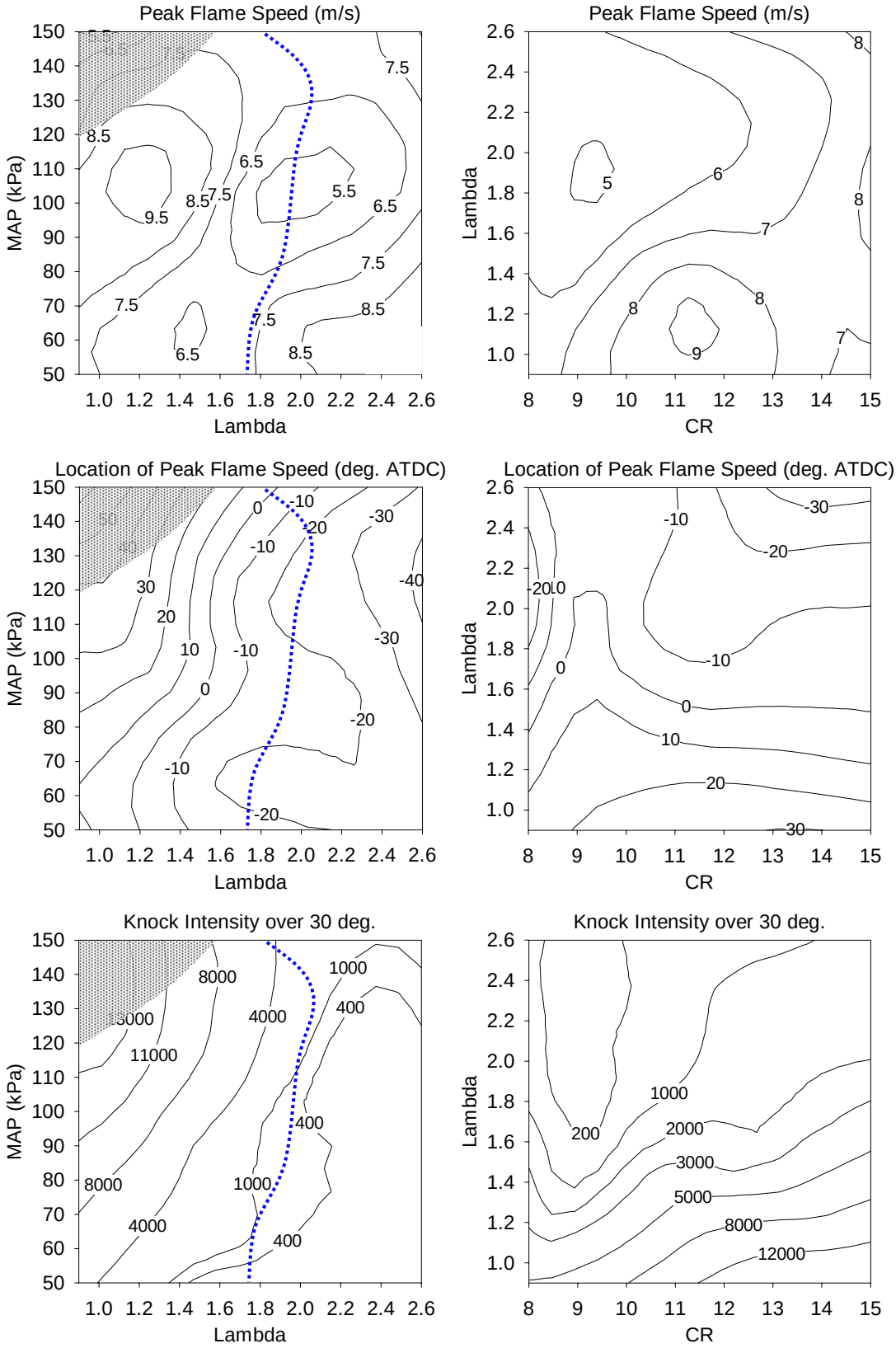

Figure 5.8: HAJI-G - (top) Peak Flame Speed, (middle) Location of Peak Flame Speed, (lower) Knock Intensity (30°). (1800r/min, MBT, (left) CR=11, (right) MAP=90kPa, dark shaded area indicates where engine was not able to operate at all)

over 30 CAD. Figure 5.8 clearly indicates that KI30 is a function of CR, MAP and λ. In general, the magnitude of Jet Knock is small since it forms as the jet enters into the main combustion chamber. As CR or MAP is increased at a given λ, KI30 also increases. At the OPL, KI≈1000, which is considerably less than the well known heavy knock (KI≈60000).

5.6.2 Peak Knock Amplitude

Peak Jet Knock amplitude in units of pressure was also monitored because it is easier to visualise than KI30. Figure 5.9 clearly shows that the pressure amplitude is a function of CR, MAP and λ. At low λ and high CR, the peak pressure oscillations are about 300kPa, however as λ increases the amplitude drops dramatically, and beyond λ=1.8, becomes less than 80kPa. As MAP increases for low levels of λ, the peak knock amplitude increases significantly up to 260kPa. However, at high λ values the peak knock amplitude is insensitive to MAP. After examining a large body of data and also inspecting in-cylinder components after testing, the effect of Jet Knock on performance, emission and durability was found to be un-measurable with conventional measuring methods.

5.6.3 Location of Peak Jet Knock

The location of peak Jet Knock occurs between 30-40 CAD after ignition (Figure 5.9). The location is relatively insensitive to CR at a given λ. It is sensitive to MAP at low λ conditions mainly because it follows the MBT behavior. Consequently, at high λ conditions the location of peak Jet Knock is also insensitive to MAP. As λ increases at a given MAP or CR the location of peak Jet Knock becomes more advanced, similar to MBT timing. Interestingly, along the OPL, which represents <=5% CoV, and ~0.1g/kWh NO_x, the location of peak Jet Knock occurs at around TDC. Generally though, peak Jet Knock occurs before peak pressure and peak MBR, and close to peak $dp/d\theta$. This means that the growth of Jet Knock amplitude is governed by pressure rise. This translates to high knock amplitudes at low λ condition as seen in Figure 5.9.

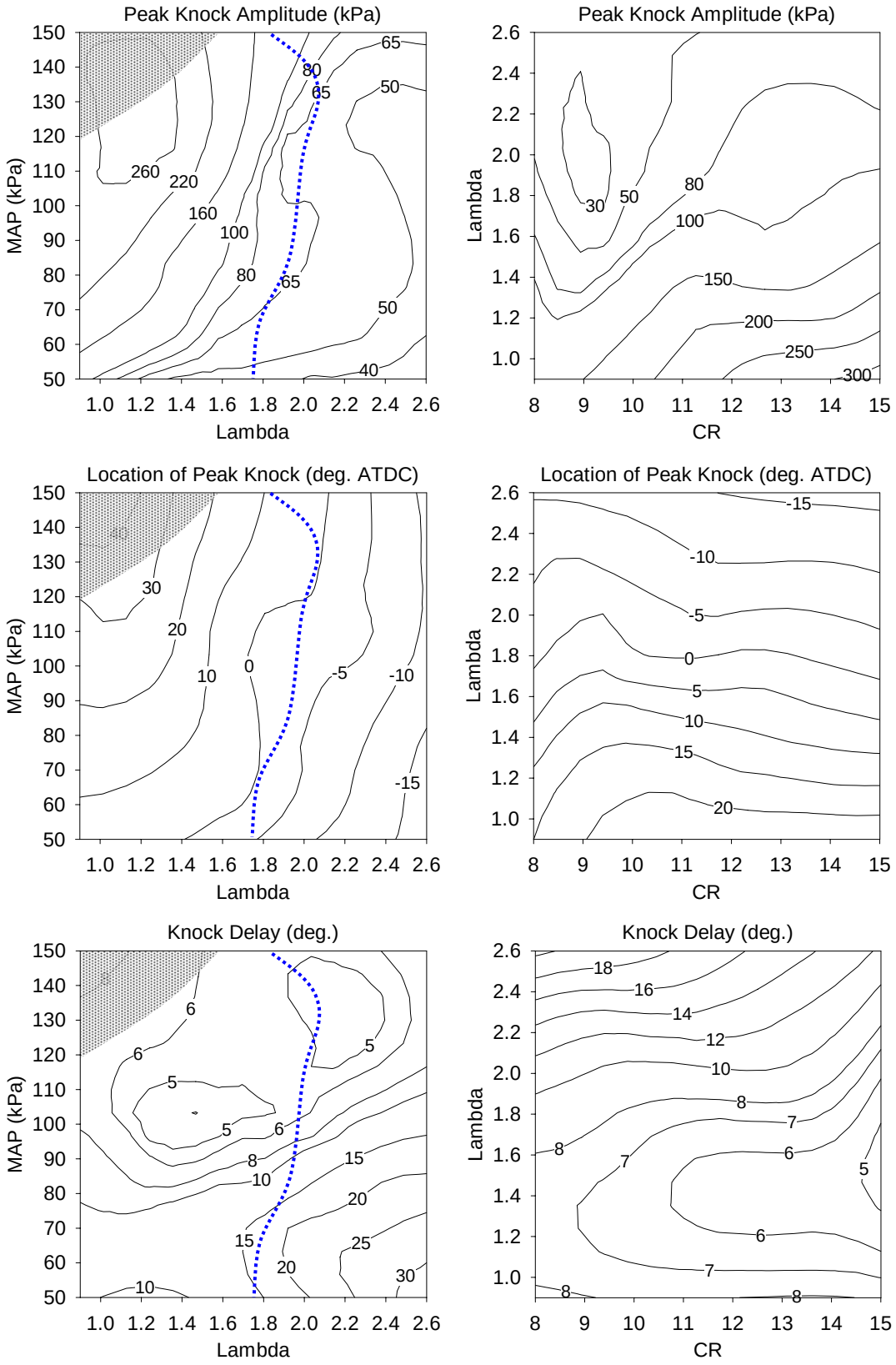

Figure 5.9: HAJI-G - (top) Peak Knock Amplitude, (middle) Location of Peak Knock, (lower) Knock Delay. (1800r/min, MBT, (left) CR=11, (right) MAP=90kPa, dark shaded area indicates where engine was not able to operate at all)

5.6.4 Jet Knock Delay

The start of Jet Knock is defined as the point where in-cylinder pressure oscillations equal or exceed 20kPa. Jet Knock is detected between 5-20 CAD after ignition (Figure 5.9), where less than 10% of the charge has burned and the flame is not fully developed. This is a typical characteristic of the Jet Knock phenomena, which differentiates it from the well known heavy knock which occurs late in the cycle and is characterised by spontaneous combustion or autoignition of the end gas. At a given λ, the knock delay is relatively insensitive to CR, however at low MAP and a given CR, it increases as λ increases.

5.6.5 Pressure at Peak Knock

As discussed in Section 5.6.3, the location of peak knock usually occurs before peak pressure. Consequently, the pressure at peak knock (Figure 5.10) is up to 1Mpa less than peak cylinder pressures (Figure 5.6). This is a unique characteristic of Jet Knock since heavy knock usually occurs at peak pressure. Interestingly the way in which CR, λ and MAP affects the magnitude of pressure at peak knock is the same as for $dp/d\theta$ (Section 5.5.3) and peak cylinder pressure (Section 5.5.1).

5.6.6 Knock Duration

The knock duration was calculated throughout the combustion period from the time when in-cylinder pressure oscillations equaled or exceeded 20kPa. At low λ, the knock duration varies little with CR (Figure 5.10). At high λ values and low CR, the Jet Knock magnitude falls below 20kPa, which is why the knock duration registered as 0 CAD. Interestingly, for any given λ, when the MAP is increased by three times (from 50kPa to 150kPa), the knock duration almost doubles (from ~40CAD to ~80CAD). This is expected since at high λ values MBT is advanced, therefore Jet Knock is subjected to the pressure rise due to compression and combustion in the combustion chamber for a longer period of time.

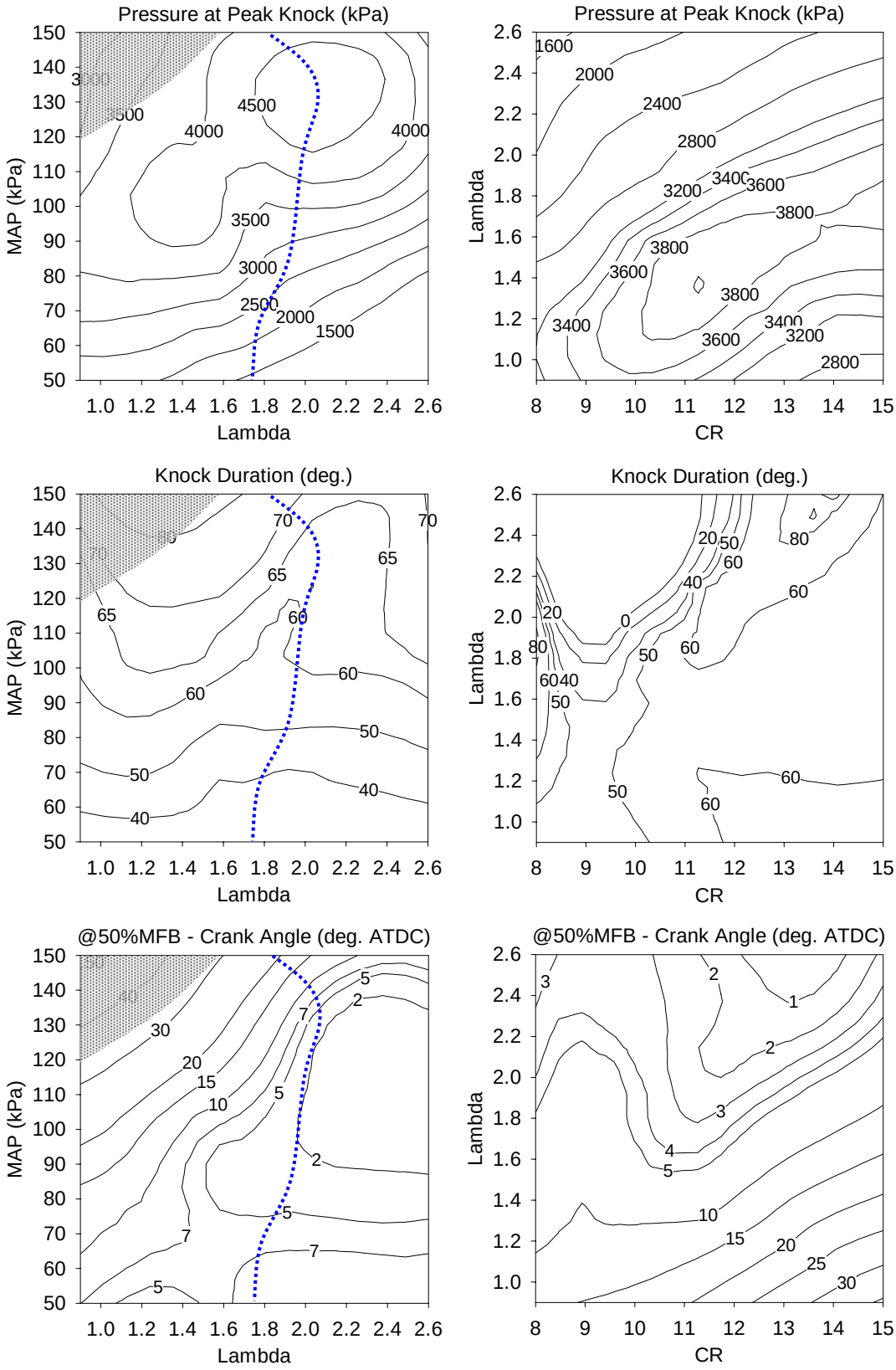

Figure 5.10: HAJI-G - (top) Pressure at Peak Knock, (middle) Knock Duration, (lower) @50%MFB - Crank Angle. (1800r/min, MBT, (left) CR=11, (right) MAP=90kPa, dark shaded area indicates where engine was not able to operate at all)

5.7 Combustion Characteristics @50% MFB

5.7.1 @50%MFB - Crank Angle (CA)

It is common for laminar and turbulent flame speeds and FSR to be examined and compared @50% MFB. This is because at this stage of combustion, the flame is fully developed, combustion is the most stable and it is also where peak MBR usually occurs. Along the OPL, the 50%MFB point is mostly situated between 2-20° ATDC (Figure 5.10). Overall, the position of 50% MFB is a function of CR, λ and MAP. The position of 50% MFB is directly related to the position of peak MBR, since 50% MFB occurs where peak MBR appears (Figure 5.5).

5.7.2 @50%MFB - Laminar Flame Speed (S_L for C_8H_{18})

The empirical approximation of laminar flame speed developed in Section 3.6.1 is valid up to 5 cm/s. Figure 5.11 shows S_L for isooctane (C_8H_{18}) which was used instead of gasoline. In general, laminar flame speed decreases at high pressures and increases at high temperatures. At a given λ, S_L does not vary much with CR, (Figure 5.11) however increasing λ for a given MAP or CR decreases combustion temperatures (Figure 5.7), consequently S_L drops by a factor of 10 when λ is doubled. The upper limit of the numerical approximation of S_L (Equation 3.20) occurs at λ=2.2. All S_L and FSR_a values above λ=2.2 should therefore be ignored.

5.7.3 @50%MFB - Turbulent Flame Speed ($S_{T,a}$)

$S_{T,a}$ is the actual flame speed in the combustion chamber and it is calculated by using Equation 3.22. At low λ values, as CR increases, the turbulent flame speed decreases, due to a reduction in laminar flame speed and an increase in burn duration (Figure 5.11). At the 50% MFB position at λ>2, as MAP or CR increases the density of the charge increases. The increase in density increases $S_{T,a}$, since the mass flux through a given flame surface area increases. Since S_L decreases as MAP is increased, one would have thought that $S_{T,a}$ would also decrease. However, this is not the case because $S_{T,a}$ is governed by u' and density, both of which increase as MAP is increased, offsetting the decrease in S_L.

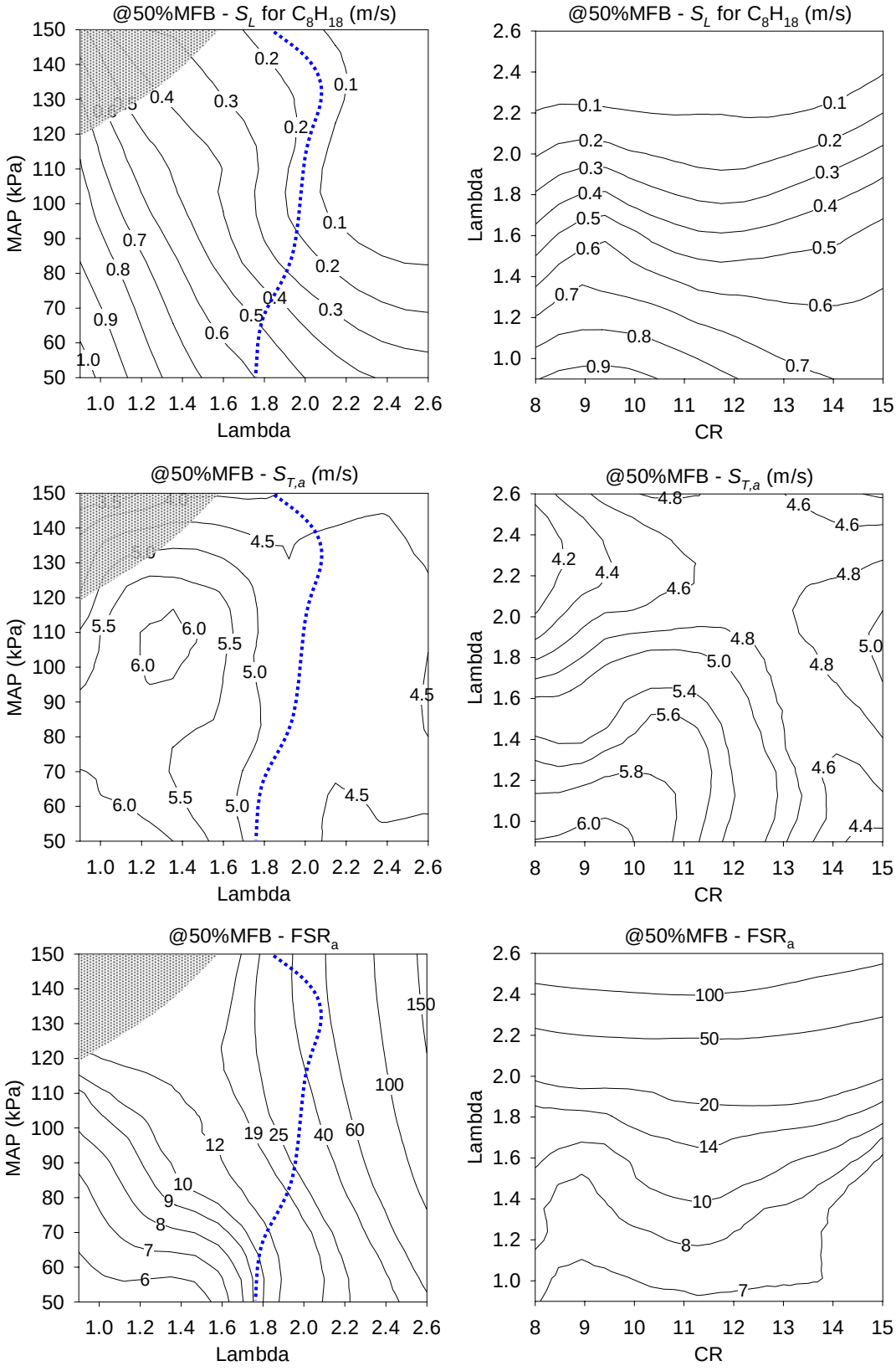

Figure 5.11: HAJI-G - (top) @50%MFB - S_L for C_8H_{18}, (middle) @50%MFB - $S_{T,a}$, (lower) @50%MFB - FSR_a. (1800r/min, MBT, (left) CR=11, (right) MAP=90kPa, dark shaded area indicates where engine was not able to operate at all)

5.7.4 @50%MFB - Flame Speed Ratio (FSR_a)

Due to the chemical and turbulence enhancement of the HAJI system, the FSR_a becomes very high as λ increases. Increasing MAP also has a positive effect on the FSR_a whereas CR has little affect. Approximately tripling MAP can double FSR_a at a given λ (Figure 5.11). As λ increases S_L decreases, consequently the flame speed ratio can increase up to 70 times, which is not observed in other homogeneously charged lean burn engines. The ability to increase the FSR_a is a special property of HAJI which is realised through its turbulence and chemical enhancement in lean mixtures.

5.7.5 @50%MFB - Turbulence Intensity (u')

Turbulence intensity is shown in Figure 5.12 and was previously shown to be a function of both CR and MAP (Equation 3.18 and 3.19). Figure 5.12 highlights how theses factors affect u' at 50%MFB where, at any given λ, a rise in CR or MAP results in an increase of u'. In both cases, this rise is due to an increase in pressure. λ has the opposite effect on u', so when the mixture becomes leaner, the turbulence intensity drops. This negative effect of λ at 50%MFB on turbulence intensity has more to do with the associated drop in combustion pressure, rather than the composition of the mixture.

5.7.6 @50%MFB - u'/S_L for C_8H_{18}

As described in Section 3.6.2, the most popular turbulent flamelet models or FSR_t models are a function of u'/S_L, consequently they are plotted on a u'/S_L vs FSR diagram (Figure 3.6). This helps to identify the regimes of combustion, which are discussed in more detail in Chapter 8.

Turbulence intensity varies from 3 to 4.4 (Figure 5.12) and S_L varies between 0.1 m/s to 1 m/s (Figure 5.11). As a result, u'/S_L varies from 4 to 50 and varies little with CR (Figure 5.12), however an increase in MAP at a given λ increases this ratio significantly. λ causes the greatest variation in u'/S_L because of its enormous effect on S_L (Figure 5.11). At high values of u'/S_L, the flame surface is subjected to

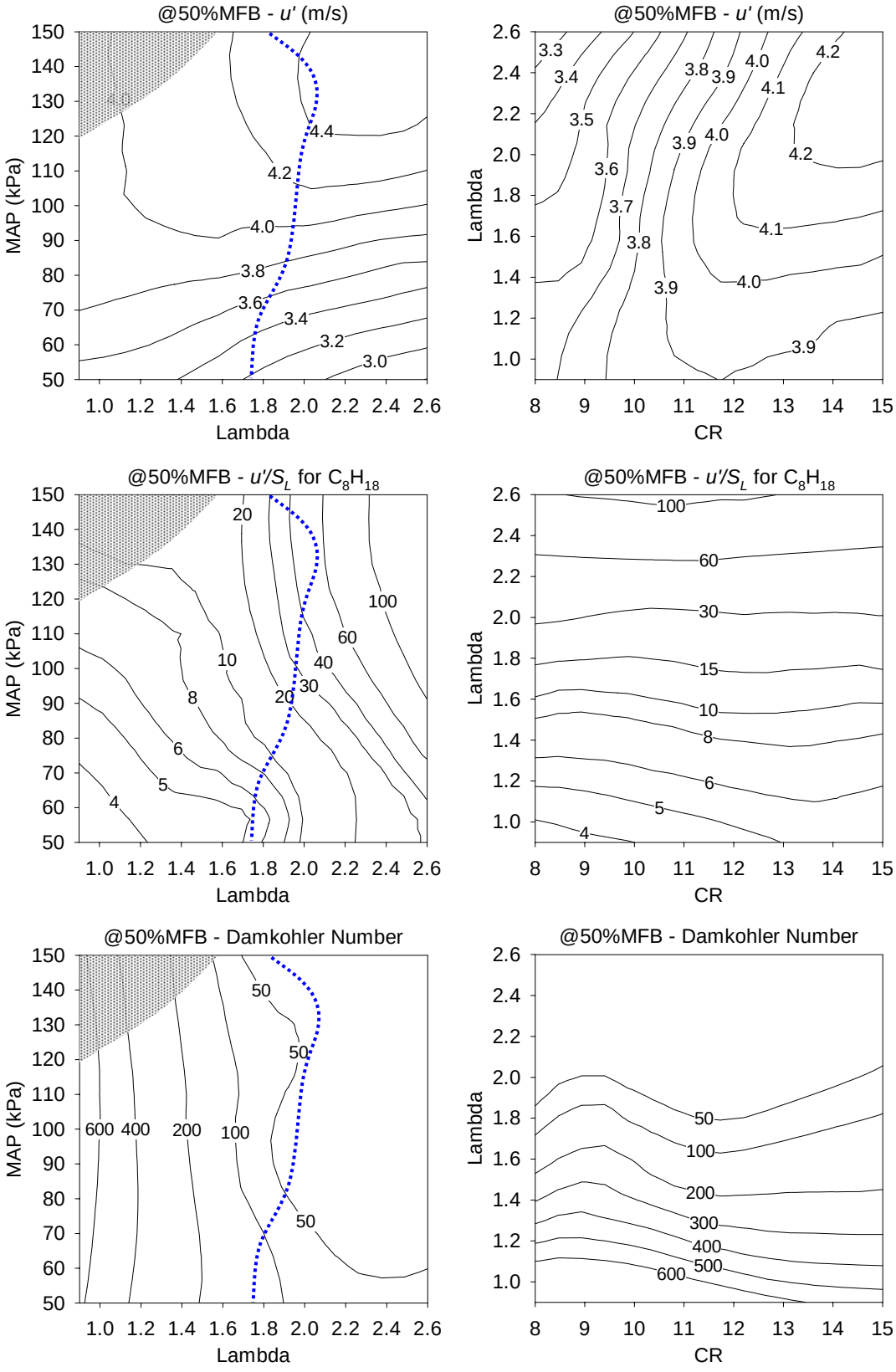

Figure 5.12: HAJI-G - (top) @50%MFB - u', (middle) @50%MFB - u'/S_L, (lower) @50%MFB - Damkohler Number. (1800r/min, MBT, (left) CR=11, (right) MAP=90kPa, dark shaded area indicates where engine was not able to operate at all)

very strong turbulence, which severely distorts the surface and therefore increases the flame surface area significantly. This increases mass flux across the flame surface area and therefore increases flame speed. This increase is very important in lean mixtures otherwise the slow oxidization rate in the flame reaction zone decreases the flame speed to very low levels, which would extend burn durations to unacceptable levels.

5.7.7 @50%MFB - Damkohler Number (*Da*)

The Damkohler number (defined in Section 3.5.3 and Equation 3.15) varies relatively little with CR and MAP (Figure 5.12). However, as λ increases, *Da* decreases dramatically from 600 to 50 in magnitude. The low Damkohler number indicates that chemical reaction at the flame front is becoming weak. This makes the jet vulnerable to distortion through turbulence. In contrast, at high *Da* the combustion process is chemically dominated and turbulence is less likely to influence flame propagation.

5.7.8 @50%MFB - Turbulent Reynolds Number (Re_T)

As shown in Figure 5.13, at low λ values the turbulent Reynolds number (defined in Equation 3.14) increases as CR increases. This is due to decreasing combustion chamber height as CR increases, which reduces the integral length scale (refer Equation 3.10). For any given λ, as MAP increases, Re_T increases due to an increase in u' and a decrease in kinematic viscosity. For any given MAP or CR, as λ increases, Re_T decreases, due predominantly to the decrease in u'. This means that at high Re_T, the combustion chamber is highly turbulent, which is advantageous when the flame is fully developed as it enhances its speed. In contrast at low Re_T the turbulence is lower in the combustion chamber, which usually occurs at low MAP. This should be monitored carefully especially at idle, since lack of turbulence can increase the 0-10% burn duration due to slow transition time from turbulent jet to turbulent flames.

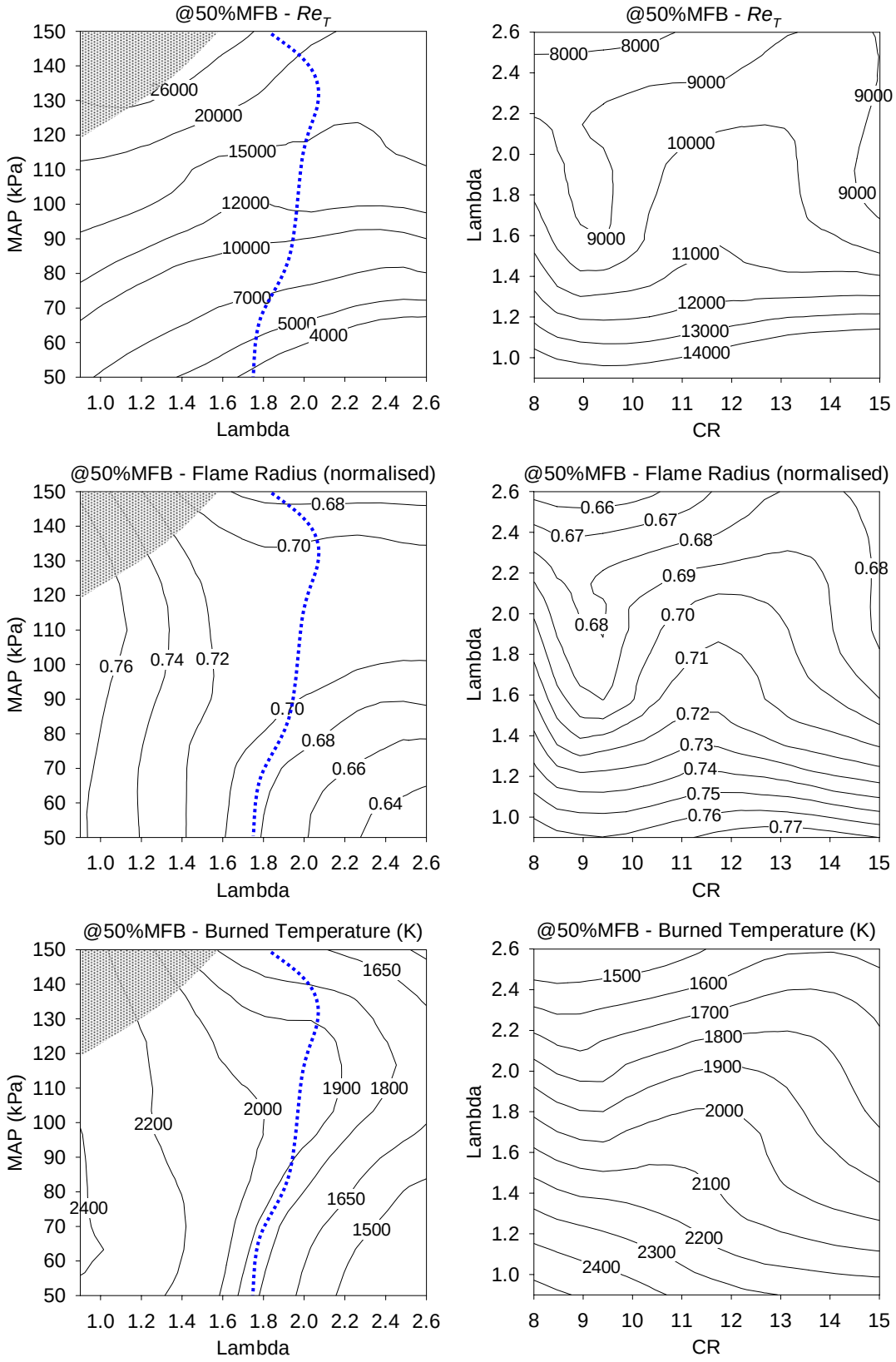

Figure 5.13: HAJI-G - (top) @50%MFB - Re Turbulent, (middle) @50%MFB - Flame Radius (normalised), (lower) @50%MFB - Burned Temperature. (1800r/min, MBT, (left) CR=11, (right) MAP=90kPa, dark shaded area indicates where engine wasn't able to operate at all)

5.7.9 @50%MFB - Flame Radius (normalised)

The normalised flame radius at 50%MFB is an indication of the percentage distance propagated by the flame with respect to the total distance propagating. This percentage does not vary much with CR and MAP as shown in Figure 5.13, however it varies from 64% to 76% throughout the λ range. The position of flame radius is heavily dependent on the density ratio between the burned and unburned mixture. The unburned mixture temperature varies less than the burned temperature which is a function of λ (Figure 5.13 and 5.7). Consequently, at high λ values where burnt mixture temperatures are low, the ratio of burned to unburned temperature is also low, so the density ratio is not as high. In fact, if the density ratio was unity, then the normalised flame radius position would tend to occur around 50% MFB.

5.7.10 @50%MFB - Burned Combustion Temperature

The actual effects of MAP, CR and λ on combustion temperatures @50%MFB (Figure 5.13) are the same as described for the peak temperature (Section 5.5.5 and Figure 5.2). The burned combustion temperatures @50%MFB are lower than the peak temperatures by 200°K at all λ values. This is especially important for NO_x formation at high temperatures in the post flame zone. In fact, a drop in 200°K would indicate that the majority of the NO_x emissions would have to form prior to 50%MFB.

5.8 Summary

This chapter is an extension of Lumsden's [143] (Sections 2.8.6 and 4.3.1) research in that it explores HAJI in gasoline mode with respect to emissions and combustion characteristics at varying CR and MAP pressures. The large body of data, all at a fixed speed of 1800 r/min, was best described with two types of contour plots: CR vs. λ at MAP=90kPa, and λ vs. MAP at CR=11.

The CR vs. λ contour plots at MAP=90kPa provide a comprehensive analysis from CR=8 to CR=15. It was found that CR=11 provides the best balance between

Table 5.2 HAJI-G outputs and characteristics at OPL.

Engine Speed (r/min)	1800	Peak MBR (%/deg)	0.032
Compression Ratio	11	Peak Pressure (kPa)	2000-5500
Lambda (λ)	1.7-2.1	Peak $dp/d\theta$ (kPa/deg)	55-155
MBT (°BTDC)	5-34	Peak Temperature (K)	1950-2050
IMEP (kPa)	200-1020	Peak Flame Speed (m/s)	5.5-7.3
CoV of IMEP (%)	2-5	Peak Knock Amplitude (kPa)	45-160
ISFC (g/kWh)	210-300	Knock Delay (°)	5-15
$\%H_2$ of Total Fuel Energy	1-3.2	@50%MFB - S_L (m/s)	0.15-0.6
ISHC (g/kWh)	10-32	@50%MFB - $S_{T,a}$ (m/s)	4-5
ISCO (g/kWh)	4-8	@50%MFB - FSR_a	9-50
$ISNO_x$ (g/kWh)	0.1	@50%MFB - u' (m/s)	3.2-4.4
(0-10%) Burn Duration	10-16	@50%MFB - u'/S_L	5.5-60
(10-90%) Burn Duration	35-38	@50%MFB - Da	50-150
(0-100%) Burn Duration	57-63	@50%MFB - Re_T	4000-23000

combustion stability, emissions and efficiency results. The λ vs. MAP contour plots at CR=11 clearly demonstrated the lean burn capability of HAJI-G operating up to λ =2.6 from MAP=50kPa to MAP=150kPa.

The OPL, positioned around λ=1.9, highlights world class NO_x emissions of ≈0.1g/kWh and CoV of IMEP<=5% for a range of load points from IMEP=200kPa (idle) to IMEP>1000kPa (WOT). Various performance measures along this line are summarised in Table 5.2. Clearly, the most important parameter affecting overall performance is λ, where λ is maintained in the range of 1.7-2.1 across the entire load range. This is lean enough to satisfy NO_x emissions targets, but not overly lean such that HCs, combustion stability and thermal efficiency are compromised. Remarkably, operating along the OPL and coupling HAJI to a boosting device manages to keep the total burn duration within ± 3 CAD and peak temperatures within ± 50K, further demonstrating the strong independence between IMEP on combustion performance.

CHAPTER 6
Results of HAJI Hydrogen

6.1 Introduction

This chapter, together with Chapter 5, fulfills objective number 2 by exploring HAJI in hydrogen main chamber mode with respect to performance, emissions and combustion characteristics. These results are novel to this thesis and presented in the form of contour plots similar to Chapter 5, as it is an excellent way to qualitatively explore the vast number of data points obtained from the experiments and combustion analysis.

The engine conditions used in this chapter are shown in table 6.1. These conditions are identical to Chapter 5; therefore back-to-back comparison can be made directly between HAJI-H_2 and HAJI-G modes.

Table 6.1 CFR engine conditions for Chapter 6 results.

Ignition Mode: HAJI-Hydrogen (HAJI-H_2)		
Speed	-	1800 r/min
Spark Timing	-	MBT
CR vs. Lambda (λ) contour plots at	-	MAP = 90 kPa
Lambda (λ) vs. MAP contour plots at	-	CR = 11 (HUCR)

The OPL (optimum performance line) is presented on all Lambda (λ) vs. MAP contour plots, which represents an operating condition where: CoV of IMEP <= 3% and NO_x ~0.1g/kWh. It must be emphasised that this represents world class combustion stability and engine out emissions for all engine load points. Similar to HAJI-G mode, CR=11 was also found to be the optimum (Appendix F.3) for HAJI-H_2 mode where performance, efficiency and emissions results are best balanced.

6.2 Performance

6.2.1 MBT - Minimum Spark Advance for Best Torque

MBT timing (Figure 6.1) (Appendix F.1) was used throughout the project to ensure maximum thermal efficiency at all operating points. Similar to HAJI-G operating mode in HAJI-H_2 mode, MBT was retarded to avoid backfire as CR or MAP was increased for a given λ (Figure 6.8). Overall, λ is the most influential parameter on MBT; as λ increases the flame stability decreases, which is compensated by the advancement of spark timing. Due to the faster burning nature of H_2, all MBT timings for HAJI-H_2 are more retarded than HAJI-G (Figure 5.1) at a given λ and MAP condition.

6.2.2 IMEP

IMEP is influenced by λ and MAP (Figure 6.1), consequently a decrease in λ or increase in MAP will increase the magnitude of IMEP. It is worth noting that in naturally aspirated mode at MAP=90kPa (WOT) the engine was backfire limited at λ=1.79, where IMEP=460kPa. The results were extrapolated out to λ=1 where IMEP≈600kPa could be achieved in the absence of backfire. However, at MAP=190 at λ=2.1 an IMEP of 1044kPa was recorded with the total elimination of backfire. This was concluded to be the result of additional cooling of air and reduction in the backflow of hot residual gases. Furthermore, along the OPL a maximum of 850kPa IMEP can be produced. This is a substantial increase in IMEP when considering that at best (backfire free), at λ=1 in naturally aspirated mode only 600kPa IMEP can be achieved.

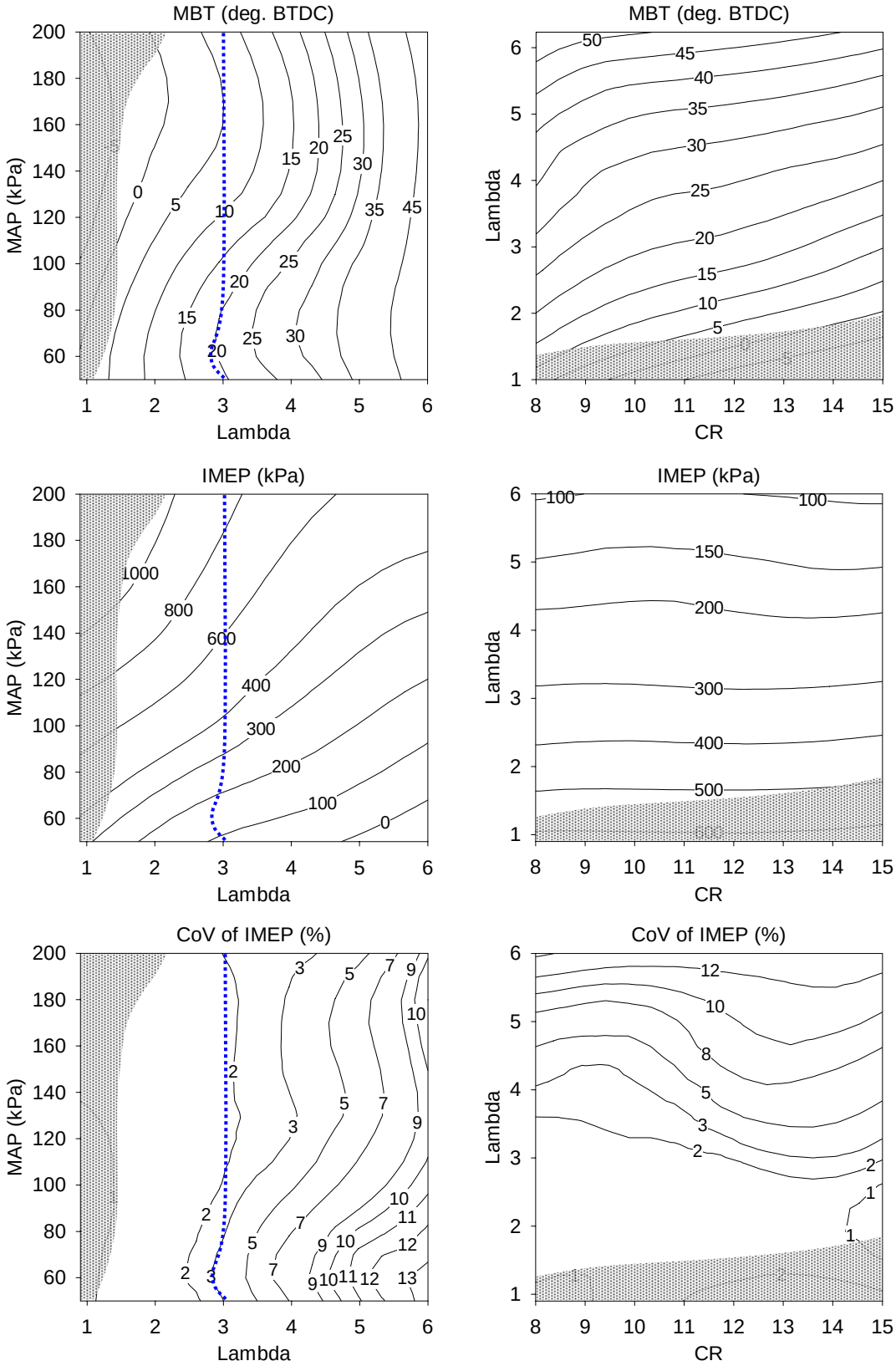

Figure 6.1: HAJI-H_2 - (top) MBT, (middle) IMEP, (lower) CoV of IMEP. (1800r/min, MBT, (left) CR=11, (right) MAP=90kPa), dark shaded area indicates backfire limited conditions)

6.2.3 CoV of IMEP

World class combustion stabilities (CoV of IMEP <=3%) were experienced up to λ=3.8 (Figure 6.1). This high stability exceeds the lean burn requirement since the OPL lies at around λ=3 in order to meet the 0.1g/kWh NO_x target at all load points.

6.2.4 Thermal Efficiency

Figure 6.2 shows that for any given λ, the maximum thermal efficiency occurs at around CR=11. Peak thermal efficiency on the CR vs. λ plot occurs at λ=2.5 and at CR=11. When observing the MAP vs. λ plot, it is clear that thermal efficiency can be further increased to 39% by boosting the MAP to 160kPa at λ=3. This means the thermal efficiency can be increase by ~30% going from a λ=1 engine operating at a MAP=90, to a λ=3 engine operating at a MAP=160kPa.

6.3 Emissions

6.3.1 ISHC - Unburned Fuel

As the engine was operated in all H_2 mode the engine out HC emissions around the OPL recorded were ~1g/kWh (or 0.32g/km). One would expect little or no HC emissions, however it is reasonable to observe these magnitudes when considering that the engine specifications allow for higher oil consumption due to the heavy duty nature of the engine. Above λ=1, the HC emissions predominantly increase due to the decrease in efficiency. Furthermore, the inaccuracy of specific HC calculations must also be noted as the sensitivity of emissions analyser to lubricating oil was assumed to be the same as gasoline (Table E.3).

6.3.2 ISCO$_2$

Since carbon is available from lubricating oil and in air (in the form of CO_2 and CO), the formation of CO_2 is between 5-15g/kWh (Figure 6.2) when operating at

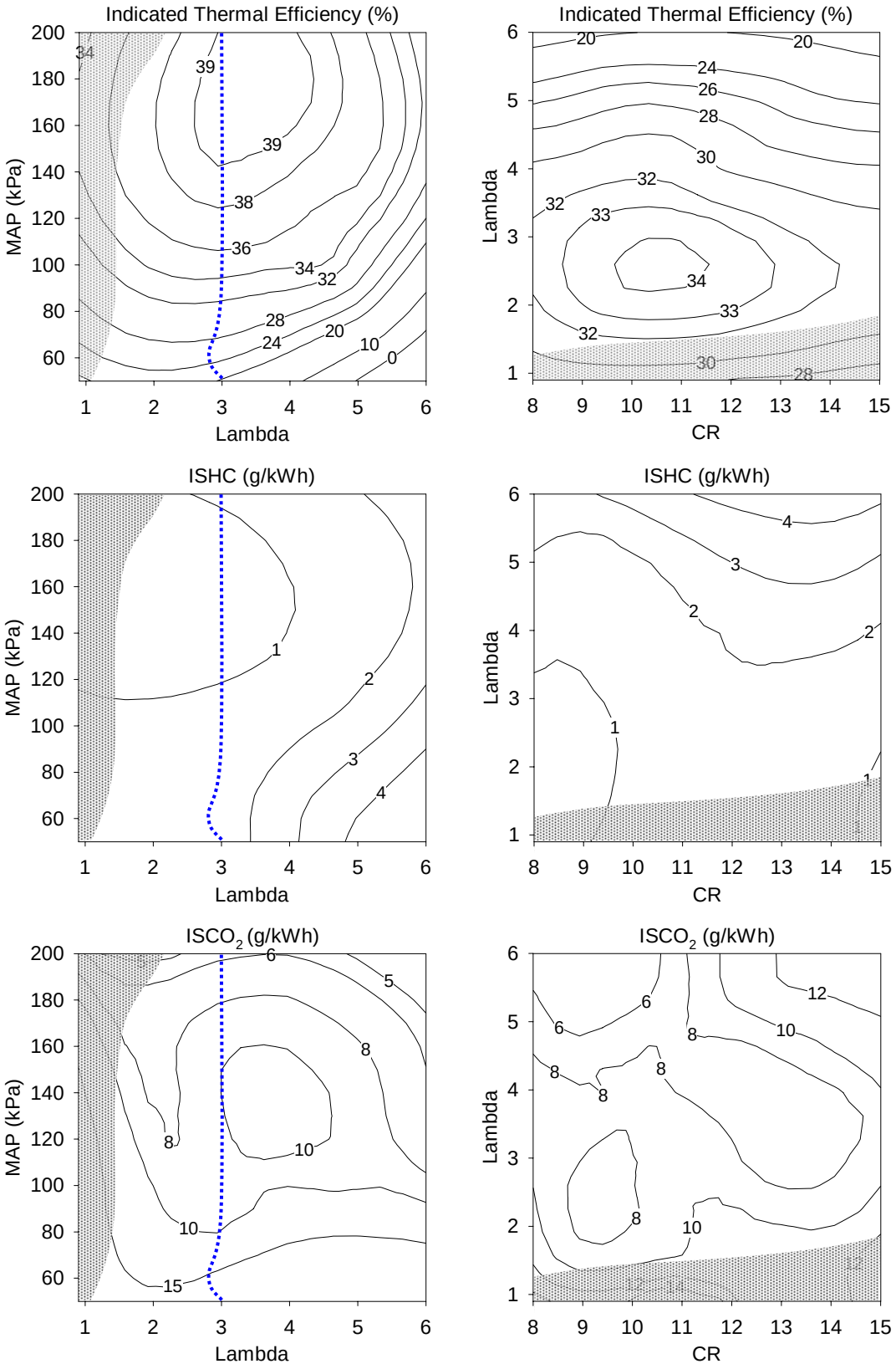

Figure 6.2: HAJI-H_2 - (top) ISFC and Thermal Efficiency, (middle) ISHC emissions, (lower) $ISCO_2$ emissions. (1800r/min, MBT, (left) CR=11, (right) MAP=90kPa), dark shaded area indicates backfire limited conditions)

or less than λ=3. This is more than 50 times less than what was observed in HAJI-G mode and therefore certainly below the proposed EU emission regulations relevant to CO_2 emissions (Figure 1.6).

6.3.3 ISCO

The formation of CO is inevitable due to the presence of lubricating oil and CO_2 in the atmosphere, which burns up in the combustion chamber (Figure 6.3). The lowest results are 0.5g/kWh, which is surprisingly high compare to HAJI-G's (Figure 5.3) lowest Figure of 1g/kWh. This is predominantly due to the inaccuracy of the ADS 9000 emission gas analyser which has a resolution of 0.01% (100ppm) (Table E.1 and E.2) for this gas, which approximately corresponds to 0.5g/kWh. Consequently, absolute magnitudes were ignored, however the presence of CO was noted.

6.3.4 NO_x

Following the OPL in Figure 6.3, the engine out NO_x in HAJI-H_2 mode is ~0.1g/kWh. This low NO_x capability is maintained at all load points while achieving exceptional combustion stabilities. The operation of a H_2 engine at near λ=1.79 should be avoided as it produces up to 18g/kWh of NO_x, which is due to the high flame temperatures of H_2 (Figure 6.7). Overall, the insensitivity of NO_x to MAP means that inlet boost can be increased beyond 200kPa if higher power output is required while maintaining 0.1g/kWh NO_x capability.

6.4 Burn Characteristics

6.4.1 (0-10%) Burn Duration

In the stable engine operating range (<3% CoV of IMEP), 0-10%burn durations are within 4-8 CAD. In contrast, the 0-10% burn duration is between 7-15 CAD at λ=6 depending on the MAP (Figure 6.3). This rapid initial burn is partially responsible for the low CoV of IMEP values at high λ, since it allows little time for turbulence to shift or affect the central surface of the flame.

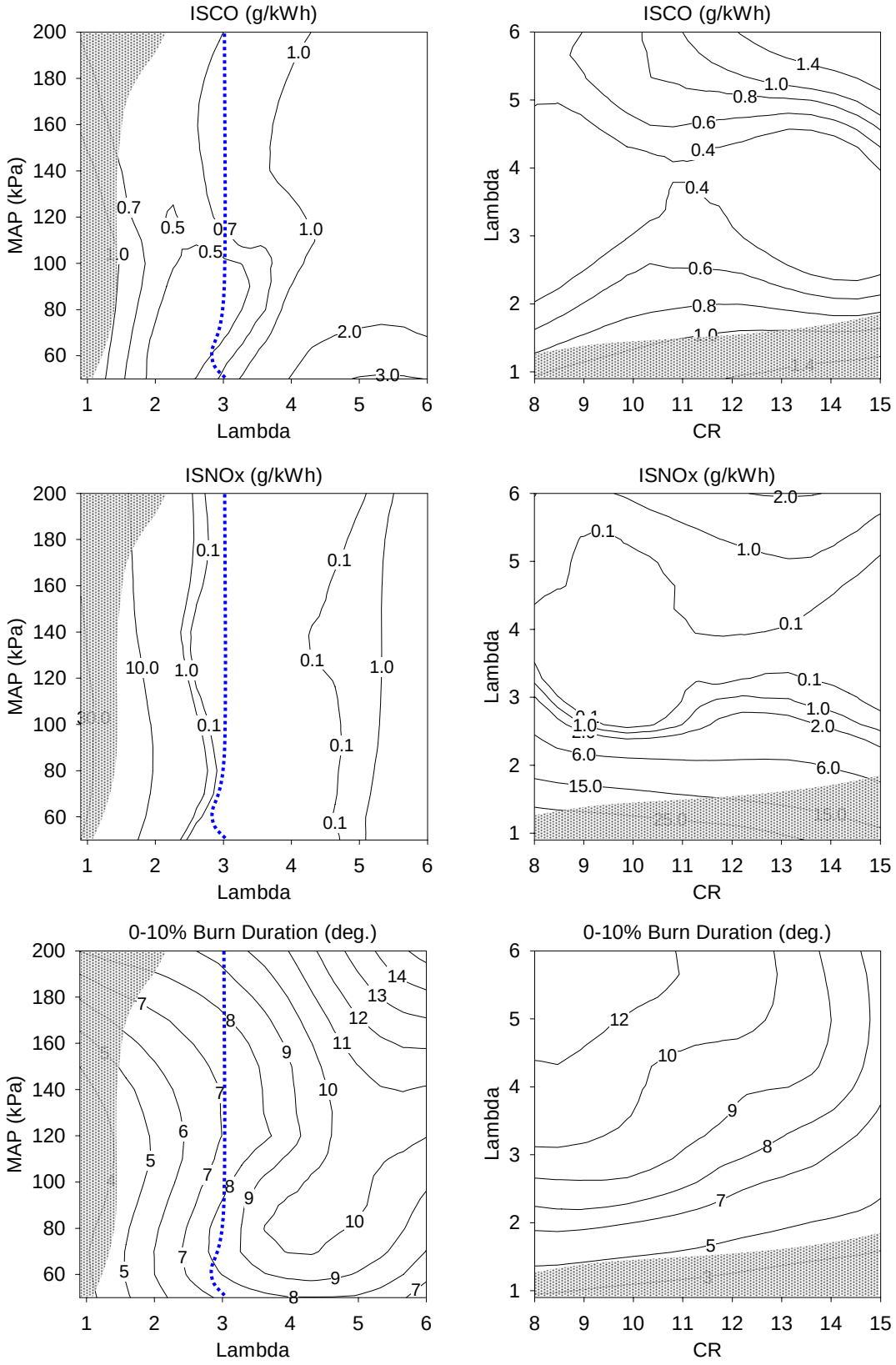

Figure 6.3: HAJI-H_2 - (top) ISCO, (middle) $ISNO_x$, (lower) 0-10% Burn Duration. (1800r/min, MBT, (left) CR=11, (right) MAP=90kPa), dark shaded area indicates backfire limited conditions)

6.4.2 (10-90%) Burn Duration

CR and MAP have little effect on the 10-90% burn duration compared to λ, which clearly determines the speed at which the charge is consumed by the fully matured flame (Figure 6.4). At low λ, the burn duration can be as short as 15 CAD and at high λ it can be as long as 45 CAD, only a 30 CAD difference between a λ=1 and λ=6 mixture. Interestingly, in both HAJI-H_2 and HAJI-G mode, the longest 10-90% burn duration is approximately 45 CAD and occurs where combustion stability deteriorates fast, namely at λ=6 and λ=2.6 respectively.

6.4.3 (0-100%) Burn Duration

The total burn duration is strongly dependent on λ and varies little with CR and MAP (Figure 6.4). Near λ=1, the flame propagates through the entire combustion chamber in less than 20 CAD and at around λ=6 it takes approximately 60 CAD. Along the OPL the total burn duration varies from 40 to 53 CAD, this is approximately 20 CAD less than what is observed in HAJI-G mode (Figure 5.4). This is interesting because in HAJI-H_2 mode this OPL is around λ=3, as opposed to λ=1.9 for HAJI-G. This indicates that for an equivalent MAP and CR at a given λ the reaction rate controlling combustion is higher for HAJI-H_2 than for HAJI-G.

6.4.4 Peak MBR

The speed of combustion is described by the mass burn rate (MBR) and, similar to HAJI-G, for HAJI-H_2 (Figure 6.4) is strongly dependent on λ. Peak MBR for HAJI-H_2 occurs at around λ=1 where up to 10% of the charge is consumed per CAD. This is due to the fact that combustion temperatures are at their maximum and the rate of reaction is therefore maximised. Along the OPL the peak MBR is between 3-4%, similar to HAJI-G mode. However, the 0-100% burn duration of HAJI-H_2 is less than HAJI-G. This indicates that the peak MBR value is not an accurate indicator of the overall burn duration. The reason HAJI-H_2 burns faster than HAJI-G overall is because in HAJI-H_2 mode the 0-10% and 90-100% burn durations are shorter than HAJI-G.

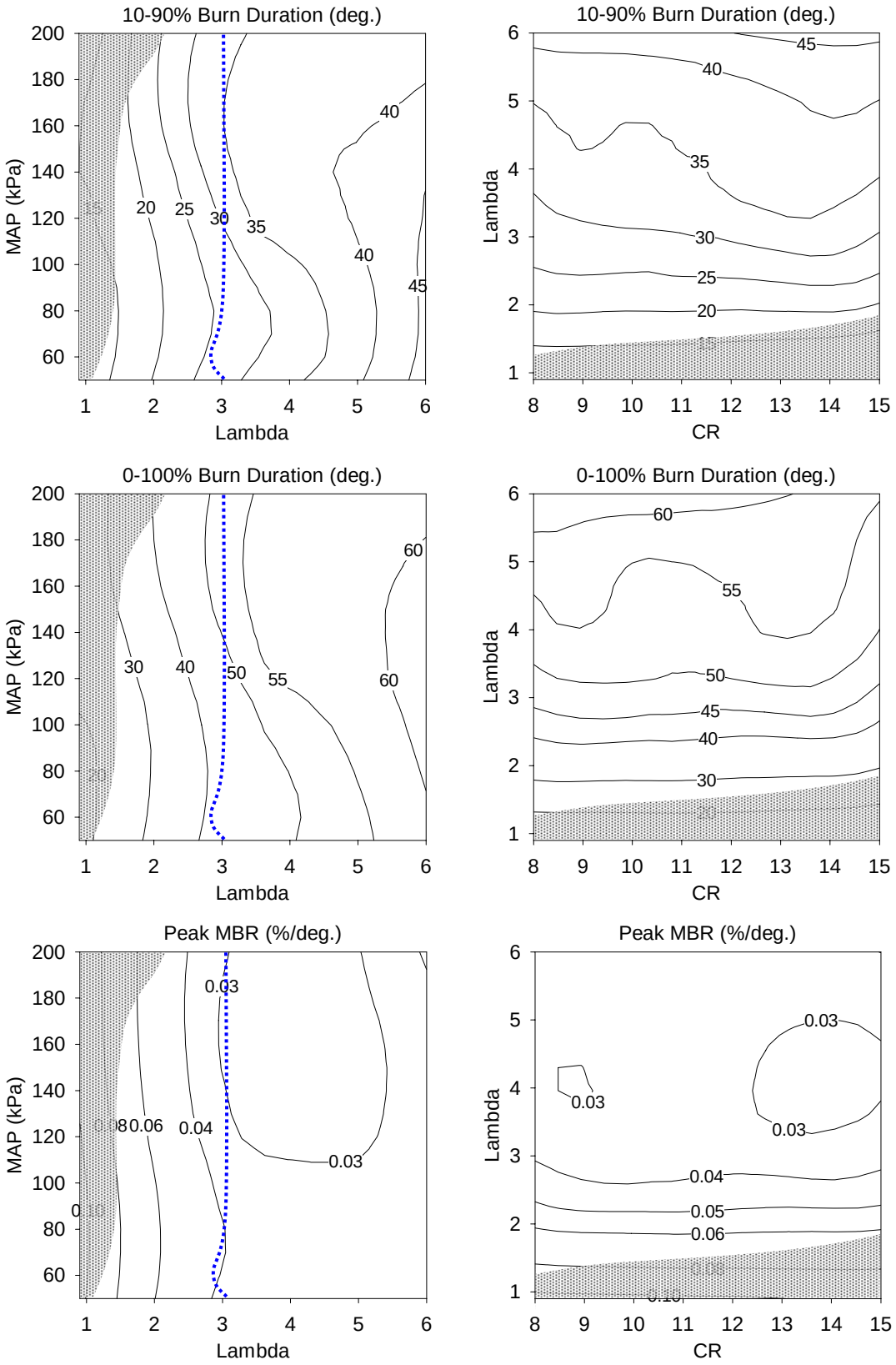

Figure 6.4: HAJI-H_2 - (top) 10-90% Burn Duration, (middle) 0-100% Burn Duration, (lower) Peak MBR. (1800r/min, MBT, (left) CR=11, (right) MAP=90kPa), dark shaded area indicates backfire limited conditions)

6.4.5 Location of Peak MBR

Peak MBR usually occurs when the flame is fully developed and combustion chamber temperature is higher than at the point of ignition. This condition is usually achieved between 50-70% MFB. The location of peak MBR for HAJI-H_2 occurs predominantly after TDC (Figure 6.5) which is similar to HAJI-G (Section 5.4.5). As λ is increased at a given MAP or CR, the location of peak MBR is advanced. In contrast, for any given λ, as CR or MAP is increased, the location of peak MBR is retarded. In fact, at λ=6, the peak MBR occurs before TDC and this is related to the MFB, cylinder temperature and pressure as explained next.

6.4.6 MFB at Peak MBR

Figure 6.5 shows the MFB at peak MBR. As λ is increased at a given CR and MAP, the MFB at peak MBR is decreased. The optimal temperature and pressure favoring peak burn rate occurs at around 50%MFB for high λ conditions. However, at low λ conditions, peak burn rate shifts closer to 65%MFB. This increase in MFB as λ decreases is thought to be the result of retarded spark timing which forces most of the charge to be burned on the expansion stroke. The rapid expansion cools the mixture and therefore more fuel is required to counteract this cooling effect in order to achieve peak MBR. It should be noted that peak MBR can never occur at or close to 100%MFB because of the cooling effects of the cylinder wall. Also, peak MBR cannot occur during the early development of the flame kernel because at that stage the flame enhancement due to turbulence is not present.

6.5 Combustion Characteristics

6.5.1 Peak Pressure

The magnitude of peak pressure (Figure 6.5) increases with increasing CR and MAP. At any given MAP the peak pressure increases up to around λ=3 and then decreases as the mixture is leaned out further. The peak pressures at λ=1, MAP=90 and at λ=3, MAP=170 are of similar order (5Mpa), however, the IMEP is about 100kPa higher and the NO_x is reduced from 30g/kWh to 0.1g/kWh at λ=3.

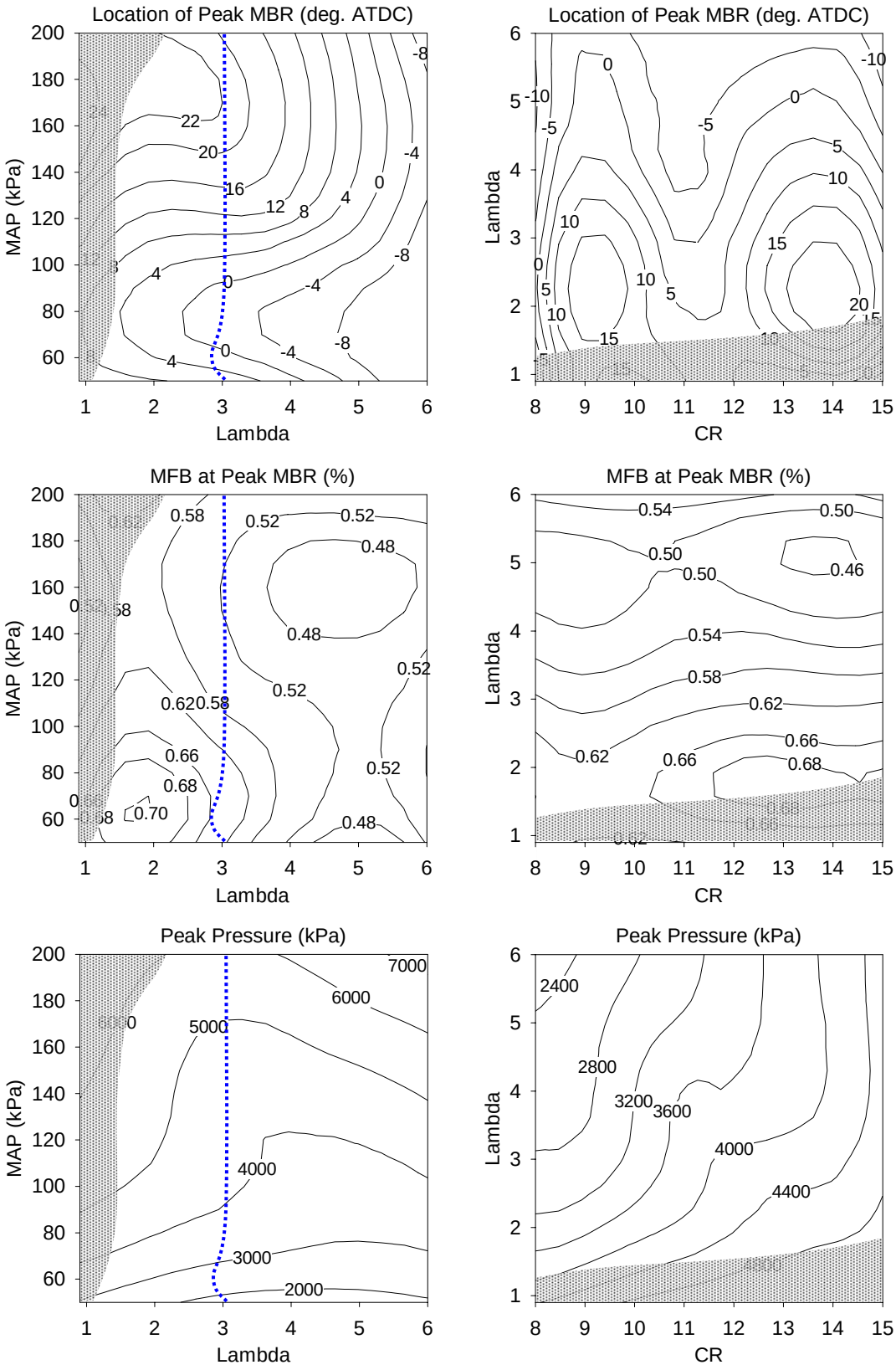

Figure 6.5: HAJI-H_2 - (top) Location of Peak MBR, (middle) MFB at Peak MBR, (lower) Peak Pressure. (1800r/min, MBT, (left) CR=11, (right) MAP=90kPa), dark shaded area indicates backfire limited conditions)

This result further validates the knowledge that pressure does not significantly effect NO_x formation.

6.5.2 Location of Peak Pressure

The location of peak pressure shown in Figure 6.6 varies from approximately 2 to 15 CAD ATDC at any given λ, which is closer to TDC than HAJI-G mode. Ideally, as per the Otto cycle, MBT and peak pressure should occur at TDC with minimum burn duration. In reality it is not possible due to the onset of knock and the slow burning of the fuel. In HAJI-H_2 mode the burn duration is short at low λ values, and, unlike HAJI-G, MBT did not have to be retarded by much to avoid backfire. Consequently, the location of peak pressure occurs close to TDC. At high λ the burn duration is longer so the spark timing must be advanced to obtain MBT. Consequently, 50% of the charge is already burnt at close to TDC. The location of peak pressure occurs at almost TDC since there is not enough energy available in the remaining charge to counteract the reduction in pressure from expansion.

6.5.3 Peak *dp/dθ*

The rate of pressure rise (*dp/dθ*) is an indicator of how fast combustion occurs. In HAJI-H_2 mode it is up to 200kPa/deg (Figure 6.6). This is expected as HAJI-H_2 mode shows high MBR and short burn duration. *dp/dθ* at low λ conditions is dominated by combustion energy release as close to TDC the contributions from the piston motion is minimal. At high λ, MBR decreases and consequently MBT becomes advanced. In these cases, *dp/dθ* is affected both by compression and combustion. Despite the additional affect of decreasing volume, the rate of pressure rise is still lower than at low λ.

6.5.4 Location of Peak *dp/dθ*

The location of *dp/dθ* depends on whether the pressure rise is compression or combustion dominated. At low λ conditions, peak pressure occurs before TDC, where MBT is retarded. As a consequence, combustion becomes mainly

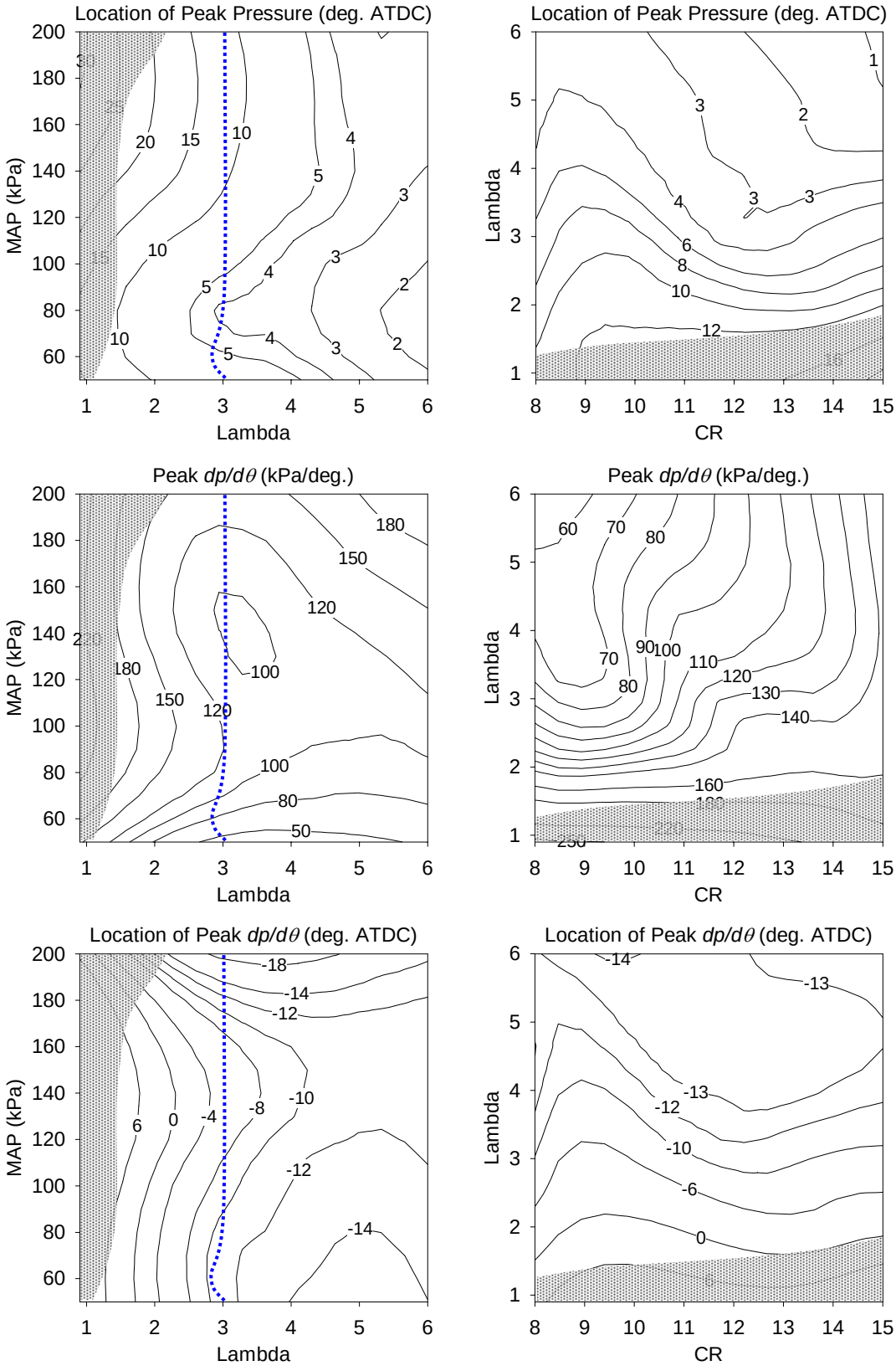

Figure 6.6: HAJI-H_2 - (top) Location of Peak Pressure, (middle) Peak Rate of Pressure Rise, (lower) Location of Peak *dp/dθ*. (1800r/min, MBT, (left) CR=11, (right) MAP=90kPa), dark shaded area indicates backfire limited conditions)

compression dominated, therefore, $dp/d\theta$ occurs before TDC. When $\lambda<2$ the cycle becomes backfire limited and MBT is retarded, hence $dp/d\theta$ occurs after TDC.

6.5.5 Peak Temperature

Combustion temperature (Figure 6.7) is mainly a function of λ, and it is unaffected by CR or MAP. The peak combustion temperature varies from 1400K to 2700K. Along the OPL, the temperature is about 1800K, which is primarily responsible for the reduction of NO_x from 30g/kWh (at $\lambda=1$) to 0.1g/kWh (at $\lambda=3$) (Figure 6.3). The insensitivity of combustion temperature to MAP is the mechanism which allows the engine to be boosted while maintaining almost zero NO_x.

6.5.6 Location of Peak Temperature

As shown in Figure 6.7, the location of peak temperature occurs near TDC for most cases and up to 33 CAD after MBT. However, when MBT occurs at or after TDC, the location of peak temperature corresponds to the location of MBT. This means that the initial flame kernel is the hottest and the average burned zone temperature declines from that point on. This happens because the burned zone is expanding rapidly while it is increasing in mass, consequently, the exothermic reaction is not able to generate enough heat to compensate for this growth in mass and size.

6.5.7 Peak Flame Speed

The location of peak flame speed (Figure 6.7) is dependent on CR, MAP and λ. High flame speeds occur in both $\lambda=1$ and $\lambda=6$ mixtures. Flame speed is influenced by density, MBR and flame surface area, hence, for a given λ, peak flame speed increases as the CR increases. However, flame speed drops as MAP is increased. This is because high pressures actually have the tendency to lower flame speeds. High flame speeds are also observed at high λ values early in the compression stroke near MBT. Here, the flame's surface is small and cylinder pressures are low, both of which have the tendency to increase flame speed.

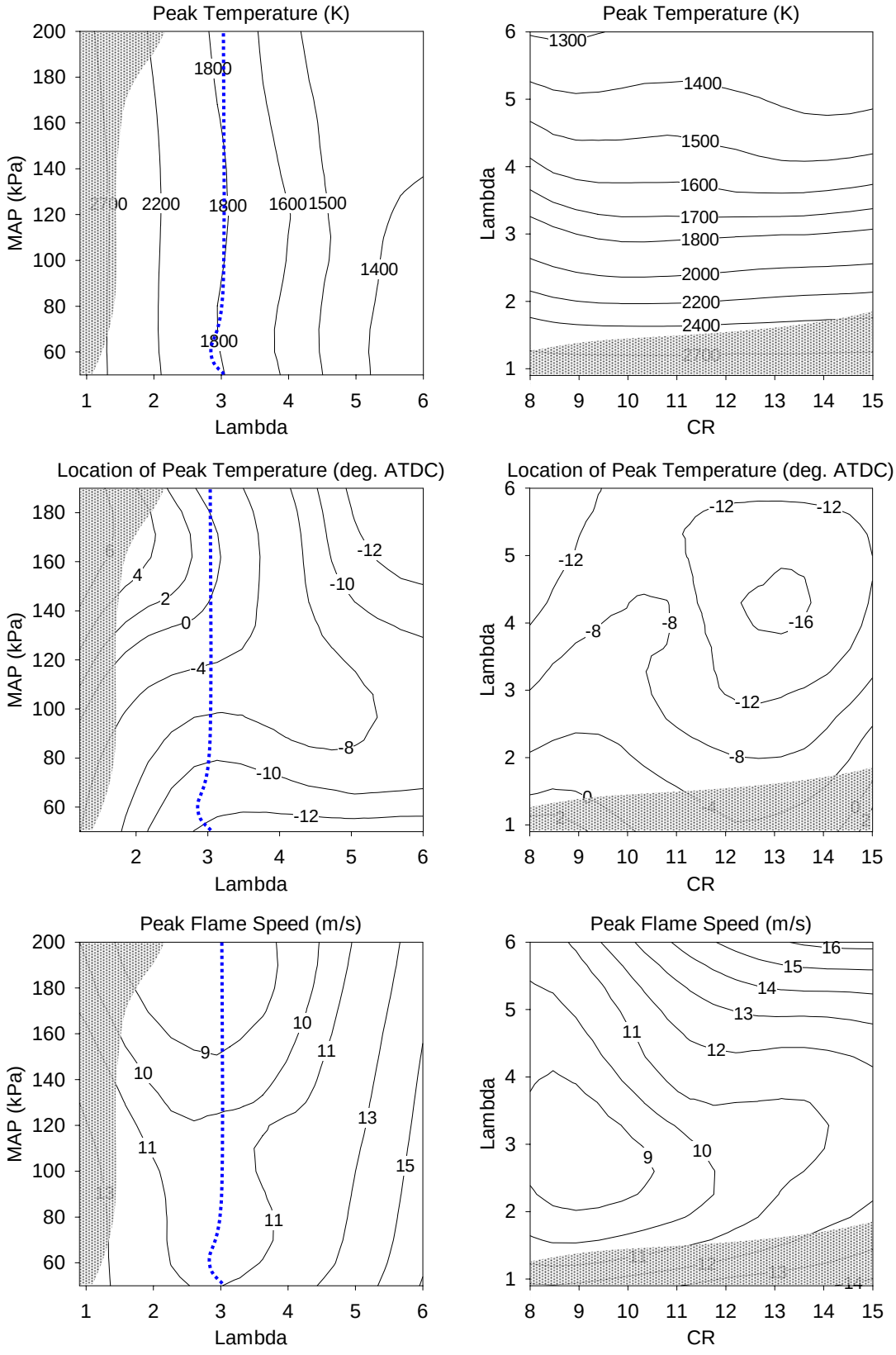

Figure 6.7: HAJI-H_2 - (top) Peak Temperature, (middle) Location of Peak Temperature, (lower) Peak Flame Speed. (1800r/min, MBT, (left) CR=11, (right) MAP=90kPa), dark shaded area indicates backfire limited conditions)

6.5.8 Location of Peak Flame Speed

The location of peak flame speed in λ=1 mixtures occurs up to 15 CAD after MBT (Figure 6.8). Since the mixture is backfire limited and MBT occurs close to TDC, the initial flame kernel does not have the capacity to release enough energy to counteract the expanding volume. Peak flame speed therefore occurs later in the fully developed flame. At high λ, the peak flame speed position occurs close to MBT. This is expected since lean mixtures, unlike λ=1 mixtures, are unable to counteract the expanding volume and therefore the optimum conditions for peak flame speeds occur near MBT. This is due to the fact that the flame kernel has a small surface area, cylinder pressures are low, and that the volume is becoming smaller since it is on the compression stroke.

6.6 Jet Knock

6.6.1 Knock Intensity - KI30

Over 30 CAD, the knock intensity factor (KI30) describes the intensity of pressure oscillation. The knock intensity of HAJI-H_2 mode (Figure 6.8) varies between 200-10000 depending on the cylinder pressure and temperature and increases with increasing MAP, CR and λ. Along the OPL, similar to HAJI-G at high loads, KI<4000, however at moderate loads KI<1000. Overall the magnitude of KI varies by a factor of 50, which is similar to the variation observed in HAJI-G mode.

6.6.2 Peak Knock Amplitude

The Jet Knock amplitude for HAJI-H_2 varies between 40-300kPa depending on λ, CR and MAP (Figure 6.8). As CR or MAP is increased at any given λ, the peak knock amplitude increases. This happens as the spark timing is retarded, which increases the density of the charge. When the jet penetrates into a dense charge it establishes a pressure wave with a larger energy density on the surface. Consequently the magnitude of Jet Knock increases. Furthermore, the momentum of the jet is somewhat greater due to the larger energy release in the prechamber due to higher density at retarded MBT. Along the OPL the magnitude of Jet Knock

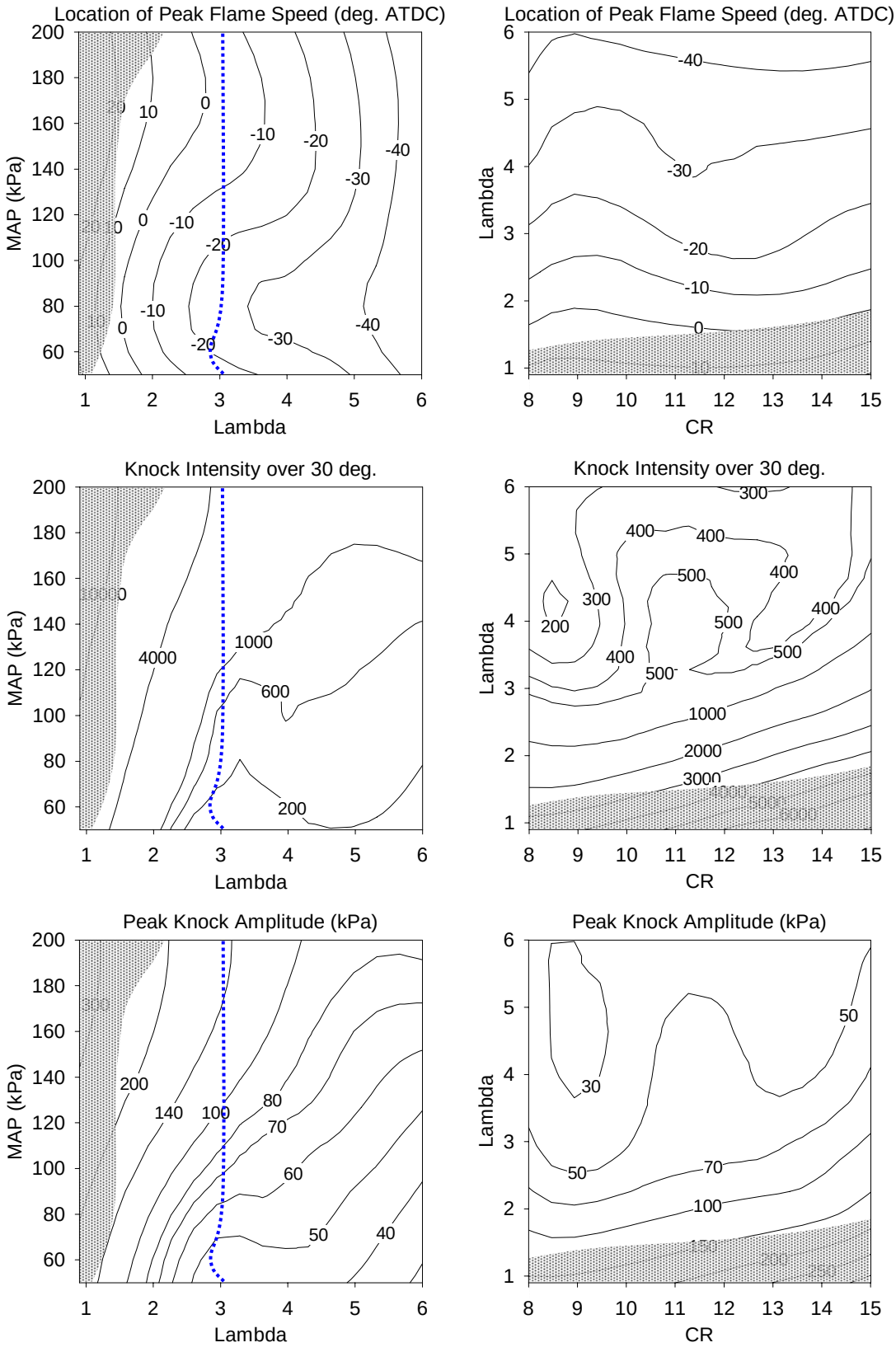

Figure 6.8: HAJI-H_2 - (top) Location of Peak Flame Speed, (middle) Knock Intensity (30°), (lower) Peak Knock Amplitude. (1800r/min, MBT, (left) CR=11, (right) MAP=90kPa), dark shaded area indicates backfire limited conditions)

varies from 50 to 140kPa, which is quite small considering heavy knock is around 850kPa.

6.6.3 Location of Peak Knock

Interestingly, in HAJI-G mode the locations of peak knock occurs at ~30-40 CAD after MBT, whereas in HAJI-H_2 mode, it occurs at ~20 CAD after MBT (Figure 6.9). This is attributed to the shorter burn duration in HAJI-H_2 mode. Along the OPL the location of peak knock varies from 10° BTDC to 5° ATDC. Similar to HAJI-G mode the location of peak knock occurs before peak pressure and peak MBR, and close to peak *dp/dθ*. This means that the location of peak knock amplitude is strongly governed by the location of peak pressure rise.

6.6.4 Knock Delay

Similar to HAJI-G mode, the start of knocking is defined when the in-cylinder pressure oscillation equals or exceeds 20kPa. In HAJI-H_2, knock delay (Figure 6.9) is relatively insensitive to MAP, decreasing with increasing CR and λ. Jet Knock in HAJI-H_2 mode was detected ~4-10 CAD after MBT, which is less than in HAJI-G mode. In general, it was expected since the initial burn duration of HAJI-H_2 is less than HAJI-G. Along the OPL, the knock delay in HAJI-H_2 mode is between 4.5-6 CAD after MBT, which is inline with the theory that the pressure wave (shock wave) is generated as the jet exits the pre-chamber.

6.6.5 Pressure at Peak Knock

The pressure at peak knock is a function of CR, MAP and λ. Because peak knock occurs before peak pressure, the magnitude of pressure at peak knock (Figure 6.9) is as much as 1000 kPa less than peak cylinder pressure (Figure 6.5). The pressure at peak knock increases with increasing MAP and CR and decreases with increasing λ. Since the location of peak pressure is closely related to the location of peak knock, the pressure at peak knock has similar behavior to peak pressure as CR, MAP and λ are varied. Along the OPL the pressure at peak knock varies from 1.5MPa to 5MPa, which is expected since the MAP varies from 50 to 200kPa.

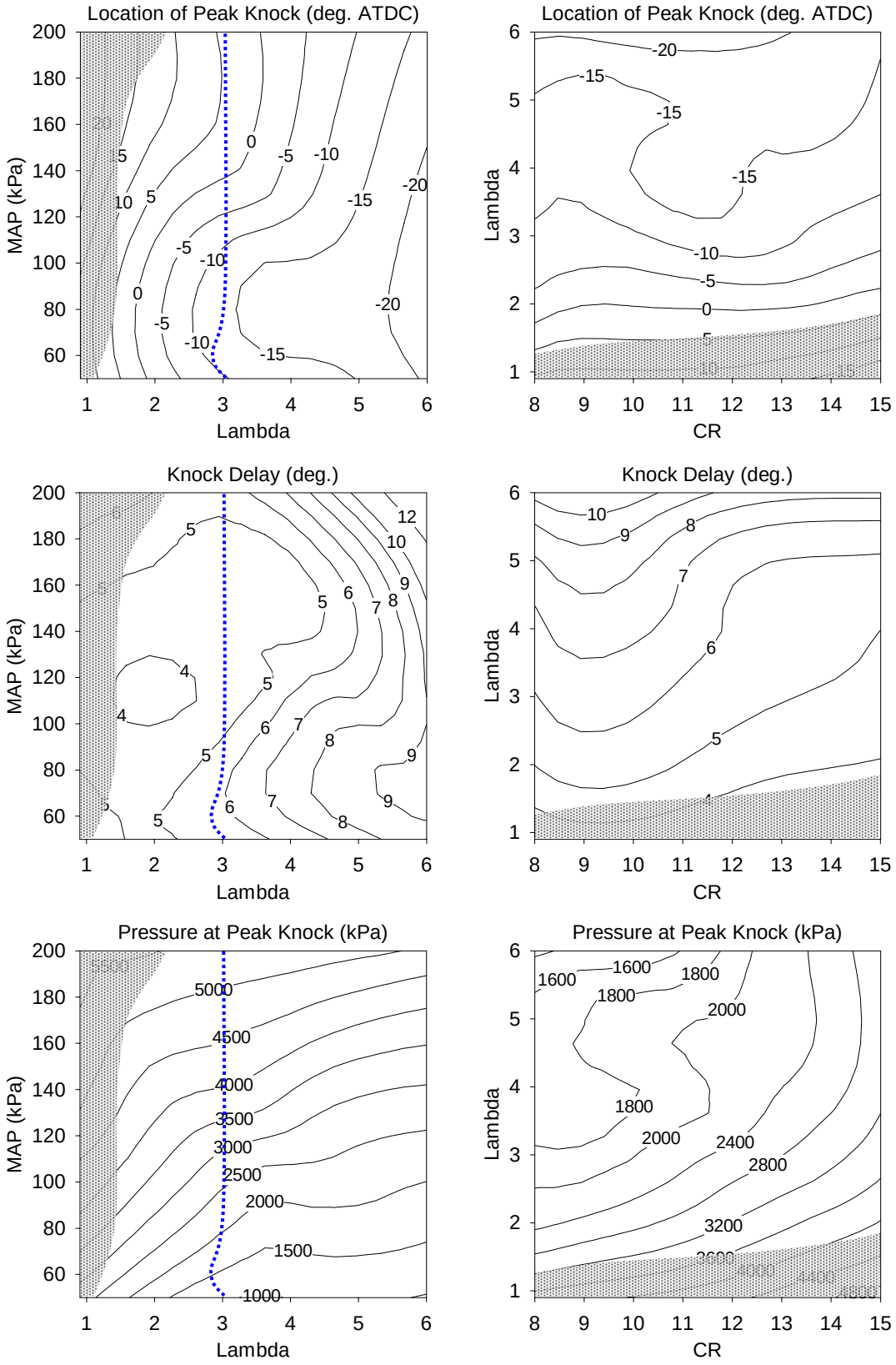

Figure 6.9: HAJI-H_2 - (top) Peak Knock Amplitude, (middle) Location of Peak Knock, (lower) Knock Delay. (1800r/min, MBT, (left) CR=11, (right) MAP=90kPa), dark shaded area indicates backfire limited conditions)

6.6.6 Knock Duration

The knock duration in HAJI-H_2 mode is complex (Figure 6.10) and two minima can be observed on the CR vs. λ plot. The first minima occurs at around CR=9 and the other at around CR=14 with peaks occurring at CR=8, 11, and 15. In general, at any given CR, knock duration is insensitive to λ and at any given MAP it varies little with λ. Increasing MAP at a given λ increases the knock duration from 30 to 50 CAD, which also corresponds to the variation observed along the OPL. In HAJI-H_2 mode, increasing MAP by 4 times doubles the knock duration, whereas in HAJI-G mode, the knock duration doubles with only a 3 fold increase in MAP.

6.7 Combustion Characteristics @50% MFB

6.7.1 @50%MFB - Crank Angle (CA)

As in HAJI-G mode, the combustion characteristics of HAJI-H_2 mode are monitored at the 50%MFB point, since a lot can be learnt about the behavior of HAJI at different CR, MAP and λ conditions. The position of the 50%MFB point advances with increasing λ. At low λ values, as MAP or CR increases, the position of the 50%MFB point becomes retarded (Figure 6.10).

6.7.2 @50%MFB - Laminar Flame Speed (S_L for H_2)

The empirical approximation of laminar flame speeds developed in Section 3.6.1 is valid to 5cm/s for hydrogen. Figure 6.10 shows S_L for hydrogen in HAJI-H_2 mode. The area below 5cm/s should be treated with caution as no theory or data is available in the literature to explain these conditions. At any given λ, the magnitude of S_L is relatively insensitive to CR and varies little with MAP. As λ increases at any given CR or MAP, the magnitude of S_L drops by a factor of 80. Along the OPL at MAP>90kPa, the calculated S_L<0.05m/s, which is unrealistically low since the mixture is actually burning at these ultra lean AFRs. Hence, the actual values of S_L are unreliable for HAJI ultra-lean mixture combustion.

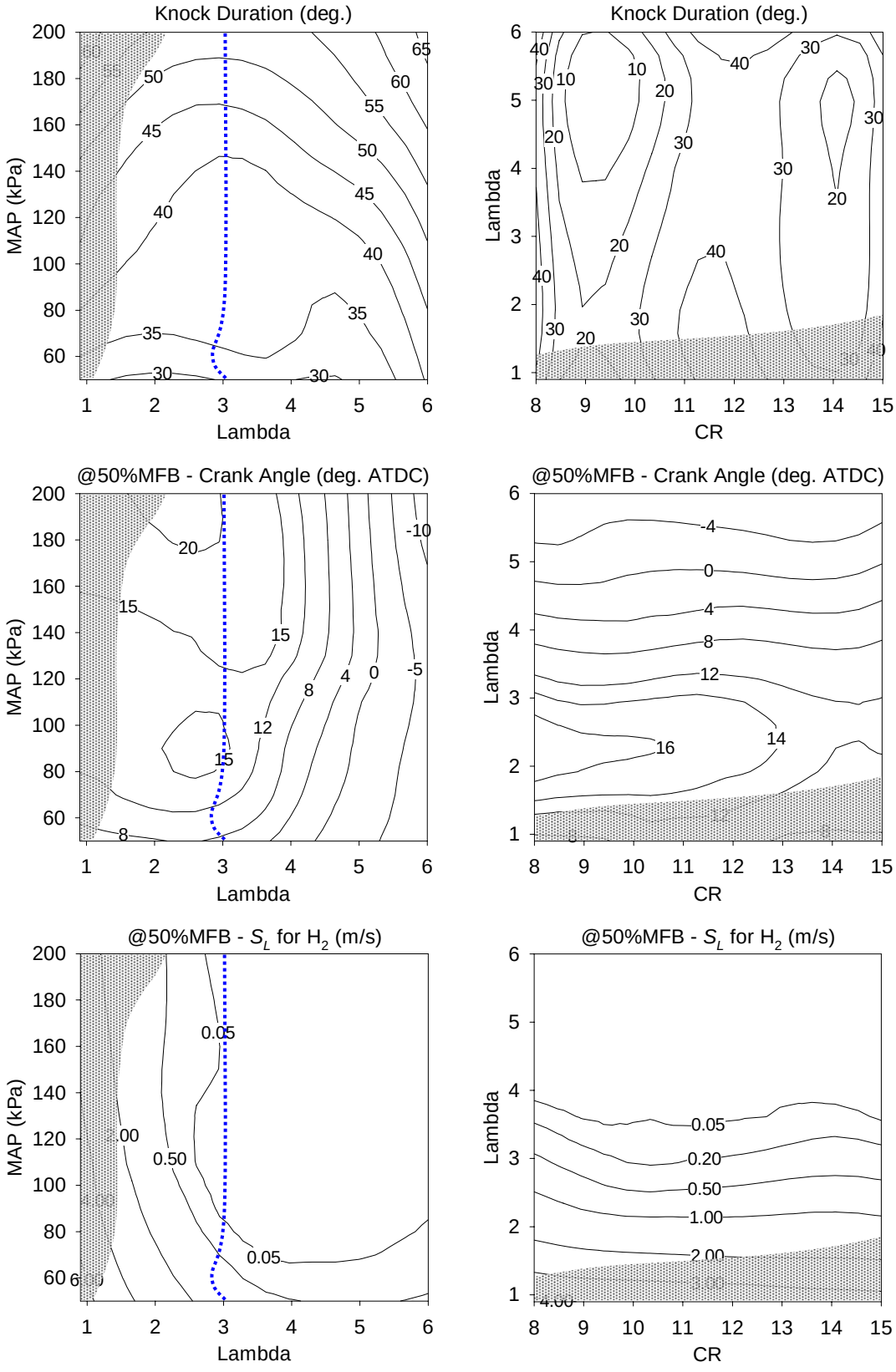

Figure 6.10: HAJI-H_2 - (top) Knock Duration, (middle) @50%MFB - Crank Angle, (lower) @50%MFB - S_L for H_2. (1800r/min, MBT, (left) CR=11, (right) MAP=90kPa), dark shaded area indicates backfire limited conditions)

6.7.3 @50%MFB - Turbulent Flame Speed ($S_{T,a}$)

$S_{T,a}$ in HAJI-H_2 mode (Figure 6.11) varies between 5 to 12m/s, which is only a 2.5 fold difference between λ=1 and λ=6. Interestingly, and in contrast to $S_{T,a}$, S_L changes by a factor of 80 under similar conditions. Overall $S_{T,a}$ is relatively insensitive to CR and MAP and therefore mainly influenced by λ. As λ increases at any given CR or MAP, the magnitude of $S_{T,a}$ decreases, which is expected as S_L decreases and burn duration increases. Along the OPL, $S_{T,a}$ is approximately 6m/s, which is quite fast considering the mixture is at $\lambda \approx 3$.

6.7.4 @50%MFB - Flame Speed Ratio (FSR_a)

The FSR_a (Figure 6.11) shows the difference between $S_{T,a}$ and S_L. FSR_a varies relatively little with CR and MAP and is primarily a function of λ. This is due to the dramatic decrease in S_L at high λ conditions. Values of FSR_a>100 should be ignored as S_L values are unreliable in that range. At low MAP along the OPL line, the FSR_a is initially around 6 but when MAP exceeds 90kPa, the magnitude of the FSR_a exceeds 100. It is worth noting that according to the Damkohler relationship, when FSR=100 the turbulent flame surface area is 100 times larger than the smooth laminar flame area. This would indicate an extraordinarily wrinkled turbulent flame in the combustion chamber, which is very unlikely in the presence of low turbulence intensity. Hence, this indicates that the chemical effects of HAJI are playing a dominant role.

6.7.5 @50%MFB - Turbulence Intensity (u')

Turbulence intensity is a function of CR and MAP. In HAJI-H_2 mode at any given λ, u' increase as CR or MAP is increased (Figure 6.11). This is predominantly driven by an increase in combustion pressures at 50%MFB. In contrast, as λ increases at any given CR or MAP the magnitude of u' decreases, which is driven by a decrease in combustion pressures. Along the OPL, u' varies from 3.2m/s to 4.6m/s. Interestingly, at high CR, as λ increases u' decreases, which is the opposite to what happens in HAJI-G mode. Turbulence intensity is determined by the rapid distortion theory and therefore u' decreases in HAJI-H_2 mode because combustion

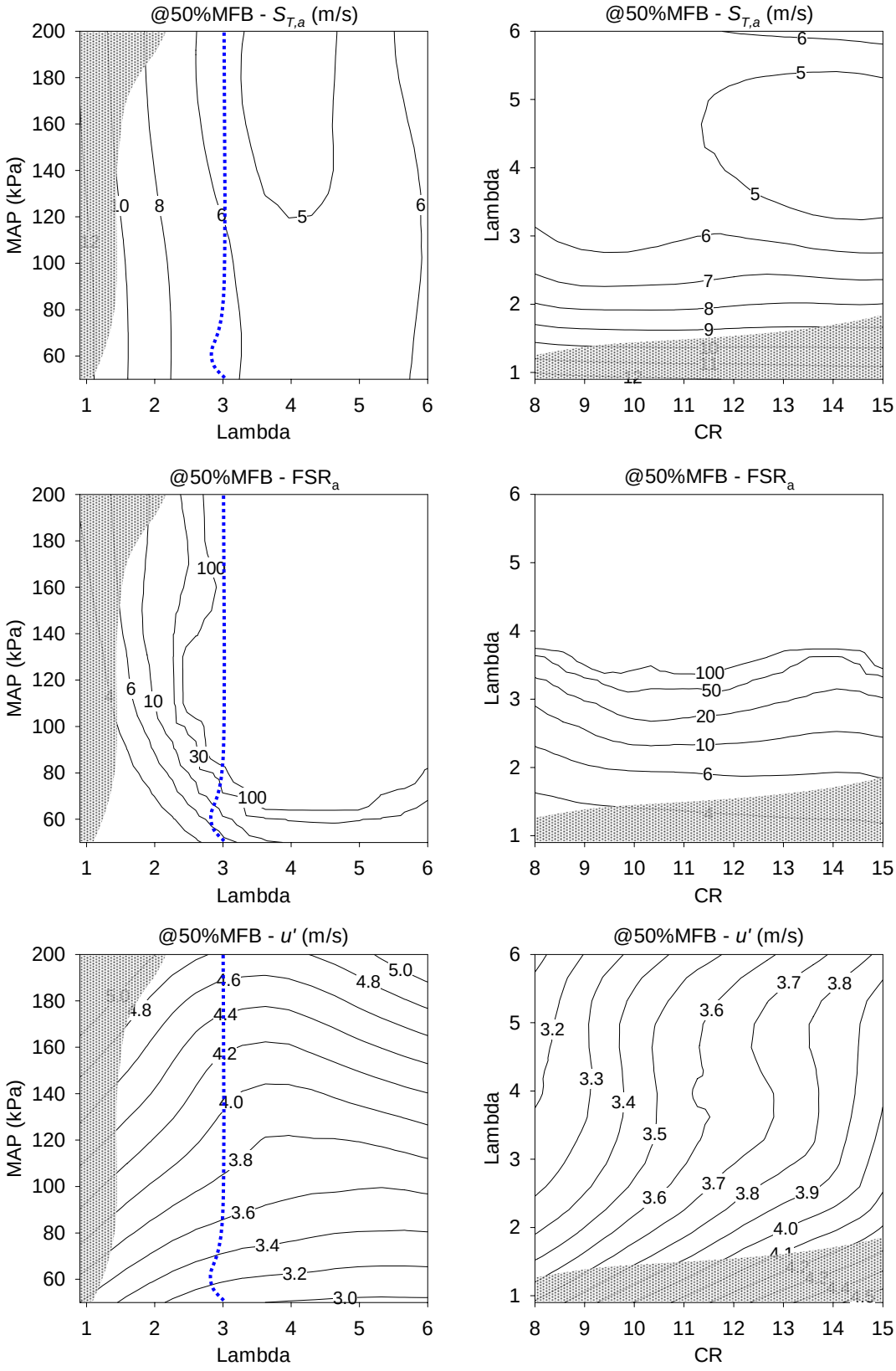

Figure 6.11: HAJI-H_2 - (top) @50%MFB - $S_{T,a}$, (middle) @50%MFB - $FSR_{a,}$ (lower) @50%MFB - u'. (1800r/min, MBT, (left) CR=11, (right) MAP=90kPa), dark shaded area indicates backfire limited conditions)

pressures at 50%MFB gradually decrease as λ increases whereas with HAJI-G, *u'* increases because combustion pressures increase as λ increases.

6.7.6 @50%MFB - u'/S_L for H_2

The u'/S_L with HAJI-H_2 is only slightly affected by CR and MAP at any given λ (Figure 6.12) but is strongly affected by λ itself. Since the magnitude of *u'* varies little, the effect of S_L controls the trend of u'/S_L on the CR vs. λ and λ vs. MAP plots. Generally, when λ<2 the magnitude of u'/S_L<6 and when λ>3, depending on MAP, u'/S_L>80. Along the OPL u'/S_L varies from 3 to >80. The behavior of HAJI-H_2 is very similar to HAJI-G mode in the sense that it is strongly controlled by λ and that there are regions on the CR vs. λ and λ vs. MAP plots where the u'/S_L values are unknown due to the lack of knowledge about S_L. As mentioned before, high u'/S_L values indicate that the flame surface is severely distorted by turbulence, which in lean mixtures is advantageous because it increases the turbulent flame speeds.

6.7.7 @50%MFB - Damkohler Number (*Da*)

The Damkohler number varies relatively little with CR and MAP (Figure 6.12). However, as λ increases, *Da* decreases dramatically, varying from 100 to 6000 as compared to 100 to 600 for HAJI-G. The higher *Da* values in HAJI-H_2 mode are due to the higher S_L and smaller flame thickness. At high *Da* values the combustion process is chemically dominated and the turbulence is less likely to influence the flame propagation. In contrast, low *Da* values occurring at high λ, indicate that the jet is vulnerable to distortion through turbulence.

6.7.8 @50%MFB - Turbulent Reynolds Number (Re_T)

At high λ values it is advantageous to have high Re_T as it enhances flame speed. The behavior of Re_T in HAJI-H_2 mode (Figure 6.12) is similar to HAJI-G mode. At a given λ, Re_T increases little as CR increases due to a decrease in the size of integral length scale. For any given λ, as MAP increases, Re_T increases due to an increase in *u'* and decrease in kinematic viscosity. For any given CR as λ increases,

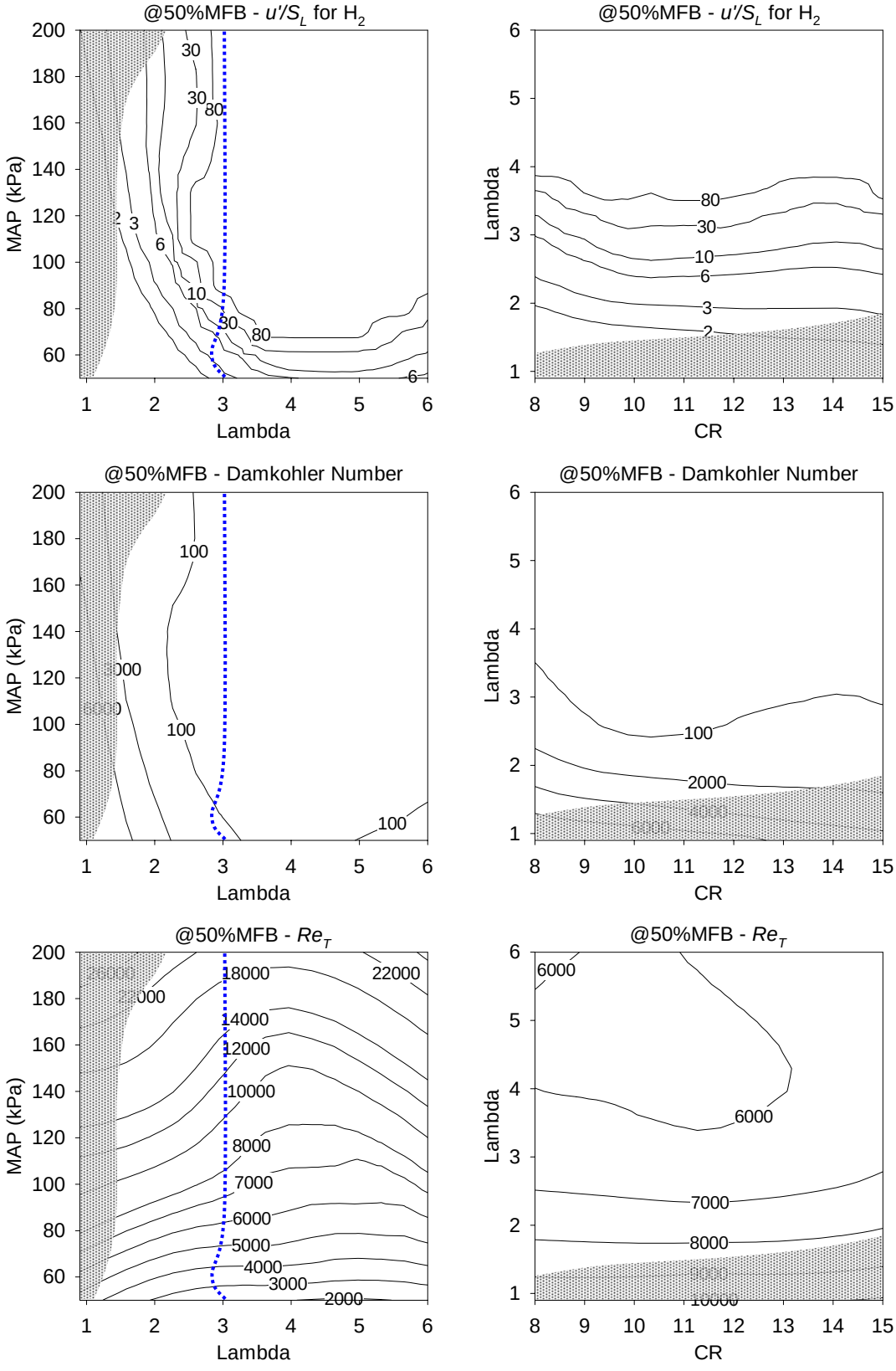

Figure 6.12: HAJI-H_2 - (top) @50%MFB - u'/S_L for H_2, (middle) @50%MFB - Damkohler Number, (lower) @50%MFB - Re Turbulent. (1800r/min, MBT, (left) CR=11, (right) MAP=90kPa), dark shaded area indicates backfire limited conditions)

Re_T decreases and this is predominantly due to the decrease in u'. Along the optimum operating line Re_T varies from 3000 to 20000 depending on MAP.

6.7.9 @50%MFB - Flame Radius (normalised)

The distance propagated by the flame varies little with CR and MAP (Figure 6.13) but varies from 62% to 74% throughout the λ range. Since the normalised flame radius depends on the density ratio between the unburned and burned gases, at low λ, values the flame position is closer to 74%. At high λ values, the unburned to burned gas density ratio is low therefore the flame position is at 62% of the normalised flame radius. The flame position should be as low as possible as it reduces the contact area between the burned gas and cylinder walls therefore reducing heat transfer.

6.7.10 @50%MFB - Burned Combustion Temperature

The actual effects of MAP, CR and λ on combustion temperatures at 50%MFB (Figure 6.13) are the same as described for peak temperature. The burned combustion temperatures at 50%MFB are lower than the peak temperatures by 100°K at high λ values and lower by 200°K at low λ values. This is a reasonable observation since at high λ values the mixture is subjected to longer post combustion compression due to more advanced ignition timing relative to λ=1.

6.8 Summary

The results presented in this chapter are novel to this thesis. For the first time the CFR engine was fitted with a HAJI unit and fueled with hydrogen alone. A large body of data was collected and processed to explore the performance, emissions and combustion characteristics of HAJI-H_2. This was achieved using two types of contour plots: CR vs. λ at MAP=90kPa and λ vs. MAP at CR=11. The CR vs. λ contour plots at MAP=90kPa and 1800 r/min provide a comprehensive analysis from CR=8 to CR=15, which is consistent with the data presentation format of Chapter 5. These plots were used to identify the optimum CR of 11 for HAJI-H_2

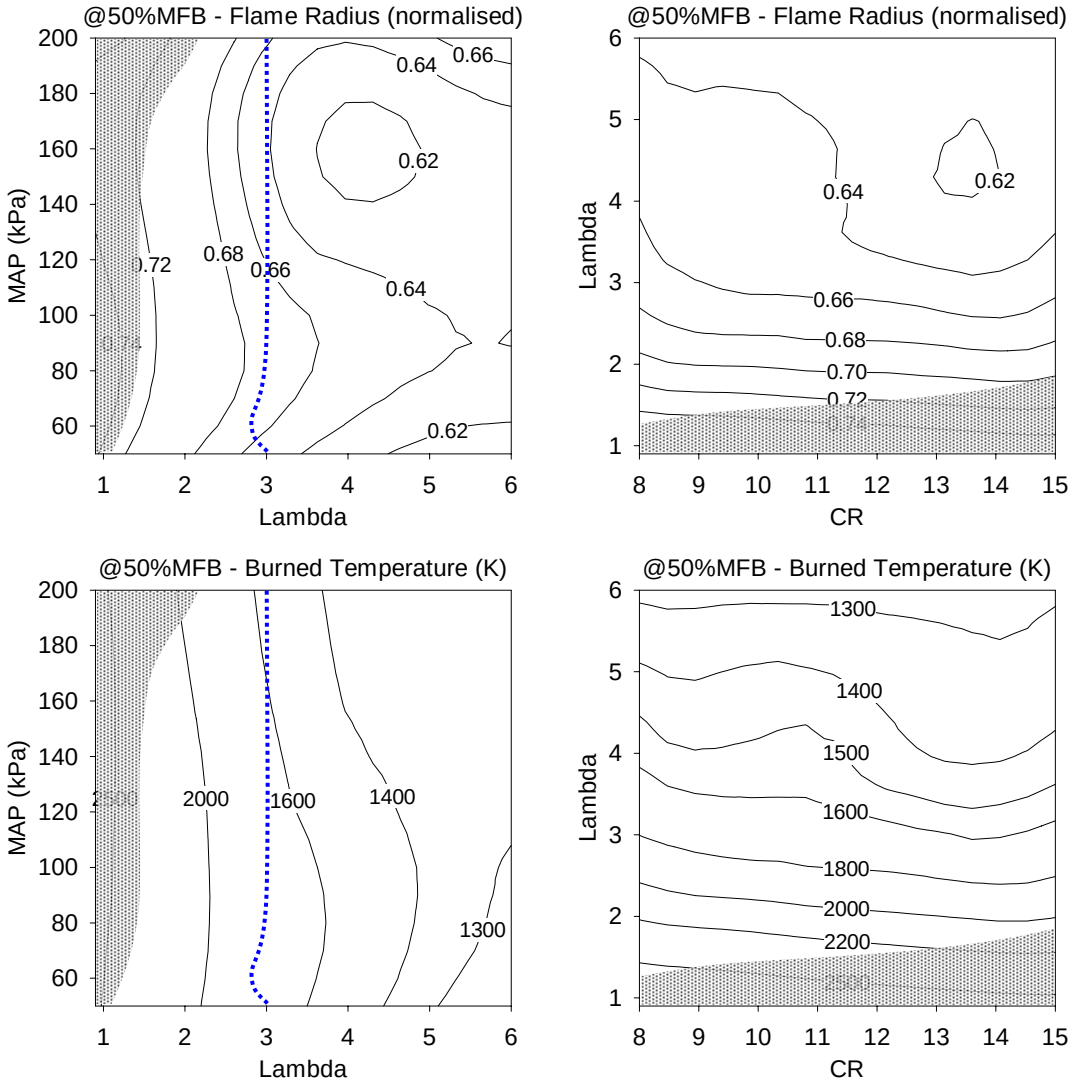

Figure 6.13: HAJI-H_2 - (top) @50%MFB - Flame Radius (normalised), (lower) @50%MFB - Burned Temperature. (1800r/min, MBT, (left) CR=11, (right) MAP=90kPa), dark shaded area indicates backfire limited conditions)

operation (same as HAJI-G) where performance, efficiency and emissions results are best balanced.

The λ vs. MAP contour plots at CR=11 operating at 1800r/min clearly demonstrated the ability of HAJI-H_2 to operate up to λ=6 from MAP=50kPa to MAP=200kPa.

In this chapter a wide range of data was explored to identify the limiting CR, MAP, and λ conditions where near zero NO_x, high combustion stability and high thermal

Table 6.2 HAJI-H_2 outputs and characteristics at OPL.

Engine Speed (r/min)	1800	Peak MBR (%/deg)	0.03-0.04
Compression Ratio	11	Peak Pressure (kPa)	2000-5800
Lambda	2.8-3.0	Peak dp/dθ (kPa/deg)	50-140
MBT (°BTDC)	5-20	Peak Temperature (K)	1800
IMEP (kPa)	100-850	Peak Flame Speed (m/s)	8.5-11.0
CoV of IMEP (%)	1.9-3.0	Peak Knock Amplitude (kPa)	50-140
Thermal Efficiency (%)	20-39	Knock Delay (°)	4.5-5.8
%H_2 of Total Fuel Energy	-	@50%MFB - S_L (m/s)	<0.05-1.50
ISHC (g/kWh)	0.8-1.8	@50%MFB - $S_{T,a}$ (m/s)	5.2-6.8
ISCO (g/kWh)	0.4-0.8	@50%MFB - FSR_a	6->100
$ISNO_x$ (g/kWh)	0.1	@50%MFB - u' (m/s)	3.1-4.7
(0-10%) Burn Duration	7-9.5	@50%MFB - u'/S_L	3->80
(10-90%) Burn Duration	25-35	@50%MFB - Da	<100-200
(0-100%) Burn Duration	40-53	@50%MFB - Re_T	3000-19000

efficiency are simultaneously realised. CR=11 and λ≈3 was shown to be the optimum operating point at which NO_x≈0.1g/kWh and CoV of IMEP<3%. These results can be achieved at all load conditions by varying MAP from 50kPa to 200kPa. The specific performance, emissions and combustion characteristics throughout the optimum operating points are summarised in Table 6.2.

CHAPTER 7
Parametric Studies

7.1 Introduction

Chapter 5 and 6 detailed the most significant experimental and diagnostic results of this project. Significant overall knowledge was obtained about the performance, emissions and the combustion characteristics of a HAJI equipped CFR engine operating in both gasoline and hydrogen modes at optimal calibration settings for spark timing, CR, and H_2 quantity. This chapter aims to examine these and other parameters in further detail to better understand how key parameters effect HAJI performance.

This chapter begins by examining the effect of nozzle length, pre-chamber H_2 quantity and engine speed on HAJI performance. Furthermore, the effects of spark timing, compression ratio and λ are examined in HAJI mode and compared to the baseline SI engine. The results of this chapter are based on data points taken at engine conditions described in Table 4.2.

Jet Knock phenomenon is re-visited for both HAJI and SI engines in the presence and absence of main chamber fuel. Lastly, the chapter concludes with a brief discussion and summary of key findings.

7.2 Parametric Studies of HAJI

7.2.1 Effect of Pre-chamber Orifice Length

The orifice length of a single nozzle pre-chamber received little attention in previous work as a design parameter and thus it was revisited in this project through quantitative analysis. Four different lengths were tested: 1.5, 3, 6 and 12mm. The following is a summary of the effect of orifice length on performance and emissions.

Combustion Stability

A 1.5mm orifice length provides stable combustion (CoV of IMEP<5%) up to around λ=1.8, whereas the 3, 6 and 12mm lengths are stable up to λ=2.1 (Figure 7.1). Overall, the 3mm orifice length provides the most stable combustion when λ>2.1. In HAJI-G mode, the optimum λ is around 1.9, which was shown by the optimum performance line in Chapter 5. This means that orifice lengths of 3, 6 and 12mm could satisfy the combustion stability requirements. Furthermore, an orifice length of 12mm may allow for a much more compact nozzle and therefore considerable packaging advantages in the cylinder head.

Thermal Efficiency

While the 1.5mm orifice believed to ignite the main chamber mixture near the exit of the orifice of the pre-chamber, it is thought that a 12mm orifice length

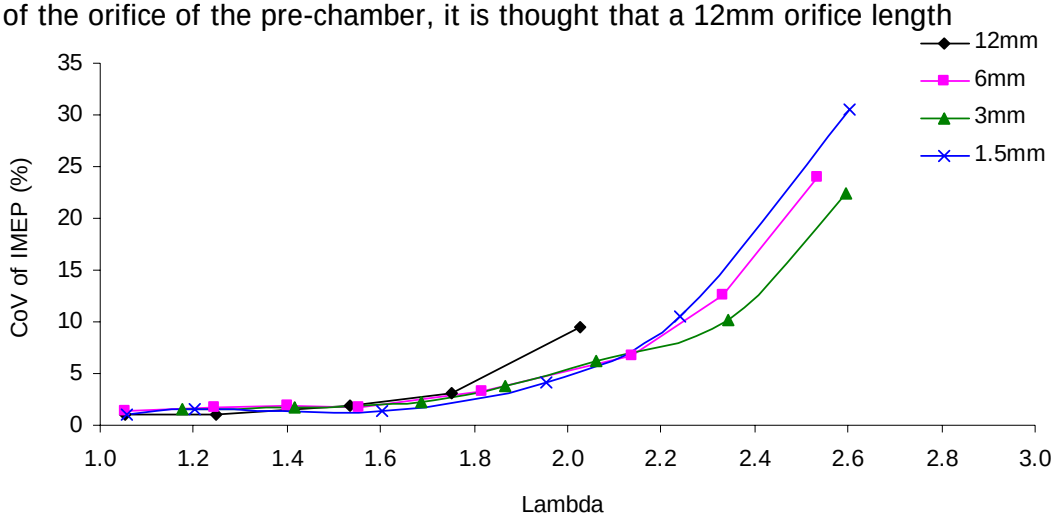

Figure 7.1: Combustion stability at different pre-chamber nozzle lengths.
(1800r/min, MBT, CR=9, MAP=90kPa)

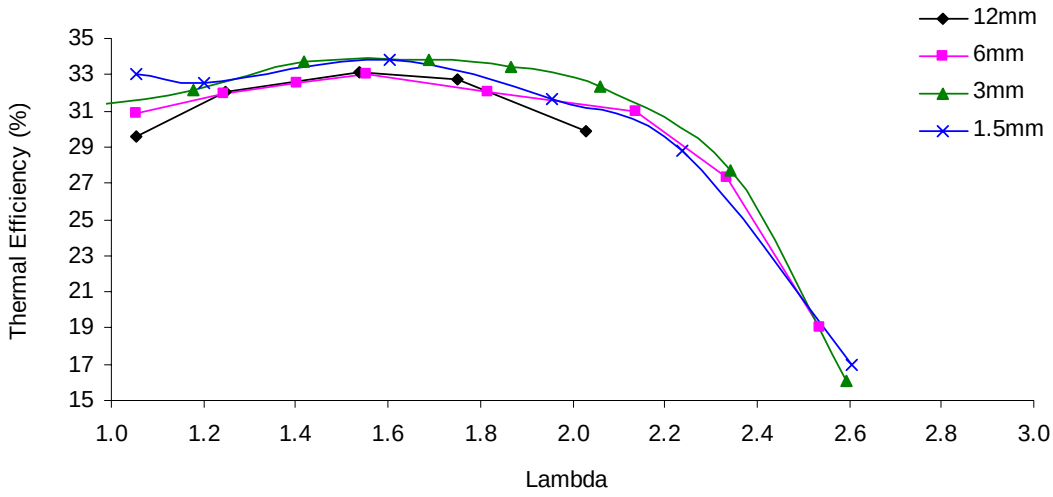

Figure 7.2: Thermal efficiency at different pre-chamber nozzle lengths.
(1800r/min, MBT, CR=9, MAP=90kPa)

establishes the center of the ignition in the opposite side of the combustion chamber. In contrast, it is believed that the 3mm orifice length concentrates the center of the combustion somewhere in the middle of the combustion chamber, which brings about the added benefit of reduced heat transfer and burn duration. These reductions are small, however enough to increase the thermal efficiency by a few percent when the 3mm length orifice is used over the 1.5mm, 6mm or 12mm orifice lengths (Figure 7.2). Interestingly, close to λ=1 where the ignitibility of the main chamber mixture is the highest and the quantity of H_2 in the pre-chamber near zero, the 1.5mm length orifice performs best. This may be because the heat rejection through the orifice is minimised. This is especially important at λ=1 because a gasoline jet shoots through the nozzle instead of a hydrogen jet and this is more likely to cool (or quench) since the quench gap of gasoline is larger than hydrogen. So if little or no hydrogen is used near λ=1, the primary fuel in the pre-chamber is gasoline at λ=1, and therefore a short orifice length is ideal.

Emissions

There was little variation in HC and CO emissions as the orifice length was varied but a noticeable affect on NO_x emissions was observed. In lean mixtures (λ>1.8), the 3mm length orifice provided the lowest NO_x, whereas the 1.5mm length generated the highest NO_x (Figure 7.3). This might be related to the different dispersion and temperature of the HAJI jet. The 1.5mm nozzle may create a more

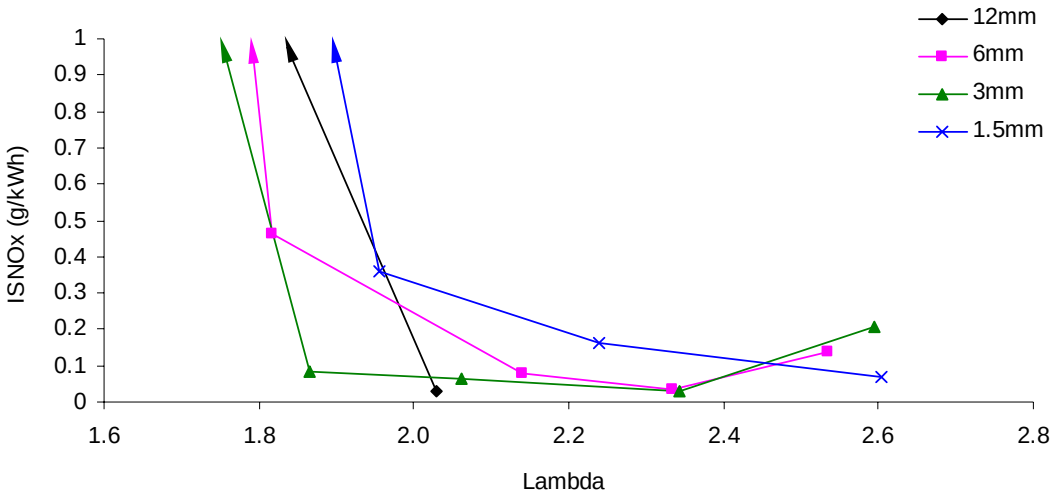

Figure 7.3: $ISNO_x$ emissions at different pre-chamber nozzle lengths.
(1800r/min, MBT, CR=9, MAP=90kPa)

dispersed jet, which means the AFR in the vicinity of the jet will be higher (similar to the main chamber charge) and more uniform, producing lower temperatures. The lower temperatures due to dispersion will however be offset by the reduced cooling effect of the short nozzle. Thus, the overall affect is that the jet temperature is relatively high, prompting the production of NO_x. In contrast the 6mm length nozzle also produced more NO_x than the 3mm length. In this case, the small dispersion of the jet may create a lower AFR near the jet and therefore increases the local temperatures. The increase in temperature should be offset by the cooling effect of the longer nozzle, but not enough in this case to produce less NO_x than the 3mm length nozzle. A 3mm nozzle length proved to be most optimum by balancing jet dispersion and orifice cooling in such a way that the temperature field in the combustion chamber was conducive to low NO_x production.

7.2.2 Effect of Pre-chamber H_2 Quantity

The effect of H_2 quantity (% of H_2 of total energy) on HAJI-G performance was examined at three different air-fuel ratios: λ=1, λ=1.6 and λ=2. The spark timing was held constant at MBT (Appendix F.1): 12, 25, and 40° BTDC, at which the optimum H_2 quantities are 0, 0.5 and 3.5%. At these conditions CoV of IMEP, efficiency and NO_x are balanced best. The main chamber fuelling rate was also held constant and the quantity of H_2 was the only parameter varied.

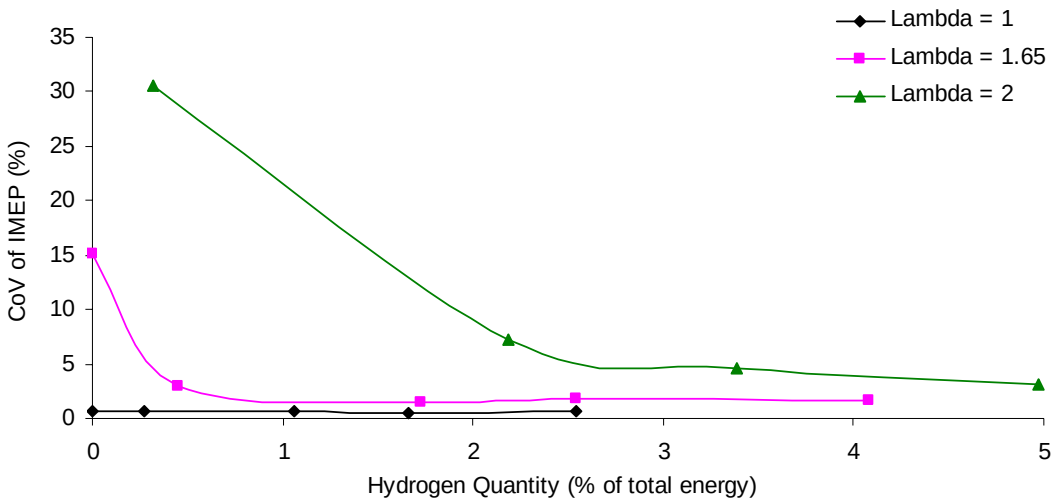

Figure 7.4: CoV of IMEP versus HAJI H_2 quantity at different Lambda values.
(1800r/min, MBT, CR=9, MAP=90kPa)

Combustion Stability

As shown in Figure 7.4, combustion stability is clearly not influenced by the H_2 quantity at λ=1. In contrast, the use of H_2 becomes a necessity to maintain good combustion stabilities in lean mixtures. When λ=1.6, the minimum H_2 quantity required is less than 0.5% but at λ=2, 3.5% is required to keep the CoV of IMEP<5%. Interestingly, if a CoV<5% is achieved at any given λ then increasing the H_2 quantity is not beneficial, since combustion stability improves very little.

From a commercial point of view, the unavailability of H_2 in vehicles has been an outstanding issue. Recently developed on-board H_2 reformers can provide >20% H_2 by volume when reforming HC based fuels. This opens up an immediate possibility of exploring the commercialisation of the HAJI system since it consumes less than 4% of H_2 at any given load point.

Thermal efficiency

The reader should be reminded that thermal efficiency throughout this thesis includes both main chamber and pre-chamber fuel used. Since the spark timing is already at MBT at λ=1 with 0% H_2 quantity, the thermal efficiency decreases as the quantity of H_2 is increased (Figure 7.5). This is extra energy which decreases the burn duration by 6.8%, advances the peak pressure location by 2 CAD and increases the magnitude of peak pressure by 4%. The extra energy could possibly

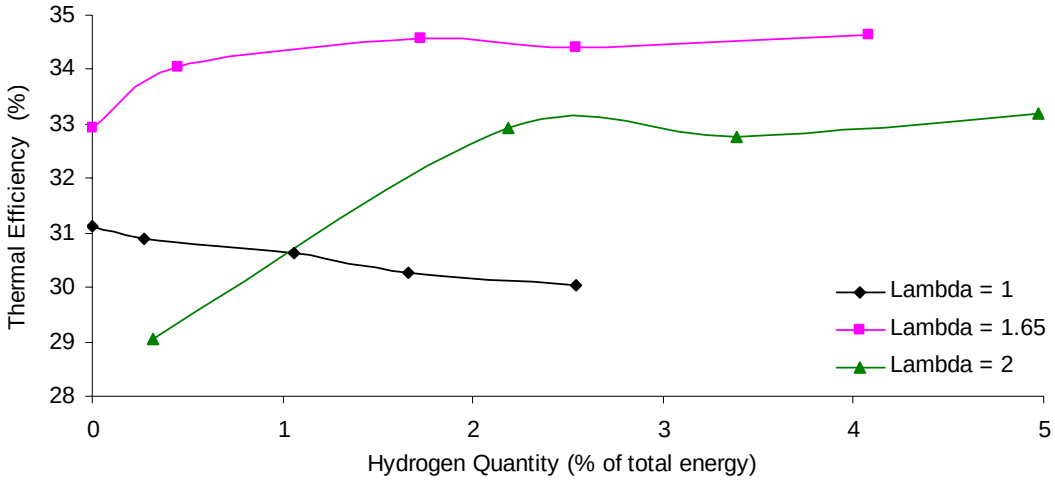

Figure 7.5: Thermal efficiency versus HAJI H_2 quantity at different Lambda values. (1800r/min, MBT, CR=9, MAP=90kPa)

be capitalized to maintain thermal efficiency by retarding the spark timing, which would in turn increase IMEP.

At λ=1.6 and λ=2, the optimum H_2 quantity is 0.5% and 3.5%. Consequently, any decrease from these percentages translates into a decrease in thermal efficiency. This deterioration could possibly be improved by simultaneously advancing spark timing to obtain a new MBT for these reduced energy cycles. In contrast, when the H_2 quantity is increased from the optimum of 0.5% and 3.5%, thermal efficiency is unchanged. This indicates that the small additional energy input is converted into useful work at high λ values without the need to readjust spark timing.

Emissions

HC and CO emissions at λ=1 are unchanged as the H_2 quantity increases. However, NO_x emissions increase by up to 21% (Figure 7.6). This could be due to the higher local temperatures generated by the presence of H_2 and by the increased concentrations of H and OH radicals in the HAJI jet, which increase the rate formation of NO_x.

At λ=1.6 and λ=2, increasing the H_2 quantity lowers CO and HC emissions due to an increase in combustion temperatures. At λ=1.6, peak temperature increases from 1995 to 2098K (Figure 7.7) which increases the NO_x emissions

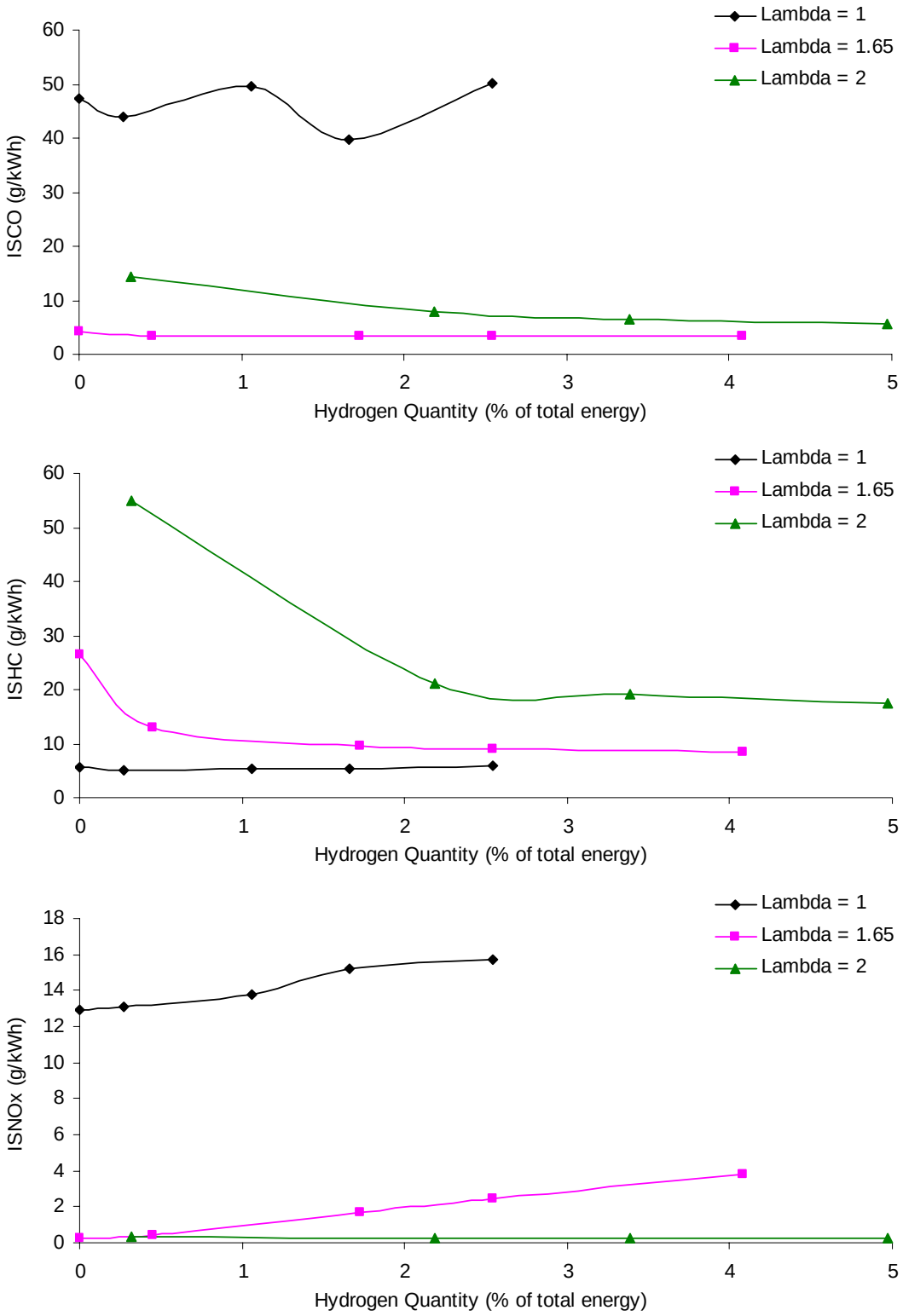

Figure 7.6: (top) ISCO, (middle) ISHC, (bottom) $ISNO_x$ emissions versus HAJI H_2 quantity at different Lambda values. (1800r/min, MBT, CR=9, MAP=90kPa) - Note in the upper figure: Fluctuation in CO is due operating at λ=1, where CO formation is extremely sensitive to air-fuel ratio (see Figure 2.1, where λ=0.99 condition produces 40% more CO than λ=1.01)

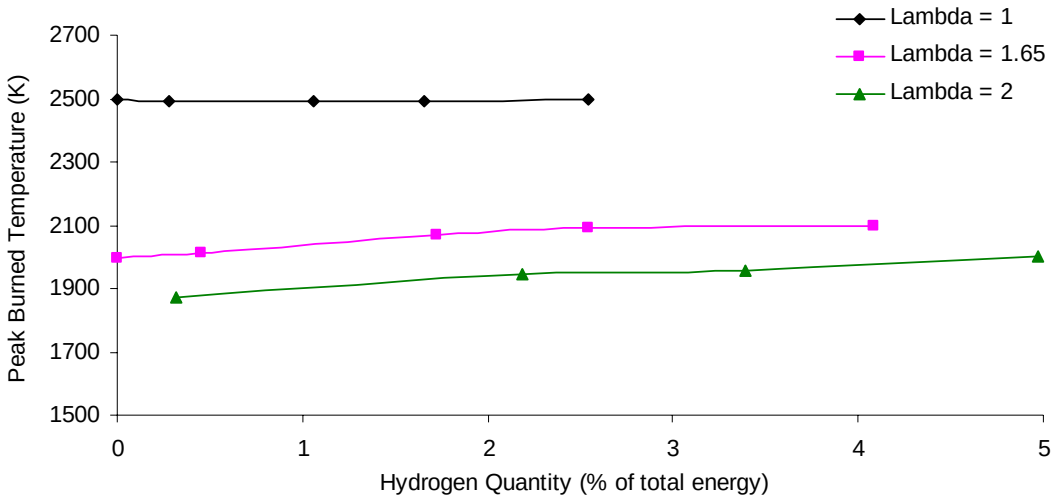

Figure 7.7: Peak burned temperature versus HAJI H_2 quantity at different Lambda values. (1800r/min, MBT, CR=9, MAP=90kPa)

from 0.3 to 3.8g/kWh. This is over a ten-fold increase in NO_x emissions, highlighting the sensitivity of NO_x to the increase in H_2 quantity from 0.5% to 4%. At λ=2, the sensitivity of NO_x to increasing H_2 quantity is negligible. Although peak combustion temperature increases from 1870 to 1999K, this has little effect on NO_x formation at λ=2 because the temperature is still low enough to keep the rate of NO_x formation low. From a commercial point of view, this insensitivity to H_2 quantity at λ=2 is very desirable, because it enables the development and implementation of a relatively easy and simple H_2 addition strategy into the ECU.

It must be noted that the magnitude of CO emissions are two times higher at λ=2 than at λ=1.65. This occurs due to the lower combustion temperatures at λ=2, where the partial oxidation of crevice, quench and oil-layer hydrocarbons emerge late in the cycle and remain incompletely oxidised. However, the higher CO should be kept in perspective because the λ=2 CO levels are one-tenth of those at λ=1.

Burn Duration

At λ=1 as the quantity of H_2 increases the total burn duration decreases by 6.8%, and the first 10% of the mass fraction burn duration decreases by 8.5% (Figure 7.8). At λ=1.6, as the H_2 quantity is increased from 0.5% to 4%, the total burn duration decreases by 21% and the 0-10% burn duration by 20%. At λ=2 the results obtained are 20% and 22% respectively.

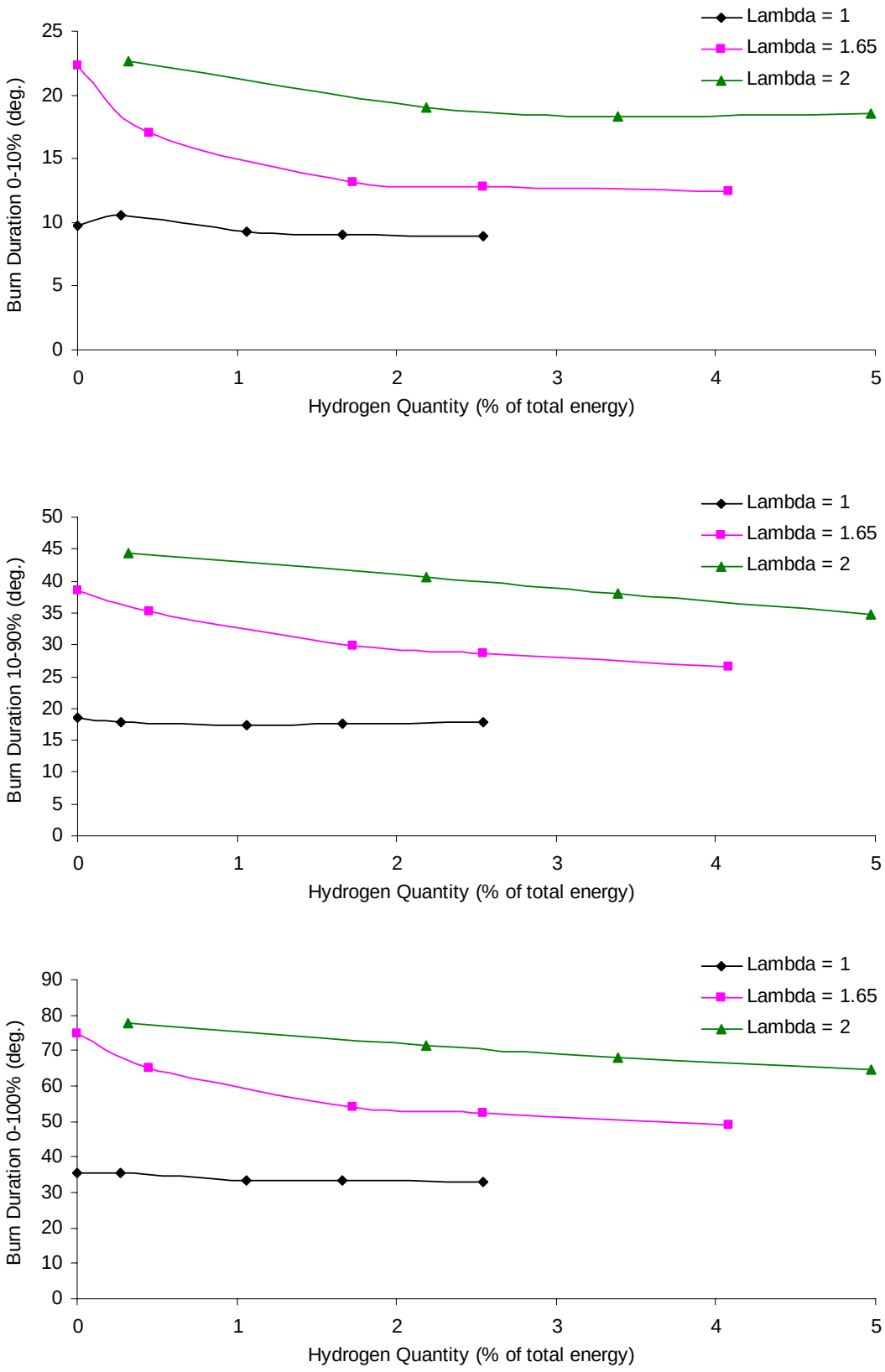

Figure 7.8: Burn duration - (top) 0-10%, (middle) 10-90%, (bottom) 0-100% versus HAJI H_2 quantity at different Lambda values. (1800r/min, MBT, CR=9, MAP=90kPa)

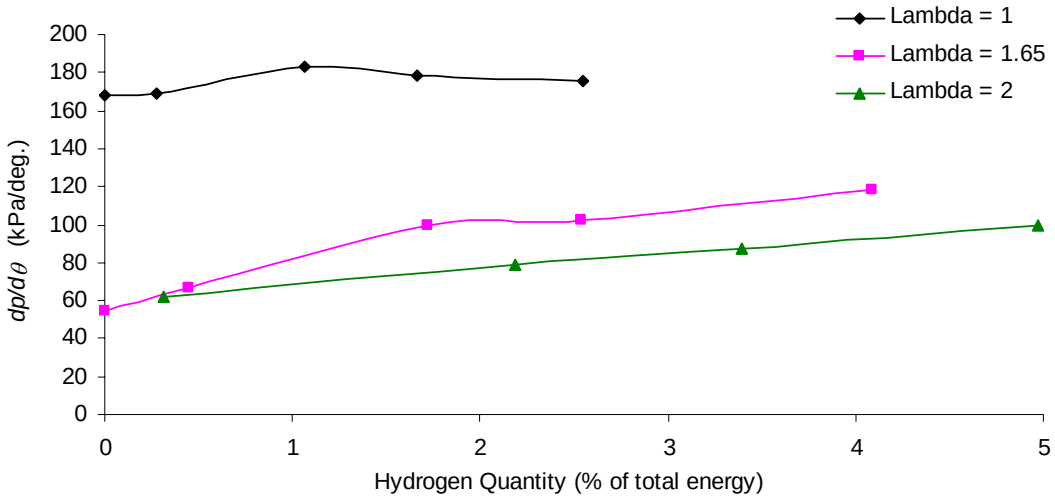

Figure 7.9: Rate of pressure rise versus HAJI H_2 quantity at different Lambda values. (1800r/min, MBT, CR=9, MAP=90kPa)

The most undesirable effect of short burn duration is that it may increase the rate of pressure rise to levels where combustion becomes audible (>500kPa/deg). Fortunately, at λ=1 where the highest pressure rise is encountered, irrespective of the H_2 quantity the rate of pressure rise is approximately around 170kPa/deg (Figure 7.9). At λ=1.6 and λ=2 the rate of pressure rise increases from 55kPa/deg. to 118kPa/deg. and from 61kPa/deg. to 100kPa/deg respectively, highlighting the effectiveness of HAJI in enhancing lean mixture burn rates.

7.2.3 Effect of Engine Speed

The effect of engine speed on HAJI performance was examined at 1200 and 1800r/min. At these two engine speeds the MAP was set to 50 and 90kPa, MBT was maintained at all λ conditions, while the H_2 quantity varied from 0% to 3.5%.

Combustion Stability

CoV of IMEP seems to decrease as the MAP is increased at both engine speeds (Figure 7.10), especially at high λ values. This is expected since the level of residual exhaust gas fraction decreases with increasing MAP. This means that the level of dilution is decreased, which in turn increases flame speed and stability, especially in the early stages of flame development. At 50kPa MAP up to λ =1.9, speed has no effect on the CoV of IMEP. As speed is decreased at MAP=50kPa

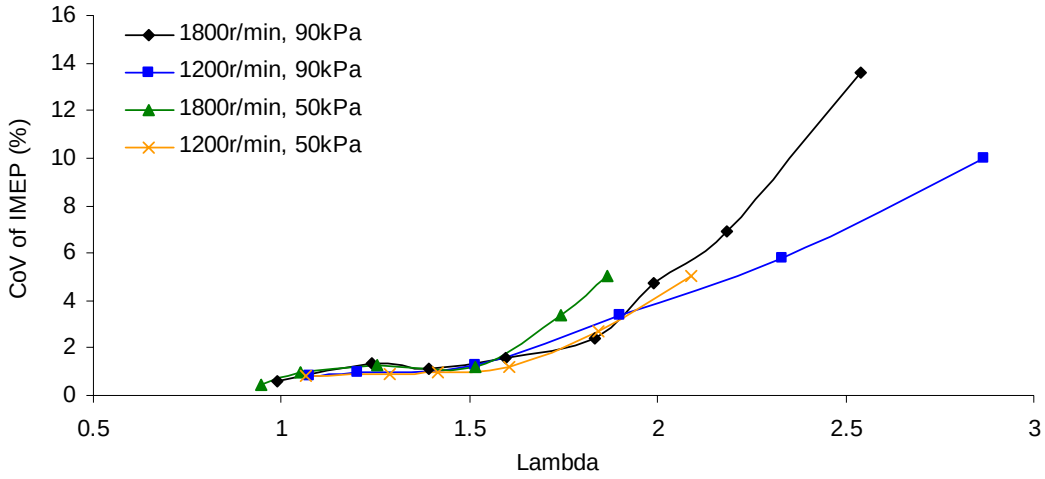

Figure 7.10: CoV of IMEP versus Lambda at different engine speeds. (MBT, CR=9)

and λ > 1.6, CoV of IMEP decreases. This is especially important when the engine idles since both speed and MAP are low at this point.

Thermal Efficiency

At a given engine speed, thermal efficiency clearly reduces as MAP decreases due to an increase in pumping losses (Figure 7.11). Interestingly, when MAP=50kPa a reduction in engine speed decreases the thermal efficiency further, instigated by an increase in residual gases. The high level of residual gases decreases the flame speed, which extends the burn duration, thereby increasing the available time for heat loss through the cylinder head, piston and walls [95]. At MAP=90kPa this phenomena is not observed because very small quantities of residual gases become trapped in the combustion chamber. At 1800r/min and λ >2, as MAP is

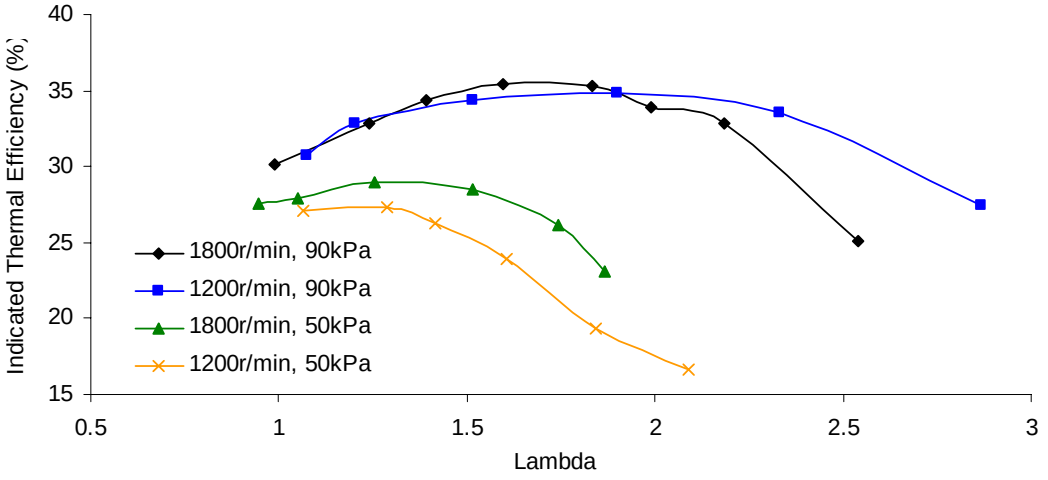

Figure 7.11: Thermal efficiency versus Lambda at different engine speeds. (MBT, CR=9)

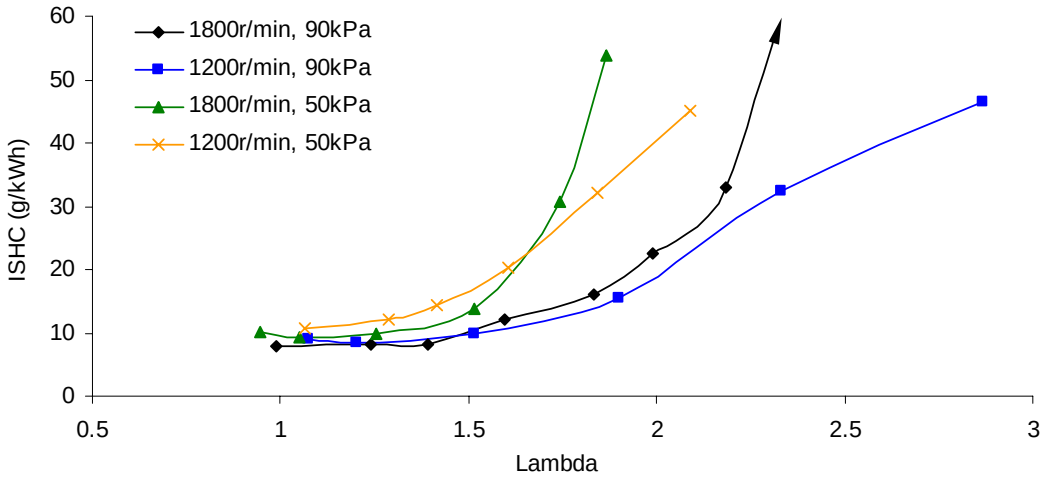

Figure 7.12: ISHC versus Lambda at different engine speeds. (MBT, CR=9)

decreased, thermal efficiency also falls. This occurs predominantly due to the reduction in combustion stability, which increases the amounts of unburned fuel.

Emissions

HC emissions increase as λ increases irrespective of engine speed or MAP (Figure 7.12). This is due to the increase in quench gap and reduced flame temperatures. HC emissions at any given λ are higher at lower MAP due to the increase of residual gas fraction in the combustion chamber, which reduces flame temperatures. As expected, there is a very strong correlation of increasing HC emissions as CoV of IMEP increases.

At MAP=90kPa, NO_x emissions vary little with engine speed, especially around the

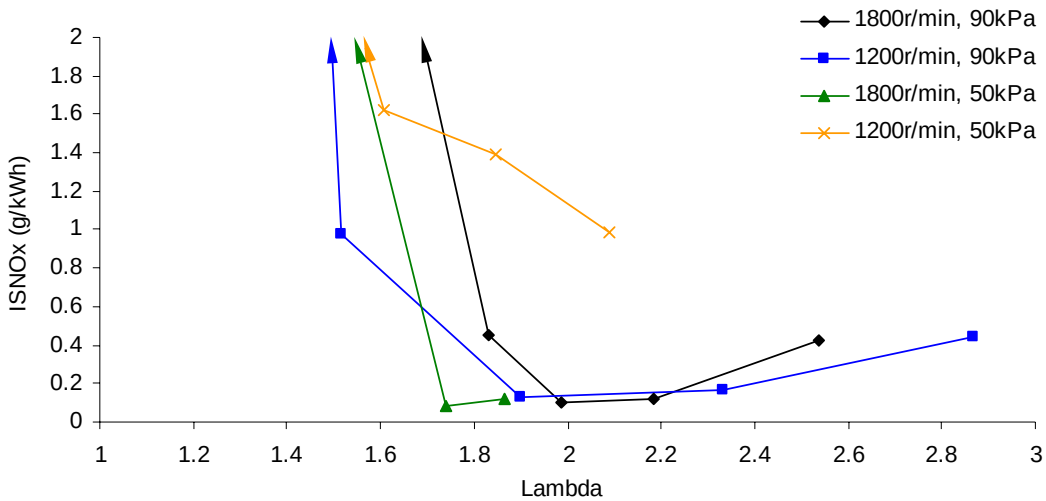

Figure 7.13: $ISNO_x$ versus Lambda at different engine speeds. (MBT, CR=9)

optimum λ of 1.9 (Figure 7.13). At MAP=50kPa as the engine speed decreases from 1800r/min to 1200r/min the NO_x emissions increase by almost 10 times. This is due to an increase in residual gas fraction at low engine speed, which decreases flame speed. This forces MBT to be advanced to 50° BTDC, which in turn increases combustion temperature. Consequently, high NO_x and low HC emissions are observed at 1200r/min at MAP=50kPa.

7.3 Parametric Studies of HAJI Compared to SI

7.3.1 Effect of Spark Timing

The effect of spark timing on HAJI performance was examined at three different air-fuel ratios (λ=1, 1.62 and 2) and compared to a λ=1 baseline SI engine. All other engine variables were held constant producing the following results.

Combustion Stability

The SI engine combustion stability increases as ignition timing is advanced (Figure 7.14) with the lowest CoV of 1.41% compared to 0.43% for HAJI at λ=1. At λ=1 HAJI also provides better combustion stability between 20°BTDC and TDC. However, at -5° and 25°BTDC HAJI becomes unacceptably unstable. At -5°BTDC, the AFR of the pre-chamber is likely to be similar to the main chamber (lot of gasoline with little H_2) and it also begins to empty since the piston is on the

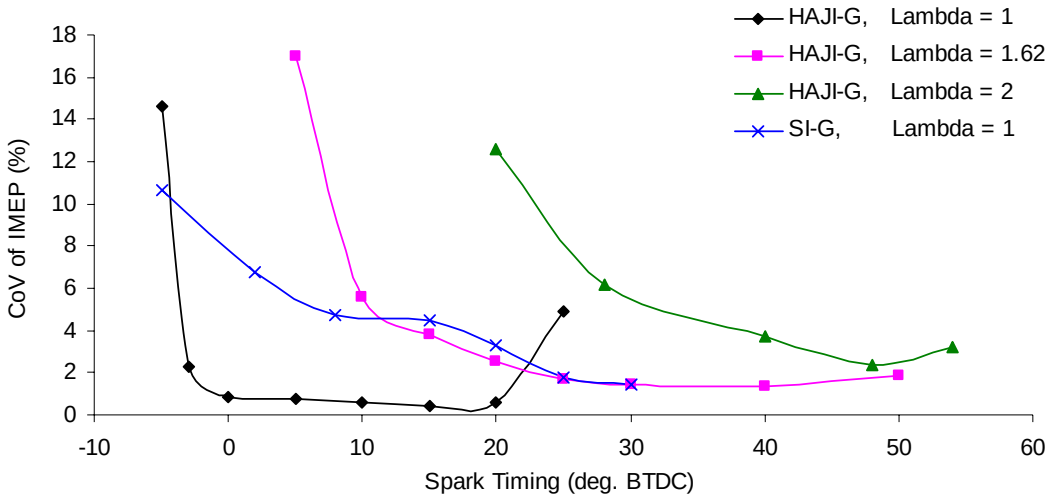

Figure 7.14: CoV of IMEP versus spark timing - HAJI compare to SI.
(1800r/min, CR=9, MAP=90kPa)

expansion stroke. This combination is believed to result in a jet that lacks momentum and active radicals; consequently the CoV climbs abruptly to 15%. Combustion also becomes unstable when the spark timing was set to 25°BTDC. This is thought to occur due to the lack of air flow from the main chamber into the pre-chamber prior to ignition, which results in an excessively fuel rich pre-chamber that has low ignitibility.

At λ=1.62 and λ=2 the CoV steadily increases as the spark timing becomes retarded. This occurs due to the simultaneous escape of H_2 into the main chamber and the leaning out of the pre-chamber as it is filled with the lean main chamber mixture. Consequently, at retarded ignition timing the H_2 jet is turned into a lean H_2-gasoline jet, lacking high flame temperature, momentum and active radicals [232]. To improve HAJI performance at retarded ignition timing, an increased quantity of hydrogen may be used to maintain an optimally rich H_2 pre-chamber.

In contrast to the λ=1 mixture, at λ=1.62 and λ=2, the spark timing can be advanced to 40° and 50° before the pre-chamber becomes excessively fuel rich. This is expected since more fresh air flows into the pre-chamber due to the lean main chamber condition.

Overall, world class combustion stabilities are achieved over 20 CAD at λ=1 in standard SI mode and depending on λ, HAJI provides a spark timing window of 20 to 35 CAD. In terms of engine optimisation, the larger spark timing window is preferred because it provides more opportunities to find a balance between optimum efficiency and emissions.

Thermal Efficiency

In SI mode, MBT occurs at 25°BTDC and thermal efficiency is extremely sensitive to timing (Figure 7.15). It varies from 17% to 31%. In contrast, the thermal efficiency of the HAJI system is relatively insensitive to spark timing at a given λ, especially around peak thermal efficiency. This means that MBT occurs over a range of spark timing rather than at a particular crank angle. This is a great advantage when the engine is simultaneously optimised for performance and low emissions since the compromisation of thermal efficiency is kept to a minimum. At

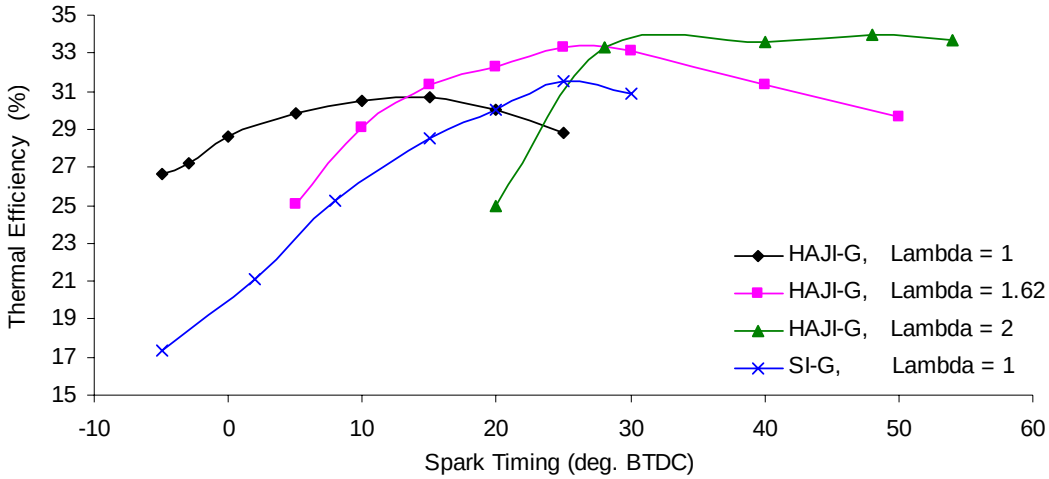

Figure 7.15: Thermal efficiency versus spark timing - HAJI compare to SI.
(1800r/min, CR=9, MAP=90kPa)

λ=1, 1.62 and 2, MBT occurs at 12°, 25° and 40°BTDC respectively and over the range of AFR and timings, the thermal efficiency varies from 25% to 34%.

Emissions

The λ=1 SI engine produces less HC emissions than the HAJI engine at λ=1, λ=1.62 and λ=2 (Figure 7.16). In general, HC emissions in the SI engine increase by up to 20% as the spark timing is retarded. In contrast, the HAJI system HC emissions strongly follow the trend of CoV of IMEP. This means higher HC emissions at retarded ignition timing and lower HC emissions at advanced ignition timing. The reason HC emissions are so high in a HAJI engine is explained by at least two mechanisms. The first is the increase in crevice volume of the HAJI pre-

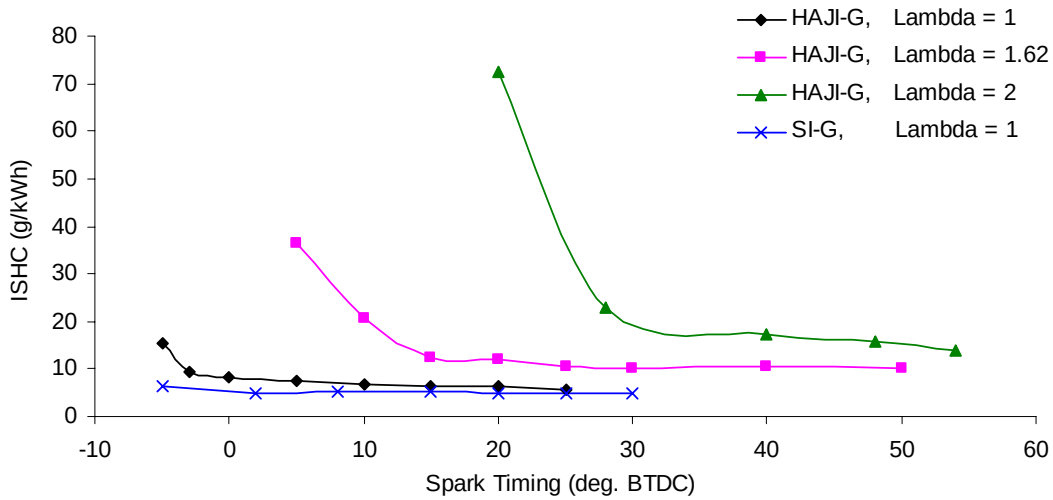

Figure 7.16: ISHC emissions versus spark timing - HAJI compare to SI.
(1800r/min, CR=9, MAP=90kPa)

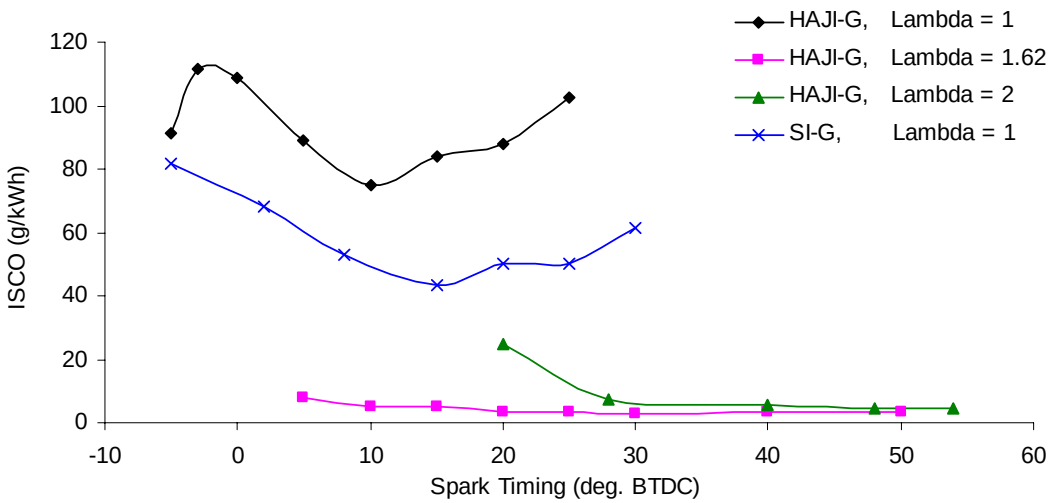

Figure 7.17: ISCO emissions versus spark timing - HAJI compare to SI. (1800r/min, CR=9, MAP=90kPa)

chamber volume and the second is the increase in quench gap as λ increases. Nevertheless, it is important to remember that even though the HAJI system can emit 3 times more HC emissions at λ=2 than the SI engine at λ=1, the thermal efficiency of HAJI over SI is still superior.

The CO emissions of HAJI at λ=1 are higher than SI (Figure 7.17) and this is because the AFR was not exactly the same and CO is extremely sensitive to AFR near λ=1. Closer inspection reveals that HAJI was actually operating at λ=0.99 and that SI was operating at λ=1.01. Experimental results indicate that a λ=0.99 mixture typically produces 40% more CO emissions than a λ=1.01 mixture (Figure

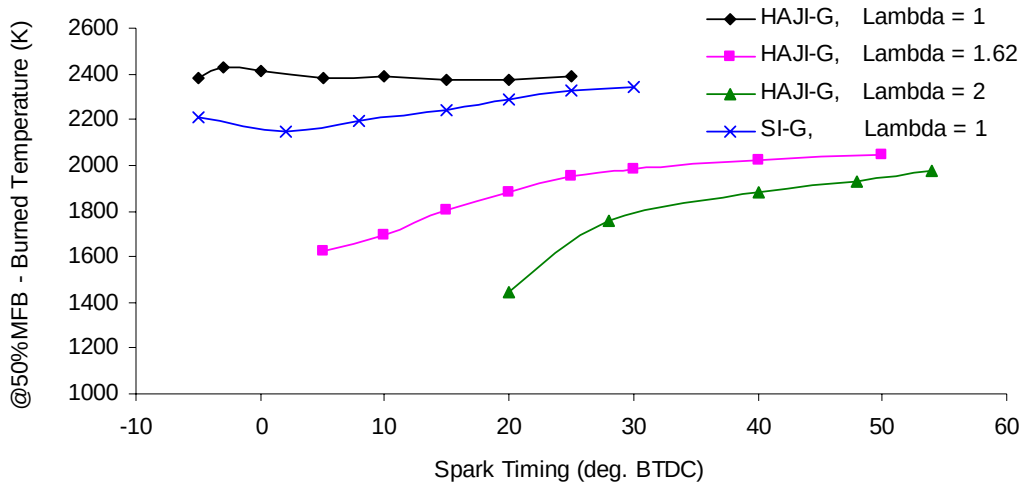

Figure 7.18: Combustion temperatures @50% MFB versus spark timing - HAJI compare to SI. (1800r/min, CR=9, MAP=90kPa)

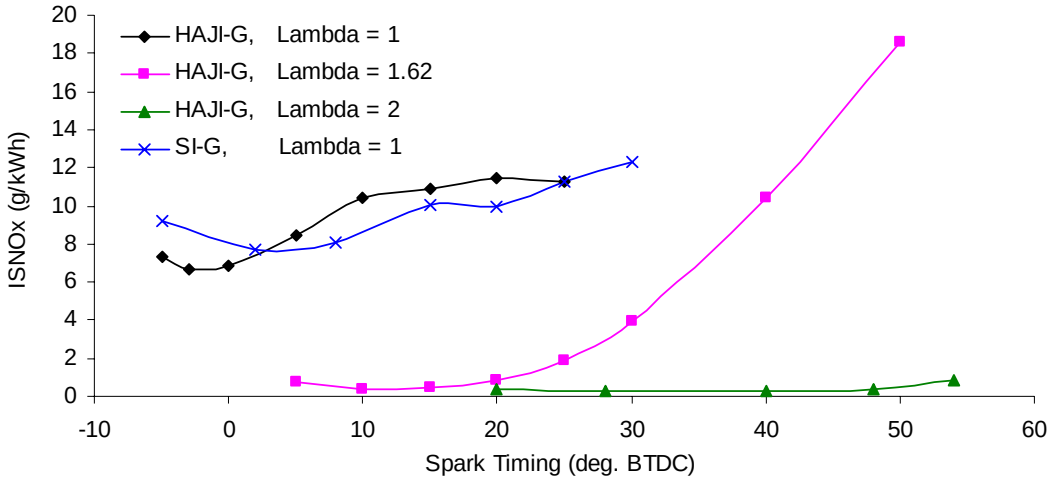

Figure 7.19: ISNO$_x$ emissions versus spark timing - HAJI compared to SI.
(1800r/min, CR=9, MAP=90kPa)

2.1). Another reason for the higher CO in HAJI mode is that the combustion temperature is slightly higher than SI (Figure 7.18), which promotes the production of CO. The λ=1.62 mixture produced the lowest CO levels but the λ=2 mixtures produced in excess of 50% more CO. The general trend for all modes is that CO increases as spark timing is retarded in lean mixtures, whereas at λ=1, the minimum CO is produced at around 10-15°BTDC and increases when spark timing is advanced or retarded from this minimum.

The NO$_x$ emissions are strongly influenced by spark timing and the rate at which NO$_x$ increase is strongly dependent on λ (Figure 7.19). At λ=1, HAJI produces more NO$_x$ than its SI counterpart, predominantly due to its higher combustion temperatures (Figure 7.18). Advancing spark timing yields a 50% increase in NO$_x$ at λ=1 and similar trends can also be observed at λ=2.

At λ=1.62, the optimum spark timing (MBT) with respect to thermal efficiency is 25°BTDC. At this point, NO$_x$= 1.92g/kWh. If the timing is retarded away from MBT to 15°BTDC, the combustion temperatures drop at 50%MFB from 1951K to 1807K, which drives the NO$_x$ emissions level down to 0.4g/kWh. This is a ~5 fold decrease in engine out NO$_x$ emissions with only a 3.2% decrease in fuel economy. This is still a 6.4% increase in fuel economy over the λ=1 SI engine. In terms of

engine optimisation, the optimum spark timing chosen will be at a NO_x output that satisfies the emissions regulations at the time of calibration.

Interestingly, at λ=1.62, the NO_x emissions can reach levels of 18g/kWh when spark timing is advanced to 50°BTDC. This is a 45 fold increase in NO_x levels over the measurements taken at 15°BTDC. This is due to the availability of high levels of O_2 and an increase in combustion temperatures and residence time, all of which yield perfect conditions for a high rate of NO_x formation.

Burn Duration

The 0-10% MFB duration is strongly influenced by spark timing at all λ conditions (Figure 7.20). Even at λ=2, HAJI consumes the mixture faster than its SI counterpart operating at λ=1. In fact at λ=1, HAJI consumes the mixture 2 times faster than the SI engine for all values of spark timing.

The 0-10% burn duration increases as spark timing is retarded in SI mode at λ=1. This might be due to the decrease in turbulence levels as the piston approaches TDC and the increase in cylinder pressure, which increases heat transfer and also reduces the magnitude of spark discharge which therefore decreases the size of the flame kernel. HAJI at λ=1 is not subjected to this phenomena since the main chamber charge is ignited by the jet. The burn duration only increases when spark timing occurs after TDC, at which point the CoV of IMEP rapidly increases. Interestingly, at λ=1.62 and λ=2, the burn duration decreases as the spark timing is retarded. This occurs due to the increase in unburned charge density. In fact from 20° to 50°, the density approximately doubles. This means that as the jet enters into the main chamber at 20° ignition timing, it could burn up to 2 times more charge than at 50° for a given flame surface area. The unburned gas temperature also increases by approximately 120°C. This increases the chemical reaction rate in the flame front and can therefore decrease the burn duration.

Overall, the 10-90% and 0-100% burn duration increases as spark timing is retarded in both HAJI and SI mode irrespective, of the λ conditions. This is due to the decrease in turbulent flame speed on the expansion stroke, which is driven by the rapidly falling temperatures and pressures. It is worth noting that the 0-100%

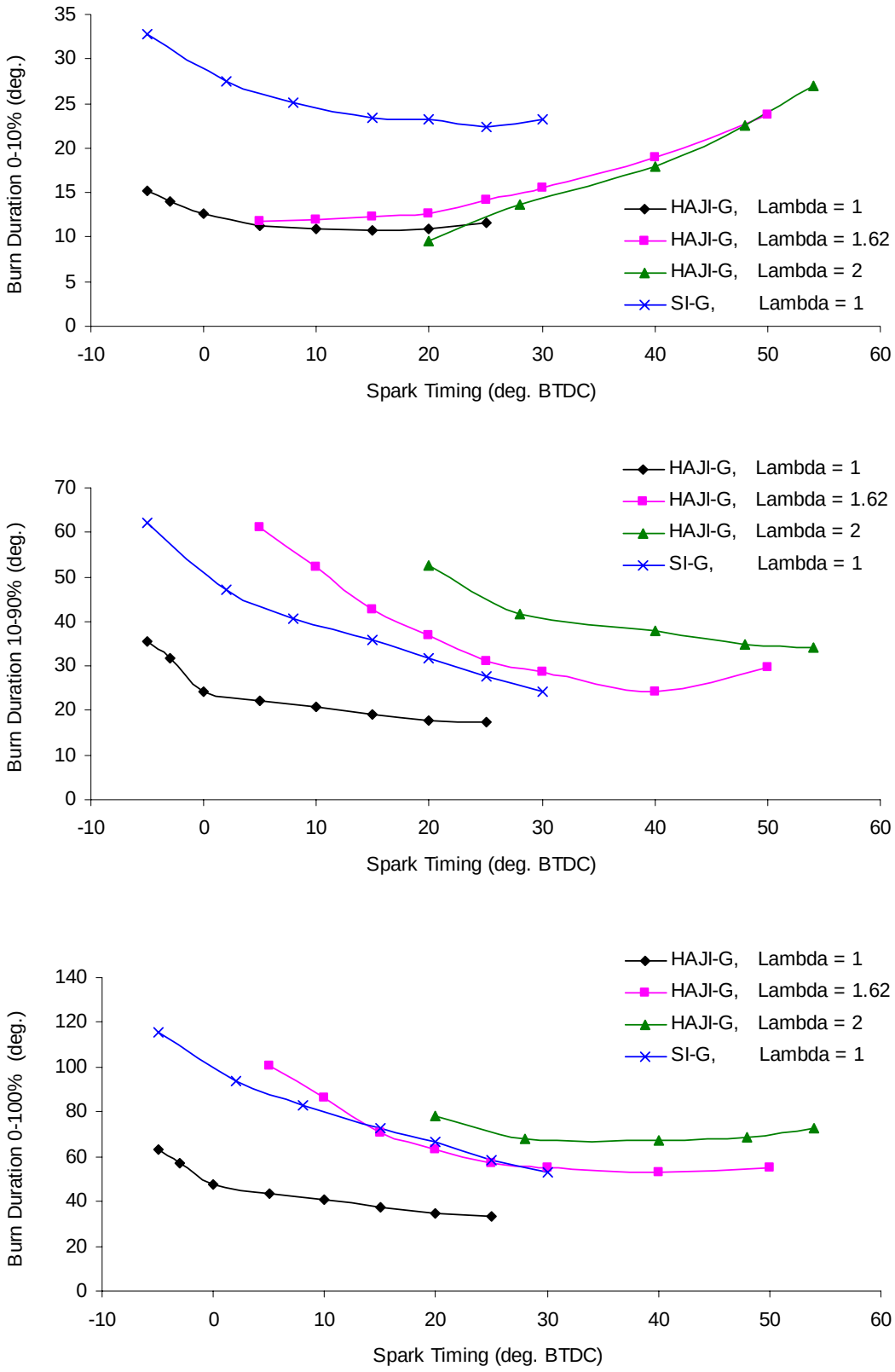

Figure 7.20: Burn duration versus spark timing, (top) 0-10%, (middle) 10-90%, (bottom) 0-100% - HAJI compared to SI. (1800r/min, CR=9, MAP=90kPa)

burn duration at λ=1 shows that HAJI burns the mixture 2 times faster than SI. This is a significant decrease in burn duration considering that the H_2 fuel flow in HAJI mode is only 0.2% of the total fuel energy. Interestingly, the total burn duration of HAJI at λ=1.62 and λ=2 stabilises after MBT, whereas at λ=1 it decreases slightly. This stabilisation of total burn duration at high λ comes from the balance of increasing burn duration at 0-10% MFB and decreasing burn duration at 10-90% MFB.

7.3.2 Effect of Compression Ratio

The effect of CR on HAJI performance was examined at three different air-fuel ratios (λ=1, 1.6 and 1.9) and compared to a λ=1 baseline SI engine. MBT was maintained at all data points while CR was varied from 8 to 15. All other engine variables were held constant, producing the following results.

CoV of IMEP

The CoV of IMEP for SI was found to be less than 5% from CR=8 to CR=13 (Figure 7.21). At CR=13, it exceeded the 5% limit and at CR=15 the engine could not operate at all due to heavy knocking; even though spark timing was retarded to 9.5° ATDC. In contrast, HAJI at λ=1 was able to operate at CR=15 with knock limited MBT occurring at 7.5°ATDC. This demonstrates some tendency for HAJI to suppress end gas knock and is most likely due to the shorter burn duration (Figure 7.25, 7.26) which decreases heat transfer to the end gas. Another factor contributing to knock suppression may be the increased turbulence intensity

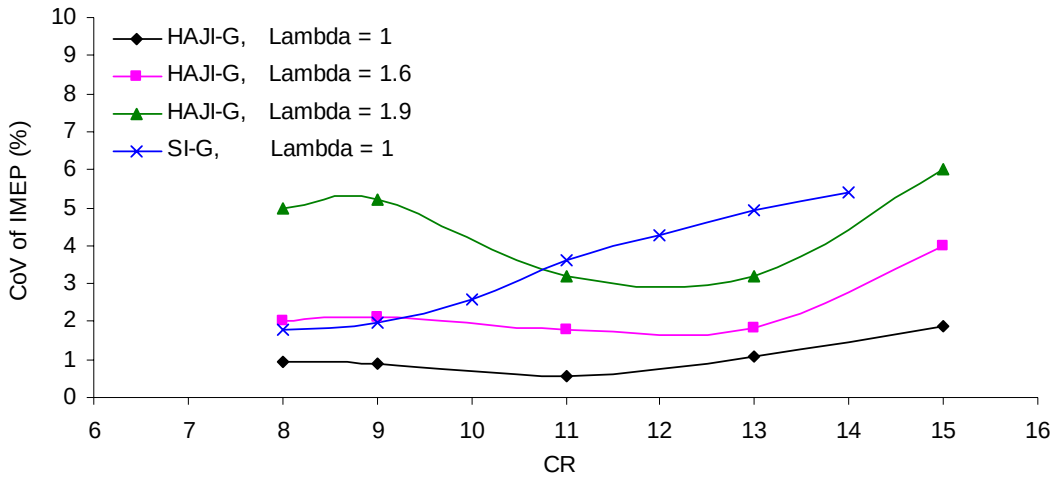

Figure 7.21: CoV of IMEP versus CR - HAJI compare to SI. (1800r/min, MBT, MAP=90kPa)

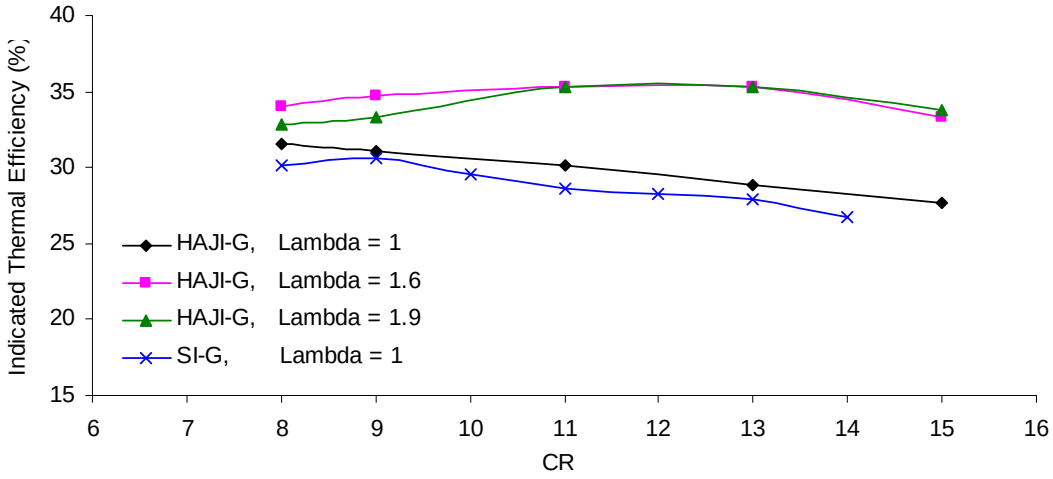

Figure 7.22: Thermal efficiency versus CR - HAJI compared to SI.
(1800r/min, MBT, MAP=90kPa)

caused by the jet, which could increase the heat transfer from the end gas to the cylinder wall. In terms of combustion stabilities, at all λ, HAJI outperforms SI when CR>=11. Only when CR<11 and λ=1.9 is HAJI outperformed by the SI engine.

Thermal Efficiency

The HUCR (Appendix F.2 and F.3) of the SI engine occurs at CR=9 and from this point onwards, as CR is increased, thermal efficiency decreases (Figure 7.22). This is due to retardation of spark timing, an increase in heat transfer and an increase in burn duration. For HAJI, the HUCR is a function of λ. At λ=1, the HUCR<8, however at λ=1.6 and λ=1.9, the HUCR occurs over a range of CR values from CR=11 to CR=13. At all CR, HAJI provides a higher thermal efficiency than the SI engine. At λ=1, this is due to the shorter burn duration and at λ=1.6 and 1.9 it is due to both the shorter burn duration and reduced combustion temperatures. In fact, HAJI operating at CR=11 and λ>=1.6 provides an improvement in thermal efficiency of over 15% compared to SI operating at CR=9. In terms of engine optimisation for thermal efficiency, this means that HAJI operating lean could provide a minimum increase of 2 CR over a standard SI engine.

Emissions

As CR increases in SI mode, the HC emissions increase (Figure 7.23) predominantly due to the increase in surface to volume ratio and increase in charge density, which pushes more unburned HC into the crevice volume. In

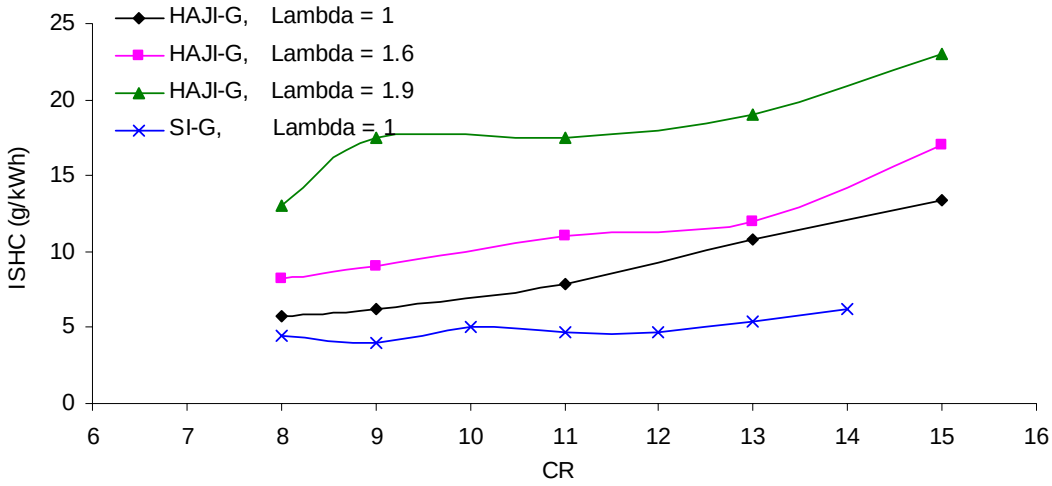

Figure 7.23: ISHC emission versus CR - HAJI compared to SI.
(1800r/min, MBT, MAP=90kPa)

general, the SI engine outperforms HAJI even at λ=1, since with HAJI, the pre-chamber functions as an extra large crevice volume as already described. Consequently, at λ=1.9 and CR=11, the HAJI engine emits more than 3.5 times more unburned HC than its SI counterpart at λ=1.

The CO emissions follow a similar pattern to HC emissions in that they increase as CR increases. However, at high λ values, HAJI produces between one-fourth and one-ninth the CO emissions compared to SI.

The NO_x emissions decrease by at least 50% when the CR is increased from 8 to

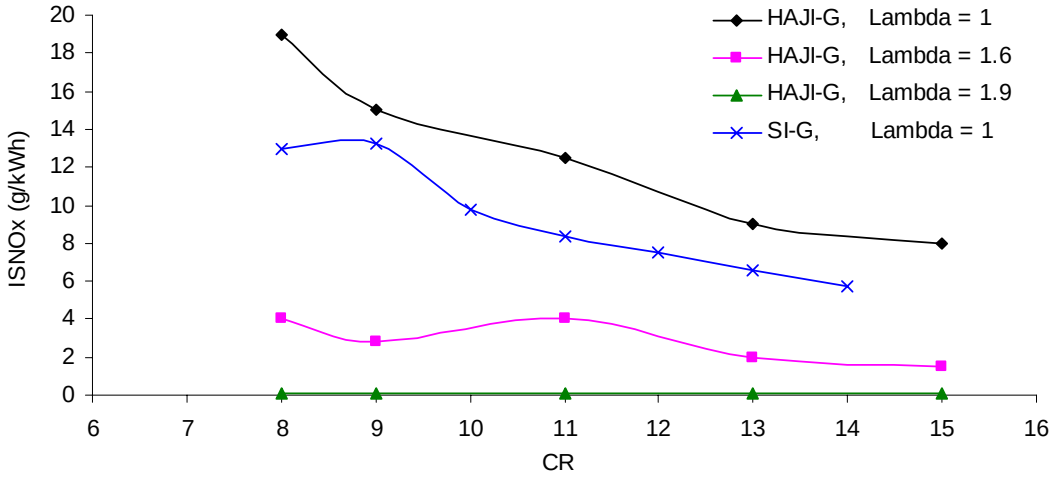

Figure 7.24: $ISNO_x$ emission versus CR - HAJI compared to SI.
(1800r/min, MBT, MAP=90kPa)

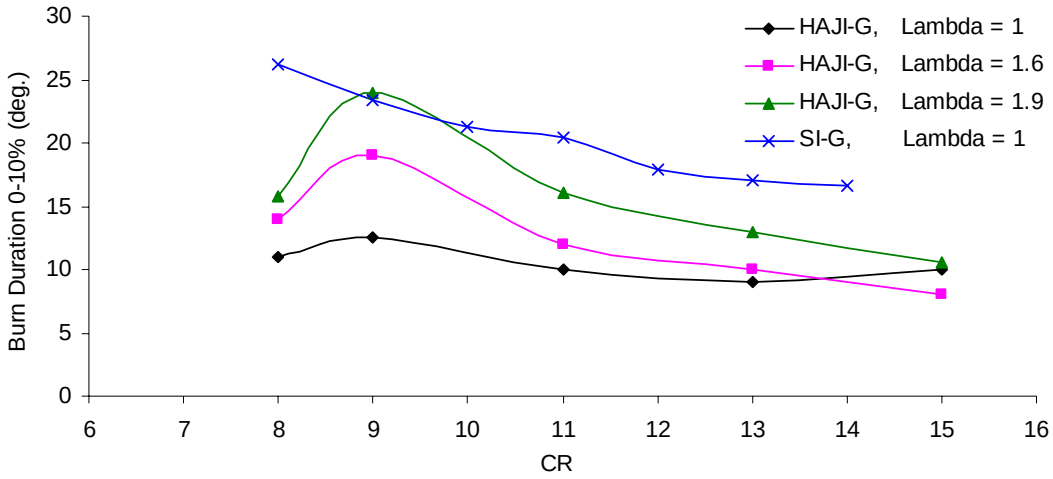

Figure 7.25: Burn Duration (0-10%) versus CR - HAJI compared to SI.
(1800r/min, MBT, MAP=90kPa)

15 in both SI and HAJI modes at λ=1 and λ=1.6 (Figure 7.24). This is predominantly due to retarded spark timing, which drops the combustion temperatures and reduces the residence time at high temperatures. At λ=1, HAJI produces more NO_x than SI at any given CR and this is due to the higher combustion temperatures caused by higher pressure produced by the shorter burn duration (Figure 7.26). Due to low combustion temperatures at λ=1.9, the rate of NO_x formation is constant throughout the CR range. Consequently, as long as HAJI operates near λ=1.9, NO_x emissions are independent of CR and CR can be optimised to balance thermal efficiency, HC emissions and combustion stability.

Burn Duration

As CR increases from CR=8 to CR=15 the burn duration of the first 10% mass fraction decreases by 36% in SI mode (Figure 7.25). In HAJI mode it decreases by 16% at λ=1, 57% at λ=1.6 and by 55% at λ=1.9. This is expected since at higher CR, the temperature and therefore the rate of fuel oxidization, is higher at the time of spark ignition since MBT occurs closer to TDC. As CR increases at λ=1, this enhancement in the burning process is not sustained through the entire burn in both HAJI and SI modes. Consequently, the total burn duration increases (Figure 7.26) and this is mainly driven by a reduction in the flame reaction zone which is caused by flame stretch and a drop in burned gas temperature due to late burning on the expansion stroke. At λ=1.6 and λ=1.9, this drop in burned gas

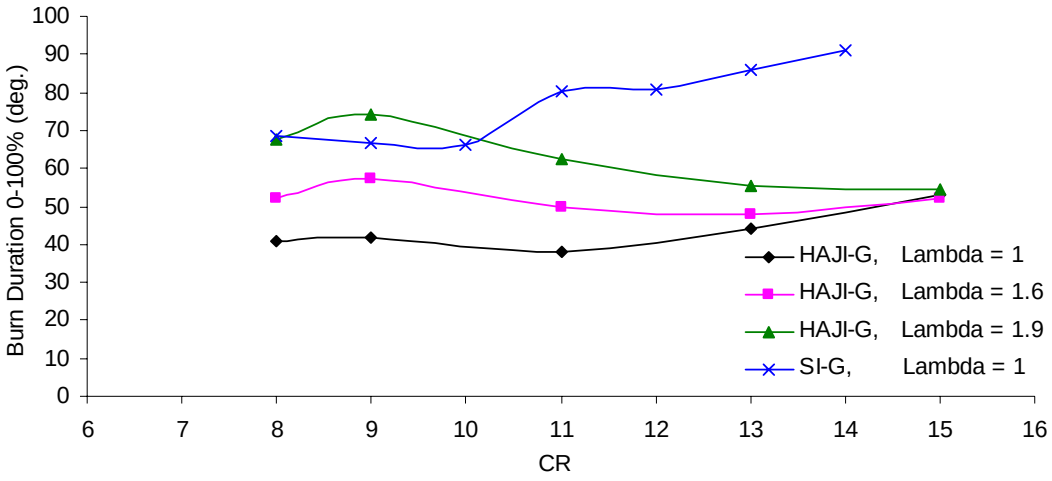

Figure 7.26: Burn Duration (0-100%) versus CR - HAJI compared to SI.
(1800r/min, MBT, MAP=90kPa)

temperature is not so pronounced, therefore, the overall burn duration actually decreases.

7.3.3 Effect of Lambda

The effect of λ on HAJI performance was examined at WOT and compared to the λ=1 baseline SI engine operating on: gasoline and H_2. MBT was maintained at all data points while λ was varied from λ=1.

CoV of IMEP

The most influential variable affecting the combustion stability of SI and HAJI is λ (Figure 7.27). SI-G performs well around stoichiometric, however it fails to operate acceptably beyond λ=1.35. SI-H_2 is backfire limited below λ=1.48 and unable to operate satisfactorily above λ=2.5. In gasoline mode at λ=1, when the SI engine was fitted with HAJI, the CoV of IMEP dropped from 1.8% to <0.9%. HAJI also extended the acceptable lean limit (<5% of CoV of IMEP) for gasoline to λ=1.9 and for H_2 to λ=4.6.

In SI-H_2 mode the engine became backfire limited at λ=1.48 and in HAJI-H_2 mode at λ=1.7, corresponding to 580kPa and 520kPa IMEP respectively. It is worth noting that backfire is a power limiting factor only at this operating point (WOT),

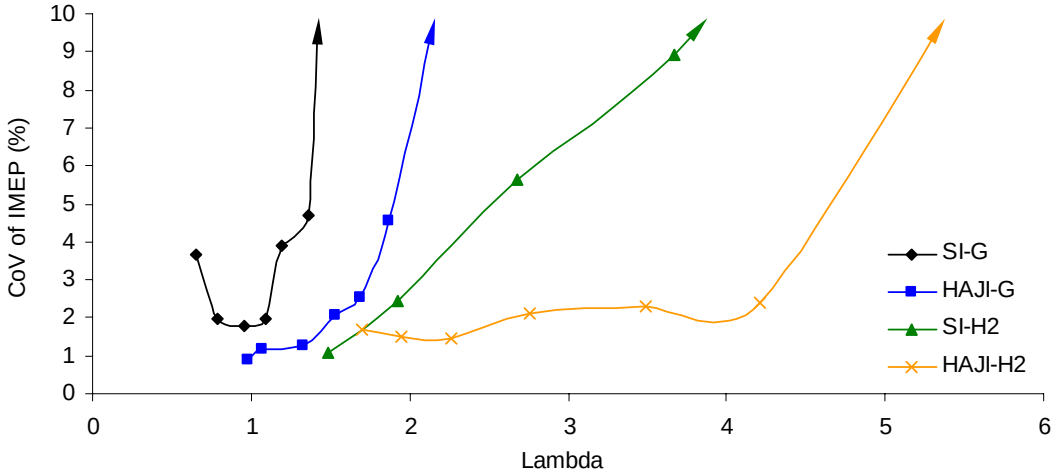

Figure 7.27: CoV of IMEP versus Lambda - HAJI compared to SI.
(1800r/min, CR=9, MBT, MAP=90kPa)

and that in lean supercharged HAJI-H_2 mode >1000kPa IMEP was developed as already discussed in Chapter 6.

Thermal Efficiency

When CoV of IMEP increases, thermal efficiency decreases for both HAJI and SI modes irrespective of the fuel type used (Figure 7.28). At low λ values in gasoline mode, SI and HAJI performance is similar. However in H_2 mode, SI provides higher thermal efficiency over HAJI, since SI is less knock and backfire limited. Overall, irrespective of the type of fuel used, HAJI provides better thermal efficiency when operated sufficiently lean. It is important to realise at this point that Figure 7.28, is a back to back study at CR=9. Therefore, the total

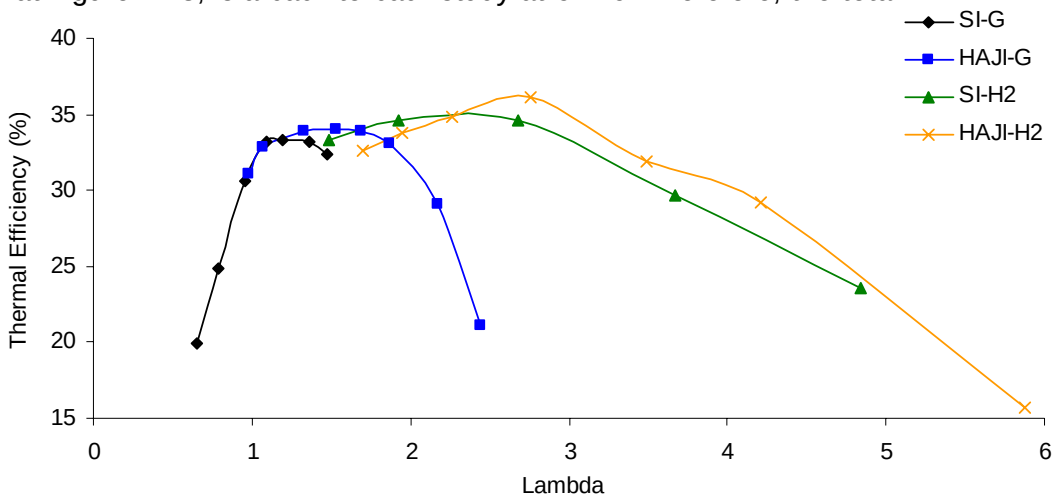

Figure 7.28: Thermal efficiency versus Lambda - HAJI compared to SI.
(1800r/min, CR=9, MBT, MAP=90kPa)

improvement in thermal efficiency that HAJI can provide by operating at CR=11 is not captured on this graph and will be discussed in Section 8.3.

Emissions

In all modes, HC emissions dramatically increase as λ increases. This is predominantly because of the increase in quench gap (Figure 7.29). When λ doubles, the laminar flame speed can decrease by as much as 6 fold, which in turn increases the quench gap by approximately the same proportion. In HAJI-G mode at λ=2, a 4-fold increase in HC emissions is observed when compared to SI at λ=1. This result is certainly lower than the expected 6 fold increase, especially when considering that the crevice volume of HAJI is larger than SI. This could be due to the additional turbulence HAJI creates in the main chamber which increases mixing near the quench gap region. This wall HC mixing might also be enhanced by the Jet Knock phenomena, which enhances the diffusion of unburned HCs from the walls and crevice volumes via pressure oscillation.

In H_2 mode, the presence of unburned HC is thought to be sourced from the lubricating oil. These specific HCs increase as λ increases due to the drop in thermal efficiency. HAJI-H_2 produces less unburned HCs compared to SI-H_2, which might be due to enhanced turbulence in the quench gap region as described above.

In gasoline mode at λ=1, CO emissions are >30g/kWh (Figure 7.30). At λ=1.5,

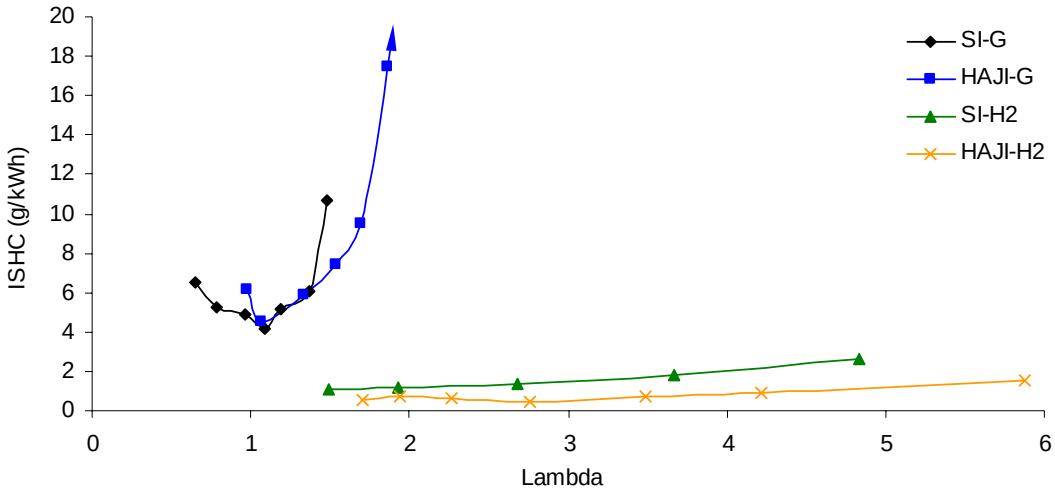

Figure 7.29: ISHC emissions versus Lambda - HAJI compared to SI.
(1800r/min, CR=9, MBT, MAP=90kPa)

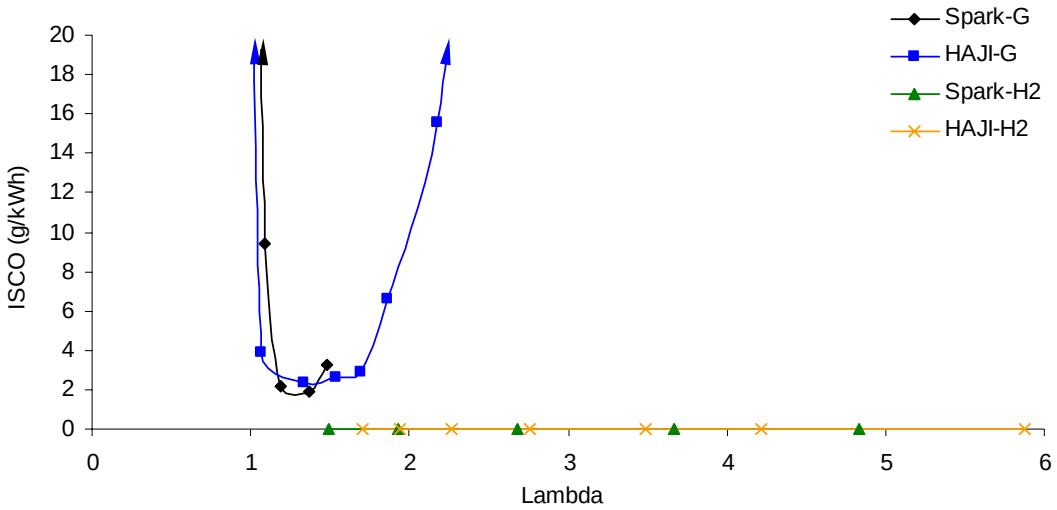

Figure 7.30: ISCO emissions versus Lambda - HAJI compared to SI.
(1800r/min, CR=9, MBT, MAP=90kPa)

CO emissions drop by 91% and at λ=1.9 by 81%. Clearly, excessively rich or lean operation is not desirable. In H_2 mode the presence of CO should be noted, however the results should be treated with caution as the resolution of the CO emissions analyser was only 100ppm and readings of 0ppm and 100ppm were obtained at these particular engine operating conditions.

In all modes around λ=1, NO_x emissions climb above 15g/kWh. As λ increases combustion temperatures drop and the rate of NO_x formation decreases dramatically (Figure 7.31). In a gasoline fueled SI engine, NO_x reduce to 5g/kWh and fueled with H_2, NO_x can be reduced to 0.54g/kWh. In contrast, HAJI in both

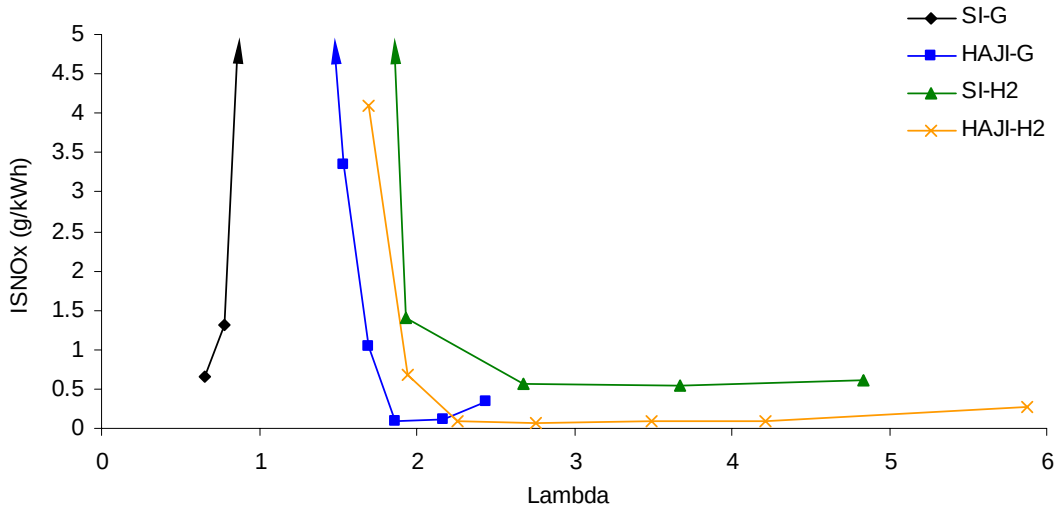

Figure 7.31: $ISNO_x$ emissions versus Lambda - HAJI compared to SI.
(1800r/min, CR=9, MBT, MAP=90kPa)

gasoline and H_2 mode can reduce the NO_x to 0.1g/kWh. In gasoline mode, this translates to a reduction of >99% in NO_x emissions over its SI counterpart and in H_2 mode to a reduction of >90%. It is worth noting that as λ increases in HAJI mode, NO_x emissions start to climb up again. This is due to the reduction in thermal efficiency and an increase in combustion temperature and residence time due to more advanced spark timing at high λ values.

Burn Duration

The enhanced burning process of HAJI over SI is shown on Figures 7.32 and 7.33. The 0-10% burn duration is dramatically reduced when the SI engine is fitted with HAJI. When fueled with gasoline at λ=1, HAJI decreases the 0-10% burn duration over SI by 37% and at λ=1.2 by 48%. When fueled with H_2 at λ=2.2, HAJI decreases the 0-10% burn duration by 50% and at λ=3 by 57%. The 0-10% burn duration is an important combustion characteristic, since combustion variability is related to this early burn phase [52]. Shorter burn duration means smaller CoV of IMEP values and since HAJI-H_2 burns the fastest at a given λ, it also provides the lowest CoV of IMEP values.

HAJI not only decreases the initial burn duration, but also decreases the total burn duration (Figure 7.33). This allows the spark timing to be retarded, which results in an increase in thermal efficiency and reduced residence time at high temperatures for less NO_x production. The greatest reduction in total burn

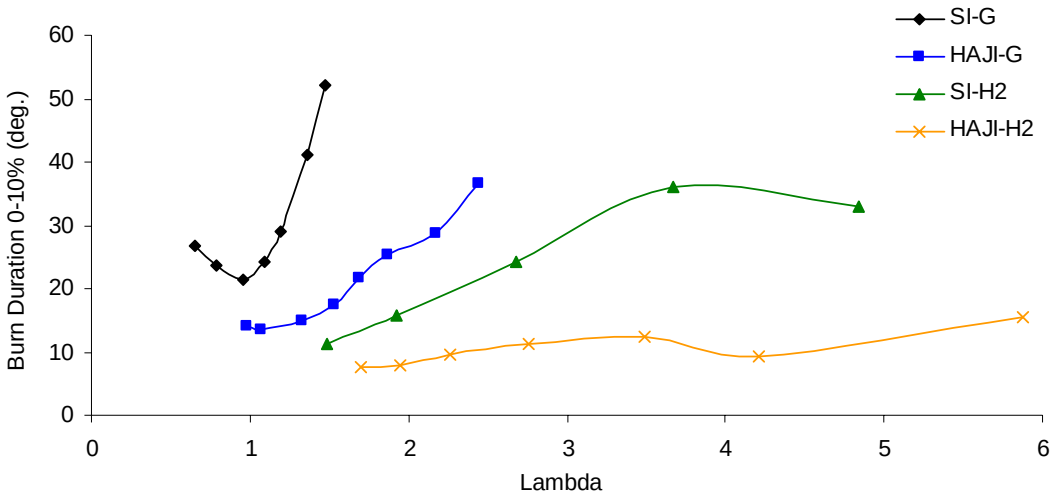

Figure 7.32: Burn duration (0-10%) versus Lambda - HAJI compared to SI. (1800r/min, CR=9, MBT, MAP=90kPa)

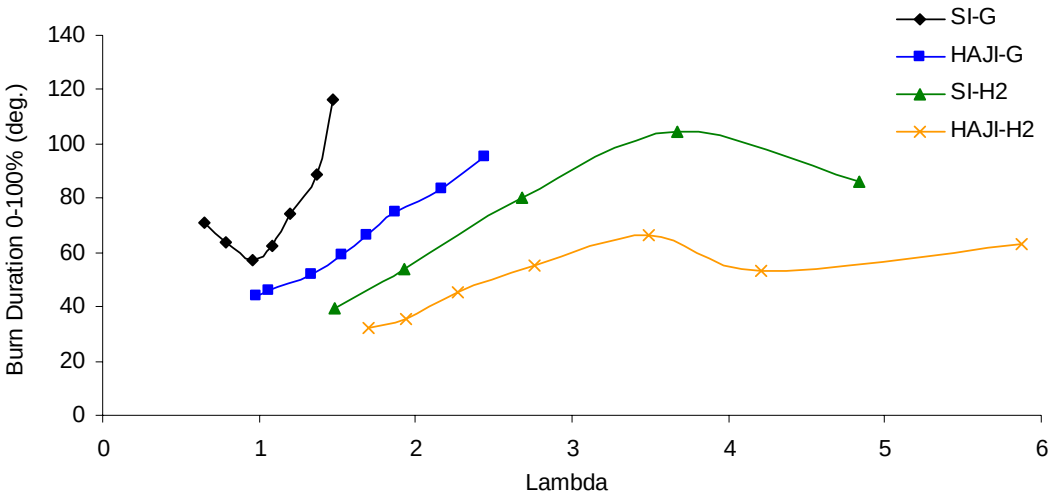

Figure 7.33: Burn duration (0-100%) versus Lambda - HAJI compared to SI. (1800r/min, CR=9, MBT, MAP=90kPa)

duration is achieved in HAJI-H_2 mode at any given λ. HAJI-G reduces the total burn duration over SI-G by up to 50% at any given λ and HAJI-H_2 reduces the total burn duration over SI-H_2 by up to 36%. In summary, the remarkable burning ability of H_2 is demonstrated in HAJI-H_2 mode at λ=6, where the total burn duration is equal to the λ=1 SI-G engine.

7.4 Jet Knock

7.4.1 The Knocking Phenomena

As described in Section 2.5.3, Jet Knock is the result of a fluid (gas or liquid) entering into a stationary fluid at or above Mach 1 and it is observed as small pressure oscillations superimposed onto a raw pressure trace (Figure 7.37). The Jet Knock phenomena in a HAJI-fitted engine was first observed by the author and throughout this thesis, an attempt was made to develop awareness and understanding of this combustion phenomenon. The previous two chapters have already highlighted how λ, MAP, and CR affect the location, duration and magnitude of Jet Knock in HAJI-G and HAJI-H_2 modes. The following section attempts to identify how Jet Knock relates to spark timing, presence of main chamber fuel, and quantity of H_2 in the pre-chamber.

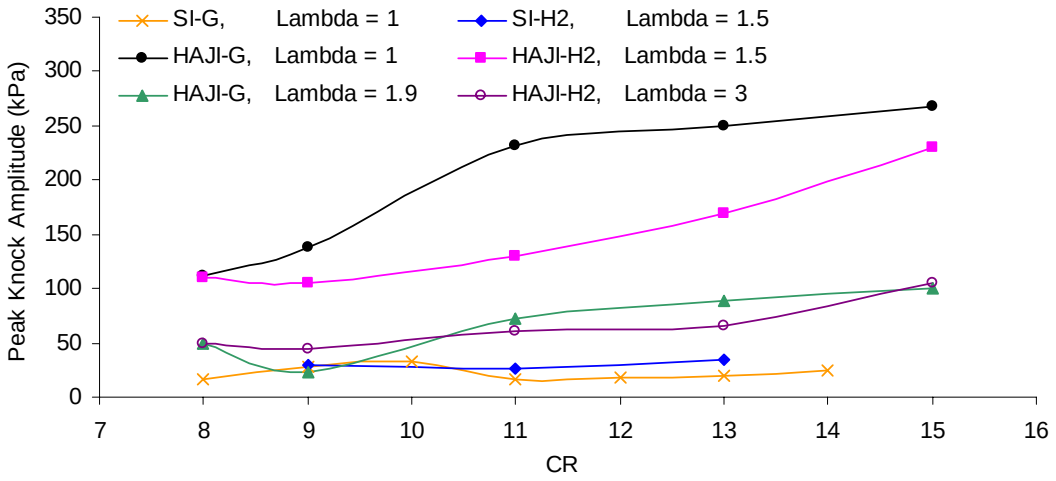

Figure 7.34: Jet Knock versus CR - HAJI compared to SI at different Lambda. (1800r/min, MAP=90kPa)

7.4.2 Pre-Chamber and Main Chamber Fueling

When the SI engine is fueled with gasoline and H_2, Jet Knock is not present. Figures 7.34 and 7.36 clearly shows the absence of any pressure disturbance throughout the combustion period. Furthermore, the maximum pressure oscillation observed in SI mode was less than 25kPa irrespective of CR and type of main chamber fuel. In contrast, in HAJI-G and HAJI-H_2 mode, Jet Knock is present at all λ values. Figures 7.34, 7.35 and 7.37 clearly show the amplitude of Jet Knock decreases as λ increases. In HAJI-G and HAJI-H_2 modes, the Jet Knock amplitude can be >250 kPa at low λ values, which is >10 times that observed in SI mode.

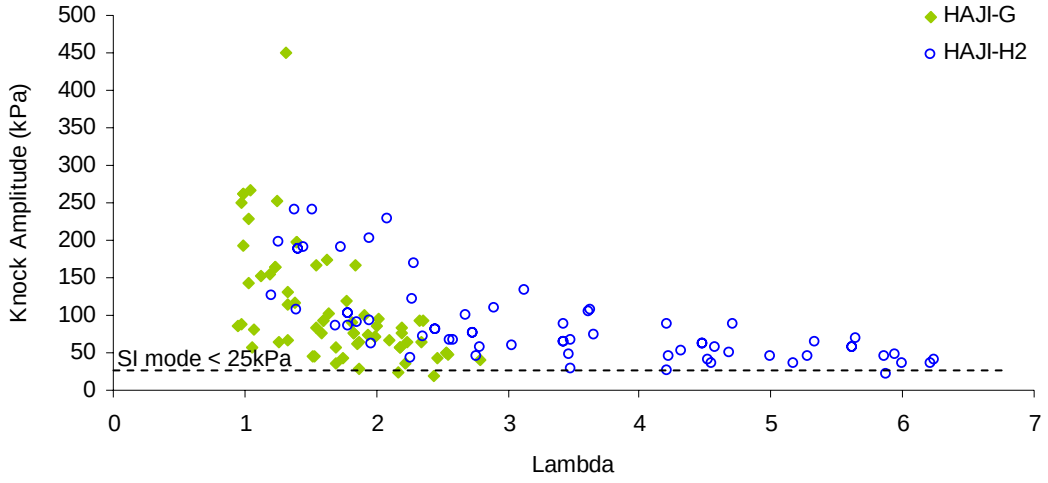

Figure 7.35: Dependence of Jet Knock on Lambda in HAJI-G and HAJI-H_2 mode at different MAP, and CR conditions. (1800r/min, MAP=90kPa)

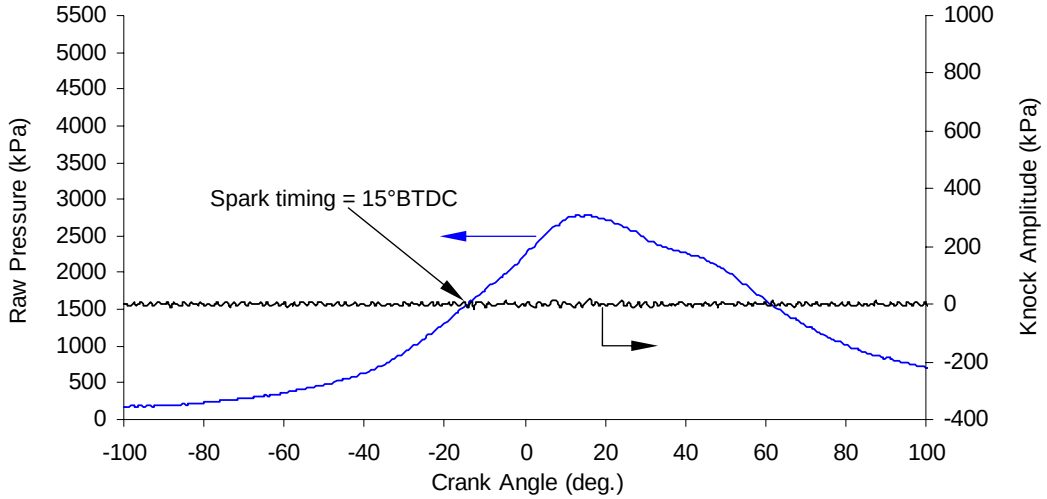

Figure 7.36: Filtered knocking versus crank angle, SI-G.

(1800r/min, CR=11, MAP=90kPa, λ=1)

The scatter in the results (Figure 7.35) is due to the dependence of Jet Knock on CR and MAP as discussed previously in Chapter 5 and 6.

The effect of CR is shown in Figure 7.34 and clearly there is an increase in Jet Knock as CR increases at a given λ. This is probably due to the increase in velocity and mass issuing from the pre-chamber at higher CR.

The rate of pressure rise was the only parameter to correlate with Jet Knock. Figure 7.38 shows the relationships between pressure rise and knocking amplitude and it is clear that when the pressure rise is <50kPa/deg., the knock amplitude is less than 50kPa. Such low pressure rise can only be achieved at high λ values or retarded spark timing. Since ignition timing strongly influences engine performance, the reduction of Jet Knock with the current nozzle configuration is impossible unless optimum efficiency and emission results are compromised.

7.4.3 Pre-Chamber Fueling Only

Through observation of Figure 7.37 (top and middle), it can be seen that the peak magnitude of the Jet Knock is influenced by the magnitude of the first pressure wave exiting the orifice at ignition [72] and by the amplification due to combustion

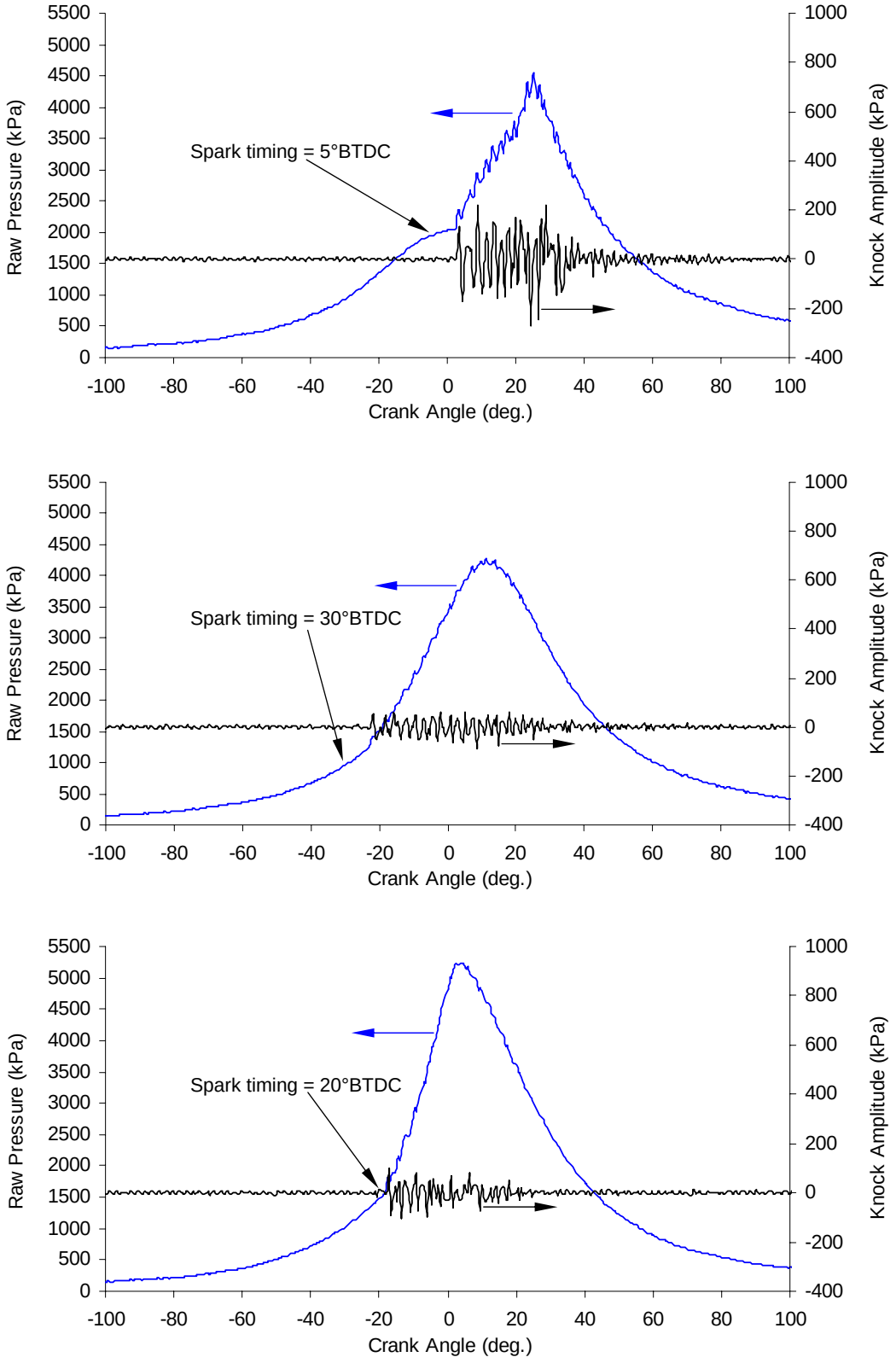

Figure 7.37: Raw and filtered pressure trace versus crank angle, (top) HAJI-G - CR=11 λ=1, (middle) HAJI-G - CR=11 λ=1.83, (bottom) HAJI-H_2 - CR=11 λ=1.8. (1800r/min, MAP=90kPa)

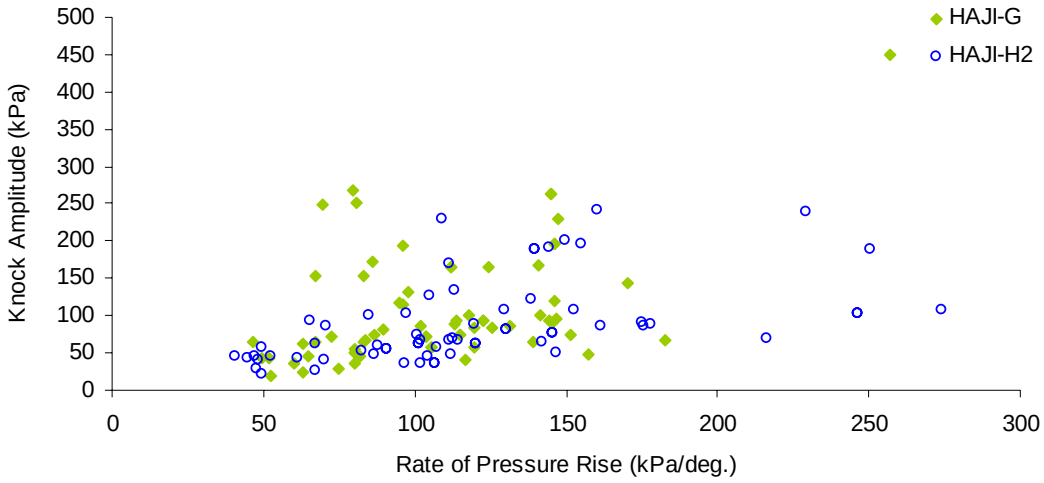

Figure 7.38: Knock amplitude versus rate of pressure rise at different MAP, and CR conditions. (1800r/min)

of main chamber fuel. Increasing the rate of pressure rise (Figure 7.38) increases the magnitude of Jet Knock, which is predominantly a result of operating at low λ conditions. As λ decreases, the pre-chamber becomes very rich and therefore generates a more intense pressure wave just after ignition.

To determine the extent to which the pre-chamber contributes to the peak knock amplitude, the engine was operated without main chamber fuel and the pre-chamber was fueled with H_2 only. Three different H_2 flows were tested (Table 7.1), which corresponds to 0.6 to 6.4% of the total fuel energy under normal engine operating conditions in HAJI-G mode.

In the absence of main chamber fuel, the first pressure wave has the largest amplitude and therefore becomes peak knock amplitude (Figure 7.39). From this

Table 7.1 Added H_2 quantity corresponding to % of total fuel energy at λ=1 and λ=2.6 in HAJI-G mode.

H_2 flow	Added H_2 of total fuel energy at λ=1	Added H_2 of total fuel energy at λ=2.4
4.9 g/h	~0.6%	~1.4%
12 g/h	~1.5%	~3.4%
23 g/h	~2.9%	~6.4%

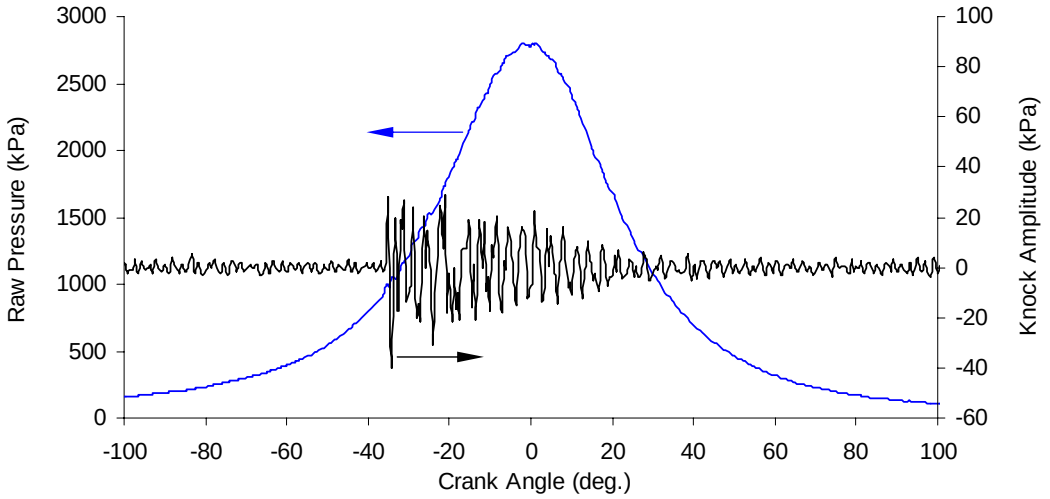

Figure 7.39: Knock amplitude versus crank angle in the absence of main chamber fuel. (1800r/min, CR=13, MAP=90kPa, H_2 flow=23g/h, spark timing=40°BTDC)

point onwards, the pressure wave attenuates due to the absence of main chamber combustion. In the absence of main chamber fuel, the amplitude of peak Jet Knock is a function of H_2 quantity, spark timing (Figure 7.40) and MAP (Figure 7.41).

As the H_2 quantity increases at a given MAP and spark timing, the magnitude of Jet Knock increases (Figure 7.40). This is predominantly attributable to the increase in pressure rise, which increases the pressure ratio between the pre-chamber and main chamber and therefore increases the jet velocity. At 0° BTDC

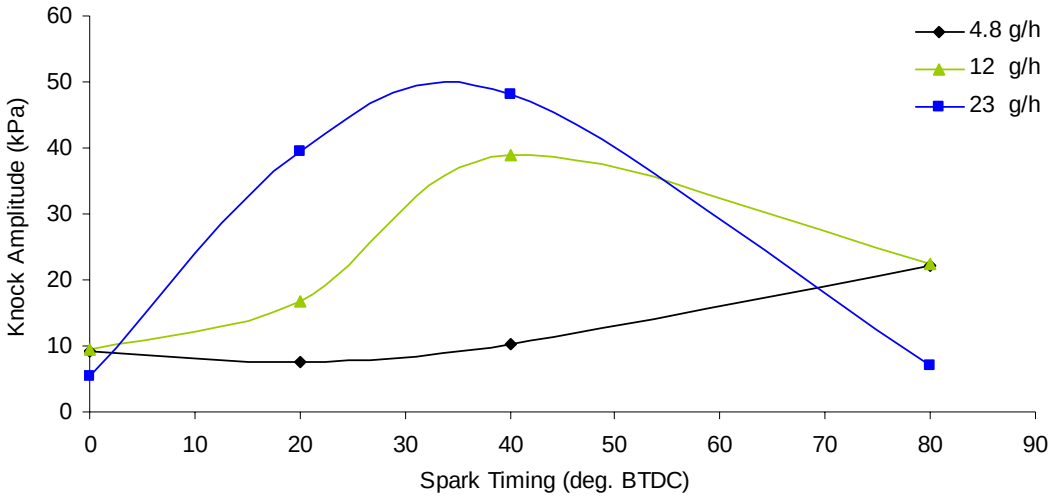

Figure 7.40: Jet Knock versus spark timing at different pre-chamber H_2 flow rates. (1800r/min, CR=13, MAP=90kPa, no main chamber fuel)

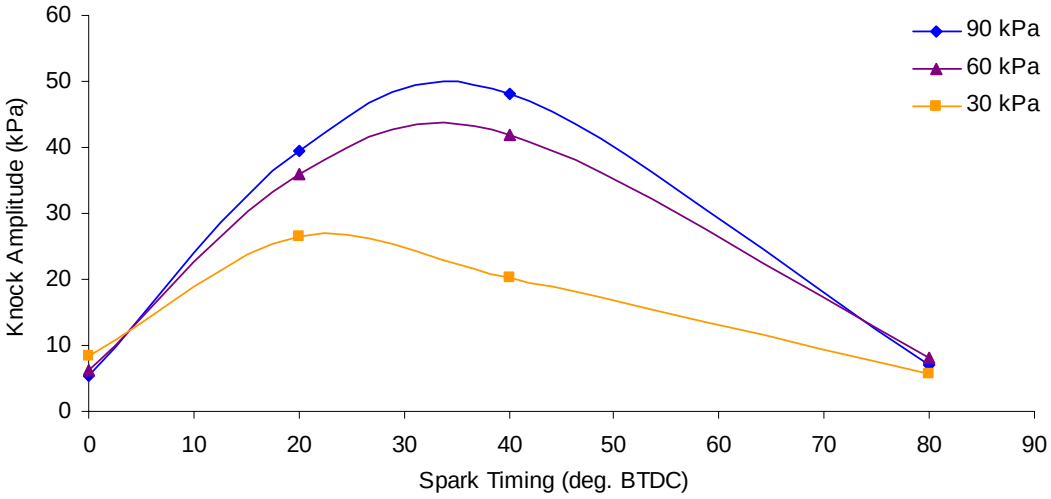

Figure 7.41: Jet Knock versus spark timing at different MAP.
(1800r/min, CR=13, pre-chamber H_2 flow rate = 23g/h, no main chamber fuel)

and 80° BTDC, the Jet Knock amplitude is the smallest. H_2 injection timing ends at 90° BTDC. Therefore at 80° BTDC, the pre-chamber is excessively rich and consequently little heat is released in the pre-chamber and the jet velocity is suspected to be low. In contrast, at 0° BTDC, the pre-chamber becomes excessively lean and since cylinder pressure at TDC is a maximum, the potential to maximise the pressure ratio across the pre-chamber and main chamber is minimised. Lastly, it is worth noting that Jet Knock amplitude decreases for a given H_2 quantity if MAP is decreased (Figure 7.41) because H_2 escapes from the pre-chamber prior to ignition.

7.4.4 Effect of Jet Knock on Performance and Emissions

With the single nozzle pre-chamber it was not possible to operate at conditions where the Jet Knock did not exist, therefore sensitivity studies on the affect on performance and emissions could not be made. Consequently, hundreds of data points were examined with the following two considerations in mind to demonstrate that Jet Knock:

1.) Could possibly increase the local heat flux, which could decrease thermal efficiency, increase thermal induced stresses and reduce the likelihood of knock by transporting heat away from the end gas.

2.) Could possibly enhance molecular diffusion, which could increase reaction rates in the flame reaction zone, and decrease HC emissions in the quench boundary layer.

As mentioned already, unfortunately, while considering the abovementioned points, no relationships were identified between Jet Knock and performance and emissions. Further investigations were out of the scope of this research; therefore recommended topics can be located in the conclusion and recommendation chapter.

7.5 General Discussion

7.5.1 Parametric Studies of HAJI

The best combustion stability, thermal efficiency and lowest NO_x emissions were achieved with a 3mm length orifice nozzle. This provides the best balance between penetration and dispersion of the HAJI jet. It also works equally well at λ=1 operation where the jet is gasoline dominated and also at high λ conditions where the jet is predominantly made up of H_2. It is important to realise that the longer the nozzle, the more likely that the jet penetrates deep enough to impinge on the opposite cylinder wall, consequently increasing heat transfer and burning lubricating oil off the walls. In contrast, short nozzles tend to disperse the jet and not enough penetration and turbulence generation is achieved.

In general, once MBT is established with the optimum H_2 quantity, then any decrease in H_2 quantity will decrease combustion stability, thermal efficiency, NO_x emissions and increase, HC and CO emissions. Any increase on top of the already established optimum H_2 quantity at a fixed ignition timing further increases combustion stability and decreases HC and CO. Thermal efficiency is unchanged at high λ values, however at λ=1, NO_x can increase dramatically. Therefore, once optimum H_2 is established, it should not be increased unless the spark timing is adjusted (retarded) simultaneously.

At high MAP, the effect of engine speed on thermal efficiency and emissions is negligible above λ=2.2. However at low MAP, as the speed is decreased the amount of residual gas fraction increases in the combustion chamber. This decreases flame speed and temperature, which forces MBT to be advanced. Consequently, NO_x emissions are higher at lower engine speeds and thermal efficiency is also penalised.

7.5.2 Parametric Studies of HAJI Compare to SI

One of the most influential parameters when optimising an engine for performance and emissions at a given air-fuel ratio is the spark timing. In SI mode, MBT occurred where CoV of IMEP was also the lowest. Emissions are not affected greatly when spark timing is deviated away from MBT. However, thermal efficiency and combustion stability can be compromised greatly, especially if timing is retarded. Similar to SI, in HAJI mode MBT occurs where CoV of IMEP is low. However, unlike SI, thermal efficiency and combustion stability are not as sensitive to spark timing. In fact at high λ values, it is possible to retard spark timing from MBT and as a result decrease NO_x emissions by >70%.

High CR is important when optimising an engine for fuel economy. At λ=1 HAJI is able to provide higher thermal efficiency at all CR values and simultaneously provide better combustion stabilities. However, more HC, CO and NO_x emissions are produced, so a λ=1 HAJI engine is not competitive with a λ=1 SI engine unless fuel economy, power and combustion stability requirements outweigh the emission constraints. In contrast, with the exception of HC emissions at high CR and λ values, HAJI provides better fuel economy, higher combustion stabilities, and lower NO_x and CO emissions. In general, optimum CR in SI mode is driven by thermal efficiency and it therefore occurs at CR=9. In HAJI mode, optimum CR is equal to 11:1, where thermal efficiency at λ=1 is equivalent to what is achieved at 9:1 in SI mode. This allows HAJI to maintain the same torque and power output as the SI engine. Furthermore, at CR=11, HAJI can further maximise thermal efficiency at high λ values and at the same time minimize NO_x emissions.

HAJI improves combustion stability at any given λ by at least 50% but also extends the lean limit by a minimum of 40% for gasoline and 84% for H_2. As it does so, the thermal efficiency improves, NO_x approach near zero values, CO decreases dramatically and HC emissions typically increase by 3.5 times for HAJI-G and decrease for HAJI-H_2. In HAJI-G mode, the optimum λ is near λ=1.9 and for HAJI-H_2 it is at λ=3 where CoV of IMEP<5%, NO_x<=0.1g/kWh. The optimum λ in SI-G mode is at λ=1 where NO_x=12g/kWh and in SI-H_2 mode the optimum AFR is at λ=2.5 where NO_x=0.78g/kWh.

7.5.3 Jet Knock

Jet Knock occurs independent of the type of fuel present in the pre-chamber as long as main chamber λ is low. The magnitude of the first pressure wave can be as high as 50kPa without the presence of main chamber fuel. However under normal operating conditions in HAJI-G and HAJI-H_2 modes, it can be as high as 250kPa, since combustion maintains and amplifies the magnitude of the pressure wave. Increasing MAP or CR tends to increase the Jet Knock amplitude. Overall, λ influences the magnitude of pressure oscillation the most.

In SI mode, Jet Knock was not observed under any condition when the engine was fueled with gasoline or H_2. Only heavy knock was observed, which manifested from the end gas region. Since heavy knock is well known to damage engines, it was avoided throughout the experimentation by retarding spark timing. In contrast, although Jet Knock was measurable, it showed no influence on performance, emissions and the durability of the engine.

7.6 Summary

This chapter examined the effects of different engine parameters on performance, emissions and combustion characteristics of the HAJI system and where appropriate, it was compared to the baseline SI engine. The engine parameters examined in particular were nozzle length, pre-chamber H_2 quantity, engine speed, spark timing, CR, and λ. Considering each parameter alone provided

greater insight into the HAJI system's sensitivity to different calibration parameters. Furthermore, it was shown in that as long as the pre-chamber was fuelled, the Jet Knock phenomena exists in HAJI combustion under most engine conditions, even in the absence of main chamber fuel.

CHAPTER 8
Combustion and Optimum HAJI vs. SI Analysis

8.1 Introduction

This chapter aims to demonstrate how the combustion temperature varies as a function of λ, and how it affects the NO_x formation at different load conditions. This was compared to a predictive NO_x model, which was implemented into the two-zone model.

Furthermore this chapter attempts to elucidate the fundamental differences between the HAJI and SI combustion processes by comparing parameters such as burn rate, flame speed and FSR. This information is then used to identify the combustion regimes in which HAJI and SI operate.

Finally, a comparison of HAJI to SI in terms of performance, emissions and combustion characteristics is presented. Chapters 5 and 6 proved the hypothesis: "That engine-out NOx emissions can be controlled at all load points, with a simultaneous improvement in thermal efficiency, by coupling HAJI with a boosting device." Therefore, to put HAJI's future into perspective, this chapter concludes by examining the usefulness of HAJI in terms of meeting future emission regulations - in particular Euro 5.

8.2 Combustion Analysis

8.2.1 Temperatures and NO_x Formation

As discussed previously, the formation of NO_x emissions is heavily dependent on λ since it controls the combustion temperature. SI engines are unable to operate at high λ values since combustion becomes unstable. Through chemical and turbulent enhancement, HAJI can provide stable operation at λ=2 and in turn reduce NO_x emission concentrations to <20ppm.

The result of burned mixture temperature and related NO_x formation for SI-G and HAJI-G mode is shown in Figure 8.1 with related engine outputs presented in Table 8.1. The results were ensemble averaged over 40 cycles and taken at MBT timing (Appendix F.1) and MAP=90kPa. The compression ratio was 9:1 for all tests, which is optimum for SI but not for HAJI which performs best at 11:1.

In reality, the temperature difference between the first and last mass fraction burned can be as much as 400K [55, 96]. The temperature profiles presented in this thesis and in Figure 8.1 show the average burned zone temperature, which assumes that there is no temperature gradient in the burned zone. Due to this assumption, peak combustion temperatures and NO_x emissions are underestimated (Table 8.1). On the other hand, this method follows the trend of experimental results. So if implemented into a predictive model, it could give a relative indication of the production of NO_x as engine parameters are varied. Furthermore, if an improvement in the accuracy of NO_x prediction is desired, then a multi-zone model calculating the actual temperature gradient in the burnt zone could be implemented.

In gasoline mode at $\lambda\approx1$, HAJI generates higher combustion temperature than SI so the amount of NO_x produced is also higher (Figure 8.1). Furthermore, HAJI produces less IMEP with a penalty on fuel economy. Therefore, at this operating point, which is at the HUCR (Appendix F.2 and F.3) for the SI engine, HAJI is outperformed. Since HAJI is not operating at the HUCR, it is less sensitive to

Table 8.1 Selected engine outputs in SI-G and HAJI-G mode at CR=9 and MAP=90kPa.

Ignition Mode	Lambda	MBT (°BTDC)	IMEP (kPa)	Thermal Efficiency (%)	CoV of IMEP (%)	NO_x actual - in exhaust (ppm)	NO_x calculated (ppm)
SI-G	1.09	23	852	33.7	1.98	3607	2318
HAJI-G	1.07	10	823	33.1	1.19	4271	3169
HAJI-G	1.33	18	688	34.1	1.25	1709	552
HAJI-G	1.53	25	609	34.2	2.06	589	87
HAJI-G	1.86	39	493	33.3	4.57	12	10
HAJI-G	2.17	45	397	29.3	10.55	12	0.2

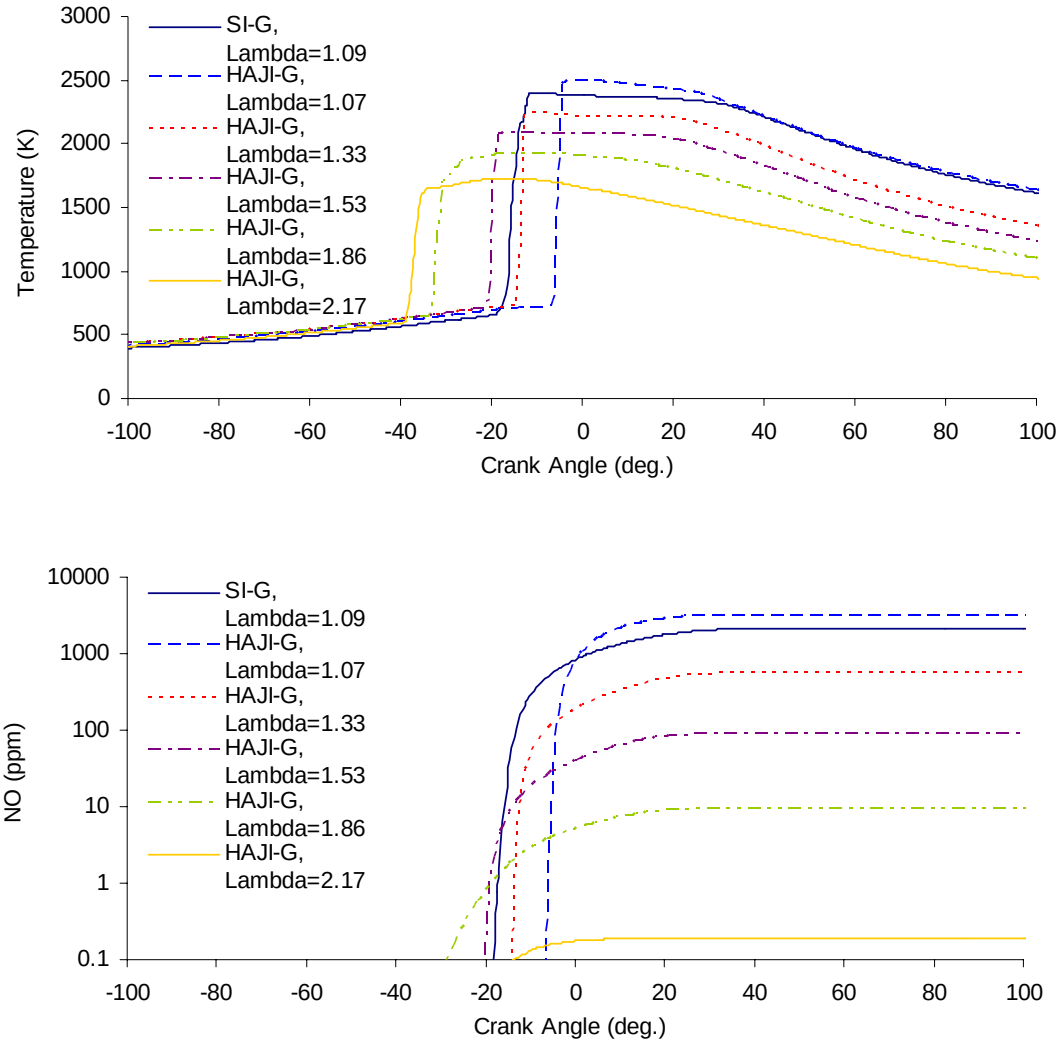

Figure 8.1: Calculated burned temperature (top) and NO (bottom) versus crank angle. SI-G vs. HAJI-G at CR=9 and MAP=90kPa, 1800r/min.

knocking. Consequently, this pushes the knock limited MBT closer to TDC, which together with the increased flame temperatures decrease the thermal efficiency overall. In contrast, as the mixture is leaned out, the fuel economy actually improves by 1.5% at λ=1.53 and NO_x drops by a factor of 7. A further increase in λ decreases the NO_x concentration at λ=1.86 by a factor of 355 over λ=1.07 conditions. As λ is increased in HAJI mode, the engine ceases to be knock limited and an improvement in thermal efficiency is observed due to more optimum MBT timing and a reduction in flame temperature.

Figure 8.1 also highlights the disadvantage of longer burn duration on NO_x production. At λ=1.86, the rate of NO_x formation is initially constant between 30°BTDC and 20°BTDC, then decreases to zero when approaching 15°ATDC. A reduction in burn duration at a given λ could further reduce NO_x emissions. Dober [55] showed that for a given λ, the fastest burning HAJI system uses central ignition with 6 nozzles. As a result, when he increased the number of nozzles from 4 to 6, he showed a decrease in combustion variability and HC emissions and halved NO_x emissions above λ=1.8.

When the main chamber was fueled with H_2, the results were similar to the gasoline results (Figure 8.2 and Table 8.2) with the exception that in both SI and HAJI mode, operation at λ=1 was impossible due to backfire. In SI mode at λ=1.48, peak burned temperatures reach 2370K, producing 4593ppm NO_x. In contrast, for HAJI mode at λ=1.7, 731ppm NO_x is produced and as λ increases NO_x emissions drop below 10ppm while fuel economy is increased by 1.6%.

Calculated NO_x emissions are approximately 2 times less than actual measured values up to λ=2.76, and a further increase in λ increased the difference even more. As described earlier, this is due to the zero dimensionality of the two-zone model where the burned zone temperature is basically the average zone temperature. Furthermore, as per previous observation in HAJI-G mode, the calculated temperature follows the trend of actual measurements which further validates the possible usefulness of a two-zone NO_x model to examine trends if implemented into a predictive model.

Table 8.2 Selected engine outputs in SI-H_2 and HAJI-H_2 mode at CR=9 and MAP=90kPa.

Ignition Mode	Lambda	MBT (°BTDC)	IMEP (kPa)	Thermal Efficiency (%)	CoV of IMEP (%)	NO_x actual - in exhaust (ppm)	NO_x calculated (ppm)
SI-H2	1.48	14	582	33.3	1.1	4593	2194
HAJI-H_2	1.69	0	520	32.7	1.07	731	306
HAJI-H_2	2.37	7.5	400	33.2	1.47	12	7
HAJI-H_2	2.76	13.5	369	33.9	2.21	9	5
HAJI-H_2	3.64	19.5	255	30.5	3.52	8	0.03
HAJI-H_2	5.88	45	81	15.7	13.3	7	4.61-E7

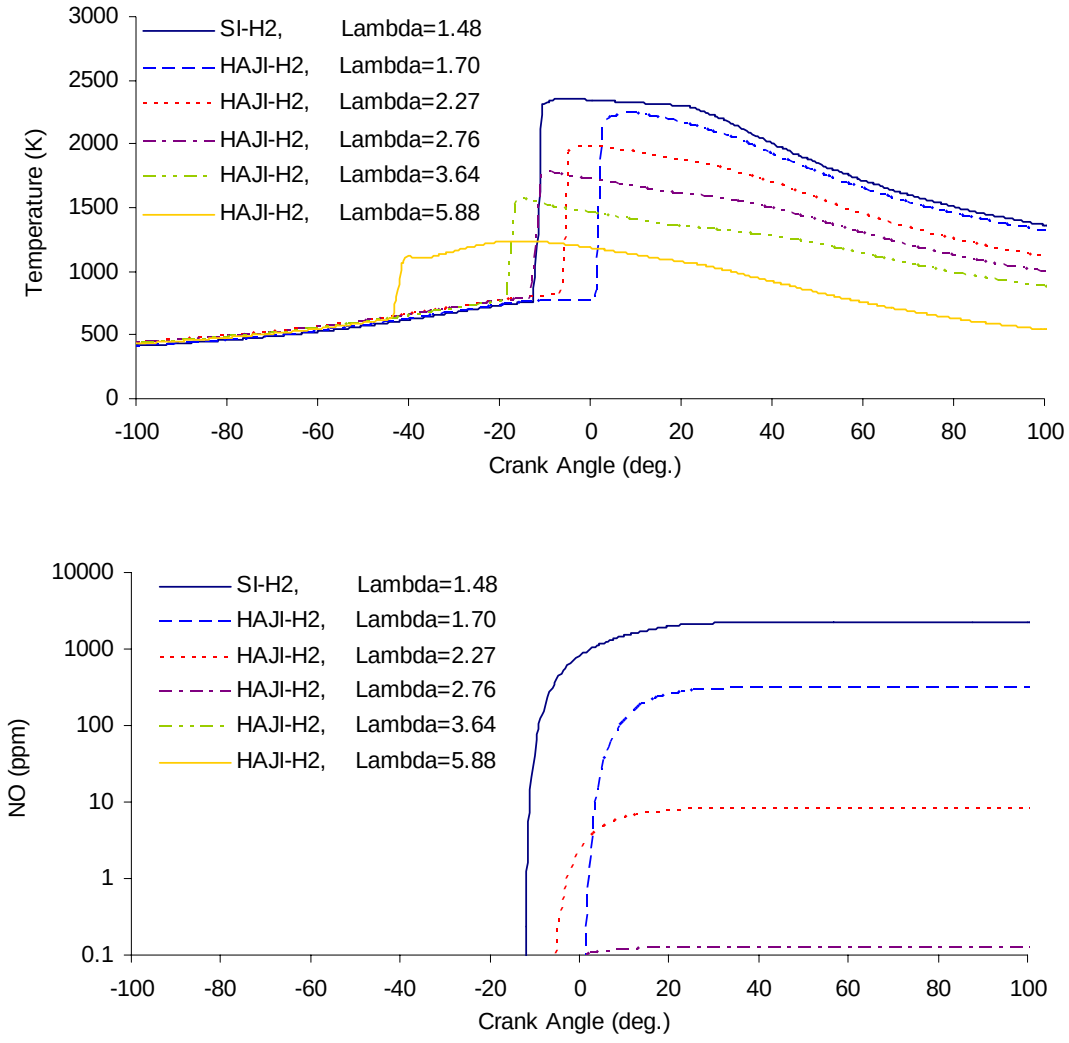

Figure 8.2: Calculated burned temperature (top) and NO (bottom) versus crank angle. SI-H_2 vs. HAJI-H_2 at CR=9 and MAP=90kPa, 1800r/min.

It is important to emphasize how low combustion temperatures actually are in HAJI mode especially when compared with combustion temperatures in the literature. Flynn et al. [68] determined that the lowest flame temperature for sustaining viable combustion in an SI engine is 1900K. At this condition, the lower limit for NO_x output is determined to be >0.7g/kWh. The results presented in this thesis have clearly highlighted the ability for HAJI to surpass these limits. In HAJI-G mode between λ=1.9 and λ=2.1, the flame temperatures vary from 1700K to 1850K. In HAJI-H_2 mode between λ=3 and λ=4, the flame temperatures vary between 1450K and 1600K, while producing only ~0.1g/kWh NO_x emissions and simultaneously improving thermal efficiency over the baseline engine. In addition to these results, Dober [55] fueled a HAJI equipped engine with propane and operated at λ=2.7, producing flame temperatures between 1390K and 1590K, while operating below 5% CoV of IMEP.

It is worth reminding the reader that at full load (WOT), regardless of main chamber fuel, SI outperforms HAJI in terms of IMEP and thermal efficiency. In addition, HAJI-G produces higher NO_x. This severe limitation was remedied by boosting the HAJI fitted engine while operating lean. SI engine was not boosted since at λ=1 it would provide similar emissions and efficiency results to its un-boosted counterpart. The result for the boosted HAJI engine versus the baseline λ=1 SI engine are shown in Table 8.3 and Figure 8.3.

As MAP increased from 90kPa to 150kPa in HAJI-G mode, λ increased from 1.07 to 2.14, and HAJI outperformed SI-G by increasing full load IMEP by 6.8% and increasing fuel economy by 8%. The significant improvement in thermal efficiency at boosted conditions occurs due to the total elimination of pumping work. The boosting device (air compressor) was assumed to have zero parasitic losses. This is a realistic assumption since turbocharged engines provide similar benefits by making use of the waste enthalpy (>30% of the fuel energy) in the exhaust. Furthermore, the 8% fuel economy improvement is not as much as what can be achieved at HAJI's optimum CR=11 and this is discussed in more detail in section 8.6.

Table 8.3 Selected engine outputs at high load conditions in SI and HAJI mode at CR=9 except HAJI-H_2 at MAP=120,150, 190kPa where CR=11.

Ignition Mode	Lambda	MAP (kPa)	IMEP (kPa)	Thermal Efficiency (%)	CoV of IMEP (%)	NO_x actual - in exhaust (ppm)	NO_x calculated (ppm)
SI-G	1.09	90	852	33.7	1.98	3607	2318
HAJI-G	1.07	90	823	33.1	1.19	4271	3169
HAJI-G	1.77	120	836	36.3	1.64	397	5
HAJI-G	2.14	150	910	36.4	3.74	30	0.3
SI-H2	1.48	90	582	33.3	1.1	4593	2194
HAJI-H_2	1.69	90	520	32.7	1.7	731	306
HAJI-H_2	2.26	120	657	37.5	1.16	31	25
HAJI-H_2	2.28	150	803	38.6	1.28	41	24
HAJI-H_2	3.13	190	806	38.7	1.8	7	0.05

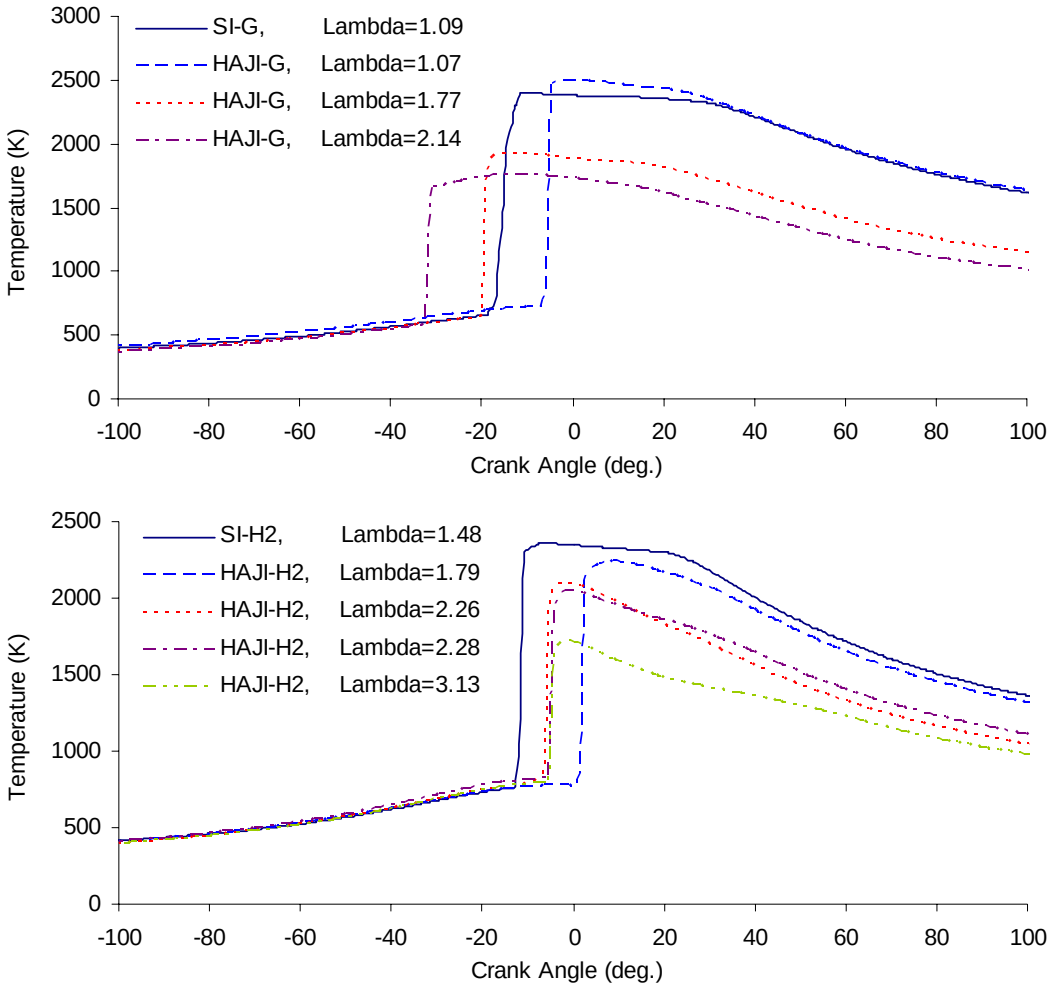

Figure 8.3: Calculated burned temperature (top) and NO (bottom) versus crank angle. SI-G vs. HAJI-G (for condition refer to Table 8.3).

In boosted lean mode (λ=2.14, MAP=150kPa), peak combustion temperatures drop dramatically (Figure 8.3) from 2500K to 1762K. This reduces NO_x concentrations by a factor of 120 (or 99.17%).

With boost, HAJI-H_2 is able to outperform its baseline naturally aspirated counterpart at high load, as long as combustion is lean. Fuel economy and IMEP improvements of 16% and 38.5% respectively were achieved in boosted HAJI-G mode. Even though IMEP was increased, backfire was not encountered during boosted operation due to the reduced ignitability of the excess air mixture and also because of the reduced peak combustion temperatures of 1720K compared to 2240K. The lower combustion temperature reduced NO_x from 4593ppm to 7ppm. Overall, HAJI is able to increase thermal efficiency at high load whilst reducing NO_x concentrations to near zero levels and maintaining excellent combustion stability (Table 8.3).

8.2.2 Burn Rates and Flame Speeds

A useful way to compare different combustion events is to examine the MFB, MBR and flame speed during the combustion event. To examine the combustion characteristic of HAJI-G and HAJI-H_2 mode and compare it to the baseline SI engine, the MFB vs. CA, MBR vs. MFB and S_T vs. flame radius diagrams are constructed for different λ conditions (Figure 8.4 and 8.5).

There are some important features of Figures 8.4 and 8.5 that should be noted. The MBR vs. MFB diagrams are independent of fuel mass burned, thus combustion characteristics of different engine modes and conditions can be compared. The speed of combustion is directly related to the MBR and by inspection, the acceleration of combustion can be observed with respect to the amount of fuel burned. Finally, the reciprocal of the area under the MBR vs. MFB curve gives the burn duration in degrees.

By comparing the MBT spark timing from Table 8.1 to the first noticeable MFB in Figure 8.4 (approximately 1% MFB), we find that the ignition delay in SI mode is

10.5CAD at λ=1.09. In contrast, at the same λ, the ignition delay for HAJI is only 7CAD, and at λ=2.17 it is only 11CAD. Interestingly, the results presented in section 5 and 6 under knock delay approximately coincide with the first 1% of the mass being consumed. Therefore the knock delay information can also serve as ignition delay data. The short ignition delay with HAJI is followed by fast consumption of the first 3% of the unburned charge, which can be observed on the MBR vs. MFB diagram. The high initial burn rates indicate that the energy release comes from both the fuel in the prechamber and the fuel first enflamed by the prechamber jet. Since the burned volume is small at this stage, the derived flame speeds are 3.5-5.5m/s. This indicates that the initial HAJI flame speed is turbulent, whereas in SI mode the flame starts off as laminar with a speed of ~0.75m/s at λ=1.09.

These results are unique to this thesis and the implication of enhanced initial flame speeds is the reason Dober [55] and Lumsden [143] used a flame speed multiplying factor to correlate the theoretical modelling results to the experimental results.

Lumsden [143] used a constant flame speed multiplying factor. At high λ values, the factor was high enough so that the theoretical initial MFB profile would match the experimental results. Unfortunately, this caused an overestimation of MBR at the latter part of the burn duration. It is therefore suspected that the variation in flame enhancement factor varies throughout the combustion event.

At λ=1.07 the peak MBR in HAJI mode is 35% higher than SI. This is interesting considering that the amount of H_2 at this condition is less than 0.5% of the total fuel energy. The pre-chamber is thought to be richer than the main chamber, therefore upon ignition the active radicals are maximised, enhancing the burn through the entire burn duration. The SI burn profile is achieved in HAJI mode when λ is between 1.53 and 1.86. Furthermore, in SI mode, peak MBR occurs at 72% MFB. However in HAJI mode at λ=1 it is closer to 63% MFB and at λ=2.17, 53%MFB. As λ increases, the peak MBR shifts towards the 50% MFB point, providing a more consistent burn rate for the duration of combustion.

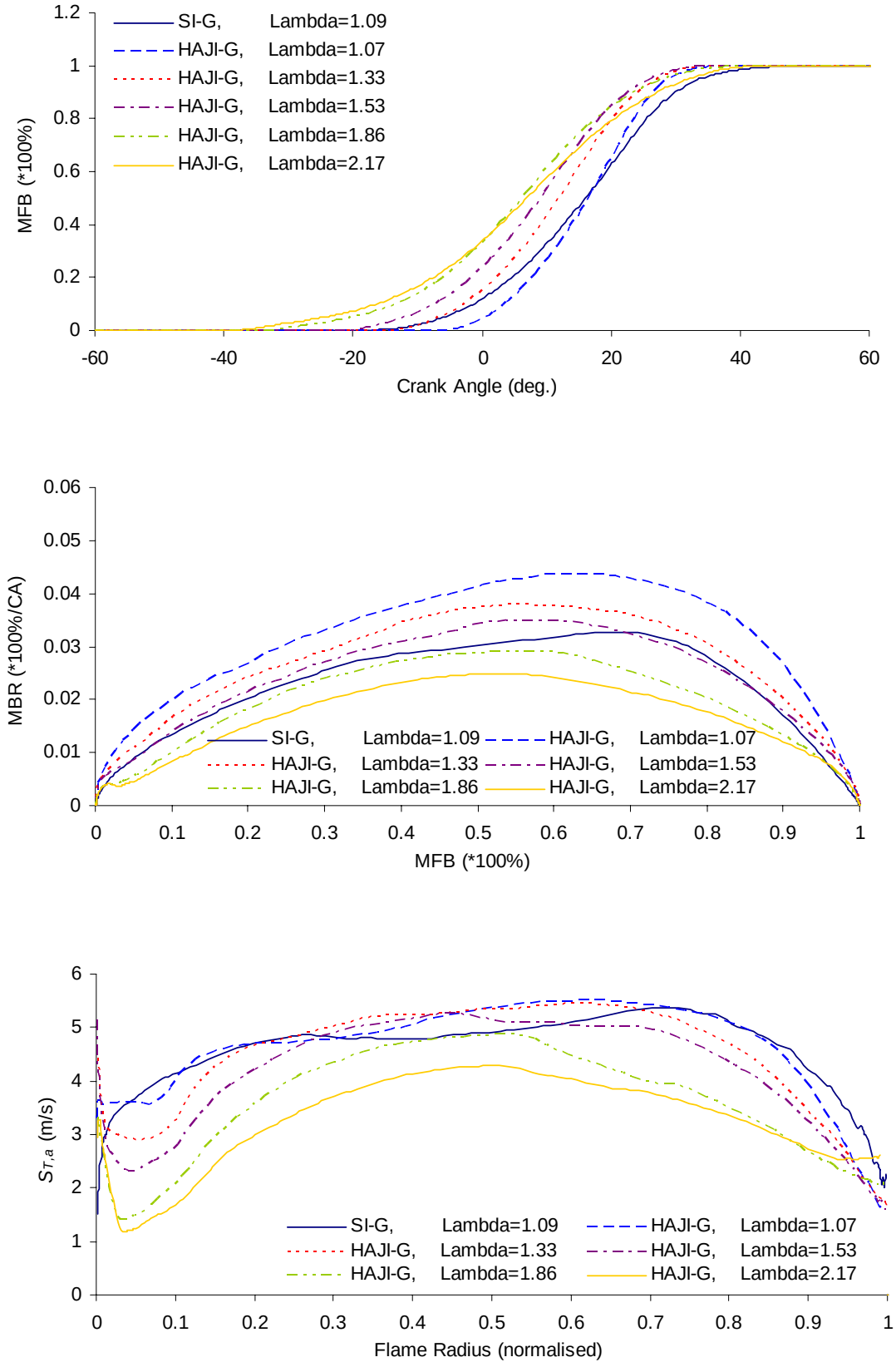

Figure 8.4: SI-G versus HAJI-G - (top) MFB vs. CA, (middle) MBR vs. MFB, (bottom) $S_{T,a}$ vs. Flame Radius. (CR=9, MAP=90kPa, 1800r/min, for more details see Table 8.1)

In SI-H_2 mode, the ignition delay is only 4.5CAD at λ=1.4, whereas in HAJI- H_2 mode at λ=1.7 and λ=5.88, the ignition delay is shorter at 3.5CAD and 4CAD respectively (Figure 8.5 with MBT data from Table 8.2).

HAJI-H_2 burns 17% faster at λ=1.7 than SI-H2 at λ=1.48 and 75% faster than SI-G at λ=1.09. Similar to gasoline mode, when the engine is fueled with hydrogen, the peak MBR moves towards the 50% MFB point. In Figure 8.5 it can be observed that the MBR is almost constant throughout the burn duration for λ>2.

With HAJI, the enhanced initial burn rate after the start of combustion occurs at all λ conditions but is accentuated the most at λ=5.88. At this very lean condition, combustion starts off fast as the jet penetrates into the combustion chamber and burns all of the charge in its path. Subsequently, at the transition point where the jet energy is dissipated and the burning of main chamber fuel begins, a deceleration in combustion can be observed momentarily. Consequently, a unique double hump can be observed on the MFB vs. MBR diagram. This fast burn rate translates into high initial flame speeds. In SI mode, 6m/s flame speeds are observed and in HAJI mode up to 9.8m/s. Other examples of high initial flame speed and a double hump in the MBR is observed in diesel and DI combustion [55, 95, 197, 232]. Interestingly, no reference was found in the literature of this combustion enhancement phenomena relating to homogeneously charged IC engines.

8.2.3 Regimes of Combustion

As shown in the previous section, one of the most useful aspects of the diagnostic two-zone model is the ability to extract useful information such as MFB, MBR, and $S_{T,a}$ from the pressure data. Using the E-CoBRA program, further manipulation of the data can provide insight into combustion parameters such as S_L, turbulence intensity, Damkohler and Reynolds number at the flame front. All of this information can be plotted to gain in-depth knowledge of the HAJI combustion process and determine how it differs from SI.

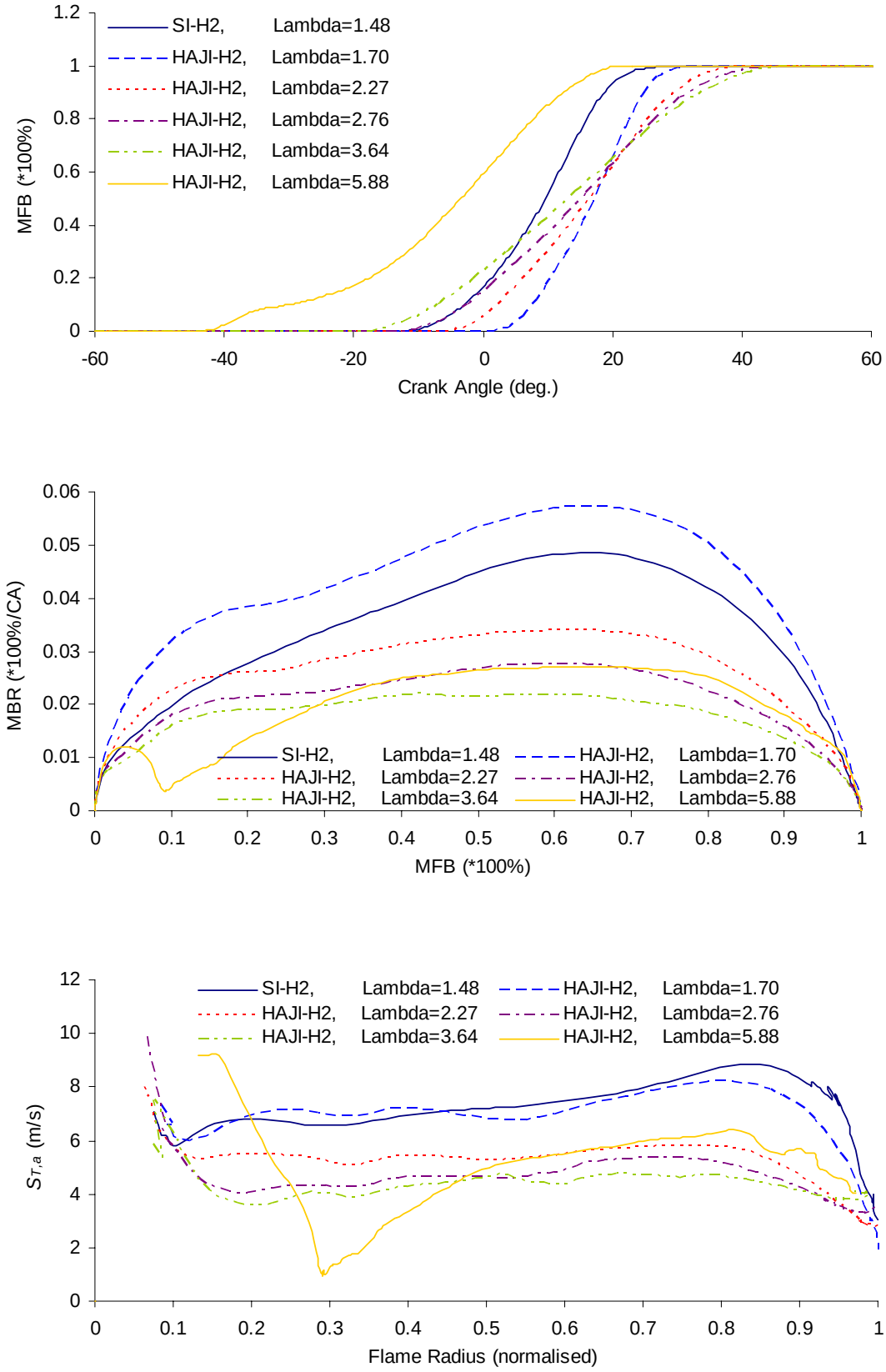

Figure 8.5: SI-H_2 versus HAJI-H_2 - (top) MFB vs. CA, (middle) MBR vs. MFB, (bottom) $S_{T,a}$ vs. Flame Radius. (CR=9, MAP=90kPa, 1800r/min, for more details see Table 8.2)

For Figures 8.6 and 8.11, data points were taken at 50%MFB. This point is convenient from the analysis point of view because the turbulence intensity level generated by the jets is expected to have attenuated to similar values measured by Lancaster in SI mode, which is more realistic to use in modelling (Section 3.5.4). The flame in the main chamber is also fully developed, therefore the effect of "developing turbulence", usually applied initially to the flame kernel, can be ignored [31, 75, 143]. Finally, the 50%MFB point is a global mapping point in academic research and in the automotive industry.

After examining many theoretical turbulent flamelet models, the most useful FSR_t model proved to be the simplest of all, which is in the form of $FSR_t=S_{T,t}/S_L=1+u'/S_L$ and plotted in Figure 8.6. This flamelet model correlates strongly with all ignition modes and all λ conditions. Furthermore, considering that all HAJI and SI data points spread around *KaLe=0.3,* it can be concluded (at least at 50%MFB) that there is a continuous flame sheet, the chemical processes are more dominant than the turbulent processes and finally, that the structure of the flame will remain largely unaltered by the turbulent flow field. Lumsden [143] also found this to be true for the entire burn duration up to λ=1.6 in gasoline mode, so Figure 8.6 is simply an extension of Lumsden's work by showing results for higher λ conditions and, more importantly, for conditions where the engine was fueled with hydrogen.

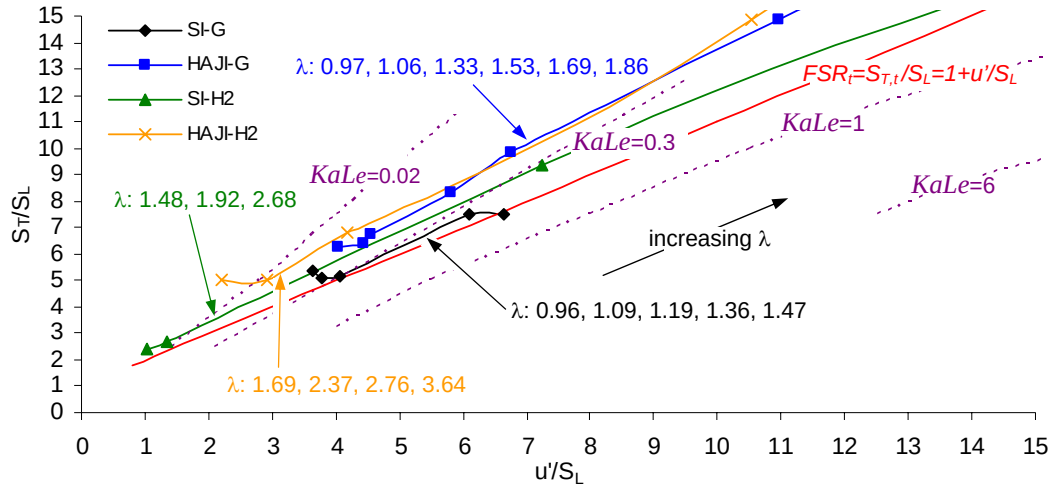

Figure 8.6: $S_{T,a}/S_L$ versus u'/S_L for HAJI and SI modes, fueled with gasoline and H_2. (all data points are at 50%MFB, CR=9, MAP=90kPa, 1800r/min, for more details see Table 8.1 and 8.2), $FSR_t=S_{T,t}/S_L=1-u'/S_L$ is also shown.

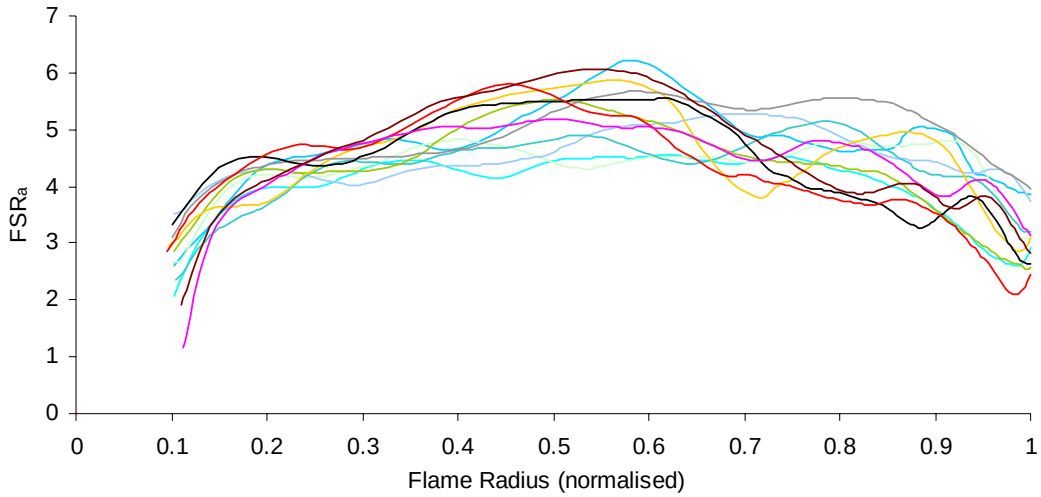

Figure 8.7: FSR_a ($S_{T,a}/S_L$) versus Flame Radius, consecutive cycles in SI-G mode, λ=1.09. (CR=9, MAP=90kPa, 1800r/min, 50%MFB is at 75% of the flame radius, for more details see Table 8.1)

$FSR_{a,t}$ increases linearly in all modes with u'/S_L, which is due to the small variation in turbulence intensity. Consequently, λ is the most influential parameter affecting the $FSR_{a,t}$. In fact, in HAJI-G mode at λ=2.17 the peak FSR_a is 50 compared to a peak FSR_a=5 for SI at λ=1 (Figure 8.7 and 8.8). However, as λ increases beyond 2.17, the laminar flame speed rapidly approaches unrealistically small values causing the FSR_a to rise to infinity. This is also the case in hydrogen mode beyond λ=3. At these very lean conditions, combustion theory fails to explain how HAJI operates even though the actual turbulence intensity was measured inside the engine by Lancaster [131] (Section 3.5.4) and the laminar flame speed model is the most sophisticated available in the literature [78, 160] (Section 3.6.1). Considering all factors, it is only logical to conclude that HAJI can operate at ultra-lean mixtures due to the chemical enhancement provided by the active radicals issued from the rich pre-chamber.

This enhancement is not captured when calculating S_L, therefore the author believes that the current S_L values are severely underestimated for gasoline fueled engines beyond λ=2 and for hydrogen fueled engines beyond λ=3. Consequently, the upper limit of $FSR_{a,t}$ by the author is considered to be around 50. The upper limit of $FSR_{a,t}$=50 is further supported by high speed Formula 1 racing engines operating up to 18,000 rev/min, giving approximately a FSR_a=60. This however

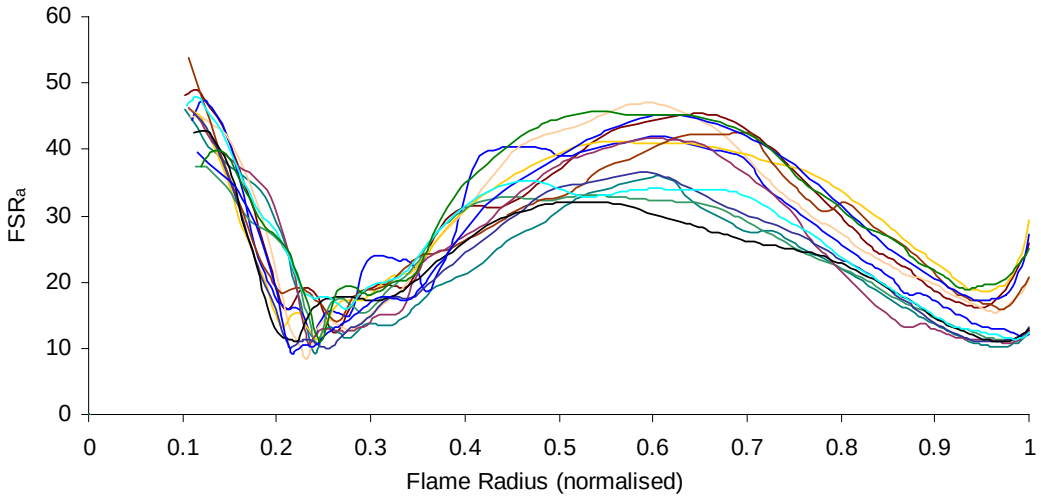

Figure 8.8: FSR_a ($S_{T,a}/S_L$) versus Flame Radius, consecutive cycles in HAJI-G mode, λ=2.17, (CR=9, MAP=90kPa, 1800r/min, 50%MFB is at 67% of the flame radius, for more details see Table 8.1)

contradicts with Bradley's [31] conclusion that the limit of turbulent flame speed in IC engine is near $FSR_{a,t}$=20, above which the flame can possibly extinguish.

Due to the complex turbulent and chemical combustion process of HAJI through a wide range of λ conditions, Lumsden [143] and Dober [55] faced a lot of difficulties predicting the flame speed of HAJI. As already mentioned, Dober and Lumsden built predictive models, which worked with limited success even when a flame speed multiplying (FSM) factor was used. The author chose to examine this flame speed multiplying factor by calculating the ratio of actual flame speed over

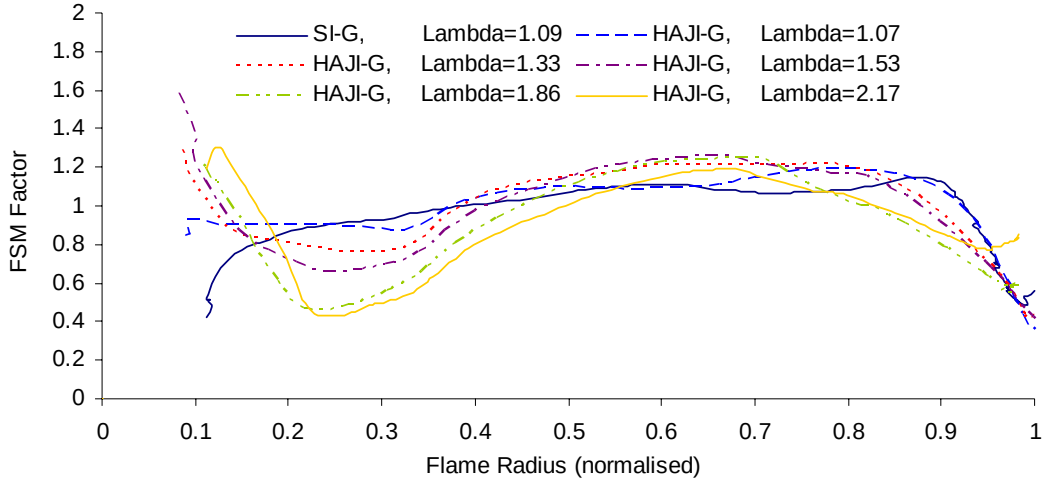

Figure 8.9: FSM Factor for SI-G and HAJI-G modes.
(CR=9, MAP=90kPa, 1800r/min, for more details see Table 8.1)

the theoretical flame speed (Equation 3.25). The theoretical flame speed was calculated using a turbulent flamelet model in the form of $FSR_t=S_{T,t}/S_L=1+u'/S_L$ chosen from a large number of models because it fits the behavior of SI and HAJI combustion the best.

The results of SI and HAJI modes are displayed in Figures 8.9 and 8.10 respectively. The FSR_t model predicts the flame speed very well for most of the combustion processes in SI mode in both gasoline and H_2 mode as shown by a steady FSM factor of 1 throughout combustion. In SI-G, mode the FSM factor is initially less than 1 and this is expected since the flame speed is laminar just after ignition (Figure 8.7). As the flame radius becomes larger than the smallest eddies, the turbulence begins to distort the flame's surface, resulting in the development of a turbulent flame. In order to correlate the FSR_t model with the early flame kernel development (i.e. FSM factor=1), the turbulence intensity relevant to the flame kernel during the combustion cycle must be known. To fix this overestimation of flame speed by the FSR_t model, Lancaster [133] was the first to develop a flame speed multiplying factor based on spectral distribution of turbulent energy. Lancaster's work was further refined by Bradley et al. [31] and Santavicca et al. [190]. Interestingly, the FSR_t model requires no modification when H_2 is used in SI mode (Figure 8.10). This might be due to the high flame speed of H_2 that causes the flame kernel to quickly develop into a turbulent flame (Figure 8.5).

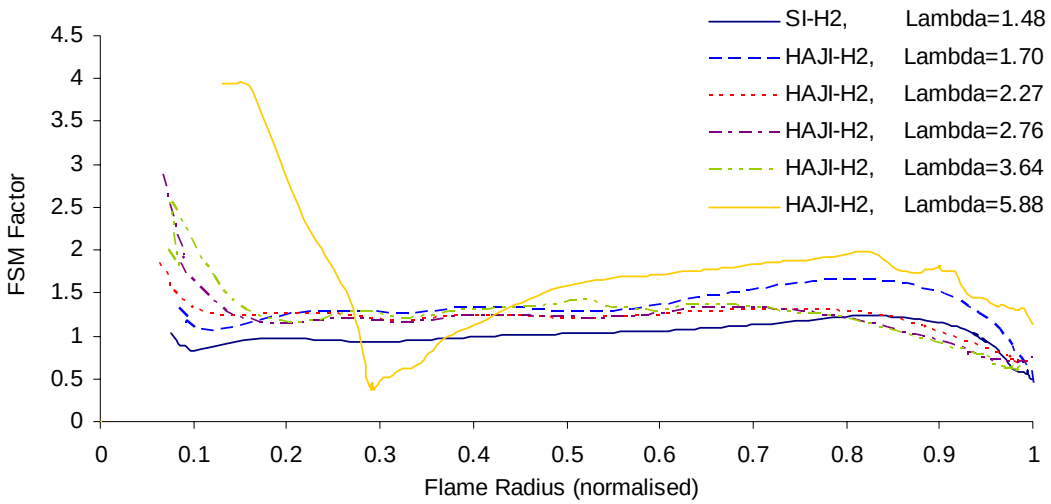

Figure 8.10: FSM Factor for SI-H_2 and HAJI-H_2 modes.
(CR=9, MAP=90kPa, 1800r/min, for more details see Table 8.2)

In HAJI-G mode at λ=1, the FSR_t model closely predicts the flame speed behavior of HAJI (Figure 8.9) (therefore FSM Factor=1). Unlike SI mode, as λ increases, the FSR_t model underestimates the flame speed enhancement level severely at the start of combustion until the flame radius reaches 20% of its maximum size. The calculated flame speed needs to be multiplied by up to 1.6 times to match with the actual flame speed (therefore FSM Factor=1.6). This enhanced flame speed is due to fast burning of the initial main chamber fuel enflamed by the jet. This shows that the initial flame speed in HAJI-G mode is turbulent rather than laminar as observed in SI mode.

The initial flame speed enhancement is independent of λ which means that even at high λ, the FSM factor is still about 1.6. At λ=1.86 and 2.17, the FSR_t model over predicts the flame speed (i.e. FSM Factor<0.5) at 25% of the maximum flame radius. This occurs at the transition point, where it is believed that the jet energy is dissipated and burning of the main chamber fuel begins. Consequently, once sufficient heat is released into the combustion chamber, the flame speed quickly accelerates up to speeds close to those predicted by the FSR_t model. At the end of combustion, the FSR_t model overestimates the flame speeds as indicated by a FSM factor falls below 1. This is observed in both SI and HAJI mode and is expected to happen because the flame approaches the cool cylinder walls where it quickly decelerates due to quenching. In fact, the flame probably stagnates momentarily until all of the fuel is consumed from the end gas, which is generally transported from the quench layer by turbulence.

In HAJI-H_2 mode, the FSR_t model underestimates the flame speed through the entire burn duration except at the end of combustion (Figure 8.10). Between 15% and 80% of the maximum flame radius, the underestimation can be compensated for by a constant such that, as λ increases, the FSM factor increases. The behavior up to 20% flame radius is similar to gasoline mode, where the jet upon engulfing the main chamber fuel, enhances the flame speed such that the FSR_t model needs to be multiplied by up to 4 times to match the actual flame speed. At λ=5.88 and 30% flame radius, the turbulent flame speed drops to 1m/s. However, the FSR_t model predicts 2.5m/s, thus giving a FSM factor=0.4. Even though this result is

similar to what was observed in HAJI-G mode at λ=2.17 the author is doubtful about the calculations. The actual flame speed of 1m/s is plausible, however the FSR_t model and therefore the FSM factor probably contain calculation errors due to the laminar flame speed being equal to ~7E-10 m/s. Such a small S_L value is not realistic as it results in FSR_t values of 1.4E-9. It should be noted that at optimal λ conditions in both gasoline and H_2 modes where laminar flame speed is sufficiently high, the values of FSR_t and FSM factor are all realistic.

Further information can be gained about HAJI combustion by examining data in the Da-Re_T domain. As shown in Figure 8.11, in SI mode both gasoline and H_2 fueled engines fall into the domain already defined by previous researchers [3, 75]. In this domain, the burned and unburned regions in the combustion chamber are separated by a flame front. Da is relatively high, which means that the flame front consumes the mixture faster than turbulence can distort or break it up. In relative terms, this means weak levels of turbulence with respect to S_L.

For HAJI-G or HAJI-H_2, as λ was increased, the Da started to decrease as u'/S_L increased. This indicates that the chemical reaction in the flame reaction zone is slow compared to the level of turbulence. Consequently, the turbulence could transport and mix the reacting mixture as the burning occurs. In fact, since u'/S_L is much greater than unity, the turbulence may produce pockets of burned and unburned mixture in the vicinity of the flame front. Additionally, as λ increases in gasoline and H_2 modes, Re_T decreases slightly due to the increase in viscosity, which is driven by the increase in density and increase in unburned mixture temperature.

8.3 Optimum HAJI Compared to SI

8.3.1 Optimum λ and MAP Conditions

This final section compares the overall performance of HAJI at optimal operating conditions to the baseline SI engine. The engine was operated at a constant speed at 1800 r/min in all cases. In SI-G and SI-H_2 mode, the compression ratio was set

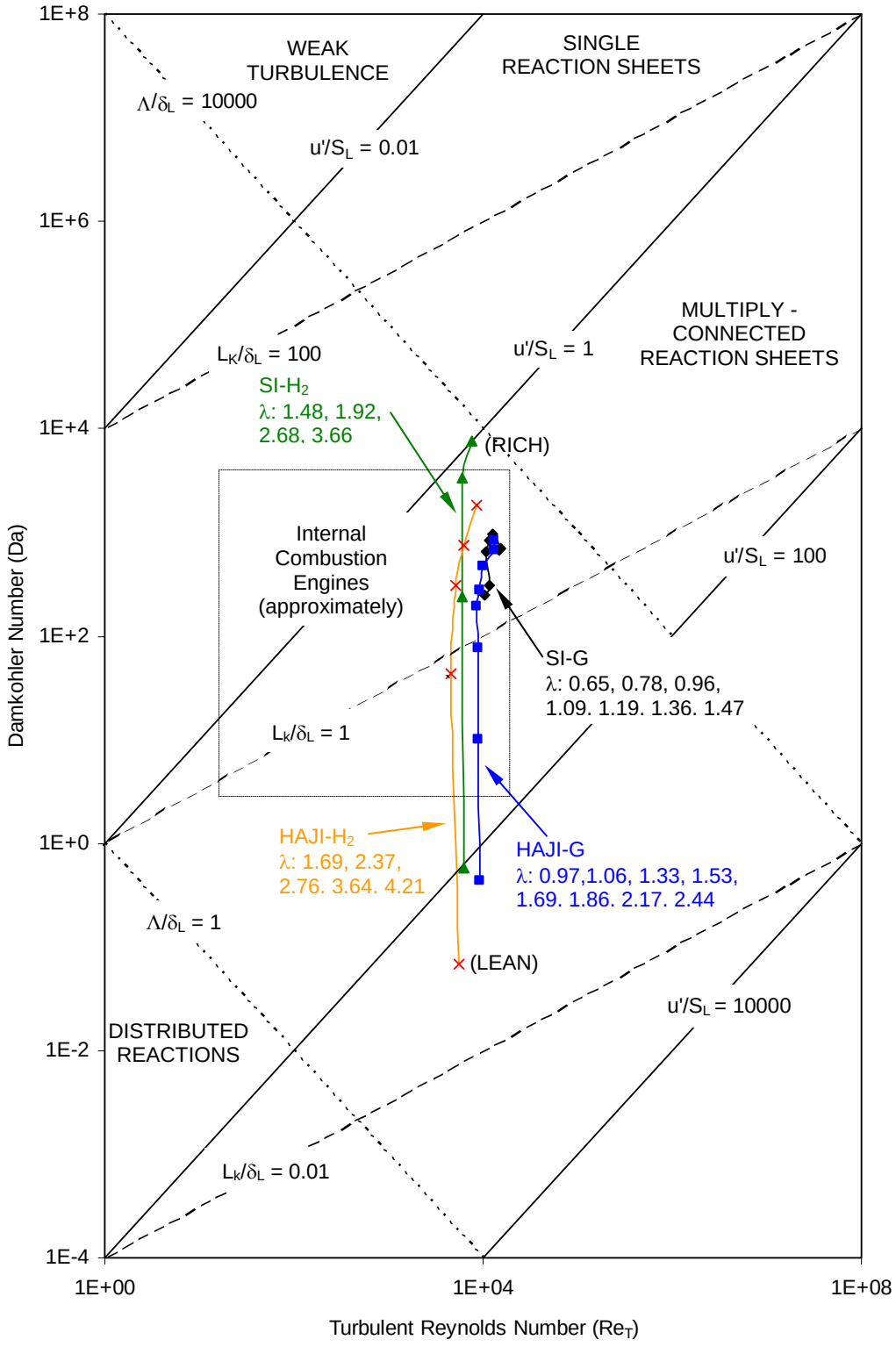

Figure 8.11: *Da* versus Re_T - HAJI compared to SI,

(all data points at 50%MFB, CR=9, MAP=90kPa, 1800r/min)

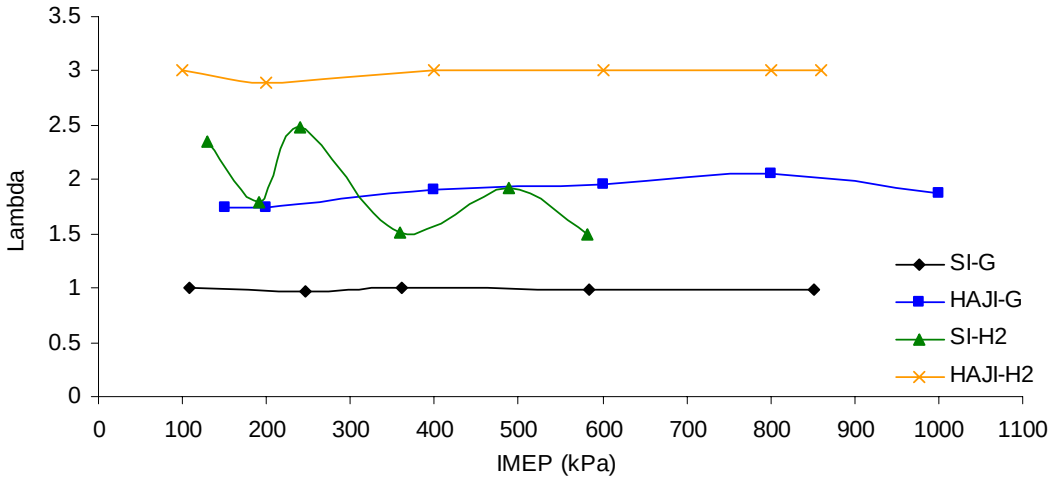

Figure 8.12: Input λ at a given load for HAJI (CR=11) and SI (CR=9) at 1800 r/min (for graphs 8.14 to 8.23).

to 9:1, which corresponded to the HUCR in SI mode for the CFR engine. In HAJI-G and HAJI-H_2 mode the compression ratio was set to 11:1. To achieve a desired load condition while maintaining less than 5% of CoV of IMEP in both HAJI and SI modes, λ and MAP were adjusted. Figure 8.12 and 8.13 show the input λ and MAP conditions at a given IMEP. For HAJI-G and HAJI-H_2 modes, this information was derived from the OPL shown on all of the graphs in Chapters 5 and 6.

It can be seen in Figure 8.12 that HAJI-G and HAJI-H_2 operate at much higher λ than SI, yet equivalent and even higher loads than SI are possible. This is achieved by increasing the MAP while keeping the fuel flow fixed at a given IMEP.

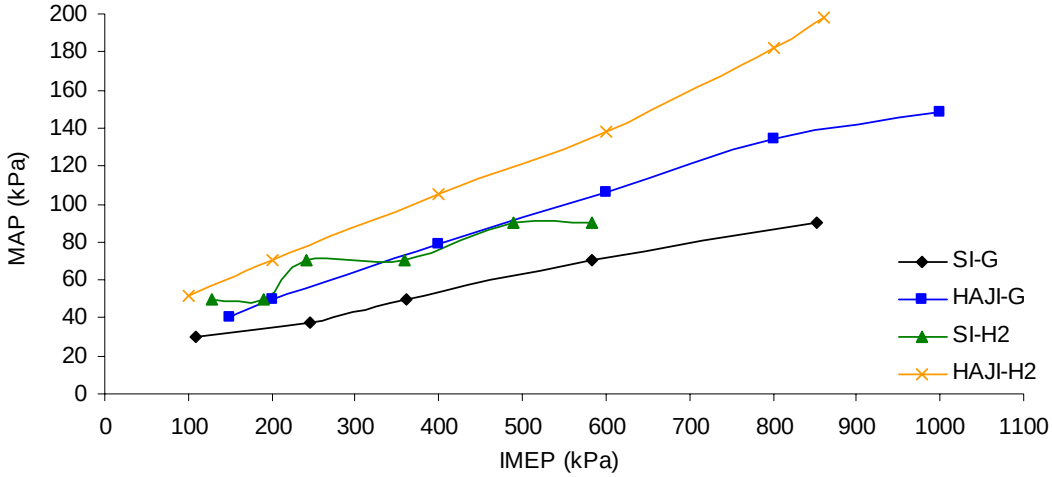

Figure 8.13: Input MAP at a given load for HAJI (CR=11) and SI (CR=9) modes at 1800 r/min and optimum λ (for graphs 8.14 to 8.23).

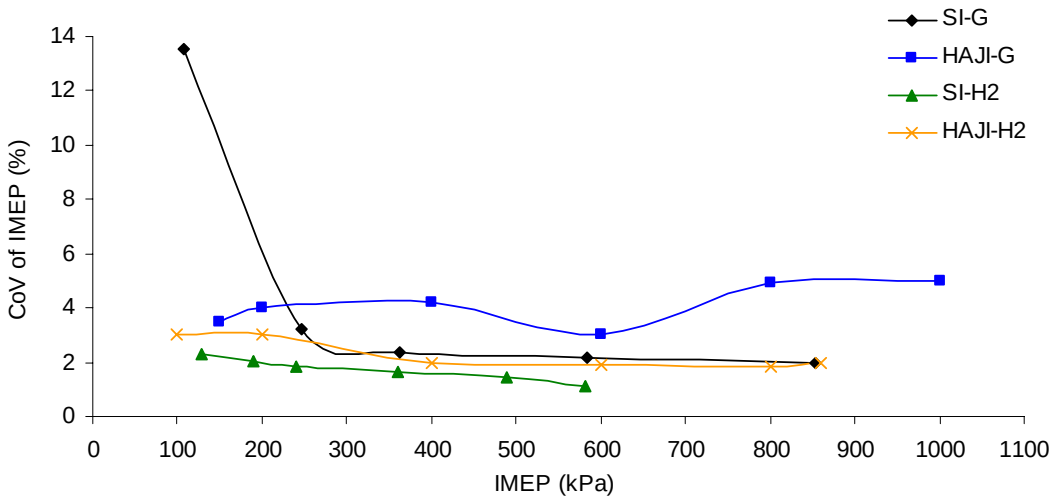

Figure 8.14: CoV of IMEP versus IMEP - HAJI compared to SI, 1800r/min, λ and MAP conditions as per Figure 8.12 and 8.13.

8.3.2 Performance

All optimum data points in SI and HAJI modes provide excellent combustion stabilities, except SI-G mode at idle (Figure 8.14) where the CoV of IMEP reaches unacceptable levels of 14%. In contrast, HAJI-G can stabilise combustion at idle and as a result it provides a ~41% improvement in thermal efficiency (Figure 8.15). In general, thermal efficiency drops as engine load decreases. This is due to the increase in pumping losses and increase in overall burn duration as a consequence of increased levels of EGR.

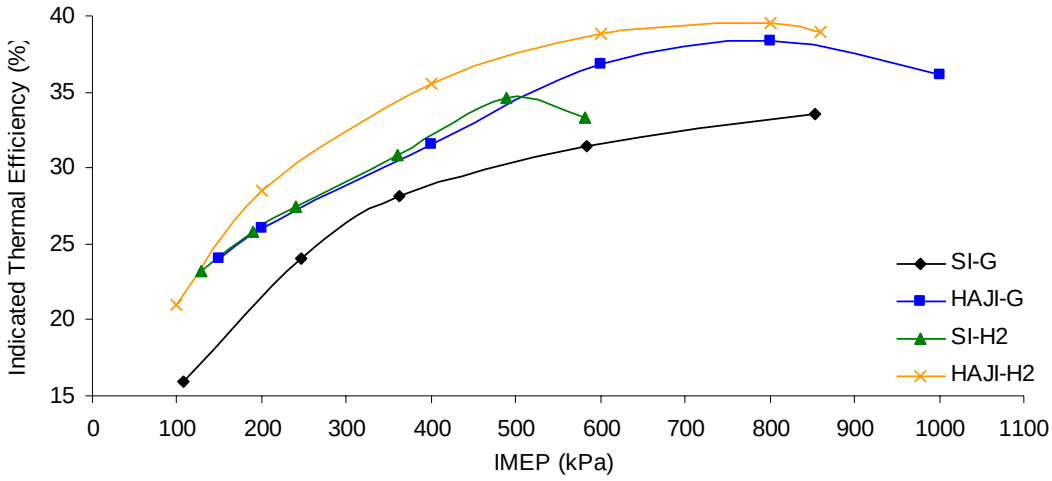

Figure 8.15: Thermal Efficiency versus IMEP - HAJI compared to SI, 1800r/min, λ and MAP conditions as per Figure 8.12 and 8.13.

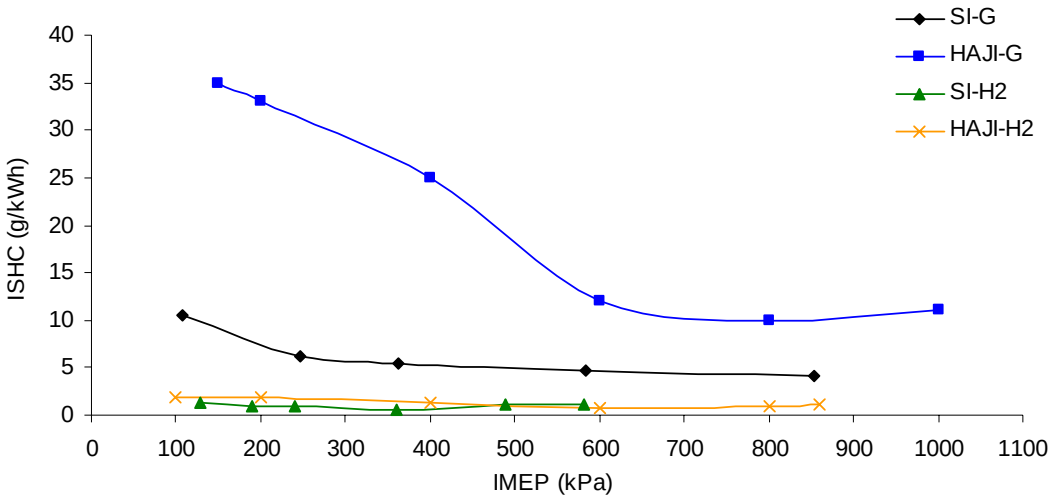

Figure 8.16: ISHC emissions versus IMEP - HAJI compared to SI, 1800r/min, λ and MAP conditions as per Figure 8.12 and 8.13.

Back to back, HAJI-G improved thermal efficiency on average by 15%, compared with SI-G and HAJI-H_2 improved thermal efficiency by 10% compared with SI-H_2. However when HAJI-H_2 is compared to SI-G then up to a 20% improvement in thermal efficiency is realised.

In SI-H_2 mode at maximum load (IMEP=582kPa), the engine was backfire limited and the thermal efficiency dropped severely. This was remedied in HAJI-H_2 mode by operating in the lean and boosted mode. Consequently, HAJI-H_2 is able to extend the backfire limited load point by 47% (IMEP=860kPa) and HAJI-G is able to extend the knock limited load point by 17%.

8.3.3 Emissions

Figure 8.16 shows the HC emissions for all modes and it is clear that HAJI emits more unburned fuel (due to large quench area and high quench gap (Section 2.2.4 and 7.3.3)) than SI despite having a higher thermally efficiency. In gasoline mode, up to 3.5 times more unburned HC are produced in HAJI-G mode over SI-G. In H_2 mode, up to 1.5g/kWh of unburned HC are produced, which is approximately ~0.5g/km. Considering that Euro 4 HC emission regulations call for 0.1g/km, these results imply that even a H_2 fueled engine would need to be fitted with a catalytic converter to satisfy the emissions legislation.

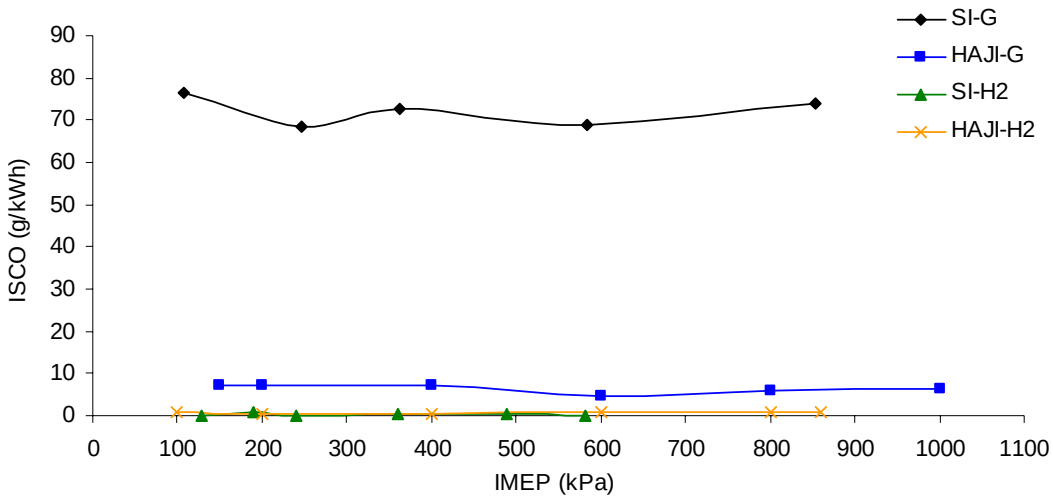

Figure 8.17: ISCO emissions versus IMEP - HAJI compared to SI, 1800r/min, λ and MAP conditions as per Figure 8.12 and 8.13.

CO emissions are predominantly controlled by λ, consequently, SI-G emits 10 times more CO emissions at all load points when compared to HAJI-G (Figure 8.17). It is important to note that this plot is very conservative at high loads (IMEP>800kPa) when comparing SI-G to HAJI-G since in reality, production engines operate at λ=0.8 at full load to protect the catalytic converter from overheating. Consequently, the CO emissions climb above 250g/kWh (Figure 2.1). HAJI-G exhaust temperatures are always low due to lean burn so <7g/kWh CO is emitted, which is a reduction >97% in CO emissions.

As expected, the H_2 fueled engines provide the lowest levels of CO since the only HC present during combustion comes from the lubricant and CO_2 in the atmosphere. As previously mentioned, the CO measurements of HAJI-H_2 and SI-H_2 are not reliable, since the measurements moved between zero and the smallest resolution (100ppm) on the emissions analyser.

HAJI-G decreases CO_2 emissions by up to 20% at all load points compared to SI-G, which is proportional to the improvement in thermal efficiency (Figure 8.18). Fueling the engine with H_2 presents the possibility of decreasing the CO_2 emissions levels to near zero. However, due to the burning up of lubricating oil and CO_2 in atmosphere, small amounts of CO_2 are also emitted in SI-H_2 and HAJI-H_2 modes. Even so, H_2 operation still offers a reduction in CO_2 emissions of over 99%.

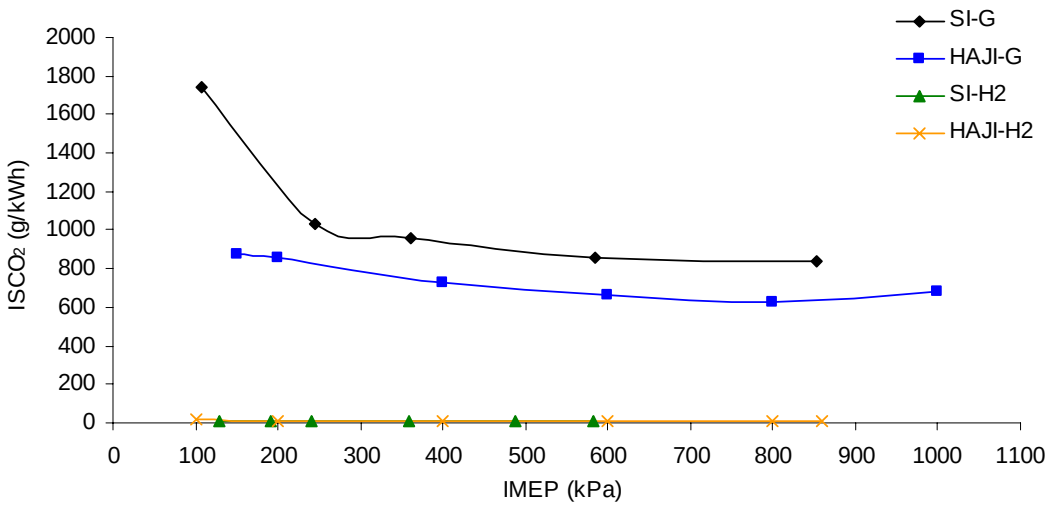

Figure 8.18: $ISCO_2$ emissions versus IMEP - HAJI compared to SI, 1800r/min, λ and MAP conditions as per Figure 8.12 and 8.13.

In SI-G mode, NO_x varies from 4.3g/kWh to 16.1g/kWh (Figure 8.19). In contrast, HAJI can maintain ~0.1g/kWh NO_x at all load points. The benefits in H_2 mode are also high when the SI engine is fitted with HAJI. SI-H_2 produces ~1g/kWh, whereas HAJI NO_x levels decrease to ~0.1g/kWh. When operating near the stoichiometric AFR in SI-H_2 mode, the NO_x output exceeds 20g/kWh. Similar high NO_x can be achieved with HAJI, so lean operation is necessary at all load points if NO_x are to be controlled.

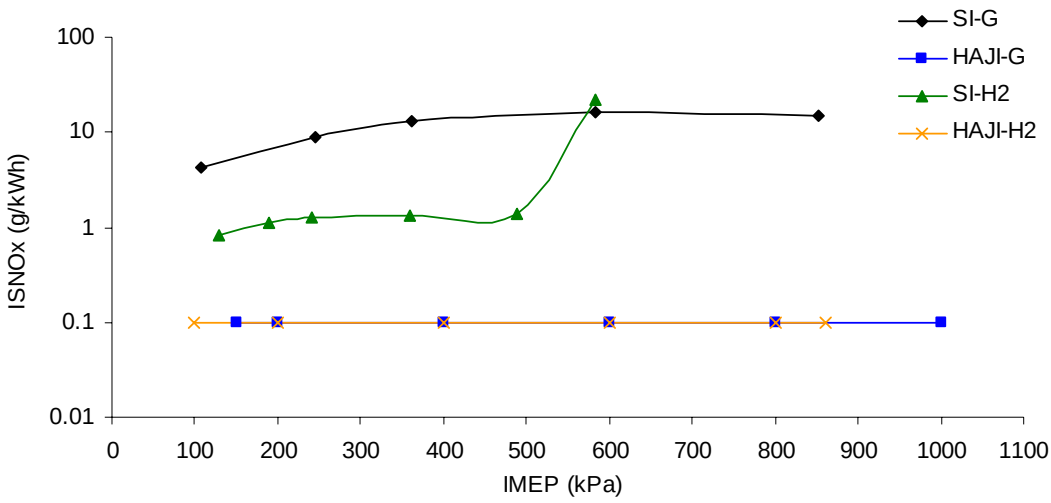

Figure 8.19: $ISNO_x$ emissions versus IMEP - HAJI compared to SI, 1800r/min, λ and MAP conditions as per Figure 8.12 and 8.13.

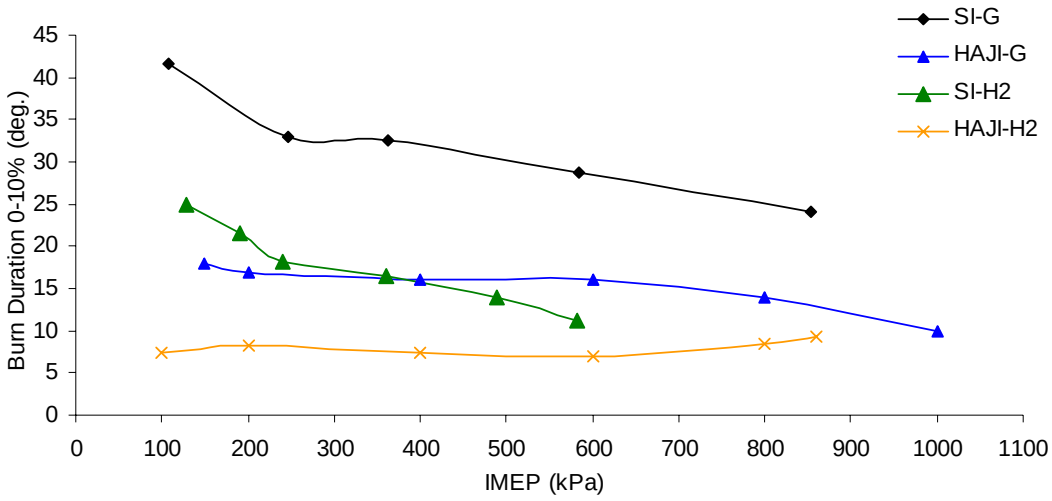

Figure 8.20: Burn Duration (0-10%) versus IMEP - HAJI compared to SI, 1800r/min, λ and MAP conditions as per Figure 8.12 and 8.13.

8.3.4 Combustion Characteristics

The previous section has clearly demonstrated that HAJI outperforms SI in terms of fuel economy, CO, CO_2, and NO_x emissions, whilst maintaining excellent levels of combustion stability. These improvements are the result of jet ignition, which decreases the initial burn duration (Figure 8.20) and also the total burn duration (Figure 8.21). Compared to SI-G which was operated at λ=1, the shorter burn durations of HAJI are achieved with leaner mixtures of λ≈1.9 in HAJI-G mode and λ≈3 in HAJI-H_2 mode. The shorter burn duration shifted MBT closer to TDC, which decreases the time available for NO_x formation and increases the thermal

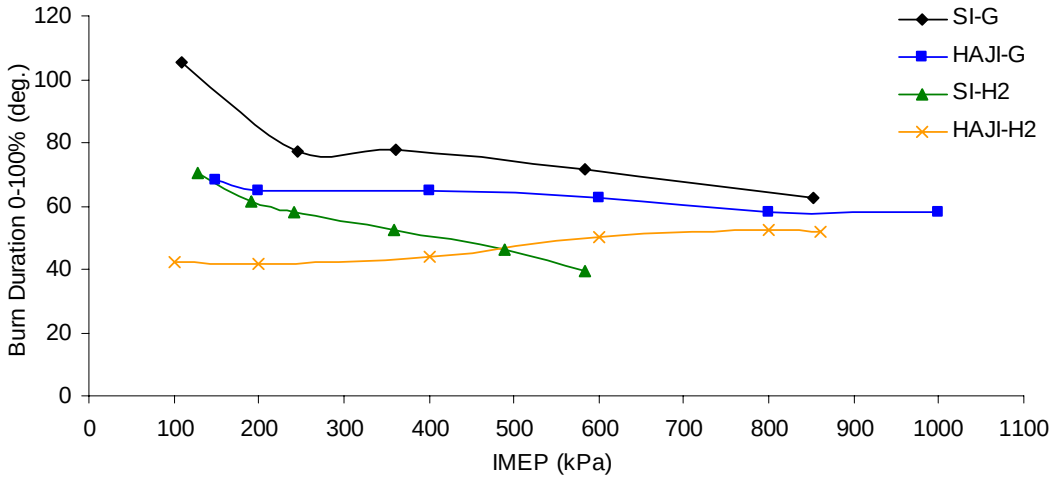

Figure 8.21: Burn Duration (0-100%) versus IMEP - HAJI compared to SI, 1800r/min, λ and MAP conditions as per Figure 8.12 and 8.13.

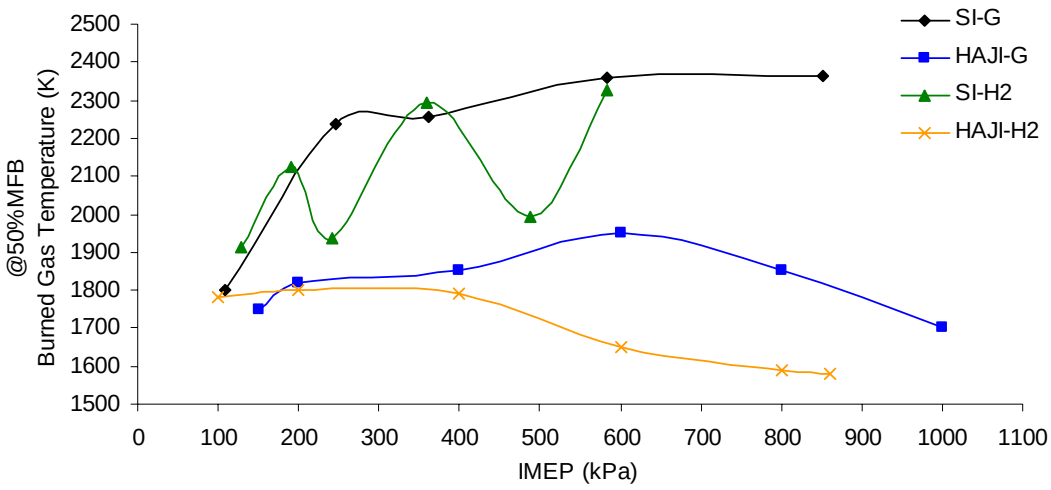

Figure 8.22: Burned Gas Temperature @50%MFB versus IMEP - HAJI compared to SI, 1800r/min, λ and MAP conditions as per Figure 8.12 and 8.13.

efficiency. The high λ conditions in both gasoline and H_2 mode decrease combustion temperature dramatically (Figure 8.22), which is the main reason for near zero engine out NO_x emissions in HAJI mode.

Figure 8.23 compares the Jet Knock amplitude for the various modes and highlights that at full load the knock amplitude of HAJI-G is only marginally higher than for SI-G. In contrast the knock amplitude of HAJI-H_2 is 3 times higher than SI-G.

8.4 HAJI Emissions and Costs to Meet Future Emissions Legislations

8.4.1 General Light-Off Emissions

Once catalytic converters achieve their optimum operating temperature, the conversion efficiency of HC, CO and NO_x is about 99.6%. The majority of the total emissions emitted over a typical drive cycle (duration of city cycle FTP = 1848 seconds) occur in the first 60 seconds (approximately 84% HC, 95% CO, and 65% NO_x [223]) and consequently, car manufacturers are predominantly concentrating on reducing start up emissions. This is difficult to achieve because a standard SI engine in cold start requires rich operation to stabilise combustion, which is the

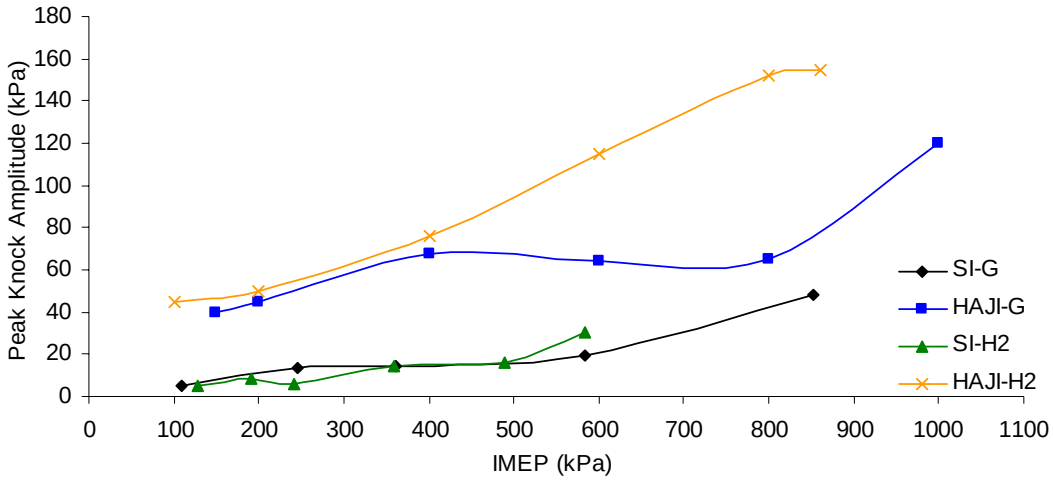

Figure 8.23: Jet Knock amplitude versus IMEP - HAJI compared to SI, 1800r/min, λ and MAP conditions as per Figure 8.12 and 8.13.

root cause of high HC and CO emissions in the first 60 seconds. Considerable amounts of NO_x emissions also accumulate in the early part of the drive cycle and the remainder in the later part predominantly at high speeds.

8.4.2 HC Emissions

Euro 4 and 5 standards require HC emissions of 0.1g/km and 0.05g/km respectively. At the optimum operating point, HAJI-G produces between 10-35g/kWh HC emissions. With a catalytic conversion efficiency of 99.6% this translates to a tail pipe HC output of 0.04-0.14g/kWh, which is approximately 0.012-0.044g/km not including accumulated emissions before light-off.

On first impression, it may seem that HAJI would fail the HC emissions test considering that HAJI produces 3.5 times more HC emission than SI. In reality HAJI would be likely to pass Euro 5, by decreasing the light off period dramatically by emitting more unburned fuel than SI, while simultaneously providing excess air into the exhaust stream. This combination is the basic principle of secondary air injection, typically used at start up in SIDI turbo and diesel turbo engines to decrease the catalyst light off period.

A more effective way to decrease start up HC emissions is to use direct fuel injection. This would dramatically reduce quench HC emissions [55]. However, careful consideration needs to be paid to particulate emissions which can form in DI engines.

The complete elimination of HC emissions at start up could be achieved by operating HAJI-G in H_2 only mode for <60 seconds until light-off occurs. Lumsden and Watson [141] operated in this mode and showed huge improvements in cold start combustion stabilities while nearly eliminating HC emissions. This would allow HAJI-G mode to reduce Euro 5 HC emission levels by 12-76% depending on the drive cycle.

8.4.3 CO Emissions

Euro 4 CO emissions are 1g/km or ~3g/kWh. HAJI-G engine out CO emissions are <7g/kWh, so with a 99.6% catalyst conversion efficiency, the tailpipe CO emissions are ~0.028g/kWh. This is approximately >97% below the Euro 4 limits not including the light-off period. Even when the complete drive cycle is considered, there are no foreseeable obstacles for HAJI to meet future Euro 5 CO emission requirements. This is because HAJI-G engine out CO emissions in steady state are 10 times less than SI-G at all load points. More importantly however, at start up HAJI-G will emit up to 100 times less CO than SI-G, since SI-G needs to operate rich (λ<0.9, CO>150g/kWh) to stabilise combustion.

8.4.4 NO_x Emissions

In SI-G mode, Euro 4 emission requirements can be achieved with a TWC converter. In SI-H_2 mode the TWC NO_x conversion efficiency falls to zero since the engine operates lean. In order to meet Euro 4, engine out NO_x need to be controlled in the cylinder. NO_x in SI-H_2 mode are ~1g/kWh with a CoV of IMEP<5% and this output does not satisfy Euro 4 requirements of 0.08g/km (or ~0.25g/kWh).

HAJI in both gasoline and H_2 mode can operate at ~0.1g/kWh. This is achieved at all load points without a catalytic converter. This consequently satisfies Euro 5 emission requirements, which is 0.04g/km.

8.4.5 CO_2 Emissions

The European Union target for CO_2 set for 2012 is 120g/km (Figure 1.6). HAJI-G mode has a better chance of achieving this considering that it is more fuel efficient than SI-G. In contrast SI-H_2, and HAJI-H_2 engines can already produce near zero CO_2 emissions.

8.4.6 Cost Impact

The unit cost of an engine fitted with HAJI would be expected to be the same as a current SIDI engine meeting Euro 4 requirement since the two technologies are very similar in terms of hardware. However, SIDI engine cost is expected to increase to meet Euro 5 requirements, due to the increase in after treatment costs. In contrast, the HAJI engine unit cost is expected to be the same for Euro 4 and Euro 5 since no additional hardware is required.

Unfortunately, the engine cost of an SI engine meeting Euro 4 and Euro 5 was not available to the author at the time of writing. However, the cost of a diesel engine was available. Up to now, HAJI has been compared mainly to SI technology although the emerging popularity of diesel engines in Europe is certainly worth noting.

The HAJI project started in 1990 when diesel engines were predominantly operating in trucks and buses. However, the market share of diesel engines in passenger cars in Europe increased from 18.6% to 44.1% from 1993 to 2003 [225]. Interestingly, the proposed diesel Euro 5 NO_x emission regulations are 2 times higher than gasoline fueled engines (0.08g/kWh) and the additional cost of a Euro 5 design for a diesel engine for passenger cars varies between 200-400 euros per car [18]. Furthermore the proposed Euro 5 limit on NO_x emissions for

heavy duty engines of 0.5g/kWh (5 times higher than current HAJI results) would cost between 1500-3000 euros depending on the engine type. Therefore, from the commercialisation point of view, the incentive to investigate HAJI in diesel applications is probably higher than for SI. In general, diesel engines are more expensive than SI engines and it would therefore be expected that after treatment costs are also higher. Based on this, the additional cost of a Euro 5 compliant SI engine is estimated to be less than 200 euros (approximately 7% increase in engine unit cost).

Since a H_2 infrastructure is not available, the most promising option is for HAJI to use an onboard H_2 reformer. Due to their inefficiency (max. efficiency=93%), fuel reforming should be kept to a minimum. Current reformers are able to generate between 20-40% H_2 by volume, which is more than adequate considering in HAJI-G mode a maximum of 3.5% is required across all load points. Despite the cost of H_2 reformers being unknown to the author, considering that a Euro 4 engine upgrade to Euro 5 is around 200 Euros then this would still make the HAJI system competitive against SI.

8.5 General Discussion

8.5.1 Combustion Analysis

Combustion temperatures are greatly influenced by λ. In both HAJI-G and HAJI-H_2 mode, it is possible to operate at sufficiently high λ values to reduce NO_x emissions to <20ppm. In naturally aspirated mode at high load, HAJI struggles to keep up with the SI engine, however when operated in lean boosted mode it significantly increases IMEP, reduces NO_x and improves thermal efficiency, while maintaining or improving combustion stability over its baseline SI counterpart.

The diagnostic two-zone combustion model was also used to calculate NO concentration and compared to measured values. Unfortunately, due to its zero dimensional nature, the model fails to predict peak combustion temperatures accurately so the predicted NO was lower than the measured values. The model

nevertheless, accurately follows the trend of measured values and is therefore a useful tool for predicting the rate of NO formation at different engine conditions prior to testing.

The ignition delay for SI-G is approximately 10.5CAD whereas for HAJI-G it is between 7.5 and 10.5CAD. When the engine is fueled with H_2, the ignition delay in SI mode reduces to 4.5CAD and in HAJI mode it varies between 3-4.5CAD depending on λ. The peak burn rate in SI mode occurs when more than 70% of the charge is consumed, whereas in HAJI mode, as λ increases this moves towards 50% MFB. At high λ values, this provides a uniform burn rate for the entire burn duration.

The unique characteristic of HAJI combustion is revealed to be the enhancement of the initial flame speed as derived from experimental pressure data with the use of the two-zone combustion model. When HAJI is compared to SI, the initial flame speed in gasoline mode is up to 7 times higher and in hydrogen mode up to 1.6 times higher.

After examining many FSR_t models, the simplest model proved to approximate the behavior of SI and HAJI the best between 20-80% of the maximum flame radius. The model is in the form of $FSR_t=S_{T,t}/S_L=1+u'/S_L$. In order for the model to be useful in a predictive sense, some adjustments were needed. Initially in SI mode, the flame speed is laminar and the FSR_t model overestimates the flame speed. This is remedied by multiplying the FSR_t model with a flame speed reducing factor based on the level of turbulence intensity relevant to the flame kernel, instead of on the overall turbulence intensity in the combustion chamber. In HAJI mode, instead of a flame reducing factor, a flame enhancing factor was needed to compensate for the rapid initial burn. This is one of the key distinguishing characteristics of HAJI, where combustion begins with a turbulent flame, unlike SI that always develops from a laminar flame. Furthermore, the actual FSRs in the SI engine are of order 6 in contrast to HAJI where they can be up to 100.

8.5.2 Comparison of Optimum HAJI to λ=1 SI

Operating at optimum λ=1.9 and 1800r/min HAJI-G was compared to λ=1 SI-G. For HAJI, low loads were achieved with mild throttling and high loads were achieved by boosting. HAJI provided excellent combustion stability (CoV of IMEP<5%), increased thermal efficiency by 15-41%, reduced CO emissions by 90%, reduced CO_2 emissions by 20% (on average) and decreased NO_x emissions by up to 99.3%. The only area where HAJI was inferior to SI was in HC emissions, increasing by up to 3.5 times, but this was not unexpected for such lean mixture combustion.

A similar analysis for HAJI-H_2 demonstrated world class combustion stability at λ=3 by operating below 3% CoV of IMEP, improved thermal efficiency by 10% over SI-H_2 and 10-25% over SI-G as well as near zero HC, CO and CO_2 emissions when compared to SI-G. Remarkably, in boosted lean mode, HAJI-H_2 produced 47% more IMEP than its SI-H_2 counterpart which was backfire limited at λ=1.48 to 582kPa IMEP.

All of the abovementioned improvements are the result of hydrogen jet ignition which, even though it operates at ultra lean AFRs, reduces the initial and total burn duration at all load points compared to baseline SI stoichiometric mode. Furthermore, the lean boosted HAJI system opens up the possibility for an engine to operate almost NO_x free without a lean NO_x catalyst whilst maintaining or improving on the maximum IMEP of its SI counterpart.

8.5.3 HAJI Emissions and Costs to Meet Future Emissions Legislations

Since NO_x is not a problem with HAJI, only a TWC would need to be fitted to control the HC and reduce CO further. CO_2 emissions decrease when operating in HAJI-G mode compared to SI-G. As expected however, near zero CO_2 emission levels can be achieved by fueling the engine with H_2.

Since the H_2 infrastructure is not available, an onboard H_2 reformer would be suitable to fuel HAJI with H_2. The cost of a reformer could be offset by the increasing cost of the SI engine, which requires an upgraded after treatment system to move from Euro 4 to Euro 5. Interestingly, if the H_2 infrastructure was ready when Euro 5 is introduced in 2010, no on board H_2 reforming would be required, and the HAJI system could reduce the cost of an engine unit compared to SI.

8.6 Summary

This chapter clearly demonstrated the decrease in combustion temperatures as λ was increased, which in turn decreased NO_x emissions. The predictive NO_x model was found to underestimate NO_x formation compared to experimental results, however it proved to be useful for qualitative analysis.

The fundamental differences between HAJI and SI combustion were identified by showing that while the SI engine starts combustion with a laminar flame, HAJI initiates combustion with a turbulent flame. Furthermore, a simple FSR_t model was found to correlate well with SI and HAJI combustion, especially within the 20-80% flame radius range. Outside of this range, a flame speed multiplying (FSM) factor was identified which compensates for the inaccuracy of the FSR_t model.

Ultimately, when HAJI was compared to SI, at all load points it was found to improve fuel economy, decrease CO, CO_2, and NO_x emissions. In gasoline mode, HAJI increased HC emissions, however in H_2 mode almost eliminates it. HAJI-G and HAJI-H_2 has the potential to meet the proposed Euro 5 emission regulations and since the system is not complex in terms of hardware, it is expected to cost the same as a Euro 4 design. Unfortunately, for now it seems that the unit cost saving of HAJI with respect to Euro 5 regulations is offset by the unavailability of H_2 fuel, which can only be remedied by generating H_2 with an onboard reformer.

CHAPTER 9
Conclusions

9.1 Introduction

The primary aim of this research was to study the performance and emission benefits of HAJI compared to SI while gaining further understanding about the combustion process of both ignition systems. After the formulation of the hypothesis, specific objectives were developed.

The tested hypotheses of this research have demonstrated that:

- Engine-out NO_x emissions could be controlled at all load points, with a simultaneous improvement in thermal efficiency over SI by operating the HAJI equipped engine under boosted (supercharged) conditions. More specifically, NO_x emission can be kept below 0.1g/kWh without aftertreatment, satisfying Euro 5 emission standards, with a simultaneous improvement in thermal efficiency.
- The flame speed multiplying factor was shown to vary throughout the combustion event because lean-mixture enhancement via HAJI is most

dominant in the early phase of combustion where active radicals and turbulence are highest.

- As long as the pre-chamber was fueled with H_2 or gasoline mixtures the small pressure oscillation “Jet Knock”, which is generated in the combustion chamber upon ignition, exists independently of whether the main chamber is fueled or not.

9.2 Research Achievements

9.2.1 Engine Development

The approach in setting up the test facilities was to make the equipment and diagnostics accurate and reliable as follows:

- An engine management system was successfully adapted to the engine, enabling the simultaneous control of direct and port fuel injectors for the pre-chamber and main chamber respectively.
- A data acquisition system enabling real-time sampling of cylinder pressure and crank angle position was adapted to the test engine. This provided real-time and post-test combustion analysis.
- All of the important instruments, sensors and outputs were calibrated and verified to ensure the acquired experimental data was both quantitatively and qualitatively accurate.

Significant New Findings

The extremely wide operating capabilities of the HAJI system was explored and compared to the baseline SI engine, from which it was concluded that:

- A single cylinder engine fitted with HAJI could be extensively operated with a homogeneous lean mixture at boosted inlet pressure conditions.
- The HAJI equipped engine fueled with H_2 in the pre-chamber had significant performance benefits over SI operation with gasoline or H_2 as the main chamber fuel.

- The independence of engine out NO_x in ultra lean conditions while varying engine load was identified.
- A simultaneous increase in thermal efficiency and a reduction of NO_x to near zero levels could be achieved across the entire load range. In addition, an increase in power output over the SI engine operating at WOT was successfully achieved by coupling HAJI with lean burn supercharging.

9.2.2 Modelling Achievements

In support of the experiments, the following analytical tools were developed and applied:

- A two-zone combustion model was developed and implemented (based on information from the literature) to interpret pressure trace and emissions data.
- The implementation of a fast equilibrium solver enables the calculation of burned and unburned mixture properties.
- Flame speeds were calculated based on the implementation of a spherical flamelet model.
- NO_x formation in a HAJI and SI engine based on the extended Zeldovich mechanism was modelled.
- The magnitude of pressure oscillation in the combustion chamber was calculated from the pressure trace, based on the adoption of a 2^{nd} order Butterworth digital filter.

9.3 Conclusions

9.3.1 Understanding

The experimental results supported by the analytical tools led to the following new insights and novel findings:

- As in SI engines, a strong relationship between combustion stability and HC emissions exists for ultra lean burn engines.

- The importance of H_2 fuel to achieve cleaner and more efficient engines in the future was revealed. Furthermore, the significant role of the HAJI system to facilitate this was identified.
- The possibility of HAJI satisfying Euro 5 emission levels with Euro 4 technology was observed.
- The independence of engine out NO_x in ultra lean conditions while varying engine load was identified.
- Flame speed analysis clearly identified and quantified the difference between SI and HAJI combustion, especially in the initial phase of combustion.
- The effect of spark timing and quantity of H_2 in the pre-chamber on the amplitude of Jet Knock was quantified.

9.3.2 Parametric Studies

The results of the parametric studies are formulated with reference to a single orifice HAJI system and the plane cylindrical, variable main chamber height of the CFR engine.

- The pre-chamber nozzle with a 3mm orifice length was identified to provide the best combustion stability, thermal efficiency and lowest NO_x emissions for the CFR engine configuration.
- Once the optimum H_2 quantity is established at MBT, then any decrease in H_2 quantity will decrease combustion stability, thermal efficiency, NO_x emissions and increase, HC, and CO emissions.
- Any increase over the already established optimum H_2 quantity at MBT, delivers minimal improvement in combustion stability and HC and CO emissions. NO_x however can increase dramatically, especially at $\lambda \approx 1.65$. Thermal efficiency is unchanged at high λ values, whereas a decrease is observed at $\lambda=1$.
- At high MAP, the effect of engine speed on thermal efficiency and emissions is negligible when the engine operates leaner than $\lambda=2.2$. However, as the speed is decreased at low MAP, NO_x emissions increase and thermal efficiency decreases.

- At λ=1 and MBT in SI mode, the combustion stability is the highest. Spark timing away from MBT has a small effect on emissions, however, thermal efficiency and CoV of IMEP can deteriorate significantly, especially if timing is retarded.
- In contrast, in HAJI mode, thermal efficiency and CoV of IMEP are not so sensitive to variations away from MBT. For example, at high λ values it is possible to retard spark timing from MBT and decrease NO_x emissions by >70%.
- Compared to SI at the same CR at λ=1, HAJI has a higher thermal efficiency and lower CoV of IMEP, but produces more HC and NO_x emissions. At high λ values, the thermal efficiency benefits are even greater and NO_x emissions are significantly lower, while HC emissions are higher.
- SI-H_2 and HAJI-H_2 operations did not suffer from knock limited MBT at any operating point predominantly due to the high ON of H_2.
- SI-G at λ=1 suffered from knock limited MBT from CR=9. Whereas HAJI-G at λ=1 was already operating with knock limited MBT at CR=8. Irrespective of this, HAJI was operating at a higher thermal efficiency over SI at any given CR, due to the shorter burn durations.
- In HAJI-G mode at any given CR or MAP, as λ increased, the knock limited MBT decreased and eventually disappeared resulting in a significant increase in thermal efficiency.
- The HUCR of a fuel strongly depends on λ. Increasing λ values increases the HUCR in a homogeneously charged engine.
- In the CFR engine the HUCR at λ=1 in SI-G mode was at CR=9. However, in HAJI-G mode at λ=1.6, the HUCR can be increased by 2 (to CR=11) and at λ=2.6 the HUCR can be increased by 6 (to CR=15).
- In SI-H_2 mode, the HUCR was at CR=9. Interestingly, due to the non optimum combustion chamber shape of the CFR engine in HAJI-H_2 mode at all λ, the HUCR only increased by 2 (to CR=11).
- HAJI reduces the ONR at constant load, which means that operating in lean boosted mode requires a lower ON fuel than operating at the same load at λ=1.

- HAJI extends the lean stability limit (CoV of IMEP<5%) to λ=2 for gasoline and λ=4 for H_2. Consequently, thermal efficiency improves and CO and NO_x emissions decrease.

9.3.3 Jet Knock

- Not observed in SI mode, Jet Knock occurs in HAJI mode due to the presence of a high speed jet exiting the pre-chamber, which produces shock waves from the throat of the nozzle.
- Jet Knock occurs for both H_2 and gasoline main chamber fuels and appears to be independent of fuel type as long as it is ignitable.
- The amplitude of the first pressure wave can be as high as 50kPa, even without the presence of main chamber fuel.
- Close to λ=1 in HAJI-G and HAJI-H_2 modes, the amplitude of pressure oscillation may be as high as 250kPa.
- Increasing MAP or CR tends to increase the Jet Knock amplitude. However, λ influences the magnitude of pressure oscillation the most.
- Most importantly, although Jet Knock was measurable, no affect on performance, emissions and the durability of the engine was detected. This is not surprising since conventional end-gas knock has a pressure oscillation amplitude between 10-30 times higher than Jet Knock.

9.3.4 Combustion Analysis

- NO_x emissions can be reduced even at high engine load points to 0.1g/kWh in both HAJI-G and HAJI-H_2 modes when operating sufficiently lean.
- The predictive NO_x model underestimated NO concentration when compared to experimental results. However, the trend of calculated values was predicted accurately.
- Ignition delay, defined as the time between spark ignition and the first 1% MFB, is reduced by up to 30% with HAJI in gasoline and H_2 modes. The ignition delay for H_2 main chamber fuel is generally half that of gasoline.

- Instead of a laminar flame as seen in SI engines, the HAJI system establishes a turbulent flame at the beginning of the combustion process. This mechanism is primarily responsible for the fast initial and overall burn duration of HAJI over SI. Consequently, the initial flame speed for HAJI in gasoline mode is up to 7 times higher and in hydrogen mode up to 1.6 times higher compared to SI.
- A simple FSR model was found to approximate the behavior of SI and HAJI the best between 20-80% of the maximum flame radius. However, in order for this model to be useful in a predictive sense, a flame speed multiplying (FSM) factor was calculated. When FSM<1, then it is a flame reducing factor and when FSM>1, then it is a flame enhancing factor. These are used to capture the inaccuracy of the FSR model in the following conditions:
    - In SI mode, the flame is initially laminar and so the FSR model overestimates the flame speed. This is remedied by multiplying the FSR model with a flame speed reducing factor. This captures the level of turbulence intensity relevant to the flame kernel instead of the overall turbulence intensity in the combustion chamber.
    - In the HAJI mode, instead of a flame reducing factor, a flame enhancing factor is used to compensate for the turbulence and chemical enhancement that the HAJI system provides.

- The actual FSR in the SI engine is about 6 whereas with HAJI it can be up as high as 100. Combustion theory postulates that this produces entrained pockets of burned and unburned mixture in the vicinity of the flame front, which is the underlying mechanism of increasing the flame surface area and therefore flame speed. However, turbulence alone cannot explain how ultra-lean mixture combustion takes place. So a model, which considers a combination of both turbulence and active species from the rich pre-chamber, is therefore required to explain the observed findings. This means that while combustion in the SI engine is controlled largely by turbulence, HAJI combustion is controlled as much by chemistry as it is by turbulence.

9.3.5 Optimum HAJI vs. Standard SI

- For gasoline operation, the optimum λ in HAJI mode is approximately λ=1.9. Light load (idle) can be achieved with mild throttling and high load (equivalent or larger than the IMEP of SI engine operating at WOT) can be achieved by boosting. HAJI provided excellent combustion stability (CoV of IMEP<5%), increased thermal efficiency by 15-41%, reduced CO emissions by 90%, reduced CO_2 emissions by 15-41% and decreased NO_x emissions by up to 99.3%. The only area where HAJI was inferior to SI was in HC emissions, which increased by up to 3.5 times, but this was not unexpected for such lean mixture combustion.
- A similar analysis for HAJI-H_2 demonstrated world class combustion stability at λ=3 by operating below 3% CoV of IMEP, improved thermal efficiency by 10% over SI-H_2 and 10-25% over SI-G as well as near zero HC, CO and CO_2 emissions compared to SI-G. Remarkably, in boosted lean mode, HAJI-H_2 produced 47% more IMEP than its SI-H_2 counterpart which was backfire limited at λ=1.48 to 582kPa IMEP.
- Clearly, a gasoline fueled engine fitted with HAJI can reduce CO_2 emissions over SI. However, reaching aggressive CO_2 emissions targets can only be achieved with an IC engine fueled by H_2.
- HAJI fitted engines have the potential to meet Euro 5 emission regulations with the equivalent of Euro 4 technology. This could prevent an increase in the unit price of SI engines when Euro 5 regulations are introduced in 2010.
- To meet Euro 5 emission legislations for gasoline fueled passenger cars, HC and CO emissions can be controlled with HAJI and a catalytic converter. NO_x emissions can be controlled by HAJI at all load points, without a catalytic converter.
- Interestingly, even if the SI-H_2 engine operates at its lean limit (CoV of IMEP<5%), it would still require a catalytic converter to meet HC and CO emissions requirements (based on the CFR results) and would also require some NO_x after treatment. A HAJI-H_2 engine however, can simultaneously meet Euro 5 NO_x emissions standards without the need for NO_x after treatment, while still achieving a world class CoV of IMEP of less than 3%.

9.4 Recommendations for Future Work

9.4.1 Experiments

This research has covered a large range of engine parameters and data space. However, in this exploration many new research avenues have surfaced. To broaden our knowledge in terms of HAJI operation, a greater range of engine parameters still need to be explored and some of these valuable topics would include:

- In this thesis with a single nozzle pre-chamber, 0.1g/kWh NO_x were achieved. It is anticipated that this could be reduced further by decreasing the burn duration with the use of up to 3 nozzles in the side-mounted CFR engine or 6 nozzles as used by Dober [55] in central ignition systems. This would further retard MBT, which would in turn reduce NO_x.
- The usage of H_2 in the HAJI system extends lean limit and improves thermal efficiency over SI. However what is the level of unburned H_2 in the exhaust in HAJI-G and HAJI-H_2 mode?
- One of the most powerful tools to improve fuel economy and control emissions in current SI engines is the use of EGR because it does not upset the operation of the catalytic converter. Based on the lean burn performance, HAJI should have an excellent EGR tolerance and this could possibly reduce the near zero NO_x emissions obtained with excess air, to zero with EGR, most likely at the expense of thermal efficiency.
- Aluminium pre-chambers can possibly erode due to the high instantaneous temperature and velocity through the nozzle. Therefore, cooling and material requirements are worth exploring and identifying.
- After a wide range of testing and inspection of engine conditions, the effects of the Jet Knock phenomena on performance, emission and durability was found to be immeasurable. Consequently, a more sensitive and specific investigation must be set up to quantify its effect in order to confirm these observations and attempt to answer the following questions: Does Jet Knock limit the HUCR? Does it reduce HC emissions due to enhanced mixing in the quench gap? Does it suppress knock due to the increased heat transfer

between the end gas and cylinder wall? What is the sensitivity of knocking amplitude to different nozzle diameters and number of holes?

- Examining the performance of HAJI at high speed (up to 8000 r/min) would further validate its usefulness or limitations. This is especially important in today's engine market since a high number of small displacement engines can only achieve high specific power outputs at high speeds.
- A DI system needs to be optimised for a HAJI engine to reduce HC emissions [55], especially at start-up. However, the associated particulate emissions must be understood for future applications.
- Onboard hydrogen generators (reformers) are now available for vehicles. Cost, size, efficiency, and complexity should be explored with respect to the HAJI system. If feasible, a system should be developed in the engine test laboratory to prove its effectiveness.
- The hydrogen jet(s) penetrate very fast and deep into the combustion chamber and depending on the jet orientation they may impinge onto the cylinder walls and their reactive ability may burn the lube oil. Bore and piston wear should be investigated as a function of jet orientation. This could possibly be carried out with standard flat crown pistons running on a global durability cycle (+400 hours) and compared to more robust bowl type pistons used in diesel engines, where the diesel jets always impinge onto the piston.
- At last a detailed study with optical imaging is suggested to examine the effects of nozzle orientation, diameter, length, number of nozzles and pre-chamber volume on jet penetration and dispersion. The effects on emissions and thermal efficiency should also be recorded.

9.4.2 Modelling

- The lean limit extension of HAJI depends on the level of combustion enhancement from turbulence intensity and the production of chemically active species. The contribution of each mechanism at different λ values and MAP conditions could be quantified with a detailed chemical combustion model. The model should be calibrated against experimental results obtained from laser induced fluoresence imaging, which could provide actual temperature profiles and OH^- concentration of the HAJI combustion.

- The NO_x model built into the two-zone combustion model followed the trend of experimental results, but severely underestimated the actual values. It is possible to extend the model by splitting the burned zone into multiple burned zones, thereby calculating a temperature gradient across the burned zone and subsequently predicting engine out NO_x emissions with greater accuracy.
- The continuous development of 3D predictive models, initiated by previous HAJI researchers such as Kyaw [128], Dober [55], and Wang [217], are important since they provide a means of validating different hypotheses about how jet ignition works. At present, this is still a long and tedious process. Further development of two-zone models should therefore be considered as they allow a researcher to conduct both theoretical investigations as well as extensive experimental work, as shown in this thesis.
- A simple combustion chamber and piston arrangement should be built into an FEA program to determine the reduction of thermal stresses on different engine components using imported temperature profiles corresponding to different λ conditions. This is important since the optimum operation of HAJI-G is at λ=1.9 and at λ=3 for HAJI-H_2, where the average combustion temperatures are significantly lower. This should drastically reduce the thermal stresses and increase engine durability or allow engine manufacturers to use less expensive engine materials.

9.4.3 Next Step to Commercialisation

After more than a decade of research and development at the University of Melbourne, the HAJI system is mature enough to be evaluated for commercialisation purposes. HAJI improves thermal efficiency at all load points, reduces thermal stresses and preliminary results indicate that a HAJI equipped engine is able to meet proposed Euro 5 emission levels with a design complexity equivalent to a Euro 4 design. The next phase for HAJI is therefore to implement all of the accumulated knowledge into one vehicle and run it through the different legislated emission drive cycles with the following setup:

Start-Up

- To achieve rapid catalyst light off in a gasoline fueled vehicle, homogeneous

operation at $\lambda \approx 1.9$ will provide approximately 3.5 times more unburned HC and excess air to the exhaust stream. This approach is similar to the well known secondary air injection concepts, or

- Until light off is achieved, operate in an all H_2 mode at $\lambda=3$. This would nearly eliminate HC and CO emissions, while producing near zero NO_x emissions [143], or
- Inject the main chamber fuel (gasoline) directly into the combustion chamber to reduce quenched and crevice source HC emissions [55].

Steady State

- Once catalyst light off has occurred at low and medium load conditions, a homogenously lean operating condition ($\lambda \approx 1.9$) should satisfy Euro 5 requirements.

High Load

- With the combination of HAJI lean burn and boosting, future emission legislations can be met. In gasoline mode at $\lambda \approx 1.9$, this would correspond to a MAP of 150kPa and in H_2 mode at $\lambda=3$ a MAP of 190kPa.

Further refinement of the HAJI system beyond Euro 5 is envisaged with the combination of existing and new techniques, which can be justified by the results of future investigations.

Furthermore, in order to demonstrate the viability of the HAJI system for high volume production, the following topics also need to be examined accurately when considering HAJI over SI: engine unit cost increase, durability/reliability of technology, packaging advantage, lead time to implement into production, robustness/flexibility of technology to meet emission regulations beyond 2010.

As a final remark, HAJI has the potential to provide a bridging technology between our current oil based economy and future H_2 economy. A lean boosted HAJI-G engine with an on-board reformer offers a near zero urban pollution output with reduced CO_2, and the same engine operating on H_2 alone can finally eliminate all of the legislated vehicle pollutants.

References

[1] AATSE (Australian Academy of Technological Sciences and Engineering), "Urban air pollution in Australia", Parkville VIC: AATSE, 1997.

[2] Abdel-Gayed, R.G., K.J. Al-Khishali, and D. Bradley, "Turbulent burning velocities and flame straining in explosions", Proc. R. Soc. Lond. A391, pp. 393-414, 1984.

[3] Abraham, J., F.A. Williams, and F.V. Bracco, "A discussion of turbulent flame structure in premixed charges", SAE 850345, 1985.

[4] ADS 9000 Super Four Gas Analyser, Operator's Manual.

[5] Ahmadi-Befrui, B., W. Brandstatter, and H. Kratochwill, "Calculation of inhomogeneous-charge combustion in a swirl-assisted lean-burn engine", SAE 910266, 1991.

[6] Aleiferis, P.G., A. M. K. P. Taylor, J. H. Whitelaw, K. Ishii, and Y. Urata, "Cyclic variations of initial flame kernel growth in a Honda VTEC-E lean-burn spark-ignition engine", SAE 2000-01-1207, 2000.

[7] Alger, T., M. Hall, and R.D. Matthews, "Effects of swirl and tumble on in-cylinder fuel distribution in a central injected DISI engine", SAE 2000-01-0533, 2000.

[8] Alkidas, A.C., R.J. Drews, and W.F. Miller, "Effects of piston crevice geometry on the steady state engine out hydrocarbon emission of a SI engine", SAE 952537, 1995.

[9] Allgeier, T., M. Klenk, T. Landenfeld, E. Conte, K. Boulouchos, and J. Czerwinski, "Advanced emission and fuel economy concept using combined injection of gasoline and hydrogen in SI-engines", SAE 2004-01-1270, 2004.

[10] Amann, A.A., "A perspective of reciprocating engine diagnostics without lasers", Progress in Energy Combustion and Science, Vol. 9, pp.239-267. 1983.

[11] Amann, C.A., "Cylinder-pressure measurement and its use in engine research", SAE 852067, 1985.

[12] American Automobile Manufacturers Association (AAMA), Motor Vehicle Facts and Figures 1996, pp.44-47, (AAMA, Washington, D.C.) 1996.

[13] American Automobile Manufacturers Association (AAMA), World Motor Vehicle Data 1993 (AAMA, Washington, D.C., 1993), p. 23, and American Automobile Manufacturers Association (AAMA), Motor Vehicle Facts and Figures 1996, p.44, (AAMA, Washington, D.C.), 1996.

[14] Andrews, G., "Environmental impact and health concerns of SI emissions", Short course on SI engines emissions, University of Leeds, November 2001.

[15] Apostolescu, N., and R. Chiriac, "A study of combustion of hydrogen-enriched gasoline in a spark ignition engine", SAE 960603, 1996.

[16] Arcoumanis, C., D.R. Hull, and J.H. Whitelaw, "An approach to charge stratification in lean-burn, spark-ignition engines", SAE 941879, 1994.

[17] Arcoumanis, C., Z. Hu, C. Vafidis, and J.H. Whitelaw, "Tumbling motion - A mechanism for turbulence enhancement in spark-ignition engines", SAE 900060, 1990.

[18] Article published by the administrator of European Federation for Transport and Environment, "Waiting for Euro 5 and Euro 6 new emission standards for passenger cars, vans and lorries", www.t-e.nu, Created on the 31st of March 2004, Accessed: 9 November 2004.

[19] Ball, J.K., R.C. Stone, and R.R. Raine, "A technique for estimating completeness of combustion and its use in modeling cycle-by-cycle variations in combustion", SAE 2000-01-0953, 2000.

[20] Barnard, J.A., and J.N. Bradley, "Flame and combustion", Chapman and Hall, 1985.

[21] Barr, P.K., and P.O. Witze, "Some limitations to the spherical flame assumption used in phenomenological engine models", SAE 880129, 1988.

[22] Beck, N.J., and R. Barkhimer, "Evolution of heavy duty natural gas engines - stoichiometric, carbureted, and spark ignited to lean burn, fuel injected and micro-pilot", SAE 972665, 1997.

[23] Berckmüller, M., H. Rottengruber, A. Eder, N. Brehm, G. Elsässer, G. Müller-Alander and C. Schwarz, "Potentials of a charged SI-Hydrogen engine", SAE 2003-01-3210, 2003.

[24] Birch, S., "Diesel vs. gasoline: the fight goes on", Automotive engineering internation online: Tech briefs, Jan. 2000, http://www.sae.org/automag/techbriefs_01-00/08.htm, Accessed: 12 August 2004.

[25] Blank, D.A., and A.A. Pouring, "Radical controlled autoignition at reduced compression ratios in a hydrogen DI diesel engine with piston micro-chambers", SAE 2004-01-1846, 2004.

[26] Boam, D.J., I.C. Finlay, T.W. Biddulph, T. Ma, R. Lee, S.H. Richarson, J. Bloomfield, J.A. Green, S. Wallace, W.A. Woods, and P. Brown. "The sources of unburnt hydrocarbon emissions from spark ignition engines during cold starts and warm-up", In Proceedings of the Institution of Mechanical Engineers, Number 208 (D01493), 1994.

[27] Boisvert, J., and P.G. Hill, "Test of thickness flame combustion estimates in a single-cylinder engine", ASME, Vol.109, pp.410-418, October 1987.

[28] Borman, G.L., and K.W. Ragland, "Combustion Engineering", McGraw-Hill, New York, 1998.

[29] Boulouchos, K., "Strategies for future engine combustion systems - homogeneous or stratified charge?", SAE 2000-01-0650, 2000.

[30] Bradley, D., and M.J. Scott, "Afterburning in spherical premixed turbulent explosions", Combustion and Flame Vol. 99, pp. 581-590, 1994.

[31] Bradley, D., J. Hynes, M. Lawes, and C. Sheppard, "Limitation to turbulence enhanced burning rates in lean burn engines", I.Mech.E. paper C46/88, 1988.

[32] Bradley, D., R.A. Hicks, M. Lawes, C.G.W. Sheppard, and R. Woolley, "The measurement of laminar burning velocities and Markstein numbers for isooctane-air and isooctane-n-heptane-air mixtures at elevated temperatures and pressures in an explosion bomb", Combustion and Flame, Vol. 115, pp. 126-144, 1998.

[33] Broge, J.L., "Tenneco comes clean", Automotive Engineering International, 2003.

[34] Bromberg, L., D.R. Cohn, A. Rabinovich, N. Alexeev, J.B. Green Jr., N. Domingo, J.M.E. Storey, R.M. Wagner and J. S. Armfield, "Experimental evaluation of SI engine operation supplemented by hydrogen rich gas from a compact plasma boosted reformer", SAE 2000-01-2206, 2000.

[35] Brunt, M.F.J., and A.L. Emtage, "Evaluation of burn rate routines and analysis errors", SAE 970037, 1997.

[36] Burden, R.L., and D.J. Faires, "Numerical Analysis", PWS-KENT Publishing Company, Boston, 1989.

[37] Carabateas, N.E., A.M.K.P. Taylor, J.H. Whitelaw, K. Ishii, K. Yoshida, and M. Matsuki, "The effect of injector and intake port design on in-cylinder fuel droplet distribution, airflow and lean-burn performance for a Honda VTEC-E engine", SAE 961923, 1996.

[38] Cartwright, A., and R. Fleck, "Cylinder pressure analysis in high performance two-stroke engines", SAE 962535, 1996.

[39] Cathcart, G., and C. Zavier, "Fundamental characteristics of an air-assisted, direct-injection combustion system as applied to 4-stroke automotive gasoline engines", SAE 2000-01-0256, 2000.

[40] Challen, J., "International engine of the year awards 2004", Cover Story, Engine Technology International, September 2004.

[41] Cheng, W.K., D. Hamrin, J.B. Heywood, S. Hochgreb, K. Min, and M. Norris, "An overview of hydrocarbon emission mechanisms on spark ignition engines", SAE 932708, 1993.

[42] Cheung, H.M, and J.B. Heywood, "Evaluation of a one-zone burn-rate analysis procedure using production SI engine pressure data", SAE 932749, 1993.

[43] Chinworth, M., "Hydrogen and the automobile", Automotive Engineering International, September 2002.

[44] Christensen, M., A. Hultqvist, and B. Johansson, "Demonstrating the multi-fuel capability of a homogeneous charge compression ignition engine with variable compression ratio", SAE 1999-01-3679, 1999.

[45] Christensen, M., B. Johansson, P. Amneus, and F. Mauss, "Supercharged homogeneous charge compression ignition", SAE 980787, 1998.

[46] Chun, K.M., and K.W. Kim, "Measurements and analysis of knock on a SI engine using the cylinder pressure and block vibration signals", SAE 940146, 1994.

[47] Clarke, D.P., C.H. Such, M.T. Overington, and P.K Das, "A lean burn turbocharged, natural gas engine for the US medium duty automotive market", SAE 921552, 1986.

[48] Dai, W., G.C. Davis, M.J. Hall, and R.D. Matthews, "Diluents and lean mixture combustion modeling for SI engines with a quasi-dimensional model", SAE 952382, 1995.

[49] Date, T., and S. Yagi, "Research and development of Honda CVCC engine", SAE 740605, 1974.

[50] Dennis, A.J., C.P. Garner, and D.H.C. Taylor, "The effect of EGR on diesel engine wear", SAE 1999-01-0839, 1999.

[51] Deslandes, J.V., "Oxidation product in engine exhausts", Thesis (Ph.D.), University of Melbourne, 1975.

[52] DeZylva, M.D., "Flame initiation as the source of variability in the SI engine", Thesis (M.Eng.Sc.), The University of Melbourne, 1992.

[53] Directive 98/69/EC of the European Parliament and of the Council of 13 October 1998 relating to the measures to be taken against air pollution by emissions from motor vehicles and amending Council Directive 70/220/EEC. Luxembourg: The European Parliament and The Council, 13 October 1998.

[54] Dober, G.G., "Ultra lean geometric control of HC emissions", Unpublished Phd Conversion Report, University of Melbourne, 1998.

[55] Dober, G.G., "Geometrical control of hydrocarbon emissions", Thesis (Ph.D.), University of Melbourne, 2002.

[56] Doyle, T.A., "Technology status of hydrogen vehicles", IEA Agreement on the Production and Utilization of Hydrogen, IEA/H2/TR1-98, 1998.

[57] Duchaussoy, Y., A. Lefebvre, and R. Bonetto, "Dilution interest on turbocharged SI engine combustion", SAE 2003-01-0629, 2003.

[58] Duffy, K., J. Kilkenny, G. Coleman, and E. Fluga, "Diesel HCCI results at Caterpillar", Deer Conference, San Diego, California, 28th August, 2002.

[59] Dunn, S., "Hydrogen future: Toward a sustainable energy system", Worldwatch paper 157, 2001.

[60] Environmental Benefits of NGVs. 2003, http://www.ngv.org, Accessed: 10 August 2004.

[61] Erickson, W.D., and R.K. Prabhu, "Rapid computation of chemical equilibrium composition: An application to hydrocarbon combustion", AIChE Journal, Vol. 32, No. 7, July 1986.

[62] Erickson, W.D., J.T. Kemper, and D.O. Allison, "A method for computing chemical-equilibrium compositions of reacting-gas mixtures by reduction to

a single iteration equation", NASA Technical Note, NASA TN D-3488, August 1966.

[63] Eriksson, L., "Documentation for the chemical equilibrium program package CHEPP", Department of Electrical Engineering, Linköping University, October 3, 2000.

[64] Estimated monetary benefits from control of various pollutants, "National environment protection measure for ambient air quality", p52, http://www.3sc.net/airqual/nepm.html, Accessed: 19 August 2001.

[65] Evans, R.L., and E.C. Tippett, "The effects of squish motion on the burn-rate and performance of a spark-ignited engine", SAE 901533, 1990.

[66] Evans, R.L., "Combustion chamber design for a lean-burn SI engine", SAE 921545, 1992.

[67] Fan, L., G. Li, Z. Han, and R. D. Reitz, "Modeling fuel preparation and stratified combustion in a gasoline direct injection engine", SAE 1999-01-0175, 1999.

[68] Flynn, F.P., G.L. Hunter, R.P. Durrett, L.A. Farrell, and W.C. Akinyemi, "Minimum engine flame temperature impacts on diesel and spark-ignition engine NOx production", SAE 2000-01-1177, 2000.

[69] Fox, J.W., W.K. Cheng, J.B. Heywood, "A model for predicting residual gas fraction in spark-ignition engines", SAE 931025, 1993.

[70] Frequently Asked Questions, Medinox FAQ, http://www.medinox.com/faq/faq2.htm, Accessed: 26 February 2003.

[71] Freund, J.B., S.K. Lele, and P. Moin, "Numerical simulation of a Mach 1.92 turbulent jet and its sound field", American Institute of Aeronautics and Astronautics. AIAA Journal. New York: Nov 2000.Vol.38, Iss. 11; pg. 2023.

[72] Fukuma, T., T. Fujita, P. Pichainarong, and S. Furuhama, "Hydrogen combustion study in direct injection hot surface ignition engine", SAE 861579, 1986.

[73] Geiger, J., S. Pischinger, R. Böwing, H.J. KoB, and J. Thiemann ,"Ignition systems for highly diluted mixtures in SI engines", SAE 1999-01-0799, 1999.

[74] Gilbert, T.R., R.V. Kirss, and G. Davies, "Chemistry: The Science in Context", W.W. Norton & Company, New York, 2004.

[75] Gillespie, L., M. Lawes, C.G.W. Sheppard, and R. Woolley, "Aspects of laminar and turbulent burning velocity relevant to SI engines", SAE 2000-01-0192, 2000.

[76] Glasson, N., G.A. Lumsden, R. Dingli, and H.C. Watson, "Development of the HAJI system for a multi-cylinder spark ignition engine", SAE 961104, 1996.

[77] Godoy, J., "Auto Emissions Killing Thousands", www.oneworld.net, Published on 3 June 2004, Accessed: 8 August 2004.

[78] Gottgens, J., F. Mauss, and N. Peters, " Analytical approximations of burning velocities and flame thickness of a lean hydrogen, methane, ethylene, ethane, acetylene, and propane flames", 24th Symposium (International) on Combustion/The Combustion Institute, pp. 129-135, 1992.

[79] Grandin, B., and H.E. Angstrom, "Replacing fuel enrichment in a turbo charged SI engine: lean burn or cooled EGR", SAE 1999-01-3505, 1999.

[80] Grant, T., "Alternative fuels for diesel and SI engines", Short course on road transport engine emissions, University of Melbourne, July 2001.

[81] Green, J.B., N. Domingo, J.M.E. Storey, R.M. Wagner, J.S. Armfield, L. Bromberg, D.R. Cohn, A. Rabinovich, and N. Alexeev, "Experimental evaluation of SI engine operation supplemented by hydrogen rich gas from a compact plasma boosted reformer", SAE 2000-01-2206, 2000.

[82] Groff, E.G., and F.A. Matekunas, "The nature of turbulent flame propagation", SAE 800133, 1980.

[83] Guezennec, Y.G., and W. Hamama, "Two-zone heat release analysis of combustion data and calibration of heat transfer correlation in an I.C engine", SAE 1999-01-0218, 1999.

[84] Gupta, H.C., and F.V. Bracco, "The origin of pressure oscillations in divided chambers engines", Combustion and Flame, Vol. 48, pp. 33-49, 1982.

[85] Gussak, L.A., "High chemical activity of incomplete combustion products and a method of prechamber torch ignition for avalanche activation of combustion in internal combustion engines", SAE 750890, 1975.

[86] Gussak, L.A., "The role of chemical activity and turbulence intensity in prechamber-torch organization of combustion of a stationary flow of a fuel-air mixture", SAE 830592, 1983.

[87] Gussak, L.A., V.P. Karpov, and Y.V. Tikhonov, "The application of lag-process in prechamber engines", SAE 790692, 1979.

[88] Guzzella, L., U. Wenger, and R. Martin, "IC-engine downsizing and pressure-wave supercharging for fuel economy", SAE 2000-01-1019, 2000.

[89] Hamilton, B., "What parameters determine octane requirement?", http://www.faqs.org/faqs/autos/gasoline-faq/part3/, Created: 15 January 2004, Accessed: 8 December 2004.

[90] Hatakeyama, S., Y. Sekiya, T. Murayama, and H. Tsunemoto, "A study of lean burn of a 4-stroke gasoline engine by the aid of low-pressure, air-assisted, in-cylinder injection-Part II", SAE 1999-01-3689, 1999.

[91] Heffel, J.W., D.C. Johnson, and C. Shelby, "Hydrogen powered Shelby Cobra: Vehicle conversion", American Hydrogen Association, Volume 13, No. 1, 2002.

[92] Heimrich, M.J., and C.C. Andrews, "On-board hydrogen generation for rapid catalyst light-off", SAE 2000-01-1841, 2000.

[93] Heisler, H., "Advanced Engine Technology." Butterworth Heinmann, 1995.

[94] Hensinger, D.M., J.A. Maxson, K. Hom, and A.K. Oppenheim, "Jet plume injection and combustion", 920414, 1992.

[95] Heywood, J.B., "Combustion and its modeling in spark-ignition engines", International Symposium, COMODIA 94, 1994.

[96] Heywood, J.B., "Internal combustion engine fundamentals", McGraw-Hill, London, 1988.

[97] Ho, C.M., and D.A. Santavicca, "Turbulence effects on early flame kernel growth", SAE 872100, 1987.

[98] Holper, P., and J. Nonnan, CSIRO Atmospheric Research - Urban and regional air pollution information sheet http://www.dar.csiro.au/info/material/airpoll.htm, Accessed: 24 January 2002.

[99] Horie, K., K. Nishizawa, T. Ogawa, S. Akazaki, and K. Miura, "The development of a high fuel economy and high performance four- valve lean burn engine", SAE 920455, 1992.

[100] Houghton, J.T. et al., eds. Climate Change 1995: The Science of Climate Change, published for the Intergovernmental Panel on Climate Change, in collaboration with the World Meteorological Organization and the United Nations Environment Programme (Cambridge University Press, Cambridge, U.K., 1996).

[101] Houston, R., and G. Cathcart, "Combustion and emissions characteristics of Orbital's combustion process applied to multi-cylinder automotive direct-injected, 4-stroke engines", SAE 980153, 1998.

[102] Im, K.S., M.C. Lai, and J. Wang, "Development process of shock waves by supersonic spray", SAE 2004-01-1769, 2004.

[103] Inoue, T., S. Matsushita, K. Nakanishi, and H. Okano, "Toyota lean combustion system - The third generation", SAE 930873, 1993.

[104] IPCC (Intergovernmental Panel on Climate Change) Third Assessment Report, 2001.

[105] Iwamoto, Y., K. Noma, O. Nakayama, T. Yamauchi, and H. Ando, "Development of gasoline direct injection engine", SAE 970541, 1997.

[106] James, D., "Hydrogen politics", Business Review Weekly, November 28 - December 4, 2002.

[107] James, E.H., "Laminar burning velocities of isooctane-air mixtures - A literature review." SAE 870170, 1987.

[108] Jeonghoon, S., S. Myoungho, and K. Wootai, "Performance evaluation of lean-burn engines by high ignition energy", Hanyang University and Hyundai Motor Company, International Pacific Conference on Automotive Engineering, Paper Number 99014, 26 May 1999.

[109] Jijun, L., W. Wu Deyu, and Z. Longbao, "An experimental investigation on a new squish jet-turbulence combustion chamber for SI engine", SAE 1999-01-3664, 1999.

[110] Jost, K., "Fuel-cell commercialization", Automotive Engineering International, September 2002.

[111] Kaelblein, T., Y.I. Jeong, and K.T. Rhee, "Knock effects on spark-ignition engine emission and performance", SAE 900712, 1990.

[112] Kanda, M., T. Baika, S. Kato, M. Iwamuro, M. Koike, and A. Saito, "Application of a new combustion concept to direct injection gasoline engine", SAE 2000-01-0531, 2000.

[113] Kashima, S., M. Nakasato, T. Sawa, M. Sugiyama, and T. Yasuhara, "Report on Auto-Related Environmental Taxes - Utilization of Auto-Related Taxes in Environmental Policy" < http://www.env.go.jp/en/rep/aret/>, Created: July 1999, Accessed: 27 January 2002.

[114] Kato, S., N. Nakamura, K. Kato, and H. Ohnaka, "High efficiency supercharger increases engine output, reduces fuel consumption through computer control", SAE 861392, 1986.

[115] Kim, J.M., Y. T. Kim, J. T. Lee, and S. Y. Lee, "Performance characteristics of hydrogen fueled engine with the direct injection and spark ignition system", SAE 952498, 1995.

[116] Kim, T., S. Noh, C. Yu, and I. Kang, "Optimization of swirl and tumble in KMC 2.4L lean burn engine", SAE 940307, 1994.

[117] Kimbara, Y., K. Shinoda, H. Koide, and N. Kobayashi, "NO_x reduction is compatible with fuel economy through Toyota's lean combustion", SAE 851210, 1985.

[118] Kiyota, Y., K. Akishino, and H. Ando, "Concept of lean combustion by barrel-stratification", SAE 920678, 1992.

[119] Komiyama, K., and J.B. Heywood, "Predicting NO_x emission and effects of exhaust gas recirculation in spark-ignition engines", SAE 730475, 1973.

[120] Konig, G., and C.G.W. Sheppard, "End gas autoignition and knock in a spark ignition engine", SAE 902135, 1990.

[121] Koyanagi, K., M. Hiruma, K. Yamane, and S. Furuhama, "Effect of hydrogen jet on mixture formation in a high-pressure injection hydrogen fueled engine with spark ignition", SAE 931811, 1993.

[122] Kreyszig, E., "Advanced engineering mathematics", John Wiley & Sons INC., New-York,1993.

[123] Kuck, H.A., V. Fleischer, and W. Schnorbus, "New 1.3L high performance SI-engine supercharged by the VW G-Lader", SAE 860102, 1986.

[124] Kühn, M., J. Abthoff, R. Kemmler, and T. Kaiser, "Influence of the inlet port and combustion chamber configuration on the lean-burn behavior of a spark-ignited gasoline engine", SAE 960608, 1996.

[125] Kume, T., Y. Iwamoto, K. Iida, M. Murakami, K. Akishino, and H. Ando, "Combustion control technologies for direct injection SI engine", SAE 960600, 1996.

[126] Kuwahara, K., K. Ueda, and H. Ando, "Mixing control strategy for engine performance improvement in a gasoline direct-injection engine", SAE 980158, 1998.

[127] Kuwahara, K., T. Watanabe, J. Takemura, S. Omori, T. Kume, and H. Ando, "Optimization of in-cylinder flow and mixing for a center-spark four-

valve engine employing the concept of barrel-stratification", SAE 940986, 1994.

[128] Kyaw, Z., "Chemical control of S.I. engine combustion", Thesis (Ph.D.), University of Melbourne, 1992.

[129] Lake, T., J. Stokes, R. Murphy, R. Osborne, and A. Schamel, "Turbocharging concepts for downsized DI gasoline engines", SAE 2004-01-0036, 2004.

[130] Lambe, S.M., "Hydrogen dual-fuel combustion", Thesis (Ph.D.), The University of Melbourne, 1991.

[131] Lancaster, D.R., "Effects of engine variables on turbulence in a spark-ignition engine", SAE 760159, 1976.

[132] Lancaster, D.R., R.B. Krieger, J.H. Lienesch, "Measurement and analysis of engine pressure data", Engine Research Dept., General Motors Research Laboratories, SAE 750026, 1975.

[133] Lancaster, D.R., R.B. Krieger, S.C. Sorenson, and W.L. Hull, "Effects of turbulence on spark ignition engine combustion", SAE 760160, 1976.

[134] Latham, S., S. Kollamthodi, P.G. Boulter, P.M. Nelson, and A.J. Hickman, "Assessment of primary NO_2 emissions, hydrocarbon speciation and particulate sizing on a range of road vehicles", TRL Limited, Project Report PR/SE/353/2001, 2001.

[135] Lavoie, G.A., "Correlations of combustion data for SI engine calculation - laminar flame speed, quench distance and global reaction rates", SAE 780229, 1978.

[136] Lawrence, J.C., "Hydrocarbon emission from a HAJI equipped ultra lean burn engine", Thesis (Ph.D.), University of Melbourne, 1999.

[137] Light-Duty Automotive Technology and Fuel Economy Trends 1975 through 2001 (EPA420-S-01-001) is available electronically on the Office of Transportation and Air Quality's (OTAQ) Web site at: http://www.epa.gov/otaq/fetrends.htm, Accessed: 27 January 2002.

[138] Linna, J.R., H. Malberg, P.J. Bennett, P.J. Palmer, T. Tian, and W.K. Cheng, "Contribution of oil layer mechanism to the hydrocarbon emissions from spark ignition engines", SAE 972892, 1997.

[139] Lu, J.H., D. Ezeboye, A. Iiyama, R. Greif, and R. F. Sawyer, "Effect of knock on time-resolved engine heat transfer", SAE 890158, 1989.

[140] Lumsden, G, and H.C. Watson, "Optimum Control of an S.I. engine with a $\lambda = 5$ capability", SAE 950689, 1995.

[141] Lumsden, G., and H.C. Watson, "HAJI operation in a hydrogen-only mode for emission control at cold start", SAE 950412, 1995.

[142] Lumsden, G., D. Eddleston, and R. Sykes, "Comparing lean burn and EGR", SAE 970505, 1997.

[143] Lumsden, G.A., "The phenomena of hydrogen assisted jet ignition", Thesis (Ph.D.), University of Melbourne, 1995.

[144] Maricq, M.M., R.H. Munoz, J. Yang, and R.W. Anderson, "Sooting tendencies in an air-forced, direct-injection, spark-ignition (DISI) engine", SAE 2000-01-0255, 2000.

[145] Matlab Reference Guide, The Math Works Inc., 1992.

[146] Matsushita, S., T. Inoue, K. Nakanishi, K. Kato, and N. Kobayashi, "Development of the Toyota lean combustion system", SAE 850044, 1985.

[147] Mattavi, J.N., and C.A. Amman, "Combustion modeling in reciprocating engines", General Motors Symposia Series, Plenum press, New York, 1980.

[148] McAlister, R., "Hydrogen today - Clean energy for a better world", American Hydrogen Association, Vol 13, No. 1, 2002.

[149] McFadden, P.D., "Combustion modelling program user's guide and operating manual", The University of Melbourne, Department of Mechanical and Manufacturing Engineering, Report T37/'78, 1978.

[150] McReynolds, L.A., L.J. Test, J.M. Snell, J. McHale, E.J. McLaughlin, R. Childes, B.R. Siegel, P.C. Ritchie, and P.J. Smith, "ASTM Manual of engine test methods for rating fuels", American Society for Testing Materials, 1952.

[151] Metghalchi, M., and J.C. Keck, "Burning velocities of air with methanol, isooctane, and indolene at high pressure and temperature", Combustion and Flame, Vol.48, pp. 191-210, 1982.

[152] Mikulic, L., "Mercedes Perspective: Future Challenges for Passenger Car Propulsion Systems", press release by DaimlerChrysler AG, 05-06-2004.

[153] Miller, J.A., and C.T. Bowman, "Mechanism and modeling of nitrogen chemistry in combustion", Prog. Energy Combust. Sci., Vol. 15, pp. 287-338, 1989.

[154] Milton, B.E., and J.C. Keck, "Laminar burning velocities in stoichiometric hydrogen and hydrogen-hydrocarbon gas mixtures", Combustion and Flame, Vol. 58, pp. 13-22, 1984.

[155] Min, K., W.K. Cheng, and J.B. Heywood, "The effects of crevices on the engine out hydrocarbon emissions in SI engines", SAE 940306, 1994.

[156] Minami, T., I. Yamaguchi, M. Shintani, K. Tsujimura, and T. Suzuki, "Analysis of fuel spray characteristics and combustion phenomena under high pressure fuel injection", SAE 900438, 1990.

[157] Monaghan, M.L., "Future gasoline and diesel engines - review", International Journal of Automotive Technology, Vol. 1, No. 1, pp. 1-8, 2000.

[158] Motor vehicle emission regulations and fuel specifications. Part 1. Summary and annual 1997/1998 update. Brussek: CONCAWE, (Report no.9/98), 1998.

[159] Mukai, K., and H. Miyazaki, "The influence of the combustion chamber head material of a gasoline engine on exhaust HC", SAE 2000-01-3072, 2000.

[160] Muller, U.C., M. Bollig, and N. Peters, "Approximations for burning velocities and Markstein numbers for lean hydrocarbon and methanol flames", Combustion and Flame, Vol. 108, pp. 349-356, 1997.

[161] Murase, E., and K. Hanada, "Enhancement of combustion by injection of radicals", SAE 2000-01-0194, 2000.

[162] Nakahira, T., M. Komori, M. Nishida, and K. Tsujimura, "The shock wave generation around diesel fuel spray with high pressure injection", SAE 920460, 1992.

[163] Nakamura, N., T. Baika, and Y. Shibata, "Multipoint spark ignition for lean combustion", SAE 852092, 1985.

[164] National Greenhouse Gas Inventory 1999, Australian Greenhouse office, http://www.greenhouse.gov.au/inventory, Accessed: February 2001.

[165] Negus, C.H., "An interactive chemical equilibrium solver for the personal computer", Thesis (M.Eng.Sc.), The faculty of the Virginia Polytechnic Institute and State University, Blacksburg, Virginia, 1997.

[166] Neiper, H.N., "Catalytic converters and chronic fatigue syndrome", Australian Health and Healing, Vol.14, No.4, p. 5-8, August 1995 - October 1995.

[167] NIST (The National Institute of Standards and Technology) Chemistry WebBook", http://webbook.nist.gov, (Accessed 21st of September, 2001).

[168] Okamoto, K., T. Ichikawa. K. Saitoh, K. Oyama, K. Hiraya, and T. Urushihara, "Study of Antiknock performance under various octane numbers and compression rations in a DISI engine", SAE 2003-01-1804, 2003.

[169] Olikara, C., and G.L. Borman, "A computer program for calculating properties of equilibrium combustion products with some application to I.C. engines", SAE 750468, 1975.

[170] Olsson, K. and B. Johansson, "Combustion chamber for natural gas SI engines part 2: combustion and emissions", SAE 950517, 1995.

[171] Oppenheim, A.K., J. Beltramo, D.W. Faris, J. A. Maxson, K. Hom, and H.E. Stewart, "Pulsed Jet Combustion - A key to controlled combustion engines", SAE 890153, 1989.

[172] Oppenheim, A.K., K. Teichman, K. Hom, and H.E. Stewart, "Jet ignition of an ultra-lean mixture", SAE 780637, 1978.

[173] Otobe, Y., O. Goto, H. Miyano, M. Kawamoto, A. Aoki, and T. Ogawa, "Honda Formula 1 turbocharged V6 1.5 liter engine", SAE 890877, 1989.

[174] Overington, M.T., and C.D. Boer, "Vehicle fuel economy-high compression ration and supercharging compared", SAE 840242, 1984.

[175] Petitjean, D., Bernardini L., Middlemass C., and Shahed S.M., "Advanced gasoline engine turbocharging technology for fuel economy improvements", SAE 2004-01-0988, 2004.

[176] Pierik, R.D., and J.F. Burkhard, "Design and development of a mechanical variable valve actuation system", SAE 2000-01-1221, 2000.

[177] Poulos, S.G., and J.B. Heywood, "The effect of chamber geometry on spark-ignition engine combustion", SAE 830334, 1983.

[178] Pozniak, D.J., "A spark ignition, lean-homogeneous combustion, engine emission control system for a small vehicle", SAE 760225, 1976.

[179] Preussner, C., C. Döring, S. Fehler, and S. Kampmann, "GDI: interaction between mixture preparation, combustion system and injector performance", SAE 980498, 1998.

[180] Rai, H.S., M.F.J Brunt, and C.P. Loader, "Quantification and reduction of IMEP error resulting from pressure transducer thermal shock in an S.I. engine", SAE 1999-01-1329, 1999.

[181] Randolph, A.L., "Cylinder-pressure-based combustion analysis in race engines", General Motors Corp., SAE 942487, 1994.

[182] Rase, E.M., and K. Hanada, "Ignition timing control of homogeneous charge compression ignition engines by pulsed flame jets", Combustion Science and Technology, 174:129-140, 2002.

[183] Rhee, K.T., and S.L. Chang, "Empirical equations for adiabatic flame temperatures for some fuel-air combustion systems", Journal of Combustion Science and Technology, Vol. 44, pp. 75-88, 1985.

[184] Robinet, C., P. Higelin, B. Moreau, O. Pajot, and J. Andrzejewski, "A new firing concept for internal combustion engines: "l'APIR"." SAE 1999-01-0621, 1999.

[185] Rodt, S., "Future diesel - Exhaust gas legislation for passenger cars, light duty commercial vehicles, and heavy duty vehicles", Federal Environmental Agency, http://www.umweltbundesamt.de, Accessed: 23 July 2003.

[186] Rogers, T.E., "Basic digital filter design routines 'Stearns & Hush' graduate digital filter design course text book", http://home.att.net/~terrence. rogers/index.htm, Created: 05 August 1997, Accessed: 16 June 2002.

[187] Russ, S., "A review of the effect of engine operating conditions on borderline knock", SAE 960497, 1996.

[188] Russ, S., E.W. Kaiser, W.O. Siegl, S.H. Podsiadlik, and K.M. Barrett, "Compression ratio and coolant temperature effects on HC emissions from a spark-ignition engine", SAE 950163, 1995.

[189] Saika, T., and K. Korematsu, "Flame propagation into ring crevice of a spark ignition engine", SAE 861528, 1986.

[190] Santavicca, D.A., D. Liou, and G.L. North, "A fractal model of turbulent flame kernel growth", SAE 900024, 1990.

[191] Schuerholz, S., D. Ellmer, St. Siemund, "Exhaust gas management", SAE 2004-01-0647, 2004.

[192] Shinagawa, T., T. Okumura, S. Furuno, and K.O. Kim, "Effects of hydrogen addition to SI engine on knock behavior", SAE 2004-01-1851, 2004.

[193] Shrestha, S.O.B., and G.A. Karim, "A predictive model for gas fueled spark ignition engine applications". SAE 1999-01-3482, 1999.

[194] Shuliang, L., F. Yongjian, and P. Pucheng, "Twice Electronic Fuel Injection (TEFI)-A new idea of lean combustion in S.I. engines", SAE 2000-01-1087, 2000.

[195] Spindt, R.S., "Air Fuel Ratios from Exhaust Gas Analysis", SAE 650507, 1965.

[196] Stanglmaier, R.H., and C.E. Roberts, "Homogeneous charge compression ignition (HCCI): Benefits, compromises, and future engine applications", SAE 1999-01-3682, 1999.

[197] Stone, R., "Introduction to internal combustion engines", Society of Automotive Engineers, Inc., Third Edition, 1999.

[198] Sun, R., R. Thomas, and C.L. Gray, "An HCCI engine: Power plant for a hybrid vehicle", SAE 2004-01-0933, 2004.

[199] Sung, N.W., and S.P. Jun, "The effect of combustion chamber geometry in a SI engine", SAE 972996, 1997.

[200] Swain, M.R., M.N. Swain, and R.R. Adt, "Considerations in the design of an inexpensive hydrogen-fueled engine", SAE 881630, 1988.

[201] Swarts, A., A. Yates, C. Viljoen, and R. Coetzer, "A further study of inconsistencies between autoignition and knock intensity in the CFR octane rating engine" SAE 2005-01-2081, 2005.

[202] Tabaczynski, R.J., C.R. Ferguson, and K. Radhakrishnan, "A turbulent entrainment model for spark-ignition engine combustion", SAE 770647, 1977.

[203] Tabaczynski, R.J., D.P. Hoult, and J.C. Keck, "High Reynolds number flow in a moving corner." Journal of Fluid Mechanics, 42:249-255, 1970.

[204] Takiguchi, M., P. Pichainarong, T. Matsushita, and S. Furuhama, "Characteristics of combustion pressure vibration in hydrogen fuel injection hot surface ignition engines", SAE 871611, 1987.

[205] Taylor, C.F., "The Internal-Combustion Engine in Theory and Practice. Vol. V2.' The MIT Press, 1985.

[206] Tomoda, T., S. Sasaki, D. Sawada, A. Saito, and H. Sami, "Development of direct-injection gasoline engine - Study of stratified mixture formation." SAE 970539, 1997.

[207] Topinka, J.A., M.D. Gerty, J.B. Heywood and J.C. Keck, "Knock behavior of a lean-burn, H_2 and CO enhanced, SI gasoline engine concept", SAE 2004-01-0975, 2004.

[208] Towers, J.M., and R.L. Hoekstra, "Engine knock, a renewed concern in motorsports", SAE 983026, 1998.

[209] Tully, E.J., and J.B. Heywood, "Lean-burn characteristics of a gasoline engine enriched with hydrogen from a plasmatron fuel reformer", SAE 2003-01-0630, 2003.

[210] Ubong, E., "Hydrogen: Properties, storage and safety", Center of Fuel Cell Research and Powertrain Integration, Flint, MI, USA, Report Number: F2004F208, 2004.

[211] University Corporation for Atmospheric Research (UCAR) and the National Oceanic and Atmospheric Administration (NOAA), Reports to the Nation: Our Changing Climate, p. 20, (UCAR, Boulder, Colorado), 1997.

[212] Urushihara, T., T. Murayama, Y. Takagi, and K.H. Lee, "Turbulence and cycle-by-cycle variation of mean velocity generated by swirl and tumble flow and their effects on combustion", SAE 950813, 1995.

[213] Vizoroglu, T.N., "Hydrogen, fuel cells, and infrastructure technologies program", Annual Report, Clean Energy Research Institute, University of Miami, 2003.

[214] Wakai, K., S. Kito, and I. Sumida, "Effect of small hydrogen jet flame on augmentation of lean combustion", SAE 931943, 1993.

[215] Wakai, K., S. Kito, and S. Shimizu, "Combustion of methanol-air mixture in a closed chamber ignited by a pulsed jet plume of hydrogen flame", International Power Engineering Conference, May 17-21, 1992.

[216] Wallace, J.S., L. Segal, and J.F. Keffer, "Lean mixture operation of hydrogen-fueled spark ignition engines", SAE 852119, 1985.

[217] Wang, D., "An Investigation of Direct Injection of Natural Gas in a Hydrogen Assisted Jet Ignition Engine ", Thesis (Ph.D.), University of Melbourne, 2004.

[218] Watson, H.C., "Cyclic variability, lean burn and hydrogen addition", Short course on road transport engine emissions, University of Melbourne, July 2001.

[219] Watson, H.C., "International patent. Application PCT/AU92/00552", 1992.

[220] Watson, H.C., "Sources of hydrocarbon emissions", Short course on SI engines emissions, University of Leeds, November 2001.

[221] Watson, H.C., and E.E. Milkins, "Cylinder head design", Modern engine developments Lecture 7246/1, University of Melbourne, 1972.

[222] Watson, H.C., E.E. Milkins, W.R.B. Martin, and J. Edsell, "An Australian hydrogen car", Department of Mechanical and Industrial Engineering, University of Melbourne, 1983.

[223] Watson, H.C., Private conversation, April 2005.

[224] Wave View manual written by David Tinker.

[225] Webster, D., and G. Andrews, "Three-way catalysts - present and future. Design and materials for warm-up and high conversion efficiency", Short course on road transport engines emissions, University of Melbourne, July 2001.

[226] Whitelaw, J. H., and H.M. Xu, "Cyclic variations in a lean-burn spark-ignition engine without and with swirl", SAE 950683, 1995.

[227] Worldwide Emission Standards, DELPHI - Automotive Technology, 2003.

[228] WRI calculation based on compiled data from various editions of: International Energy Agency, Energy Statistics and Balances of Non-OECD Countries and Energy Statistics and Balances of OECD Countries (Organisation for Economic Co- Operation and Development, Paris, various editions).

[229] Wylen, G.V., R. Sonntag, and C. Borgnakke, "Fundamentals of classical thermodynamics", 4th edition, John Wiley & Sons, Inc., New York, 1994.

[230] Yang, J., E.W. Kaiser, W.O. Siegl, and R.W. Anderson, "Effects of port-injection timing and fuel droplet size on total and speciated exhaust hydrocarbon emissions", SAE 930711, 1993.

[231] Yates, A.B.Y., A. Swarts, and C.L. Viljoen, "Correlating auto-ignition delays and knock-limited spark-advance data for different types of fuel", SAE 2005-01-2083, 2005.

[232] Zakis, G., "Alternative ignition system for CNG in Diesel Applications", Thesis (M.Eng.Sc.), University of Melbourne, 2003.

[233] Zhang, Y., Private conversation, August 2001.

[234] Zinner, K., "Supercharging of internal combustion engines", Springer-Verlag Berlin Heidelberg New York, 1978.

Appendix A
Mixture Properties and Regulations

A.1 Properties of Air-Fuel Mixtures

Table A.1 Combustion and transport properties of fuel mixtures with air [213].

Property of Fuel	Gasoline	Hydrogen	Methane	Propane
Specific gravity at NTP	4.0	0.07	0.55	1.52
Normal boiling point (K)	310 - 478	20.3	111.6	231
Density of liquid at NTP	0.7	0.0708	0.4225	0.5077
Density ratio, NTP liquid / NTP gas	150	845	649	259
Diffusion coefficient in NTP air (cm^2/s)	0.05	0.61	0.16	0.1
Diffusion velocity in NTP air (mm/s)	0.17	2.0	0.51	0.34

Property of Fuel	Gasoline	Hydrogen	Methane	Propane
Quenching gap in NTP air (mm)	2.0	0.64	2.03	1.78
Limits of flammability in air (vol. %)	1.4 - 6.0	4.0 - 75.0	5.3 - 15.0	2.2 - 9.5
Limits of flammability in air, by equivalence ratio	0.75 - 3.79	0.10 - 7.14	0.53 - 1.68	0.54 - 2.5
Limits of detonation in oxygen (vol.%)	1.1 - 3.3	18.3 - 59.0	6.3 - 13.5	3.4 - 35.0
Minimum energy for ignition in air (mJ)	0.24	0.02	0.29	0.305
Autoignition temp. (K)	501 - 744	858	813	740
Flame temp. (K)	2470	2318	2148	2248
Maximum burning velocity in NTP air (cm/s)	37 - 43	278	37 - 45	43 - 52
Thermal Conductivity @400K W/mK		0.167272	0.030859	0.0139
Energy of stoichiometric mixture (mJ/m^3)	3.91	3.58	3.58	3.79

A.2 Health Effect of Pollutants

Table A.2 Engine emissions and their effect on health [98].

Pollutant	Sources	Health effects
Carbon monoxide	Motor vehicles, burning of fossil fuels.	Blood absorbs carbon monoxide more readily than oxygen, reducing the amount of oxygen being carried through the body. Carbon monoxide can produce tiredness and headaches. People with heart problems are particularly at risk.
Sulfur dioxide	Coal and oil burning power stations, mineral ore processing and chemical manufacture.	Attacks the throat and lungs. People with breathing problems can suffer severe illness.
Nitrogen dioxide	Fuel combustion.	Affects the throat and lungs.
Volatile organic compounds	Motor vehicles, fuel combustion, solvent use.	Some VOCs cause eye and skin irritation, headaches or nausea, while some are classed as carcinogens.
Ozone	Formed from nitrogen oxides and hydrocarbons in sunny conditions. Released by motor vehicles and industry.	Ozone attacks the tissue of the throat and lungs and irritates the eyes.
Lead	Exhaust gases from motor vehicles that use leaded petrol, smelters.	Lead from air particles can enter lungs then be absorbed into the blood stream. Over a period, lead can affect the nervous system and the body's ability to produce blood.
Particles	Motor vehicles, burning of plant materials, bushfires.	May cause breathing difficulties and worsen respiratory diseases. Some particles contain cancer-producing materials.

A.3 Emission Regulations

Table A.3 Current and future light-duty emission regulations for Europe [158].

	Pollutant	Limits (g/km) 1996 -> Euro2[1)]	Limits (g/km) 2000 -> Euro3[2)]	Limits (g/km) 2005 -> Euro4[2)]
Gasoline	CO	2.2	2.3	1.0
	HC	-	0.2	0.1
	$HC+NO_x$	0.5	-	-
	NO_x	-	0.15	0.08
Diesel	CO	1	0.64	0.5
	$HC+NO_x$	0.7/0.9[3)]	0.56	0.3
	NO_x	-	0.5	0.25
	Particulates	0.08/0.10[3)]	0.05	0.025

1) Test starts with 40 second idling without exhaust sampling.
2) Engine and exhaust sampling started simultaneously.
3) IDI/DI diesel.

Table A.4 Current and future US Federal emissions regulations and Californian standards for light-duty vehicles [158, 227].

Category	CO g/mile	NMHC/NMOG[3] g/mile	NO_x g/mile	Formaldehyde[4] g/mile	Particulates[5] g/mile
Tier I Gasoline	3.4 (4.2)[6]	0.25 (0.31)	0.1 (0.6)	--- (---)	--- (---)
Tier I Diesel	--- (4.2)	--- (0.31)	--- (1.0)	--- (---)	--- (0.08)
$TLEV_1$	3.4 (4.2)	0.125 (0.156)	0.4 (0.6)	0.015 (0.018)	--- (0.08)
LEV_1	3.4 (4.2)	0.075 (0.090)	0.2 (0.3)	0.015 (0.018)	--- (0.08)
$ULEV_1$	1.7 (2.1)	0.04 (0.055)	0.2 (0.3)	0.008 (0.011)	--- (0.04)
ZEV_1	0.0	0.0	0.0	0.0	0.0
LEV_2	3.4(4.2)	0.075(0.090)	0.05(0.07)	0.015(0.018)	(0.01)
$ULEV_2$	1.7(2.1)	0.040(0.055)	0.05(0.07)	0.008(0.011)	(0.01)
$SULEV_2$	(1.0)	(0.01)	(0.02)	(0.004)	(0.01)
ZEV_2	0.0	0.0	0.0	0.0	0.0

1) Emissions categories phasing out 2004-2007.
2) Emission limits phasing in 2004 onwards.
3) NMOG= reactivity corrected values for alternative fuelled vehicles.
4) Methanol and flexible-fuel vehicles only.
5) Diesels only.
6) Limits for 50.000 miles with 100.000 miles in parentheses.

Table A.5 Proposed Euro 5 emission regulations for passenger cars and light-duty commercial vehicles. Proposed to be effective from 2010 [185].

Vehicle class/group	Reference weight RW (kg)	CO g/km	HC g/km	NO_x g/km	Particulate mass g/km
		Petrol Diesel	Petrol Diesel	Petrol Diesel	
Passenger cars	All	1	0.05	0.04/0.08	0.0025
Light-duty commercial vehicles	RW≤1305	1	0.08	0.08	0.0025
	1305<RW ≤1760	1		0.08	0.0025
	1760<1305	1.25		0.1	0.0032

Note: The implementation of these limit values is technically realisable by 2005. Germany is of the opinion that according to political agreements with France, standards for the future reduction of NO_x and particulate emissions for diesel passenger cars should be implemented in due time and should be made obligatory starting 2010.

A.4 Euro 5 Emissions in g/kWh

Emissions are actually legislated distance specific, however, experimental results produce power specific emissions. Therefore, the g/km emissions values need to be converted to g/kWh to find the limiting values relevant to the experimental results.

Assuming a conservative fuel consumption of 10 Liters/100km for a passenger car and a conservatively high average thermal efficiency of 36%, this would equate to the following kWh per 100km:

10(Liters/100km) * 0.736(kgm^{-3}) * 44000 ($kJkg^{-1}$) * 0.36 (thermal efficiency) / 3600 = 32.38 kWh/100km

This can be converted to more relevant units of km/kWh:

100/32.38 = 3.08 km/kWh

Therefore:

Euro 5 NO_x = 0.04(g/km) * 3.08 (km/kWh) = 0.123 g/kWh

Euro 5 HC = 0.05(g/km) * 3.08 (km/kWh) = 0.154 g/kWh

Euro 5 CO = 1 (g/km) * 3.08 (km/kWh) = 3.08 g/kWh

Appendix B
Engine Technology and Fundamentals

B.1 Spark-Ignition Direct-Injected (SIDI) Engines

B.1.1 Injectors and Spray Patterns

As discussed in Chapter 2.8.2, SIDI is complex for two main reasons: the short times available for the preparation of the mixture prior to combustion and the desire to stratify the air-fuel mixture using the fuel spray and interacting gas dynamics. The three typical spray patterns used in DI are shown in Figure B.1.

Interestingly, tests done in 1997-98 [179] with multi-hole, diesel-like injectors gave poor homogenisation of the fuel in gasoline SIDI engines. The outward opening injectors also performed poorly in terms of homogenising the fuel with air. At the time, Bosch and Toyota believed that the inward opening swirl type injectors were the best as they provided better breakup of fuel without the increased penetration, and generated better droplet size distribution than an equivalent single holed nozzle [179, 206]. Since 1998, Bosch has developed a multi-hole injector for SIDI applications that is superior to the swirl type injector

Figure B.1: Typical spray patterns of different atomization concepts, (left) multi-hole, (middle) outward opening, (right) inward opening swirl type, [179].

as it provides flexible spray arrangements and variability in the number of spray holes. Consequently, its greatest benefit is a reduction in soot formation.

There are currently many types of DI combustion systems, all of which are characterized by the in-cylinder air motion, the fuel injector type and the piston shape. The three most common DI systems are the wall guided, charge motion or air guided, and spray/jet guided (Figure B.2) [39]. In each system, a different mechanism dominates the transportation of the fuel into the region of the spark. All three mechanisms are complex in design and more expensive than PFI.

The first commercial adaptation of the direct injection stratified charge engine was in the early 1930's. The Hesselman engine was touted as a high-power spark-ignition fuel-injection engine. It operated on fuel oil with a then high compression ratio of 7.5 and produced a maximum BMEP of 861 kPa.

Since the Hasselman engine, Mercedes-Benz, Mitsubishi, Nissan, Toyota and GM have also put SIDI engines into production [90]. Some of these will be discussed hereon. Due to the rapid advancements in GDI technology, the technical literature

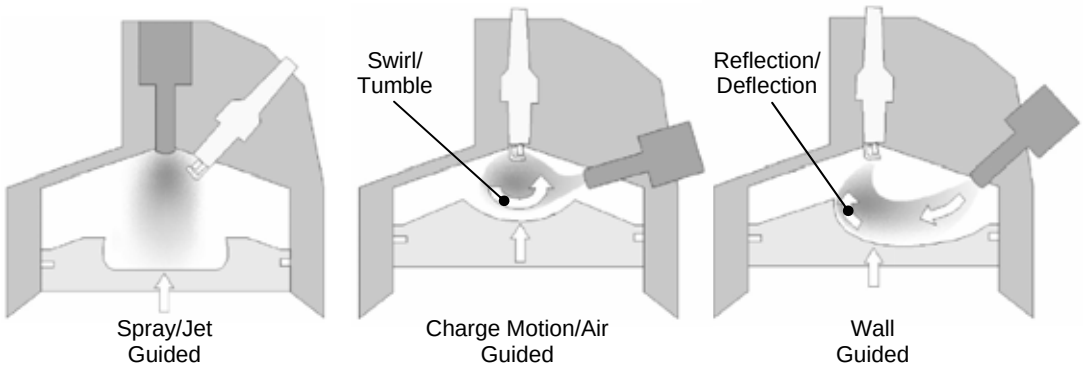

Figure B.2: Direct injection combustion systems [39].

from the major manufacturers is made available only after the technology is put into production. Consequently, the following short literature review is limited to published material up to recent years. It nevertheless provides an excellent background on technologies that were accepted and pursued by the industry in the era when HAJI was developed.

B.1.2 Mitsubishi

In the 1990's, Mitsubishi trademarked the term GDI and took the lead in direct injection engine development and production. Mitsubishi adopted a wall guided DI system called barrel stratification (Figure B.2 - right side) where a side injector sprays onto a spherical cavity in the piston and is reflected toward the spark plug [118, 125, 126, 127]. This arrangement eliminates problems with liquid fuel or over rich mixtures around the spark plug. The principal factor controlling the mixing is the fuel spray or gaseous mixture reflecting off the cavity wall which is subjected to the fuel spray momentum.

Since Mitsubishi's method is controlled by tumble, it is little affected by the engine speed and therefore allows adequate mixing over a wide speed range. The engine operates at CR=12 and in stratified mode by late injection at light load and low speed. This is in contrast with homogeneous mode in which there is early injection at higher loads and speeds. Kuwahara et al. [126] concluded that the GDI technology combined with two injections per cycle eliminates soot by burning it up efficiently utilising the air, radical and heat generated by the lean mixture. Mitsubishi currently offers a range of GDI engines around the world, however in January of 2003, citing emissions problems and high cost, Mitsubishi announced the discontinuation of their development GDI engines.

B.1.3 Toyota

Twenty years ago at Toyota, Kimbara et al. [117] and Matsushita et al. [146] developed a lean combustion system that featured a helical port, swirl control valve and sequential port fuel injection. The combustion chamber setup is similar

to Figure B.2 (left side) with swirl generated (not shown on Figure B.2), and without the DI injector. They claimed 10-15% improvement in thermal efficiency and HC emissions of 0.18 g/mile compared to today's 0.011g/mile for $ULEV_2$. A fuel economy of 3.6 litre/100km was achieved (constant 60 km/h cruising). A further improvement by Inoue et al. [103] improved fuel economy by 10%, and reduced NO_x emissions by 30%.

In 1997, Tomoda et al. [206] fitted this engine with a swirl nozzle type direct injector (Figure B.1-left) and achieved, depending on the NO_x reduction, a 10-20% improvement in thermal efficiency between 0 to 450kPa BMEP. This SIDI engine also needs to transition between stratified lean and homogeneous stoichiometric modes, which is performed at higher loads and speeds primarily to avoid smoke.

In 2000, Toyota changed direction in their DI technology. Kanda et al. [112] developed a new combustion process (NCP) with a fan-shaped fuel spray and a combustion chamber with a shell-shaped cavity in the piston. This extended the stratified combustion mode, allowing it to switch at a higher r/min and load. Consequently, when it was compared to the previous SIDI engine equipped with swirl control valve (SCV) and a helical port, they concluded that the NCP provided a 20% increase in fuel economy whilst satisfying the Japanese emission regulations at the time.

B.1.4 Honda

In 1992, Honda developed their own version of a swirl assisted lean combustion system similar to Toyota's system described earlier. They called it VTEC-E. Horie et al. [99] achieved a fuel economy improvement of 8-12% depending on the type of drive cycle. Carabateas et al. [37] in 1996 examined the effect of a twin jet air injector design and a transfer passage between the two intake ports, still using the VTEC-E cylinder head and valvetrain. They concluded a decrease in NO_x, and CoV of IMEP was possible with no improvements in HC emissions [6, 37].

B.1.5 SIDI - Air Assisted

Since combustion in SIDI engines are strongly controlled by the detail of the sprays, an alternative way to atomize the fuel is by causing the air to collide with the fuel. The fundamental concept of air assisted fuel injectors is to reduce the stratification gradients in the combustion chamber [39].

In 1998, Houston and Cathcart [101] of Orbital engineering tested Orbital's air assisted fuel injector with the combination of a lipped piston crown with a high squish region to stratify the fuel air mixture away from the piston walls. The results at part load conditions (corresponding to a vehicle speed of 40 km/h) were a 34% improvement in fuel consumption and a reduction in NO_x and HC emissions in comparison to baseline port injected engines even when the engine operated lean. Further development at Orbital [39] in 2000 showed that the Orbital air assisted direct injector worked as a spray guided combustion system (Figure B.2-left) and was superior to other systems. Orbital was confident about dominating some of the lean burn market but this has not happened to date.

In 2000, Maricq et al. [144] at Ford examined the sooting (PM) tendencies in an air-assisted SIDI engine. They concluded that as fuel injection is retarded, at a fixed AFR, PM emissions declined to a minimum at an injection time well within the compression stroke, after which they rapidly increased. In a heavily stratified mixture, the PM increase can be attributed to a growing number of rich zones that occur in a progressively more inhomogeneous fuel mixture. Air assist provided less PM emissions over non-air-assisted DI at almost all injection timings, except where mode switching occurred between stratified and homogeneous mixtures.

B.2 Turbulence Mechanisms

B.2.1 Squish

Squish is the result of charge moving from the cylinder walls towards the center of the combustion chamber as the piston approaches the cylinder head near TDC.

The amount of charge and the velocity (referred to as squish velocity) pushed towards the center of the combustion chamber depends on the squish area and clearance between the piston and cylinder head. Peak squish velocity usually occurs at 5-10 degrees BTDC [93, 96].

Squish type combustion chambers reduce the tendency for knock due to shorter flame path and burn duration, as well as increased heat transfer from the end gas [205]. Strategically placed slots on the piston surface can create squish jets (Figure B.3) which can further increase the turbulence intensity and therefore increase the thermal efficiency, reduce NO_x, HC and CO and increase combustion stability in lean mixtures [65, 109]. Squish area must be designed with great care as it can increase HC emissions due to the possibility of flame quench in areas of high surface to volume ratio near TDC. On the other hand, squish can reduce HC emissions by pushing all of the unburned air fuel mixture away from the cylinder wall into the hot burned mixture where it may oxidise. Also, the increased level of turbulence decreases the quench gap, allowing the flame to approach close to the walls [28].

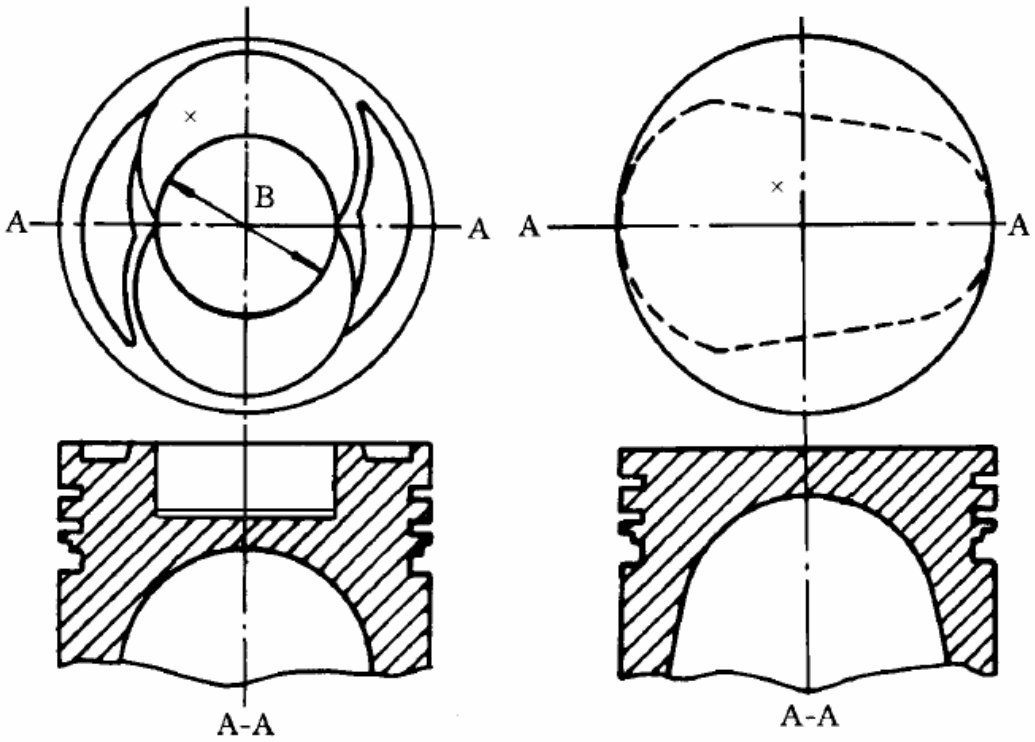

Figure B.3: (left) Squish jet-turbulence combustion chamber, (right) bathtub combustion chamber - popular in China [109].

B.2.2 Tumble

Tumble motion is a rotational flow motion in the combustion chamber that is perpendicular to the cylinder axis. Tumble can increase the mean level of turbulence intensity, enhancing burn rates, probably better than squish or swirl [223]. In the past, tumble was difficult to generate, however with today's modern electronics both the new Audi A6 and the Mercedes 3.5-liter V6 are equipped with tumble flaps in the intake ducts.

The stronger the tumbling motion, the more the kinetic energy is released during its breakdown [17]. This motion is widely adopted especially in DI engines to strategically position the fuel cloud in the vicinity of the spark plug [67]. It must be implemented with care as it can create high fuel concentrations around the spark plug [7]. This can lead to spark plug failure due to carbon build up.

Interestingly, it was found by Kanda et al. [112] that weak tumble gives the lowest fuel consumption in a DI engine. This is somewhat expected since low tumble DI engines would provide minimum or no additional mixing of the air-fuel mixture and would also suffer from poorly evaporated fuel droplets. In contrast, in homogeneously charged SI engines, the air-fuel mixture is already mixed before it enters into the combustion chamber and therefore it does not require this additional complexity of tumble motion to be controlled.

B.2.3 Swirl

Swirling motion is a rotational motion in the combustion chamber about the cylinder axis. In the past, swirl was easy to generate in the combustion chamber by deactivating one of the intake valves in a 4-valve engine. This method to generate turbulence in the combustion chamber was widely pursued to extend the lean flammability limits of lean burn engines [103, 116, 117].

Swirl increases the turbulence intensity through rotational motion and precession [226] as well as during the gradual dissipation throughout the combustion and

expansion process [96]. Interestingly, Urushihara et al. [212] have found that in a steady state test for the same angular momentum, swirl generates less turbulence than tumble. Swirl increases the burning rate and the rate of pressure rise and also increases combustion stability through the higher convection velocities and turbulence levels generated [226].

Appendix C
Engine Calibration

C.1 Compression Ratio Calibration and TDC Alignment

The special feature of the CFR engine is its variable compression ratio. The clearance volume can be varied over a wide range by varying the clearance height. A micrometer is attached to the sliding cylinder head and to the fixed engine block, which measures the clearance height. Deslandes [51] calibrated the currently used CFR engine's micrometer reader to the compression ratio:

$$CR = \frac{4.5 + 0.237 + micro}{0.237 + micro} \tag{C.1}$$

where: *CR* = compression ratio

micro = micrometer setting (in inch)

He estimated the accuracy of the calibration to be ±0.65%. As the CFR engine is a fixed head engine, a check was only performed on this calibration. The author checked the calibration with a piece of plasticine. It was placed inside the combustion chamber through the spark plug hole and the piston was moved to

TDC. This squashed the plastacine piece, which upon removal, allowed the height to be measured and compared to Equation C.1. An agreement between the two was found within an acceptable range of 0.8% - 1.5%.

In order to correctly phase the cylinder pressure to crankshaft position, the location of TDC must be determined. There are three popular methods to determine TDC. Method one uses a dial indicator on the piston. The engine is then rotated clockwise and anticlockwise taking consecutive readings. TDC is the midpoint between equal dial indicator readings. Then this midpoint is aligned with the TDC marker on the flywheel [132]. The estimated accuracy of this measurement is ±0.1 CAD. Amann [11] suggests transmitting microwave energy into a motoring cylinder through the spark plug hole - assuming spark plug is located in line with cylinder. This produces sharp resonance peaks on either side of TDC. He also claimed an accuracy of ±0.1 CAD. The third method involves examining the log-Pressure vs. log-Volume diagram (Figure C.1 and C.2). Observing features of P-V diagram reveal information about the accuracy of the phasing. These rules are summarised below [11, 132]

- Peak pressure should occur between 0.5° - 1.5° BTDC (due to heat loss on the compression stroke [132]). At low compression ratios closer to 0.5° and higher compression ratios closer to 1.5°. Less than 0.5° pressure is too retarded, more than 1.5° pressure too advanced with respect to TDC.

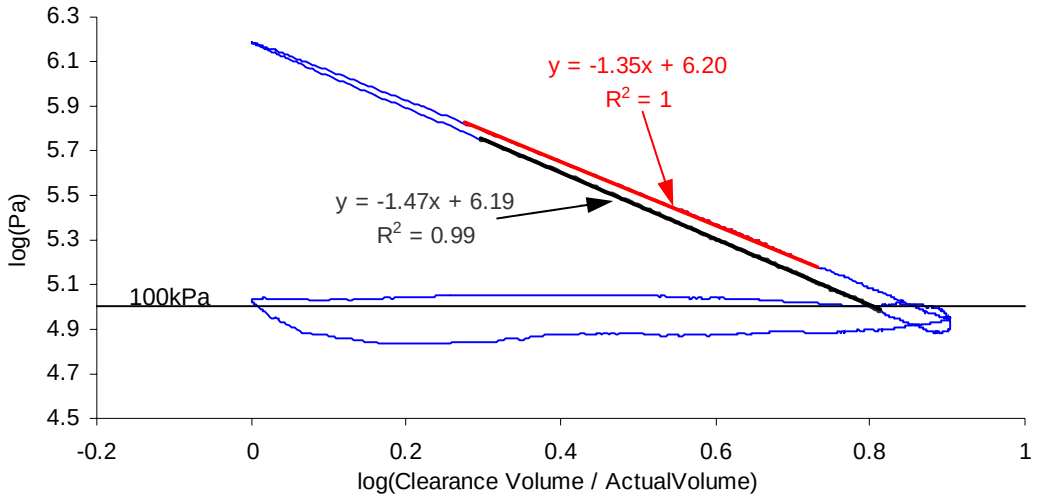

Figure C.1: Motoring trace @WOT, 1800r/min, CR = 8, drift compensated, single cycle, results from E-CoBRA.

- Exhaust pressure should be above 100 KPa towards end of stroke. Below 100 kPa indicates reference pressure too low. Also if the first part of the compression line on a log-log plot is curved then CR in not adjusted properly, hence calculated clearance volume is wrong.
- If the end of the compression line is curved, then wrong clearance volume is assigned. Compression ratio value must be checked.
- If compression and expansion lines cross over, this indicates that pressure is excessively retarded (peak pressure occurring BTDC) with respect to volume.
- Polytropic compression index should fall in between 1.24 and 1.35 depending on engine speed, mixture composition and turbulence levels.
- At WOT, the expansion line at BDC should not dip below the induction line. Upon occurrence, the amplifier time constant must be adjusted to medium or long.

Following these rules, one should be able to get the phasing to within 0.2 CAD accuracy. Lancaster el at. [132] indicates that a phase accuracy of 0.2 or 0.3 CAD is required in order to keep IMEP errors below 1% for spark ignition engines or engines with a long burn duration. Normally the pressure transducer is subjected to thermal shock, which was ameliorated by the use of a coating of RTV [132]. This can reduce thermal shock related IMEP errors by 75%, otherwise errors of up to 5% in gross IMEP and 70% in PMEP can occur [180]. In this research, most data is taken in lean conditions where burn duration is considerably long. Most of the data is also quantitatively analysed rather then qualitatively, which requires a high standard of accuracy in calibrations.

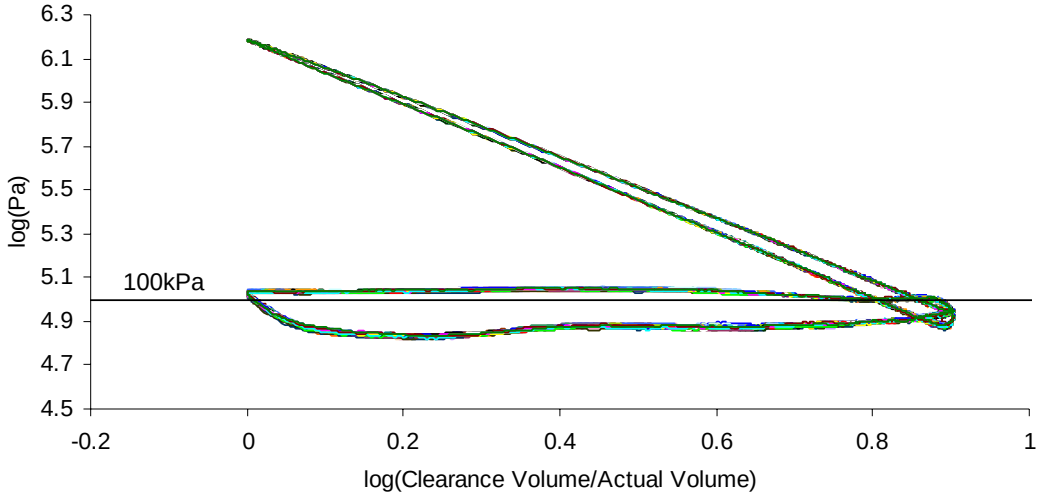

Figure C.2: Motoring trace - 40 cycles - engine conditions same as Figure C.1.

C.2 Fuel and Air Flow Calibration

C.2.1 Airflow

Airflow was measured volumetrically using a calibrated orifice between two surge tanks. The orifice was calibrated experimentally (Figure C.3) with the engine running at 1800r/min. Mass flow was varied by throttling the engine. A theoretical calibration was performed using the British Standard BS 1042 from which calibration constants were determined based on the orifice geometry. An acceptable agreement between the two methods was found in the range of +/- 1.5%.

C.2.2 Gasoline Fuel Flow

The gasoline fuel was port injected using a standard Bosch automotive fuel injector (model number CDH 275). The flow rate of the injector at 2.5 bar gauge pressure is given by:

$$\textit{Flow Rate (mg/pulse)} = 2.6 * \textit{(injector pulse time in ms)} \qquad \text{(C.2)}$$

The fuel flow was also measured volumetrically using a sight glass and stopwatch, confirming Equation C.2. The estimated error of this method is <2% at λ=1 and <1% at λ=2.

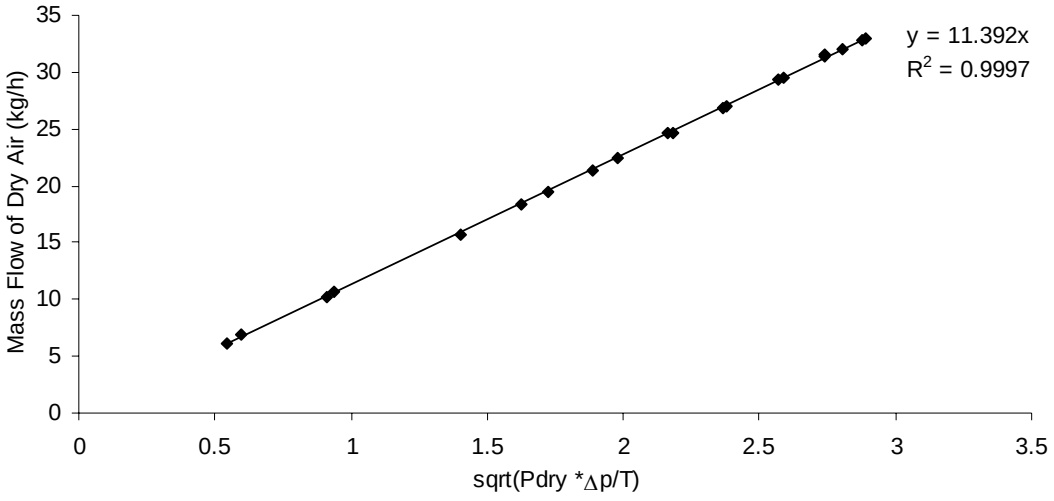

Figure C.3: Experimental air orifice flow calibration curve: P_{dry} = Ambient atmospheric pressure, Δp = H_2O pressure drop across the orifice, T = Ambient air temperature.

C.2.2 Hydrogen Fuel Flow

C.2.2.1 Pre-chamber H_2 Fuel Flow

Hydrogen in the HAJI pre-chamber is injected with a Siemens prototype direct injector. The mass flow rate through the HAJI unit was measured with a digital Brooks 5860E gas flow meter calibrated for hydrogen.

C.2.2.2 Main Chamber H_2 Fuel Flow METHOD 1

Main chamber hydrogen was administered into the intake port. The mass flow of hydrogen was calculated from the intake mass flow of air and the AFR form the exhaust gas analyzer. This was calculated from the $\%O_2$ concentration in the exhaust (Figure C.4). The AFR of hydrogen from the $\%O_2$ concentration was derived as follows:

$$AFR_{H_2} = \frac{34.07\left[\%O_2 - 1\right]}{\frac{100}{21}\%O_2 - 1} \tag{C.3}$$

This method proved to be extremely accurate up to λ =3.5 with less then 2% error and at λ =4.2 with less then 5% error with respect to METHOD 2, which is explained next.

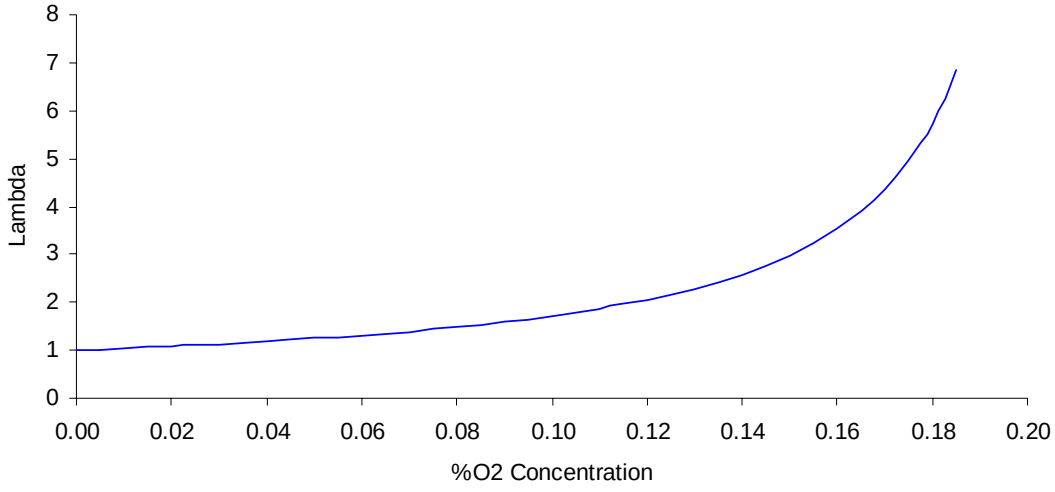

Figure C.4: Hydrogen λ as a function of exhaust O_2 concentration, λ = AFR_{H2} / 34.07.

C.2.2.3 Main Chamber H_2 Fuel Flow METHOD 2

A more accurate method to calculate the mass flow rate of H_2 fuel flow administered into the intake port is through calibrated sonic nozzles. The flow through the nozzle was first calibrated by measuring the volumetric flow through a gas EMAIL meter and multiplying it by the density of H_2 at the lab temperature and pressure (calibration condition). In order to maintain high accuracy in calculating H_2 flow, 6 different nozzles were calibrated (Figure C.5).

Zakis [232] derived an equation for the mass flow through a calibrated sonic nozzle to compensate for daily temperature and pressure variations in the engine test cell. This is as follows:

$$\dot{m} = \left(\frac{\sqrt{T_c}}{\sqrt{T_t}} \right) A[P_g + P_t - P_c] + C \qquad \text{(C.4)}$$

where: 'A' and 'C' are calibration coefficients and constants as shown in Figure C.5

P_g = gauge pressure (psi)

P_t = ambient pressure on test day (psi)

P_c = ambient pressure on calibration day (psi)

T_t = upstream temperature of H_2 on test day (K)

T_c= upstream temperature of H_2 during calibration (K)

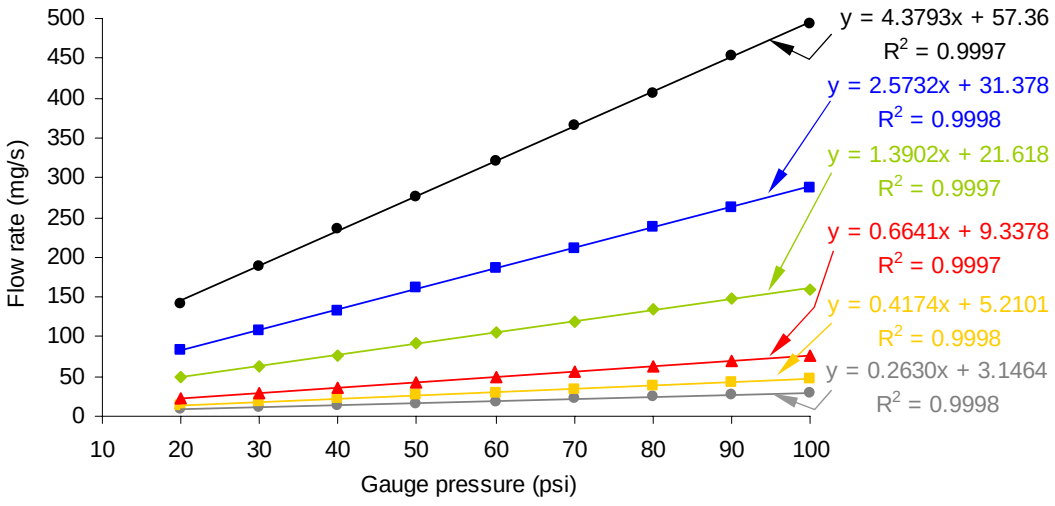

Figure C.5: Mass flow rate of H_2 as a function of upstream gauge pressure.

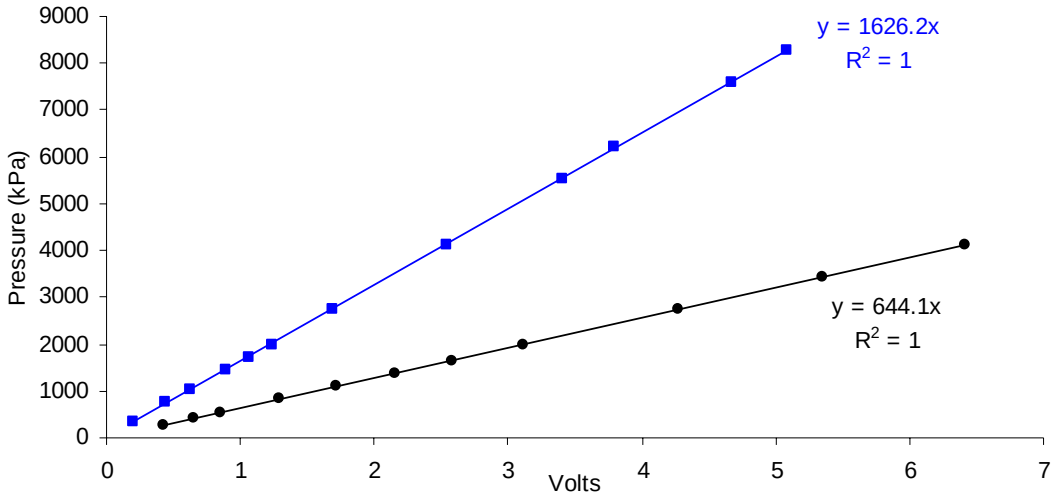

Figure C.6: Pressure transducer calibration graph, (Type: Kistler 601B Sensitivity: 0.5pc/unit, Range: 200 units/Volt for y=644.1x, 500 units/Volt for y=1626.2x).

C.3 Cylinder Pressure Measurements

The cylinder pressure within the combustion chamber was measured using a Kistler 601B1 transducer connected to a 462-A-05 PCP charge amplifier. The transducer was calibrated using a dead weight tester at regular intervals. Figure C.6 shows a sample calibration of the system for low pressure conditions, which occur under low compression ratios or lean air-fuel ratios. This setting provides a pressure resolution of 1.57 kPa/digital count. A higher setting was also used for high compression ratio or stoichiometric conditions with a resolution of 3.97 KPa/digital count, which is adequate for MFB analysis. The pressure signal is smoothed using a double 5-point average technique, proven to be adequate for MFB and MBR calculations [181].

Appendix D
Combustion Modelling

D.1 Geometric Relationships Used in Modelling

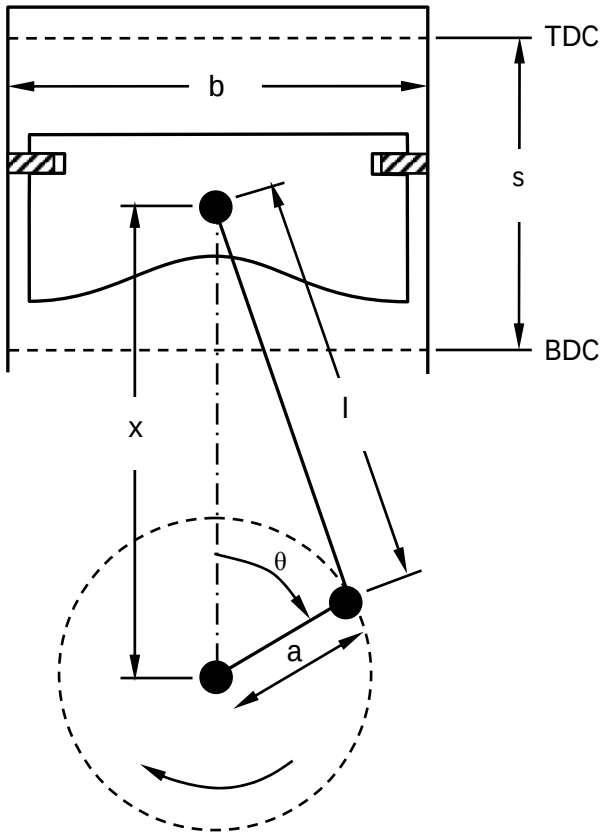

Figure D.1: Basic geometry of the reciprocating IC engine.

As shown in Figure D.1, variables which define the engine geometry are as follows:

b = bore, *s* = stroke, *a* = crank radius *= s/2*

l = connecting rod length, *R = l/a,* r_c = compression ratio

x = distance between crank shaft axis and piston pin axis

V_s = swept volume, V_c = clearance volume, $r_c = 1+(V_s/V_c)$

$$x = \sqrt{l^2 + a^2 \sin^2 \theta} + a\cos\theta \tag{D.1}$$

Combustion chamber area (plane cylindrical combustion chamber):

$$A = \frac{\pi}{2}b^2 + \pi b\frac{s}{2}\left[R + 1 - \cos\theta - (R^2 - \sin^2\theta)^{1/2} + \left(\frac{2}{r_c - 1}\right)\right] \tag{D.2}$$

Combustion chamber volume and its derivative:

$$V = \frac{V_s}{r_c - 1} + \frac{V_s}{2}\left[R + 1 - \cos\theta - (R^2 - \sin^2\theta)^{1/2}\right] \tag{D.3}$$

$$\frac{dV}{d\theta} = \frac{V_s}{2}\sin\theta\left[1 + \cos\theta(R^2 - \sin^2\theta)^{-1/2}\right] \tag{D.4}$$

Note: To convert from m^3/rads to m^3/deg, need to multiply the equation above by PI/180.

Mean piston speed:

$$S_p = 2sN \tag{D.5}$$

D.2 Combustion Modelling

D.2.1 Compression and Expansion Process

The Single-Zone model (Figure D.2) operates throughout the compression and expansion part of the cycle and is governed by the same equation. The heat transfer to the working fluid is positive, and the work transfer from the working fluid is positive.

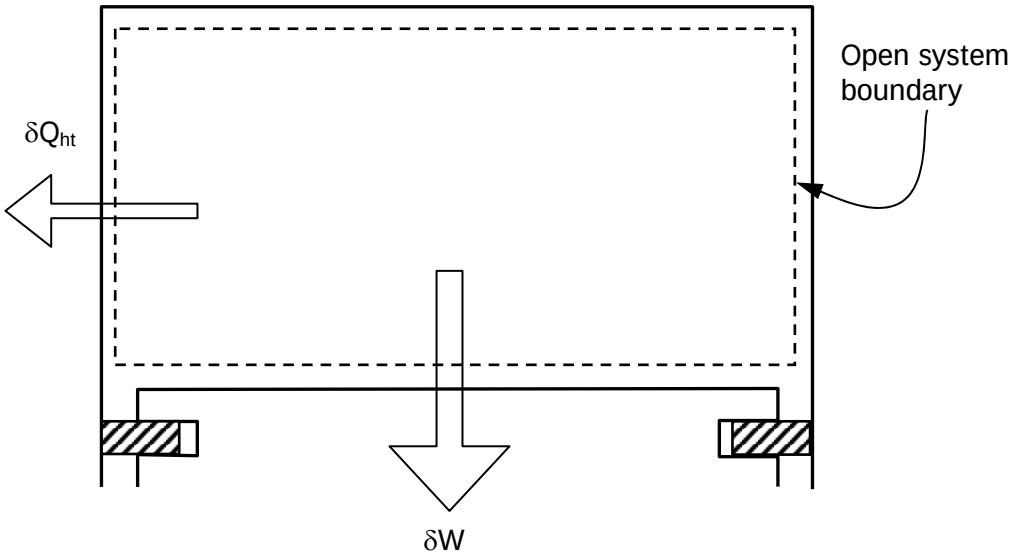

Figure D.2: Open system boundary for Single-Zone combustion chamber.

The differential first law for this model for a small crank angle change is:

$$\frac{dQ}{d\theta} - \frac{dW}{d\theta} = \frac{dU}{d\theta} \tag{D.6}$$

$$\frac{dQ}{d\theta} - P\frac{dV}{d\theta} = mc_v\frac{dT}{d\theta} \tag{D.7}$$

From the ideal gas equation $PV = mRT$

$$m\frac{dT}{d\theta} = \frac{1}{R}\left[P\frac{dV}{d\theta} + V\frac{dP}{d\theta}\right] \tag{D.8}$$

$$\frac{dU}{d\theta} = \frac{c_v}{R}\left[P\frac{dV}{d\theta} + V\frac{dP}{d\theta}\right] \tag{D.9}$$

The first law now becomes:

$$\frac{dQ}{d\theta} - P\frac{dV}{d\theta} = \frac{c_v}{R}\left[P\frac{dV}{d\theta} + V\frac{dP}{d\theta}\right] \tag{D.10}$$

Rearranging:

$$\frac{dQ}{d\theta} - \left[1 + \frac{c_v}{R}\right]P\frac{dV}{d\theta} = \frac{c_v}{R}V\frac{dP}{d\theta} \tag{D.11}$$

$$\frac{dP}{d\theta} = \frac{1}{V}\left[\frac{R}{c_v}\frac{dQ}{d\theta} - \left(1 + \frac{R}{c_v}\right)P\frac{dV}{d\theta}\right] \tag{D.12}$$

Note for D.12: $R = C_p - C_v$ and $R/C_v = (C_p/C_v) - 1$

Now from (D.8)

$$\frac{dT}{d\theta} = T\left[\frac{1}{V}\frac{dV}{d\theta} + \frac{1}{P}\frac{dP}{d\theta}\right] \tag{D.13}$$

Equation D.12 and D.13 are the governing equations for the compression and expansion part of the cycle.

D.2.2 Combustion Process

The two-zone model (Figure D.3) operates the combustion part of the cycle. The heat transfer to the working fluid is positive, and the work transfer from the working fluid is positive. The energy equation for the whole system changed at any instant of time (corresponding to a CA) is described by the first law:

$$\frac{dU}{d\theta} = \frac{dQ}{d\theta} - \frac{dW}{d\theta} \tag{D.14}$$

$$mc_v \frac{dT}{d\theta} = \frac{dQ}{d\theta} - P\frac{dV}{d\theta} \tag{D.15}$$

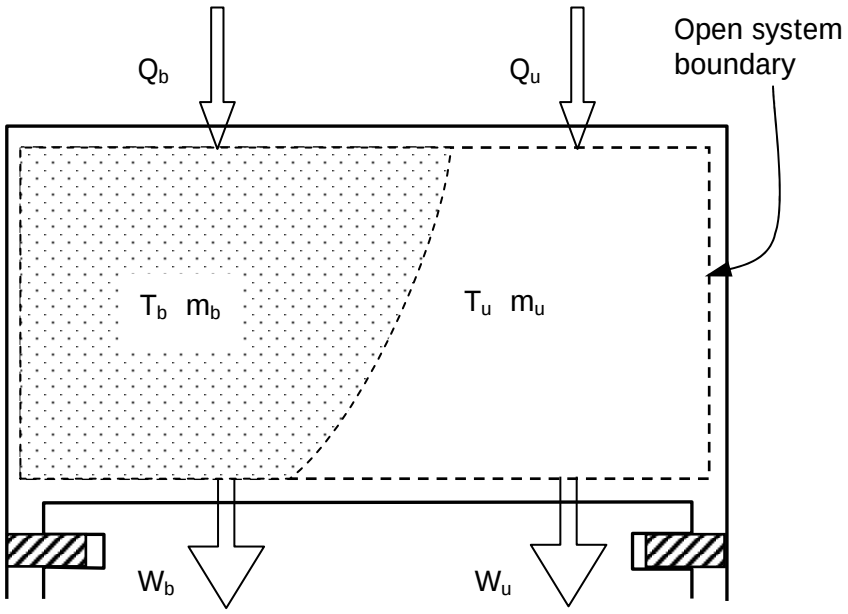

Figure D.3: Open system boundary for Two-Zone combustion chamber.

Internal energy of the system:

$$U = m_u u_u + m_b u_b \tag{D.16}$$

Differentiating D.16 yields

$$\frac{dU}{d\theta} = m_u \frac{du_u}{d\theta} + u_u \frac{dm_u}{d\theta} + m_b \frac{du_b}{d\theta} + u_b \frac{dm_b}{d\theta} \tag{D.17}$$

Mass conservation:

$$m = m_u + m_b \qquad \Rightarrow \qquad \frac{dm_u}{d\theta} = -\frac{dm_b}{d\theta} \tag{D.18}$$

Applying D.18 to D.17 and combine it with D.15 (Note: $u_u = c_{vu}\, dT$)

$$(u_b - u_u)\frac{dm_b}{d\theta} + m_u c_{v_u} \frac{dT_u}{d\theta} + m_b c_{v_b} \frac{dT_b}{d\theta} + P\frac{dV}{d\theta} - \frac{dQ}{d\theta} = 0 \tag{D.19}$$

Volume conservation

$$V = V_u + V_b \qquad \frac{dV}{d\theta} = \frac{dV_u}{d\theta} + \frac{dV_b}{d\theta} \tag{D.20}$$

From $PV=mRT$ using the product rule

$$P\frac{dV}{d\theta} + V\frac{dP}{d\theta} = mR\frac{dT}{d\theta} + RT\frac{dm}{d\theta} \tag{D.21}$$

$$\frac{1}{V}\frac{dV}{d\theta} = \frac{1}{T}\frac{dT}{d\theta} + \frac{1}{m}\frac{dm}{d\theta} - \frac{1}{P}\frac{dP}{d\theta} \tag{D.22}$$

Differential equation of state:

$$\frac{dV_u}{d\theta} = V_u\left[\frac{1}{m_u}\frac{dm_u}{d\theta} + \frac{1}{T_u}\frac{dT_u}{d\theta} - \frac{1}{P}\frac{dP}{d\theta}\right] \tag{D.23}$$

$$\frac{dV_b}{d\theta} = V_b\left[\frac{1}{m_b}\frac{dm_b}{d\theta} + \frac{1}{T_b}\frac{dT_b}{d\theta} - \frac{1}{P}\frac{dP}{d\theta}\right] \tag{D.24}$$

In D.23 and D.24, replace V/T with mR/P (since $PV=mRT$) and substitute D.23 and D.24 into D.20 while applying D.18

$$\frac{dV}{d\theta} = \left[\frac{V_b}{m_b} - \frac{V_u}{m_u}\right]\frac{dm_b}{d\theta} + \frac{R_u m_u}{P}\frac{dT_u}{d\theta} + \frac{R_b m_b}{P}\frac{dT_b}{d\theta} - \frac{V}{P}\frac{dP}{d\theta} \tag{D.25}$$

Applying the first law to the unburned zone

$$\frac{du_u}{d\theta} = \frac{1}{m_u}\frac{dQ_u}{d\theta} - Pv_u\left[\frac{1}{T_u}\frac{dT_u}{d\theta} - \frac{1}{P}\frac{dP}{d\theta}\right] \tag{D.26}$$

Expanding the bracket of 26 and applying $c_p = R + c_v$

$$m_u c_{p_u}\frac{dT_u}{d\theta} = V_u\frac{dP}{d\theta} + \frac{dQ_u}{d\theta} \tag{D.27}$$

From D.19, D.25, and D.27

$$\frac{dT_u}{d\theta} = \frac{V_u}{m_u c_{p_u}}\frac{dP}{d\theta} + \frac{1}{m_u c_{p_u}}\frac{dQ_u}{d\theta} \tag{D.28}$$

$$\frac{dT_b}{d\theta} = \frac{P}{m_b R_b}\left[\frac{dV}{d\theta} - \frac{\left(R_b T_b - R_u T_u\right)}{P}\frac{dm_b}{d\theta} - \frac{R_u V_u}{P c_{p_u}}\frac{dP}{d\theta} - \frac{R_u}{P c_{p_u}}\frac{dQ_u}{d\theta} + \frac{V}{P}\frac{dP}{d\theta}\right] \tag{D.29}$$

$$\begin{aligned}\frac{dP}{d\theta} = \frac{-1}{\left[\frac{c_{v_u}}{c_{p_u}}V_u - \frac{c_{v_b}R_u}{R_b c_{p_u}}V_u + \frac{c_{v_b}}{R_b}V\right]}\Bigg\langle &\left[1+\frac{c_{v_b}}{R_b}\right]P\frac{dV}{d\theta} - \frac{dQ}{d\theta} \\ &+\left[\left(u_b - u_u\right) - c_{v_b}\left(T_b - \frac{R_u}{R_b}T_u\right)\right]\frac{dm_b}{d\theta} \\ &+\left[\frac{c_{v_u}}{c_{p_u}} - \frac{c_{v_b}}{R_b}\frac{R_u}{c_{p_u}}\right]\frac{dQ_u}{d\theta}\Bigg\rangle\end{aligned} \tag{D.30}$$

where: $R_{gas} = \frac{n}{m}R_{universal}$ $\quad c_v = c_p - R$ $\quad u = h - RT$

D.3 Heat Transfer

The following equations are used to account for convection and radiation (5% of total heat transfer) assuming a one-dimensional heat flow through the cylinder wall, piston and cylinder head [83, 96].

$$\frac{dQ}{d\theta} = \frac{dQ_u}{d\theta} + \frac{dQ_b}{d\theta} \tag{D.31}$$

$$\frac{dQ_u}{d\theta} = \frac{30A_u}{N}\left[h_{c_u}\left(T_{g_u} - T_w\right) + \beta\sigma\left(T_{g_u}^4 - T_w^4\right)\right] \tag{D.32}$$

$$\frac{dQ_b}{d\theta} = \frac{30A_b}{N}\left[h_{c_b}\left(T_{g_b} - T_w\right) + \beta\sigma\left(T_{g_b}^4 - T_w^4\right)\right] \tag{D.33}$$

where: A = surface area, N = r/min

h_c = convective heat transfer coefficient

β = 0.6, σ = Stefan-Boltzmann constant = 5.67*10^{-8} (W/m^2*K^4)

Note: Equation D.31 results in joules/radians. It must be converted to joules/degrees, just like Equation D.4 (to get joules/degrees multiply by $PI/180$).

To be more precise, the following has to be considered for each zone. The total heat transfer in each zone is the sum of the heat transfer between gas and cylinder, gas and cylinder head, gas and piston, and lastly the heat transfer between the two zones. Therefore, the heat transfer for the unburned and burned zones become:

$$\frac{dQ_u}{d\theta} = \frac{dQ_{cylinder}}{d\theta} + \frac{dQ_{cylinder\_head}}{d\theta} + \frac{dQ_{piston}}{d\theta} + \frac{dQ_{zone}}{d\theta} \tag{D.34}$$

$$\frac{dQ_b}{d\theta} = \frac{dQ_{cylinder}}{d\theta} + \frac{dQ_{cylinder\_head}}{d\theta} + \frac{dQ_{piston}}{d\theta} + \frac{dQ_{zone}}{d\theta} \tag{D.35}$$

Woschni Heat Transfer coefficient (must apply to both burned and unburned zones)

$$h_c = 3.26 D^{-0.2} P^{0.8} T^{-0.55} \omega^{0.8} \tag{D.36}$$

where: D = diameter of piston, P = cylinder pressure in (kPa)

T = zone temperature (K)

Average gas velocity (ms^{-1}) (This is same for both burned and unburned zones)

$$\omega = C_1 S_P + C_2 \frac{V_d T_r}{P_r V_r} \left(P - P_m \right) \tag{D.37}$$

where: V_d = displaced volume in (m^3), V_r (m^3), T_r (K), P_r (Pa) represents the known state of the working gas related to inlet closure or ignition, S_p = average linear engine speed, P_m = corresponding motoring pressure in the absence of combustion, C_1 = 6.18 for gas

exchange, C_1 = 2.28 for compression and expansion, C_2 = 0 for gas exchange and compression, C_2 = 3.24*10^{-3}(m/sK) for combustion and expansion [96].

D.4 Flame Geometry and Wall Area Calculations

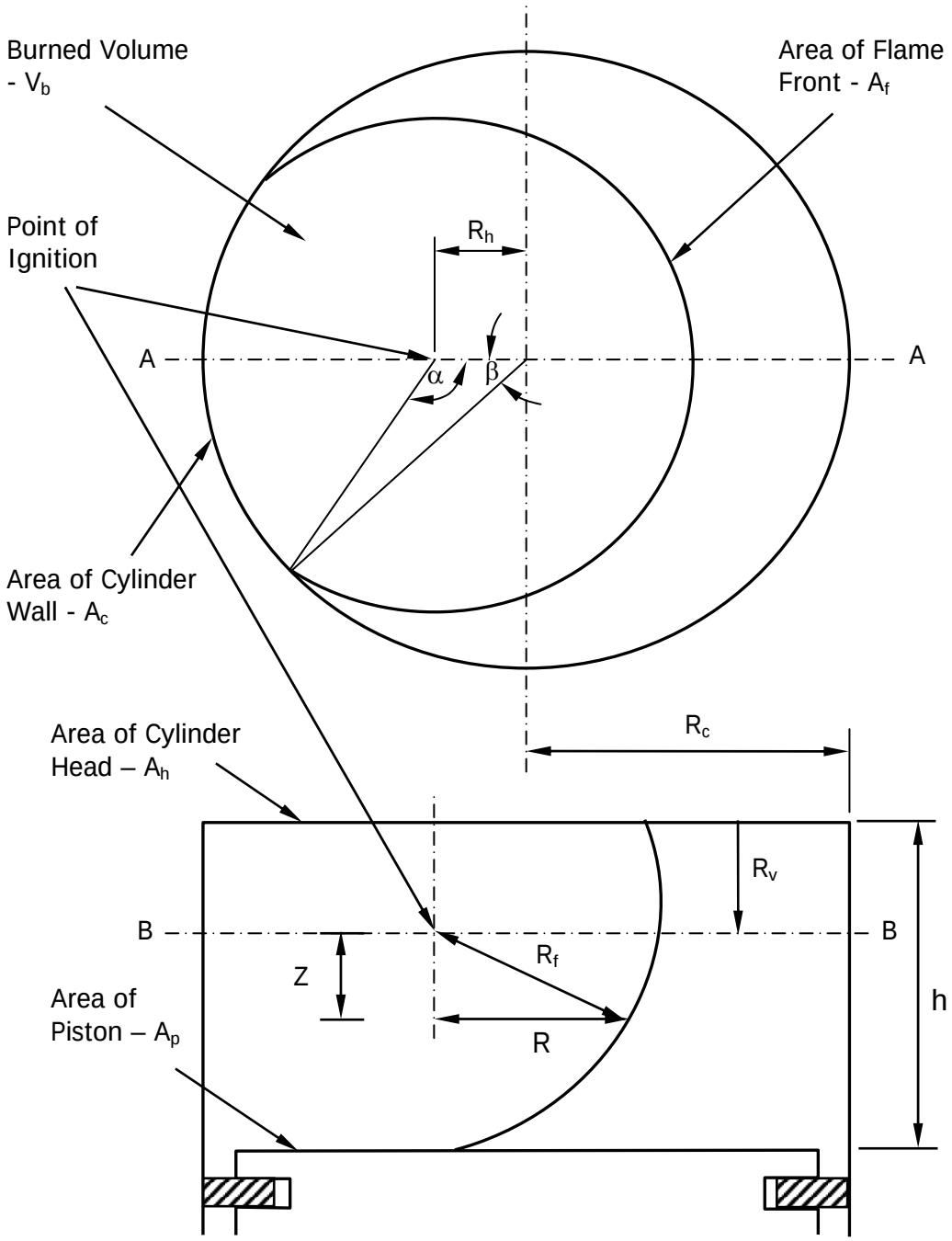

Figure D.4: Spherical flame geometry in a disc type combustion chamber.

$$\cos\alpha = \frac{R^2 + R_h^2 - R_c^2}{2RR_h} \quad \text{(D.38)} \qquad \cos\beta = \frac{R_c^2 + R_h^2 - R^2}{2R_cR_h} \quad \text{(D.38)}$$

$$R = \sqrt{R_f^2 - z^2} \quad \text{(D.39)}$$

In order to reduce computation time, the symmetry about A-A and B-B must be realised (Figure D.4).

Burned Gas Volume:

$$V_b = \int_0^h \left[\alpha R^2 + \beta R_c^2 - R_c R_h \sin\beta\right] dz \quad \text{(D.40)}$$

Flame Front Area:

$$A_f = 2R\int_0^h \alpha dz \quad \text{(D.41)}$$

Burned Wall Area:

$$Wall\_Area = A_c + A_h + A_p \quad \text{(D.42)}$$

$$A_c = 2R_c\int_0^h \beta dz \quad \text{(D.43)} \qquad A_h = \alpha R^2 + \beta R_c^2 - R_c R_h \sin\beta \quad \text{(D.44)}$$

$$A_p = \alpha\left(R_f^2 - (h - R_v)^2\right) + \beta R_c^2 - R_c R_h \sin\beta \quad \text{(D.45)}$$

These equations were implemented into VBA and validated against Poulos et al. [177]. The results for the above equations (Figures D.5, D.6 and D.7) are more accurate for a disc combustion chamber (same as the CFR engine) than Poulos results, however, his 'flat triangular' approximation can be used for a hemi, open, and bowl in piston type combustion chambers.

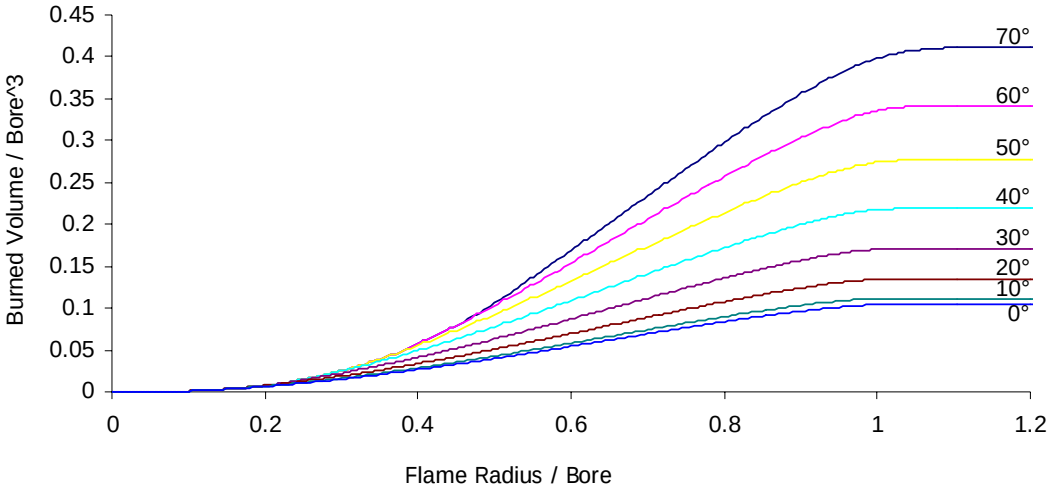

Figure D.5: Burned volume vs. flame radius at different crank angle (BTDC) for the side ignition CFR SI engine, disc chamber, bore=80mm, stroke=79.58mm, connecting rod length=140mm, CR=8.5. (results from E-CoBRA)

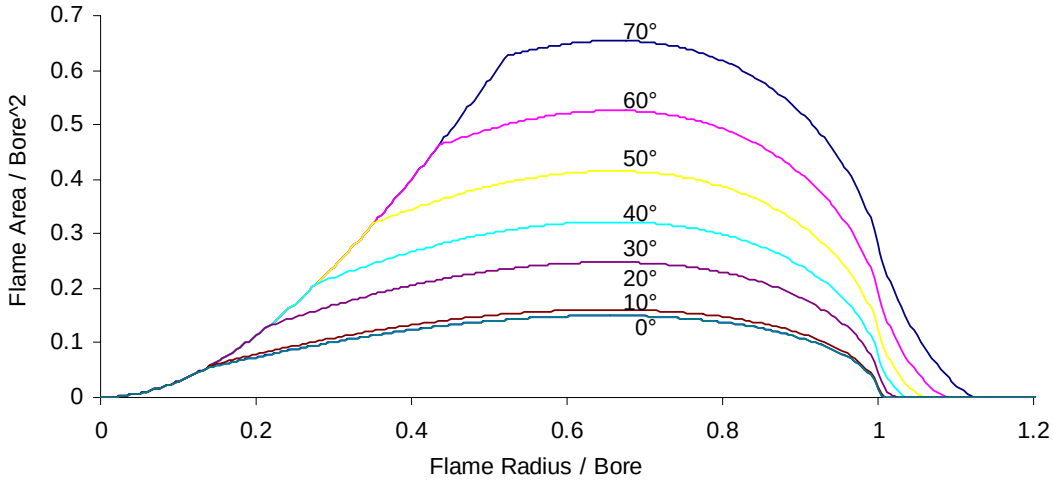

Figure D.6: Flame area vs. flame radius at different crank angle (BTDC) for the side ignition CFR SI engine, disc chamber, bore=80mm, stroke=79.58mm, connecting rod length=140mm, CR=8.5. (results from E-CoBRA)

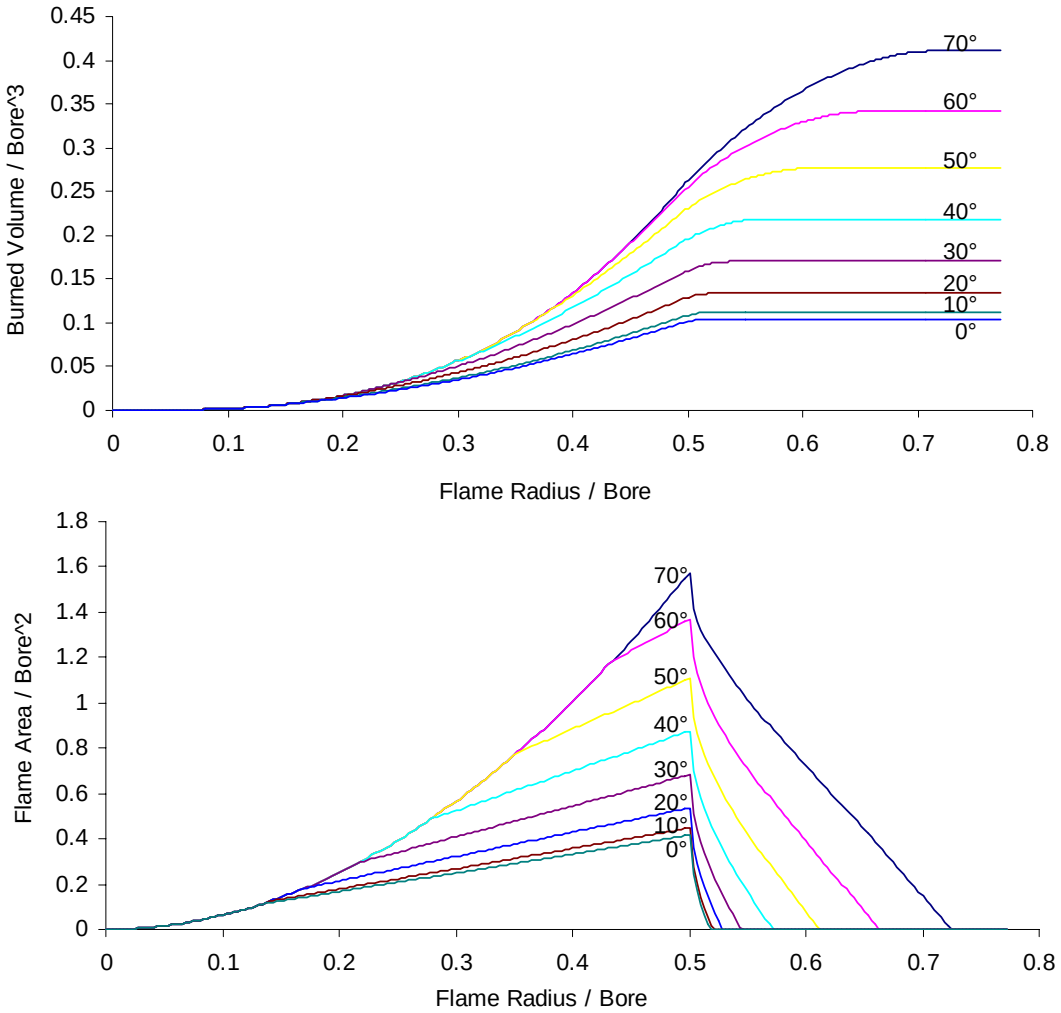

Figure D.7: (top) Burned volume vs. flame radius, (bottom) Flame area vs. flame radius, at different crank angle (BTDC) for the central ignition CFR SI engine, disc chamber, bore=80mm, stroke=79.58mm, connecting rod length=140mm, CR=8.5. (results from E-CoBRA)

D.5 Numerical Integration

Five different methods were evaluated for solving the differential Equations of 28, 29, and 30:

- Improved Euler method (2nd order, predictor-corrector)
- Runge-Kutta (4th and 5th order)
- Adams-Moulton (4th and 5th order, predictor-corrector)

The Adams-Bashford predictor solves the equations explicitly with high accuracy and speed. Euler, Runge-Kutta, and Adams-Moulton methods require a derivative at the point of interest and work well with functions where the values of all variables are known explicitly. Equations 28, 29, and 30 contain variables that depend on each other. For example $dp/d\theta$ is a function of c (specific heat). However, c is a function of T, therefore T has to be determined first. The only logical and computationally efficient way is to use a method that predicts c or $dp/d\theta$ based on previously calculated values. The Adams-Bashford method fits this description and can be combined with an integrated cubic Newton backward polynomial to form the predictor formula, hence becoming the Adams-Moulton method. The Adams-Moulton method only requires an extra line of calculation, however it can increase accuracy by up to 10 times over the Adams-Bashford method. Also, being an implicit method means that it is numerically stable [122].

The Adams-Bashford explicit method (predictor)

$$y_{n+1} = y_n + \frac{h}{720}\left[1901 f_n - 2774 f_{n-1} + 2616 f_{n-2} - 1274 f_{n-3} + 251 f_{n-4}\right] \quad \text{(D.46)}$$

Adams-Moulton implicit method (corrector)

$$y_{n+1} = y_n + \frac{h}{720}\left[251 f_{n+1} + 646 f_n - 264 f_{n-1} + 106 f_{n-2} - 19 f_{n-3}\right] \quad \text{(D.47)}$$

where: h = step size (mostly dx), f = derivative of function

f_{n+1} = derivative at y_{n+1} from Adams-Bashford

n = point of consideration, $n+1$ = approx. of next point

Truncation Error

$$Error = \frac{27}{502}\frac{C-P}{h} \tag{D.48}$$

where: C = value of corrector, P = value of predictor

h = step size

D.6 Chemical Equilibrium Composition Modelling

The following section describes a method of rapid computation of chemical equilibrium composition applicable to hydrogen and hydrocarbon combustion developed by Erickson and Prabhu at NASA [61]. The author re-derived, modified and implemented the method into VBA (sample results of the working program are shown on Figures D.7, D.8, and D.9). The re-derivation was especially important since Equations D.64 and D.68 were published with a typing error, producing inaccurate results. The reason this method was used is because it is up to 80 times faster then the often-used free-energy minimization method. The chemical system is composed of four elements (C, H, O, N) and ten reacting species are assigned indices i = 1,2...10 in the following order: H_2O, CO_2, CO, O_2, H_2, N_2, H, O, OH, and NO. Starting with an appropriate set of equilibrium equations and elemental equations, the ten equations are reduced to two equations and then to a single equation containing one unknown variable.

For a reacting gas mixture containing ten species composed of four chemical elements there are six independent chemical reactions that can be written. The following set of independent reactions are chosen:

$CO + H_2O$	$\rightarrow$	$CO_2 + H_2$	[1]
$2CO_2$	$\rightarrow$	$2CO + O_2$	[2]
H_2+O_2	$\rightarrow$	$2OH$	[3]
H_2	$\rightarrow$	$2H$	[4]
O_2	$\rightarrow$	$2O$	[5]
O_2+N_2	$\rightarrow$	$2NO$	[6]

The following describes the solution procedure of the product species for a given input:

1.) Input parameters:

- Temperature (T, kelvin)
- Density (ρ, kg/m^3)
- Equivalence Ratio (ϕ)
- H/C ratio
- mol CO/ mol CO_2 ratio (ξ = initial guess)
- Nitrogen/Oxygen ratio (air = 79/21)

2.) Compute constants:

Chemical equilibrium constants Kp were curve fitted in DataFit using the famous vapor pressure model *"exp(a+b/x+c*log(x))"*

$$CO + H_2O \rightarrow CO_2 + H_2 \quad \text{(D.49)}$$

*T < 800 → K1 = Exp(-11.5723745 + 5255.72032 / T + 0.96398354 * Log(T))*

*T <= 2600 → K1 = Exp(-11.927269 + 5193.65214 / T + 1.02850772 * Log(T))*

*T <= 6000 → K1 = Exp(-9.90914812 + 4728.77893 / T + 0.79405057 * Log(T))*

$$2CO_2 \rightarrow 2CO + O_2 \quad \text{(D.50)}$$

*T < 800 → K2= Exp(15.4600070 - 67772.0986 / T + 0.77535057 * Log(T))*

*T <= 6000 → K2= Exp(30.2986377 - 69188.1029 / T - 1.18303008 * Log(T))*

K2= K2 P_o / (Density * R_{uni} * T)*

$$H_2 + O_2 \rightarrow 2OH \quad \text{(D.51)}$$

*T < 800 → K3 = Exp(4.81617915 - 9554.57691 / T - 0.14234455 * Log(T))*

*T <= 2700 → K3= Exp(6.42554150 - 9664.76907 / T - 0.36267753 * Log(T))*

*T <= 6000 → K3 = Exp(8.40910545 - 10346.7118 / T - 0.58193587 * Log(T))*

$$H_2 \rightarrow 2H \quad \text{(D.52)}$$

*T < 800 → K4 = Exp(1.96193395 - 51996.3266 / T + 1.48000464 * Log(T))*

*T <= 2500 → K4= Exp(4.62582493 - 52329.0289 / T + 1.14258246 * Log(T))*

*T <= 6000 → K4 = Exp(11.8839457 - 54344.0182 / T + 0.31650772 * Log(T))*

*K4 = K4 * P_o / (Density * R_{uni} * T)*

$O_2 \rightarrow 2O$ (D.53)

*T < 800 → K5= Exp(4.80924042 - 59545.6966 / T + 1.39032710 * Log(T))*

*T <= 3000 → K5= Exp(10.9084500 - 60205.2613 / T + 0.59937809 * Log(T))*

*T <= 6000 → K5 = Exp(15.2261961 - 61463.4378 / T + 0.11118509 * Log(T))*

*K5= K5 * P_o / (Density * R_{uni} * T)*

$O_2+N_2 \rightarrow 2NO$ (D.54)

*T < 800 → K6 = Exp(2.73981886 - 21709.6133 / T + 0.03721003 * Log(T))*

*T <= 3000 → K6 = Exp(3.13453339 - 21774.4906 / T - 0.00959753 * Log(T))*

*T <= 6000 → K6 = Exp(6.89000288 - 22968.6081 / T - 0.42951512 * Log(T))*

*Ka = (K4 / (K2 * K3)) ^ 0.5* (D.55) , *Kb = (K2 * K5) ^ 0. 5* (D.56)

*Kc = K1 * K2 * K3* (D.57), *Kd = K2 * K6* (D.58)

Table D.1 Constant coefficients a_{mn}.

N	a_{0n}	a_{1n}	a_{2n}
0	_____	*-Kc*	_____
1	σ_H^2	*-2(2σ_H+KaKc)*	*4*
2	_____	*-(4$\sigma_H K_1$+Ka^{2}Kc)*	*8K_1*
3	_____	_____	*4K_1^2*

where: σ_i = mole number of species i, (mol of species i / kg mixture)

σ_H, σ_O, σ_N, σ_C = mole numbers of elements

Table D.2 Constant coefficients f_{mn} and g_{0n}.

n	f_{0n}	f_{1n}	g_{0n}
0	*2K_2*	_____	*1*
1	*2K_2(Ka+1)+Kb*	_____	*Ka+1*
2	*2σ_c+ σ_H - σ_o + (Ka+1)Kb+2K_2Ka*	*-1*	*Ka*
3	*σ_c+ σ_H - σ_o + (2σ_c - σ_o + Kb)Ka*	*Ka – 2K_1 - 1*	_____
4	*(σ_c+ σ_o)Ka*	*Ka – 2K_1*	_____

3.) Iteration loop starts here

$$a_m = \sum_{n=0}^{3} a_{mn}\xi^n \qquad m = 0, 1, 2 \tag{D.59}$$

$$f_m = \sum_{n=0}^{4} f_{mn}\xi^n \qquad m = 0, 1 \tag{D.60}$$

$$g_0 = \sum_{n=0}^{2} g_{0n}\xi^n \tag{D.61}$$

$$\sigma_{10} = K_d\left(\left[1+8\sigma_N\xi^2 / K_d\right]^{1/2} - 1\right)/ 4\xi^2 \tag{D.62}$$

$$b_1 = f_1 \tag{D.63}$$

$b_0 = f_0 + g_0\,\sigma_{10}\,\xi^2$ *Corrected (original was: $b_0 = f_0 - g_0\,\sigma_{10}\,\xi^2$)* (D.64)

$$F(\xi) = a_2\,b_0^2 - a_1\,b_1\,b_0 + a_0\,b_1^2 = 0 \tag{D.65}$$

$$F'(\xi) = b_0^2\,a'_2 - b_1 b_0\,a_1' + b_1^2\,a_0' + (2a_0\,b_1 - a_1\,b_0)\,b_1' + (2a_2\,b_0 - a_1\,b_1)\,b_0' \tag{D.66}$$

$$a_m^{'} = \sum_{n=1}^{3} n a_{mn}\xi^{n-1} \qquad m = 0, 1, 2 \tag{D.67}$$

$$b_0^{'} = \sum_{n=1}^{4} n f_{0n}\xi^{n-1} + 2\sigma_N\,g_0\xi\,/(1+8\sigma_N\xi^2 / K_d)^{1/2} + \sigma_{10}\xi^2\sum_{n=1}^{2} n g_{0n}\xi^{n-1} \tag{D.68}$$

D.68 is the corrected equation, the original equation was:

$$b_0^{'} = \sum_{n=1}^{4} n f_{0n}\xi^{n-1} - 2\sigma_N\,g_0\xi\,/(1+8\sigma_N\xi^2 / K_d)^{1/2} - \sigma_{10}\xi^2\sum_{n=1}^{2} n g_{0n}\xi^{n-1}$$

$$b_1^{'} = f_1^{'} = \sum_{n=2}^{4} n f_{1n}\xi^{n-1} \tag{D.69}$$

$$\xi_{l+1} = \xi_l - F(\xi_l) / F'(\xi_l) \tag{D.70}$$

$$|(y_i)_{l+1} - (y_i)_l| \le ERROR \tag{D.71}$$

$$1 - ((\xi_l - F(\xi_l) / F'(\xi_l)) / \xi_l) \le ERROR \tag{D.72}$$

Iteration loop finishes here

4.) Compute final composition

$\sigma_1 = -b_0 / b_1$ (D.73) ; $\sigma_2 = \sigma_C / (\xi + 1)$ (D.74); $\sigma_3 = \xi\sigma_C / (\xi + 1)$ (D.75)

$\sigma_4 = K2 / \xi^2$ (D.76); $\sigma_5 = K1\ \sigma_1\ \xi$ (D.77); $\sigma_6 = (\sigma_N - \sigma_{10})/2$ (D.78)

$\sigma_7 = (K4/K2K3)^{1/2} / \xi$ (D.79); $\sigma_8 = (K2K5)^{1/2} / \xi$ (D.80)

$\sigma_9 = (\sigma_H - 2(1 + K1\xi)\ \sigma_1\ ) / (Ka\xi + 1)$ (D.81)

5.) For all species the thermodynamic properties such as specific heat and enthalpy are in the form of the "Shomate Equation" [167]. The accuracy of this format is equivalent to the more popular NASA polynomials.

It is important to note the expression of specific heat when the composition changes through a series of equilibrium states.

$$c_p = \sum_i x_i c_p + h_i \frac{\partial x}{\partial T}$$ (D.82) where: x_i = mole fraction of specie

h_i = enthalpy of specie

The second term $h_i \frac{\partial x}{\partial T}$ takes into account the dissociation of molecules at higher temperatures. It approaches zero if the composition is frozen and the components in the mixture are ideal gases (then also the mixture is an ideal gas).

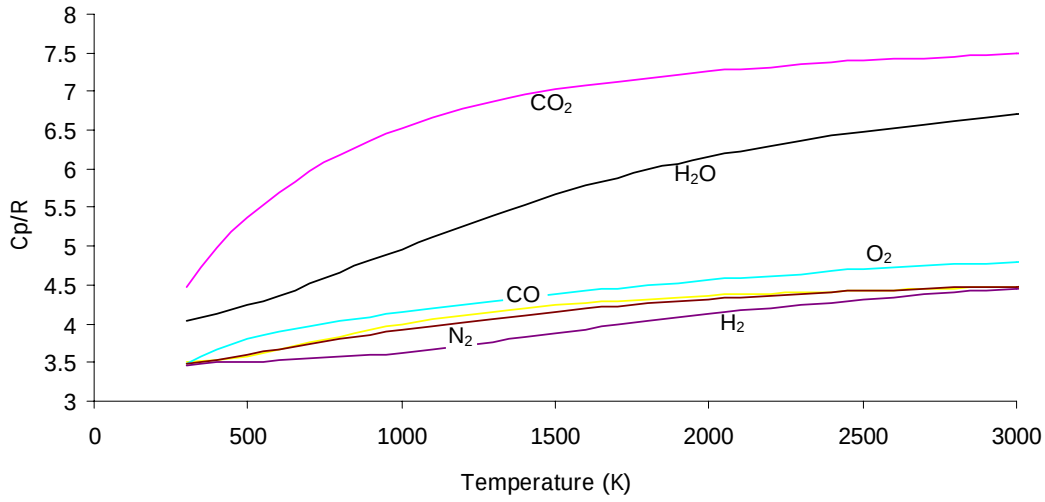

Figure D.7: Specific heat at constant pressure c_p/R, as a function of temperature for species CO2, H2O, O2, N2, H2, and CO, (from http://webbook.nist.gov)

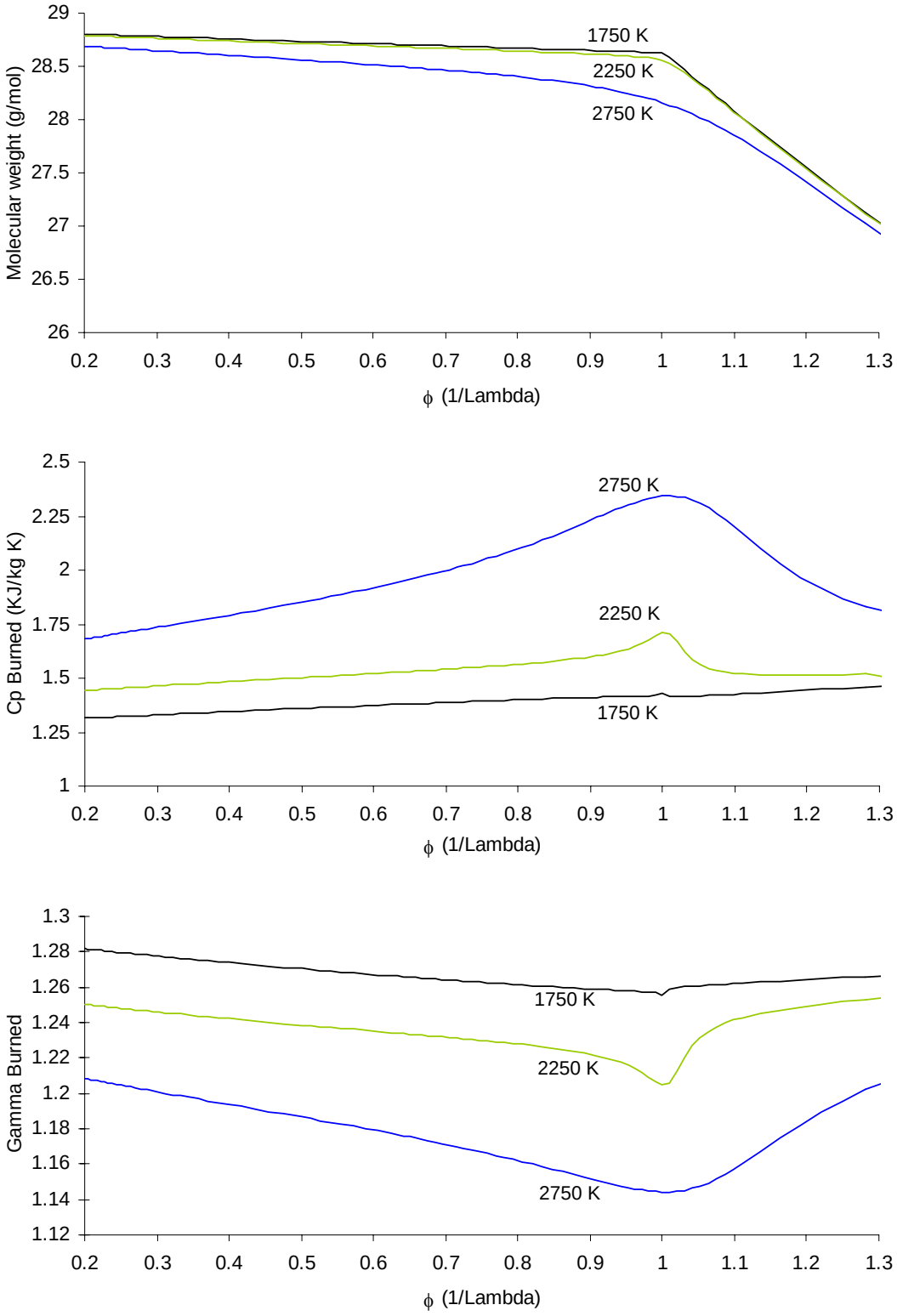

Figure D.8: Fuel – Isooctane, equilibrium burned gases as function of equivalence ratio at T = 1750, 2250, and 2750 K, at 30 atm, (top) molecular weight, (middle) specific heat, (bottom) ratio of specific heats. (results from E-CoBRA)

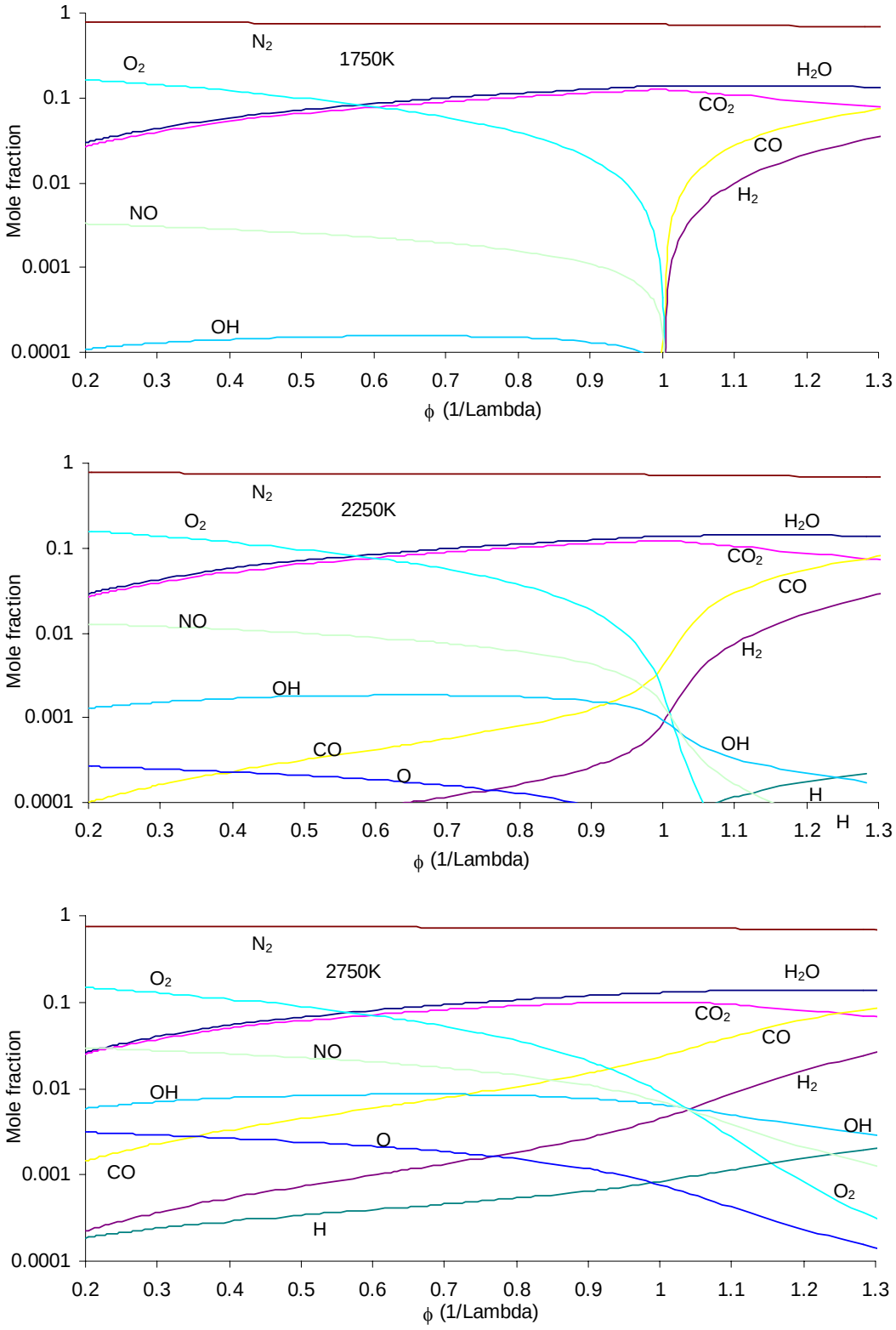

Figure D.9: Fuel – Mole fraction of equilibrium combustion products of isooctane-air mixture as function of equivalence ratio at T = (top) 1750, (middle) 2250, and (bottom) 2750 K. (results from E-CoBRA)

Appendix E
Exhaust Gas Analysis

E.1 ADS 9000 Exhaust Gas Analyser

Throughout the experiments, the ADS 9000 exhaust gas emission analyser was used to measure HC, CO, CO_2, O_2, and NO. The method of measurements for HC, CO, and CO_2 is performed by NDIR (Non Dispersive Infrared) and for O_2 and NO by an electrochemical cell. The ADS 9000 calculates the AFR based on the algorithm described by Spindt [195]. The range and accuracy of the ADS 9000 is shown in Table E.1 and E.2.

Table E.1: ADS 9000 measurement range and resolution.

Measurement Ranges		
Channel	Range	Resolution
HC	0 - 10,000 ppm	1 ppm
CO	0 - 10%	0.01%
CO_2	0 - 20%	0.01%
O_2	0 - 23%	0.1%
NO	0 - 4000 ppm	1 ppm
Temp	0 - 150°C	1°C
RPM	0 - 10,000 r/min	10 r/min
AFR	5 - 20	0.01
Lambda (λ)	0.5 - 2.0	0.001
CO Correction	0 - 10%	0.01%

Table E.2: ADS 9000 resolution for different ranges.

Accuracy		
Channel	Range	Resolution
HC	0 - 240 ppm	±11 ppm
CO	0.00 - 1.00%	±0.05% Absolute
	1.00 - 2.00%	±0.06% Absolute
CO_2	0.00 - 16.00%	±0.40% Absolute
O_2	0.00 - 2.00%	±0.10% Absolute
	2.01 - 23.00%	±5.00% Relative
NO	0 - 1000 ppm	±32 ppm
	1001 - 2000 ppm	±60 ppm
	2001 - 4000 ppm	±120 ppm

The following must be noted in order to avoid errors in measurements:

- The repeatability of HC, CO, and CO_2 is one-half of the accuracy limits specified in Table E.2.
- Environmental (operating) temperature is between 2 to 40°C.
- Environmental (operating) 0 to 85% relative humidity (non-condensing).
- Environmental (operating) altitude is between -300 to 2100m.
- Warm up time is less than 6 minutes, which is followed by an auto electronic calibration.
- The gas samples must be dry because water can damage the NDIR systems. This was achieved by a water separating system, which was part of the ADS 9000 exhaust gas emission analyser.

E.2 Emission Correction

In collaboration with Zakis [232] and Dober [55], the author has developed a number of pre-sampling and post-sampling procedures to ensure that the absolute magnitude of concentration of emissions is correct. The following is a summary of these procedures.

E.2.1 Eliminating Air Leakage

As air leaks into the exhaust sample gas, it will dilute the mixture resulting in an inaccurate AFR and emissions concentration reading. To avoid this, an airtight

system was developed between the exhaust system and the emission analyser. This was further improved by maintaining a positive gauge pressure in the exhaust system at all times and by using the shortest possible tube between the exhaust manifold and emission analyser with an internal diameter >8mm.

E.2.2 Correcting for Hydrocarbon Type

All HC values presented in this thesis are quoted in hexane (C_6). The ADS 9000 counts carbon atoms and every 6^{th} carbon atom is displayed as 1 unburned HC molecule. It displays HC concentrations as hexane (C_6) independent of the type of HC fuel used. Therefore, if one uses propane (C_3H_8) and the analyser displays 1000ppm HC, then this corresponds to 1000 ppm HC in hexane (C_6), however, it is 2000 ppm HC in propane (C_3). It does not matter what the HC concentration is being quoted as long as it is identified as C_6 , C_3, or some other type of HC. Otherwise specific emission values can not be calculated.

E.2.3 ADS 9000 Sensitivity to Different Hydrocarbons

The ADS 9000 can detect propane (C_3H_8) HC with 100% consistency, however it fails to detect other types of HC with the same success rate. Therefore, Dober [55] and Zakis [232] have determined a sensitivity factor for different fuel types, which needs to be multiplied to the values displayed by the ADS 9000 to get the correct HC concentrations. They have done this by performing a back-to-back concentration study between the ADS 9000 and the F.F.I.D. (fast flame ionization detector), which has a near 100% detection rate irrespective of the HC type. The result of this study is shown in Table E.3.

Table E.3: ASD9000 -NDIR sensitivity to various fuels [55, 232].

Hydrocarbon Type	Static sensitivity Factor	Dynamic sensitivity Factor
Natural Gas	2.97	3.03
Butane	0.89	0.89
Propane	1	-
Gasoline	2.29	-

E.3 AFR Calculation

The ADS 9000 could not accurately calculate the AFR because it is unable to compensate for the sensitivity to different HCs and cannot recognize hydrogen as a fuel. The following expressions were developed to compensate for this and were implemented into VBA.

$$z[FUEL] + m_a[AIR] \rightarrow aCO_2 + bH_2O + cN_2 + dO_2 + eH_yC_k + fCO + gNO_x \quad \text{(E.1)}$$

where:

[balance the C's] : $z\ [\Sigma\ C's] = a + ek + f$ (E.2)

[balance the H's] : $z[\Sigma\ H's] = 2b + ey$ (E.3)

[balance the O's] : $z[\ \Sigma\ O's\ ] + 2m_a = 2a + b + 2d + f + gx$ (E.4)

rearranging we obtain:

$$z = a + ek + \frac{f}{\left[\sum C's\right]} \quad \text{(E.5)}$$

$$b = z\left[\sum H's\right] - \frac{ey}{2} \quad \text{(E.6)}$$

$$m_a = a + \frac{b}{2} + d + \frac{f}{2} + \frac{gx}{2} - \frac{z\left[\sum O's\right]}{2} \quad \text{(E.7)}$$

$$\frac{A}{F}_{mass} = \frac{m_a\left(1 + \frac{79}{21}\right)M_{AIR}}{zM_{FUEL}} \quad \text{(E.8)}$$

where: M_{FUEL} = molecular mass of the total composition

M_{AIR} = molecular mass of air = 28.96 kJ/kmol

For pure H_2, Equation E.8 simplifies to the following already shown in Equation C.3

$$AFR_{H_2} = \frac{34.07\left[\%O_2 - 1\right]}{\frac{100}{21}\%O_2 - 1} \quad \text{(E.9)}$$

All of the above equations were implemented into VBA with the following interface displayed in Figure E.1.

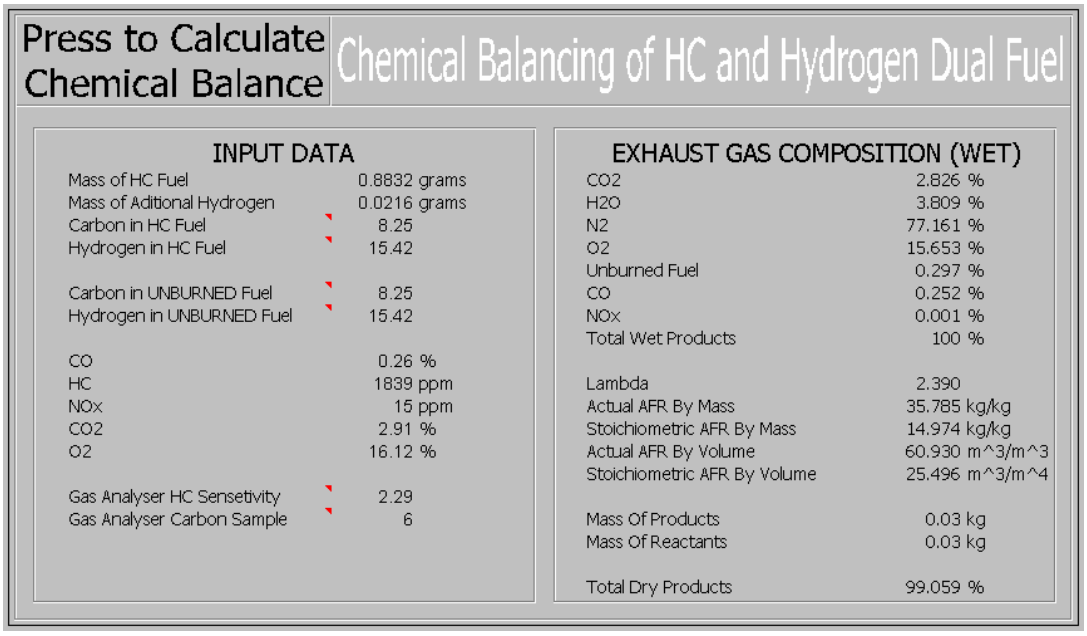

Figure E.1 AFR calculator interface in Excel (programmed in VBA).

E.4 Indicated Emissions Calculation

$$Indicated\_Specific\_Emission = ISFC(1+AFR)\left(\frac{n_s}{n_p}\right)\left(\frac{M_s}{M_p}\right) \qquad \text{(E.10)}$$

where: n_p = moles of total products

n_s = moles of sample product

M_p = molecular mass of products

M_s = molecular mass of sample product (e.g. NO, CO, HC etc.)

AFR= air-fuel ratio

ISFC = indicated specific fuel consumption (g/kWh)

Note: n_s/n_p is usually given in ppm

Appendix F
Operating Variables and Concept Behind Analysis

F.1 MBT

F.1.1 Definition

Spark timing at a given air-fuel ratio has a significant effect on torque, emissions and efficiency as described in Section 7.3.1. In general the optimum spark timing is referred to as MBT. There are at least two popular definitions of MBT used throughout the literature. Heywood [96] defines it as the *maximum brake torque* as the abbreviation suggest. Stone [197] defines MBT as the *minimum advance for best torque*. Maximum brake torque can occur over a few degrees, so there is some ambiguity on exactly where MBT occurs if Heywood's definition is used. Historically, Heywood's definition has been very popular, however the overwhelming interest in engine emissions and thermal efficiency has forced engine controlling parameters such as MBT, to be defined more accurately and hence Stone's definition is currently preferred.

Interestingly, from both the abovementioned definitions of MBT, it is impossible to foretell whether or not the spark timing at maximum brake torque is knock limited. Furthermore, if MBT is achieved but no knock is encountered then it is

difficult to know how many CAD spark timing can be further advanced (this is known as the knock margin) before knock is encountered.

In this thesis, MBT was defined as the minimum spark advance for best torque. This means that at the extreme operating conditions (i.e.: supercharging and high CR), many of the data points are knock limited.

Observing the results in Chapters 5, 6, 7 and 8, the knock limited spark timing is not identified as it is not essential information to fulfill the principal objective of this research, which was to experimentally demonstrate the performance, emissions and thermal efficiency benefits of HAJI over its SI counterpart. It should be noted that the knowledge about MBT being knock limited or not is simply a property of the combustion system at a given operating condition similar to peak pressure, MFB, and combustion temperatures. However, the impact of knock limited MBT on efficiency and engine durability is important and therefore discussed next.

F.1.2 Knock Limited MBT Results

The author believes that it is essential to understand under what conditions a combustion system is knock limited because it indicates that the engine is operating below its highest theoretical thermal efficiency. If the engine is not knock limited, then it is equally important to understand the size of the knock margin because it provides knowledge about the likelihood of occurrence of knock. Knock margin is critical information that must be well comprehended since engine ageing, manufacturing tolerances and untested operating conditions [197] can reduce the knock margin, which eventually results in knock. Certainly, heavy engine knock must be avoided as it can damage the engine and this topic is discussed in detail in Section 2.5, whereas light knock may only be of annoyance to the vehicles occupants.

To investigate and discuss the topic of knock limited MBT in great detail is out of the scope of this thesis, however a starting point is defined here by identifying

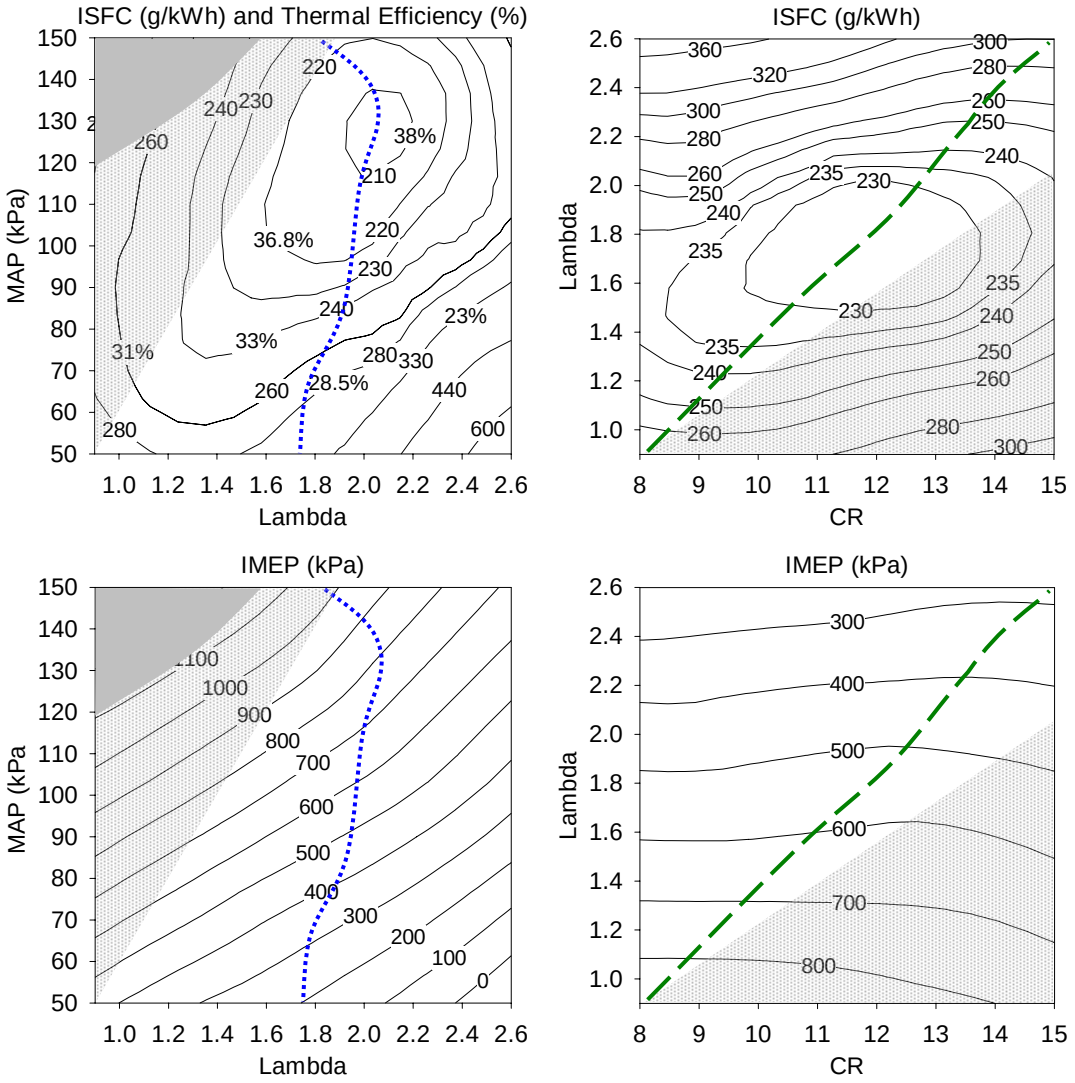

Figure F.1: (top) Indicated thermal efficiency (bottom) IMEP as a function of Lambda, CR and MAP, HAJI-G, 1800 r/min, (top/bottom left) CR=11, dotted line indicates the OPL, (top/bottom right) MAP=90, dashed line indicates HUCR, light shaded area is knock limited MBT, dark shaded area indicates where engine was not able to operate at all. The graph is the results of 35 data points.

knock limited MBT regions for the results presented in Chapter 5 and 6, accompanied by a brief discussion.

Figure F.1 shows the thermal efficiency of HAJI-G mode as a function of CR, MAP and λ. The optimum performance line (OPL - dotted line) is also shown on the MAP vs. Lambda contour plot. The dark shaded area indicates engine conditions where the engine was not able to operate at all, due to either heavy knock or misfire. Light shaded areas are an indication of where MBT was knock limited (i.e.:

zero knock margin). Along the OPL, MBT is not knock limited, which provides some level of knock margin depending on the operating condition. The actual value of the knock margin was not recorded, however it can be concluded with high confidence that the closer the operating point is to the shaded area, the smaller the knock margin becomes.

In the HAJI-H_2 mode (Figure F.2) the engine was not knock limited at any of the operating points, which is expected since the octane number of H_2 is 140 [207].

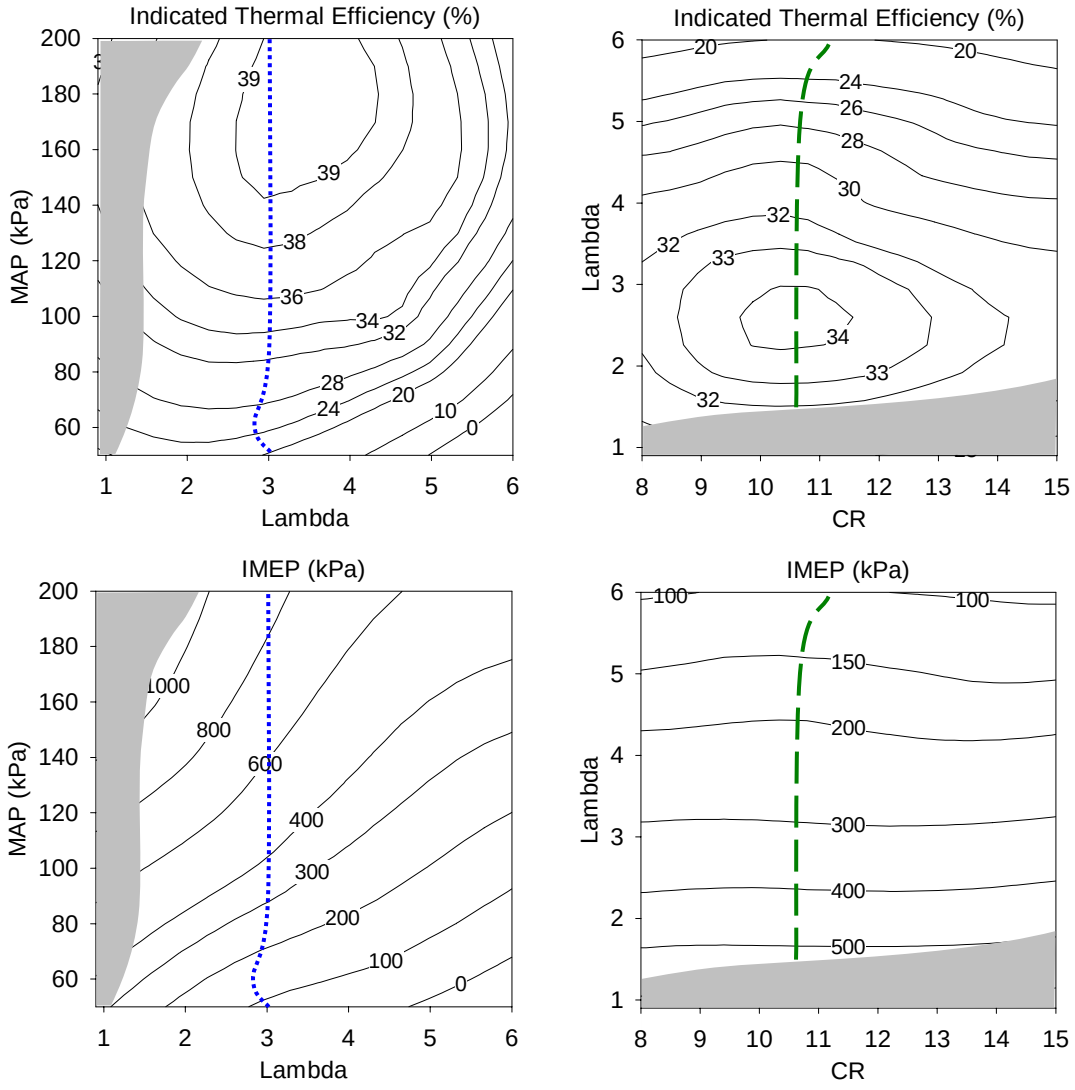

Figure F.2: (top) Indicated thermal efficiency (bottom) IMEP as a function of Lambda, CR and MAP, HAJI-H_2, 1800 r/min, (top/bottom left) CR=11, dotted line indicates is the OPL, (top/bottom right) MAP=90, dashed line indicates HUCR, dark shaded area indicates where engine was not able to operate at all due to backfire. The graph is the results of 35 data points.

Unfortunately the engine did suffer from the well known backfire problem, which was discussed briefly in Section 2.9.

Overall, it is important to realise that thermal efficiency drops in knock limited areas. Figure F.1 (top - right) shows that in HAJI-G mode at any given λ, the boundary of the knock limited area (light shaded area) almost lines up with the HUCR line. In theory, if MBT is not knock limited at a given λ, then the highest thermal efficiency should be achieved at the highest CR, which means that the boundary of the knock limited area should line up with the HUCR line. As observed in Figure F.1 (top - right), this was not achieved in the CFR engine, due to the influence of combustion chamber shape on thermal efficiency. The cylindrical combustion chamber shape of the CFR engine is not optimum for high CR operation. This is further validated by the results obtained in HAJI-H_2 mode (Figure F.2 - right), where the HUCR line runs between CR=10 and CR=11, yet it should be at CR=15 since the engine is not knock limited at any given operating point.

F.2 Octane Number Requirement (ONR)

Preventing knock limited MBT or increasing the knock margin can be achieved by reducing the octane number requirement (ONR) of the engine. In the literature, most of the results published on ONR (Table F.1) are based on experimental results [89, 157, 168, 187, 201, 205, 207, 231]. The range tested from which these results were developed is also presented in Table F.1. It is worth noting that most parameters exhibit a strong linear relationship within the range tested, however extrapolating ONR outside of this range should be performed with caution.

The effects of different parameters on ONR are extremely complex (Table F.1). In this research, it is demonstrated that a lean boosted HAJI engine is capable of producing equal or more IMEP than its SI counterpart. Consequently, one of the intriguing questions Table F.1 raises is, “How does the ONR change at a constant IMEP (i.e. mixture is becoming lean while boosting)?” Topinka et al. [207] experimentally determined that the ONR increases when maintaining

Table F.1 The effect of various parameters on the octane number requirement (ONR) of an engine [89, 157, 168, 187, 201, 205, 207, 231].

Parameters	Octane Number Requirement (ONR)	Range Tested	Reference
Spark advance	increase 1 ONR / 1° knock limited spark advance	0-30 CAD	[89, 187]
Intake Air Temperature	increase 1 ONR / 7 °C	20-90 °C	[89, 187]
Air-Fuel Ratio	peaks around 5% rich of stoichiometric, decreases 2 ONR / 0.1 λ)	12 - 26 AFR	[157, 187, 207]
MAP	increase 3-4 ONR / 10kPa	85 - 135 kPa	[187, 207]
Compression Ratio	increase 5 ONR/ CR	5 - 12 CR	[89, 157, 187, 201, 231]
Exhaust Back Pressure	increase 1 ONR / 30 kPa	0 - 65 kPa	[187]
Coolant Temperature	increase 1 ONR / 10 °C	70 - 110 °C	[187]
Altitude	decrease 1.4 ONR/300m decrease 2.5 ONR/300m	0 - 1800m 1800 - 3600m	[89]
Humidity	decrease 1 ONR when increasing relative humidity from 40% to 50% at 30°C		[89]
Engine Deposits	increase 6-9 ONR over life of engine	0 - 25000km	[89]
Excessive Oil Consumption	increase up to 12 ONR depending on driving style		[89]
H_2 Addition	decrease 1 ONR / 1% H_2 added	0 - 12% H_2 added	[207]
Type of Fuel Injection	decrease 4 ONR when DISI used over MPI		[168]
Increasing Squish	decrease up to 5 ONR as squish area increases	0 - 67% squish area	[205]
Combustion Chamber Shape	decrease up to 15 ONR from cylindrical to modern type (hemispherical head)	7.8-11 CR	[201]

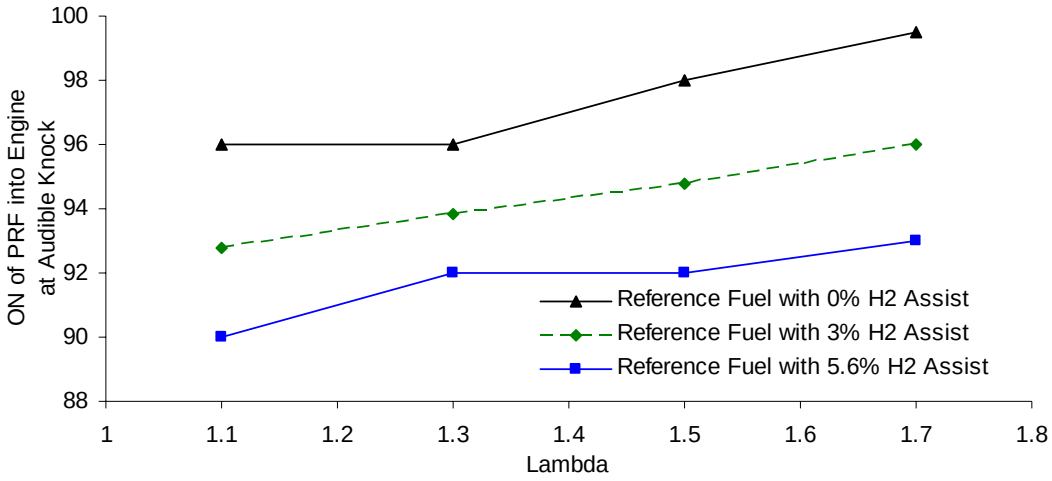

Figure F.3: Decrease in primary reference fuel (PRF) octane number at the audible knock limit with and without H_2 addition. All data points are at 850kPa IMEP [207].

constant IMEP as the mixture was made leaner (Figure F.3). Topinka et al. also showed for constant IMEP that for every percent of fuel energy replaced by H_2, the ONR decreased by one at constant IMEP (Figure F.3). This means that the ONR for a SI-G engine operating at λ=1.1 (no H_2 added) should be the equivalent to HAJI-G engine operating at λ=1.7 when 3% H_2 is added. In contrast, the results of this thesis actually suggest that the ONR decreases at constant IMEP. This can be seen in Figure F.1 (lower - left), where in HAJI-G mode near λ=1, MBT is knock limited, which can be avoided by increasing the ON of the fuel. However, following any of the constant IMEP lines it can be clearly seen that while the mixture becomes lean and the intake manifold pressure increases, MBT is no longer knock limited. This indicates that in HAJI-G mode the ONR decreases as the mixture is made leaner at constant load.

Similar trends can be observed in HAJI-H_2 mode (Figure F.2 lower - left) where the mixture near λ=1 is backfire limited, however along a constant load line as the mixture becomes lean and boosted, MBT never actually becomes knock limited. This further supports the fact that at a constant load in HAJI mode, to lower NO_x emissions and improve thermal efficiency by operating in lean boosted (supercharged) mode does not increase the ONR.

The experiments conducted by Topinka et al. [207] in an SI engine at λ=1.7 with and without H_2 addition would produce high CoV of IMEP (see Figure 2.19),

therefore the burn duration of the mixture is anticipated to be very long. As a consequence, one of the fundamental reasons why Topinka et al. would have experienced an increase in ONR as the mixture becomes lean and boosted is because the extended burn duration increases the time available to transfer heat into the end-gas and also increases the residence time of the end-gas at high temperature. This mechanism of end gas heating causes the mixture to be more susceptible to knock. In contrast, HAJI can reduce the burn duration in such lean mixtures better than SI operating at λ=1. As an example, Figure 8.21 demonstrates that the total burn duration of HAJI-G operating at λ=1.9 is less than SI-G operating at λ=1 at all load points.

In summary HAJI reduces the ONR at constant load, which means that operating in lean boosted mode requires a lower ON fuel than operating at the same load at λ=1. This tendency of HAJI to reduce knock in lean mixtures is possible because the jet ignition can stabilise combustion in lean mixtures and reduce burn duration. Moreover addition of H_2 reduces the probability of knock by decreasing burn duration even further [192] and because hydrogen's ON is higher than that of gasoline.

F.3 HUCR

By definition at a given λ the highest useful compression ratio (HUCR) occurs at the CR where the thermal efficiency is the highest (Figure F.1 and F.2 top - right). In general to achieve this MBT is usually not knock limited. Due to this reason when knock limited MBT is mentioned at a given engine condition then it is well known that thermal efficiency of the engine is not maximised. The most obvious action to improve the thermal efficiency of an engine which operates at knock limited MBT is to either lower the CR or increase the ON of the fuel, both allowing more optimal spark timing.

The thermal efficiency of an engine varies considerably with load, speed, and ambient conditions. For this reason, it is difficult to know at what conditions the engine's thermal efficiency should be maximized, especially if the complexity of Table F.1 is considered. The ONR of an engine depends on many variables so to

design an engine which is free of knock at all conditions requires calibration at the point where ONR is the highest. One example of this would be trailer-towing up a hill with an engine which already covered 50000kms in low humidity with 40°C ambient air temperatures. However, only small fraction of the population would subject their vehicles to such conditions. Consequently at any other times the engine would be operating at conditions where the ONR is significantly lower hence the engine thermal efficiency would not be maximised at those conditions.

The above discussion only considered thermal efficiency to be important when determining the HUCR. Emissions change significantly as CR is varied (Section 7.3.2), therefore when determining the HUCR the effect of CR on NO_x, HC and CO need to be considered as emission regulations become more stringent. Due to the high complexity of this problem, the most efficient way to determine the HUCR of an engine is to map it at different CRs and then perform a test on the NEDC (or similar) to obtain results for fuel consumption and emissions. Clearly the highest CR that achieves the desired emissions regulations is what would be considered as the HUCR.

It should be emphasised that mapping an engine at a given CR is extremely time consuming. In this thesis mapping at each CR was performed by moving through approximately 5 spark timings, 5 MAPs, 7 air-fuel ratios and 4 H_2 pre-chamber quantities, giving over 700 data points. Overall 5 CRs were mapped with gasoline and H_2 fuel representing approximately 3500 data points. In the automotive industry the test matrix is even more complex when considering variable cam timing, variable valve lift, piston shape and injector selection to name a few.

In this thesis the optimum CR (or HUCR) was determined with a simple method. From the beginning of the project the engine variables such as CR, MAP, spark timing, pre-chamber H_2 quantity, and λ were chosen as these are the most fundamental and influential parameters in combustion development work. Then the OPL was determined on the MAP vs. λ contour plots by setting a limit on combustion variation (<5% CoV of IMEP), and setting a limit on NO_x (<0.1g/kWh). When these conditions were met, then the OPL was positioned where thermal efficiency was the highest. The OPL was established for all 5 CRs

and then by visual inspecting the MAP vs. λ contour plots, CR=11 was chosen because it provided the best balance between efficiency and emissions.

F.4 Concepts Behind Analysis

The fundamental theory behind the two-zone combustion model is explained in detail in Chapter 3. The combustion modelling equations are described in Appendix D and the source code can be found in Appendix G. The results of the modelling are presented in Chapters 5, 6, 7, and 8. The purpose of this section is to visually describe the behavior of different output parameters from the combustion analysis as a function of crank angle rotation. Results for λ=1 and λ=1.85 are presented on Figures F.4, F.5, and F.6, to provide a better sense of how key parameters (such as pressure, MFB, flame speed etc...) vary during combustion, and variables such as peak pressure, location of 50% MFB, combustion duration [35], peak temperature etc... are also identified.

As explained in Section 4.5.2 the analysis was carried out by analysing 40 consecutive individual cycles, which were used to developed ensemble average diagrams. As an example Figure F.4 (top) shows the 40 individual cycles for pressure vs. CA for λ=1, λ=1.85 and motoring condition. The thick lines represent the ensemble average of all three conditions. All of the other figures in this chapter (Figures F.4, F.5, and F.6) were developed the same way. Therefore each data point for peak pressure, location of 50% MFB, peak temperature etc... shown in this chapter as well as in Chapter 7 and 8 are a result of the ensemble average of 40 consecutive cycles. This technique was used to ensure with 99.9% confidence that the population mean differed from the sample mean by no more than +/- 3% [132]. When the author analysed sets of ten 40 cycle sequences at low λ values the IMEP varied less than +/- 1% and at high λ values less than 2%.

Finally it is worth noting that the CoV of IMEP of the motoring cycle (Figure F.4 - top) is 1.2% (less than +/-2kPa variation in PMEP), not zero as one would think. This occurs since the pressure resolution is about 1.57 kPa/digital count (Section C.3) and because piezo-electric transducers have a poor response when they are not subjected to a significant change in pressure (as in the pumping loop).

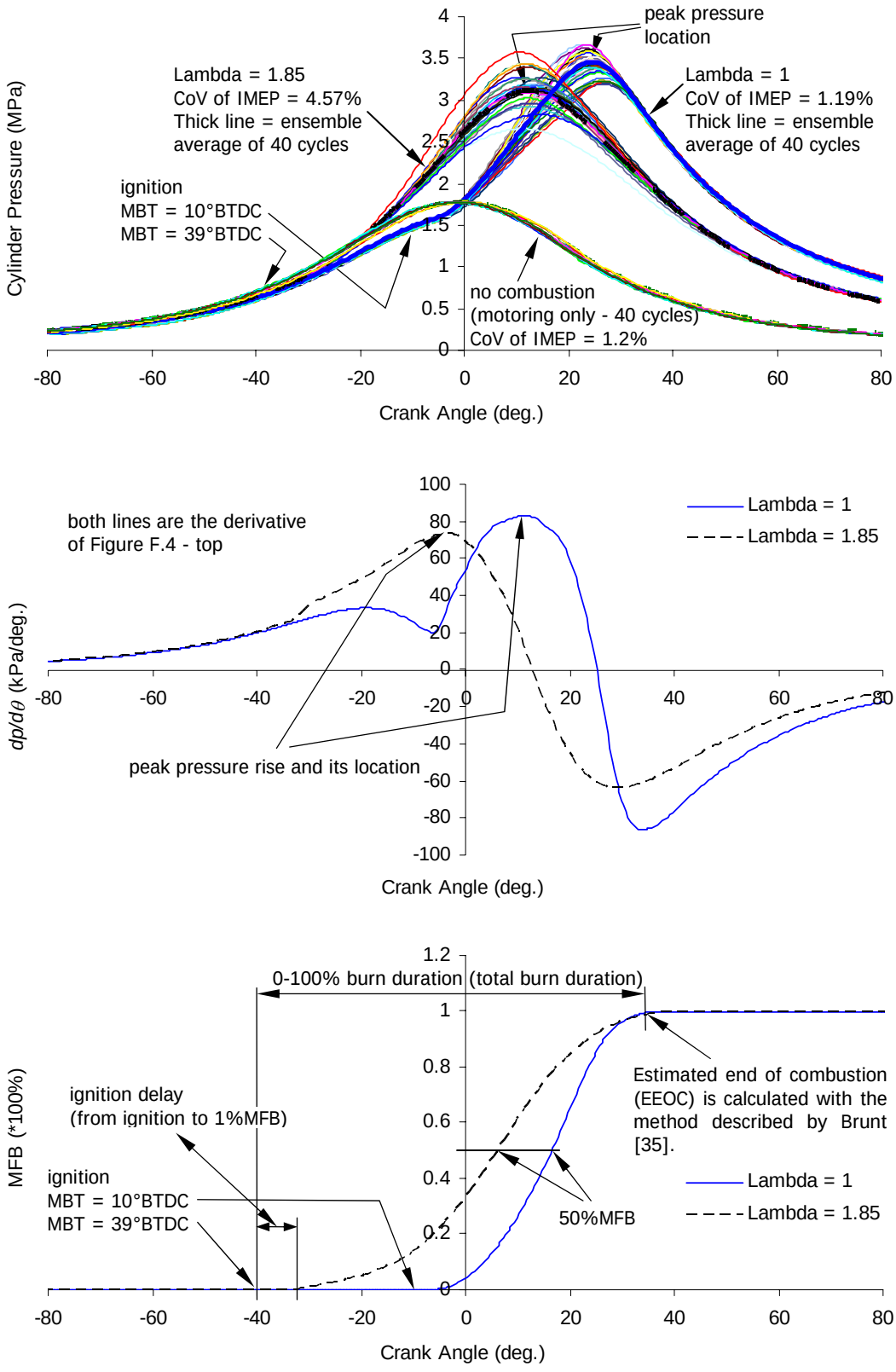

Figure F.4 (top) Cylinder pressure, (middle) $dp/d\theta$, (bottom) MFB versus CA, HAJI-G, CR=9, MAP=90kPa, each solid line is the average of 40 cycles (filtered pressure trace).

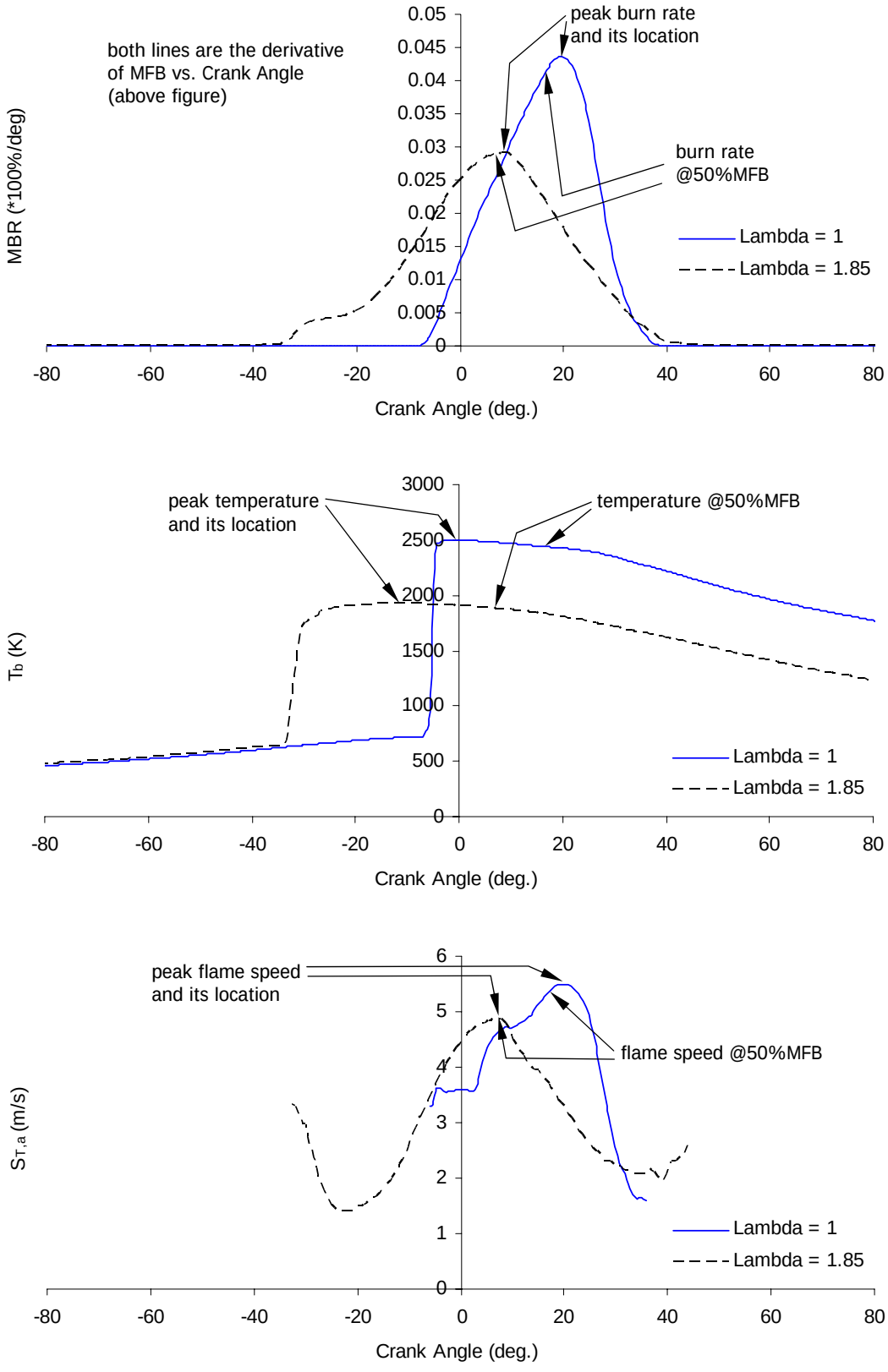

Figure F.5: (top) MBR, (middle) T_b, (bottom) $S_{T,a}$, versus CA, HAJI-G, CR=9, MAP=90kPa, each line is the average of 40 cycles.

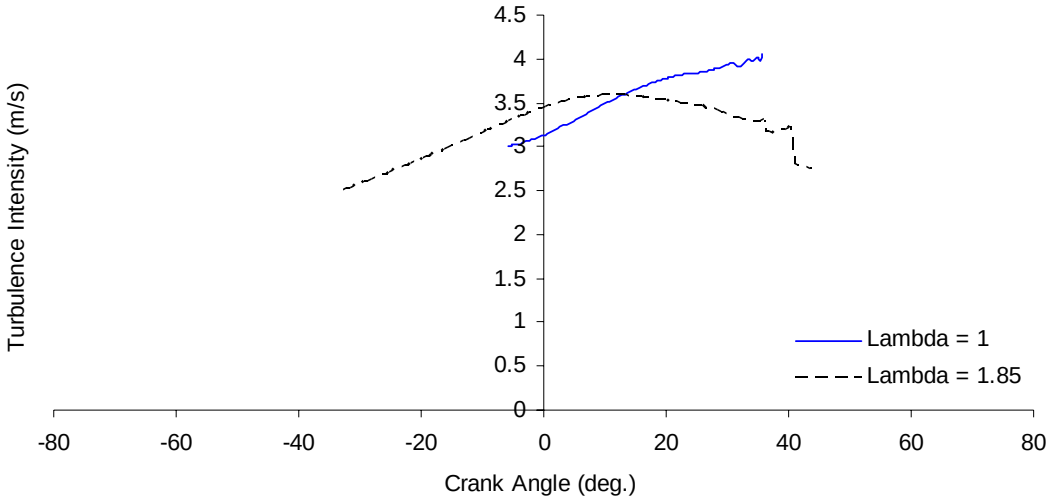

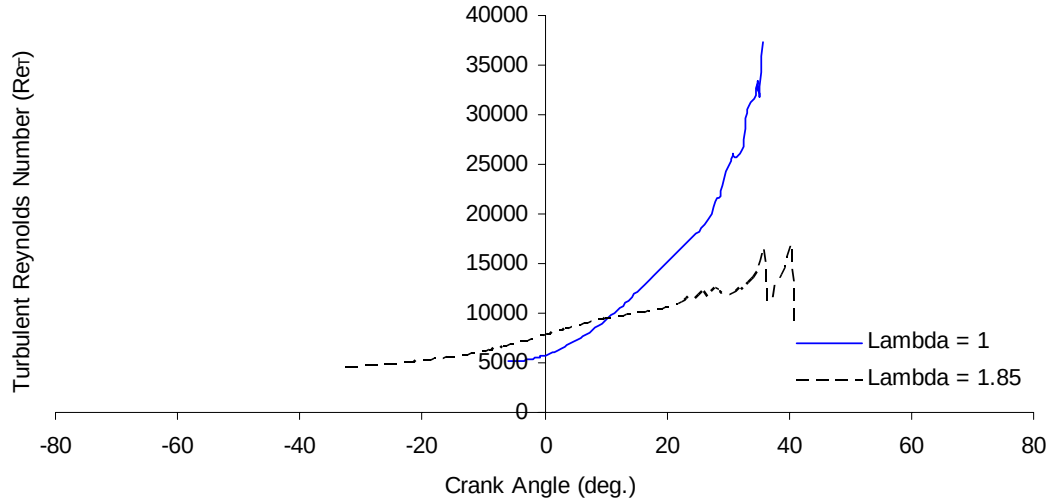

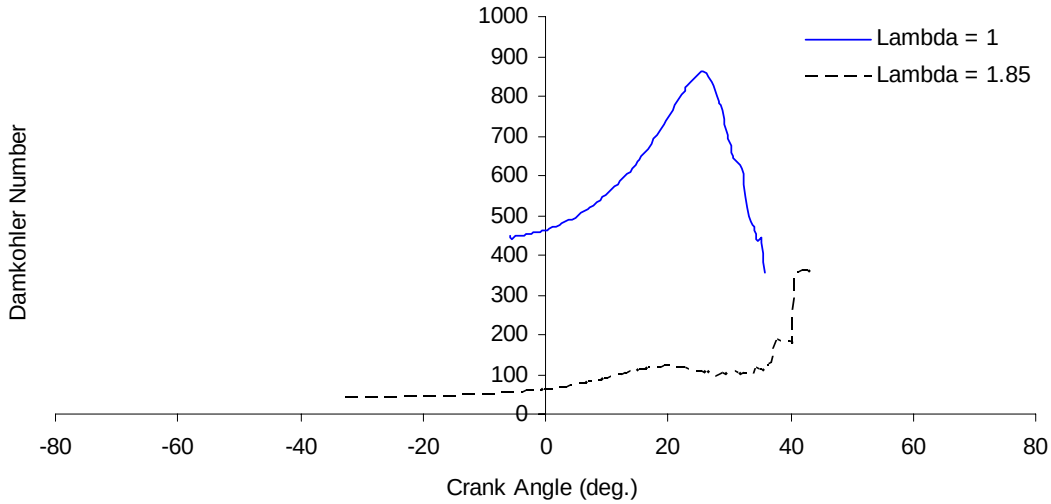

Figure F.6: (top) Turbulence Intensity, (middle) Turbulent Reynolds number, (bottom) Damkohler number versus CA, HAJI-G, CR=9, MAP=90kPa, each line is the average of 40 cycles.

Appendix G
E-CoBRA Programming Files

G.1 Programming in VBA

E-CoBRA was developed in Excel 2000. The simple functions were programmed in cells, however, most of the complex functions were programmed into Visual Basic Application (VBA). Excel with VBA was chosen over other programming languages for the following reasons:

- The multisheet orientation makes it easy to organise elements of the application and store it in a single file.
- Complex problems can be easily programmed into VBA's scripting language.
- Excel makes it easy to add controls such as buttons, list boxes, and option boxes to worksheets. Implementing such controls often requires no programming at all.
- Excel has powerful 2D graphing functions.
- The author's prior extensive experience with excel and VBA.

In total, over 7000 lines of computer code were written by the author to analyse experimental combustion pressure traces. Over 500 data points were analysed on a Pentium III 833MHz PC and it took 1.5 hours to setup and run 1 data point consisting of 40 cycles. The analysis of each data point resulted in an output of over 100 parameters, these included: IMEP, PMEP, CoV of IMEP, thermal efficiency, MFB, MBR, peak temperature and its location, peak pressure rise and its location, peak flame speed and its location, burn duration (0-100%, 0-10%, 0-90%, 10-90%), knock amplitude and its location, knock intensity, predicted NOx, specific characteristics at 50% MFB, TDC, and 30mm flame radius etc...The following are the modules implemented into VBA. The implementation of these modules consumed an estimated 35% of the total project time.

G.2 Adiabatic Flame Temperature

```
Option Explicit     'forces the declaration of all variables
Option Base 1       'the address of first element in array is 1


Private A111 As Double, A112 As Double, A113 As Double
Private A121 As Double, A122 As Double, A123 As Double
Private A131 As Double, A132 As Double, A133 As Double
Private A211 As Double, A212 As Double, A213 As Double
Private A221 As Double, A222 As Double, A223 As Double
Private A231 As Double, A232 As Double, A233 As Double
Private A311 As Double, A312 As Double, A313 As Double
Private A321 As Double, A322 As Double, A323 As Double
Private A331 As Double, A332 As Double, A333 As Double


'=========================================
'U.C. Muller, M.Bollig, and N. Peters, "Approximations for Burning
'Velocities and Markstein Numbers for Lean Hydrocarbon and 'Methanol
Flames", Combustion and Flame, '1997, Vol. 108, pp. 349-356
'=========================================
'There are 35 other fuel's coefficient listed in the paper 'Limitation/Range:
temp is b/w 298K to self ignition, pressure is b/w 1 ' to 100atm, 'Lambda
is b/w stoichiometric and lean flammability limit ' (CAN NOT CALC. rich),
accuracy within much less than 1%
'=========================================
Public Function AdiabaticFlameTemperatureHydrogen(Lambda As Double,
_
                                UnburnedTemperature As Double, _
                                ReactionPressure As Variant) As Double
Dim Phi As Double
Const NumberOfCarbonAtoms As Double = 0

Dim a11 As Double, a12 As Double, a13 As Double
Dim a21 As Double, a22 As Double, a23 As Double
Dim A31 As Double, A32 As Double, A33 As Double
Dim a1 As Double, a2 As Double, A3 As Double
If Lambda < 1 Then
Lambda = 1
End If
Phi = 1 / Lambda
UnburnedTemperature = (UnburnedTemperature + 273.15) / 298
'nondimensional form of unburned temperature T = T/298(K)
ReactionPressure = ReactionPressure / 101.325       'nondimensional form
of reaction pressure p=p/1atm

If Phi < 0.6 And Phi > 0.13 Or Phi = 0.13 Then

 A111 = 2471.5,  A112 = 177.18,  A113 = 152.454,  A121 = 0,  A122 = 0,
A123 = 0,  A131 = 0,  A132 = 0,  A133 = 0,  A211 = 0.5562,  A212 = -
0.0596,  A213 = -0.0457,  A221 = 0,  A222 = 0,  A223 = 0,  A231 = 0,
A232 = 0,  A233 = 0,  A311 = 0.1035,  A312 = -0.0093,  A313 = -0.0106,
, A321 = 0, A322 = 0,  A323 = 0,  A331 = 0,  A332 = 0,  A333 = 0

ElseIf Phi < 1 And Phi > 0.6 Or Phi = 1 Or Phi = 0.6 Then

 A111 = 2392.94, A112 = 126.287,  A113 = 80.335,  A121 = 32.0662,
A122 = 14.5362,  A123 = 11.8463,  A131 = -2.4776,  A132 = -1.1117,
A133 = 0.3428,  A211 = 0.3889,  A212 = -0.1453,  A213 = -0.0493, A221
= 0.0521,  A222 = 0.017,  A223 = -0.0219,  A231 = -0.00365,  A232 = -
0.0004,  A233 = 0.00339,  A311 = -0.1443,  A312 = -0.1174,  A313 =
0.0449,  A321 = 0.0678,  A322 = 0.0122,  A323 = -0.0484,  A331 = -
0.00424,  A332 = 0.00124,  A333 = 0.00561,

End If

a11 = A111 + A112 * Log(UnburnedTemperature) + A113 *
Log(UnburnedTemperature) ^ 2
a12 = A121 + A122 * Log(UnburnedTemperature) + A123 *
Log(UnburnedTemperature) ^ 2
a13 = A131 + A132 * Log(UnburnedTemperature) + A133 *
Log(UnburnedTemperature) ^ 2

a21 = A211 + A212 * Log(UnburnedTemperature) + A213 *
Log(UnburnedTemperature) ^ 2
a22 = A221 + A222 * Log(UnburnedTemperature) + A223 *
Log(UnburnedTemperature) ^ 2
a23 = A231 + A232 * Log(UnburnedTemperature) + A233 *
Log(UnburnedTemperature) ^ 2

A31 = A311 + A312 * Log(UnburnedTemperature) + A313 *
Log(UnburnedTemperature) ^ 2
A32 = A321 + A322 * Log(UnburnedTemperature) + A323 *
Log(UnburnedTemperature) ^ 2
A33 = A331 + A332 * Log(UnburnedTemperature) + A333 *
Log(UnburnedTemperature) ^ 2

a1 = a11 + a12 * Log(ReactionPressure) + a13 * Log(ReactionPressure)
^ 2
```

```
a2 = a21 + a22 * Log(ReactionPressure) + a23 * Log(ReactionPressure)
^ 2
A3 = A31 + A32 * Log(ReactionPressure) + A33 * Log(ReactionPressure)
^ 2

AdiabaticFlameTemperatureHydrogen = a1 * (1 + a2 * Log(Phi) + A3 *
Log(Phi) ^ 2) - 273.15

End Function

Public Function AdiabaticFlameTemperatureC8H18(Lambda As Double, _
                                UnburnedTemperature As Double, _
                                ReactionPressure As Variant) As Double
Dim Phi As Double
Const NumberOfCarbonAtoms As Double = 0

Dim a11 As Double, a12 As Double, a13 As Double
Dim a21 As Double, a22 As Double, a23 As Double
Dim A31 As Double, A32 As Double, A33 As Double
Dim a1 As Double, a2 As Double, A3 As Double
If Lambda < 1 Then
Lambda = 1
End If
Phi = 1 / Lambda
UnburnedTemperature = (UnburnedTemperature + 273.15) / 298
'nondimensional form of unburned temperature T = T/298(K)
ReactionPressure = ReactionPressure / 101.325       'nondimensional form
of reaction pressure p=p/1atm

A111 = 2296.17, A112 = 130.125, A113 = 82.11, A121 = 26.6138
A122 = 15.0791, A123 = 9.8686, A131 = -2.0203, A132 = -1.1573
A133 = 0.6696, A211 = 0.4821, A212 = -0.171, A213 = -0.0786
A221 = 0.0439,  A222 = 0.0245, A223 = -0.0211, A231 = -0.00312
A232 = -0.00127, A233 = 0.00355, A311 = -0.0304, A312 = -0.1405
A313 = 0.0051, A321 = 0.0512, A322 = 0.0261, A323 = -0.0409, A331 =
-0.00344, A332 = -0.00084, A333 = 0.00521,

a11 = A111 + A112 * Log(UnburnedTemperature) + A113 *
Log(UnburnedTemperature) ^ 2
a12 = A121 + A122 * Log(UnburnedTemperature) + A123 *
Log(UnburnedTemperature) ^ 2
a13 = A131 + A132 * Log(UnburnedTemperature) + A133 *
Log(UnburnedTemperature) ^ 2

a21 = A211 + A212 * Log(UnburnedTemperature) + A213 *
Log(UnburnedTemperature) ^ 2
a22 = A221 + A222 * Log(UnburnedTemperature) + A223 *
Log(UnburnedTemperature) ^ 2
a23 = A231 + A232 * Log(UnburnedTemperature) + A233 *
Log(UnburnedTemperature) ^ 2

A31 = A311 + A312 * Log(UnburnedTemperature) + A313 *
Log(UnburnedTemperature) ^ 2
A32 = A321 + A322 * Log(UnburnedTemperature) + A323 *
Log(UnburnedTemperature) ^ 2
A33 = A331 + A332 * Log(UnburnedTemperature) + A333 *
Log(UnburnedTemperature) ^ 2

a1 = a11 + a12 * Log(ReactionPressure) + a13 * Log(ReactionPressure)
^ 2
a2 = a21 + a22 * Log(ReactionPressure) + a23 * Log(ReactionPressure)
^ 2
A3 = A31 + A32 * Log(ReactionPressure) + A33 * Log(ReactionPressure)
^ 2

AdiabaticFlameTemperatureC8H18 = a1 * (1 + a2 * Log(Phi) + A3 *
Log(Phi) ^ 2) - 273.15

End Function
```

G.3 Phase and Align Pressure Trace with TDC

```
Sub AlignTDC()

Dim TDC, BDC, T As Variant
Dim Message, Style, Title, Help, Response
Dim ThreeSixtyFiveDegrees As Double

    'First Align Data'.
    T = AlignData
    If T = False Then
    MsgBox "Could NOT Detect a Good Start in 1000 Rows" & _
                        "First check the rows manually and then check the
code as well."
            Exit Sub
    End If

    'Second find TDC
    TDC = FindTopDeadCenter()

    If TDC = False Then
                MsgBox " Sorry. User must have canceled. Locate TDC
                manually or try again. "
                 Worksheets("INPUT").Activate
                    Range("A1").Select
               Exit Sub
    End If

    Message = "Do you want to align row number " & TDC & " TDC to
TRUE TDC?"
        Style = vbYesNo + vbQuestion + vbDefaultButton2
'vbQuestion,vbExclamation,vbCritical,vbInformation
          Title = "Align TDC"

              Response = MsgBox(Message, Style, Title)

    If Response = vbYes Then
       'In this case we don't need to use special paste because it's row
data.
Worksheets("INPUT").Range(Cells(TDC, 5), Cells(65000, 5)).Copy
ActiveSheet.Paste Destination:=Worksheets("INPUT").Range(Cells(61, 5),
Cells(65000 + 61 - TDC, 5))

Worksheets("INPUT").Range(Cells(TDC, 4), Cells(65000, 4)).Copy
ActiveSheet.Paste Destination:=Worksheets("INPUT").Range(Cells(61, 4),
Cells(65000 + 61 - TDC, 4))

       'Call Function to calculate the corresponding angle
       ConvertSawtoothToAngle
    Else
MsgBox " Sorry. User must have canceled. Execute procedure manually. "
          Worksheets("INPUT").Activate
             Range("A1").Select
           Exit Sub
    End If

    BDC = FindBDC()

       If BDC = 0 Then
             MsgBox "Did NOT find BDC degrees. Check Manually."
                Exit Sub
       Else
Worksheets("INPUT").Range(Cells(BDC, 5), Cells(65000, 5)).Copy
ActiveSheet.Paste Destination:=Worksheets("INPUT").Range(Cells(61, 5),
Cells(65000 + 61 - BDC, 5))

Worksheets("INPUT").Range(Cells(BDC, 4), Cells(65000, 4)).Copy
ActiveSheet.Paste Destination:=Worksheets("INPUT").Range(Cells(61, 4),
Cells(65000 + 61 - BDC, 4))

                'Call Function to calculate the corresponding angle
                ConvertSawtoothToAngle
                   Worksheets("INPUT").Activate
                      Range("A1").Select
       End If

End Sub

Function FindTopDeadCenter()

Dim TDC, TDCNew As Variant
Dim i As Double
Dim Message, Style, Title, Help, Response
Dim Message2, Title2, Default

i = 1

MyString = "No"
TDCNew = False
Confirmation = False

a = Worksheets("INPUT").Range("e61:e2000")
VoltMax = Application.WorksheetFunction.Max(a)
VoltMin = Application.WorksheetFunction.Min(a)

Do While TDCNew = False Or Confirmation = False


   While ((a(i, 1) - VoltMin) / (a(i + 1, 1) + ((VoltMax - VoltMin) / 2) -
VoltMin)) < 1.5 And T = 0
       i = i + 1

       If i = 1500 Then
          MsgBox "Could NOT find TDC in 1 cycle. Try manually."
          Exit Do
       End If
   Wend

   If TDCNew = 0 Then
```

```
        TDC = i + 60
        Worksheets("INPUT").Activate
        Cells(TDC, 5).Select
    Else
        TDC = TDCNew
        Worksheets("INPUT").Activate
        Cells(TDC, 5).Select
    End If

    Message = "Is " & TDC & " cell corresponds to TDC?" & _
            " If YES press OK. If NOT then find the TDC manually" & _
            " then type in the row number below. Or just press" & _
            " cancel if you want to exit."
    Default = "" & TDC
    Title = "Manual TDC input"
    TDCNew = Application.InputBox(Message, Title, Default)

    If TDCNew = True Then
    Worksheets("INPUT").Activate
    Cells(TDCNew, 5).Select
    Else
    Exit Do
    End If

    Message2 = "Please Confirm " & TDCNew & " position is correct."
    Style = vbYesNo + vbQuestion + vbDefaultButton2
'vbQuestion,vbExclamation,vbCritical,vbInformation
    Title2 = "Confirming TDC"
    Response = MsgBox(Message2, Style, Title2)

    If Response = vbYes Then
        Confirmation = True
    Else
        Confirmation = False
    End If

Loop

FindTopDeadCenter = TDCNew

End Function
Sub ConvertSawtoothToAngle()

Dim a, b As Variant
Dim i, NumberOfCycles, Increments, row As Integer
i = 3
Increments = 1500 'Number of data point for one cycle

        'Input Sawtooth signal in volts
        a = Worksheets("INPUT").Range(Cells(61, 5), Cells(61 + Increments
+ 100, 5))
        'Output of angle
        b = Worksheets("INPUT").Range(Cells(61, 8), Cells(61 + Increments
+ 100, 8))
        b(1, 1) = -175 'initialise angle

        FirstToothAngle = b(1, 1)

        FirstToothPosition = 1 'initialise first tooth position

While FirstToothPosition < Increments


    'It will stay in the loop until all conditions are satisfied
    'When it is finished in the loop i = tip of the triangle
    i = i + 1 'from previous cycle i finished on the tip of the tooth so we
bump it over.
    Do Until a(i, 1) > a(i + 1, 1) And _
            a(i, 1) > a(i - 1, 1) And _
        a(i + 1, 1) < a(i + 2, 1) And _
        a(i - 1, 1) > a(i - 2, 1) And _
        a(i + 2, 1) < a(i + 3, 1) And _
        a(i - 2, 1) > a(i - 3, 1)

    i = i + 1
    Loop

    SecondToothPosition = i

    DiffBwTwoToothPosition = SecondToothPosition - FirstToothPosition

    'It is possible that there is 9 data points between 2 teeth. But it is also
possible to have 11 points.
    If DiffBwTwoToothPosition <= 12 Then
    SecondToothAngle = FirstToothAngle + 5
    ElseIf DiffBwTwoToothPosition <= 23 Then
    SecondToothAngle = FirstToothAngle + 10
    ElseIf DiffBwTwoToothPosition <= 33 Then
    SecondToothAngle = FirstToothAngle + 15
    ElseIf DiffBwTwoToothPosition <= 43 Then
    SecondToothAngle = FirstToothAngle + 20
    ElseIf DiffBwTwoToothPosition <= 53 Then
    SecondToothAngle = FirstToothAngle + 25
    ElseIf DiffBwTwoToothPosition <= 63 Then
    SecondToothAngle = FirstToothAngle + 30
    ElseIf DiffBwTwoToothPosition <= 73 Then
    SecondToothAngle = FirstToothAngle + 35
    ElseIf DiffBwTwoToothPosition > 73 Then
    row = 61 + FirstToothPosition
    MsgBox "Check data Manually, because there are 7 faulty teeth in a
row." & _
            "Faulty tooth is around row number " & row & "."
        Exit Sub
    End If

    b(SecondToothPosition, 1) = SecondToothAngle

    DiffBwTwoToothAngle = FirstToothAngle - SecondToothAngle

    AngleIncrement = DiffBwTwoToothAngle / DiffBwTwoToothPosition

    T = 1
    While T < DiffBwTwoToothPosition

    b(FirstToothPosition + T, 1) = FirstToothAngle - (T * AngleIncrement)

    T = T + 1
    Wend

FirstToothAngle = SecondToothAngle
FirstToothPosition = SecondToothPosition
Wend

Worksheets("INPUT").Range(Cells(61, 8), Cells(61 + Increments + 100,
8)) = b

'Automatically calculates everything in the open workbook
SpeedCalculation

End Sub

'At this point -175 degrees corresponds to TDC.
Private Function FindBDC()   'As Integer

Dim row, ColumnAngle, ColumnPressure As Integer
Dim PressureVoltMax, PressureVoltMin, PressureVoltAtTDC,
PressureVoltAtBDC As Double
Dim PressureVolt As Variant
Dim angle As Variant
row = 62
ColumnAngle = 8
angle = 0

    PressureVoltAtTDC = Worksheets("INPUT").Cells(61, 4).Value
        PressureVolt = Worksheets("INPUT").Range("d61:d1500")
PressureVoltMax = Application.WorksheetFunction.Max(PressureVolt)
PressureVoltMin = Application.WorksheetFunction.Min(PressureVolt)
'Estimating the maximum voltage at BDC
PressureVoltAtBDC = PressureVoltMin + ((PressureVoltMax -
PressureVoltMin) * 0.2)

    If PressureVoltAtTDC < PressureVoltAtBDC Then
        FindAngle = 5
    Else
        FindAngle = 365
    End If

        angle = Worksheets("INPUT").Range("h1:h1520").Value
        Do Until angle(row, 1) = FindAngle Or angle(row, 1) > FindAngle

            row = row + 1
'Angle = Worksheets("INPUT").Cells(row, ColumnAngle).Value

                If row = 2000 Then
                    MsgBox "BDC was NOT detected in 2000 rows." & _
                            "First check the rows manually and then check
the code as well."
                        Exit Do
                End If
            Loop

    'MsgBox "Angle at BDC  " & Angle(row, 1)
If row = 2000 Then
FindBDC = 0
Else
FindBDC = row
End If

End Function

Private Function AlignData()

Dim a, b As Variant
Dim i, Increments As Integer
```

```
i = 3
Increments = 1500 'Number of data point for one cycle

        'Input Sawtooth signal in volts
 a = Worksheets("INPUT").Range(Cells(61, 5), Cells(61 + Increments +
100, 5))
        'Output of angle
b = Worksheets("INPUT").Range(Cells(61, 8), Cells(61 + Increments +
100, 8))
        b(1, 1) = -175 'initialise angle

        FirstToothAngle = b(1, 1)

        FirstToothPosition = 1 'initialise first tooth position

    'It will stay in the loop until all conditions are satisfied
    'When it is finished in the loop i = tip of the triangle
    i = i + 1 'from previous cycle i finished on the tip of the tooth so we
bump it over.
    Do Until a(i, 1) > a(i + 1, 1) And _
            a(i, 1) > a(i - 1, 1) And _
        a(i + 1, 1) < a(i + 2, 1) And _
        a(i - 1, 1) > a(i - 2, 1) And _
        a(i + 2, 1) < a(i + 3, 1) And _
        a(i - 2, 1) > a(i - 3, 1)

    i = i + 1
        If i = 1000 Then
           Exit Do
        End If
    Loop

'In this case we don't need to use special paste because it's row data.
        If i < 1000 Then
        'We need the tip of the wave
        i = i - 1
            Worksheets("INPUT").Range(Cells(61 + i, 5), Cells(65000,
5)).Copy
                ActiveSheet.Paste
Destination:=Worksheets("INPUT").Range(Cells(61, 5), Cells(65000 - i, 5))

Worksheets("INPUT").Range(Cells(61 + i, 4), Cells(65000, 4)).Copy
ActiveSheet.Paste Destination:=Worksheets("INPUT").Range(Cells(61, 4),
Cells(65000 - i, 4))
        End If

If i = 2000 Then
AlignData = False
Else
AlignData = True
ConvertSawtoothToAngle
End If

End Function
```

G.4 Analyse User Defined Cycles

```
'This function calls the Progress Indicator. Progress Indicator Calls
NumberOfCycle
Sub StartProressIndicatorAndAnalysis2()
'UserForm2.StartUpPosition = 3
UserForm2.Show
End Sub

'\This program comes up with a progress indicator.
Sub UpdateProgress2(Pct, Cycle, TotalCycle)
    With UserForm2
        .Label2.Caption = Format(Cycle, "0")
        .Label4.Caption = Format(TotalCycle, "0")
        .FrameProgress.Caption = Format(Pct, "0%")
        .LabelProgress.Width = Pct * (.FrameProgress.Width - 3)
        .Repaint
    End With
End Sub

'UserForm2.Show

'This function prompts the user for the number of cycles
'to be analysed
Sub NumberOfCycle()

Dim N As Variant
Dim Message, Title, Default

Message = "Number of Cycles to Analyse?" & _
          "Type in an integer between 0-40."
   Title = "Analyses up to 40 cycles."
      Default = "1"
         N = InputBox(Message, Title, Default, 2000, 2500)

            If N <= 0 Or N > 40 Or N = False Then
               'Turn OFF Progress Indicator and display message.
               Unload UserForm2
                  MsgBox "Sorry. No Analysis has been made." & _
                     "Next time type in an integer between 0-40. OR Do
Not press cancel."
                        Exit Sub
            End If

'Call function MoveDate to copy-paste data onto OUTPUT sheet
MoveData (N)

End Sub

'Make sure that the copy-paste areas are correct.
Private Sub MoveData(TotalCycleNumber As Integer)

Dim i, row, column, RowIndicated, ColumnIndicated, Cycle As Integer

i = 0
row = 0             'Offset = 0
column = 0
RowIndicated = 0
ColumnIndicated = 0

Worksheets("OUTPUT").Range("ah3:cb92").ClearContents
Worksheets("OUTPUT").Range("a101:fg65520").ClearContents

Do

   'Call Progress indicator
      Cycle = i + 1
      PctDone = Cycle / TotalCycleNumber
         Call UpdateProgress2(PctDone, Cycle, TotalCycleNumber)

Call ConvertSawtoothToAngle
Call Butter 'knock analysis
Call EngineSimulation 'Two-Zone engine simulation
Call SpeedCalculation 'calculates everything in the open workbook

'This will increase the speed of calculation by 25%
Application.ScreenUpdating = False

'Make sure that the copy-paste ranges are equal size.
'Copy-Paste Indicated OUTPUT data
Worksheets("Engine Modeling Output").Range("f5:f94").Copy
Worksheets("OUTPUT").Range("Am3:am92") _
.Offset(rowOffset:=RowIndicated, columnOffset:=ColumnIndicated) _
.PasteSpecial Paste:=xlPasteValues

'Copy-Paste ANGLE
Worksheets("ANALYSIS").Range("t2:t1500").Copy
Worksheets("OUTPUT").Range("b100:b1598") _
.Offset(rowOffset:=row, columnOffset:=column) _
.PasteSpecial Paste:=xlPasteValues

'Copy-Paste VOLUME
Worksheets("ANALYSIS").Range("v2:v1500").Copy
Worksheets("OUTPUT").Range("c100:c1598") _
.Offset(rowOffset:=row, columnOffset:=column) _
.PasteSpecial Paste:=xlPasteValues

'Copy-Paste PRESSURE
Worksheets("ANALYSIS").Range("w2:w1500").Copy
Worksheets("OUTPUT").Range("d100:d1598") _
.Offset(rowOffset:=row, columnOffset:=column) _
.PasteSpecial Paste:=xlPasteValues

'Copy-Paste LOGPRESSURE
Worksheets("ANALYSIS").Range("ad2:ad1500").Copy
Worksheets("OUTPUT").Range("e100:e1598") _
.Offset(rowOffset:=row, columnOffset:=column) _
.PasteSpecial Paste:=xlPasteValues

'Copy-Paste LOGVOLUME
Worksheets("ANALYSIS").Range("ae2:ae1500").Copy
Worksheets("OUTPUT").Range("f100:f1598") _
.Offset(rowOffset:=row, columnOffset:=column) _
.PasteSpecial Paste:=xlPasteValues

'Copy-Paste MFB
Worksheets("ANALYSIS").Range("an2:an1500").Copy
Worksheets("OUTPUT").Range("g100:g1598") _
.Offset(rowOffset:=row, columnOffset:=column) _
.PasteSpecial Paste:=xlPasteValues

'Copy-Paste MBR
```

```
Worksheets("ANALYSIS").Range("ap2:ap1500").Copy
Worksheets("OUTPUT").Range("h100:h1598") _
.Offset(rowOffset:=row, columnOffset:=column) _
.PasteSpecial Paste:=xlPasteValues

'Copy-Paste TORQUE
Worksheets("ANALYSIS").Range("aq2:aq1500").Copy
Worksheets("OUTPUT").Range("i100:i1598") _
.Offset(rowOffset:=row, columnOffset:=column) _
.PasteSpecial Paste:=xlPasteValues

'Copy-Paste dpdth
Worksheets("ANALYSIS").Range("au2:au1500").Copy
Worksheets("OUTPUT").Range("j100:j1598") _
.Offset(rowOffset:=row, columnOffset:=column) _
.PasteSpecial Paste:=xlPasteValues

'Copy-Paste PRESSURE VOLTAGE
Worksheets("INPUT").Range("d58:d1556").Copy
Worksheets("OUTPUT").Range("k98:k1596") _
.Offset(rowOffset:=row, columnOffset:=column) _
.PasteSpecial Paste:=xlPasteValues

'Copy-Paste SAWTOOTH WAVE VOLTAGE
Worksheets("INPUT").Range("e58:e1556").Copy
Worksheets("OUTPUT").Range("l98:l1596") _
.Offset(rowOffset:=row, columnOffset:=column) _
.PasteSpecial Paste:=xlPasteValues

'++++++FROM TWO-ZONE MODELING

'Copy-Paste Tu
Worksheets("Engine Modeling Output").Range("j200:j1698").Copy
Worksheets("OUTPUT").Range("m101:m1599") _
.Offset(rowOffset:=row, columnOffset:=column) _
.PasteSpecial Paste:=xlPasteValues

'Copy-Paste Tb
Worksheets("Engine Modeling Output").Range("y200:y1698").Copy
Worksheets("OUTPUT").Range("n101:n1599") _
.Offset(rowOffset:=row, columnOffset:=column) _
.PasteSpecial Paste:=xlPasteValues

'Copy-Paste Mean Temp.
Worksheets("Engine Modeling Output").Range("z200:z1698").Copy
Worksheets("OUTPUT").Range("o101:o1599") _
.Offset(rowOffset:=row, columnOffset:=column) _
.PasteSpecial Paste:=xlPasteValues

'Copy-Paste Adiabatic Flame Temp.
Worksheets("Engine Modeling Output").Range("aa200:aa1698").Copy
Worksheets("OUTPUT").Range("p101:p1599") _
.Offset(rowOffset:=row, columnOffset:=column) _
.PasteSpecial Paste:=xlPasteValues

'Copy-Paste NOppm rate controlled method 1
Worksheets("Engine Modeling Output").Range("ab200:ab1698").Copy
Worksheets("OUTPUT").Range("q101:q1599") _
.Offset(rowOffset:=row, columnOffset:=column) _
.PasteSpecial Paste:=xlPasteValues

'Copy-Paste NOppm rate controlled method 1
Worksheets("Engine Modeling Output").Range("ac200:ac1698").Copy
Worksheets("OUTPUT").Range("r101:r1599") _
.Offset(rowOffset:=row, columnOffset:=column) _
.PasteSpecial Paste:=xlPasteValues

'Copy-Paste NOppm equilibrium
Worksheets("Engine Modeling Output").Range("ad200:ad1698").Copy
Worksheets("OUTPUT").Range("s101:s1599") _
.Offset(rowOffset:=row, columnOffset:=column) _
.PasteSpecial Paste:=xlPasteValues

'Copy-Paste Flame Area
Worksheets("Engine Modeling Output").Range("ae200:ae1698").Copy
Worksheets("OUTPUT").Range("t101:t1599") _
.Offset(rowOffset:=row, columnOffset:=column) _
.PasteSpecial Paste:=xlPasteValues

'Copy-Paste St
Worksheets("Engine Modeling Output").Range("af200:af1698").Copy
Worksheets("OUTPUT").Range("u101:u1599") _
.Offset(rowOffset:=row, columnOffset:=column) _
.PasteSpecial Paste:=xlPasteValues

'Copy-Paste Flame Radius
Worksheets("Engine Modeling Output").Range("ag200:ag1698").Copy
Worksheets("OUTPUT").Range("v101:v1599") _
.Offset(rowOffset:=row, columnOffset:=column) _
.PasteSpecial Paste:=xlPasteValues

'Copy-Paste (St/Sl)actualC8H18
Worksheets("Engine Modeling Output").Range("aj200:aj1698").Copy
Worksheets("OUTPUT").Range("w101:w1599") _
.Offset(rowOffset:=row, columnOffset:=column) _
.PasteSpecial Paste:=xlPasteValues

'Copy-Paste (St/Sl)actualH2
Worksheets("Engine Modeling Output").Range("ak200:ak1698").Copy
Worksheets("OUTPUT").Range("x101:x1599") _
.Offset(rowOffset:=row, columnOffset:=column) _
.PasteSpecial Paste:=xlPasteValues

'Copy-Paste (St/Sl)theoretical
Worksheets("Engine Modeling Output").Range("al200:al1698").Copy
Worksheets("OUTPUT").Range("y101:y1599") _
.Offset(rowOffset:=row, columnOffset:=column) _
.PasteSpecial Paste:=xlPasteValues

'Copy-Paste FERI Factor Lumsden
Worksheets("Engine Modeling Output").Range("an200:an1698").Copy
Worksheets("OUTPUT").Range("z101:z1599") _
.Offset(rowOffset:=row, columnOffset:=column) _
.PasteSpecial Paste:=xlPasteValues

'Copy-Paste TaylorLengthScale Lumsden
Worksheets("Engine Modeling Output").Range("ao200:ao1698").Copy
Worksheets("OUTPUT").Range("aa101:aa1599") _
.Offset(rowOffset:=row, columnOffset:=column) _
.PasteSpecial Paste:=xlPasteValues

'Copy-Paste Re Turbulent Lumsden
Worksheets("Engine Modeling Output").Range("ap200:ap1698").Copy
Worksheets("OUTPUT").Range("ab101:ab1599") _
.Offset(rowOffset:=row, columnOffset:=column) _
.PasteSpecial Paste:=xlPasteValues

'Copy-Paste Damkohler Lumsden
Worksheets("Engine Modeling Output").Range("aq200:aq1698").Copy
Worksheets("OUTPUT").Range("ac101:ac1599") _
.Offset(rowOffset:=row, columnOffset:=column) _
.PasteSpecial Paste:=xlPasteValues

'Copy-Paste Turbulent Intensity Lumsden
Worksheets("Engine Modeling Output").Range("ar200:ar1698").Copy
Worksheets("OUTPUT").Range("ad101:ad1599") _
.Offset(rowOffset:=row, columnOffset:=column) _
.PasteSpecial Paste:=xlPasteValues

'Copy-Paste dR/dt (flame speed - derivative of flame radius wrt. time)
Worksheets("Engine Modeling Output").Range("bd200:bd1698").Copy
Worksheets("OUTPUT").Range("ae101:ae1599") _
.Offset(rowOffset:=row, columnOffset:=column) _
.PasteSpecial Paste:=xlPasteValues

'Copy-Paste knocking noise
Worksheets("Butterworth").Range("d45:d1543").Copy
Worksheets("OUTPUT").Range("af101:af1599") _
.Offset(rowOffset:=row, columnOffset:=column) _
.PasteSpecial Paste:=xlPasteValues

'Copy-Paste Laminar Flame Speed C8H18
Worksheets("Engine Modeling Output").Range("ah200:ah1698").Copy
Worksheets("OUTPUT").Range("ag101:ag1599") _
.Offset(rowOffset:=row, columnOffset:=column) _
.PasteSpecial Paste:=xlPasteValues

'Copy-Paste Laminar Flame Speed H2
Worksheets("Engine Modeling Output").Range("ai200:ai1698").Copy
Worksheets("OUTPUT").Range("ah101:ah1599") _
.Offset(rowOffset:=row, columnOffset:=column) _
.PasteSpecial Paste:=xlPasteValues

'Copy-Paste dNO/dt
Worksheets("Engine Modeling Output").Range("be200:be1698").Copy
Worksheets("OUTPUT").Range("am101:am1599") _
.Offset(rowOffset:=row, columnOffset:=column) _
.PasteSpecial Paste:=xlPasteValues

'Copy-Paste Burned Volume Fraction
Worksheets("Engine Modeling Output").Range("bb200:bb1698").Copy
Worksheets("OUTPUT").Range("an101:an1599") _
.Offset(rowOffset:=row, columnOffset:=column) _
.PasteSpecial Paste:=xlPasteValues

'Copy-Paste Burned Mass Faction
Worksheets("Engine Modeling Output").Range("bc200:bc1698").Copy
Worksheets("OUTPUT").Range("ao101:ao1599") _
.Offset(rowOffset:=row, columnOffset:=column) _
.PasteSpecial Paste:=xlPasteValues

'Copy-Paste TurbIntZeroLANCASTER
Worksheets("Engine Modeling Output").Range("bf200:bf1698").Copy
Worksheets("OUTPUT").Range("ap101:ap1599") _
```

```
.Offset(rowOffset:=row, columnOffset:=column) _
.PasteSpecial Paste:=xlPasteValues

'Copy-Paste TurbIntLANCASTER
Worksheets("Engine Modeling Output").Range("bg200:bg1698").Copy
Worksheets("OUTPUT").Range("aq101:aq1599") _
.Offset(rowOffset:=row, columnOffset:=column) _
.PasteSpecial Paste:=xlPasteValues

'Copy-Paste TurbConstLANCASTER
Worksheets("Engine Modeling Output").Range("bh200:bh1698").Copy
Worksheets("OUTPUT").Range("ar101:ar1599") _
.Offset(rowOffset:=row, columnOffset:=column) _
.PasteSpecial Paste:=xlPasteValues

'Copy-Paste SlUnStrech
Worksheets("Engine Modeling Output").Range("bi200:bi1698").Copy
Worksheets("OUTPUT").Range("as101:as1599") _
.Offset(rowOffset:=row, columnOffset:=column) _
.PasteSpecial Paste:=xlPasteValues


'Copy-Paste FSR_LANCASTER
Worksheets("Engine Modeling Output").Range("bj200:bj1698").Copy
Worksheets("OUTPUT").Range("at101:at1599") _
.Offset(rowOffset:=row, columnOffset:=column) _
.PasteSpecial Paste:=xlPasteValues

'Copy-Paste FSRActual
Worksheets("Engine Modeling Output").Range("bk200:bk1698").Copy
Worksheets("OUTPUT").Range("au101:au1599") _
.Offset(rowOffset:=row, columnOffset:=column) _
.PasteSpecial Paste:=xlPasteValues

'Copy-Paste FERI_Factor_LANCASTER
Worksheets("Engine Modeling Output").Range("bl200:bl1698").Copy
Worksheets("OUTPUT").Range("av101:av1599") _
.Offset(rowOffset:=row, columnOffset:=column) _
.PasteSpecial Paste:=xlPasteValues

'Copy-Paste StLANCASTER
Worksheets("Engine Modeling Output").Range("bm200:bm1698").Copy
Worksheets("OUTPUT").Range("aw101:aw1599") _
.Offset(rowOffset:=row, columnOffset:=column) _
.PasteSpecial Paste:=xlPasteValues

'Copy-Paste SlLUMSDAN STRETCHED
Worksheets("Engine Modeling Output").Range("bn200:bn1698").Copy
Worksheets("OUTPUT").Range("ax101:ax1599") _
.Offset(rowOffset:=row, columnOffset:=column) _
.PasteSpecial Paste:=xlPasteValues

'Copy-Paste TaylorLengthScaleLANCASTER
Worksheets("Engine Modeling Output").Range("bo200:bo1698").Copy
Worksheets("OUTPUT").Range("ay101:ay1599") _
.Offset(rowOffset:=row, columnOffset:=column) _
.PasteSpecial Paste:=xlPasteValues

'Copy-Paste ReTurbLANCASTER
Worksheets("Engine Modeling Output").Range("bp200:bp1698").Copy
Worksheets("OUTPUT").Range("az101:az1599") _
.Offset(rowOffset:=row, columnOffset:=column) _
.PasteSpecial Paste:=xlPasteValues

'Copy-Paste DamkohlerLANCASTER
Worksheets("Engine Modeling Output").Range("bq200:bq1698").Copy
Worksheets("OUTPUT").Range("ba101:ba1599") _
.Offset(rowOffset:=row, columnOffset:=column) _
.PasteSpecial Paste:=xlPasteValues

'Copy-Paste uSlC8H18Lumsden
Worksheets("Engine Modeling Output").Range("br200:br1698").Copy
Worksheets("OUTPUT").Range("bb101:bb1599") _
.Offset(rowOffset:=row, columnOffset:=column) _
.PasteSpecial Paste:=xlPasteValues

'Copy-Paste uSlH2Lumsden
Worksheets("Engine Modeling Output").Range("bs200:bs1698").Copy
Worksheets("OUTPUT").Range("bc101:bc1599") _
.Offset(rowOffset:=row, columnOffset:=column) _
.PasteSpecial Paste:=xlPasteValues

'Copy-Paste uSlC8H18Lancaster
Worksheets("Engine Modeling Output").Range("bt200:bt1698").Copy
Worksheets("OUTPUT").Range("bd101:bd1599") _
.Offset(rowOffset:=row, columnOffset:=column) _
.PasteSpecial Paste:=xlPasteValues

'Copy-Paste uSlH2Lancaster
Worksheets("Engine Modeling Output").Range("bu200:bu1698").Copy
Worksheets("OUTPUT").Range("be101:be1599") _
.Offset(rowOffset:=row, columnOffset:=column) _
.PasteSpecial Paste:=xlPasteValues

'Copy-Paste FlameRadiusNORMALIZED
Worksheets("Engine Modeling Output").Range("bv200:bv1698").Copy
Worksheets("OUTPUT").Range("bf101:bf1599") _
.Offset(rowOffset:=row, columnOffset:=column) _
.PasteSpecial Paste:=xlPasteValues

'Update screen
Application.ScreenUpdating = True

i = i + 1

'Call Function DeleteRows from this module. It also makes sure that
'it does not delete the last calculation. DeleteRows gets the next cycle
If i < TotalCycleNumber Then
DeleteCycles (i)
End If

'If we analyse more then one cycle then we need to update
'the offset parameters to avoid copy-pasting data over each other
row = row + 1500
   column = 0
      RowIndicated = 0
         ColumnIndicated = ColumnIndicated + 1

Loop Until i = TotalCycleNumber

   'Turn OFF Progress Indicator
   Unload UserForm2

'Automatically calculates everything in the open workbook
SpeedCalculation

End Sub

'++++++++++++++++++++++++++++++++++++++++++++++
++++++++++++++++++++++++++++
'The sole purpose of the code below is to find the next cycle on the
'input sheet and copy and paste it into the right cells so
'that the analysis can be carried out.
'
'      WARNING!!!!!!      WARNING!!!!!!      WARNING!!!!!!
'
'The code below highly relies on the following:
'Cycle always starts from row 61. Therefore any insertion or deletion
'of rows must be adjusted here. It also therefore obvious that function
'FindStartOfCycle has very little function. In fact the only thing it is
'good for is to put an alert message on is the cycle does not start from
'row 61.
'The pressure voltage always has to be in column d
'Sawtooth voltage always has to be in column e
'If you want to change it then it must be changed here as well
'++++++++++++++++++++++++++++++++++++++++++


Private Sub DeleteCycles(Cycle As Integer)

Dim N, StartCycle, EndCycle As Integer

N = 0
EndCycle = FindEndOfCycle(Cycle)
StartCycle = FindStartOfCycle()


'If EndCycle <1475 than We not copy-paste the entire cycle.
If StartCycle = 0 Or EndCycle = 0 Or EndCycle < 1475 Then

   MsgBox "Did NOT delete anything. Check cut-paste range. End of cycle
maybe not in range."
   Exit Sub

Else
   'This will increase the speed of calculation by 25%
   Application.ScreenUpdating = False
   Sheets("INPUT").Select
   Range("A1").Select
   'Make sure that the copy-paste ranges are equal size.
   'Also if ranges are adjusted then the while loop counter
   'must be updated as well.
 Worksheets("INPUT").Range(Cells(EndCycle,  4),  Cells(65000,  4)).Copy
ActiveSheet.Paste  Destination:=Worksheets("INPUT").Range(Cells(61,  4),
Cells(65000 - EndCycle + 61, 4))

   Worksheets("INPUT").Range(Cells(EndCycle, 5), Cells(65000, 5)).Copy
   ActiveSheet.Paste Destination:=Worksheets("INPUT").Range(Cells(61,
5), Cells(65000 - EndCycle + 61, 5))

   Application.ScreenUpdating = True

End If
```

```
End Sub

Private Function FindEndOfCycle(Cycle As Integer) As Integer

Dim row, column As Integer
Dim angle As Variant
row = 1000
column = 8

   angle = Worksheets("INPUT").Range("h1:h1520").Value
   Do
     row = row + 1
     'Angle = Worksheets("INPUT").Cells(row, column).Value

        If row = 2000 Then
        MsgBox "End of cycle (545deg.) was NOT detected in 2000 rows."
& _
        "First check the rows manually and then check the code as well."
        Exit Do
        End If

   Loop Until angle(row, 1) = 545 Or angle(row, 1) > 545 'loops until
angle = 545 or becomes larger

If row = 2000 Then
FindEndOfCycle = 0
Else
FindEndOfCycle = row
End If

End Function

Private Function FindStartOfCycle() As Integer

Dim row, column As Integer
Dim angle As Variant

row = 60
column = 8

angle = Worksheets("INPUT").Range("h1:h1520").Value
   Do
     row = row + 1
     'Angle = Worksheets("INPUT").Cells(row, column).Value

        If row = 500 Then
MsgBox "Start of Cycle (-175deg.) was NOT detected in 500" & _
        "rows. First check the rows manually and then check the code as
well."
        Exit Do
        End If

  Loop Until angle(row, 1) = -175 Or angle(row, 1) > -175

            If Not (row = 61) Then
MsgBox "Someone inserted a row on this sheet. Start of cycle" & _
            "should be from row 61. If you want to change it then in" &
_
"DeleteRow the range have to be changed as well, otherwise it will NOT
delete properly"
            row = 500
            End If

  'MsgBox "FindStartOfCycle Angle  " & Angle(row, 1)
If row = 500 Then
FindStartOfCycle = 0
Else
FindStartOfCycle = row
End If

End Function

'Ask user which Data Set to see
Sub ViewRawData()

Dim N As Variant
Dim Message, Title, Default

Message = "Which Cycle's Data do you want to see?" & _
        "Type in an integer between 0-40." & _
          "If you don't see any data then RUN 'Analyse Cycle' first."
   Title = "View Row Data"

      Default = "1"

        N = InputBox(Message, Title, Default)

          If N <= 0 Or N > 40 Or N = False Then
            MsgBox "Sorry. Nothing selected." & _
              "Next time type in an integer between 0-40. Or Do NOT
press cancel."
                Exit Sub
            End If

Worksheets("OUTPUT").Activate
Range("A100").Offset(rowOffset:=(1500 * (N - 1)),
columnOffset:=0).Select

End Sub
```

G.5 Average Cycles

```
Option Explicit     'forces the declaration of all variables
Option Base 1       'the address of first element in array is 1

Sub AverageCombustion()

Dim Data() As Variant

Dim T As Double, a As Double, i As Double, Avg As Variant, b As Double, x
As Double
Dim c As Double
Dim DataAverage() As Variant
ReDim DataAverage(1590, 57)

Data = Worksheets("OUTPUT").Range("b101:bf61000").Value

i = 1, b = 0,a = 0, T = 0, c = 1

 While c <= 57
      i = 1
      While i < 1500
         x = 1, b = 0, a = 0, T = 0, Avg = ""
         While x <= 40
              If IsEmpty(Data(i + b, c)) = "False" And IsNumeric(Data(i
+ b, c)) Then
                 a = a + 1
                 T = T + Data(i + b, c)
                 Avg = T / a
              End If
           b = b + 1500
           x = x + 1
         Wend

      DataAverage(i, c) = Avg

      i = i + 1
      Wend

 c = c + 1
 Wend

'sheet must be activated first, otherwise the command
Sheets("OUTPUT").Select
Range("b100").Select
Worksheets("OUTPUT").Range("b101:bf1590").Value = DataAverage

Sheets("OUTPUT").Select
Range("w16").Select
End Sub
```

G.6 Chemical Equilibrium

```
'=========================================
'The following program based on the paper called RAPID COMPUTATION
OF CHEMICAL EQUILIBRIUM COMPOSITION: An Application to
Hydrocarbon Combustion W.D. Erickson (NASA-Langley Research Center)
and R.K. Prabhu (PRC Kentron,Inc)
'Published in AIChE Journal July 1986 Vol.32,No.7
'=========================================
'=                    Implemented and Modified by Ferenc Hamori
'=                          University of Melbourne
'=                            (-:June - 2002:-)
'=========================================
'                     MODIFICATIONS TO ORIGINAL ALGORITHM
'All equations have been fully re-derived.
'No modifications have been made except two:
'Equation 33 (on page 1083 in the above reference)= b0 = f0 -(g0*(mol
of H2O)*(mol ratio of CO/CO2))
'This should be the following:
'b0 = f0 +(g0*(mol of H2O)*(mol ratio of CO/CO2))
'consequently the derivative of b0, which is b0' OR in this program refer to
as 'db0, should have "POSITIVE" coefficients front of each of its terms
'this must have been a typing error since it is a simple derivation
'With the above modifications the published results are reproduced
exactly.
'=========================================
```

```
Option Explicit     'forces the declaration of all variables
Option Base 1       'the address of first element in array is 1

'public declaration can be used by all modules in the workbook
'privte declaration can be used by only the module is has been declared

Private Const Po As Double = 100325    'standard state pressure (Pa)
Private Const Runi As Double = 8.31451 'universal gas constant (J/molK)

'Fundamentals of Physics Extended (Halliday, Resnick ...) Appendix D p.A7
Private Const MassH2O As Double = 18.01534  'molecular mass g/mol
Private Const MassCO2 As Double = 44.00995  'molecular mass g/mol
Private Const MassCO As Double = 28.01055   'molecular mass g/mol
Private Const MassO2 As Double = 31.9988    'molecular mass g/mol
Private Const MassH2 As Double = 2.01594    'molecular mass g/mol
Private Const MassN2 As Double = 28.0134    'molecular mass g/mol
Private Const MassH As Double = 1.00797     'molecular mass g/mol
Private Const MassO As Double = 15.9994     'molecular mass g/mol
Private Const MassOH As Double = 17.00737   'molecular mass g/mol
Private Const MassNO As Double = 30.0061    'molecular mass g/mol
Private Const MassC As Double = 12.01115    'molecular mass g/mol
Private Const MassN As Double = 14.0067     'molecular mass g/mol

Private CpH2O() As Double           'specific heat (J/mol K)
Private CpCO2() As Double           'specific heat (J/mol K)
Private CpCO() As Double            'specific heat (J/mol K)
Private CpO2() As Double            'specific heat (J/mol K)
Private CpH2() As Double            'specific heat (J/mol K)
Private CpN2() As Double            'specific heat (J/mol K)
Private CpH() As Double             'specific heat (J/mol K)
Private CpO() As Double             'specific heat (J/mol K)
Private CpOH() As Double            'specific heat (J/mol K)
Private CpNO() As Double            'specific heat (J/mol K)
Private CpC() As Double             'specific heat (J/mol K)
Private CpN() As Double             'specific heat (J/mol K)
Private CpAverage() As Double       'average burned Cp (J/mol K)
Private MolecularWeightAverage() As Double 'average molecular weight of
burned mixture
Private GammaAverage() As Double    'R=Cp-Cv , Gamma = Cp/Cv ,
MolecularWeight = Runi/Rgas

Private UnburnedCpAverage() As Double
Private UnburnedMolecularWeightAverage() As Double
Private UnburnedGammaAverage() As Double
Private UnburnedEnthalpyAverage() As Double

Private EnthalpyH2O() As Double     'enthalpy (J/mol K)
Private EnthalpyCO2() As Double     'enthalpy (J/mol K)
Private EnthalpyCO() As Double      'enthalpy (J/mol K)
Private EnthalpyO2() As Double      'enthalpy (J/mol K)
Private EnthalpyH2() As Double      'enthalpy (J/mol K)
Private EnthalpyN2() As Double      'enthalpy (J/mol K)
Private EnthalpyH() As Double       'enthalpy (J/mol K)
Private EnthalpyO() As Double       'enthalpy (J/mol K)
Private EnthalpyOH() As Double      'enthalpy (J/mol K)
Private EnthalpyNO() As Double      'enthalpy (J/mol K)
Private EnthalpyC() As Double       'enthalpy (J/mol K)
Private EnthalpyN() As Double       'enthalpy (J/mol K)
Private EnthalpyAverage() As Double 'enthalpy (J/mol K)

Private Tmin As Double              'minimum temperature (K)
Private Tmax As Double              'maximum temperature (K)
Private Tstep As Double             'stepsize in temperature (K)
Private Density As Double           'density (kg/m^3)
Private FuelWeight As Double        'molecular weight of fuel (g/mol)
Private FuelEnthalpyOfFormation As Double 'fuel's enthalpy of formation at
25deg. (KJ/Kmol)
Private Hp() As Double              'enthalpy of formation of product kJ/kmol
Private Hr() As Double              'enthalpy of formation of reactant kJ/kmol
Private HpMinusHr() As Double       ' Hp - Hr
Private AdibaticFlameTemp As Double ' adiabatic flame temperature (K)
Private FuelAirTemp As Double       'fuel air temperature
Private UnburnedFuelAirTemp As Double 'unburned fuel air temperature
(K)
Private FuelType As Variant         'type of fuel
Private NumberOfCarbon As Double    'number of carbon in the fuel
Private NumberOfHydrogen As Double  'number of hydrogen atom in HC
fuel
Private FuelEnthalpy() As Double    'enthalpy of fuel
Private FuelSpecificHeat() As Double 'specific heat of fuel
Private VaryFuelAirTemp As Variant  'the unburned fuel air temperature
can be fixed or varied
Private HrPerfect() As Double       'Hr of combustion without dissociation
Private HpPerfect() As Double       'Hp of combustion without dissociation
Private CalorificPerfect() As Double 'calorific value of perfect combustion
Private AdibaticFlameTempPerfect As Double 'adiabatic flame temperature
without dissociation

Private aa As Double
Private bb As Double
Private cc As Double
Private dd As Double
Private ee As Double
Private ff As Double

Private molHmolC As Double          'mol H / mol C
Private molNmolO As Double          'mol N / mol O
Private molCOmolCO2 As Double       'mol CO / mol CO2
Private RatiomolCOmolCO2() As Double 'mol CO / mol CO2 for printing
Private RmolO As Double             'reactant mol of Oxygen
Private RmolC As Double             'reactant mol of Carbon
Private RmolH As Double             'reactant mol of Hydrogen
Private RmolN As Double             'reactant mol of Nitrogen

Private PmolH2O() As Double         'product mol of H2O (mol
Private PmolCO2() As Double         'product mol of CO2
Private PmolCO() As Double          'product mol of CO
Private PmolO2() As Double          'product mol of O2
Private PmolH2() As Double          'product mol of H2
Private PmolN2() As Double          'product mol of N2
Private PmolH() As Double           'product mol of H
Private PmolO() As Double           'product mol of O
Private PmolOH() As Double          'product mol of OH
Private PmolNO() As Double          'product mol of NO
Private PmassTOTAL() As Double      'mass of the product in grams
Private PmolTOTAL() As Double       'total number of mols in product
Private RmolTOTAL As Double         'mass of reactants in grams

Private Lambda As Double            'actual AFR / stoichiometric AFR
Private Phi As Double               '1 / Lambda

Private ErrorLimit As Double        'error limit

Private K1() As Double              'equilibrium constant of reaction
CO+H2O=CO2+H2 (nondimensional)
Private K2() As Double              'equilibrium constant of reaction
2CO2=2CO+O2 (mol/kg)
Private K3() As Double              'equilibrium constant of reaction
H2+O2=2OH (nondimensional)
Private K4() As Double              'equilibrium constant of reaction H2=2H
(mol/kg)
Private K5() As Double              'equilibrium constant of reaction O2=2O
(mol/kg)
Private K6() As Double              'equilibrium constant of reaction
O2+N2=2NO (nondimensional)
Private Ka() As Double              'Ka=(K4/(K2K3))^0.5
Private Kb() As Double              'Kb=(K2K5)^0.5
Private Kc() As Double              'Kc=K1K2K3
Private Kd() As Double              'Kd=K2K6

'constant coefficients
Private a00 As Double, a01 As Double, a02 As Double, a03 As Double
Private a10 As Double, a11 As Double, a12 As Double, a13 As Double
Private a20 As Double, a21 As Double, a22 As Double, a23 As Double
Private f00 As Double, f01 As Double, f02 As Double, f03 As Double, f04
As Double
Private f10 As Double, f11 As Double, f12 As Double, f13 As Double, f14
As Double
Private g00 As Double, g01 As Double, g02 As Double, g03 As Double, g04
As Double
Private a0 As Double, a1 As Double, a2 As Double
Private f0 As Double, f1 As Double
Private g0 As Double
Private da0 As Double, da1 As Double, da2 As Double
Private db0 As Double, db1 As Double
Private b0 As Double, b1 As Double

Private FunctionOFCOtoCO2 As Double 'function of CO/CO2
Private dFunctionOFCOtoCO2 As Double 'derivative of the function
FunctionOFCOtoCO2

Private TotalSteps As Double        'total steps between min and max
temperature
Private N() As Double               'number of iteration

'This program comes up with a progress indicator.
'UserForm2 calls Main_ChemicalEquilibriumCompositionInput
'to see it for your self go to UserForm2 right click and go to properties
Sub StartProressIndicatorAndAnalysis4()
UserForm4.Show
End Sub

Sub Main_ChemicalEquilibriumCompositionInput()

'get input from "Equilibrium Table Input" worksheet
GetInput

'resize arrays dynamically
ResizeArrays

'calculate mol numbers of carbon hydrogen oxygen and nitrogen
MolNumbersOf_C_H_O_N

'start iteration
```

```
IterationLoop

'Turn OFF Progress Indicator
Unload UserForm4

PrintToScreen

End Sub
 Sub GetInput()

Dim Temp As Double

If Engine_Simulation.Combustion = "off" Then
'Tmax = Worksheets("Equilibrium Table Input").Range("e6").Value
Tmax =
Engine_Simulation.BurnedTemperature(Engine_Simulation.CyclePosition)
Else
Tmax =
Engine_Simulation.BurnedTemperature(Engine_Simulation.CyclePosition +
1)
End If
'Tstep = Worksheets("Equilibrium Table Input").Range("e7").Value
Tstep = 0.01
'Tmin = Worksheets("Equilibrium Table Input").Range("e5").Value
Tmin = Tmax - 0.01
'Lambda = Worksheets("Equilibrium Table Input").Range("e8").Value
Lambda = Engine_Simulation.Lambda
'Density = Worksheets("Equilibrium Table Input").Range("e9").Value
Density =
Engine_Simulation.BurnedGasDensity(Engine_Simulation.CyclePosition)
'molHmolC = Worksheets("Equilibrium Table Input").Range("e14").Value
molHmolC = 4
'molNmolO = Worksheets("Equilibrium Table Input").Range("e15").Value
molNmolO = Engine_Simulation.VolumeFractionOfN2toO2
'molCOmolCO2 = Worksheets("Equilibrium Table
Input").Range("e16").Value
molCOmolCO2 = 2000
'ErrorLimit = Worksheets("Equilibrium Table Input").Range("e18").Value
ErrorLimit = 0.0000000001
'FuelWeight = Worksheets("Equilibrium Table Input").Range("e19").Value
FuelWeight = 16.043
'FuelEnthalpyOfFormation = Worksheets("Equilibrium Table
Input").Range("e20").Value
FuelEnthalpyOfFormation = -74873
'FuelAirTemp = Worksheets("Equilibrium Table
Input").Range("e21").Value
FuelAirTemp = Tmax
'FuelType = Worksheets("Equilibrium Table Input").Range("e11").Value
FuelType = Engine_Simulation.MainChamberFuel
'VaryFuelAirTemp = Worksheets("Equilibrium Table
Input").Range("e22").Value
VaryFuelAirTemp = "yes"
'UnburnedFuelAirTemp = Worksheets("Equilibrium Table
Input").Range("e23").Value
UnburnedFuelAirTemp =
Engine_Simulation.UnburnedTemperature(Engine_Simulation.CyclePosition
)

'If VaryFuelAirTemp = "yes" Then
'MsgBox "Hr and Hp values of all Fuels are valid up 3500K." & _
'       "Results above 3500K are inconclusive!"
'End If

If FuelType = "Methane" Then
Temp = 1
ElseIf FuelType = "Propane" Then
Temp = 2
ElseIf FuelType = "Isooctane" Then
Temp = 3
ElseIf FuelType = "Gasoline 1" Then
Temp = 4
ElseIf FuelType = "Gasoline 2" Then
Temp = 5
ElseIf FuelType = "Diesel" Then
Temp = 6
ElseIf FuelType = "Hydrogen" Then
Temp = 7
Else
Temp = 0
MsgBox "Fuel type is not recognised. Default settings will be used off the
screen."
End If

If Temp > 0 Then
NumberOfCarbon = Worksheets("Equilibrium Table Input").Cells(4 +
Temp, 11).Value
NumberOfHydrogen = Worksheets("Equilibrium Table Input").Cells(4 +
Temp, 12).Value
molHmolC = Worksheets("Equilibrium Table Input").Cells(4 + Temp,
13).Value
FuelWeight = Worksheets("Equilibrium Table Input").Cells(4 + Temp,
14).Value
FuelEnthalpyOfFormation = Worksheets("Equilibrium Table Input").Cells(4
+ Temp, 15).Value
aa = Worksheets("Equilibrium Table Input").Cells(4 + Temp, 16).Value
bb = Worksheets("Equilibrium Table Input").Cells(4 + Temp, 17).Value
cc = Worksheets("Equilibrium Table Input").Cells(4 + Temp, 18).Value
dd = Worksheets("Equilibrium Table Input").Cells(4 + Temp, 19).Value
ee = Worksheets("Equilibrium Table Input").Cells(4 + Temp, 20).Value
ff = Worksheets("Equilibrium Table Input").Cells(4 + Temp, 21).Value
End If

Phi = 1 / Lambda
TotalSteps = (Abs(Tmax - Tmin) / Tstep) + 1    'example -2,-1,0,1,2,
which is (2+2)+1=5 total steps

End Sub
'dynamically  resize arrays
Private Sub ResizeArrays()

ReDim K1(TotalSteps)
ReDim K2(TotalSteps)
ReDim K3(TotalSteps)
ReDim K4(TotalSteps)
ReDim K5(TotalSteps)
ReDim K6(TotalSteps)
ReDim Ka(TotalSteps)
ReDim Kb(TotalSteps)
ReDim Kc(TotalSteps)
ReDim Kd(TotalSteps)
ReDim N(TotalSteps)
ReDim PmolH2O(TotalSteps)
ReDim PmolCO2(TotalSteps)
ReDim PmolCO(TotalSteps)
ReDim PmolO2(TotalSteps)
ReDim PmolH2(TotalSteps)
ReDim PmolN2(TotalSteps)
ReDim PmolH(TotalSteps)
ReDim PmolO(TotalSteps)
ReDim PmolOH(TotalSteps)
ReDim PmolNO(TotalSteps)
ReDim N(TotalSteps)
ReDim PmolTOTAL(TotalSteps)
ReDim PmassTOTAL(TotalSteps)
ReDim RatiomolCOmolCO2(TotalSteps)
ReDim HpMinusHr(TotalSteps)
ReDim Hp(TotalSteps)
ReDim Hr(TotalSteps)
ReDim FuelEnthalpy(TotalSteps)
ReDim FuelSpecificHeat(TotalSteps)
ReDim HrPerfect(TotalSteps)
ReDim HpPerfect(TotalSteps)
ReDim CalorificPerfect(TotalSteps)
ReDim CpAverage(TotalSteps)
ReDim MolecularWeightAverage(TotalSteps)
ReDim GammaAverage(TotalSteps)

ReDim CpH2O(TotalSteps)
ReDim CpCO2(TotalSteps)
ReDim CpCO(TotalSteps)
ReDim CpO2(TotalSteps)
ReDim CpH2(TotalSteps)
ReDim CpN2(TotalSteps)
ReDim CpH(TotalSteps)
ReDim CpO(TotalSteps)
ReDim CpOH(TotalSteps)
ReDim CpNO(TotalSteps)
ReDim CpC(TotalSteps)
ReDim CpN(TotalSteps)

ReDim EnthalpyH2O(TotalSteps)
ReDim EnthalpyCO2(TotalSteps)
ReDim EnthalpyCO(TotalSteps)
ReDim EnthalpyO2(TotalSteps)
ReDim EnthalpyH2(TotalSteps)
ReDim EnthalpyN2(TotalSteps)
ReDim EnthalpyH(TotalSteps)
ReDim EnthalpyO(TotalSteps)
ReDim EnthalpyOH(TotalSteps)
ReDim EnthalpyNO(TotalSteps)
ReDim EnthalpyC(TotalSteps)
ReDim EnthalpyN(TotalSteps)
ReDim EnthalpyAverage(TotalSteps)

ReDim UnburnedCpAverage(TotalSteps)
ReDim UnburnedMolecularWeightAverage(TotalSteps)
ReDim UnburnedGammaAverage(TotalSteps)
ReDim UnburnedEnthalpyAverage(TotalSteps)

End Sub
'important to note that the composition is calculated for 1 kg of
'substance NOT 1kg or 1mol of fuel
Private Sub MolNumbersOf_C_H_O_N()
```

```
RmolO = 500 / (MassO / 2 + (MassN2 / 2) * molNmolO / 2 + Phi *
((MassC + molHmolC) / (4 * MassH + molHmolC)))
RmolC = 2 * MassH * RmolO * Phi / (4 * MassH + molHmolC)
RmolH = 2 * MassH * (RmolO * Phi - 2 * MassH * RmolC)
RmolN = (1000 - MassC * RmolC - RmolH - MassO *RmolO) / (MassN2/ 2)

RmolTOTAL = MassO * RmolO + MassC * RmolC + MassH * RmolH +
(MassN2 / 2) * RmolN

End Sub
Private Sub IterationLoop()

Dim i As Long, j As Long
Dim TempBurned As Double
Dim y1 As Double
Dim ErrorActual As Double
Dim Temp As Double, tempy As Double
Dim quadratic As Double
Dim PctDone As Double
Dim HpMinusHrSmallest As Double
Dim RO2 As Double
Dim RN2 As Double
Dim PCO2 As Double
Dim PN2 As Double
Dim PH2O As Double
Dim PO2 As Double
Dim CalorificPerfectSmallest As Double

HpMinusHrSmallest = 1000000000000#
CalorificPerfectSmallest = 1000000000000#
Temp = molCOmolCO2
i = 1
TempBurned = Tmin
While TempBurned <= Tmax

   'calculates chemical equilibrium constants
   ChemicalEquilibriumConstants i, TempBurned
   'calculate constants based on Ka,Kb,Kc,Kd, and molC,molH,molO,molN
   ConstantCoefficients i

      y1 = Temp
      j = 1
      molCOmolCO2 = Temp 'COToCO2Predictor(T)
      ErrorActual = 1
      While ErrorActual >= ErrorLimit
      am_fm_g0

      PmolNO(i) = Kd(i) * ((1 + 8 * RmolN * molCOmolCO2 ^ 2 / Kd(i)) ^
0.5 - 1) / (4 * molCOmolCO2 ^ 2)

      b1 = f1
      b0 = f0 + (g0 * PmolNO(i) * molCOmolCO2 ^ 2)

      'calculate the derivative of am,b0,b1
      dam_db0_db1 i

      FunctionOFCOtoCO2 = a2 * b0 ^ 2 - a1 * b1 * b0 + a0 * b1 ^ 2

      dFunctionOFCOtoCO2 = b0 ^ 2 * da2 - _
                  b1 * b0 * da1 + _
                  b1 ^ 2 * da0 + _
                  (2 * a0 * b1 - a1 * b0) * db1 + _
                  (2 * a2 * b0 - a1 * b1) * db0

      y1 = molCOmolCO2 - FunctionOFCOtoCO2 / dFunctionOFCOtoCO2
      ErrorActual = 1 - (y1 / molCOmolCO2)
      molCOmolCO2 = y1
      j = j + 1
      N(i) = j1
      Wend

      PmolCO2(i) = Abs(RmolC / (molCOmolCO2 + 1))
      PmolCO(i) = Abs(molCOmolCO2 * RmolC / (molCOmolCO2 + 1))
      PmolO2(i) = Abs(K2(i) / (molCOmolCO2 ^ 2))
      PmolN2(i) = Abs((RmolN - PmolNO(i)) / 2)
      PmolO(i) = Abs((K2(i) * K5(i)) ^ 0.5 / molCOmolCO2)
      PmolH2O(i) = Abs(-b0 / b1)
PmolOH(i) = Abs((RmolH - 2 * PmolH2O(i) * (1 + K1(i) * molCOmolCO2))
            / (Ka(i) * molCOmolCO2 + 1))
PmolH(i) = Abs(((K4(i) / (K2(i) * K3(i))) ^ 0.5 * molCOmolCO2 *
PmolOH(i)))
      PmolH2(i) = Abs(K1(i) * PmolH2O(i) * PmolCO(i) / PmolCO2(i))

      RatiomolCOmolCO2(i) = molCOmolCO2
PmassTOTAL(i) = (MassNO * PmolNO(i) + MassCO2 * PmolCO2(i) +
MassCO * PmolCO(i) + MassO2 * PmolO2(i) + MassN2 * PmolN2(i) +
MassO * PmolO(i) + MassH2 * PmolH2(i) + MassOH * PmolOH(i) +
MassH * PmolH(i) + MassH2O * PmolH2O(i))

'calculate the enthalpy of formation, at a given temp Hr=Hp, this
temperature is the adiabatic flame temperature,
'the following includes dissociation
      If VaryFuelAirTemp = "yes" Then
      FuelAirTemp = TempBurned
      End If

      If FuelType = "Hydrogen" Then

            Hr(i) = (((RmolH) * (HTwo(FuelAirTemp, i)) / 2) + _
                  (RmolO * OTwo(FuelAirTemp, i) / 2) + _
                  (RmolN * NTwo(FuelAirTemp, i) / 2)) * (2 / RmolH)

'all enthalpy values are zero at 298 therefore h0 must be add to it
            Hp(i) = (PmolNO(i) * (90291 + NO(TempBurned, i)) + _
                  PmolCO2(i) * (-393522 + COTwo(TempBurned, i)) + _
                  PmolCO(i) * (-110527 + CO(TempBurned, i)) + _
                  PmolO2(i) * (OTwo(TempBurned, i)) + _
                  PmolN2(i) * (NTwo(TempBurned, i)) + _
                  PmolO(i) * (249170 + O(TempBurned, i)) + _
                  PmolH2(i) * (HTwo(TempBurned, i)) + _
                  PmolOH(i) * (38987 + OH(TempBurned, i)) + _
                  PmolH(i) * (217999 + Hydrogen(TempBurned, i)) + _
                  PmolH2O(i) * (-241826 + HTwoO(TempBurned, i))) * _
                  (2 / RmolH)
      Else
         'Hr and Hp is per kmol of fuel
            Hr(i) = (((RmolC / NumberOfCarbon) *
(EnthalpyAndSpecificHeat(FuelAirTemp, i))) + _
                  (RmolO * OTwo(FuelAirTemp, i) / 2) + _
                  (RmolN * NTwo(FuelAirTemp, i) / 2)) *
(NumberOfCarbon / RmolC)
'all enthalpy values are zero at 298 therefore h0 must be add to it
            Hp(i) = (PmolNO(i) * (90291 + NO(TempBurned, i)) + _
                  PmolCO2(i) * (-393522 + COTwo(TempBurned, i)) + _
                  PmolCO(i) * (-110527 + CO(TempBurned, i)) + _
                  PmolO2(i) * (OTwo(TempBurned, i)) + _
                  PmolN2(i) * (NTwo(TempBurned, i)) + _
                  PmolO(i) * (249170 + O(TempBurned, i)) + _
                  PmolH2(i) * (HTwo(TempBurned, i)) + _
                  PmolOH(i) * (38987 + OH(TempBurned, i)) + _
                  PmolH(i) * (217999 + Hydrogen(TempBurned, i)) + _
                  PmolH2O(i) * (-241826 + HTwoO(TempBurned, i))) * _
                  (NumberOfCarbon / RmolC)

      End If
      'when you divide by the fuel weight then the result is the calorific
value of
      'the fuel in KJ/kg, basically to convert from j/mol to j/g OR kJ/kg
      HpMinusHr(i) = (Hr(i) - Hp(i)) / (FuelWeight)

      If Abs(HpMinusHr(i)) < HpMinusHrSmallest Then
      AdibaticFlameTemp = TempBurned
      HpMinusHrSmallest = Abs(HpMinusHr(i))
      End If

      'the following calculates perfect combustion. No dissociation
      'Van Wylen p.559
      If FuelType = "Hydrogen" Then
         RO2 = Lambda * 0.5
         RN2 = RO2 * molNmolO
         PCO2 = 0
         PN2 = RO2 * molNmolO
         PH2O = 1
         PO2 = Lambda - 1
      Else
         RO2 = Lambda * (NumberOfCarbon + NumberOfHydrogen / 4)
         RN2 = Lambda * (NumberOfCarbon + NumberOfHydrogen / 4) *
molNmolO
         PCO2 = NumberOfCarbon
         PN2 = RO2 * molNmolO
         PH2O = NumberOfHydrogen / 2
      PO2 = (Lambda - 1) * (NumberOfCarbon + NumberOfHydrogen / 4)
      End If

      If FuelType = "Hydrogen" Then

      HrPerfect(i) = HTwo(FuelAirTemp, i) + _
                  RO2 * OTwo(FuelAirTemp, i) + _
                  RN2 * NTwo(FuelAirTemp, i)
      Else

      HrPerfect(i) = EnthalpyAndSpecificHeat(FuelAirTemp, i) + _
                  RO2 * OTwo(FuelAirTemp, i) + _
                  RN2 * NTwo(FuelAirTemp, i)
      End If
      'all enthalpy values are zero at 298 therefore h0 must be add to it
      HpPerfect(i) = PCO2 * (-393522 + COTwo(TempBurned, i)) + _
                  PN2 * (NTwo(TempBurned, i)) + _
                  PH2O * (-241826 + HTwoO(TempBurned, i)) + _
                  PO2 * OTwo(TempBurned, i)
      'dividing with fuel weight will give the calorific value
      CalorificPerfect(i) = (HrPerfect(i) - HpPerfect(i)) / FuelWeight

      If Abs(CalorificPerfect(i)) < CalorificPerfectSmallest Then
```

```
        AdibaticFlameTempPerfect = TempBurned
        CalorificPerfectSmallest = Abs(CalorificPerfect(i))
        End If

         'to make sure all the Cp and enthalpy vales are correctly
        'stored in the arrays for printing purposes
        NO TempBurned, i
        COTwo TempBurned, i
        CO TempBurned, i
        OTwo TempBurned, i
        NTwo TempBurned, i
        O TempBurned, i
        HTwo TempBurned, i
        OH TempBurned, i
        Hydrogen TempBurned, i
        HTwoO TempBurned, i
        EnthalpyAndSpecificHeat FuelAirTemp, i

        'calculate average burned Cp value (J/mol K)
        PmolTOTAL(i) = PmolNO(i) + PmolCO2(i) + PmolCO(i) + _
                       PmolO2(i) + PmolN2(i) + PmolO(i) + _
                       PmolH2(i) + PmolOH(i) + PmolH(i) + PmolH2O(i)

        'to calculate Cp: SUM ( molar fraction * Cp + Enthalpy * (derivative
molar fraction wrt. temperature)
        'we skip i=1 because we don't have information on i=0
        'OR we can calculate the enthalpy at T1 and T2 then Cp=DH/DT
        If i = 1 Then
        'CpAverage(i) = (CpNO(i) * (PmolNO(i) / PmolTOTAL(i))) + _
                       (CpCO2(i) * (PmolCO2(i) / PmolTOTAL(i))) + _
                       (CpCO(i) * (PmolCO(i) / PmolTOTAL(i))) + _
                       (CpO2(i) * (PmolO2(i) / PmolTOTAL(i))) + _
                       (CpN2(i) * (PmolN2(i) / PmolTOTAL(i))) + _
                       (CpO(i) * (PmolO(i) / PmolTOTAL(i))) + _
                       (CpH2(i) * (PmolH2(i) / PmolTOTAL(i))) + _
                       (CpOH(i) * (PmolOH(i) / PmolTOTAL(i))) + _
                       (CpH(i) * (PmolH(i) / PmolTOTAL(i))) + _
                       (CpH2O(i) * (PmolH2O(i) / PmolTOTAL(i)))
        'all enthalpy values are zero at 298 therefore h0 must be add to it
        EnthalpyAverage(i) = ((90291 + EnthalpyNO(i)) * (PmolNO(i) /
PmolTOTAL(i))) + _
                             ((-393522 + EnthalpyCO2(i)) * (PmolCO2(i) /
PmolTOTAL(i))) + _
                             ((-110527 + EnthalpyCO(i)) * (PmolCO(i) /
PmolTOTAL(i))) + _
                             (EnthalpyO2(i) * (PmolO2(i) / PmolTOTAL(i))) + _
                             (EnthalpyN2(i) * (PmolN2(i) / PmolTOTAL(i))) + _
                             ((249170 + EnthalpyO(i)) * (PmolO(i) /
PmolTOTAL(i))) + _
                             (EnthalpyH2(i) * (PmolH2(i) / PmolTOTAL(i))) + _
                             ((38987 + EnthalpyOH(i)) * (PmolOH(i) /
PmolTOTAL(i))) + _
                             (EnthalpyH(i) * (PmolH(i) / PmolTOTAL(i))) + _
                             ((-241826 + EnthalpyH2O(i)) * (PmolH2O(i) /
PmolTOTAL(i)))

        Else


        'CpAverage(i) = (CpNO(i) * (PmolNO(i) / PmolTOTAL(i)) + _
                        (90291 + EnthalpyNO(i)) * ((PmolNO(i) / PmolTOTAL(i))
- (PmolNO(i - 1) / PmolTOTAL(i - 1))) / Tstep) + _
                        (CpCO2(i) * (PmolCO2(i) / PmolTOTAL(i)) + _
                        (-393522 + EnthalpyCO2(i)) * ((PmolCO2(i) /
PmolTOTAL(i)) - (PmolCO2(i - 1) / PmolTOTAL(i - 1))) / Tstep) + _
                        (CpCO(i) * (PmolCO(i) / PmolTOTAL(i)) + _
                        (-110527 + EnthalpyCO(i)) * ((PmolCO(i) / PmolTOTAL(i))
- (PmolCO(i - 1) / PmolTOTAL(i - 1))) / Tstep) + _
                        (CpO2(i) * (PmolO2(i) / PmolTOTAL(i)) + _
                        EnthalpyO2(i) * ((PmolO2(i) / PmolTOTAL(i)) - (PmolO2(i
- 1) / PmolTOTAL(i - 1))) / Tstep) + _
                        (CpN2(i) * (PmolN2(i) / PmolTOTAL(i)) + _
                        EnthalpyN2(i) * ((PmolN2(i) / PmolTOTAL(i)) - (PmolN2(i
- 1) / PmolTOTAL(i - 1))) / Tstep) + _
                        (CpO(i) * (PmolO(i) / PmolTOTAL(i)) + _
                        (249170 + EnthalpyO(i)) * ((PmolO(i) / PmolTOTAL(i)) -
(PmolO(i - 1) / PmolTOTAL(i - 1))) / Tstep) + _
                        (CpH2(i) * (PmolH2(i) / PmolTOTAL(i)) + _
                        EnthalpyH2(i) * ((PmolH2(i) / PmolTOTAL(i)) - (PmolH2(i
- 1) / PmolTOTAL(i - 1))) / Tstep) + _
                        (CpOH(i) * (PmolOH(i) / PmolTOTAL(i)) + _
                        (38987 + EnthalpyOH(i)) * ((PmolOH(i) / PmolTOTAL(i)) -
(PmolOH(i - 1) / PmolTOTAL(i - 1))) / Tstep) + _
                        (CpH(i) * (PmolH(i) / PmolTOTAL(i)) + _
                        EnthalpyH(i) * ((PmolH(i) / PmolTOTAL(i)) - (PmolH(i - 1)
/ PmolTOTAL(i - 1))) / Tstep) + _
                        (CpH2O(i) * (PmolH2O(i) / PmolTOTAL(i)) + _
                        (-241826 + EnthalpyH2O(i)) * ((PmolH2O(i) /
PmolTOTAL(i)) - (PmolH2O(i - 1) / PmolTOTAL(i - 1))) / Tstep)

       'all enthalpy values are zero at 298 therefore h0 must be add to it
        EnthalpyAverage(i) = ((90291 + EnthalpyNO(i)) * (PmolNO(i) /
PmolTOTAL(i))) + _
                             ((-393522 + EnthalpyCO2(i)) * (PmolCO2(i) /
PmolTOTAL(i))) + _
                             ((-110527 + EnthalpyCO(i)) * (PmolCO(i) /
PmolTOTAL(i))) + _
                             (EnthalpyO2(i) * (PmolO2(i) / PmolTOTAL(i))) + _
                             (EnthalpyN2(i) * (PmolN2(i) / PmolTOTAL(i))) + _
                             ((249170 + EnthalpyO(i)) * (PmolO(i) /
PmolTOTAL(i))) + _
                             (EnthalpyH2(i) * (PmolH2(i) / PmolTOTAL(i))) + _
                             ((38987 + EnthalpyOH(i)) * (PmolOH(i) /
PmolTOTAL(i))) + _
                             (EnthalpyH(i) * (PmolH(i) / PmolTOTAL(i))) + _
                             ((-241826 + EnthalpyH2O(i)) * (PmolH2O(i) /
PmolTOTAL(i)))

       'Cp=DH/DT
        CpAverage(i) = (EnthalpyAverage(i) - EnthalpyAverage(i - 1)) / Tstep

         'this is in g/mol OR kg/kmol
        MolecularWeightAverage(i) = (MassNO * (PmolNO(i) /
PmolTOTAL(i))) + _
                                    (MassCO2 * (PmolCO2(i) / PmolTOTAL(i))) + _
                                    (MassCO * (PmolCO(i) / PmolTOTAL(i))) + _
                                    (MassO2 * (PmolO2(i) / PmolTOTAL(i))) + _
                                    (MassN2 * (PmolN2(i) / PmolTOTAL(i))) + _
                                    (MassO * (PmolO(i) / PmolTOTAL(i))) + _
                                    (MassH2 * (PmolH2(i) / PmolTOTAL(i))) + _
                                    (MassOH * (PmolOH(i) / PmolTOTAL(i))) + _
                                    (MassH * (PmolH(i) / PmolTOTAL(i))) + _
                                    (MassH2O * (PmolH2O(i) / PmolTOTAL(i)))

        'convert from J/molK to kJ/KgK
        CpAverage(i) = CpAverage(i) / MolecularWeightAverage(i)
        'R=Cp-Cv , Gamma = Cp/Cv , MolecularWeight = Runi/Rgas
        GammaAverage(i) = CpAverage(i) / (CpAverage(i) - (Runi /
MolecularWeightAverage(i)))

        'to convert from J/mol to J/g, (J/mol)/(g/mol)= J/g = kJ/kg
        EnthalpyAverage(i) = EnthalpyAverage(i) /
MolecularWeightAverage(i)

        End If

'=======calculate unburned properties===========
        'first calculate Cp and Enthalpy of Unburned Gas
        OTwo UnburnedFuelAirTemp, i
        NTwo UnburnedFuelAirTemp, i
        HTwo UnburnedFuelAirTemp, i

        EnthalpyAndSpecificHeat UnburnedFuelAirTemp, i

        UnburnedMolecularWeightAverage(i) = (((Phi / (NumberOfCarbon +
NumberOfHydrogen / 4)) * FuelWeight + _
                              MassO2 + molNmolO * MassN2) / _
  ((Phi / (NumberOfCarbon + NumberOfHydrogen / 4)) + 1 + molNmolO))

        'same answer different method
        'UnburnedMolecularWeightAverage(i) = ((RmolC /
NumberOfCarbon+RmolH/2) * FuelWeight + _
RmolO * MassO2 / 2 +   RmolN * MassN2 / 2) /
((RmolC / NumberOfCarbon) + (RmolO + RmolN) / 2)

        If FuelType = "Hydrogen" Then

UnburnedCpAverage(i) = ((Phi / (NumberOfCarbon + NumberOfHydrogen
/ 4)) * CpH2(i) * FuelWeight + CpO2(i) + molNmolO * CpN2(i)) /
((Phi / (NumberOfCarbon + NumberOfHydrogen / 4)) + 1 + molNmolO)

        Else

UnburnedCpAverage(i) = ((Phi / (NumberOfCarbon + NumberOfHydrogen
/ 4)) * FuelSpecificHeat(i) * FuelWeight +  CpO2(i) + molNmolO *
CpN2(i)) /  ((Phi / (NumberOfCarbon + NumberOfHydrogen / 4)) + 1 +
molNmolO)

        End If

        'convert from J/molK to kJ/KgK
        UnburnedCpAverage(i) = UnburnedCpAverage(i) /
UnburnedMolecularWeightAverage(i)

        UnburnedGammaAverage(i) = UnburnedCpAverage(i) /
(UnburnedCpAverage(i) - (Runi / UnburnedMolecularWeightAverage(i)))
         'MsgBox "UnburnedGammaAverage(i) " & UnburnedGammaAverage(i)

        If FuelType = "Hydrogen" Then
UnburnedEnthalpyAverage(i) = ((Phi / (NumberOfCarbon +
NumberOfHydrogen / 4)) * EnthalpyH2(i) + EnthalpyO2(i) + molNmolO *
EnthalpyN2(i)) / ((Phi / (NumberOfCarbon + NumberOfHydrogen / 4)) + 1
+ molNmolO)
```

```
        Else
UnburnedEnthalpyAverage(i) = ((Phi / (NumberOfCarbon +
NumberOfHydrogen / 4)) * FuelEnthalpy(i) + EnthalpyO2(i) + molNmolO
* EnthalpyN2(i)) / ((Phi / (NumberOfCarbon + NumberOfHydrogen / 4)) +
1 + molNmolO)
        'same answer different method
        'UnburnedEnthalpyAverage(i) = ((RmolC / NumberOfCarbon) *
FuelEnthalpy(i) + RmolO * EnthalpyO2(i) / 2 + RmolN * EnthalpyN2(i) /
2) / ((RmolC / NumberOfCarbon) + (RmolO + RmolN) / 2)
        End If

        'to convert from j/mol to j/g = kJ/kg
        UnburnedEnthalpyAverage(i) = UnburnedEnthalpyAverage(i) /
UnburnedMolecularWeightAverage(i)

        OTwo TempBurned, i
        NTwo TempBurned, i
        HTwo UnburnedFuelAirTemp, i
        EnthalpyAndSpecificHeat FuelAirTemp, i

    i = i + 1
    TempBurned = TempBurned + Tstep
   Wend

If Engine_Simulation.Combustion = "off" Then
'============DATA FOR ENGINE SIMULATION========
Engine_Simulation.BurnedEnthalpy(Engine_Simulation.CyclePosition) =
EnthalpyAverage(i - 1)
Engine_Simulation.BurnedCp(Engine_Simulation.CyclePosition) =
CpAverage(i - 1) * 1000
Engine_Simulation.BurnedGamma(Engine_Simulation.CyclePosition) =
GammaAverage(i - 1)
Engine_Simulation.BurnedMolecularWeight(Engine_Simulation.CyclePositio
n) = MolecularWeightAverage(i -
1Engine_Simulation.BurnedTemperature(Engine_Simulation.CyclePosition)
= Tmax
Engine_Simulation.UnburnedEnthalpy(Engine_Simulation.CyclePosition) =
UnburnedEnthalpyAverage(i - 1)
Engine_Simulation.UnburnedCp(Engine_Simulation.CyclePosition) =
UnburnedCpAverage(i - 1) * 1000
Engine_Simulation.UnburnedGamma(Engine_Simulation.CyclePosition) =
UnburnedGammaAverage(i - 1)
Engine_Simulation.UnburnedMolecularWeight(Engine_Simulation.CyclePosi
tion) = UnburnedMolecularWeightAverage(i - 1)
Engine_Simulation.UnburnedTemperature(Engine_Simulation.CyclePosition
) = UnburnedFuelAirTemp
Engine_Simulation.O2molfrac(Engine_Simulation.CyclePosition) =
PmolO2(i - 1) / PmolTOTAL(i - 1)
Engine_Simulation.N2molfrac(Engine_Simulation.CyclePosition) =
PmolN2(i - 1) / PmolTOTAL(i - 1)
Engine_Simulation.Omolfrac(Engine_Simulation.CyclePosition) = PmolO(i -
1) / PmolTOTAL(i - 1)
Engine_Simulation.H2molfrac(Engine_Simulation.CyclePosition) =
PmolH2(i - 1) / PmolTOTAL(i - 1)
Engine_Simulation.OHmolfrac(Engine_Simulation.CyclePosition) =
PmolOH(i - 1) / PmolTOTAL(i - 1)
Engine_Simulation.Hmolfrac(Engine_Simulation.CyclePosition) = PmolH(i -
1) / PmolTOTAL(i - 1)
Engine_Simulation.NOmolfrac(Engine_Simulation.CyclePosition) =
PmolNO(i - 1) / PmolTOTAL(i - 1)
Engine_Simulation.COmolfrac(Engine_Simulation.CyclePosition) =
PmolCO(i - 1) / PmolTOTAL(i - 1)
Engine_Simulation.CO2molfrac(Engine_Simulation.CyclePosition) =
PmolCO2(i - 1) / PmolTOTAL(i - 1)
Engine_Simulation.H2Omolfrac(Engine_Simulation.CyclePosition) =
PmolH2O(i - 1) / PmolTOTAL(i - 1)

'MsgBox "UnburnedTemperature(CyclePosition) after 1  " &
UnburnedTemperature(CyclePosition)
'MsgBox "UnburnedTemperature(CyclePosition) after 2  " &
UnburnedFuelAirTemp
'============DATA FOR ENGINE SIMULATION========
Else 'this means that combustion and expansion is "on"
'============DATA FOR ENGINE SIMULATION====
Engine_Simulation.BurnedEnthalpy(Engine_Simulation.CyclePosition + 1)
= EnthalpyAverage(i - 1)
Engine_Simulation.BurnedCp(Engine_Simulation.CyclePosition + 1) =
CpAverage(i - 1) * 1000
Engine_Simulation.BurnedGamma(Engine_Simulation.CyclePosition + 1) =
GammaAverage(i - 1)
Engine_Simulation.BurnedMolecularWeight(Engine_Simulation.CyclePositio
n + 1) = MolecularWeightAverage(i - 1)
Engine_Simulation.BurnedTemperature(Engine_Simulation.CyclePosition +
1) = Tmax                'burned temperature (m^3)
Engine_Simulation.UnburnedEnthalpy(Engine_Simulation.CyclePosition +
1) = UnburnedEnthalpyAverage(i - 1)
Engine_Simulation.UnburnedCp(Engine_Simulation.CyclePosition + 1) =
UnburnedCpAverage(i - 1) * 1000
Engine_Simulation.UnburnedGamma(Engine_Simulation.CyclePosition + 1)
= UnburnedGammaAverage(i - 1)
Engine_Simulation.UnburnedMolecularWeight(Engine_Simulation.CyclePosi
tion + 1) = UnburnedMolecularWeightAverage(i - 1)
Engine_Simulation.UnburnedTemperature(Engine_Simulation.CyclePosition
+ 1) = UnburnedFuelAirTemp
Engine_Simulation.O2molfrac(Engine_Simulation.CyclePosition + 1) =
PmolO2(i - 1) / PmolTOTAL(i - 1)
Engine_Simulation.N2molfrac(Engine_Simulation.CyclePosition + 1) =
PmolN2(i - 1) / PmolTOTAL(i - 1)
Engine_Simulation.Omolfrac(Engine_Simulation.CyclePosition + 1) =
PmolO(i - 1) / PmolTOTAL(i - 1)
Engine_Simulation.H2molfrac(Engine_Simulation.CyclePosition + 1) =
PmolH2(i - 1) / PmolTOTAL(i - 1)
Engine_Simulation.OHmolfrac(Engine_Simulation.CyclePosition + 1) =
PmolOH(i - 1) / PmolTOTAL(i - 1)
Engine_Simulation.Hmolfrac(Engine_Simulation.CyclePosition + 1) =
PmolH(i - 1) / PmolTOTAL(i - 1)
Engine_Simulation.NOmolfrac(Engine_Simulation.CyclePosition + 1) =
PmolNO(i - 1) / PmolTOTAL(i - 1)
Engine_Simulation.COmolfrac(Engine_Simulation.CyclePosition + 1) =
PmolCO(i - 1) / PmolTOTAL(i - 1)
Engine_Simulation.CO2molfrac(Engine_Simulation.CyclePosition + 1) =
PmolCO2(i - 1) / PmolTOTAL(i - 1)
Engine_Simulation.H2Omolfrac(Engine_Simulation.CyclePosition + 1) =
PmolH2O(i - 1) / PmolTOTAL(i - 1)

'MsgBox "UnburnedTemperature(CyclePosition) after 1  " &
UnburnedTemperature(CyclePosition)
'MsgBox "UnburnedTemperature(CyclePosition) after 2  " &
UnburnedFuelAirTemp
'============DATA FOR ENGINE SIMULATION============
End If

End Sub

Private Sub ConstantCoefficients(i As Long)

a00 = 0, a01 = RmolH ^ 2, a02 = 0, a03 = 0,

a10 = -Kc(i), a11 = -2 * (2 * RmolH + Ka(i) * Kc(i))
a12 = -(4 * RmolH * K1(i) + Ka(i) ^ 2 * Kc(i)), a13 = 0

a20 = 0, a21 = 4, a22 = 8 * K1(i), a23 = 4 * K1(i) ^ 2

f00 = 2 * K2(i), f01 = 2 * K2(i) * (Ka(i) + 1) + Kb(i)
f02 = 2 * RmolC + RmolH - RmolO + (Ka(i) + 1) * Kb(i) + 2 * K2(i) *
Ka(i)
f03 = RmolC + RmolH - RmolO + (2 * RmolC - RmolO + Kb(i)) * Ka(i)
f04 = (RmolC - RmolO) * Ka(i)

f10 = 0, f11 = 0, f12 = -1, f13 = Ka(i) - 2 * K1(i) – 1, f14 = Ka(i) - 2 *
K1(i)

g00 = 1, g01 = Ka(i) + 1, g02 = Ka(i), g03 = 0, g04 = 0

End Sub

Private Sub am_fm_g0()

a0 = a00 * molCOmolCO2 ^ 0 +  a01 * molCOmolCO2 ^ 1 + _
    a02 * molCOmolCO2 ^ 2 +  a03 * molCOmolCO2 ^ 3

a1 = a10 * molCOmolCO2 ^ 0 +  a11 * molCOmolCO2 ^ 1 + _
    a12 * molCOmolCO2 ^ 2 +  a13 * molCOmolCO2 ^ 3

a2 = a20 * molCOmolCO2 ^ 0 +  a21 * molCOmolCO2 ^ 1 + _
    a22 * molCOmolCO2 ^ 2 +  a23 * molCOmolCO2 ^ 3

f0 = f00 * molCOmolCO2 ^ 0 + f01 * molCOmolCO2 ^ 1 + _
    f02 * molCOmolCO2 ^ 2 +  f03 * molCOmolCO2 ^ 3 + _
    f04 * molCOmolCO2 ^ 4

f1 = f10 * molCOmolCO2 ^ 0 +  f11 * molCOmolCO2 ^ 1 + _
    f12 * molCOmolCO2 ^ 2 +  f13 * molCOmolCO2 ^ 3 + _
    f14 * molCOmolCO2 ^ 4

g0 = g00 * molCOmolCO2 ^ 0 +  g01 * molCOmolCO2 ^ 1 + _
    g02 * molCOmolCO2 ^ 2

End Sub

Private Sub dam_db0_db1(i As Long)

da0 = 1 * a01 * molCOmolCO2 ^ (1 - 1) +  2 * a02 * molCOmolCO2 ^ (2
- 1) +  3 * a03 * molCOmolCO2 ^ (3 - 1)

da1 = 1 * a11 * molCOmolCO2 ^ (1 - 1) +  2 * a12 * molCOmolCO2 ^ (2
- 1) +  3 * a13 * molCOmolCO2 ^ (3 - 1)

da2 = 1 * a21 * molCOmolCO2 ^ (1 - 1) + 2 * a22 * molCOmolCO2 ^ (2
- 1) + 3 * a23 * molCOmolCO2 ^ (3 - 1)
```

```
db0 = (1 * f01 * molCOmolCO2 ^ (1 - 1) +  2 * f02 * molCOmolCO2 ^ (2
- 1) + 3 * f03 * molCOmolCO2 ^ (3 - 1) + 4 * f04 * molCOmolCO2 ^ (4 -
1)) + (2 * RmolN * g0 * molCOmolCO2 / (1 + 8 * RmolN * molCOmolCO2
^ 2 / Kd(i)) ^ 0.5) + ((PmolNO(i) * molCOmolCO2 ^ 2) * _
 (1 * g01 * molCOmolCO2 ^ (1 - 1) + 2 * g02 * molCOmolCO2 ^ (2 - 1)))

db1 = 2 * f12 * molCOmolCO2 ^ (2 - 1) + 3 * f13 * molCOmolCO2 ^ (3 -
1) +  4 * f14 * molCOmolCO2 ^ (4 - 1)

End Sub

'calculates chemical equilibrium constants
Private Sub ChemicalEquilibriumConstants(i As Long, T As Double)

If T < 800 Then

K1(i) = Exp(-11.57237455 + 5255.720327 / T + 0.963983548 * Log(T))
ElseIf T <= 2600 Then
K1(i) = Exp(-11.9272694 + 5193.652143 / T + 1.028507725 * Log(T))
ElseIf T <= 6000 Then
K1(i) = Exp(-9.909148122 + 4728.778939 / T + 0.794050571 * Log(T))
End If

If T < 800 Then
K2(i) = Exp(15.46000703 - 67772.09865 / T + 0.775350574 * Log(T))
ElseIf T <= 6000 Then
K2(i) = Exp(30.29863775 - 69188.10297 / T - 1.183030086 * Log(T))
End If

K2(i) = K2(i) * Po / (Density * Runi * T)

If T < 800 Then
K3(i) = Exp(4.816179157 - 9554.576917 / T - 0.142344554 * Log(T))
ElseIf T <= 2700 Then
K3(i) = Exp(6.425541503 - 9664.769073 / T - 0.362677534 * Log(T))
ElseIf T <= 6000 Then
K3(i) = Exp(8.409105456 - 10346.71181 / T - 0.581935879 * Log(T))
End If

If T < 800 Then
K4(i) = Exp(1.961933959 - 51996.32664 / T + 1.480004645 * Log(T))
ElseIf T <= 2500 Then
K4(i) = Exp(4.625824934 - 52329.02896 / T + 1.142582468 * Log(T))
ElseIf T <= 6000 Then
K4(i) = Exp(11.88394574 - 54344.01821 / T + 0.316507726 * Log(T))
End If

K4(i) = K4(i) * Po / (Density * Runi * T)

If T < 800 Then
K5(i) = Exp(4.809240422 - 59545.69665 / T + 1.390327107 * Log(T))
ElseIf T <= 3000 Then
K5(i) = Exp(10.90845007 - 60205.26137 / T + 0.599378092 * Log(T))
ElseIf T <= 6000 Then
K5(i) = Exp(15.22619616 - 61463.43787 / T + 0.111185095 * Log(T))
End If

K5(i) = K5(i) * Po / (Density * Runi * T)

If T < 800 Then
K6(i) = Exp(2.739818862 - 21709.61337 / T + 0.037210039 * Log(T))
ElseIf T <= 3000 Then
K6(i) = Exp(3.134533396 - 21774.49065 / T - 0.009597538 * Log(T))
ElseIf T <= 6000 Then
K6(i) = Exp(6.890002885 - 22968.60817 / T - 0.429515129 * Log(T))
End If

Ka(i) = (K4(i) / (K2(i) * K3(i))) ^ 0.5
Kb(i) = (K2(i) * K5(i)) ^ 0.5
Kc(i) = K1(i) * K2(i) * K3(i)
Kd(i) = K2(i) * K6(i)

End Sub

Private Sub PrintToScreen()

Application.ScreenUpdating = False

Dim i As Long
Dim j As Long
Dim T As Double
Dim TempArray() As Variant

ReDim TempArray(1 To TotalSteps + 20, 1 To 55)

'temperature
TempArray(4, 2) = "Temperature (K)"
'H2O
TempArray(4, 3) = "1-H2O (mol/kg)"
TempArray(4, 3 + 23) = "1-H2O (Cp-j/molK)"
TempArray(4, 3 + 36) = "1-H2O (h-j/molK)"
'CO2
TempArray(4, 4) = "2-CO2 (mol/kg)"
TempArray(4, 4 + 23) = "2-CO2 (Cp-j/molK)"
TempArray(4, 4 + 36) = "2-CO2 (h-j/molK)"
'C0
TempArray(4, 5) = "3-CO (mol/kg)"
TempArray(4, 5 + 23) = "3-CO (Cp-j/molK)"
TempArray(4, 5 + 36) = "3-CO (h-j/molK)"
'O2
TempArray(4, 6) = "4-O2 (mol/kg)"
TempArray(4, 6 + 23) = "4-O2 (Cp-j/molK)"
TempArray(4, 6 + 36) = "4-O2 (h-j/molK)"
'H2
TempArray(4, 7) = "5-H2 (mol/kg)"
TempArray(4, 7 + 23) = "5-H2 (Cp-j/molK)"
TempArray(4, 7 + 36) = "5-H2 (h-j/molK)"
'N2
TempArray(4, 8) = "6-N2 (mol/kg)"
TempArray(4, 8 + 23) = "6-N2 (Cp-j/molK)"
TempArray(4, 8 + 36) = "6-N2 (h-j/molK)"
'H
TempArray(4, 9) = "7-H (mol/kg)"
TempArray(4, 9 + 23) = "7-H (Cp-j/molK)"
TempArray(4, 9 + 36) = "7-H (h-j/molK)"
'O
TempArray(4, 10) = "8-O (mol/kg)"
TempArray(4, 10 + 23) = "8-O (Cp-j/molK)"
TempArray(4, 10 + 36) = "8-O (h-j/molK)"
'OH
TempArray(4, 11) = "9-OH (mol/kg)"
TempArray(4, 11 + 23) = "9-OH (Cp-j/molK)"
TempArray(4, 11 + 36) = "9-OH (h-j/molK)"
'NO
TempArray(4, 12) = "10-NO (mol/kg)"
TempArray(4, 12 + 23) = "10-NO (Cp-j/molK)"
TempArray(4, 12 + 36) = "10-NO (h-j/molK)"
'iteration
TempArray(4, 13) = "iteration"
'total grams/kg mixture
TempArray(4, 14) = "product grams/kg"
'total reactant mols/kg mixture
TempArray(4, 15) = "reactant grams"
'ratio of CO / CO2
TempArray(4, 16) = "ratio of CO / CO2"
'Hp-Hr
TempArray(4, 17) = "Hp - Hr"
'adiabatic flame temperature
TempArray(4, 18) = "Adiabatic Flame Temp. (K)"
'Hr
TempArray(4, 19) = "Hr"
'Hp
TempArray(4, 20) = "Hp"
'Fuel Specific Heat
TempArray(4, 21) = "Fuel Specific Heat"
'Hr perfect combustion
TempArray(4, 22) = "Hr Perfect"
'Hp perfect combustion
TempArray(4, 23) = "Hp Perfect"
'calorific value at perfect combustion
TempArray(4, 24) = "CalorificPerfect"
'adiabatic flame temperature of perfect combustion NO DISSOCIATION
TempArray(4, 25) = "Adiabatic Flame Temp. Perfect"

i = 1
T = Tmin
While T <= Tmax

    'temperature
    TempArray(4 + i, 2) = T
    'H2O
    TempArray(4 + i, 3) = PmolH2O(i) / PmolTOTAL(i)
    'CO2
    TempArray(4 + i, 4) = PmolCO2(i) / PmolTOTAL(i)
    'C0
    TempArray(4 + i, 5) = PmolCO(i) / PmolTOTAL(i)
    'O2
    TempArray(4 + i, 6) = PmolO2(i) / PmolTOTAL(i)
    'H2
    TempArray(4 + i, 7) = PmolH2(i) / PmolTOTAL(i)
    'N2
    TempArray(4 + i, 8) = PmolN2(i) / PmolTOTAL(i)
    'H
    TempArray(4 + i, 9) = PmolH(i) / PmolTOTAL(i)
    'O
    TempArray(4 + i, 10) = PmolO(i) / PmolTOTAL(i)
    'OH
    TempArray(4 + i, 11) = PmolOH(i) / PmolTOTAL(i)
    'NO
    TempArray(4 + i, 12) = PmolNO(i) / PmolTOTAL(i)
    'iteration
    TempArray(4 + i, 13) = N(i)
    'total products grams/kg mixture
    TempArray(4 + i, 14) = PmassTOTAL(i)
```

```
        'total reactant mols/kg mixture
        TempArray(4 + i, 15) = RmolTOTAL
        'ratio of CO / CO2
        TempArray(4 + i, 16) = RatiomolCOmolCO2(i)
        'Hp-Hr
        TempArray(4 + i, 17) = HpMinusHr(i)
        'adiabatic flame temperature
        TempArray(4 + i, 18) = AdibaticFlameTemp
        'Hr
        TempArray(4 + i, 19) = Hr(i)
        'Hp
        TempArray(4 + i, 20) = Hp(i)
        'Fuel Specific heat
        TempArray(4 + i, 21) = FuelSpecificHeat(i)
        'Hr perfect combustion
        TempArray(4 + i, 22) = HrPerfect(i)
        'Hp perfect combustion
        TempArray(4 + i, 23) = HpPerfect(i)
        'calorific value at perfect combustion
        TempArray(4 + i, 24) = CalorificPerfect(i)
        'adiabatic flame temperature of perfect combustion NO
DISSOCIATION
        TempArray(4 + i, 25) = AdibaticFlameTempPerfect

        'adiabatic flame temperature
        TempArray(1, 1) = "Adiabatic Flame Temp. (K)"
        TempArray(1, 2) = AdibaticFlameTemp
        TempArray(2, 1) = "Adiabatic Flame Temp. NO Dissociation (K)"
        TempArray(2, 2) = AdibaticFlameTempPerfect
        'TempArray(3, 1) = (PmolNO(i) + PmolCO2(i) + PmolCO(i) + _
                    PmolO2(i) + PmolN2(i) + PmolO(i) + _
                    PmolH2(i) + PmolOH(i) + PmolH(i) + PmolH2O(i))

        'Cp of all the species
        TempArray(4 + i, 26) = CpH2O(i)
        TempArray(4 + i, 27) = CpCO2(i)
        TempArray(4 + i, 28) = CpCO(i)
        TempArray(4 + i, 29) = CpO2(i)
        TempArray(4 + i, 30) = CpH2(i)
        TempArray(4 + i, 31) = CpN2(i)
        TempArray(4 + i, 32) = CpH(i)
        TempArray(4 + i, 33) = CpO(i)
        TempArray(4 + i, 34) = CpOH(i)
        TempArray(4 + i, 35) = CpNO(i)
        TempArray(4, 36) = "Cp Average (KJ/KgK)"
        TempArray(4 + i, 36) = CpAverage(i)
        TempArray(4, 37) = "Gamma Average"
        TempArray(4 + i, 37) = GammaAverage(i)
        TempArray(4, 38) = "Molecular Weight Average (g/mol)"
        TempArray(4 + i, 38) = MolecularWeightAverage(i)

        'enthalpy
        TempArray(4 + i, 39) = EnthalpyH2O(i)
        TempArray(4 + i, 40) = EnthalpyCO2(i)
        TempArray(4 + i, 41) = EnthalpyCO(i)
        TempArray(4 + i, 42) = EnthalpyO2(i)
        TempArray(4 + i, 43) = EnthalpyH2(i)
        TempArray(4 + i, 44) = EnthalpyN2(i)
        TempArray(4 + i, 45) = EnthalpyH(i)
        TempArray(4 + i, 46) = EnthalpyO(i)
        TempArray(4 + i, 47) = EnthalpyOH(i)
        TempArray(4 + i, 48) = EnthalpyNO(i)
        TempArray(4 + i, 49) = EnthalpyC(i)
        TempArray(4 + i, 50) = EnthalpyN(i)

        TempArray(4 + i, 51) = UnburnedCpAverage(i)
        TempArray(4, 51) = "Unburned CpAverage"
        TempArray(4 + i, 52) = UnburnedMolecularWeightAverage(i)
        TempArray(4, 52) = "Unburned Molecular Weight Average"
        TempArray(4 + i, 53) = UnburnedGammaAverage(i)
        TempArray(4, 53) = "UnburnedGammaAverage"
        TempArray(4 + i, 54) = UnburnedEnthalpyAverage(i)
        TempArray(4, 54) = "UnburnedEnthalpyAverage kJ/kg"
        TempArray(4, 55) = "EnthalpyAverage kJ/kg"
        TempArray(4 + i, 55) = EnthalpyAverage(i)

'to print out on 58 rows only we need to divide total steps by 58
'we need o round because we do not want fractions
i = i + 1 ' Round(i / 58)
T = T + Tstep
Wend
Sheets("Equilibrium Table Output").Select
Range("A1").Select
Worksheets("Equilibrium Table Output").Range(Cells(1, 1),
Cells(TotalSteps + 20, 55)).Value = TempArray
'Sheets("Graph Output").Select
'Range("A1").Select
Sheets("Equilibrium Table Output").Select
Range("A1").Select
Application.ScreenUpdating = True

End Sub
```

```
'progress indicator
Private Sub UpdateProgress4(PctDone, T, Tmax)
    With UserForm4
        .Label2.Caption = Format(T, "0.0")
        .Label4.Caption = Format(Tmax, "0.0")
        .FrameProgress.Caption = Format(PctDone, "0.0%")
        .LabelProgress.Width = PctDone * (.FrameProgress.Width - 3)
        .Repaint
    End With
End Sub

'all equations are in the form of the "Shomate Equation"
Public Function NTwo(x As Double, tt As Long) As Double

Dim hh As Double
Dim Cp As Double
Dim Temperature As Double
Const a As Double = 26.092, Const b As Double = 8.218801
Const c As Double = -1.976141, Const d As Double = 0.159274
Const e As Double = 0.044434, Const f As Double = -7.98923

Temperature = x / 1000

   'Cp = heat capacity (J/mol*K)
    Cp = a + b * Temperature + c * Temperature ^ 2 + _
        d * Temperature ^ 3 + e / Temperature ^ 2
   'h = standard enthalpy (kJ/mol)
    hh = a * Temperature +  b * Temperature ^ 2 / 2 + _
        c * Temperature ^ 3 / 3 +  d * Temperature ^ 4 / 4 - _
        e / Temperature + f

CpN2(tt) = Cp
'to convert from kJ/mol to J/mol, kJ/mol = 1000*J/mol
EnthalpyN2(tt) = hh * 1000

NTwo = hh * 1000
End Function
Private Function OTwo(x As Double, tt As Long) As Double

Dim hh As Double
Dim Cp As Double
Dim Temperature As Double
Const a As Double = 29.659, Const b As Double = 6.137261
Const c As Double = -1.186521, Const d As Double = 0.09578
Const e As Double = -0.219663, Const f As Double = -9.861391

Temperature = x / 1000

   'Cp = heat capacity (J/mol*K)
    Cp = a + b * Temperature + c * Temperature ^ 2 + _
        d * Temperature ^ 3 + e / Temperature ^ 2
   'h = standard enthalpy (kJ/mol)
    hh = a * Temperature + _
        b * Temperature ^ 2 / 2 +  c * Temperature ^ 3 / 3 + _
        d * Temperature ^ 4 / 4 -  e / Temperature + f
CpO2(tt) = Cp
'to convert from kJ/mol to J/mol, kJ/mol = 1000*J/mol
EnthalpyO2(tt) = hh * 1000

OTwo = hh * 1000

End Function
Private Function O(x As Double, tt As Long) As Double

Dim hh As Double
Dim Cp As Double
Dim Temperature As Double
Const a As Double = 21.1861, Const b As Double = -0.502314
Const c As Double = 0.168694, Const d As Double = -0.008962
Const e As Double = 0.075664, Const f As Double = 243.1306

Temperature = x / 1000

   'Cp = heat capacity (J/mol*K)
    Cp = a + b * Temperature + c * Temperature ^ 2 + _
        d * Temperature ^ 3 + e / Temperature ^ 2
   'h = standard enthalpy (kJ/mol)
    hh = a * Temperature + _
        b * Temperature ^ 2 / 2 + c * Temperature ^ 3 / 3 + _
        d * Temperature ^ 4 / 4 -  e / Temperature + f

CpO(tt) = Cp
'to convert from kJ/mol to J/mol, kJ/mol = 1000*J/mol
EnthalpyO(tt) = hh * 1000 - 249170

O = hh * 1000 - 249170

End Function
Private Function COTwo(x As Double, tt As Long) As Double

Dim hh As Double, Dim Cp As Double, Dim Temperature As Double
```

```
Const a As Double = 24.99735, Const b As Double = 55.18696
Const c As Double = -33.69137, Const d As Double = 7.948387
Const e As Double = -0.136638, Const f As Double = -403.6075
Const g As Double = 58.16639, Const h As Double = 2.720074
Const i As Double = -0.492289, Const j As Double = 0.038844
Const k As Double = -6.447293, Const l As Double = -425.9186

Temperature = x / 1000
'temperature 1.2 or 1.7 or 1.5 represents 1200K, 1700K, 1500K
If Temperature < 1.2 Then

   'Cp = heat capacity (J/mol*K)
    Cp = a + b * Temperature + c * Temperature ^ 2 + _
        d * Temperature ^ 3 + e / Temperature ^ 2
   'hh = standard enthalpy (kJ/mol)
    hh = a * Temperature +  b * Temperature ^ 2 / 2 +  c * Temperature
^ 3 / 3 +  d * Temperature ^ 4 / 4 -  e / Temperature + f

Else

    'Cp = heat capacity (J/mol*K)
    Cp = g + h * Temperature + i * Temperature ^ 2 + j * Temperature ^
3 + k / Temperature ^ 2
    'h = standard enthalpy (kJ/mol)
    hh = g * Temperature + _
        h * Temperature ^ 2 / 2 + i * Temperature ^ 3 / 3 + _
        j * Temperature ^ 4 / 4 - k / Temperature + l

End If

CpCO2(tt) = Cp
'to convert from kJ/mol to J/mol, kJ/mol = 1000*J/mol
EnthalpyCO2(tt) = hh * 1000 + 393522

COTwo = hh * 1000 + 393522

End Function

Private Function CO(x As Double, tt As Long) As Double

Dim hh As Double, Dim Cp As Double
Dim Temperature As Double, Const a As Double = 25.56759
Const b As Double = 6.09613, Const c As Double = 4.054656
Const d As Double = -2.671301, Const e As Double = 0.131021
Const f As Double = -118.0089, Const g As Double = 35.1507
Const h As Double = 1.300095, Const i As Double = -0.205921
Const j As Double = 0.01355, Const k As Double = -3.28278
Const l As Double = -127.8375,

Temperature = x / 1000
'temperature 1.2 or 1.7 or 1.5 represents 1200K, 1700K, 1500K
If Temperature < 1.3 Then

   'Cp = heat capacity (J/mol*K)
    Cp = a + b * Temperature + c * Temperature ^ 2 + d * Temperature
^ 3 + e / Temperature ^ 2
   'hh = standard enthalpy (kJ/mol)
    hh = a * Temperature + b * Temperature ^ 2 / 2 +  c * Temperature
^ 3 / 3 +  d * Temperature ^ 4 / 4 -  e / Temperature + f

Else

    'Cp = heat capacity (J/mol*K)
    Cp = g + h * Temperature + i * Temperature ^ 2 + _
        j * Temperature ^ 3 + k / Temperature ^ 2
    'h = standard enthalpy (kJ/mol)
    hh = g * Temperature + h * Temperature ^ 2 / 2 + _
        i * Temperature ^ 3 / 3 + j * Temperature ^ 4 / 4 - _
        k / Temperature + l
End If

CpCO(tt) = Cp
'to convert from kJ/mol to J/mol, kJ/mol = 1000*J/mol
EnthalpyCO(tt) = hh * 1000 + 110527

CO = hh * 1000 + 110527
End Function
Private Function HTwoO(x As Double, tt As Long) As Double

Dim hh As Double, Dim Cp As Double, Dim Temperature As Double
Const a As Double = 30.092, Const b As Double = 6.832514
Const c As Double = 6.793435, Const d As Double = -2.53448
Const e As Double = 0.082139, Const f As Double = -250.881
Const g As Double = 41.96426, Const h As Double = 8.622053
Const i As Double = -1.49978, Const j As Double = 0.098119
Const k As Double = -11.15764, Const l As Double = -272.1797

Temperature = x / 1000
'temperature 1.2 or 1.7 or 1.5 represents 1200K, 1700K, 1500K
If Temperature < 1.7 Then

   'Cp = heat capacity (J/mol*K)
    Cp = a + b * Temperature + c * Temperature ^ 2 + d * Temperature
^ 3 + e / Temperature ^ 2
   'hh = standard enthalpy (kJ/mol)
    hh = a * Temperature + b * Temperature ^ 2 / 2 + _
        c * Temperature ^ 3 / 3 + d * Temperature ^ 4 / 4 - _
        e / Temperature + f

Else

    'Cp = heat capacity (J/mol*K)
    Cp = g + h * Temperature + i * Temperature ^ 2 + _
        j * Temperature ^ 3 + k / Temperature ^ 2
    'h = standard enthalpy (kJ/mol)
    hh = g * Temperature + h * Temperature ^ 2 / 2 +         i *
Temperature ^ 3 / 3 + j * Temperature ^ 4 / 4 - k / Temperature + l

End If

CpH2O(tt) = Cp
'to convert from kJ/mol to J/mol, kJ/mol = 1000*J/mol
EnthalpyH2O(tt) = hh * 1000 + 241826

HTwoO = hh * 1000 + 241826
End Function

Private Function OH(x As Double, tt As Long) As Double

Dim hh As Double, Dim Cp As Double, Dim Temperature As Double
Const a As Double = 32.27768, Const b As Double = -11.36291
Const c As Double = 13.60545, Const d As Double = -3.846486
Const e As Double = -0.001335, Const f As Double = 29.75113
Const g As Double = 28.74701, Const h As Double = 4.714489
Const i As Double = -0.814725, Const j As Double = 0.054748
Const k As Double = -2.747829, Const l As Double = 26.41439

Temperature = x / 1000
'temperature 1.2 or 1.7 or 1.5 represents 1200K, 1700K, 1500K
If Temperature < 1.3 Then

   'Cp = heat capacity (J/mol*K)
    Cp = a + b * Temperature + c * Temperature ^ 2 + d * Temperature
^ 3 + e / Temperature ^ 2
   'hh = standard enthalpy (kJ/mol)
    hh = a * Temperature + b * Temperature ^ 2 / 2 + _
        c * Temperature ^ 3 / 3 + d * Temperature ^ 4 / 4 - _
        e / Temperature + f

Else

    'Cp = heat capacity (J/mol*K)
    Cp = g + h * Temperature + i * Temperature ^ 2 + j * Temperature ^
3 + k / Temperature ^ 2
    'h = standard enthalpy (kJ/mol)
    hh = g * Temperature + h * Temperature ^ 2 / 2 + i * Temperature ^
3 / 3 + j * Temperature ^ 4 / 4 - k / Temperature + l
End If

CpOH(tt) = Cp
'to convert from kJ/mol to J/mol, kJ/mol = 1000*J/mol
EnthalpyOH(tt) = hh * 1000 - 38987

OH = hh * 1000 - 38987
End Function
'the reason the 10th order polynomial is used instead of the "Shomate
Equation"
'is because there is a large error associated at 1500K see:
'http://webbook.nist.gov/cgi/cbook.cgi?ID=C1333740&Type=JANAFG&Plot
=on&Units=SI&Mask=1#JANAFG
Private Function HTwo(x As Double, tt As Long) As Double

'constants for enthalpy
Const a As Double = 3.79147804130657E-32
Const b As Double = -1.22144863322508E-27
Const c As Double = 1.68074904780168E-23
Const d As Double = -1.27904185278065E-19
Const e As Double = 5.77314503694717E-16
Const f As Double = -1.50143513372571E-12
Const g As Double = 1.78259524177014E-09
Const h As Double = 6.17936620170937E-07
Const i As Double = -2.13429430625896E-03
Const j As Double = 30.334693248086
Const k As Double = -8902.85886883742
'constants for Cp
Const aH2 As Double = -2.00021565050997E-34
Const bH2 As Double = 7.15702862376145E-30
Const cH2 As Double = -1.11608367296818E-25
Const dH2 As Double = 9.92694414741561E-22
Const eH2 As Double = -5.52771925065681E-18
Const fH2 As Double = 1.98676455639382E-14
Const gH2 As Double = -4.5686144104651E-11
Const hhH2 As Double = 6.39514429415845E-08
```

```
Const iH2 As Double = -4.88525894406929E-05
Const jH2 As Double = 0.019560053641675
Const kH2 As Double = 25.9949865093975

' Cp heat capacity (J/mol K)
CpH2(tt) = ((((((((((aH2 * (x ^ 10)) + (bH2 * (x ^ 9))) + (cH2 * (x ^
8))) + (dH2 * (x ^ 7))) + (eH2 * (x ^ 6))) + (fH2 * (x ^ 5))) + (gH2 * (x
^ 4))) + (hhH2 * (x ^ 3))) + (iH2 * (x ^ 2))) + (jH2 * x)) + kH2)
'enthalpy (j / molK)
EnthalpyH2(tt) = ((((((((((a * (x ^ 10)) + (b * (x ^ 9))) + (c * (x ^ 8)))
+ (d * (x ^ 7))) + (e * (x ^ 6))) + (f * (x ^ 5))) + (g * (x ^ 4))) + (h *
(x ^ 3))) + (i * (x ^ 2))) + (j * x)) + k)

HTwo = EnthalpyH2(tt)

End Function

Private Function Hydrogen(x As Double, tt As Long) As Double

Dim hh As Double, Dim Cp As Double,  Dim Temperature As Double
Const a As Double = 20.78603, Const b As Double = 4.850638 * 10 ^ -10
Const c As Double = -1.582916 * 10 ^ -10, Const d As Double =
1.525102 * 10 ^ -11, Const e As Double = 3.196347 * 10 ^ -11
Const f As Double = 211.802

Temperature = x / 1000

  'Cp = heat capacity (J/mol*K)
   Cp = a + b * Temperature + c * Temperature ^ 2 + d * Temperature
^ 3 + e / Temperature ^ 2
  'h = standard enthalpy (kJ/mol)
   hh = a * Temperature + b * Temperature ^ 2 / 2 + _
      c * Temperature ^ 3 / 3 + d * Temperature ^ 4 / 4 - _
      e / Temperature + f

CpH(tt) = Cp
'to convert from kJ/mol to J/mol, kJ/mol = 1000*J/mol
EnthalpyH(tt) = hh * 1000 - 217999

Hydrogen = hh * 1000 - 217999
End Function

Private Function NO(x As Double, tt As Long) As Double

Dim hh As Double, Dim Cp As Double, Dim Temperature As Double
Const a As Double = 23.83491, Const b As Double = 12.58878
Const c As Double = -1.139011, Const d As Double = -1.497459
Const e As Double = 0.214194, Const f As Double = 83.35783
Const g As Double = 35.99169, Const h As Double = 0.95717
Const i As Double = -0.148032, Const j As Double = 0.009974
Const k As Double = -3.004088, Const l As Double = 73.10787

Temperature = x / 1000
'temperature 1.2 or 1.7 or 1.5 represents 1200K, 1700K, 1500K
If Temperature < 1.2 Then

  'Cp = heat capacity (J/mol*K)
   Cp = a + b * Temperature + c * Temperature ^ 2 + d * Temperature
^ 3 + e / Temperature ^ 2
  'hh = standard enthalpy (kJ/mol)
   hh = a * Temperature + _
      b * Temperature ^ 2 / 2 + c * Temperature ^ 3 / 3 + _
      d * Temperature ^ 4 / 4 -  e / Temperature + f

Else

   'Cp = heat capacity (J/mol*K)
   Cp = g + h * Temperature + i * Temperature ^ 2 + j * Temperature ^
3 + k / Temperature ^ 2
   'h = standard enthalpy (kJ/mol)
   hh = g * Temperature + h * Temperature ^ 2 / 2 + i * Temperature ^
3 / 3 + j * Temperature ^ 4 / 4 - k / Temperature + l

End If

CpNO(tt) = Cp
'to convert from kJ/mol to J/mol, kJ/mol = 1000*J/mol
EnthalpyNO(tt) = hh * 1000 - 90291

NO = hh * 1000 - 90291

End Function

'this is from Heywood p.132 everything is in kcal/gmol
'the range is 300-3500K
Public Function EnthalpyAndSpecificHeat(x As Double, tt As Long) As
Double

Dim FEnthalpy As Double, Dim FSpecificHeat As Double
Dim Temperature As Double

Temperature = x / 1000

FEnthalpy = aa * Temperature + bb * Temperature ^ 2 / 2 + _
        cc * Temperature ^ 3 / 3 + dd * Temperature ^ 4 / 4 - _
        ee / Temperature +  ff

FSpecificHeat = aa + bb * Temperature + cc * Temperature ^ 2 + _
            dd * Temperature ^ 3 + ee / Temperature ^ 2

'4.1868 to convert from cal to J, the units are J/molK then divide by
FuelWeight
'to get J/g K = KJ/Kg K
FSpecificHeat = FSpecificHeat * 4.1868 / FuelWeight

'4.1868 to convert from kcal to kJ, the units are J/molK
FEnthalpy = FEnthalpy * 4.1868 * 1000

FuelEnthalpy(tt) = FEnthalpy
FuelSpecificHeat(tt) = FSpecificHeat

'4.1868 to convert from kcal to kJ, the units are J/molK
EnthalpyAndSpecificHeat = FEnthalpy

End Function

'this faction is decrease the number of iteration
Public Function COToCO2Predictor(x As Double) As Double
  '300-2800K +0.000037
  'Const a As Double = -2.45310294394045E-33
  'Const b As Double = 3.81784844315712E-29
  'Const c As Double = -2.54905095732239E-25
  'Const d As Double = 9.55862835484467E-22
  'Const e As Double = -2.20935842957574E-18
  'Const f As Double = 3.269946921217E-15
  'Const g As Double = -3.12813243381074E-12
  'Const h As Double = 1.90597642226248E-09
  'Const i As Double = -7.06860186231247E-07
  'Const j As Double = 1.43947506847198E-04
  'Const k As Double = -1.22199019668508E-02

  'Dim result As Double
  '300-6000K +0.021
  Const a As Double = 2.63571870033261E-34
  Const b As Double = -9.49059777925098E-30
  Const c As Double = 1.39595919081419E-25
  Const d As Double = -1.10222127163298E-21
  Const e As Double = 5.20444189340915E-18
  Const f As Double = -1.53310809117115E-14
  Const g As Double = 2.83848924435241E-11
  Const h As Double = -3.23058480825727E-08
  Const i As Double = 2.13298375758298E-05
  Const j As Double = -7.24999148167707E-03
  Const k As Double = 0.946903394070906
  Dim result As Double

  result = ((((((((((a * (x ^ 10)) + (b * (x ^ 9))) + (c * (x ^ 8))) + (d *
(x ^ 7))) + (e * (x ^ 6))) + (f * (x ^ 5))) + (g * (x ^ 4))) + (h * (x ^
3))) + (i * (x ^ 2))) + (j * x)) + k)
  COToCO2Predictor = result + 0.021

End Function
```

G.7 Engine Simulation

```
Option Explicit     'forces a declaration of all variables
Option Base 1       'first element in array is 1

'public declaration can be used by all modules in the workbook
'privte declaration can be used by only the module is has been declared
Private Const PI As Double = 3.14159265358979
Private Const DEGS  As Double = 57.2957795130823
Private Const RADS As Double = 1.74532925199433E-02
Private Const SIGMA As Double = 0.0000000567          'W/(m^2*K^4)
Private Const Po As Double = 100325                   'pressure (Pa)
Private Const Runi As Double = 8.31451                '(J/molK)
Private Const IVO As Double = 370                     '10deg. ATDC OR 370
ATDC NOTE: 0deg. is at TDC combustion
Private Const IVC As Double = -146                    '34deg. ABDC OR -146
ATDC NOTE: 0deg. is at TDC combustion
Private Const EVO As Double = 140                     '40deg. BBDC OR 140
ATDC NOTE: 0deg. is at TDC combustion
Private Const EVC As Double = 375                     '15deg. ATDC OR 375
ATDC NOTE: 0deg. is at TDC combustion
Private Const NUMBER_OF_DATA_POINTS As Double = 1500    'pressure
trace is 0.5 resolution, therefore 720deg. has less than 1500 data point in
one cycle
Private Const AVERAGE_WALL_TEMP As Double = 380               'wall
temperature (K)
```

```
Public BurnedInternalEnergy() As Double              'burned gas internal
energy (kJ/kgK)
Public BurnedEnthalpy() As Double                    'burned gas enthalpy
(kJ/kg)
Public BurnedCp() As Double                          'burned gas Cp (kJ/kgK)
Public BurnedCv() As Double                          'burned gas Cv (kJ/kgK)
Public BurnedGamma() As Double                       'burned gas gamma
Public BurnedRgas() As Double                        '(J/kgK)
Public BurnedMolecularWeight() As Double             '(g/mol)
Public BurnedVolume() As Double                      '(m^3)
Public BurnedTemperature() As Double                 '(K)
Public BurnedHeatTransferCoefficient() As Double
Public BurnedGasDensity() As Double                  '(kg/m^3)

Public BurnedCylinderArea() As Double                '(m^2)
Public BurnedCylinderHeadArea() As Double            '(m^2)
Public BurnedPistonArea() As Double                  '(m^2)

Public UnburnedInternalEnergy() As Double            '(kJ/kgK)
Public UnburnedEnthalpy() As Double                  '(kJ/kg)
Public UnburnedCp() As Double                        'Cp (kJ/kgK)
Public UnburnedCv() As Double                        'Cv (kJ/kgK)
Public UnburnedGamma() As Double
Public UnburnedRgas() As Double                      '(J/kgK)
Public UnburnedMolecularWeight() As Double           '(g/mol)
Public UnburnedVolume() As Double                    '(m^3)
Public DerivativeUnburnedVolume() As Double          '(m^3/deg.)
Public UnburnedTemperature() As Double               '(K)
Public UnburnedTemperature2() As Double
Public UnburnedHeatTransferCoefficient() As Double
Public UnburnedHeatTransferRate() As Double
Public UnburnedGasDensity() As Double                '(kg/m^3)

Public UnburnedCylinderArea() As Double              'm^2)
Public UnburnedCylinderHeadArea() As Double          '(m^2)
Public UnburnedPistonArea() As Double                '(m^2)

Public CylinderPressure As Variant                   '(Pa)
Public DerivativeCylinderPressure As Variant
Public CrankAngle As Variant                         'degrees
Public VolumeAtCrankAngle As Variant                 '(cc)
Public DerivativeVolumeAtCrankAngle() As Double      'm^3/deg.)
Public MotoringPressure As Variant                   '(Pa)

Private SlC8H18() As Double              'laminar flame speed (m/s)
Private SlH2() As Double                 'laminar flame speed (m/s)
Private Sl() As Double
Public TurbulentFlameSpeed() As Double' turbulent flame speed (m/s)
Public FlameSpeed() As Double            'actual flame speed (m/s)
Private FlameRadius() As Double          'flame radius (m)
Private FlameSurfaceArea() As Double     'flame surface area (m^2)
Private AdiabaticFlameTemperature() As Double        '(K)
Private FlameSpeedRatioActualC8H18() As Double
Private FlameSpeedRatioActualH2() As Double
Private FlameSpeedRatioTheoretical() As Double
'Private FlameSpeedRatioTheoreticalH2() As Double

Public MFB As Variant                    'mass fraction burned (%)
Public MBR As Variant                    'mass burned rate (/deg.)
Public FERI_Factor() As Double  'flame enhancing reaction intensity Factor

Public CylinderArea As Double            'cylinder area (m^2)
Public CylinderHeadArea As Double        'cylinder head area (m^2)
Public PistonArea As Double              'piston area (m^2)
Public CombustionChamberArea() As Double             '(m^2)
'Public CombustionChamberVolume() As Double           '(m^3)
Public VolumeSwept As Double             'swept volume (m^3)
Public VolumeClearance As Double         'clearance volume (m^3)
Public MaximumVolume As Double           'clearance + swept volume (m^3)
Private CR As Double                     'compression ratio
Private Bore As Double                               'bore (m)
Private Stroke As Double                             'stroke (m)
Private ConRodLength As Double           'connecting rod length (m)
Private MeanPistonSpeed As Double        'mean piston speed (m/s)
Public RPM As Double                     'engine speed (r/min)
Private MBT As Double  'minimum spark advance best torque (deg. BTDC)
Private MAP As Double                    'manifold pressure (kPa)
Private PeakPressureLocation As Double

Private AFR As Double                    'air fuel ratio
Private Phi As Double                    'AFR stoichiometric/AFR
Public Lambda As Double                  '1/PHI
Private StoichiometricAFR As Double      'stoichiometric air fuel ratio

Private EngineOutCO As Double                        'CO (%)
Private EngineOutHC As Double                        'HC (ppm)
Private EngineOutNOx As Double                       'NOx (ppm)
Private EngineOutCO2 As Double                       'CO2 (%)
Private EngineOutO2 As Double                        'O2 (%)

Private EquilibriumCO() As Double                    'CO (%)
Private EquilibriumHC() As Double                    'HC (ppm)
Private EquilibriumNOx() As Double                   'NOx (ppm)
Private EquilibriumCO2() As Double                   'CO2 (%)
Private EquilibriumO2() As Double                    'O2 (%)

Public O2molfrac() As Double
Public N2molfrac() As Double
Public Omolfrac() As Double
Public H2molfrac() As Double
Public OHmolfrac() As Double, Public Hmolfrac() As Double
Public NOmolfrac() As Double, Public COmolfrac() As Double
Public CO2molfrac() As Double, Public H2Omolfrac() As Double

Private CrankAngleAtEquilibriumEqualEngineOutCO As Double
Private CrankAngleAtEquilibriumEqualEngineOutHC As Double
Private CrankAngleAtEquilibriumEqualEngineOutNOx As Double
Private CrankAngleAtEquilibriumEqualEngineOutCO2 As Double
Private CrankAngleAtEquilibriumEqualEngineOutO2 As Double

Private PeakTemperature As Double      'peak cycle temperature (K)
Private LocationOfPeakTemperature As Double          '(deg.ATDC)
Private MFBatPeakTemperature As Double
Private MBRatPeakTemperature As Double
Private PeakFlameSpeed As Double
Private LocationOfPeakFlameSpeed As Double           '(deg. ATDC)
Private MFBatPeakFlameSpeed As Double
Private MBRatPeakFlameSpeed As Double
Private TotalBurnTime As Double                      '(deg.)
Private MFB_0_10 As Double                           '(deg.)
Private MFB_0_90 As Double                           '(deg.)
Private MFB_10_90 As Double                          '(deg.)
Private PeakMBR As Double                            '(/deg.)
Private LocationOfPeakMBR As Double                  'l(deg.)
Private ResidualGasMassFraction As Double
Public VolumeFractionOfN2toO2 As Double
Private AirFlow As Double                            '(kg/h)
Private FuelFlow As Double                           '(kg/h)
Public MassOfCharge As Double                        '(kg)
Public MainChamberFuel As Variant      '(Hydrogen or Isooctane)
Public CyclePosition As Double         'position of in one cycle
Private TemperatureAtIVC As Double
Private VolumeAtIVC As Double
Private PressureAtIVC As Double
Public Combustion As Variant
Public dydx1() As Double
Public AltBurnedTemp() As Double
Public BurnedTempForGraph() As Double
Public MeanTemperature() As Double
Public NOppm() As Double
Public NOppm2() As Double
Public TaylorLengthScale() As Double
Public ReTurb() As Double
Public Damkohler() As Double
Public TurbulentIntensity() As Double
Public BurnedVolumeFraction() As Double
Public BurnedMassFraction() As Double
Public dRdt() As Double
Public dNOdth() As Double
Public UnburnedGasDensityAt45deg As Double
Public TurbIntZeroLANCASTER() As Double
Public TurbIntLANCASTER() As Double
Public TurbConstLANCASTER() As Double
Public SlUnStrech() As Double
Public FSR_LANCASTER() As Double
Public FSRActual() As Double
Public FERI_Factor_LANCASTER() As Double
Public StLANCASTER() As Double
Public TaylorLengthScaleLANCASTER() As Double
Public ReTurbLANCASTER() As Double
Public DamkohlerLANCASTER() As Double
Public uSlC8H18Lumsden() As Double
Public uSlH2Lumsden() As Double
Public uSlC8H18Lancaster() As Double
Public uSlH2Lancaster() As Double
Public FlameRadiusNORMALIZED() As Double

'bring up to screen progress indicator
Sub StartProressIndicatorAndAnalysis5()
UserForm5.Show
End Sub

Sub EngineSimulation()

Dim StartTime As Double

'start Timing
StartTime = Timer

'resize arrays dynamically
ResizeArraysDynamically

'get engine data
GetInputData
```

```
'run analysis
RunAnalysis

'double indicator bar
'StuffAround

'turn OFF progress indicator
'Unload UserForm5

Call PrintAnalysisToScreen
'this will delete zeros and errors. good for graphing
Call DeleteZEROandERRORS

Call SpeedCalculation

MsgBox "It has taken " & Format(Timer - StartTime, ".0000") & " seconds
to run analysis."
Sheets("ANALYSIS").Select
Range("a1").Select

End Sub

Sub ResizeArraysDynamically()

ReDim BurnedInternalEnergy(NUMBER_OF_DATA_POINTS)
ReDim BurnedEnthalpy(NUMBER_OF_DATA_POINTS)
ReDim BurnedCp(NUMBER_OF_DATA_POINTS)
ReDim BurnedCv(NUMBER_OF_DATA_POINTS)
ReDim BurnedGamma(NUMBER_OF_DATA_POINTS)
ReDim BurnedRgas(NUMBER_OF_DATA_POINTS)
ReDim BurnedMolecularWeight(NUMBER_OF_DATA_POINTS)
ReDim BurnedVolume(NUMBER_OF_DATA_POINTS)
ReDim BurnedTemperature(NUMBER_OF_DATA_POINTS)
ReDim BurnedHeatTransferCoefficient(NUMBER_OF_DATA_POINTS)
ReDim BurnedGasDensity(NUMBER_OF_DATA_POINTS)
ReDim BurnedCylinderArea(NUMBER_OF_DATA_POINTS)
ReDim BurnedCylinderHeadArea(NUMBER_OF_DATA_POINTS)
ReDim BurnedPistonArea(NUMBER_OF_DATA_POINTS)
ReDim UnburnedInternalEnergy(NUMBER_OF_DATA_POINTS)
ReDim UnburnedEnthalpy(NUMBER_OF_DATA_POINTS)
ReDim UnburnedCp(NUMBER_OF_DATA_POINTS)
ReDim UnburnedCv(NUMBER_OF_DATA_POINTS)
ReDim UnburnedGamma(NUMBER_OF_DATA_POINTS)
ReDim UnburnedRgas(NUMBER_OF_DATA_POINTS)
ReDim UnburnedMolecularWeight(NUMBER_OF_DATA_POINTS)
ReDim UnburnedVolume(NUMBER_OF_DATA_POINTS)
ReDim DerivativeUnburnedVolume(NUMBER_OF_DATA_POINTS)
ReDim DerivativeVolumeAtCrankAngle(NUMBER_OF_DATA_POINTS)
ReDim UnburnedTemperature(NUMBER_OF_DATA_POINTS)
ReDim UnburnedTemperature2(NUMBER_OF_DATA_POINTS)
ReDim UnburnedHeatTransferCoefficient(NUMBER_OF_DATA_POINTS)
ReDim UnburnedHeatTransferRate(NUMBER_OF_DATA_POINTS)
ReDim UnburnedGasDensity(NUMBER_OF_DATA_POINTS)
ReDim UnburnedCylinderArea(NUMBER_OF_DATA_POINTS)
ReDim UnburnedCylinderHeadArea(NUMBER_OF_DATA_POINTS)
ReDim UnburnedPistonArea(NUMBER_OF_DATA_POINTS)
ReDim SlC8H18(NUMBER_OF_DATA_POINTS)
ReDim SlH2(NUMBER_OF_DATA_POINTS)
ReDim Sl(NUMBER_OF_DATA_POINTS)
ReDim TurbulentFlameSpeed(NUMBER_OF_DATA_POINTS)
ReDim FlameSpeed(NUMBER_OF_DATA_POINTS)
ReDim FlameRadius(NUMBER_OF_DATA_POINTS)
ReDim AdiabaticFlameTemperature(NUMBER_OF_DATA_POINTS)
ReDim FlameSurfaceArea(NUMBER_OF_DATA_POINTS)
ReDim FlameSpeedRatioActualC8H18(NUMBER_OF_DATA_POINTS)
ReDim FlameSpeedRatioActualH2(NUMBER_OF_DATA_POINTS)
ReDim FlameSpeedRatioTheoretical(NUMBER_OF_DATA_POINTS)
ReDim MFB(NUMBER_OF_DATA_POINTS)
ReDim MBR(NUMBER_OF_DATA_POINTS)
ReDim FERI_Factor(NUMBER_OF_DATA_POINTS)
ReDim CombustionChamberArea(NUMBER_OF_DATA_POINTS)
ReDim EquilibriumCO(NUMBER_OF_DATA_POINTS)
ReDim EquilibriumHC(NUMBER_OF_DATA_POINTS)
ReDim EquilibriumNOx(NUMBER_OF_DATA_POINTS)
ReDim EquilibriumCO2(NUMBER_OF_DATA_POINTS)
ReDim EquilibriumO2(NUMBER_OF_DATA_POINTS)
ReDim O2molfrac(NUMBER_OF_DATA_POINTS)
ReDim N2molfrac(NUMBER_OF_DATA_POINTS)
ReDim Omolfrac(NUMBER_OF_DATA_POINTS)
ReDim H2molfrac(NUMBER_OF_DATA_POINTS)
ReDim OHmolfrac(NUMBER_OF_DATA_POINTS)
ReDim Hmolfrac(NUMBER_OF_DATA_POINTS)
ReDim NOmolfrac(NUMBER_OF_DATA_POINTS)
ReDim COmolfrac(NUMBER_OF_DATA_POINTS)
ReDim CO2molfrac(NUMBER_OF_DATA_POINTS)
ReDim H2Omolfrac(NUMBER_OF_DATA_POINTS)
ReDim dydx1(NUMBER_OF_DATA_POINTS)
ReDim AltBurnedTemp(NUMBER_OF_DATA_POINTS)
ReDim BurnedTempForGraph(NUMBER_OF_DATA_POINTS)
ReDim MeanTemperature(NUMBER_OF_DATA_POINTS)
ReDim NOppm(NUMBER_OF_DATA_POINTS)
ReDim NOppm2(NUMBER_OF_DATA_POINTS)
ReDim TaylorLengthScale(NUMBER_OF_DATA_POINTS)
ReDim ReTurb(NUMBER_OF_DATA_POINTS)
ReDim Damkohler(NUMBER_OF_DATA_POINTS) As Double
ReDim TurbulentIntensity(NUMBER_OF_DATA_POINTS)
ReDim BurnedVolumeFraction(NUMBER_OF_DATA_POINTS)
ReDim BurnedMassFraction(NUMBER_OF_DATA_POINTS)
ReDim dRdt(NUMBER_OF_DATA_POINTS)
ReDim dNOdth(NUMBER_OF_DATA_POINTS)
ReDim TurbIntZeroLANCASTER(NUMBER_OF_DATA_POINTS) As Double
ReDim TurbIntLANCASTER(NUMBER_OF_DATA_POINTS) As Double
ReDim TurbConstLANCASTER(NUMBER_OF_DATA_POINTS) As Double
ReDim SlUnStrech(NUMBER_OF_DATA_POINTS) As Double
ReDim FSR_LANCASTER(NUMBER_OF_DATA_POINTS) As Double
ReDim FSRActual(NUMBER_OF_DATA_POINTS) As Double
ReDim FERI_Factor_LANCASTER(NUMBER_OF_DATA_POINTS) As Double
ReDim StLANCASTER(NUMBER_OF_DATA_POINTS) As Double
ReDim TaylorLengthScaleLANCASTER(NUMBER_OF_DATA_POINTS) As
Double
ReDim ReTurbLANCASTER(NUMBER_OF_DATA_POINTS) As Double
ReDim DamkohlerLANCASTER(NUMBER_OF_DATA_POINTS) As Double
ReDim uSlC8H18Lumsden(NUMBER_OF_DATA_POINTS) As Double
ReDim uSlH2Lumsden(NUMBER_OF_DATA_POINTS) As Double
ReDim uSlC8H18Lancaster(NUMBER_OF_DATA_POINTS) As Double
ReDim uSlH2Lancaster(NUMBER_OF_DATA_POINTS) As Double
ReDim FlameRadiusNORMALIZED(NUMBER_OF_DATA_POINTS) As Double

End Sub

Sub GetInputData()

Dim constC As Double

Bore = Worksheets("Engine Modeling Input").Range("d14").Value / 1000
Stroke = Worksheets("Engine Modeling Input").Range("d15").Value / 1000
ConRodLength = Worksheets("Engine Modeling
Input").Range("d16").Value
RPM = Worksheets("Engine Modeling Input").Range("i6").Value
CR = Worksheets("Engine Modeling Input").Range("i7").Value
MAP = Worksheets("Engine Modeling Input").Range("i8").Value
Lambda = Worksheets("Engine Modeling Input").Range("i9").Value
MBT = Worksheets("Engine Modeling Input").Range("i10").Value * (-1)
StoichiometricAFR = Worksheets("Engine Modeling
Input").Range("i14").Value
EngineOutCO = Worksheets("Engine Modeling Input").Range("i39").Value
EngineOutHC = Worksheets("Engine Modeling Input").Range("i40").Value
EngineOutNOx = Worksheets("Engine Modeling
Input").Range("i41").Value
EngineOutCO2 = Worksheets("Engine Modeling
Input").Range("i42").Value
EngineOutO2 = Worksheets("Engine Modeling Input").Range("i43").Value
AirFlow = Worksheets("Engine Modeling Input").Range("i17").Value
FuelFlow = Worksheets("Engine Modeling Input").Range("i18").Value
PeakPressureLocation = Worksheets("ANALYSIS").Range("c26").Value

EngineOutCO = Worksheets("Engine Modeling Input").Range("i39").Value
* 10000
EngineOutHC = Worksheets("Engine Modeling Input").Range("i40").Value
EngineOutNOx = Worksheets("Engine Modeling
Input").Range("i41").Value
EngineOutCO2 = Worksheets("Engine Modeling
Input").Range("i42").Value * 10000
EngineOutO2 = Worksheets("Engine Modeling Input").Range("i43").Value
* 10000

MainChamberFuel = Worksheets("Engine Modeling
Input").Range("d18").Value

CrankAngle = Worksheets("ANALYSIS").Range("t3:t1460").Value
CylinderPressure = Worksheets("ANALYSIS").Range("w3:w1460").Value
VolumeAtCrankAngle =
Worksheets("ANALYSIS").Range("v3:v1460").Value
DerivativeCylinderPressure =
Worksheets("ANALYSIS").Range("au3:au1460").Value
MFB = Worksheets("ANALYSIS").Range("an3:an1460").Value
MBR = Worksheets("ANALYSIS").Range("ap3:ap1460").Value
MotoringPressure = Worksheets("ANALYSIS").Range("al3:al1460").Value

    constC = 1
    While constC < 1458
    'to convert to Pa
    CylinderPressure(constC, 1) = CylinderPressure(constC, 1) * 1000000
    'to convert to m^3
    VolumeAtCrankAngle(constC, 1) = VolumeAtCrankAngle(constC, 1) /
1000000
    'to convert to Pa/deg.
    DerivativeCylinderPressure(constC, 1) =
DerivativeCylinderPressure(constC, 1) * 1000
    'to convert to (Pa)
    MotoringPressure(constC, 1) = MotoringPressure(constC, 1) * 1000000

    constC = constC + 1
```

```
    Wend

End Sub

Sub RunAnalysis()

Dim constA As Double
Dim Method1EqualsMethod2 As Variant
Dim CalculatedWoschniCoeff As Variant, Dim dth As Double

Dim dzero As Double, dslope As Double, ht As Double, li As Double, FracD
As Double, Dim dmin As Double, uzero As Double, ut As Double, kv As
Double, lg As Double, Dim strechb As Double, lk As Double, dt As Double,
eo As Double, ei As Double, Dim Sturb As Double, Dim FlameRadiusMAX
As Double

VolumeSwept = (Stroke) * (PI * ((Bore) ^ 2) / 4)
VolumeClearance = VolumeSwept / (CR - 1)
MaximumVolume = VolumeSwept + VolumeClearance
Phi = 1 / Lambda
MeanPistonSpeed = 2 * Stroke * RPM / 60

'convert air and fuel flow to kg/cycle
AirFlow = AirFlow / (RPM * 60 / 2)
FuelFlow = FuelFlow / (RPM * 60 / 2)

'calculate exhaust residual fraction
Call ExhaustGasMassFraction
'total mass = air + fuel + (residual fraction*total mass)
MassOfCharge = (AirFlow + FuelFlow) / (1 - ResidualGasMassFraction)
'MsgBox "ResidualGasMassFraction " & ResidualGasMassFraction
'MsgBox "MassOfCharge " & MassOfCharge

'=COMPRESSION STARTS HERE UP UNTIL MBT====
CalculatedWoschniCoeff = "no"
CylePosition = 1
While MFB(CylePosition, 1) < 0.002
    Combustion = "off"
    Call SetBurnedPropertiesToZERO

  UnburnedVolume(CylePosition) = VolumeAtCrankAngle(CylePosition, 1)

  UnburnedCylinderArea(CylePosition) = (PI * (Bore ^ 2) / 2) + (PI *
Bore*Stroke/2)*(ConRodLength/(Stroke / 2)+1-
Cos(CrankAngle(CylePosition, 1) * PI / 180) - ((ConRodLength / (Stroke /
2)) ^ 2 - Sin(CrankAngle(CylePosition, 1) * PI / 180) ^ 2) ^ 0.5 + (2 /
(CR - 1)))

 DerivativeUnburnedVolume(CylePosition) = (VolumeSwept *
Sin(CrankAngle(CylePosition, 1) * PI / 180) / 2) *
(1 + (Cos(CrankAngle(CylePosition, 1) * PI / 180) *
(((ConRodLength / (Stroke / 2)) ^ 2 - Sin(CrankAngle(CylePosition, 1) *
PI / 180) ^ 2) ^ (-0.5))))

DerivativeUnburnedVolume(CylePosition) =
DerivativeUnburnedVolume(CylePosition) / (180 / PI)
DerivativeVolumeAtCrankAngle(CylePosition) =
DerivativeUnburnedVolume(CylePosition)

'one point ahead
DerivativeUnburnedVolume(CylePosition + 1) = (VolumeSwept *
Sin(CrankAngle(CylePosition + 1, 1) * PI / 180) / 2) *
(1 + (Cos(CrankAngle(CylePosition + 1, 1) * PI / 180) *
(((ConRodLength / (Stroke / 2)) ^ 2 - Sin(CrankAngle(CylePosition + 1,
1) * PI / 180) ^ 2) ^ (-0.5))))

DerivativeUnburnedVolume(CylePosition + 1) =
DerivativeUnburnedVolume(CylePosition + 1) / (180 / PI)
DerivativeVolumeAtCrankAngle(CylePosition + 1) =
DerivativeUnburnedVolume(CylePosition + 1)

UnburnedCylinderHeadArea(CylePosition) = (PI * Bore ^ 2) / 4
UnburnedPistonArea(CylePosition) =
UnburnedCylinderHeadArea(CylePosition)
UnburnedGasDensity(CylePosition) = MassOfCharge /
UnburnedVolume(CylePosition)

'need to provide some value in order for the equilibrium calculation to
work obviously these are zero before ignition
BurnedGasDensity(CylePosition) = UnburnedGasDensity(CylePosition)
BurnedTemperature(CylePosition) = 2000

'this if statement limits method 1 to calculate up to 11 data point, which
becomes method 2's initial condition. method 2 does not require the
equilibrium solver therefore it is 45 times faster
    Method1EqualsMethod2 = "yes"
    If CylePosition < 11 Then

'if method 1 is calculating/active then obviously method 1 and method 2
    'values should be kept separate
    Method1EqualsMethod2 = "no"
    constA = 1
    UnburnedTemperature(CylePosition) = 350
     While constA < 3

        Call Main_ChemicalEquilibriumCompositionInput

UnburnedRgas(CylePosition) = (UnburnedCp(CylePosition) * (1 - (1 /
UnburnedGamma(CylePosition))))

UnburnedTemperature(CylePosition) = CylinderPressure(CylePosition, 1)
* VolumeAtCrankAngle(CylePosition, 1) /  (MassOfCharge *
UnburnedRgas(CylePosition))

        'to initialise values for method 2
        If CylePosition < 10 Then
UnburnedTemperature2(CylePosition) =
UnburnedTemperature(CylePosition)
        End If

      constA = constA + 1
      Wend
    End If

'this method (method 2) also calculates the unburned temperature before
ignition, this however assumes that the chemical composition does not
change on the compression stroke. It is 45 times faster than the previous
method.
    If CylePosition > 5 Then
    Call CalculateUnburnedTemperature2(Method1EqualsMethod2)
    UnburnedCp(CylePosition) = UnburnedCp(CylePosition - 2)
    End If

    If CrankAngle(CylePosition, 1) > MBT - 6 Then
    Call Main_ChemicalEquilibriumCompositionInput
    UnburnedRgas(CylePosition) = (UnburnedCp(CylePosition) * (1 - (1 /
UnburnedGamma(CylePosition))))
    End If

 'calculate reference temperature volume and pressure for WOSCHNI heat
transfer coefficient
If CrankAngle(CylePosition, 1) >= IVC And CalculatedWoschniCoeff =
"no" Then
        TemperatureAtIVC = UnburnedTemperature(CylePosition)
        VolumeAtIVC = VolumeAtCrankAngle(CylePosition, 1)
        PressureAtIVC = CylinderPressure(CylePosition, 1)
        CalculatedWoschniCoeff = "yes"
        End If
If CrankAngle(CylePosition, 1) >= IVC Then
            'calculated unburned gas heat transfer rate
             Call HeatTransfer
End If

BurnedTempForGraph(CylePosition) =
UnburnedTemperature2(CylePosition)

CylePosition = CylePosition + 1
Wend


'====IGNITION STARTS NOW=====

CylePosition = CylePosition - 1

BurnedRgas(CylePosition) = 289 'as an initial value

UnburnedTemperature(CylePosition) =
UnburnedTemperature(CylePosition - 1)


If MainChamberFuel = "Isooctane" Then
BurnedTemperature(CylePosition) =
AdiabaticFlameTemperatureC8H18(Lambda,
UnburnedTemperature(CylePosition) - 273.15,
CylinderPressure(CylePosition, 1) / 1000)
BurnedTemperature(CylePosition) = BurnedTemperature(CylePosition)
+ 273.15
ElseIf MainChamberFuel = "Hydrogen" Then
BurnedTemperature(CylePosition) =
AdiabaticFlameTemperatureHydrogen(Lambda,
UnburnedTemperature(CylePosition) - 273.15,
CylinderPressure(CylePosition, 1) / 1000)
BurnedTemperature(CylePosition) = BurnedTemperature(CylePosition)
+ 273.15
Else
MsgBox "CAN NOT DETECT FUEL TYPE"
End If
'++++++++++++++++++++++
BurnedTemperature(CylePosition) = BurnedTemperature(CylePosition)
BurnedTemperature(CylePosition) =
Main_ChemicalEquilibriumCompositionInput2
'++++++++++++++++++++++
BurnedTemperature(CylePosition - 1)=BurnedTemperature(CylePosition)
```

```
BurnedGasDensity(CyclePosition) = CylinderPressure(CyclePosition, 1) /
(BurnedRgas(CyclePosition) * BurnedTemperature(CyclePosition))

BurnedVolume(CyclePosition) = BurnedRgas(CyclePosition) *
BurnedTemperature(CyclePosition) * MassOfCharge * MFB(CyclePosition,
1) / CylinderPressure(CyclePosition, 1)

UnburnedVolume(CyclePosition) = VolumeAtCrankAngle(CyclePosition, 1) -
BurnedVolume(CyclePosition)

Call Main_ChemicalEquilibriumCompositionInput

UnburnedRgas(CyclePosition) = (UnburnedCp(CyclePosition) * (1 - (1 /
UnburnedGamma(CyclePosition))))

   Combustion = "on"
   While MFB(CyclePosition, 1) < 0.98

   UnburnedCylinderArea(CyclePosition) = (PI * (Bore ^ 2) / 2) +
(PI * Bore * Stroke / 2) * (ConRodLength / (Stroke / 2) + 1 -
Cos(CrankAngle(CyclePosition, 1) * PI / 180) - ((ConRodLength / (Stroke /
2)) ^ 2 - Sin(CrankAngle(CyclePosition, 1) * PI / 180) ^ 2) ^ 0.5 +
(2 / (CR - 1)))

DerivativeVolumeAtCrankAngle(CyclePosition) = (VolumeSwept *
Sin(CrankAngle(CyclePosition, 1) * PI / 180) / 2) * (1 +
(Cos(CrankAngle(CyclePosition, 1) * PI / 180) *
(((ConRodLength / (Stroke / 2)) ^ 2 - Sin(CrankAngle(CyclePosition, 1) *
PI / 180) ^ 2) ^ (-0.5))))

DerivativeVolumeAtCrankAngle(CyclePosition) =
DerivativeVolumeAtCrankAngle(CyclePosition) / (180 / PI)


        Call HeatTransfer
        Call CalculateBurnedTemperature
BurnedTempForGraph(CyclePosition - 1) =
BurnedTemperature(CyclePosition - 1)

      CyclePosition = CyclePosition + 1

   Wend

'+++++++++++++++EXPANSION START++++++++++++++++++++
                CyclePosition = CyclePosition - 2
                While CrankAngle(CyclePosition, 1) < 180
 "
                  Combustion = "off"

 UnburnedVolume(CyclePosition) = VolumeAtCrankAngle(CyclePosition, 1)

UnburnedCylinderArea(CyclePosition) = (PI * (Bore ^ 2) / 2) +
(PI * Bore * Stroke / 2) * (ConRodLength / (Stroke / 2) + 1 -
Cos(CrankAngle(CyclePosition, 1) * PI / 180) -
((ConRodLength / (Stroke / 2)) ^ 2 - Sin(CrankAngle(CyclePosition, 1) *
PI / 180) ^ 2) ^ 0.5 + (2 / (CR - 1)))

DerivativeUnburnedVolume(CyclePosition) = (VolumeSwept *
Sin(CrankAngle(CyclePosition, 1) * PI / 180) / 2) *(1 +
(Cos(CrankAngle(CyclePosition, 1) * PI / 180) *
(((ConRodLength / (Stroke / 2)) ^ 2 - Sin(CrankAngle(CyclePosition, 1) *
PI / 180) ^ 2) ^ (-0.5))))

DerivativeUnburnedVolume(CyclePosition) =
DerivativeUnburnedVolume(CyclePosition) / (180 / PI)
DerivativeVolumeAtCrankAngle(CyclePosition) =
DerivativeUnburnedVolume(CyclePosition)

'one point ahead
DerivativeUnburnedVolume(CyclePosition + 1) = (VolumeSwept *
Sin(CrankAngle(CyclePosition + 1, 1) * PI / 180) / 2) *
(1 + (Cos(CrankAngle(CyclePosition + 1, 1) * PI / 180) *
(((ConRodLength / (Stroke / 2)) ^ 2 - Sin(CrankAngle(CyclePosition + 1,
1) * PI / 180) ^ 2) ^ (-0.5))))

DerivativeUnburnedVolume(CyclePosition + 1) =
DerivativeUnburnedVolume(CyclePosition + 1) / (180 / PI)
DerivativeVolumeAtCrankAngle(CyclePosition + 1) =
DerivativeUnburnedVolume(CyclePosition + 1)

UnburnedCylinderHeadArea(CyclePosition) = (PI * Bore ^ 2) / 4
UnburnedPistonArea(CyclePosition) =
UnburnedCylinderHeadArea(CyclePosition)
UnburnedGasDensity(CyclePosition) = MassOfCharge /
UnburnedVolume(CyclePosition)

'need to provide some value for in order for the equilibrium calculation to
work 'obviously these are zero before ignition
BurnedGasDensity(CyclePosition) = UnburnedGasDensity(CyclePosition)
BurnedTemperature(CyclePosition)=BurnedTempForGraph(CyclePosition-
1)

If CyclePosition > 5 Then
Call CalculateUnburnedTemperature2(Method1EqualsMethod2)
End If
'need to provide some value for in order for the equilibrium calculation to
work obviously these are zero before ignition
BurnedGasDensity(CyclePosition) = UnburnedGasDensity(CyclePosition)
'BurnedTemperature(CyclePosition) = 2000
Call Main_ChemicalEquilibriumCompositionInput

BurnedTempForGraph(CyclePosition) =
UnburnedTemperature2(CyclePosition)
BurnedRgas(CyclePosition) = (BurnedCp(CyclePosition) * (1 - (1 /
BurnedGamma(CyclePosition))))
UnburnedRgas(CyclePosition) = (UnburnedCp(CyclePosition) * (1 - (1 /
UnburnedGamma(CyclePosition))))

UnburnedCp(CyclePosition) = UnburnedCp(CyclePosition - 2)
BurnedCp(CyclePosition) = BurnedCp(CyclePosition - 2)
CyclePosition = CyclePosition + 1
Wend

'+++++++EXPANSION FINISH++++++++++++++++++

CyclePosition = 1
While CrankAngle(CyclePosition, 1) < -45
CyclePosition = CyclePosition + 1
Wend
UnburnedGasDensityAt45deg = UnburnedGasDensity(CyclePosition)

'calculate mean temperature, NO, Flame Area, Flame Radius, Flame Speed
CyclePosition = 1
While CyclePosition < 680

MeanTemperature(CyclePosition) = (MassOfCharge * (1 -
MFB(CyclePosition, 1)) * UnburnedTemperature(CyclePosition) *
UnburnedCp(CyclePosition) + MassOfCharge * MFB(CyclePosition, 1) *
BurnedTemperature(CyclePosition) * BurnedCp(CyclePosition)) /
(MassOfCharge * (1 - MFB(CyclePosition, 1)) * UnburnedCp(CyclePosition)
+ MassOfCharge * MFB(CyclePosition, 1) * BurnedCp(CyclePosition))

 'calculate NO
   If CyclePosition < 5 Then
   NOppm(CyclePosition) = 0
   Else
   dth = CrankAngle(CyclePosition, 1) - CrankAngle(CyclePosition - 1, 1)

   'rate controlled NO in ppm
NOppm(CyclePosition)=NOZeldovich(RPM,dth,NOppm(CyclePosition - 1), _
BurnedTempForGraph(CyclePosition), CylinderPressure(CyclePosition, 1), _
O2molfrac(CyclePosition), N2molfrac(CyclePosition), _
Omolfrac(CyclePosition), OHmolfrac(CyclePosition), molfrac(CyclePosition))

NOppm2(CyclePosition) = NOZeldovich2(RPM, dth, NOppm2(CyclePosition
- 1), BurnedTempForGraph(CyclePosition), CylinderPressure(CyclePosition,
1), O2molfrac(CyclePosition), N2molfrac(CyclePosition),
Omolfrac(CyclePosition), OHmolfrac(CyclePosition), molfrac(CyclePosition))

 'equilibrium NO to convert to ppm
NOmolfrac(CyclePosition) = NOmolfrac(CyclePosition) * 1000000

If CrankAngle(CyclePosition, 1) > PeakPressureLocation Then

        If COmolfrac(CyclePosition + 1) * 1000000 > EngineOutCO And _
          COmolfrac(CyclePosition - 1) * 1000000 < EngineOutCO Or _
          COmolfrac(CyclePosition + 1) * 1000000 < EngineOutCO And _
          COmolfrac(CyclePosition - 1) * 1000000 > EngineOutCO Then

          CrankAngleAtEquilibriumEqualEngineOutCO =
CrankAngle(CyclePosition, 1)
        End If

        If NOmolfrac(CyclePosition + 1) > EngineOutNOx And _
          NOmolfrac(CyclePosition - 1) < EngineOutNOx Or _
          NOmolfrac(CyclePosition + 1) < EngineOutNOx And _
          NOmolfrac(CyclePosition - 1) > EngineOutNOx Then

          CrankAngleAtEquilibriumEqualEngineOutNOx =
CrankAngle(CyclePosition, 1)
         End If

        If CO2molfrac(CyclePosition + 1) * 1000000 > EngineOutCO2
And  CO2molfrac(CyclePosition - 1) * 1000000 < EngineOutCO2 Or
CO2molfrac(CyclePosition + 1) * 1000000 < EngineOutCO2 And _
          CO2molfrac(CyclePosition - 1) * 1000000 > EngineOutCO2
Then

CrankAngleAtEquilibriumEqualEngineOutCO2 = CrankAngle(CyclePosition,
1)
         End If

        If O2molfrac(CyclePosition + 1) * 1000000 > EngineOutO2 And _
          O2molfrac(CyclePosition - 1) * 1000000 < EngineOutO2 Or _
```

```
            O2molfrac(CyclePosition + 1) * 1000000 < EngineOutO2 And _
            O2molfrac(CyclePosition - 1) * 1000000 > EngineOutO2 Then

CrankAngleAtEquilibriumEqualEngineOutO2=CrankAngle(CyclePosition, 1)
          End If

       End If

       COmolfrac(CyclePosition - 2) = COmolfrac(CyclePosition - 2)
       CO2molfrac(CyclePosition - 2) = CO2molfrac(CyclePosition - 2)
       O2molfrac(CyclePosition - 2) = O2molfrac(CyclePosition - 2)
N2molfrac(CyclePosition - 2) = N2molfrac(CyclePosition - 2) * 1000000
Omolfrac(CyclePosition - 2) = Omolfrac(CyclePosition - 2) * 1000000
H2molfrac(CyclePosition - 2) = H2molfrac(CyclePosition - 2) * 1000000
OHmolfrac(CyclePosition - 2) = OHmolfrac(CyclePosition - 2) * 1000000
Hmolfrac(CyclePosition - 2) = Hmolfrac(CyclePosition - 2) * 1000000
H2Omolfrac(CyclePosition - 2) = H2Omolfrac(CyclePosition - 2) * 1000000

    End If

If BurnedVolume(CyclePosition) <= 0 Or
UnburnedTemperature(CyclePosition) > 1200 Then
    FlameSurfaceArea(CyclePosition) = 0,  FlameSpeed(CyclePosition) = 0
FlameRadius(CyclePosition) = 0, BurnedVolumeFraction(CyclePosition) = 0
BurnedMassFraction(CyclePosition) = 0,  dRdt(CyclePosition) = 0
          dNOdth(CyclePosition) = 0
       Else

'flame Area
FlameSurfaceArea(CyclePosition) =
FlameArea(BurnedVolume(CyclePosition), CrankAngle(CyclePosition, 1))

'flame speed
FlameSpeed(CyclePosition) = FlameSt(CylinderPressure(CyclePosition, 1),
UnburnedTemperature(CyclePosition), MFB(CyclePosition + 1, 1) -
MFB(CyclePosition, 1), FlameSurfaceArea(CyclePosition), RPM,
MassOfCharge, UnburnedRgas(CyclePosition + 1))

       'flame radius
       FlameRadius(CyclePosition) =
FlameRf(BurnedVolume(CyclePosition), CrankAngle(CyclePosition, 1))

'laminar flame H2 and C8H18
SlH2(CyclePosition) = LaminarFlameSpeedH2(Lambda,
UnburnedTemperature(CyclePosition) - 273.15,
CylinderPressure(CyclePosition, 1) / 1000) / 100
SlC8H18(CyclePosition) = LaminarFlameSpeedC8H18(Lambda,
UnburnedTemperature(CyclePosition) - 273.15,
CylinderPressure(CyclePosition, 1) / 1000) / 100

FlameSpeedRatioActualC8H18(CyclePosition) = FlameSpeed(CyclePosition)
/ SlC8H18(CyclePosition)
FlameSpeedRatioActualH2(CyclePosition) = FlameSpeed(CyclePosition) /
SlH2(CyclePosition)
BurnedVolumeFraction(CyclePosition) = BurnedVolume(CyclePosition) /
VolumeAtCrankAngle(CyclePosition, 1)

  BurnedMassFraction(CyclePosition) = (CylinderPressure(CyclePosition, 1)
* BurnedVolume(CyclePosition) / (BurnedRgas(CyclePosition + 1) *
BurnedTemperature(CyclePosition))) / MassOfCharge

dRdt(CyclePosition - 1) = (FlameRadius(CyclePosition) -
FlameRadius(CyclePosition - 2)) / ((CrankAngle(CyclePosition, 1) -
CrankAngle(CyclePosition - 2, 1)) / (360 * RPM / 60))

dNOdth(CyclePosition) = (NOppm2(CyclePosition) - NOppm2(CyclePosition
- 1)) / dth

  '++++++++++++FRACTAL++++++

If MainChamberFuel = "Isooctane" Then
        Sl(CyclePosition) = SlC8H18(CyclePosition)
             'adiabatic flame temperature
AdiabaticFlameTemperature(CyclePosition) =
AdiabaticFlameTemperatureC8H18(Lambda,
UnburnedTemperature(CyclePosition) - 273.15,
CylinderPressure(CyclePosition, 1) / 1000)  + 273.15
FSRActual(CyclePosition) = FlameSpeedRatioActualC8H18(CyclePosition)
        Else
        Sl(CyclePosition) = SlH2(CyclePosition)
             'adiabatic flame temperature
AdiabaticFlameTemperature(CyclePosition) =
AdiabaticFlameTemperatureHydrogen(Lambda,
UnburnedTemperature(CyclePosition) - 273.15,
CylinderPressure(CyclePosition, 1) / 1000) + 273.15
FSRActual(CyclePosition) = FlameSpeedRatioActualH2(CyclePosition)
        End If
SlUnStrech(CyclePosition) = Sl(CyclePosition)

          'for lambda 1 fractal dimension vs. flame radius
          dzero = 2.3314
          dslope = -0.0079434

          'ht = height of combustion chamber, li=integral length scale
          ht = 4 * VolumeAtCrankAngle(CyclePosition, 1) / (PI * Bore ^ 2)
          li = ht / 2
FracD = FractalD3(Lambda, FlameRadius(CyclePosition) * 1000) 'dzero +
dslope * FlameRadius(CyclePosition)*1000

          If FracD > 2.35 Then
          FracD = 2.35
          End If
          If FracD < 2 Then
          FracD = 2
          End If

          'average combustion chamber turbulence
          uzero = 0.5 * MeanPistonSpeed / 2
dmin = (2 * Sl(CyclePosition) + 2.36 * uzero) / (Sl(CyclePosition) + uzero)
          If FracD < dmin Then
          FracD = dmin
          End If
          'turbulence level with relevant to flame kernel
          ut = Sl(CyclePosition) * (2 - FracD) / (FracD - 2.36)

          'calculate stretched flame speed
          'kinematic viscosity kv
          'inner cutoff ei
          lk = 0.0001
          ei = 0.0001
          'kolmogorov length scale lk
kv = (0.00001 * (0.715 + UnburnedTemperature(CyclePosition) * (0.0044
+ UnburnedTemperature(CyclePosition) * (-0.00000113 +
UnburnedTemperature(CyclePosition) * 0.000000000185)))) /
UnburnedGasDensity(CyclePosition)

dt = (CrankAngle(CyclePosition + 1, 1) - CrankAngle(CyclePosition, 1)) _
               / (360 * RPM / 60)

'stretch multiplier for laminar flame speed
strechb = (1 - ((uzero ^ 3 / li / kv) ^ 0.5 * (lk / ei) ^ 0.6666 + 2 /
FlameRadius(CyclePosition) * (FlameRadius(CyclePosition) -
FlameRadius(CyclePosition - 1)) dt) * kv / Sl(CyclePosition) ^ 2)

          If strechb <= 0 Then
          strechb = 1
          End If

          Sl(CyclePosition) = Sl(CyclePosition) * strechb

          'outer cutoff eo
          If FlameRadius(CyclePosition) / 2 < li Then
          eo = FlameRadius(CyclePosition) / 2
          Else
          eo = li
          End If

kv = (0.00001 * (0.715 + UnburnedTemperature(CyclePosition) * (0.0044
+ UnburnedTemperature(CyclePosition) * (-0.00000113 +
UnburnedTemperature(CyclePosition) * 0.000000000185))))  /
UnburnedGasDensity(CyclePosition)

          lk = ((kv / ut) ^ 3 * li) ^ 0.25
          'gibson scale
          lg = li * (Sl(CyclePosition) / ut) ^ 3

          If lk < lg Then
          ei = lk
          Else
          ei = lg
          End If

          If ei > eo Then
          ei = eo
          End If

Sturb = Sl(CyclePosition) * (eo / ei) ^ (FracD - 2)
          FlameSpeedRatioTheoretical(CyclePosition) = Sturb /
Sl(CyclePosition)

          FERI_Factor(CyclePosition) = FSRActual(CyclePosition) _
                              / FlameSpeedRatioTheoretical(CyclePosition)

          TaylorLengthScale(CyclePosition) = (40.4 * kv * li / ut) ^ 0.5 /
Sl(CyclePosition)
          ReTurb(CyclePosition) = ut * li / kv
          'SAE 850345
          Damkohler(CyclePosition) = (li / ut) * (SlUnStrech(CyclePosition) /
(kv / SlUnStrech(CyclePosition)))

          TurbulentIntensity(CyclePosition) = ut

'++++++++++++++++++FRACTAL FINISH++++++++++++++
```

```
'++TURBULENT INTENSITY & FLAME SPEED CALCULATION BASED ON
LANCASTER u' MEASUREMENTS+++++
'+++++START++++++++++++++++++


TurbIntZeroLANCASTER(CyclePosition) = 1.7 + (((((0.0012 * RPM -
0.2267) - 1.57) / 1.57)  + (((0.0083264 * MAP + 0.94107069) - 1.70) /
1.70) + (((0.03783582 * CR + 1.1319092) - 1.46) / 1.46) ) * 1.7)

TurbIntLANCASTER(CyclePosition)=TurbIntZeroLANCASTER(CyclePosition)
* ((UnburnedGasDensity(CyclePosition) / UnburnedGasDensityAt45deg) ^
(1 / 3))

TurbConstLANCASTER(CyclePosition) = 1
StLANCASTER(CyclePosition) = SlUnStrech(CyclePosition) +
TurbConstLANCASTER(CyclePosition) * TurbIntLANCASTER(CyclePosition)

FSR_LANCASTER(CyclePosition) = StLANCASTER(CyclePosition) /
SlUnStrech(CyclePosition)
FERI_Factor_LANCASTER(CyclePosition) = FSRActual(CyclePosition) _
                                / FSR_LANCASTER(CyclePosition)

'SAE 850345
TaylorLengthScaleLANCASTER(CyclePosition) = (40.4 * kv * li /
TurbIntLANCASTER(CyclePosition)) ^ 0.5 / SlUnStrech(CyclePosition)
ReTurbLANCASTER(CyclePosition) = TurbIntLANCASTER(CyclePosition) *
li / kv
DamkohlerLANCASTER(CyclePosition) = (li
/TurbIntLANCASTER(CyclePosition)) * (SlUnStrech(CyclePosition) / (kv /
SlUnStrech(CyclePosition)))

uSlC8H18Lumsden(CyclePosition) = TurbulentIntensity(CyclePosition) /
SlC8H18(CyclePosition)
uSlH2Lumsden(CyclePosition) = TurbulentIntensity(CyclePosition) /
SlH2(CyclePosition)
uSlC8H18Lancaster(CyclePosition) = TurbIntLANCASTER(CyclePosition) /
SlC8H18(CyclePosition)
uSlH2Lancaster(CyclePosition) = TurbIntLANCASTER(CyclePosition) /
SlH2(CyclePosition)

      End If
CyclePosition = CyclePosition + 1
Wend

FlameRadiusMAX = Application.WorksheetFunction.Max(FlameRadius)
CyclePosition = 1
While CyclePosition < 650
FlameRadiusNORMALIZED(CyclePosition) = FlameRadius(CyclePosition) /
FlameRadiusMAX
CyclePosition = CyclePosition + 1
'MsgBox "FlameRadiusNORMALIZED(CyclePosition) " &
FlameRadiusNORMALIZED(CyclePosition)

Wend

End Sub

Sub CalculateBurnedTemperature()

'y0 = the point we want to find
'y1= 1 point before y1 = 1 step before y0
'y2= 2 points before y2 = 2 steps before y0
'y3= 3 points before y3 = 3 steps before y0
'y4= 4 points before y4 = 4 steps before y0

Dim y0_predicted, y0  As Double
Dim i, y1, dydx, dydx0, dydx2, dydx3, dydx4, dydx5, dx As Double
Dim dth, Pressure, Volume, Vu, dpdth, mb, Rb, dvdth, Tb, Tu, Ru,
dmbdth, Cpu, dQudth, dydx9, dydx8 As Double
'Dim dydx1 As Double

dth = CrankAngle(CyclePosition + 1, 1) - CrankAngle(CyclePosition, 1)
'MsgBox "dth  " & dth
Pressure = CylinderPressure(CyclePosition, 1)
'MsgBox "Pressure  " & Pressure
dpdth = DerivativeCylinderPressure(CyclePosition, 1)
'MsgBox "dpdth  " & dpdth
Volume = VolumeAtCrankAngle(CyclePosition, 1)
'MsgBox "Volume  " & Volume
Vu = UnburnedVolume(CyclePosition)
'MsgBox "Vu  " & Vu
mb = MFB(CyclePosition, 1)
'MsgBox "mb  " & mb
Rb = BurnedRgas(CyclePosition)
'MsgBox "Rb  " & Rb
dvdth = DerivativeVolumeAtCrankAngle(CyclePosition)
'MsgBox "dvdth  " & dvdth
Tb = BurnedTemperature(CyclePosition)
'MsgBox "Tb  " & Tb
Tu = UnburnedTemperature(CyclePosition)
'MsgBox "Tu  " & Tu
Ru = UnburnedRgas(CyclePosition)
'MsgBox "Ru  " & Ru
dmbdth = MBR(CyclePosition, 1)
'MsgBox "dmbdth  " & dmbdth
Cpu = UnburnedCp(CyclePosition)
'MsgBox "Cpu  " & Cpu
dQudth = UnburnedHeatTransferRate(CyclePosition)
'MsgBox "dQudth  " & dQudth



dydx1(CyclePosition) = (CylinderPressure(CyclePosition, 1) /
(MFB(CyclePosition, 1) * MassOfCharge * BurnedRgas(CyclePosition))) * _
                        (DerivativeVolumeAtCrankAngle(CyclePosition) + _
                          ((BurnedRgas(CyclePosition) *
BurnedTemperature(CyclePosition) - UnburnedRgas(CyclePosition) *
UnburnedTemperature(CyclePosition)) * (MassOfCharge *
MBR(CyclePosition, 1) / CylinderPressure(CyclePosition, 1))) - _
                           (UnburnedRgas(CyclePosition) *
UnburnedVolume(CyclePosition) *
DerivativeCylinderPressure(CyclePosition, 1) /
(CylinderPressure(CyclePosition, 1) * UnburnedCp(CyclePosition))) - _
                           (UnburnedRgas(CyclePosition) *
UnburnedHeatTransferRate(CyclePosition) /
(CylinderPressure(CyclePosition, 1) * UnburnedCp(CyclePosition))) + _
                           (VolumeAtCrankAngle(CyclePosition, 1) *
DerivativeCylinderPressure(CyclePosition, 1) /
CylinderPressure(CyclePosition, 1)) _
                          )


dydx1(CyclePosition) = dydx1(CyclePosition) * (2 * PI / 180)

If dydx1(CyclePosition) < 0 Then
dydx1(CyclePosition) = 0
End If

If CrankAngle(CyclePosition, 1) <= MBT + 3 Then
   BurnedTemperature(CyclePosition + 1) =
BurnedTemperature(CyclePosition) + dydx1(CyclePosition) * dth
Else
   dydx2 = (CylinderPressure(CyclePosition - 1, 1) / (MFB(CyclePosition -
1, 1) * MassOfCharge * BurnedRgas(CyclePosition - 1))) * _
                        (DerivativeVolumeAtCrankAngle(CyclePosition - 1) +
_
                          ((BurnedRgas(CyclePosition - 1) *
BurnedTemperature(CyclePosition - 1) - UnburnedRgas(CyclePosition - 1)
* UnburnedTemperature(CyclePosition - 1)) * (MassOfCharge *
MBR(CyclePosition - 1, 1) / CylinderPressure(CyclePosition - 1, 1))) - _
                           (UnburnedRgas(CyclePosition - 1) *
UnburnedVolume(CyclePosition - 1) *
DerivativeCylinderPressure(CyclePosition - 1, 1) /
(CylinderPressure(CyclePosition - 1, 1) * UnburnedCp(CyclePosition - 1))) -
_
                           (UnburnedRgas(CyclePosition - 1) *
UnburnedHeatTransferRate(CyclePosition - 1) /
(CylinderPressure(CyclePosition - 1, 1) * UnburnedCp(CyclePosition - 1)))
+ _
                           (VolumeAtCrankAngle(CyclePosition - 1, 1) *
DerivativeCylinderPressure(CyclePosition - 1, 1) /
CylinderPressure(CyclePosition - 1, 1)) _
                          )


   dydx2 = dydx2 * (2 * PI / 180)

   dydx3 = (CylinderPressure(CyclePosition - 2, 1) / (MFB(CyclePosition -
2, 1) * MassOfCharge * BurnedRgas(CyclePosition - 2))) * _
                        (DerivativeVolumeAtCrankAngle(CyclePosition - 2) +
_
                          ((BurnedRgas(CyclePosition - 2) *
BurnedTemperature(CyclePosition - 2) - UnburnedRgas(CyclePosition - 2)
* UnburnedTemperature(CyclePosition - 2)) * (MassOfCharge *
MBR(CyclePosition - 2, 1) / CylinderPressure(CyclePosition - 2, 1))) - _
                           (UnburnedRgas(CyclePosition - 2) *
UnburnedVolume(CyclePosition - 2) *
DerivativeCylinderPressure(CyclePosition - 2, 1) /
(CylinderPressure(CyclePosition - 2, 1) * UnburnedCp(CyclePosition - 2))) -
_
                           (UnburnedRgas(CyclePosition - 2) *
UnburnedHeatTransferRate(CyclePosition - 2) /
(CylinderPressure(CyclePosition - 2, 1) * UnburnedCp(CyclePosition - 2)))
+ _
                           (VolumeAtCrankAngle(CyclePosition - 2, 1) *
DerivativeCylinderPressure(CyclePosition - 2, 1) /
CylinderPressure(CyclePosition - 2, 1)) _
                          )


   dydx3 = dydx3 * (2 * PI / 180)

   dydx4 = (CylinderPressure(CyclePosition - 3, 1) / (MFB(CyclePosition -
3, 1) * MassOfCharge * BurnedRgas(CyclePosition - 3))) * _
```

```
                    (DerivativeVolumeAtCrankAngle(CyclePosition - 3) +
_
                    ((BurnedRgas(CyclePosition - 3) *
BurnedTemperature(CyclePosition - 3) - UnburnedRgas(CyclePosition - 3)
* UnburnedTemperature(CyclePosition - 3)) * (MassOfCharge *
MBR(CyclePosition - 3, 1) / CylinderPressure(CyclePosition - 3, 1))) - _
                    (UnburnedRgas(CyclePosition - 3) *
UnburnedVolume(CyclePosition - 3) *
DerivativeCylinderPressure(CyclePosition - 3, 1) /
(CylinderPressure(CyclePosition - 3, 1) * UnburnedCp(CyclePosition - 3))) -
_
                    (UnburnedRgas(CyclePosition - 3) *
UnburnedHeatTransferRate(CyclePosition - 3) /
(CylinderPressure(CyclePosition - 3, 1) * UnburnedCp(CyclePosition - 3)))
+ _
                    (VolumeAtCrankAngle(CyclePosition - 3, 1) *
DerivativeCylinderPressure(CyclePosition - 3, 1) /
CylinderPressure(CyclePosition - 3, 1)) _
                    )


   dydx4 = dydx4 * (2 * PI / 180)


   dydx5 = (CylinderPressure(CyclePosition - 4, 1) / (MFB(CyclePosition -
4, 1) * MassOfCharge * BurnedRgas(CyclePosition - 4))) * _
                    (DerivativeVolumeAtCrankAngle(CyclePosition - 4) +
_
                    ((BurnedRgas(CyclePosition - 4) *
BurnedTemperature(CyclePosition - 4) - UnburnedRgas(CyclePosition - 4)
* UnburnedTemperature(CyclePosition - 4)) * (MassOfCharge *
MBR(CyclePosition - 4, 1) / CylinderPressure(CyclePosition - 4, 1))) - _
                    (UnburnedRgas(CyclePosition - 4) *
UnburnedVolume(CyclePosition - 4) *
DerivativeCylinderPressure(CyclePosition - 4, 1) /
(CylinderPressure(CyclePosition - 4, 1) * UnburnedCp(CyclePosition - 4))) -
_
                    (UnburnedRgas(CyclePosition - 4) *
UnburnedHeatTransferRate(CyclePosition - 4) /
(CylinderPressure(CyclePosition - 4, 1) * UnburnedCp(CyclePosition - 4)))
+ _
                    (VolumeAtCrankAngle(CyclePosition - 4, 1) *
DerivativeCylinderPressure(CyclePosition - 4, 1) /
CylinderPressure(CyclePosition - 4, 1)) _
                    )


   dydx5 = dydx5 * (2 * PI / 180)

   'Adams-Bashford predictor
   BurnedTemperature(CyclePosition + 1) =
BurnedTemperature(CyclePosition) + _
    ((dth / 720) * (1901 * dydx1(CyclePosition) - 2774 * dydx2 + 2616 *
dydx3 - 1274 * dydx4 + 251 * dydx5))
   'MsgBox "BurnedTemperature(CyclePosition + 1) FIRST " &
BurnedTemperature(CyclePosition + 1)


End If
      BurnedVolume(CyclePosition + 1) = BurnedRgas(CyclePosition) *
BurnedTemperature(CyclePosition + 1) * MassOfCharge *
MFB(CyclePosition + 1, 1) _
                    / CylinderPressure(CyclePosition + 1, 1)

      BurnedGasDensity(CyclePosition + 1) =
CylinderPressure(CyclePosition + 1, 1) / (BurnedRgas(CyclePosition) *
BurnedTemperature(CyclePosition + 1))

 Call Main_ChemicalEquilibriumCompositionInput

      UnburnedRgas(CyclePosition + 1) = (UnburnedCp(CyclePosition + 1)
* (1 - (1 / UnburnedGamma(CyclePosition + 1))))

      BurnedRgas(CyclePosition + 1) = (BurnedCp(CyclePosition + 1) * (1
- (1 / BurnedGamma(CyclePosition + 1))))

      BurnedVolume(CyclePosition + 1) = BurnedRgas(CyclePosition + 1)
* BurnedTemperature(CyclePosition + 1) * MassOfCharge *
MFB(CyclePosition + 1, 1) _
                    / CylinderPressure(CyclePosition + 1, 1)

      BurnedGasDensity(CyclePosition + 1) =
CylinderPressure(CyclePosition + 1, 1) / (BurnedRgas(CyclePosition + 1) *
BurnedTemperature(CyclePosition + 1))

      UnburnedVolume(CyclePosition + 1) =
VolumeAtCrankAngle(CyclePosition + 1, 1) - BurnedVolume(CyclePosition
+ 1)

      UnburnedTemperature(CyclePosition + 1) =
CylinderPressure(CyclePosition + 1, 1) * UnburnedVolume(CyclePosition +
1) / _
                    (MassOfCharge * (1 - MFB(CyclePosition + 1,
1)) * UnburnedRgas(CyclePosition + 1))

      If UnburnedTemperature(CyclePosition + 1) < 500 Then
      UnburnedTemperature(CyclePosition + 1) =
BurnedTemperature(CyclePosition + 1)
      UnburnedTemperature2(CyclePosition + 1) =
BurnedTemperature(CyclePosition + 1)

      End If
If CrankAngle(CyclePosition, 1) >= MBT + 3 Then
   'Adams-Moulton corrector
   dydx0 = (CylinderPressure(CyclePosition + 1, 1) / (MFB(CyclePosition +
1, 1) * MassOfCharge * BurnedRgas(CyclePosition + 1))) * _
                    (DerivativeVolumeAtCrankAngle(CyclePosition + 1) +
_
                    ((BurnedRgas(CyclePosition + 1) *
BurnedTemperature(CyclePosition + 1) - UnburnedRgas(CyclePosition +
1) * UnburnedTemperature(CyclePosition + 1)) * (MassOfCharge *
MBR(CyclePosition + 1, 1) / CylinderPressure(CyclePosition + 1, 1))) - _
                    (UnburnedRgas(CyclePosition + 1) *
UnburnedVolume(CyclePosition + 1) *
DerivativeCylinderPressure(CyclePosition + 1, 1) /
(CylinderPressure(CyclePosition + 1, 1) * UnburnedCp(CyclePosition +
1))) - _
                    (UnburnedRgas(CyclePosition + 1) *
UnburnedHeatTransferRate(CyclePosition + 1) /
(CylinderPressure(CyclePosition + 1, 1) * UnburnedCp(CyclePosition +
1))) + _
                    (VolumeAtCrankAngle(CyclePosition + 1, 1) *
DerivativeCylinderPressure(CyclePosition + 1, 1) /
CylinderPressure(CyclePosition + 1, 1)) _
                    )


   dydx0 = dydx0 * (2 * PI / 180)

   BurnedTemperature(CyclePosition + 1) =
BurnedTemperature(CyclePosition) + _
   ((dth / 720) * (251 * dydx0 + 646 * dydx1(CyclePosition) - 264 *
dydx2 + 106 * dydx3 - 19 * dydx4))

    'MsgBox "BurnedTemperature(CyclePosition + 1) FINAL " &
BurnedTemperature(CyclePosition + 1)

      BurnedVolume(CyclePosition + 1) = BurnedRgas(CyclePosition) *
BurnedTemperature(CyclePosition + 1) * MassOfCharge *
MFB(CyclePosition + 1, 1) _
                    / CylinderPressure(CyclePosition + 1, 1)

      BurnedGasDensity(CyclePosition + 1) =
CylinderPressure(CyclePosition + 1, 1) / (BurnedRgas(CyclePosition) *
BurnedTemperature(CyclePosition + 1))

 Call Main_ChemicalEquilibriumCompositionInput

      UnburnedRgas(CyclePosition + 1) = (UnburnedCp(CyclePosition + 1)
* (1 - (1 / UnburnedGamma(CyclePosition + 1))))

      BurnedRgas(CyclePosition + 1) = (BurnedCp(CyclePosition + 1) * (1
- (1 / BurnedGamma(CyclePosition + 1))))

      BurnedVolume(CyclePosition + 1) = BurnedRgas(CyclePosition + 1)
* BurnedTemperature(CyclePosition + 1) * MassOfCharge *
MFB(CyclePosition + 1, 1) _
                    / CylinderPressure(CyclePosition + 1, 1)

      BurnedGasDensity(CyclePosition + 1) =
CylinderPressure(CyclePosition + 1, 1) / (BurnedRgas(CyclePosition + 1) *
BurnedTemperature(CyclePosition + 1))

      UnburnedVolume(CyclePosition + 1) =
VolumeAtCrankAngle(CyclePosition + 1, 1) - BurnedVolume(CyclePosition
+ 1)

      UnburnedTemperature(CyclePosition + 1) =
CylinderPressure(CyclePosition + 1, 1) * UnburnedVolume(CyclePosition +
1) / _
                    (MassOfCharge * (1 - MFB(CyclePosition + 1,
1)) * UnburnedRgas(CyclePosition + 1))

      UnburnedGasDensity(CyclePosition + 1) =
CylinderPressure(CyclePosition + 1, 1) / (UnburnedRgas(CyclePosition +
1) * UnburnedTemperature(CyclePosition + 1))

      If UnburnedTemperature(CyclePosition + 1) < 500 Then
      UnburnedTemperature(CyclePosition + 1) =
BurnedTemperature(CyclePosition + 1)
      UnburnedTemperature2(CyclePosition + 1) =
BurnedTemperature(CyclePosition + 1)
      End If
```

```
End If


End Sub'Integrate using Adams-Bashford-Moulton 5th order method
Private Sub CalculateUnburnedTemperature2(Method1EqualsMethod2)

'y0 = the point we want to find
'y1= 1 point before y1 = 1 step before y0
'y2= 2 points before y2 = 2 steps before y0
'y3= 3 points before y3 = 3 steps before y0
'y4= 4 points before y4 = 4 steps before y0

Dim i, dydx0, dydx1, dydx2, dydx3, dydx4, dydx5, dth As Double

dth = CrankAngle(CyclePosition + 1, 1) - CrankAngle(CyclePosition, 1)

 dydx1 = UnburnedTemperature2(CyclePosition) * _
      (DerivativeVolumeAtCrankAngle(CyclePosition) /
VolumeAtCrankAngle(CyclePosition, 1) + _
       DerivativeCylinderPressure(CyclePosition, 1) /
CylinderPressure(CyclePosition, 1))
' MsgBox "dydx1  " & dydx1

 dydx2 = UnburnedTemperature2(CyclePosition - 1) * _
      (DerivativeVolumeAtCrankAngle(CyclePosition - 1) /
VolumeAtCrankAngle(CyclePosition - 1, 1) + _
       DerivativeCylinderPressure(CyclePosition - 1, 1) /
CylinderPressure(CyclePosition - 1, 1))
 'MsgBox "dydx2  " & dydx2
 dydx3 = UnburnedTemperature2(CyclePosition - 2) * _
      (DerivativeVolumeAtCrankAngle(CyclePosition - 2) /
VolumeAtCrankAngle(CyclePosition - 2, 1) + _
       DerivativeCylinderPressure(CyclePosition - 2, 1) /
CylinderPressure(CyclePosition - 2, 1))
 'MsgBox "dydx3  " & dydx3
 dydx4 = UnburnedTemperature2(CyclePosition - 3) * _
      (DerivativeVolumeAtCrankAngle(CyclePosition - 3) /
VolumeAtCrankAngle(CyclePosition - 3, 1) + _
       DerivativeCylinderPressure(CyclePosition - 3, 1) /
CylinderPressure(CyclePosition - 3, 1))
 'MsgBox "dydx4  " & dydx4
 dydx5 = UnburnedTemperature2(CyclePosition - 4) * _
      (DerivativeVolumeAtCrankAngle(CyclePosition - 4) /
VolumeAtCrankAngle(CyclePosition - 4, 1) + _
       DerivativeCylinderPressure(CyclePosition - 4, 1) /
CylinderPressure(CyclePosition - 4, 1))
'MsgBox "dydx5  " & dydx5
   'Adams-Bashford predictor
   UnburnedTemperature2(CyclePosition + 1) = _
                              UnburnedTemperature2(CyclePosition) + _
   ((dth / 720) * (1901 * dydx1 - 2774 * dydx2 + 2616 * dydx3 - 1274 *
dydx4 + 251 * dydx5))

   'Adams-Moulton corrector
   dydx0 = UnburnedTemperature2(CyclePosition + 1) * _
     (DerivativeVolumeAtCrankAngle(CyclePosition + 1) /
VolumeAtCrankAngle(CyclePosition + 1, 1) + _
       DerivativeCylinderPressure(CyclePosition + 1, 1) /
CylinderPressure(CyclePosition + 1, 1))

 UnburnedTemperature2(CyclePosition + 1) =
UnburnedTemperature2(CyclePosition) + _
   ((dth / 720) * (251 * dydx0 + 646 * dydx1 - 264 * dydx2 + 106 *
dydx3 - 19 * dydx4))

   'MsgBox "UnburnedTemperature2(CyclePosition + 1)" &
UnburnedTemperature2(CyclePosition + 1)

   If Method1EqualsMethod2 = "yes" Then
   UnburnedTemperature(CyclePosition + 1) =
UnburnedTemperature2(CyclePosition + 1)
   UnburnedTemperature(CyclePosition) =
UnburnedTemperature2(CyclePosition)
   End If

End Sub

Sub HeatTransfer()

Call Hc_WOSCHNI

UnburnedHeatTransferRate(CyclePosition) = (30 *
UnburnedCylinderArea(CyclePosition) / RPM) *
(UnburnedHeatTransferCoefficient(CyclePosition) *
(UnburnedTemperature(CyclePosition) - AVERAGE_WALL_TEMP) +
0.6 * SIGMA * (UnburnedTemperature(CyclePosition) ^ 4 -
AVERAGE_WALL_TEMP ^ 4))

UnburnedHeatTransferRate(CyclePosition) =
UnburnedHeatTransferRate(CyclePosition) * PI / 180
'MsgBox "UnburnedHeatTransferRate(CyclePosition)  " &
UnburnedHeatTransferRate(CyclePosition)

End Sub
'function Hc_WOSCHNI calculates the heat transfer coefficient using the
'WOSCHNI theory. Heywood p679
Sub Hc_WOSCHNI()

Dim C1, C2 As Double
Dim w As Double     'w= average gas velocity in cylinder
Dim Tr, Vr, Pr, Vd, Pm, P, Tg, Sp, angle, ign, m As Double

m = 0.8
Tr = TemperatureAtIVC
Vr = VolumeAtIVC
Pr = PressureAtIVC
Vd = VolumeAtCrankAngle(CyclePosition, 1)
Pm = MotoringPressure(CyclePosition, 1)
P = CylinderPressure(CyclePosition, 1)
Tg = UnburnedTemperature(CyclePosition)
Sp = MeanPistonSpeed
angle = CrankAngle(CyclePosition, 1)
ign = MBT

'-146 inlet valve closes
If angle < -146 And angle >= -180 Then

   C1 = 6.18
   C2 = 0
   w = (C1 * Sp) + (C2 * Vd * Tr * (P - Pm) / (Pr * Vr))

   ElseIf angle < ign And angle >= -146 Then

   C1 = 2.28
   C2 = 0
   w = (C1 * Sp) + (C2 * Vd * Tr * (P - Pm) / (Pr * Vr))

   ElseIf angle < 0 And angle >= ign Then

   C1 = 2.28
   C2 = 3.24 * (10 ^ -3)
   w = (C1 * Sp) + (C2 * Vd * Tr * (P - Pm) / (Pr * Vr))

   '120 exhaust  valve opens
   ElseIf angle < 120 And angle >= 0 Then

   C1 = 2.28
   C2 = 3.24 * (10 ^ -3)
   w = (C1 * Sp) + (C2 * Vd * Tr * (P - Pm) / (Pr * Vr))

   ElseIf angle <= 540 And angle >= 120 Then

   C1 = 6.18
   C2 = 0
   w = (C1 * Sp) + (C2 * Vd * Tr * (P - Pm) / (Pr * Vr))

End If

'Unusually pressure is required in KPa, therefore P/1000
'3.26 = Calibration Constant 0-100 SAE 1999-01-0218

UnburnedHeatTransferCoefficient(CyclePosition) = 20 * _
(Bore ^ (m - 1)) * ((P / 1000) ^ m) * (w ^ m) * (Tg ^ (0.75 - (1.62 *
m)))

End Sub
Private Sub InitialiseChemicalEquilibriumCalculation()

'Tstep
 Worksheets("Equilibrium Table Input").Range("e7").Value = 0.01
'Tmax
Worksheets("Equilibrium Table Input").Range("e6").Value = 1800
'Tmin
Worksheets("Equilibrium Table Input").Range("e5").Value = 1800 - 0.01
'Lambda
Worksheets("Equilibrium Table Input").Range("e8").Value = 1 'Lambda
'Density
Worksheets("Equilibrium Table Input").Range("e9").Value = 1.2
'molHmolC
Worksheets("Equilibrium Table Input").Range("e14").Value = 4
'molNmolO
Worksheets("Equilibrium Table Input").Range("e15").Value = 79 / 21
'VolumeFractionOfN2toO2
'molCOmolCO2
Worksheets("Equilibrium Table Input").Range("e16").Value = 2000
'ErrorLimit
Worksheets("Equilibrium Table Input").Range("e18").Value =
0.0000000001
'FuelWeight
Worksheets("Equilibrium Table Input").Range("e19").Value = 16.043
'FuelEnthalpyOfFormation
Worksheets("Equilibrium Table Input").Range("e20").Value = -74873
'FuelAirTemp
Worksheets("Equilibrium Table Input").Range("e21").Value = 1800
```

```
'FuelType
Worksheets("Equilibrium Table Input").Range("e11").Value =
MainChamberFuel
'VaryFuelAirTemp
Worksheets("Equilibrium Table Input").Range("e22").Value = "yes"
'Unburned FuelAirTemp
Worksheets("Equilibrium Table Input").Range("e23").Value =
UnburnedTemperature(CyclePosition)

End Sub
'up until ignition burned properties are zero
Private Sub SetBurnedPropertiesToZERO()

 BurnedInternalEnergy(CyclePosition) = 0
 BurnedEnthalpy(CyclePosition) = 0
 BurnedCp(CyclePosition) = 0
 BurnedCv(CyclePosition) = 0
 BurnedGamma(CyclePosition) = 0
 BurnedRgas(CyclePosition) = 0
 BurnedMolecularWeight(CyclePosition) = 0
 BurnedVolume(CyclePosition) = 0
 BurnedTemperature(CyclePosition) = 0
 BurnedHeatTransferCoefficient(CyclePosition) = 0
 BurnedGasDensity(CyclePosition) = 0

 BurnedCylinderArea(CyclePosition) = 0
 BurnedCylinderHeadArea(CyclePosition) = 0
 BurnedPistonArea(CyclePosition) = 0

 SlC8H18(CyclePosition) = 0
 SlH2(CyclePosition) = 0
 TurbulentFlameSpeed(CyclePosition) = 0
 FlameSpeed(CyclePosition) = 0
 FlameRadius(CyclePosition) = 0
 FlameSurfaceArea(CyclePosition) = 0
 AdiabaticFlameTemperature(CyclePosition) = 0
 FlameSpeedRatioActualC8H18(CyclePosition) = 0
 FlameSpeedRatioActualH2(CyclePosition) = 0
 FlameSpeedRatioTheoretical(CyclePosition) = 0
 FERI_Factor(CyclePosition) = 0

TaylorLengthScaleLANCASTER(CyclePosition) = 0
ReTurbLANCASTER(CyclePosition) = 0
DamkohlerLANCASTER(CyclePosition) = 0

TurbIntZeroLANCASTER(CyclePosition) = 0
TurbIntLANCASTER(CyclePosition) = 0
TurbConstLANCASTER(CyclePosition) = 0
SlUnStrech(CyclePosition) = 0
FSR_LANCASTER(CyclePosition) = 0
FSRActual(CyclePosition) = 0
FERI_Factor_LANCASTER(CyclePosition) = 0
StLANCASTER(CyclePosition) = 0

End Sub

Sub ExhaustGasMassFraction()

Dim MassOfAirPerCycle As Double
Dim VolumeOfAirPerCycle As Double
Dim MassFractionOfAir As Double
Dim TempMassFracN2 As Double, TempMassFracO2 As Double
Dim MassFractionOfN2 As Double, MassFractionOfO2 As Double
Dim VolumeFractionOfN2 As Double, VolumeFractionOfO2 As Double
Dim OF As Double

'SAE 931025 (CFR engine has approx 70deg. overlap and 6.5mm valve lift
this makes the 'over lap factor equal to 2.32 (CFR cam details
SAE760159))

OF = (1.45 / 82.55) * (107 + 7.8 * 70 + 70 ^ 2) * (25 * 6.5 / (82.55 ^
2))

ResidualGasMassFraction = ((1.266 * OF / RPM) * ((MAP / 101.3) ^ (-
0.87)) * (Abs(101.3 - MAP) ^ 0.5)) + (0.632 * Phi * ((MAP / 101.3) ^ -
0.74) / CR)
'mass fraction of air = total mass - residual gas - fuel
MassFractionOfAir = 1 - ResidualGasMassFraction -  ((1 -
ResidualGasMassFraction) / ((StoichiometricAFR * Lambda) + 1))

'mass fraction of atmospheric air
TempMassFracN2 = 0.79 * 28 / (0.79 * 28 + 0.21 * 32)
TempMassFracO2 = 0.21 * 32 / (0.79 * 28 + 0.21 * 32)

'mass fraction of N2 and O2 in cylinder
MassFractionOfN2 = (ResidualGasMassFraction + (MassFractionOfAir *
TempMassFracN2)) / (ResidualGasMassFraction + MassFractionOfAir)
'MsgBox "MassFractionOfN2   " & MassFractionOfN2
MassFractionOfO2 = ((MassFractionOfAir * TempMassFracO2)) /
(ResidualGasMassFraction + MassFractionOfAir)
VolumeFractionOfN2 = (MassFractionOfN2 / 28) / ((MassFractionOfN2 /
28) + (MassFractionOfO2 / 32))
VolumeFractionOfO2 = (MassFractionOfO2 / 32) / ((MassFractionOfN2 /
28) + (MassFractionOfO2 / 32))

VolumeFractionOfN2toO2 = VolumeFractionOfN2 / VolumeFractionOfO2

'MsgBox "VolumeFractionOfN2toO2   " & VolumeFractionOfN2toO2

'the following method also can calculate the residual mass fraction (SAE
972889)
'Dim Vevc As Double
'Dim Vevo As Double
'Dim Pevc As Double
'Dim Pevo As Double
'Dim i As Double
''find pressure and volume at EVO
'i = 1
'Do Until CrankAngle(i, 1) = EVO Or CrankAngle(i, 1) > EVO
'i = i + 1
'Loop
'Pevo = CylinderPressure(i, 1)
'Vevo = VolumeAtCrankAngle(i, 1)
'find pressure and volume at EVC
'i = 1
'Do Until CrankAngle(i, 1) = EVC Or CrankAngle(i, 1) > EVC
'i = i + 1
'Loop
'Pevc = CylinderPressure(i, 1)
'Vevc = VolumeAtCrankAngle(i, 1)
'ResidualGasMassFraction = ((Vevc / Vevo) * (Pevc / Pevo)) ^ (1 / 1.32)
'MsgBox "ResidualGasMassFraction 2  " & ResidualGasMassFraction
End Sub

Sub PrintAnalysisToScreen()

Application.ScreenUpdating = False

Sheets("Engine Modeling Output").Select
Range("A1").Select
'Worksheets("Engine Modeling Output").Range("f71").Value =
UnburnedEnthalpy(1)
'Worksheets("Engine Modeling Output").Range("f73").Value =
BurnedEnthalpy(1)
'Worksheets("Engine Modeling Output").Range("f74").Value =
BurnedCp(1)
'Worksheets("Engine Modeling Output").Range("f75").Value =
BurnedGamma(1)
'Worksheets("Engine Modeling Output").Range("f76").Value =
BurnedMolecularWeight(1)
'Worksheets("Engine Modeling Output").Range("f77").Value =
BurnedTemperature(1)
'Worksheets("Engine Modeling Output").Range("f79").Value =
UnburnedEnthalpy(1)
'Worksheets("Engine Modeling Output").Range("f80").Value =
UnburnedCp(1)
'Worksheets("Engine Modeling Output").Range("f81").Value =
UnburnedGamma(1)
'Worksheets("Engine Modeling Output").Range("f82").Value =
UnburnedMolecularWeight(1)
'Worksheets("Engine Modeling Output").Range("f83").Value =
UnburnedTemperature(1)

Sheets("Engine Modeling Output").Select
Range("A1").Select

Worksheets("Engine Modeling Output").Range(Cells(200, 3),
Cells(NUMBER_OF_DATA_POINTS, 3)).Value _
= CrankAngle
Worksheets("Engine Modeling Output").Range(Cells(200, 4),
Cells(NUMBER_OF_DATA_POINTS, 4)).Value _
= VolumeAtCrankAngle
Worksheets("Engine Modeling Output").Range(Cells(200, 5),
Cells(NUMBER_OF_DATA_POINTS, 5)).Value = _
Application.WorksheetFunction.Transpose(DerivativeUnburnedVolume)
Worksheets("Engine Modeling Output").Range(Cells(200, 6),
Cells(NUMBER_OF_DATA_POINTS, 6)).Value = _
Application.WorksheetFunction.Transpose(UnburnedCylinderArea)
Worksheets("Engine Modeling Output").Range(Cells(200, 7),
Cells(NUMBER_OF_DATA_POINTS, 7)).Value = _
Application.WorksheetFunction.Transpose(UnburnedCylinderHeadArea)
Worksheets("Engine Modeling Output").Range(Cells(200, 8),
Cells(NUMBER_OF_DATA_POINTS, 8)).Value = _
Application.WorksheetFunction.Transpose(UnburnedPistonArea)
Worksheets("Engine Modeling Output").Range(Cells(200, 9),
Cells(NUMBER_OF_DATA_POINTS, 9)).Value = _
Application.WorksheetFunction.Transpose(UnburnedGasDensity)
Worksheets("Engine Modeling Output").Range(Cells(200, 10),
Cells(NUMBER_OF_DATA_POINTS, 10)).Value = _
Application.WorksheetFunction.Transpose(UnburnedTemperature)
Worksheets("Engine Modeling Output").Range(Cells(200, 11),
Cells(NUMBER_OF_DATA_POINTS, 11)).Value = _
Application.WorksheetFunction.Transpose(UnburnedTemperature2)
```

```
Worksheets("Engine Modeling Output").Range(Cells(200, 12),
Cells(NUMBER_OF_DATA_POINTS, 12)).Value _
= CylinderPressure
Worksheets("Engine Modeling Output").Range(Cells(200, 13),
Cells(NUMBER_OF_DATA_POINTS, 13)).Value _
= DerivativeCylinderPressure
Worksheets("Engine Modeling Output").Range(Cells(200, 14),
Cells(NUMBER_OF_DATA_POINTS, 14)).Value = _
Application.WorksheetFunction.Transpose(dydx1)
Worksheets("Engine Modeling Output").Range(Cells(200, 15),
Cells(NUMBER_OF_DATA_POINTS, 15)).Value _
= Application.WorksheetFunction.Transpose(BurnedTemperature)
Worksheets("Engine Modeling Output").Range(Cells(200, 16),
Cells(NUMBER_OF_DATA_POINTS, 16)).Value _
= Application.WorksheetFunction.Transpose(UnburnedTemperature)
 Worksheets("Engine Modeling Output").Range(Cells(200, 17),
Cells(NUMBER_OF_DATA_POINTS, 17)).Value _
= Application.WorksheetFunction.Transpose(BurnedVolume)
  Worksheets("Engine Modeling Output").Range(Cells(200, 18),
Cells(NUMBER_OF_DATA_POINTS, 18)).Value _
= Application.WorksheetFunction.Transpose(UnburnedVolume)
Worksheets("Engine Modeling Output").Range(Cells(200, 19),
Cells(NUMBER_OF_DATA_POINTS, 19)).Value _
= Application.WorksheetFunction.Transpose(BurnedGasDensity)
 Worksheets("Engine Modeling Output").Range(Cells(200, 20),
Cells(NUMBER_OF_DATA_POINTS, 20)).Value _
= Application.WorksheetFunction.Transpose(UnburnedGasDensity)
Worksheets("Engine Modeling Output").Range(Cells(200, 21),
Cells(NUMBER_OF_DATA_POINTS, 21)).Value _
= Application.WorksheetFunction.Transpose(BurnedRgas)
Worksheets("Engine Modeling Output").Range(Cells(200, 22),
Cells(NUMBER_OF_DATA_POINTS, 22)).Value _
= Application.WorksheetFunction.Transpose(UnburnedRgas)
Worksheets("Engine Modeling Output").Range(Cells(200, 23),
Cells(NUMBER_OF_DATA_POINTS, 23)).Value _
=
Application.WorksheetFunction.Transpose(UnburnedHeatTransferCoefficie
nt)
Worksheets("Engine Modeling Output").Range(Cells(200, 24),
Cells(NUMBER_OF_DATA_POINTS, 24)).Value _
= Application.WorksheetFunction.Transpose(AltBurnedTemp)
Worksheets("Engine Modeling Output").Range(Cells(200, 25),
Cells(NUMBER_OF_DATA_POINTS, 25)).Value _
= Application.WorksheetFunction.Transpose(BurnedTempForGraph)
Worksheets("Engine Modeling Output").Range(Cells(200, 26),
Cells(NUMBER_OF_DATA_POINTS, 26)).Value _
= Application.WorksheetFunction.Transpose(MeanTemperature)
Worksheets("Engine Modeling Output").Range(Cells(200, 27),
Cells(NUMBER_OF_DATA_POINTS, 27)).Value _
= Application.WorksheetFunction.Transpose(AdiabaticFlameTemperature)
Worksheets("Engine Modeling Output").Range(Cells(200, 28),
Cells(NUMBER_OF_DATA_POINTS, 28)).Value _
= Application.WorksheetFunction.Transpose(NOppm)
Worksheets("Engine Modeling Output").Range(Cells(200, 29),
Cells(NUMBER_OF_DATA_POINTS, 29)).Value _
= Application.WorksheetFunction.Transpose(NOppm2)
Worksheets("Engine Modeling Output").Range(Cells(200, 30),
Cells(NUMBER_OF_DATA_POINTS, 30)).Value _
= Application.WorksheetFunction.Transpose(NOmolfrac)
Worksheets("Engine Modeling Output").Range(Cells(200, 31),
Cells(NUMBER_OF_DATA_POINTS, 31)).Value _
= Application.WorksheetFunction.Transpose(FlameSurfaceArea)
Worksheets("Engine Modeling Output").Range(Cells(200, 32),
Cells(NUMBER_OF_DATA_POINTS, 32)).Value _
= Application.WorksheetFunction.Transpose(FlameSpeed)
Worksheets("Engine Modeling Output").Range(Cells(200, 33),
Cells(NUMBER_OF_DATA_POINTS, 33)).Value _
= Application.WorksheetFunction.Transpose(FlameRadius)
Worksheets("Engine Modeling Output").Range(Cells(200, 34),
Cells(NUMBER_OF_DATA_POINTS, 34)).Value _
= Application.WorksheetFunction.Transpose(SlC8H18)
Worksheets("Engine Modeling Output").Range(Cells(200, 35),
Cells(NUMBER_OF_DATA_POINTS, 35)).Value _
= Application.WorksheetFunction.Transpose(SlH2)
Worksheets("Engine Modeling Output").Range(Cells(200, 36),
Cells(NUMBER_OF_DATA_POINTS, 36)).Value _
=
Application.WorksheetFunction.Transpose(FlameSpeedRatioActualC8H18)
Worksheets("Engine Modeling Output").Range(Cells(200, 37),
Cells(NUMBER_OF_DATA_POINTS, 37)).Value _
= Application.WorksheetFunction.Transpose(FlameSpeedRatioActualH2)
Worksheets("Engine Modeling Output").Range(Cells(200, 38),
Cells(NUMBER_OF_DATA_POINTS, 38)).Value _
= Application.WorksheetFunction.Transpose(FlameSpeedRatioTheoretical)
Worksheets("Engine Modeling Output").Range(Cells(200, 39),
Cells(NUMBER_OF_DATA_POINTS, 39)).Value _
= Application.WorksheetFunction.Transpose(FlameSpeedRatioTheoretical)
Worksheets("Engine Modeling Output").Range(Cells(200, 40),
Cells(NUMBER_OF_DATA_POINTS, 40)).Value _
= Application.WorksheetFunction.Transpose(FERI_Factor)
Worksheets("Engine Modeling Output").Range(Cells(200, 41),
Cells(NUMBER_OF_DATA_POINTS, 41)).Value _
= Application.WorksheetFunction.Transpose(TaylorLengthScale)
Worksheets("Engine Modeling Output").Range(Cells(200, 42),
Cells(NUMBER_OF_DATA_POINTS, 42)).Value _
= Application.WorksheetFunction.Transpose(ReTurb)
Worksheets("Engine Modeling Output").Range(Cells(200, 43),
Cells(NUMBER_OF_DATA_POINTS, 43)).Value _
= Application.WorksheetFunction.Transpose(Damkohler)
Worksheets("Engine Modeling Output").Range(Cells(200, 44),
Cells(NUMBER_OF_DATA_POINTS, 44)).Value _
= Application.WorksheetFunction.Transpose(TurbulentIntensity)

Worksheets("Engine Modeling Output").Range("f66").Value = _
CrankAngleAtEquilibriumEqualEngineOutCO
Worksheets("Engine Modeling Output").Range("f68").Value = _
CrankAngleAtEquilibriumEqualEngineOutNOx
Worksheets("Engine Modeling Output").Range("f69").Value = _
CrankAngleAtEquilibriumEqualEngineOutCO2
Worksheets("Engine Modeling Output").Range("f70").Value = _
CrankAngleAtEquilibriumEqualEngineOutO2


Worksheets("Engine Modeling Output").Range(Cells(200, 45),
Cells(NUMBER_OF_DATA_POINTS, 45)).Value _
= Application.WorksheetFunction.Transpose(COmolfrac)
Worksheets("Engine Modeling Output").Range(Cells(200, 46),
Cells(NUMBER_OF_DATA_POINTS, 46)).Value _
= Application.WorksheetFunction.Transpose(CO2molfrac)
Worksheets("Engine Modeling Output").Range(Cells(200, 47),
Cells(NUMBER_OF_DATA_POINTS, 47)).Value _
= Application.WorksheetFunction.Transpose(O2molfrac)
Worksheets("Engine Modeling Output").Range(Cells(200, 48),
Cells(NUMBER_OF_DATA_POINTS, 48)).Value _
= Application.WorksheetFunction.Transpose(N2molfrac)
Worksheets("Engine Modeling Output").Range(Cells(200, 49),
Cells(NUMBER_OF_DATA_POINTS, 49)).Value _
= Application.WorksheetFunction.Transpose(Omolfrac)
Worksheets("Engine Modeling Output").Range(Cells(200, 50),
Cells(NUMBER_OF_DATA_POINTS, 50)).Value _
= Application.WorksheetFunction.Transpose(H2molfrac)
Worksheets("Engine Modeling Output").Range(Cells(200, 51),
Cells(NUMBER_OF_DATA_POINTS, 51)).Value _
= Application.WorksheetFunction.Transpose(OHmolfrac)
Worksheets("Engine Modeling Output").Range(Cells(200, 52),
Cells(NUMBER_OF_DATA_POINTS, 52)).Value _
= Application.WorksheetFunction.Transpose(Hmolfrac)
Worksheets("Engine Modeling Output").Range(Cells(200, 53),
Cells(NUMBER_OF_DATA_POINTS, 53)).Value _
= Application.WorksheetFunction.Transpose(H2Omolfrac)

Worksheets("Engine Modeling Output").Range(Cells(200, 54),
Cells(NUMBER_OF_DATA_POINTS, 54)).Value _
= Application.WorksheetFunction.Transpose(BurnedVolumeFraction)
Worksheets("Engine Modeling Output").Range(Cells(200, 55),
Cells(NUMBER_OF_DATA_POINTS, 55)).Value _
= Application.WorksheetFunction.Transpose(BurnedMassFraction)
Worksheets("Engine Modeling Output").Range(Cells(200, 56),
Cells(NUMBER_OF_DATA_POINTS, 56)).Value _
= Application.WorksheetFunction.Transpose(dRdt)
Worksheets("Engine Modeling Output").Range(Cells(200, 57),
Cells(NUMBER_OF_DATA_POINTS, 57)).Value _
= Application.WorksheetFunction.Transpose(dNOdth)


Worksheets("Engine Modeling Output").Range(Cells(200, 58),
Cells(NUMBER_OF_DATA_POINTS, 58)).Value _
= Application.WorksheetFunction.Transpose(TurbIntZeroLANCASTER)
Worksheets("Engine Modeling Output").Range(Cells(200, 59),
Cells(NUMBER_OF_DATA_POINTS, 59)).Value _
= Application.WorksheetFunction.Transpose(TurbIntLANCASTER)
Worksheets("Engine Modeling Output").Range(Cells(200, 60),
Cells(NUMBER_OF_DATA_POINTS, 60)).Value _
= Application.WorksheetFunction.Transpose(TurbConstLANCASTER)
Worksheets("Engine Modeling Output").Range(Cells(200, 61),
Cells(NUMBER_OF_DATA_POINTS, 61)).Value _
= Application.WorksheetFunction.Transpose(SlUnStrech)
Worksheets("Engine Modeling Output").Range(Cells(200, 62),
Cells(NUMBER_OF_DATA_POINTS, 62)).Value _
= Application.WorksheetFunction.Transpose(FSR_LANCASTER)
Worksheets("Engine Modeling Output").Range(Cells(200, 63),
Cells(NUMBER_OF_DATA_POINTS, 63)).Value _
= Application.WorksheetFunction.Transpose(FSRActual)
Worksheets("Engine Modeling Output").Range(Cells(200, 64),
Cells(NUMBER_OF_DATA_POINTS, 64)).Value _
= Application.WorksheetFunction.Transpose(FERI_Factor_LANCASTER)
Worksheets("Engine Modeling Output").Range(Cells(200, 65),
Cells(NUMBER_OF_DATA_POINTS, 65)).Value _
= Application.WorksheetFunction.Transpose(StLANCASTER)

Worksheets("Engine Modeling Output").Range(Cells(200, 66),
Cells(NUMBER_OF_DATA_POINTS, 66)).Value _
= Application.WorksheetFunction.Transpose(Sl)
```

```
Worksheets("Engine Modeling Output").Range(Cells(200, 67),
Cells(NUMBER_OF_DATA_POINTS, 67)).Value _
=
Application.WorksheetFunction.Transpose(TaylorLengthScaleLANCASTER)
Worksheets("Engine Modeling Output").Range(Cells(200, 68),
Cells(NUMBER_OF_DATA_POINTS, 68)).Value _
= Application.WorksheetFunction.Transpose(ReTurbLANCASTER)
Worksheets("Engine Modeling Output").Range(Cells(200, 69),
Cells(NUMBER_OF_DATA_POINTS, 69)).Value _
= Application.WorksheetFunction.Transpose(DamkohlerLANCASTER)


Worksheets("Engine Modeling Output").Range(Cells(200, 70),
Cells(NUMBER_OF_DATA_POINTS, 70)).Value _
= Application.WorksheetFunction.Transpose(uSlC8H18Lumsden)
Worksheets("Engine Modeling Output").Range(Cells(200, 71),
Cells(NUMBER_OF_DATA_POINTS, 71)).Value _
= Application.WorksheetFunction.Transpose(uSlH2Lumsden)
Worksheets("Engine Modeling Output").Range(Cells(200, 72),
Cells(NUMBER_OF_DATA_POINTS, 72)).Value _
= Application.WorksheetFunction.Transpose(uSlC8H18Lancaster)
Worksheets("Engine Modeling Output").Range(Cells(200, 73),
Cells(NUMBER_OF_DATA_POINTS, 73)).Value _
= Application.WorksheetFunction.Transpose(uSlH2Lancaster)

Worksheets("Engine Modeling Output").Range(Cells(200, 74),
Cells(NUMBER_OF_DATA_POINTS, 74)).Value _
= Application.WorksheetFunction.Transpose(FlameRadiusNORMALIZED)


'CrankAngle(CyclePosition, 1)
'UnburnedVolume (CyclePosition)

'sheet must be activated first, otherwise the command
"Worksheets("Fla...." does not work
'Sheets("Equilibrium Table Output").Select
'Range("A1").Select
'Worksheets("Equilibrium Table Output").Range(Cells(1, 1),
Cells(TotalSteps + 20, 55)).Value = TempArray
'Sheets("Graph Output").Select
'Range("A1").Select
'Sheets("Equilibrium Table Output").Select
'Range("A1").Select
Application.ScreenUpdating = True

End Sub
```

G.8 Flame Area

```
Option Explicit              'forces a declaration of all variables
Option Base 1                'first element in array is 1

'public declaration can be used by all modules in the workbook
'privte declaration can be used by only the module is has been declared
Private Const PI As Double = 3.14159265358979
Private Const DEGS  As Double = 57.2957795130823
Private Const RADS As Double = 1.74532925199433E-02
Private CR As Double         'compression ratio
Private Bore As Double       'bore (m)
Private Stroke As Double     'stroke (m)
Private ConRod As Double     'connecting rod length (m)
Private StartComb As Double              'start of combustion (deg.)
Private EndComb As Double                'end of combustion (deg.)
Private StepCA As Double                 'crank angle step size (deg.)
Private StepRF As Double                  'flame radius step size (m)
Private Rfs As Double        'flame kernel radius at start of combustion (m)
Private Rh As Double          'horizontal displacement of ignition point from
the center of combustion chamber (m)
Private Rv As Double         'vertical displacement of ignition point from the
cylinder head (m)
Private StepItegration As Double         'integration step to calculate
volume and surface area (m)
Private Vt() As Double                   'total volume from start of
combustion to end, at every step (m^3)
Private Vs As Double                     'swept volume (m^3)
Private At() As Double                   'total area from start of
combustion to end, at every step (m^2)
Private TotalSteps As Double             'total number of incremental
steps from start of combustion to end
Private R As Double                      'R is a ration of conrod/crank
radius

'burned volume and area properties
Private VbTotal() As Double              'total burned volume
Private AfTotal() As Double              'total flame surface area
Private AwbTotal() As Double             'total burned wall area
Private AhbTotal() As Double             'total burned cylinder head area
Private ApbTotal() As Double             'total burned piston area
Private AcbTotal() As Double             'total burned cylinder area

'unburned volume and area properties
Private VuTotal() As Double              'total unburned volume
Private AwuTotal() As Double             'total unburned wall area
Private AhuTotal() As Double    'total unburned cylinder head area
Private ApuTotal() As Double             'total unburned piston area
Private AcuTotal() As Double             'total unburned cylinder area

'This program comes up with a progress indicator.
Sub StartProressIndicatorAndAnalysis3()
UserForm3.Show
End Sub

Sub Main_FlameTableInput()

'get input from "Flame Table Input worksheet
GetInput

'check is flame center located below the piston at TDC
If CheckFlameCenter = False Then
Unload UserForm3
Exit Sub
End If

'calculate total volume at each crank angle
TotalVolume

'calculate total surface area at each crank angle
TotalSurfaceArea

'calculate burned and unburned volume and surface areas
BurnedVolumeAndFlameAndWallArea

PrintToScreen

End Sub

Private Sub GetInput()

CR = Worksheets("Flame Table Input").Range("e5").Value
Bore = Worksheets("Flame Table Input").Range("e6").Value / 1000
Stroke = Worksheets("Flame Table Input").Range("e7").Value / 1000
ConRod = Worksheets("Flame Table Input").Range("e8").Value / 1000

StartComb = Worksheets("Flame Table Input").Range("e10").Value
EndComb = Worksheets("Flame Table Input").Range("e11").Value
StepCA = Worksheets("Flame Table Input").Range("e12").Value
StepRF = Worksheets("Flame Table Input").Range("e13").Value / 1000
StepItegration=Worksheets("Flame Table Input").Range("e14").Value/
1000
Rh = Worksheets("Flame Table Input").Range("e15").Value / 1000
Rv = Worksheets("Flame Table Input").Range("e16").Value / 1000
Rfs = Worksheets("Flame Table Input").Range("e17").Value / 1000

TotalSteps = (Abs(StartComb - EndComb) / StepCA) + 1    'example -2,-
1,0,1,2, which is (2+2)+1=5 total steps
R = ConRod / (Stroke / 2)
Vs = (PI * (Bore ^ 2) / 4) * Stroke

End Sub
'Calculates volume at each crank angle step
Private Sub TotalVolume()

Dim i As Integer
Dim CA As Double, th As Double           'CA=Crank Angle, th = angle
Dim Volume() As Double                   'volume at each step
ReDim Volume(TotalSteps)'dynamically resizing the array Volume

i = 1
CA = StartComb
While CA <= EndComb
th = CA * PI / 180

Volume(i) = ((Vs / (CR - 1)) + ((Vs / 2) * (R + 1 - Cos(th) - (R ^ 2 -
(Sin(th) ^ 2)) ^ 0.5)))

i = i + 1
CA = CA + StepCA
Wend
'NOTE: if volume is *1000000 then the results are in cc, otherwise m^3
Vt = Volume()

End Sub
'Calculates volume at each crank angle step
Private Sub TotalSurfaceArea()

Dim i As Integer
Dim CA As Double, th As Double  'CA=Crank Angle, th = angle
Dim Area() As Double            'area at each step
ReDim Area(TotalSteps)          'dynamically resizing the array Area

i = 1
CA = StartComb
```

```
While CA <= EndComb
th = CA * PI / 180

Area(i) = ((PI * Bore ^ 2) / 2) + ((PI * Bore * Stroke / 2) * (R + 1 -
Cos(th) - (R ^ 2 - (Sin(th) ^ 2)) ^ 0.5 + (2 / (CR - 1))))

i = i + 1
CA = CA + StepCA
Wend
'area in m^2
At = Area()

End Sub
Private Sub BurnedVolumeAndFlameAndWallArea()

Dim i As Integer
Dim j As Integer
Dim CA As Double, th As Double 'CA=Crank Angle, th = angle in radians
Dim Alpha As Double                    'angle in radians
Dim Betta As Double                    'angle in radians
Dim dz As Double                       'in meters
Dim z As Double              'distance from point of ignition
Dim VbIncrement As Double   'burned gas volume at dz incremented
Dim Vb As Double             'burned gas volume total at a given CA
Dim Rf As Double                       'radius of flame
Dim MaxRf As Double                    'maximum radius of flame
Dim AfIncrement As Double    'flame front area at dz incremented
Dim Af As Double             'flame front area at a given CA
Dim Awb As Double                      'total burned wall area
Dim h As Double              'distance between piston and cylinder head
(m)
Dim Ahb As Double                       'area of burned head
Dim Apb As Double                      'area of burned piston
Dim Acb As Double                      'area of burned cylinder
Dim PctDone As Double                  'percent done, for counting
Dim r1 As Double                       'radius at z position
Dim r2 As Double                       'radius at z+dz position
Dim arc As Double                      'arc length between R1 and R2
radius, which separated by dz

're-dimension the private arrays dynamically
ReDimensionArrays

j = 1
i = 1
CA = StartComb
'integration to calculate burned gas volume and flame front area at every
CA
While CA <= EndComb

'Call Progress indicator
PctDone = ((i - 1) * StepCA) / Abs(StartComb - EndComb)
Call UpdateProgress3(PctDone, CA, (EndComb))

'convert to radians
th = CA * PI / 180
'calculate distance between cylinder head and piston
h = 4 * Vt(i) / (PI * Bore ^ 2)


'the maximum flame radius is from the point of ignition to the corner
'of the piston and cylinder
MaxRf = (((Rh + Bore / 2) ^ 2 + h ^ 2) ^ 0.5) * 1.2

'this puts a limitation on the maximum flame radius, otherwise the
program comes up
'with a "subscript out of range error"
If MaxRf / StepRF > 250 Then
MaxRf = StepRF * 249
End If

      j = 1
      Rf = Rfs          'initial flame kernel diameter in (m)
      While Rf < MaxRf

''''''''''''''''''''''''''''BOTTOM HALF OF FLAME''''''''''''''''''''''''''''''''''

Vb = 0, Af = 0, z = 0, dz = StepItegration, Ahb = 0,  Apb = 0
Acb = 0,  Awb = 0
'integration to calculate burned gas volume and flame front area at a
given CA
            While z < Rf

            r1 = (Rf ^ 2 - z ^ 2) ^ 0.5
               'if ratio >= 1 than "acos(ratio) = zero", which means flame
not touching cylinder wall
               'the flame radius is smaller or equal to distance
               'b/w source of ignition and closer wall
               If r1 <= ((Bore / 2) - Rh) Then
               Alpha = PI
               Betta = 0
               'the flame radius is larger or equal to distance
               'b/w source of ignition and the furthest point on cylinder
wall
               ElseIf r1 >= ((Bore / 2) + Rh) Then
               Alpha = 0
               Betta = PI
               'flame is touching the wall somewhere
ElseIf r1 > ((Bore / 2) - Rh) And r1 < ((Bore / 2) + Rh)  Then
               Alpha = Application.WorksheetFunction.Acos((r1 ^ 2 + Rh
^ 2 - (Bore / 2) ^ 2) / (2 * r1 * Rh))
               Betta = Application.WorksheetFunction.Acos(((Bore / 2) ^ 2
+ Rh ^ 2 - r1 ^ 2) / (2 * (Bore / 2) * Rh))
               Else
MsgBox "Problem with Alpha and Betta calculation"
Dim prompt
prompt = CA & "     " & r1 & ""
End If

'burned gas volume
If z <= h - Rv Then
Vb = Vb + ((Alpha * r1 ^ 2 + Betta * (Bore / 2) ^ 2 - (Bore / 2) * Rh *
Sin(Betta)) * dz)
End If
'flame front area Note: surface area of segment of a sphere is = PI*D*h
'adding up small areas of based on R1 does not work because it
underestimates
'the total area by 20% one way to solve it is below. it calculates the arc
length between each step. OR just go with the exact solution  S = PI*D*h
If z <= h - Rv Then
Af = Af + (2 * Rf * Alpha * dz)
End If
'calculates incrementally the burned cylinder area
If z <= h - Rv Then
Acb = Acb + (Bore * Betta * dz)
End If
'calculate burned piston area only when z = h
If z >= h - Rv And Apb = 0 Then
Apb = (Alpha * (Rf ^ 2 - (h - Rv) ^ 2)) + (Betta * (Bore / 2) ^ 2) - ((Bore
/ 2) * Rh * Sin(Betta))
End If

z = z + dz
Wend

 ''''''''''''''''''''''''''''''''''''''TOP HALF''''''''''''''''''''''''''''''''''''''''''''''''


z = 0
dz = StepItegration

'integration to calculate burned gas volume and flame front area at a
given CA
While z < Rf 'And Rv >= 0

 r1 = (Rf ^ 2 - z ^ 2) ^ 0.5
'if ratio >= 1 than "acos(ratio) = zero", which means flame not touching
cylinder wall
'the flame radius is smaller or equal to distance
'b/w source of ignition and closer wall
If r1 <= ((Bore / 2) - Rh) Then
     Alpha = PI
     Betta = 0
'the flame radius is larger or equal to distance
'b/w source of ignition and the furthest point on cylinder wall
ElseIf r1 >= ((Bore / 2) + Rh) Then
      Alpha = 0
      Betta = PI
'flame is touching the wall somewhere
ElseIf r1 > ((Bore / 2) - Rh) And r1 < ((Bore / 2) + Rh) Then
Alpha = Application.WorksheetFunction.Acos((r1 ^ 2 + Rh ^ 2 - (Bore / 2)
^ 2) / (2 * r1 * Rh))
Betta = Application.WorksheetFunction.Acos(((Bore / 2) ^ 2 + Rh ^ 2 - r1
^ 2) / (2 * (Bore / 2) * Rh))
Else
MsgBox "Problem with Alpha and Betta calculation"
Dim prompt2
prompt2 = CA & "     " & r1 & ""
MsgBox (prompt)
End If
'burned gas volume
If z < Rv Then
Vb = Vb + ((Alpha * r1 ^ 2 + Betta * (Bore / 2) ^ 2 - (Bore / 2) * Rh *
Sin(Betta)) * dz)
End If

If z < Rv Then
Af = Af + (2 * Rf * Alpha * dz)
End If
'calculates incrementally the burned cylinder area
If z < Rv Then
Acb = Acb + (Bore * Betta * dz)
End If

z = z + dz
```

```
Wend

Awb = Acb + Ahb + Apb

'burned volume and area properties
VbTotal(i, j) = Vb                    'total burned volume
AfTotal(i, j) = Af                    'total flame surface area
AwbTotal(i, j) = Awb                  'total burned wall area
AhbTotal(i, j) = Ahb                  'total burned cylinder head area
ApbTotal(i, j) = Apb                  'total burned piston area
AcbTotal(i, j) = Acb                  'total burned cylinder area
'unburned volume and area properties
VuTotal(i, j) = Vt(i) - Vb            'total unburned volume
AwuTotal(i, j) = At(i) - Awb          'total unburned wall area
AhuTotal(i, j) = ((PI * Bore ^ 2) / 4) – Ahb 'total unburned cylinder head
area
ApuTotal(i, j) = ((PI * Bore ^ 2) / 4) - Apb  'total unburned piston area
AcuTotal(i, j) = (PI * Bore * h) - Acb      'total unburned cylinder area

      j = j + 1
      Rf = Rf + StepRF
      Wend

i = i + 1
CA = CA + StepCA
Wend
'Turn OFF Progress Indicator
Unload UserForm3

End Sub
Private Sub ReDimensionArrays()

Dim MaxStepRf As Double

'The method below efficiently re-dimensions the array, however this mean
that each row 'will be different in length, which creates difficulties when
one wants to count up it is easy to over-run the length of array
maximum cylinder volume MaxVolume = (Vs / (CR - 1)) + Vs
'maximum distance between cylinder head and piston h = 4 * MaxVolume
/ (PI * Bore ^ 2) the maximum flame radius is from the point of ignition
to the corner 'of the piston and cylinder 'MaxRf = ((Bore ^ 2 + h ^ 2) ^
0.5) maximum number of steps, simply divide maximum flame radius with
flam radius step size MaxStepRf = MaxRf / StepRF

MaxStepRf = 250
'burned volume and area properties
ReDim VbTotal(1 To TotalSteps, 1 To MaxStepRf)   'total burned volume
ReDim AfTotal(1 To TotalSteps, 1 To MaxStepRf)  'total flame surface area
ReDim AwbTotal(1 To TotalSteps, 1 To MaxStepRf) 'total burned wall area
ReDim AhbTotal(1 To TotalSteps, 1 To MaxStepRf)  'total burned cylinder
head area
ReDim ApbTotal(1 To TotalSteps, 1 To MaxStepRf) 'total unburned piston
area
ReDim AcbTotal(1 To TotalSteps, 1 To MaxStepRf)  'total burned cylinder
area
'unburned volume and area properties
ReDim VuTotal(1 To TotalSteps, 1 To MaxStepRf) 'total unburned volume
ReDim AwuTotal(1 To TotalSteps, 1 To MaxStepRf) 'total unburned wall
area
ReDim AhuTotal(1 To TotalSteps, 1 To MaxStepRf) 'total unburned
cylinder head area
ReDim ApuTotal(1 To TotalSteps, 1 To MaxStepRf)  'total unburned piston
area
ReDim AcuTotal(1 To TotalSteps, 1 To MaxStepRf) 'total unburned
cylinder area

End Sub
'check flame center position with respect to piston position
'flame center always have to be located above the piston
Private Function CheckFlameCenter()
Dim h As Double
Dim VolumeTDC As Double 'volume at TDC

VolumeTDC = Vs / (CR - 1)
h = 4 * VolumeTDC / (PI * Bore ^ 2)

If h > Rv Then
CheckFlameCenter = True
Else
MsgBox "Flame center is located below the piston at TDC." & _
" Make sure Rv is smaller than " & h & " (m)." & _
" NO CALCULATIONS HAVE BEEN MADE!"
CheckFlameCenter = False
End If

End Function

Private Sub PrintToScreen()

Application.ScreenUpdating = False

Dim i As Long, Dim j As Long, Dim CA As Double, th As Double, th =
angle, Dim row As Long, Dim column As Long, Dim Rf As Double
Dim NumberOfOutputs As Long, Dim TempArray() As Variant

'allocates 20 spaces for each crank angle output
NumberOfOutputs = 20
ReDim TempArray(1 To (TotalSteps * 20), 1 To 255)

row = 0, column = 0, i = 1, CA = StartComb
While CA <= EndComb

'crank angle
TempArray(5 + row, 2) = CA

'title crank angle
TempArray(5 + row, 1) = "Crank Angle"
'total volume
TempArray(6 + row, 2) = Vt(i)
'title total volume
TempArray(6 + row, 1) = "Total Volume"
'total area
TempArray(7 + row, 2) = At(i)
'title total area
TempArray(7 + row, 1) = "Total Area"
'flame radius

TempArray(5 + row, 5) = "Flame Radius"
'title total burned volume
TempArray(6 + row, 5) = "Total Burned Volume"
'title total surface flame area
TempArray(7 + row, 5) = "Total Flame Surface Area"
'title total burned wall area
TempArray(8 + row, 5) = "Total Burned Wall Area"
'title total burned cylinder head area
TempArray(9 + row, 5) = "Total Burned Cylinder Head Area"
'title total burned piston area
TempArray(10 + row, 5) = "Total Burned Piston Area"
'title total burned cylinder area
TempArray(11 + row, 5) = "Total Burned Cylinder Area"

'title total unburned volume
TempArray(12 + row, 5) = "Total Unburned Volume"
'title total unburned wall area
TempArray(13 + row, 5) = "Total Unburned Wall Area"
'title total unburned cylinder head area
TempArray(14 + row, 5) = "Total Unburned Cylinder Head Area"
'title total unburned piston area
TempArray(15 + row, 5) = "Total Unburned Piston Area"
'title total unburned cylinder area
TempArray(16 + row, 5) = "Total Unburned Cylinder Area"

      j = 1
      Rf = Rfs
      While j < 249   '255 is the total length of a sheet so, 255-5-1=249

      'flame radius
      TempArray(5 + row, 5 + j) = Rf
      Rf = Rf + StepRF
      'total burned volume
      TempArray(6 + row, 5 + j) = VbTotal(i, j)
      'title total surface flame area
      TempArray(7 + row, 5 + j) = AfTotal(i, j)
      'title total burned wall area
      TempArray(8 + row, 5 + j) = AwbTotal(i, j)
      'title total burned cylinder head area
      TempArray(9 + row, 5 + j) = AhbTotal(i, j)
      'title total burned piston area
      TempArray(10 + row, 5 + j) = ApbTotal(i, j)
      'title total burned cylinder area
      TempArray(11 + row, 5 + j) = AcbTotal(i, j)

      'title total unburned volume
      TempArray(12 + row, 5 + j) = VuTotal(i, j)
      'title total unburned wall area
      TempArray(13 + row, 5 + j) = AwuTotal(i, j)
      'title total unburned cylinder head area
      TempArray(14 + row, 5 + j) = AhuTotal(i, j)
      'title total unburned piston area
      TempArray(15 + row, 5 + j) = ApuTotal(i, j)
      'title total unburned cylinder area
      TempArray(16 + row, 5 + j) = AcuTotal(i, j)

      j = j + 1
      Wend

i = i + 1
CA = CA + StepCA
row = row + NumberOfOutputs
Wend
'sheet must be activated first, otherwise the command
"Worksheets("Fla...." does not work
Sheets("Flame Table Output").Select
```

```
Range("A1").Select
Worksheets("Flame Table Output").Range(Cells(1, 1), Cells((TotalSteps *
NumberOfOutputs), 255)).Value = TempArray
Application.ScreenUpdating = True

End Sub

'progress indicator
Private Sub UpdateProgress3(Pct, Cycle, TotalCycle)
   With UserForm3
      .Label2.Caption = Format(Cycle, "0.0")
      .Label4.Caption = Format(TotalCycle, "0.0")
      .FrameProgress.Caption = Format(Pct, "0.0%")
      .LabelProgress.Width = Pct * (.FrameProgress.Width - 3)
      .Repaint
   End With
End Sub
```

G.9 Flame Area Lookup

```
Option Explicit     'forces the declaration of all variables
Option Base 1       'the address of first element in array is 1

Function FlameArea(Vb As Double, CA As Variant) As Double

Dim aa As Double, N As Double, T As Double
Dim FlameAngle() As Double

Dim BurnedVolume1 As Variant, BurnedVolume2 As Variant,
BurnedVolume3 As Variant, Dim NumberOfAngles, CA1, CA2, AreaF1,
AreaF2 As Double, Dim FlameArea1, FlameArea2, Vb11, Vb12, Vb21,
Vb22, AreaF11, AreaF12, AreaF21, AreaF22 As Double,

NumberOfAngles = (Abs(Worksheets("Flame Table
Input").Range("e10").Value  - Worksheets("Flame Table
Input").Range("e11").Value) / Worksheets("Flame Table
Input").Range("e12").Value) + 5
ReDim FlameAngle(NumberOfAngles + 10)
'find angles and put them in order
T = 0
N = 1
   While N < NumberOfAngles
FlameAngle(N) = Worksheets("Flame Table Output").Cells(5 + T, 2).Value

   T = T + 20
   N = N + 1
   Wend
'find angle to which actual crank angle is the closest
      N = 0
      Do
      N = N + 1
      Loop Until FlameAngle(N) >= CA
      If N = 1 Then
      MsgBox "Have more angle before calculation start. Now the first
angle equal to the calculated angle"
      End If

      CA1 = FlameAngle(N)
      CA2 = FlameAngle(N - 1)
 'extract flame volumes and areas
         If FlameAngle(N) = CA Then
BurnedVolume1 = Worksheets("Flame Table Output").Range("f6:is6")
.Offset(rowOffset:=((N - 1) * 20), columnOffset:=0)
FlameArea1 = Worksheets("Flame Table Output").Range("f7:is7") _
             .Offset(rowOffset:=((N - 1) * 20), columnOffset:=0)

BurnedVolume2 = Worksheets("Flame Table Output").Range("f6:is6") _
                      .Offset(rowOffset:=(((N - 1) * 20)), columnOffset:=0)
FlameArea2 = Worksheets("Flame Table Output").Range("f7:is7")
.Offset(rowOffset:=(((N - 1) * 20)), columnOffset:=0)

CA2 = CA

ElseIf FlameAngle(N) > CA Then
BurnedVolume1 = Worksheets("Flame Table Output").Range("f6:is6") _
 .Offset(rowOffset:=((N - 1) * 20), columnOffset:=0)
BurnedVolume2 = Worksheets("Flame Table Output").Range("f6:is6") _
           .Offset(rowOffset:=(((N - 1) * 20) - 20), columnOffset:=0)
FlameArea1 = Worksheets("Flame Table Output").Range("f7:is7") _
             .Offset(rowOffset:=((N - 1) * 20), columnOffset:=0)
FlameArea2 = Worksheets("Flame Table Output").Range("f7:is7")
.Offset(rowOffset:=(((N - 1) * 20) - 20), columnOffset:=0)
         Else
         MsgBox "Actual angle is not found!"
         End If

            T = 0
            Do
            T = T + 1
            Loop Until BurnedVolume1(1, T) >= Vb Or T = 248
Vb11 = BurnedVolume1(1, T)
Vb12 = BurnedVolume1(1, T - 1)
AreaF11 = FlameArea1(1, T)
AreaF12 = FlameArea1(1, T - 1)

T = 0
Do
   T = T + 1
   Loop Until BurnedVolume2(1, T) >= Vb Or T = 248
   Vb21 = BurnedVolume2(1, T)
   Vb22 = BurnedVolume2(1, T - 1)
   AreaF21 = FlameArea2(1, T)
   AreaF22 = FlameArea2(1, T - 1)

AreaF1 = AreaF12 + (((Vb - Vb12) / (Vb11 - Vb12)) * (AreaF11 -
AreaF12))
AreaF2 = AreaF22 + (((Vb - Vb22) / (Vb21 - Vb22)) * (AreaF21 -
AreaF22))

If CA2 = CA Then
    CA1 = CA2 - 1 'just to avoid overflow, not good to divide by zero
    End If

FlameArea = AreaF2 - (((CA - CA2) / (CA1 - CA2)) * (AreaF2 - AreaF1))

End Function

Function FlameSt(P As Variant, T As Double, MBR As Variant, Af As
Double, RPM, mass As Double, Rgas As Double) As Double

Dim Density As Double
Dim Burnrate As Double

Density = P / (Rgas * T)
'mass burn rate with respect to time
Burnrate = MBR * mass / (60 / (RPM * 360))

'this is massflow = density * area * velocity, this is less then dr/dt
FlameSt = Burnrate / (Density * Af)

End Function

Function FlameRf(Vb As Double, CA As Variant) As Double

Dim aa As Double, N As Double, T As Double
Dim FlameAngle() As Double

Dim BurnedVolume1 As Variant, BurnedVolume2 As Variant,
BurnedVolume3 As Variant, Dim NumberOfAngles, CA1, Rfall1, Rfall2, CA2
As Double, Dim FlameArea1, FlameArea2, Vb11, Vb12, Vb21, Vb22, Rf11,
Rf12, Rf21, Rf22 As Double, Dim Rf1, Rf2 As Double

NumberOfAngles = (Abs(Worksheets("Flame Table
Input").Range("e10").Value  - Worksheets("Flame Table
Input").Range("e11").Value) / Worksheets("Flame Table
Input").Range("e12").Value) + 5

ReDim FlameAngle(NumberOfAngles + 10)
'find angles and put them in order
T = 0
N = 1
While N < NumberOfAngles
FlameAngle(N) = Worksheets("Flame Table Output").Cells(5 + T, 2).Value

T = T + 20
N = N + 1
Wend
'find angle to which actual crank angle is the closest
N = 0
Do
N = N + 1
Loop Until FlameAngle(N) >= CA
If N = 1 Then
MsgBox "Have more angle before calculation start. Now the first angle
equal to the calculated angle"
End If

CA1 = FlameAngle(N)
CA2 = FlameAngle(N - 1)

'MsgBox "STOP"
'extract flame volumes and radius
If FlameAngle(N) = CA Then
BurnedVolume1 = Worksheets("Flame Table Output").Range("f6:is6") _
          .Offset(rowOffset:=((N - 1) * 20), columnOffset:=0)
            Rfall1 = Worksheets("Flame Table Output").Range("f5:is5") _
             .Offset(rowOffset:=((N - 1) * 20), columnOffset:=0)

BurnedVolume2 = Worksheets("Flame Table Output").Range("f6:is6") _
                     .Offset(rowOffset:=(((N - 1) * 20)), columnOffset:=0)
Rfall2 = Worksheets("Flame Table Output").Range("f5:is5") _
                     .Offset(rowOffset:=(((N - 1) * 20)), columnOffset:=0)
```

```
        CA2 = CA

ElseIf FlameAngle(N) > CA Then
          BurnedVolume1 = Worksheets("Flame Table
Output").Range("f6:is6") _
          .Offset(rowOffset:=((N - 1) * 20), columnOffset:=0)
          BurnedVolume2 = Worksheets("Flame Table
Output").Range("f6:is6") _
          .Offset(rowOffset:=(((N - 1) * 20) - 20), columnOffset:=0)
            Rfall1 = Worksheets("Flame Table Output").Range("f5:is5") _
            .Offset(rowOffset:=((N - 1) * 20), columnOffset:=0)
            Rfall2 = Worksheets("Flame Table Output").Range("f5:is5") _
            .Offset(rowOffset:=(((N - 1) * 20) - 20), columnOffset:=0)
Else
MsgBox "Actual angle is not found!"
End If

T = 0
Do
T = T + 1
Loop Until BurnedVolume1(1, T) >= Vb Or T = 248
Vb11 = BurnedVolume1(1, T)
Vb12 = BurnedVolume1(1, T - 1)
Rf11 = Rfall1(1, T)
Rf12 = Rfall1(1, T - 1)

T = 0
Do
T = T + 1
Loop Until BurnedVolume2(1, T) >= Vb Or T = 248
Vb21 = BurnedVolume2(1, T)
Vb22 = BurnedVolume2(1, T - 1)
Rf21 = Rfall2(1, T)
Rf22 = Rfall2(1, T - 1)

Rf1 = Rf12 + (((Vb - Vb12) / (Vb11 - Vb12)) * (Rf11 - Rf12))
Rf2 = Rf22 + (((Vb - Vb22) / (Vb21 - Vb22)) * (Rf21 - Rf22))

If CA2 = CA Then
CA1 = CA2 - 1 'just to avoid overflow, not good to divide by zero
End If

FlameRf = Rf2 - (((CA - CA2) / (CA1 - CA2)) * (Rf2 - Rf1))

End Function
```

G.10 Fractal

```
Public Function FractalD3(x1 As Double, x2 As Double) As Double
'x1 = Lambda
'x2 = Flame Radius (mm)
'-----------------------------------------------------------------
'  DataFit version 8.0.32
'  Date Created: Oct 28 2003
'  Time Created: 09:05:28 PM
'  This function returns a predicted f(x) value
'  for the function
a+b*x1+c*x2+d*x1^2+e*x2^2+f*x1*x2+g*x1^3+h*x2^3+i*x1*x2^2+
j*x1^2*x2.
'  The independent variables x1, x2, .. xn are passed in the
'  array x(), where x(1) = x1, et.
'  for the function
a+b*x1+c*x2+d*x1^2+e*x2^2+f*x1*x2+g*x1^3+h*x2^3+i*x1*x2^2+
j*x1^2*x2.
'  Regression Statistics:
'  R2 = 0.970982195403432
'  Adjusted R2 = 0.970965866765107
'  Standard Error = 1.33698628362781E-02
'-----------------------------------------------------------------

Const a As Double = -0.267451195437264
Const b As Double = 5.23869354864423
Const c As Double = 3.02780272732975E-02
Const d As Double = -3.3514972871816
Const e As Double = -3.7632405357793E-04
Const f As Double = -5.24377309212588E-02
Const g As Double = 0.690770688160316
Const h As Double = -3.70988898089173E-15
Const i As Double = 3.94521556704519E-04
Const j As Double = 1.49767044807074E-02
Dim result As Double

result = ((((((((a + (b * x1)) + (c * x2)) + (d * (x1 ^ 2))) + _
              (e * (x2 ^ 2))) + ((f * x1) * x2)) +  (g * (x1 ^ 3))) + (h *
(x2 ^ 3))) +  ((i * x1) * (x2 ^ 2))) + ((j * (x1 ^ 2)) * x2))

FractalD3 = result

End Function
```

G.11 Import Text File

```
Sub ImportTextUsingXlDialogOpen()

 '\ use this approach to prompt user for text wizard values

Application.ScreenUpdating = False
Application.DisplayAlerts = False


'\ display open file dialog and copy to new (temporary workbook)
'On error resume next - traps for user clicking cancel in the import dialog
'Error number is 1004 - is so exit the procedure
On Error Resume Next
If Application.Dialogs(xlDialogOpen).Show("*.txt") Then
If Err.Number = 1004 Then
Exit Sub
      End If
ActiveSheet.UsedRange.Select       'select imported text in temporary
workbook
      Selection.Copy                    ' copy to clipboard
      ActiveWorkbook.Close              ' close temporary workbook
      Worksheets("INPUT").Select        ' Select input worksheet
      Range("B61:B65536").Select
      ActiveSheet.Paste
      Worksheets("INPUT").Range("B1524:c65536").ClearContents
      'Worksheets.Add
      'Range("A1") = "Dialogs(xlDialogOpen) Method"
      'Range("A2").Select
      'ActiveSheet.Paste                '\ paste text into your workbook
   End If

 Application.ScreenUpdating = True
Application.DisplayAlerts = True
End Sub
```

G.12 Knock Analysis

```
'In this knock modules only the arrays start/base from 0 NOT 1
'This Macro was recorded 5/8/97 by Terrence E. Rogers
(http://home.att.net/~terrence.rogers/index.htm)
'This is basic digital filter design using routines that have been copied
'from 'Stearns & Hush' graduate digital filter design course text book.
'The original routines were implemented in Fortran.  Synthesis and
Analysis 'were separate but are here combined.
' The author modified and implemented into combustion analyser

Sub Butter()
SpeedCalculation

Dim Sn(2), Zn(2), T(2)    'complex scratch variables
Dim a1, b1 As Range 'to make handling of arrays A & B easier
Set a1 = Range("A")
Set b1 = Range("B")
Fc = Range("Fc").Value  'more convenience
filt_type$ = Range("type").Value    'more convenience
ns = Range("ns").Value  'even more convenience
Style = vbOKOnly + vbCritical + vbDefaultButton1    'style for alert boxes
PI = 3.14159265358979

'clear previous output
b1.Clear
   a1.Clear

'Check input parameters for conformity
If filt_type$ <> "low" And filt_type$ <> "high" Then
Response = MsgBox("type must be high or low", Style, "Error", "", 1000)
Exit Sub
ElseIf filt_type$ = "low" Then
itype = 1
Else
itype = 2
End If
If Fc <= 0 Or Fc >= 0.5 Then
Response = MsgBox("Fc out of range:0 to 0.5", Style, "Error", "", 1000)
Exit Sub
End If
If ns > 10 Then
Response = MsgBox("10 sections maximum", Style, "Error", "", 1000)
Exit Sub
End If

'Calculation of coefficients
wcp = Tan(PI * Fc)
```

```
For N = 1 To ns
Temp = PI * (2 * N + 2 * ns - 1) / (4 * ns)
Call cpx_exp(0, Temp, Sn(1), Sn(2))
Sn(1) = Sn(1) * wcp
Sn(2) = Sn(2) * wcp
Call cpx_div(1 + Sn(1), Sn(2), 1 - Sn(1), -Sn(2), Zn(1), Zn(2))
       b1(N, 1) = ((2 - itype) * wcp * wcp + (itype - 1) * 1) / (1 - 2 *
Sn(1) + wcp * wcp)
b1(N, 2) = (3 - 2 * itype) * 2 * b1(N, 1)
b1(N, 3) = b1(N, 1)
Range("A").Cells(N, 1).Value = -2 * Zn(1)
Range("A").Cells(N, 2).Value = Zn(1) ^ 2 + Zn(2) ^ 2
Next N
'now execute filter function
Filt
'find start and end of knock
FindStartAndEndOfKnock
'Automatically calculates everything in the open workbook
SpeedCalculation
'Calculate
Sheets("ANALYSIS").Select
Range("A1").Select

End Sub

Sub cpx_mult(r1, C1, r2, C2, r3, c3)
   r3 = r1 * r2 - C1 * C2
   c3 = r1 * C2 + r2 * C1
End Sub

Sub cpx_exp(r1, C1, r2, C2)
   r2 = Exp(r1) * Cos(C1)
   C2 = Exp(r1) * Sin(C1)
End Sub

Sub cpx_div(r1, C1, r2, C2, r3, c3)
   denom = r2 ^ 2 + C2 ^ 2
   r3 = (r1 * r2 + C1 * C2) / denom
   c3 = (C1 * r2 - r1 * C2) / denom
End Sub

'Sub Filt()
'   This is a filtering routine which uses the cascaded canonical
'   filter coefficients generated in Sub Butter().  It assumes that
'   input parameter limit testing has been performed by Sub Butter().
'   If this routine is used separately, one must add these checks.
'
'   The routine is written to access data in named ranges.  These
'   ranges are:
'       A,              B,          ns,             xn
'       A coef array,   B array,    no.sections,    input signal
'       yn
'       filter output
'
'   rev 1.2 3 Sept 97 T. Rogers
'       corrected bug causing data from ytemp(128) to roll into next
'       section xtemp(3)...did not init shift(1) and shift(2)to 0.
'       Extended analysis back to sample 1 although Fourier works best
'       if first sample is 0.

Sub Filt()
Dim a1, b1, xn, yn As Range 'to make handling of arrays A & B easier
Set a1 = Range("A")
Set b1 = Range("B")
Set xn = Range("xn")
Set yn = Range("yn")
ns = Range("ns").Value  'even more convenience
Count = Range("count").Value 'number of samples
Dim ytemp(2000)   'temporary storage for filter output
Dim xtemp(2000)   'temporary storage for filter input between sections
                  'change size of these arrays if x[n] or y[n] size change
                  'Must be same as Count variable.  This is only location
                  'that must change.  Other points use 'Count' but array
                  'sizes must be integer.
Dim shift(2)    'shift register in filter.

For i = 1 To ns  'repeat for each cascade section
shift(1) = 0
shift(2) = 0
If i = 1 Then  'initialize input data. Could use ytemp() & filter in
For j = 1 To Count  'place but this is easier to think about.
xtemp(j) = xn(j)    'first section data is x[n]
Next j
      Else
         For j = 1 To Count
            xtemp(j) = ytemp(j)    'second section data is old output
           Next j
       End If
  'main filter loop
For j = 1 To Count  'no output until 2 delays
Sum = xtemp(j) - a1(i, 1) * shift(1) - a1(i, 2) * shift(2)
ytemp(j) = b1(i, 1) * Sum + b1(i, 2) * shift(1) + b1(i, 3) * shift(2)
shift(2) = shift(1)
shift(1) = Sum
       Next j
   Next i

'sheet must be activated first, otherwise the command
"Worksheets("Fla...." does not work
Sheets("Butterworth").Select
Range("A1").Select
'a one dimensional array must be transposed before printing it as a
column
Worksheets("Butterworth").Range(Cells(45, 4), Cells(2044, 4)).Value = _
Application.WorksheetFunction.Transpose(ytemp)
SpeedCalculation
End Sub

Sub FindStartAndEndOfKnock()

Dim ButterAngle As Double, Dim ButterPressure As Double
Dim ButterNoise As Double, Dim KnockOnsetAndEnd As Double

Dim ButterAngleTemp As Variant, Dim ButterPressureTemp As Variant
Dim ButterNoiseTemp As Variant, Dim Tconst As Double

'get input from Butterworth sheet
ButterAngleTemp =
Worksheets("Butterworth").Range("b37:b1470").Value
ButterPressureTemp =
Worksheets("Butterworth").Range("c37:c1470").Value
ButterNoiseTemp = Worksheets("Butterworth").Range("d37:d1470").Value
KnockOnsetAndEnd = Worksheets("Butterworth").Range("c8").Value

'find start of knock
i = 200 'start around point of ignition
Do Until i > 1470 - 37

If ButterNoiseTemp(i, 1) > KnockOnsetAndEnd Then
Exit Do
End If

i = i + 1
Loop

ButterNoise = ButterNoiseTemp(i, 1)
ButterAngle = ButterAngleTemp(i, 1)
ButterPressure = ButterPressureTemp(i, 1)

Worksheets("Butterworth").Range("c15").Value = ButterNoise
Worksheets("Butterworth").Range("c16").Value = ButterPressure
Worksheets("Butterworth").Range("c17").Value = ButterAngle

'find end of knock
i = 618 'start around point of ignition
Do Until i < 200

If ButterNoiseTemp(i, 1) > KnockOnsetAndEnd Then
Exit Do
End If

i = i - 1
Loop

ButterNoise = ButterNoiseTemp(i, 1)
ButterAngle = ButterAngleTemp(i, 1)
ButterPressure = ButterPressureTemp(i, 1)

Worksheets("Butterworth").Range("c20").Value = ButterNoise
Worksheets("Butterworth").Range("c21").Value = ButterPressure
Worksheets("Butterworth").Range("c22").Value = ButterAngle
End Sub
```

G.13 Laminar Flame Speed

```
Option Explicit     'forces the declaration of all variables
Option Base 1       'the address of first element in array is 1

'J. Gottgens, F. Mauss and N. Peters, "Analytic Approximations of Burning
Velocities and Flame Thicknesses of Lean Hydrogen, Methane, Ethylene,
Ethane, Acetylene, and 'Propane Flames", Twenty-Fourth Symposium
(International) on Combustion/The Combustion _
'Institute, 1992 p.129-135
'U.C. Muller, M.Bollig, and N. Peters, "Approximations for Burning
Velocities and Markstein Numbers for Lean Hydrocarbon and Methanol
Flames", Combustion and Flame, '1997, Vol. 108, pp. 349-356
'There are 9 fuel's coefficients are listed in these papers:
'CH4, C2H2, C2H4, C2H6, C3H8, CH3OH, C7H16, C8H18, H2
```

```
'Also calculates flame thickness, inner layer characteristic
temperature(chemistry takes place
'around this temperature and above) and thermal conductivity

Function LaminarFlameSpeedH2(Lambda As Double, _
                    UnburnedTemperature As Double, _
                    ReactionPressure As Variant) As Double

'Approximation Coefficients for Burning Velocity (FOR HYDROGEN)
Const FlameConst_B As Double = 30044.1  '(bar)
Const FlameConst_E As Double = 10200.9 '(K)
Const FlameConst_F As Double = 1292880 '(cm/s)
Const FlameConst_G As Double = 2057.56 '(K)
Const FlameConst_m As Double = 1.08721
Const FlameConst_n  As Double = 3.5349
Dim Phi As Double
Dim MassFractionUnburnedGas As Double
Dim InnerLayerTemp As Double
Dim AdibaticFlameTempHydrogen As Double

If Lambda < 1 Then
Lambda = 1
End If

Phi = 1 / Lambda
UnburnedTemperature = UnburnedTemperature + 273.15 'convert to
kelvin
ReactionPressure = ReactionPressure / 100          'convert to bar

InnerLayerTemp = -FlameConst_E / (Log(ReactionPressure /
FlameConst_B)) 'in kelvin

'mass fraction of fuel in the unburned gas Stoichiometric AFR for H2 =
34.486160397445
MassFractionUnburnedGas = Phi / (34.486160397445 + Phi)

'call function to calculate adiabatic flame temp. of H2
AdibaticFlameTempHydrogen =
AdiabaticFlameTemperatureHydrogen(Lambda, _
UnburnedTemperature - 273.15, ReactionPressure * 100) + 273.15

If AdibaticFlameTempHydrogen - InnerLayerTemp <= 0 Then
AdibaticFlameTempHydrogen = InnerLayerTemp + 1
End If

LaminarFlameSpeedH2 = FlameConst_F * MassFractionUnburnedGas ^
FlameConst_m * _
                Exp(-FlameConst_G / InnerLayerTemp) * _
                (UnburnedTemperature / InnerLayerTemp) * _
                (((AdibaticFlameTempHydrogen - InnerLayerTemp) / _
(AdibaticFlameTempHydrogen - UnburnedTemperature)) ^ FlameConst_n)

End Function

Function LaminarFlameSpeedC8H18(Lambda As Double,
UnburnedTemperature As Double, ReactionPressure As Variant) As Double

'Approximation Coefficients for Burning Velocity (FOR HYDROGEN)
Const FlameConst_B As Double = 38000000  '(bar)
Const FlameConst_E As Double = 20906 '(K)
Const FlameConst_F As Double = 2926 '(cm/s)
Const FlameConst_G As Double = -25.6 '(K)
Const FlameConst_m As Double = 0.5578
Const FlameConst_n  As Double = 2.5214
Dim Phi As Double
Dim MassFractionUnburnedGas As Double
Dim InnerLayerTemp As Double
Dim AdibaticFlameTempC8H18 As Double

If Lambda < 1 Then
Lambda = 1
End If

Phi = 1 / Lambda
UnburnedTemperature = UnburnedTemperature + 273.15 'convert to
kelvin
ReactionPressure = ReactionPressure / 100          'convert to bar

InnerLayerTemp = -FlameConst_E / (Log(ReactionPressure /
FlameConst_B)) 'in kelvin
'mass fraction of fuel in the unburned gas Stoichiometric AFR for H2 =
34.486160397445
MassFractionUnburnedGas = Phi / (15.4877510118749 + Phi)

'call function to calculate adiabatic flame temp. of H2
AdibaticFlameTempC8H18 = AdiabaticFlameTemperatureC8H18(Lambda,
      UnburnedTemperature - 273.15, ReactionPressure * 100) + 273.15

If AdibaticFlameTempC8H18 - InnerLayerTemp <= 0 Then
AdibaticFlameTempC8H18 = InnerLayerTemp + 1
End If

LaminarFlameSpeedC8H18 = FlameConst_F * MassFractionUnburnedGas
^ FlameConst_m * Exp(-FlameConst_G / InnerLayerTemp) *
(UnburnedTemperature / InnerLayerTemp) *
(((AdibaticFlameTempC8H18 - InnerLayerTemp) /
(AdibaticFlameTempC8H18 - UnburnedTemperature)) ^ FlameConst_n)

End Function
```

G.14 NOx formation

```
'Combustion Engineering by Borman and Ragland p.127
Function NOZeldovich(RPM As Double, dth As Double, NOppm As Double,
T As Double, P As Variant, _
                XO2 As Double, XN2 As Double, XO As Double, _
                XOH As Double, XH As Double) As Double

Dim K1, K2, K3, K4, K5, K6, MOL, O2, N2, O, H2O, OH, h, rNO
Dim R, NO

dt = dth / (360 * RPM / 60)

R = 82.05   'cm3 atm / (gmol K)
K1 = 180000000000000# * Exp(-38370 / T),
K2 = 38000000000000# * Exp(-425 / T)
K3 = 18000000000# * T * Exp(-4680 / T)
K4 = 3800000000# * T * Exp(-20820 / T)
K5 = 71000000000000# * Exp(-450 / T)
K6 = 1700000000000000# * Exp(-24560 / T)
'p=p/100000 to convert to atm
MOL = (P / 100000) / (R * T)

O2 = XO2 * MOL
N2 = XN2 * MOL
O = XO * MOL
OH = XOH * MOL
h = XH * MOL
NO = (NOppm / 1000000) * MOL 'convert to moles from ppm
'eq 4.21 for steady state N
N = (K1 * O * N2 + K4 * NO * O + K6 * NO * h) / (K3 * O2 + K2 * NO +
K5 * OH)
'integrate eq 4.18
rNO = K1 * O * N2 + K3 * N * O2 + K5 * N * OH - K2 * NO * N - K4 *
NO * O - K6 * NO * h
rNO = rNO * dt

NO = rNO / MOL * 1000000# 'ppm
'MsgBox "stop"
NOZeldovich = NOppm + NO

End Function

'Combustion Engineering by Borman and Ragland p.127
Function NOZeldovich2(RPM As Double, dth As Double, NOppm As Double,
T As Double, P As Variant, _
                XO2 As Double, XN2 As Double, XO As Double, _
                XOH As Double, XH As Double) As Double

Dim K1, K2, K3, K4, K5, K6, MOL, O2, N2, O, H2O, OH, h, rNO
Dim R, NO

dt = dth / (360 * RPM / 60)

R = 82.05   'cm3 atm / (gmol K)
K1 = 180000000000000# * Exp(-38370 / T)
K2 = 3270000000000# * T ^ 0.3
K3 = 6400000000# * T * Exp(-6280 / (T * R))
K4 = 703000000000# * T * Exp(-19446 / T) / 298
K5 = 38000000000000#
K6 = 170000000000000# * Exp(-24560 / T)

'p=p/100000 to convert to atm
MOL = (P / 100000) / (R * T)

O2 = XO2 * MOL
N2 = XN2 * MOL
O = XO * MOL
OH = XOH * MOL
h = XH * MOL
NO = (NOppm / 1000000) * MOL 'convert to moles from ppm
'eq 4.21 for steady state N
N = (K1 * O * N2 + K4 * NO * O + K6 * NO * h) / (K3 * O2 + K2 * NO +
K5 * OH)
'integrate eq 4.18
rNO = K1 * O * N2 + K3 * N * O2 + K5 * N * OH - K2 * NO * N - K4 *
NO * O - K6 * NO * h
rNO = rNO * dt

NO = rNO / MOL * 1000000# 'ppm
'MsgBox "stop"
NOZeldovich2 = NOppm + NO
```

```
End Function
```

G.15 Simple MFB and IMEP Calculation

```
'Rassweller and Withrow model SAE 970037 paper (appendix)
'p_rise calculates the pressure rise due to combustion
'why normalize the pressure rise wrt Vr SAE 2000-01-0953 p.2
Function p_rise(p1 As Double, v1 As Double, p2 As Double, v2 As Double,
Vr As Double, ncompression As Double, nexpansion As Double, angle As
Double) As Double

Dim DP As Double 'Change in pressure due to combustion
'p1 = pressure at considered angle
'v1= volume at considered angle also vr =reference volume at TDC
'p2 = pressure before considered angle
'v2 = volume before considered angle

'to convert to Pa and m^3
p1 = p1 * 1000000
p2 = p2 * 1000000
v1 = v1 / 1000000
v2 = v2 / 1000000

If angle < 0 Then
DP = (p1 - (((v2 / v1) ^ ncompression) * p2)) * (v2 / Vr)
Else
DP = (p1 - (((v2 / v1) ^ nexpansion) * p2)) * (v2 / Vr)
End If
If DP < 0 Then
DP = 0
End If
p_rise = DP

End Function
Function p_motor(v1 As Double, p2 As Double, v2 As Double,
ncompression As Double, nexpansion As Double, angle As Double) As
Double

Dim p1  As Double
'p1 = pressure at considered angle
'v1= volume at considered angle also vr =reference volume at TDC
'p2 = pressure before considered angle
'v2 = volume before considered angle

'to convert to Pa and m^3
p2 = p2 * 1000000
v1 = v1 / 1000000
v2 = v2 / 1000000

If angle < 0 Then
p1 = ((v2 / v1) ^ ncompression) * p2
Else
p1 = ((v2 / v1) ^ nexpansion) * p2
End If

p_motor = p1 / 1000000

End Function
'++++++++++++++++++++++++++++++++++++++++++++++++
++++++++++++++++++++++++++++++++
'work function calculates the area under the given line segment
'the method is based on SAE 750026 (1975) paper
'also see 960609
Function work(v1 As Double, v2 As Double, p1 As Double, p2 As Double)
As Double

Dim a As Double

'a simple way of calculating the area under a line segment
'work = 0.5 * (p2 + p1) * (v1 - v2)

'a better approximation of area under a Polytropic expansion or
compression where n = 1.4 is the following. this is very useful when the
angle step size is large. In our case the angle step size is 0.5 deg. and the
difference is '0.002% in torque and IMEP

a = (v1 - v2) / (v1 + v2)

work = (p2 * v2 + p1 * v1) * (a + ((1 / 3) * (a ^ 3)))

End Function

Private Function FindClosestValue(Value As Double, column1 As Variant,
column2 As Variant, LengthOfColumn) As Double

Dim row, RowIndex As Integer
Dim Number As Double
row = 0
RowIndex = 0
NumberAtRowIndex = -1000000000

   While row < LengthOfColumn
     row = row + 1
     Number = column1(row)

     If Abs(Number - Value) < Abs(NumberAtRowIndex - Value) Then
     NumberAtRowIndex = Number
     RowIndex = row
     End If
   Wend

FindClosestValue = column2(row)

End Function
```

G.16 Speedup Calculation

```
Sub SpeedCalculation()

Application.ScreenUpdating = False

'Automatically calculates everything in the open workbook
Calculate

Application.ScreenUpdating = True

End Sub
```

“The Stone Age did not end because we ran out of stones, and the oil age will not end because we run out of oil.”

Don Huberts (CEO of Shell Hydrogen - 2000)